General Disclaimer

One or more of the Following Statements may affect this Document

- This document has been reproduced from the best copy furnished by the organizational source. It is being released in the interest of making available as much information as possible.

- This document may contain data, which exceeds the sheet parameters. It was furnished in this condition by the organizational source and is the best copy available.

- This document may contain tone-on-tone or color graphs, charts and/or pictures, which have been reproduced in black and white.

- This document is paginated as submitted by the original source.

- Portions of this document are not fully legible due to the historical nature of some of the material. However, it is the best reproduction available from the original submission.

FINAL TECHNICAL REPORT

ADVANCED APPLICATION FLIGHT EXPERIMENTS PRECISION ATTITUDE DETERMINATION SYSTEM

REPORT NO. 22817-6002-RU-00

31 MARCH 1976

VOLUME II

SYSTEM TESTS

CONTRACT NO. NAS1-12894

Prepared for

NATIONAL AERONAUTICS AND SPACE ADMINISTRATION
LANGLEY RESEARCH CENTER
HAMPTON, VIRGINIA 23665

TRW
DEFENSE AND SPACE SYSTEMS GROUP

ONE SPACE PARK • REDONDO BEACH, CALIFORNIA 90278

FINAL TECHNICAL REPORT

ADVANCED APPLICATION FLIGHT EXPERIMENTS
PRECISION ATTITUDE DETERMINATION SYSTEM

REPORT NO. 22817-6002-RU-00

31 MARCH 1976

VOLUME II
SYSTEM TESTS

CONTRACT NO. NAS1-12894

Prepared for

NATIONAL AERONAUTICS AND SPACE ADMINISTRATION
LANGLEY RESEARCH CENTER
HAMPTON, VIRGINIA 23665

TRW
DEFENSE AND SPACE SYSTEMS GROUP

ONE SPACE PARK • REDONDO BEACH, CALIFORNIA 90278

FOREWORD

This document constitutes the TRW Defense and Space Systems Group final technical report to NASA Langley Research Center for the Application of Precision Attitude Determination Systems to the Earth Resources Survey (AAFE) Program. Prepared under NASA contract NAS1-12894, the report is being presented in two volumes, of which this is Volume II:

- Volume I — Strapdown Star Tracker Development
- Volume II — System Tests.

This report reflects the contributions of a number of previous efforts performed both under NASA contract (NAS5-21111) and independently by TRW. In the area of system design and analysis these efforts are summarized in the following final technical reports:

- PPCS System Design and Analysis, 13900-6012-RO-01, NASA/GSFC, NAS5-21111, 1 July 1972.
- PADS System Design and Analysis (Two-Axis Gimbal Star Tracker), 13900-6014-RU-00, NASA/GSFC, NAS5-21111, 1 July 1973.
- PADS System Design and Analysis (Single-Axis Gimbal Star Tracker), 13900-6016-RU-00, NASA/GSFC, NAS5-21111, 1 July 1974.
- PADS System Design and Analysis (Strapdown Star Tracker), 99994-6316-RU-00, TRW Report, 23 December 1975.

In the area of hardware development the following reports have been published:

- PPCS Star Tracker Test, 13900-6013-RU-00, NASA/GSFC, NAS5-21111, 1 July 1972.
- PADS Star Tracker Test, 13900-6015-RU-00, NASA/GSFC, NAS5-21111, 1 July 1973.

TRW employees who contributed to this final report include: F.J. Belsky, D.I. Brubaker, R.E. Edwards, R.L. Farrenkopf, R.F. Gates, R.J. Mann, K.J. McAloon, and J.G. Zaremba.

Approved by: K. J. McAloon
K.J. McAloon
Project Manager

Approved by: W. A. Finley
W.A. Finley, Manager
Control and Senior Systems Laboratory

CONTENTS

CONTENTS (Continued)

CONTENTS (Continued)

ILLUSTRATIONS

ILLUSTRATIONS (CONTINUED)

ILLUSTRATIONS (CONTINUED)

ILLUSTRATIONS (CONTINUED)

TABLES

1. INTRODUCTION AND SUMMARY

Since 1970 TRW has been engaged in activities related to precision attitude determination systems (PADS) for spacecraft applications under company, NASA, and USAF funding. In addition to extensive analyses of such systems, developmental efforts have been undertaken in the areas of star trackers and software algorithms. Engineering model gimbal and strapdown star trackers were developed and tested along with computer simulations of the effectiveness of various algorithm approaches.

In 1974 NASA/LaRC awarded TRW a contract to perform a laboratory test of the performance capability of an engineering model PADS. The test objective which evolved subsequently was to test two such systems, one using a strapdown star tracker, the other using a single-axis gimbal star tracker. The simulated orbit configuration was to be that of a PADS aboard a three-axis stabilized, earth-pointed satellite in geosynchronous orbit. The performance goal was to demonstrate 0.001 degree (1σ) per axis accuracy for both the strapdown and gimbal PADS. A secondary program objective was the fabrication, assembly, and unit test of the strapdown star tracker for the system test. The majority of the design of this tracker had already been accomplished.

A functional block diagram of PADS is presented in Figure 1-1. PADS, mounted aboard a spacecraft, provides estimates of the inertial attitude of the spacecraft axes. The PADS sensors are:

- A star tracker which provides periodic updates of the spacecraft attitude relative to identified stars.
- Gyros which provide a continuous indication of the relative inertial attitude of the spacecraft.

In addition to the sensors, a digital computer (either on-board or ground-based) implements the software algorithms which combine the redundant sensor signals and compute the spacecraft inertial attitude.

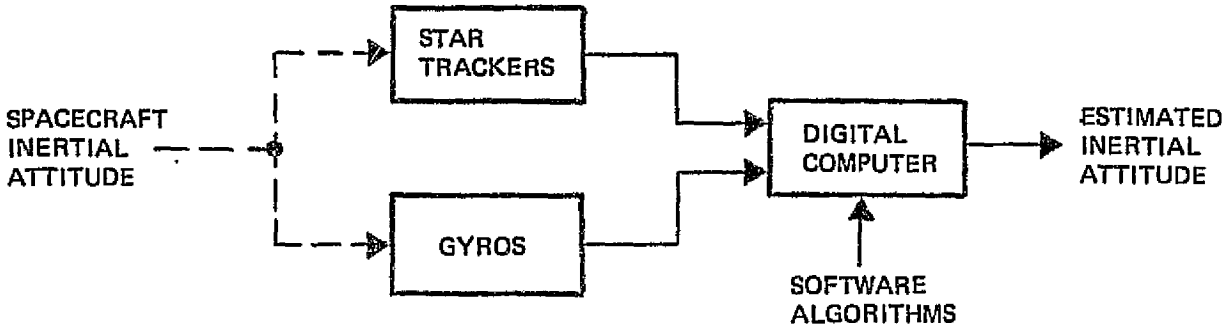

Figure 1-1. Precision Attitude Determination System (PADS)

The PADS engineering model hardware components tested in the laboratory are shown in Figure 1-2. These components consist of:

- A strapdown star tracker developed by TRW
- A single-axis gimbal star tracker also developed by TRW
- A three-axis inertial reference unit furnished by NASA.

The PADS software algorithms were implemented offline in a CDC 6500 digital computer.

In orbit the strapdown star tracker uses the orbit rate of the satellite for star availability. The developed strapdown star tracker has a star magnitude sensitivity requirement of 8 M_V in order to provide frequent star updates at geosynchronous rate. A small 1^0 by 1^0 field of view resulted from the accuracy requirement of 0.001 degree.

The single-axis gimbal star tracker is a modification of a two-axis tracker developed by TRW on a USAF program. In its modified state it has a $1/2^0$ by $1/2^0$ field of view which can be gimbaled through $\pm 45^0$. In view of the larger effective field of view of the tracker, its star magnitude sensitivity requirement is only 3.5 M_V.

The original intent was that NASA would furnish an engineering model of a three-axis inertial reference assembly using the Bendix 64 PM RIG gyro. However, schedule difficulties precluded delivery of this assembly, and the engineering model Inertial Reference Unit (IRU) from the Orbiting Astronomical Observatory program was substituted. Although nominally a higher performance unit, a somewhat anomalous behavior of the IRU gyros resulted in it being roughly equivalent to the Bendix specified performance.

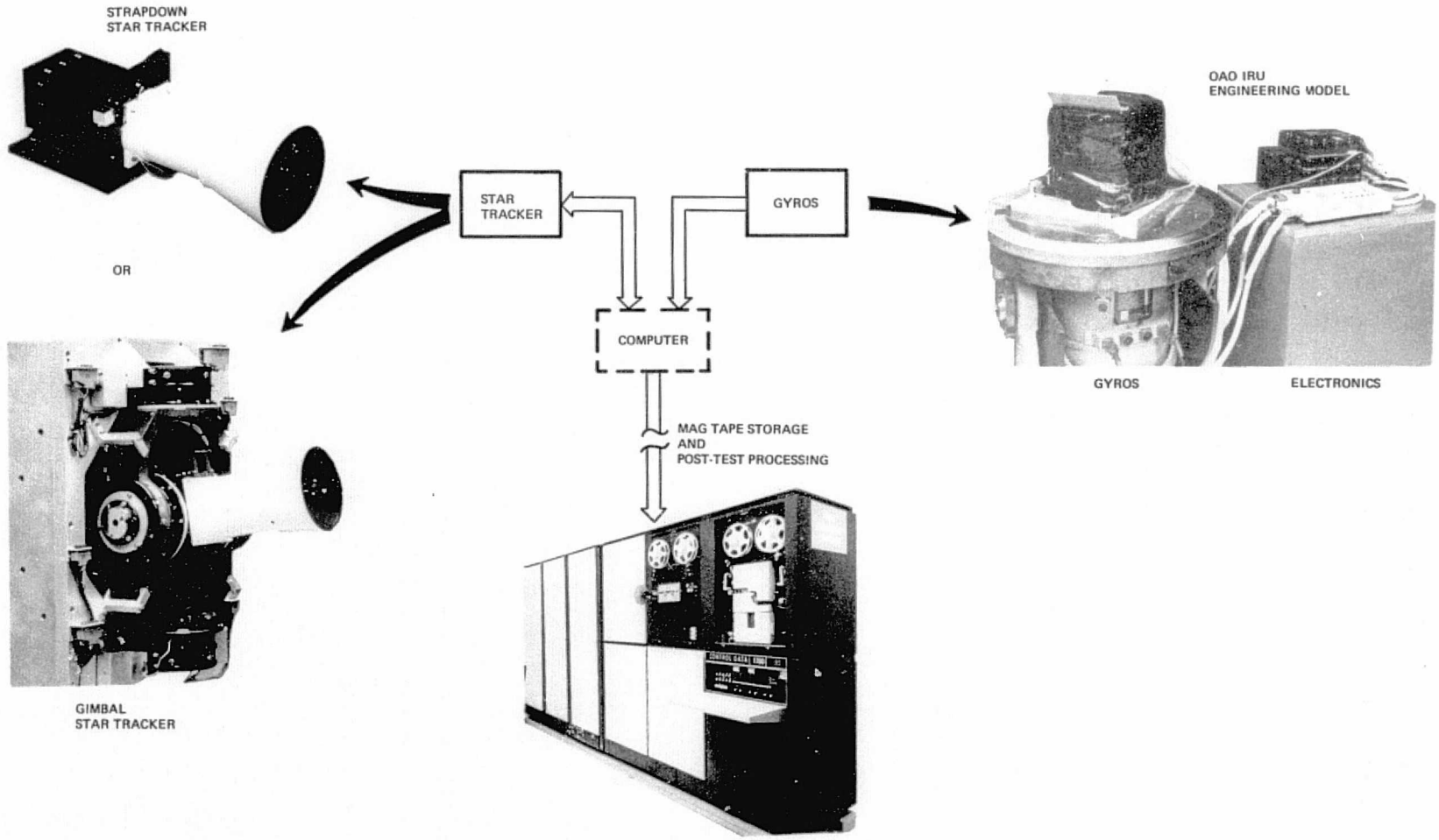

Figure 1-2. PADS Hardware Components

Since the primary emphasis of the laboratory evaluation was on the accuracy of the star trackers and the effectiveness of the software algorithms in processing actual sensor signals, it was considered adequate to implement the algorithms offline in a CDC 6500 digital computer. The sensor signals were time-tagged and stored on magnetic tape during the test, and then processed post-test using FORTRAN coded algorithms.

The precision test facility in which the PADS tests were performed is shown in Figure 1-3. A ground-fixed test configuration was implemented both because of the geosynchronous orbit simulation requirement and the extremely high accuracy demanded from the laboratory instrumentation. In this configuration the PADS reference axes were stationary in the laboratory axes and the collimated star beams were moved relative to the laboratory, or PADS, axes. Knowledge of the inertial motion of the laboratory, plus measurement of the attitude of the star beams relative to the laboratory axes by laboratory instrumentation, provided the reference coordinates against which the PADS attitude estimates were compared.

Both the strapdown and gimbal PADS laboratory tests were successfully completed. In each case a ten day test was performed following an initial alignment procedure. During the ten days four evenly spaced attitude determination test runs were made. Each run was four to five hours long.

Post-test data processing and evaluation showed that both systems met the performance goal of 0.001 degree (1σ) per axis. Based on star availability data, 20 minute star update intervals were selected to minimize gyro induced errors while still providing a high probability (>97%) of star acquisition. The rms accuracy obtained with each system, normalized to equal components for all axes, was:

- Strapdown PADS: 2.3 arc second (rms) per axis
- Gimbal PADS: 3.6 arc second (rms) per axis.

These results were obtained without any limitations in star separation geometry.

In view of the test results obtained, the program was considered very successful, not only because a difficult laboratory evaluation was completed as planned, but because both PADS met their performance goals.

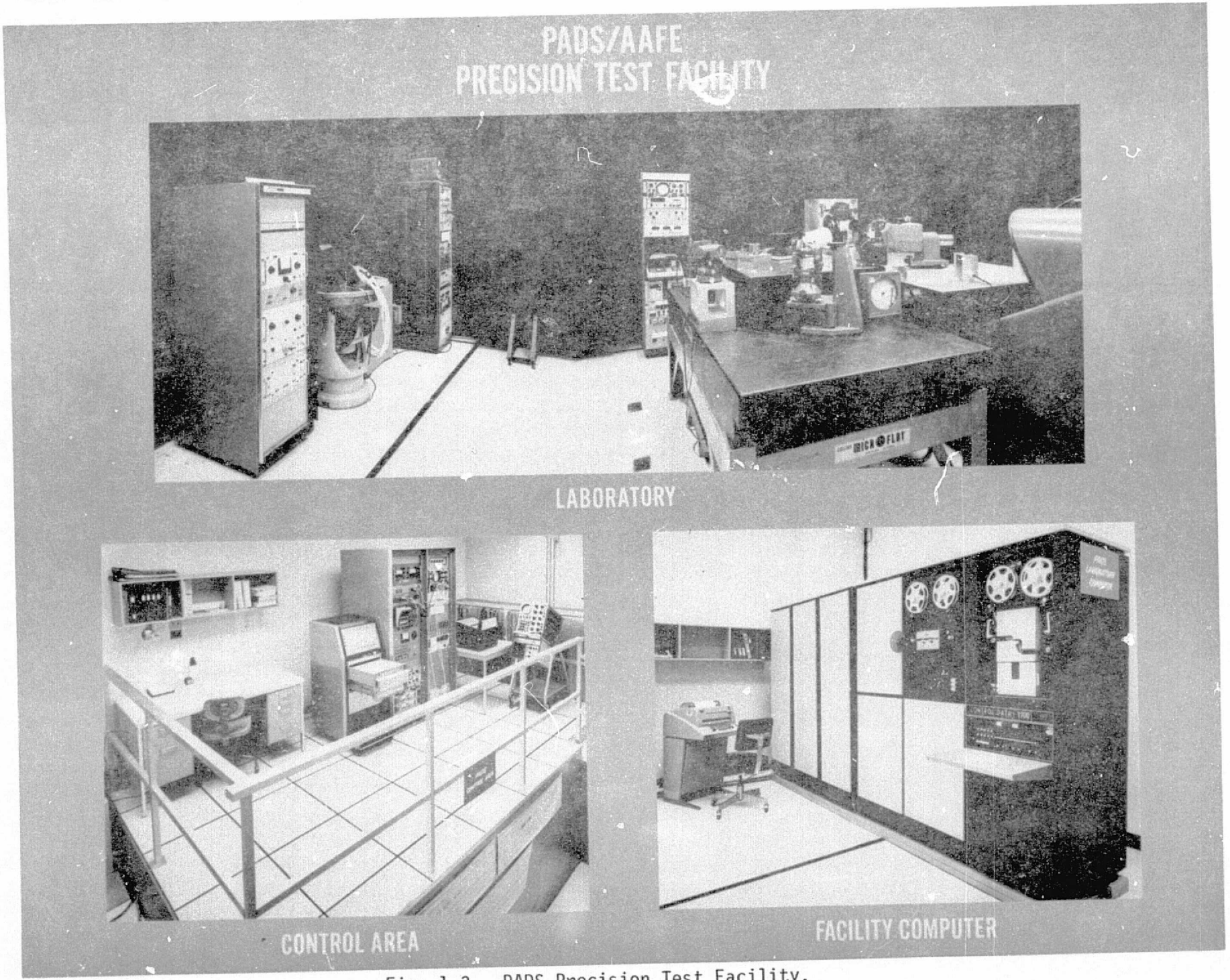

Fig. 1-3. PADS Precision Test Facility.

2. TEST OBJECTIVE

The purpose of the PADS system tests was to measure the performance capability of each of two PADS, one using a strapdown star tracker, the other using a single-axis gimbal star tracker. The performance evaluation was conducted in the laboratory under simulated orbit conditions. These conditions consisted of the stellar optical stimuli and inertial attitude rates which would be experienced on a three-axis stabilized, earth-pointed satellite in geosynchronous orbit.

The primary focus of the evaluation was on the contribution to the total system accuracy by the star trackers, and the effectiveness of the software algorithms in functioning with actual sensor signals.

The performance criteria for the laboratory tests was the accuracy with which the PADS estimated its attitude throughout the test period relative to the inertial attitude of the laboratory at the start of the test. A ground-fixed laboratory test was performed in which the PADS axes remained stationary in the laboratory coordinates. Star stimuli were simulated by moving the star line of sight relative to the laboratory coordinates. A direct means of evaluating the PADS performance was obtained from: 1) true knowledge of the laboratory inertial attitude as a function of time, and 2) precise measurement of the star line of sights relative to the laboratory, and hence inertial, coordinates.

The performance goal for PADS was a steady state accuracy of 0.001 degree (1σ) per axis. For the purposes of this program the one sigma two-axis or three-axis goal is defined as the RSS of the single axis goals.

The laboratory environment was benign in terms of temperature and vibration. No bright object sources were simulated. Satellite attitude control rates were not simulated. Evaluation of these effects was considered more properly relegated to the component test or design simulation level.

3. DESCRIPTION OF PADS

Brief descriptions of the PADS hardware and software are given in this section. Detailed design information for the system components has been documented during previous efforts and programs and is referenced in the following descriptions.

PADS provides estimates of the inertial attitude of its reference axes. A functional block diagram of PADS is shown in Figure 1-1. The star trackers provide periodic absolute attitude updates. The gyros provide continuous relative attitude data. The computer implements the software algorithms which combine these redundant sensor signals and estimate inertial attitude.

The following paragraphs describe in detail the specific PADS components which were tested. Descriptions of the strapdown star tracker, the gimbal star tracker, and the gyros are given along with comments regarding their origin and level of development. In view of the offline data processing which was performed, a description of a flight suitable digital computer was not relevant. The software algorithms are described, but their adaptability to a flight computer is not discussed, again because it was not relevant to this test program. This latter topic has been covered, however, in previous studies described in the foreword.

3.1 HARDWARE

The PADS hardware which was tested in the laboratory is illustrated in Figure 1-2. Two PADS configurations were tested, one using a strapdown star tracker, the other a gimbal star tracker. The same inertial reference unit was used for each configuration. This unit contained three gyros which had their input axes mounted orthogonal to each other. Since the emphasis of the test program was directed toward the performance capability of the star trackers and the effectiveness of the software algorithms, a flight-suitable computer was not used. Instead, the sensor data was collected on magnetic tape during the test using a CDC 1700 computer, and then processed post-test using a CDC 6500 computer.

3.1.1 Strapdown Star Tracker

An extensive description of the strapdown star tracker (SST) is presented in Volume I of this report. Detailed descriptions of the design are given along with extensive design analyses and test results.

The star tracker is a high accuracy, high sensitivity sensor with the performance characteristics listed in Table 3-1. The tracker has been designed to meet the PADS requirement to track 8 M_V stars with 3 arc seconds accuracy. Engineering model level of development has been achieved.

The star tracker uses an image dissector tube as its basic detector because the high sensitivity and resolution available from this instrument is consistent with the PADS requirements. The ITT F4012 image dissector was selected because of its proven reliability in space applications.

Table 3-1. SST Design Parameters

Field of View	1^o by 1^o
Sensitivity	10 Mv G0(6000^oK)
Photodetector	
Type	ITT F4012
Usable Photocathode Area	12.7 mm
Aperture Diameter	0.254 mm
Optics	
Type	Cassegrain
Focal Length	50.8 cm
Aperture	60 cm^2
Instantaneous Field of View	103 arc sec
Electronics	
Position Output	12 bit serial word
Magnitude Output	10 bit serial word
Update Time	0.1 sec
Functional Performance	
Maximum Acquisition Time	13.6 sec
Maximum Track Rate	0.02 ^{o}/sec
Accuracy (with FOV and Temp. Comp.)	
Line of Sight to EO Axes	
Noise (1σ)(single sample)	3.0 arc sec (8 Mv)
Fixed (1σ)	2.0 arc sec
EO Axes to Optical Reference	
Bias (3σ)	5.1 arc sec
Bias Stability (3σ)	1.3 arc sec
Size	12.7 x 12.7 x 56 cm
Weight	5 kg
Power (using CMOS logic)	4.6 watts

Photon counting is used as a detection technique because it provides superior sensitivity over that achievable with conventional analog techniques.

The search, track, and mode control electronics are completely digital, not only to complement the photon counting technique, but to eliminate those errors associated with the conventional analog implementations.

The entire electro-optical structure has been made from graphite/epoxy composite material in order to minimize all thermal distortions. This material has a linear coefficient of thermal expansion which is 100 times less than that of aluminum.

A functional block diagram of the SST is shown in Figure 3-1. An explanation of the diagram is facilitated by considering four functional groupings:

- Signal generation
- Acquisition
- Track
- Control.

Signal Generation. Photons received from the star or target are focused by the optics to a spot on the photocathode of the image dissector. The resulting signal from the anode of the tube is processed by the video detector. For weak signals, the output of the video detector will be logic level pulses corresponding to the emission of electrons from the photocathode. For strong signals, in the presence of the cruciform spatial modulation pattern, the output will be a squarewave at the modulation frequency.

Acquisition. Acquisition is achieved by scanning the 1^{o} by 1^{o} FOV with a discrete raster pattern produced by the acquisition scan generator. For normal acquisition the pattern is a 64 x 64 dot matrix which is completed in less than 14 seconds. Proximity to a star is detected by the star presence circuit. This circuit counts the number of photoelectrons at each dwell point in the scan matrix. In the presence of a star, a dwell count significantly higher than the background noise count will be measured. By commanding the differential count necessary to indicate a star, stars equal to or greater than selected magnitudes may be acquired and tracked.

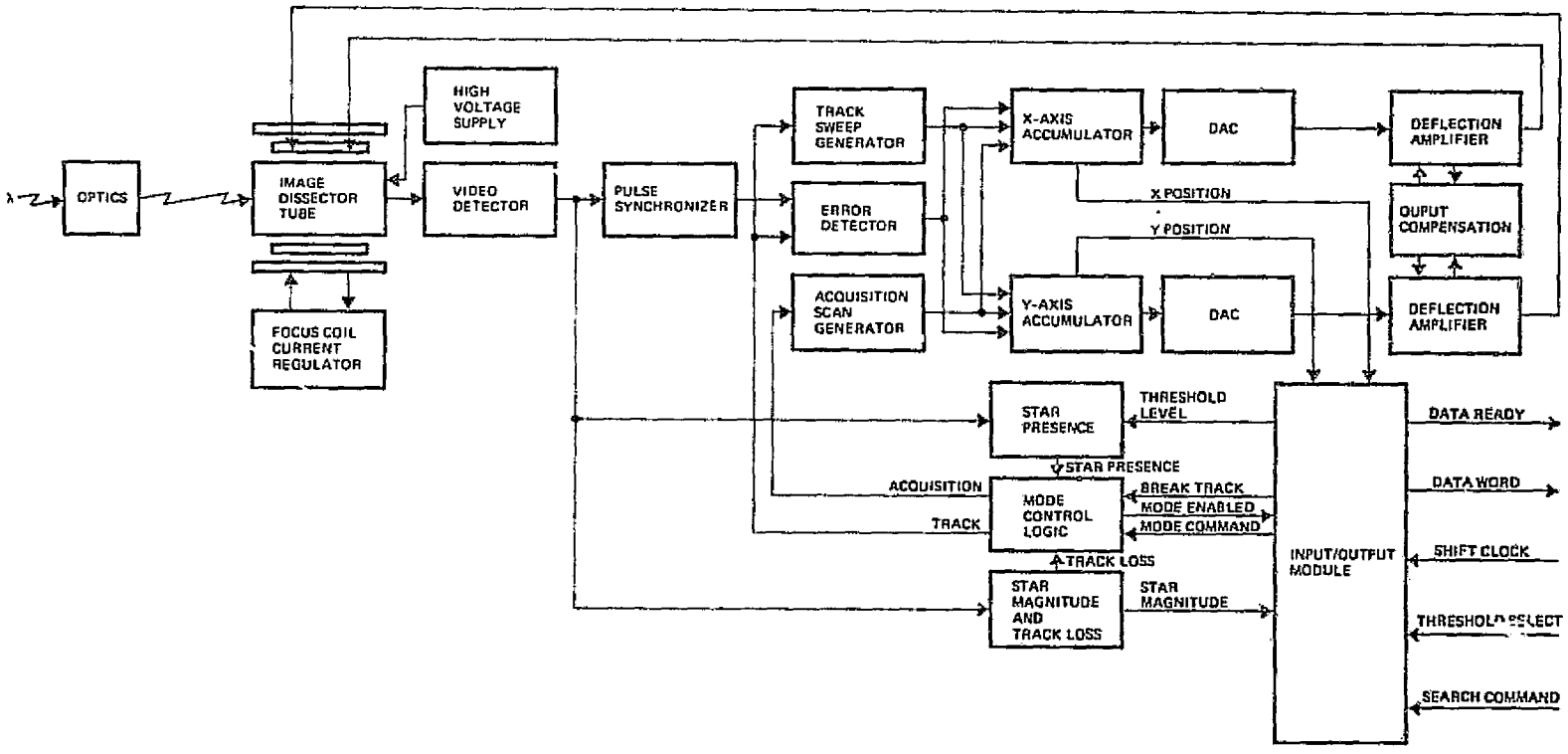

Figure 3-1. Star Tracker Block Diagram

Track. Track is initiated by a signal from the star presence circuit. The track sweep generator starts eight continuous cruciform patterns at the position at which track was entered. If the star magnitude and track loss circuit does not indicate that a star is being tracked, then the acquisition scan is continued. The pulse synchronization circuit is the key element in enabling the tracker to track either bright or dim stars. In the case of dim stars, the circuit will produce pulses on a one-to-one basis with photoelectron pulses. By counting pulses in synchronization with the cruciform track sweep, the percentage duty cycle of the pulse width modulated (PWM) information is computed in the error detector circuit. On the other hand, bright stars will produce a squarewave at the video detector output which reflects the PWM information. By gating this signal with a high frequency clock, the information content is retained in the form of clock pulses instead of photoelectron pulses, and the percent duty cycle is again computed in the error detector circuit. By timesharing the error detector only one circuit is needed to compute the error for both axes. At the end of each cruciform pattern the computed error for each axis is summed with the number in the accumulator for that axis. Each accumulator drives a DAC which in turn drives the deflection amplifiers. Star magnitude is measured by the star magnitude and track loss circuit.

Control. The tracker mode control is implemented by the mode control logic. The inputs to this circuit are:

1) Star presence
2) Track loss
3) Search
4) Zero.

The last two signals are manual controls. A manual switch to disable the track loss signal is also provided.

3.1.2 Gimbal Star Tracker

The PADS requirement is for a single-axis gimbal star tracker. However, programmatic considerations necessitated the use of a two-axis star/landmark tracker developed under an Air Force contract. A detailed design description of this unit is given in reference. (1) To make the tracker compatible to

the PADS requirements, the outer gimbal was mechanically locked and the landmark function was inhibited. The remaining star tracker functions represent the same technology developed previously by TRW for a single-axis gimbal star tracker.(2) The following description applies only to the modified tracker.

The PADS gimbal star tracker (GST) consists of a Star Sensor Unit (SSU) mounted within a single degree of freedom Sensor Gimbal Unit (SGU). The SSU incorporates the optics, detector, and supporting electronics. The SGU is an exceptionally precise and stable mount providing gimbal drive for null tracking stars and precision angular readout of the gimbal. The GST interfaces with the Sensor Electronics Assembly (SEA) which provides the gimbal angle processing and servo drive signals. The performance characteristics of the GST are shown in Table 3-2.

3.1.2.1 Star Sensor Unit

The SSU is a high accuracy star sensor designed to track 3.5 M_V stars with arc second accuracy. The SSU uses an image dissector tube together with conventional analog search and track electronics.

The optical design results from a tradeoff between the desire for a short focal length to obtain small size and weight, and the requirement to maintain arc-second level accuracy. The selected design is a Cassegrain telescope utilizing aluminum optics.

A bright object sensor and shutter assembly are incorporated in the sensor along with the high voltage power supply. The high voltage power supply will be incapacitated by the bright object sensor when the sun is within the 45 degree field, and also, a rotary solenoid will be actuated which will close the shutter in front of the photocathode.

The sensor assembly has been designed with great care for thermal symmetry to provide maximum thermal-mechanical stability. In particular, the electronics are equally spread around the tube assembly. The high voltage power supply and line voltage converter, behind the tube assembly and the flange mounting, provide symmetrical heat transfer through the structure into the mounting plate.

Table 3-2. GST Design Parameters

Field of View	0.5 x 0.5 deg
Gimbal Freedom	Up to ±60 deg
Sensitivity	+3.5 m_V
Bandwidth	25 Hz
Optics	
Focal Length	84 cm
Aperture	54 cm^2
IFOV	84 arc sec
Detector	F4012 RP
Minimum Sun Angle	45 deg
Accuracy (1σ, per axis)	
Sensor	
Electronic Bias	0.14 arc sec
Thermo-Mechanical (Random)	0.46 arc sec
Noise Equivalent Angle	1.2 arc sec
Gimbal and Encoder	
Alignment	0.71 arc sec
Thermo-Mechanical Stability	0.28 arc sec
Inductosyn	0.86 arc sec
Readout Electronics	
Bias	0.42 arc sec
Random	0.42 arc sec
Noise and Quantization	0.3 arc sec
Size	30 x 51 x 16 cm
Weight	13.6 kgm
Power	17 W

The image dissector, deflection yoke, focus coil, and high voltage biasing network are all contained in a single, integral, encapsulated assembly. The outer structure of this assembly consists of the necessary magnetic shielding to prevent stray fields, or the earth's field, from affecting the image dissector, and is mechanically indexed directly to the optics. The electronics are contained on four flex-print interconnected printed circuit boards which are installed in the housing as a subassembly around the tube assembly.

A functional block diagram of the SSU is shown in Figure 3-2. The following paragraphs explain the sensor operation.

Video Processor. The video processor performs the following functions. During the search mode, automatic gain and threshold control circuits select only the largest video pulse present and send it to the mode control logic. When in the track mode of operation, the image dissector video is shaped into a digital pulsewidth-modulated signal and is fed to the demodulator. A digital star-presence signal and an analog star-magnitude signal are also developed.

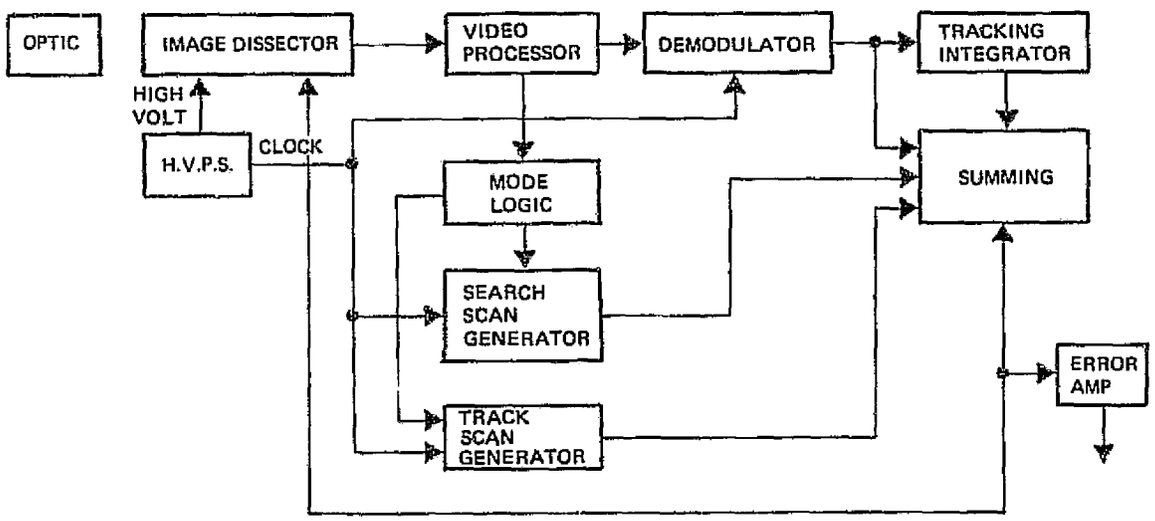

(ONLY ONE ERROR CHANNEL IS SHOWN)

Figure 3-2. Functional Block Diagram of Star Sensor Unit

Mode Control Logic. The mode control logic establishes the mode of operation: search or track. The timing of the search cycle, the gating of the tracking loop, and search-scan waveforms are also controlled by the mode logic.

Demodulator. The demodulator circuits consist of timing gates to process the pulsewidth-modulated video and precision voltage switches which develop the tracking loop correction error voltage at the input to the tracking integrator.

Tracking Integrators. This circuit consists of an integration stage (op-amp) which provides correcting dc voltages to the deflection generator to keep the star image centered in the image-dissector aperture by taking the integral of the error demodulator output.

Scan Generator. The scan generator provides three separate circuit functions. A triangular waveform is generated by a counter-integrator combination and is used as the track mode scan waveform. Two binary counters and D/A converters are used to develop the stairstep-type search mode scan waveforms. The above scan waveforms and the dc-correcting voltage from the tracking integrator are summed in current dividers to provide the deflection coil current required.

Error Amplifier. The dc component of the deflection coil current is determined by a current sampling resistor and the corresponding voltage is then amplified and filtered to give the required output pointing error gradient.

3.1.2.2 Sensor Gimbal Unit

The single degree of freedom gimbal assembly utilizes a proven single ball/flexure suspension system and Inductosyn readout. The gimbal is formed by identical drive housing assemblies attached on each side of the star sensor unit. The drive housings incorporate the suspension/bearing system, drive motors, Inductosyn encoders, and data link.

The use of identical drives on both ends of each axis is motivated by the desire to obtain mechanical and thermal symmetry. The star sensor mass is centered between the supporting bearings of the gimbal. Nearly identical

power dissipation in each housing minimizes thermal gradient variations. Further, zero structural slope mounting points are chosen so that one-g distortions result in translation only – not in angular rotations. With this approach, testing can be accomplished with negligible errors due to gravity induced droop.

Gimbal Suspension

The gimbal design features a one-ball bearing configuration. The geometry of this scheme provides self-alignment features and facilitates the fabrication of the gimbal system by providing inherent reference for the establishment of the rotational axis of the gimbal.

The desired axis is established by a line of contact of the balls with the cone surfaces of their retaining cups. The accuracy of the gimbal axis is set by the cups radii of contact and the ball sphericity. Since the ball sphericity can be obtained to two parts in a million and the cups radius of contact is established by lapping, and since all other critical surfaces are indexed to the payloads balls, the achievement of very accurate alignment is possible. The suspension consists of two single spherical balls supporting the payload. Each ball locates itself via two cone type cups. One cup (rotating retainer) is located on each side of the payload and the other cup (stationary retainer) is inclined 40 minutes of arc with respect to the center line passing through the centers of the spherical balls; the stationary cup cone is eccentrically offset with respect to the centerline of the cylindrical shaft containing the cone. The shaft element is housed in the bore of the flexure, which is an intermediate element between the retainer and the gimbal frame.

Drive Motors

Each gimbal motor drive assembly is identical in performance and general configuration. It consists of a two phase permanent magnet motor and appropriate support structure. The motor has 24 poles and 4 skewed slots between pole spaces. The commutation to the motor is provided by the Inductosyn resolver signal which is conditioned to provide the required power in terms of sine and cosine functions with periods satisfying the number of poles (12 speed). Interconnecting of the sine and cosine inputs to the respective motor winding results in a brushless motor exhibiting dc torquer characteristics.

Inductosyn Encoders

The angular rotation of each gimbal is measured using a precision Inductosyn. The Inductosyn is a pair of discs, in this case 5 inches in diameter, which are mounted such as to rotate coaxially with respect to one another with facing surfaces in close proximity. The facing surfaces have printed conductors, forming winding circuits which may be flux linked, disc-to-disc. One disc, designated the rotor, has a single winding; the other, the stator, has two windings. The winding geometry is arranged so that the transformation coupling from rotor to stator varies trigonometrically with relative disc rotation. The two stator windings are in mechanical quadrature to one another. Thus, the device is electrically identical to a synchro resolver, except for a very low coupling efficiency and for a larger number of poles than are normally found in a conventional resolver.

Data Link

The data link provides transmission of electrical signals across the gimbals without excessive restraint torques. The design utilizes an "S" folded conductor strip which is attached at the ends of and slides between a cylindrical stationary member attached to the housing sleeve and a smaller diameter cylindrical component (the rotating member) attached to the motor shaft. The inner and the outer members are lined with nylon rings to provide electrical insulation and mechanical guide for the rolamite action of a 6 conductor strip. There are four such strips providing the capability of $\pm 60^{\circ}$ motion with restraints not exceeding 36 gm-cm. Both the stationary and the rotating members of this assembly are made from beryllium. Appropriate electrical connectors (miniature) are attached to the periphery of the rotating and stationary component. The data link itself is so designed that it can be removed from the system without disturbing the various electrical interconnections.

3.1.2.3 Sensor Electronics Assembly

The Sensor Electronics Assembly provides encoding of the Inductosyn gimbal angle signals and implements the controller/drive for the gimbal motors. Figure 3-3 shows the SEA functional block diagram for one of the two gimbal axes. The Inductosyn Electronics has as its function the excitation and processing of both multi-speed and single-speed Inductosyn output signals to derive the precision measure of gimbal angle. The Drive Electronics provides for loop compensation and appropriate commutation, and and motor power drive functions.

Inductosyn Electronics

An Inductosyn is analogous to a resolver. It has a primary, the rotor, which is sinusoidally excited at some frequency, 10.3 kHz in this case. It has two secondary (stator) output signals of the same frequency, whose amplitudes are trigonometrically amplitude-related to the device's mechanical angle:

$$V_s = kV_e \sin n\theta \sin \omega_e t$$

$$V_c = kV_e \cos n\theta \sin \omega_e t$$

where θ is the mechanical angle, V_e is the rotor excitation amplitude, and ω_e is its frequency. The transformation ratio, k, is extremely small for an Inductosyn, such that the output signal is only a few millivolts. Each Inductosyn has a single-speed and a 256 speed set of windings. The speed ratio, n, is unity for the single-speed section and 256 for the multi-speed section. Thus, the single-speed outputs advance one electrical revolution for each mechanical revolution, while the multi-speed signals advance 256 electrical revolutions for the same mechanical rotation. By processing both pairs of signals an extremely high resolution can be achieved.

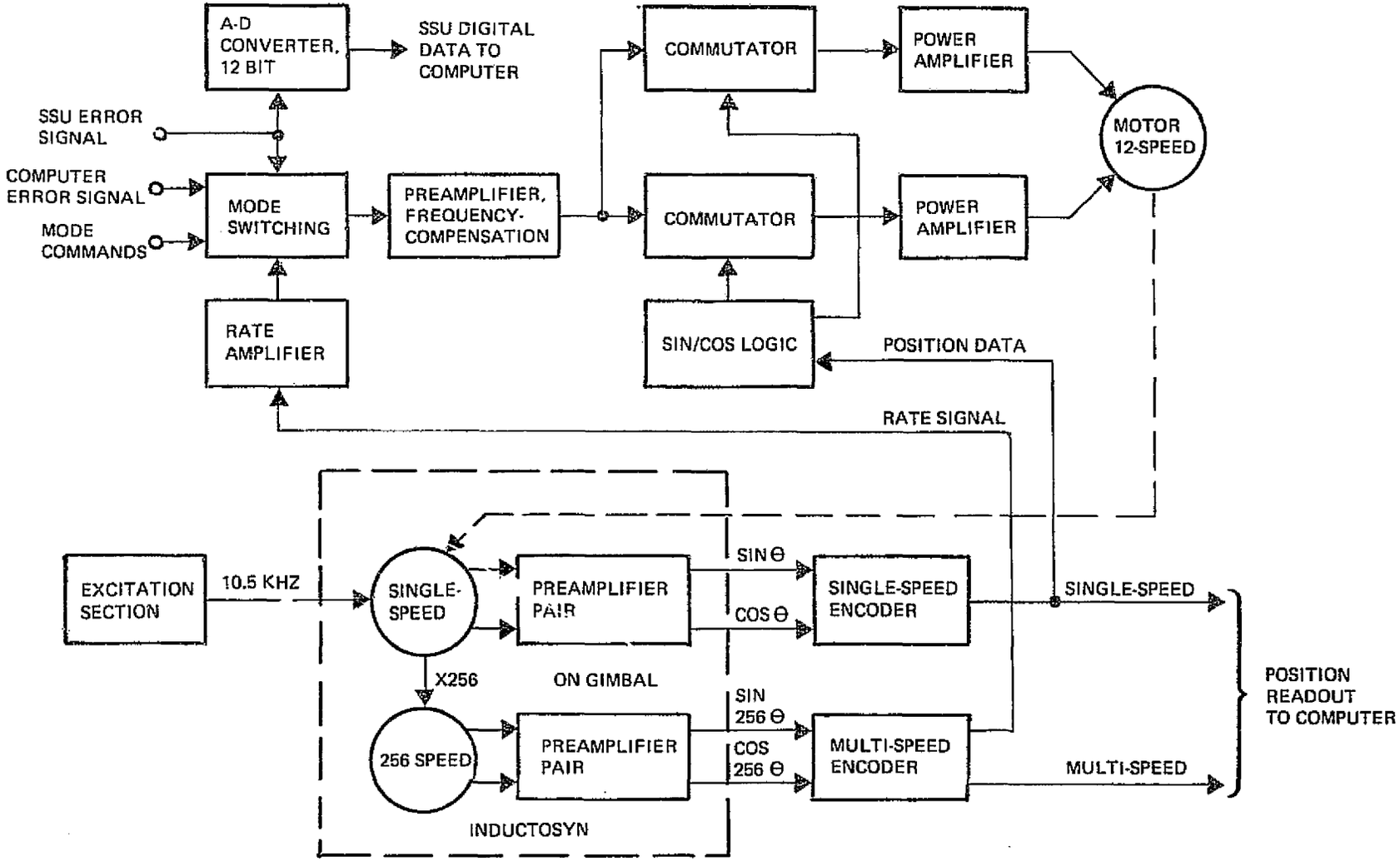

Figure 3-3. Sensor Electronics Assembly Functional Block Diagram

The Inductosyn signals are amplified by special preamplifiers located on the gimbal, and the resultant signals transmitted to the SEA for further processing. Within the SEA, the signals are converted from amplitude to phase format. Each pair, as decribed above is converted to a phase pair:

$$V_A = V \sin (\omega_e t + n\theta)$$

$$V_B = V \sin (\omega_e t - n\theta)$$

Thus, gimbal angle information now resides in the relative phase of the signals, in "double-angle" form, i.e., the relative phase between V_A and V_B changes twice as fast as $n\theta$. These signals are then converted to standard logic signals, A and B, for use by the encoder logic. The amplitude-to-phase converters are specially designed to preserve the inherent Inductosyn accuracy. A computer analysis has shown a worst-case error of ±0.03 degree electrical for the converter itself, excluding pre-amplifier gain variations and zero-crossing detector propagation delay variations.

The Encoder section is used to digitally measure the relative phases of the A and B signals from the amplitude-to-phase converters, and thus, to develop a digital quantity representing the gimbal angles.

Gimbal Control Electronics

The control electronics has two modes which are commanded by an external computer:

1) Slew

2) Track.

In tne slew mode a servo summing junction is implemented in the computer using the desired position profile and the SEA inductosyn readout. The error signal from this junction is used to drive the gimbal servo electronics. A rate signal can also be commanded by the computer to augment the gimbal response performance. Operationally, this mode is used to position the gimbal so that a star will be in the field of view of the SSU.

If the SSU acquires a star, it will send a track signal to the computer. The computer in turn will command the gimbal control electronics into the track mode. Here the vertical deflection signal from the SSU is used as the error signal to the gimbal servo electronics. The electronics will drive the gimbal motor until the SSU signal is nulled, i.e., the star is positioned midway between the top and bottom of the field of view.

The servo design consists of a proportional plus integral mechanization which eliminates gimbal hangoff due to static bearing friction. In both modes the servo is damped by a rate signal derived from the inductosyn information. The rate loop is also implemented with a proportional plus integral design to compensate for running bearing friction.

3.1.3 Inertial Reference Assembly

The original plan for the PADS program was to receive a gyro assembly for the laboratory tests from NASA/Goddard Space Flight Center (GSFC). This assembly would have used the Bendix 64 PM RIG gyro in a configuration similar to that for the International Ultraviolet Explorer Satellite. However, procurement difficulties experienced by GSFC prevented use of this gyro assembly on the PADS program. In its place GSFC subtituted an engineering model version of the Orbiting Astronomical Observatory Inertial Reference Unit (OAO/IRU). A detailed design description of this unit is given in reference (3). The following description is extracted from this reference and is limited to only those aspects relevent to the PADS testing.

3.1.3.1 General Description

The IRU used in the laboratory tests consists of two packages: an Inertial Package (IP) and an Electronics Package (EP). A test console was also supplied by GSFC which provided an electronic interface capability with the IRU.

The test console provided all the necessary commands and power to operate the IRU. Aside from the start-up and shut-down procedures, the only interfaces with the test console during the PADS tests were manual changes to the R-Term compensation for all three gyros. These changes simplified the quick look display of the gyro performance during the testing.

A data interface unit was added to the test console by GSFC to transmit the gyro outputs to the PADS data collection system. Each output consists of a 16 bit word representing the inertial rotation about the gyro input axis. The scaling is nominally 0.075 arc sec/count. The 16 bit word turns over after approximately 1.4 degrees.

IP

The IP is a temperature controlled cube 9 inches on a side. It weighs 18 kg and contains three precision gyros, their control and readout electronics, a frequency source assembly which provides the precision frequency for all the electronics in the IRU and temperature control electronics. Attached to the IP are radiator plates which conduct heat away from the IP. Each radiator is approximately 7.6 x 22.9 cm in area.

The gyros mounted in the IP were fabricated at MIT. They are MIT designed adaptations of the inertial grade 2FBG-6F floated gyro. The 2FBG-6F gyro was modified for the OAO mainly by simplifying its construction and by improving its data bandwidth capability. The gyros are operated with binary pulse restrained torque loops. Torque data from the gyros are processed as rate integrals (i.e., angles) in the EP and converted to digital signals. The IRU's reference position about each axis can either be reset or changed incrementally. The resets are enabled by programmed commands. Incremental changes in position are limited to one axis at a time.

For the PADS tests the IRU was operated only in the HOLD mode. During this mode, the rate capability is 15 arc sec/sec, or earth rate. The indicated rate of each gyro output can be digitally compensated in the EP (referred to as R-Term compensation).

The gyro electronics, temperature control, and frequency source electronics consist of potted cordwood modules and discrete components, assembled into the following subassemblies: Frequency Source Assembly, Temperature Control Assembly, Auxiliary Temperature Control Assembly, Torque Generator End Assembly (TGEA) and Signal Generator End Assembly (SGEA). Each gyro has a TGEA and SGEA mounted with it, and tuned to it, to provide proper gyro parameters. A total of 21 cordwood modules is used in each IP.

EP

The EP is a rectangular assembly, 22.9 x 38.1 x 15.2 cm weighing 17.3 kgm, made up of 3 electronic trays and an annex attached to tray 1. Contained in the 3 trays and annex are 63 potted cordwood modules and a number of discrete components, power transistors, transformers etc.

The EP contains analog, digital and hybrid electronics. There are 17 major electronics blocks including: power supplies, control units, input/out units, logic and conditioning units.

3.1.3.2 IRU Performance

The IRU was tested at GSFC by personnel from Charles Stark Draper Laboratory prior to delivery to TRW for the PADS tests. This testing is described in Appendix C of this report. In summary, the tests showed that the performance of all three gyros was degraded. The z(yaw) gyro was especially bad.

Following setup and integration at TRW, the IRU performance was again observed and found to be different from that measured at GSFC. This encouraged efforts to improve the IRU. Two actions undertaken did improve the performance:

1) A rewiring of the power interface

2) A change in the thermal configuration.

The performance was again measured by CSDL and found to be significantly improved. These results are also described in Appendix C.

The gyro performance is described in Appendix C in terms of power spectral density (PSD) curves. Another method which was used to characterize the random drift of the gyros is to plot the standard deviation of the gyro attitude as a function of sample time. Figure 3-4 illustrates the approach which was taken. The standard deviation was calculated as:

$$S = \left[\frac{1}{N} \sum_{i=1}^{N} \left(\partial\theta_i - \frac{1}{N} \sum_{j=1}^{N} \partial\theta_j \right) \right]^{1/2}$$

where

N = the total number of samples

$\partial\theta$ = the attitude change over a sample time Δt.

Figures 3-5 through 3-7 show the standard deviation plotted as a function of sample time for the three gyros. The data was derived from two runs taken on 5 September 1975 and 19 September 1975. The first run duration was three hours and gyro attitude was recorded every one second. The second run duration was 60 hours and the data was recorded every 100 seconds. When available, 50 samples were used to compute the standard deviation.

Figure 3-4. Characterization of Gyro Random Drift

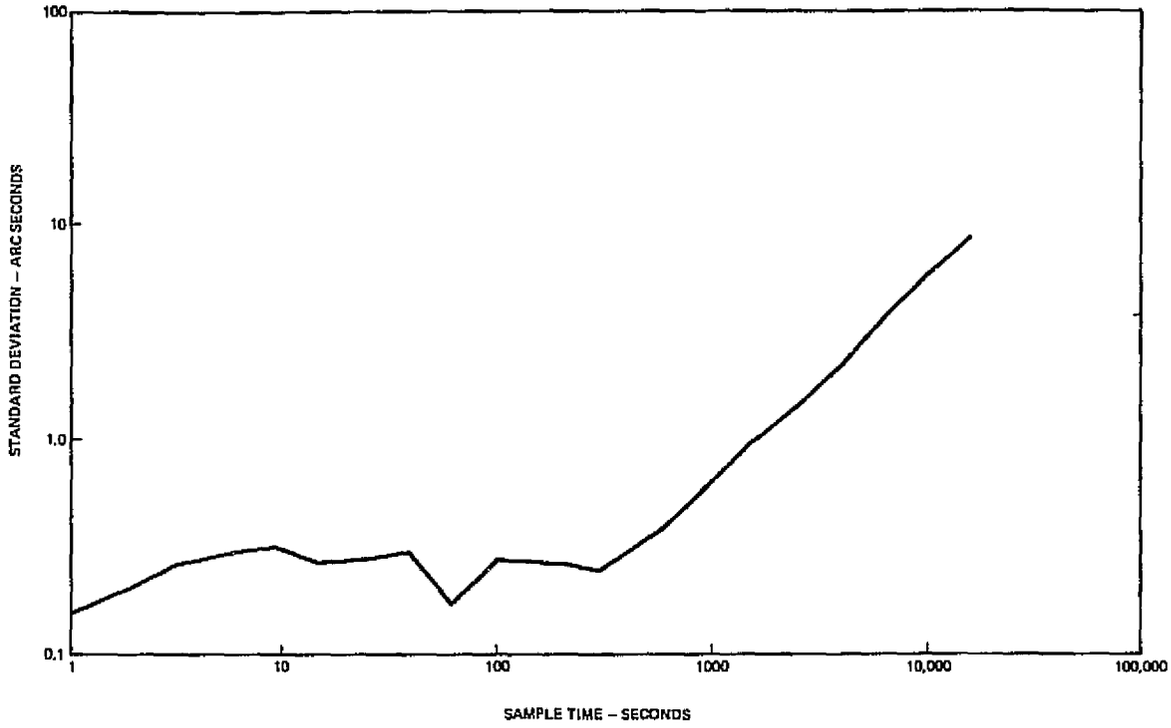

Figure 3-5. X Gyro Random Drift

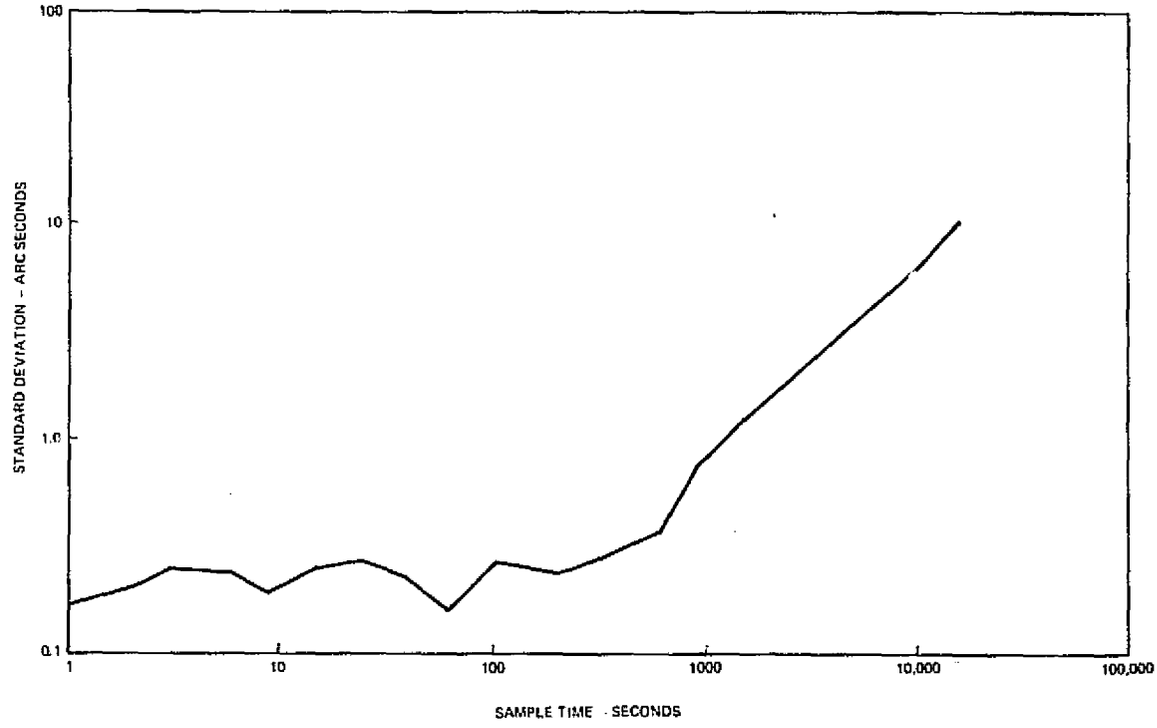

Figure 3-6. Y Gyro Random Drift

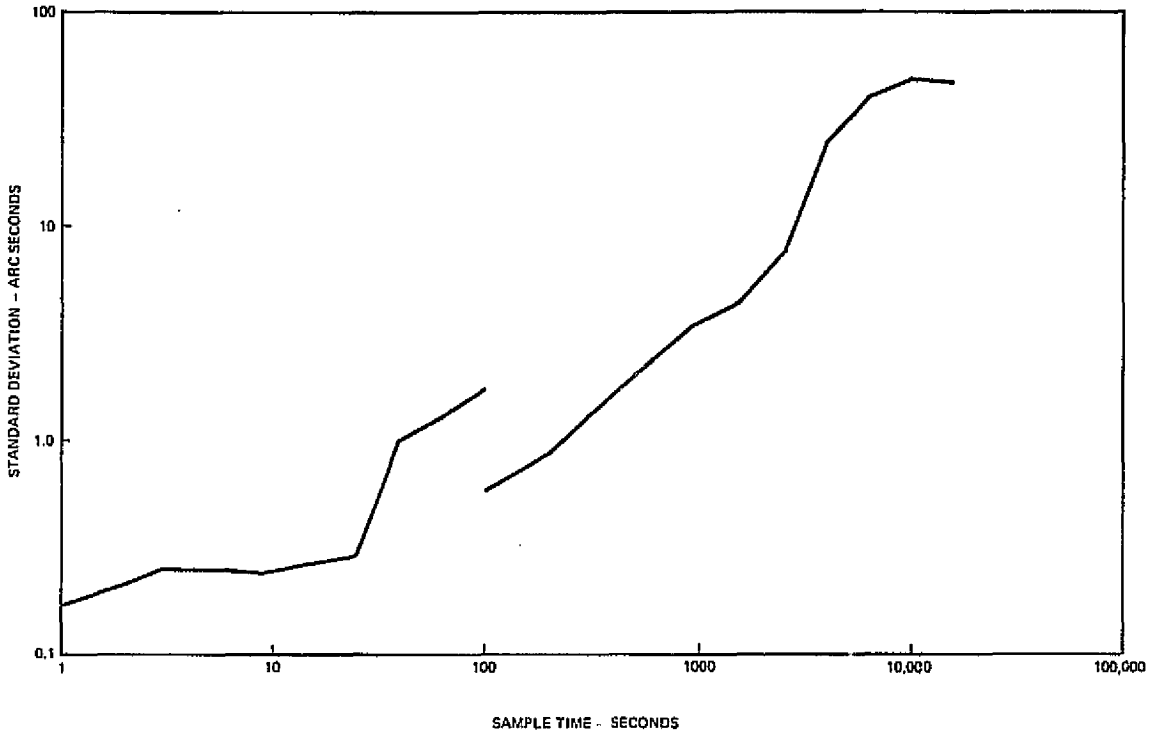

Figure 3-7. Z Gyro Random Drift

The figures indicate that the standard deviations after 20 minutes for the x and y gyros are 0.8 and 1.0 arc seconds, respectively. By coincidence, these values are remarkably close to the value measured for the originally considered Bendix gyros, namely, 0.4 arc seconds.[4] Also by coincidence, both the x and y gyros and the Bendix gyros have a slope of plus one (log-log plot) for 20 minute and longer samples. These similarities between the malfunctioning IRU x and y gyros and the Bendix gyro confirmed the decision to run the PADS tests with the IRU.

The standard deviation for the z gyro is 4 arc seconds at the 20 minute sample time, and its slope is erratic. While this performance is not ideal, it is close enough to the desired level for the gyro to be used in the system tests. In the evaluations of the system tests results in Sections 9 and 10, the effect of the poor performance of the z gyro on system accuracy is pointed out.

A final comment is appropriate regarding the performance of the x and y gyros. The time plots of gyro drift rate in Appendix C clearly indicate that the dominant error characteristic is a squarewave variation with a

period of approximately 17 hours. It is this characteristic which produces the slope of plus one in Figures 3-5 and 3-6. Although unknown in origin, this error is definitely deterministic in appearance.

3.2 SOFTWARE

The software design is, in general, characterized by achieving desired system performance with the minimum of equation complexity. Throughout the equation development, for example, models derived to compensate for systematic errors in the on-board system are simplified to the level consistent with desired performance. In most cases, for example, this resulted in only first-order terms being retained.

The software is designed to perform executive functions (program control, self-test, system test, etc.), attitude determination, and pointing control in the case of the gimbal star tracker. The attitude determination software derives inertial attitude by integration of the gyro outputs, and employs a Kalman filter for periodic updates to bound the errors. Development of the attitude determination equations required a variety of tradeoffs to determine the appropriate algorithms and design approach. On the other hand, development of equations for transformations, star selection, and gimbal pointing is straightforward, although algebraically complex.

Choice was available for selection of the kinematic variables used to propagate rate through the required numerical integration. Euler symmetric parameters were selected, as opposed to direction cosines, based upon the use of a four, rather than nine, parameter system of equations; also, the periodic renormalization that must be performed to combat computer roundoff error is much simpler. A closed form solution is utilized, under the constraint that the vehicle rate can be assumed constant over each integration interval. The closed form solution tends to inhibit the truncation error that would normally exist in the power series representation. Design analysis was also conducted to establish the integration step size and the effect of computer (roundoff and truncation) errors.

The Kalman filter state vector was limited to six elements (three attitude variables and three gyro biases) to minimize the problem dimensionality while achieving desired performance. Additional states (such as alignment/scale factor parameters in gyros and trackers) were found

not to be justified based upon inherent accuracy/stability and/or relative sensitivity. The extended Kalman filter formulation is utilized where linearization takes place about the previous attitude estimate.

The Kalman filter requires a priori definition of the initial state error covariance matrix, the measurement noise covariance matrix, and the state noise covariance matrix. The initial error covariance matrix reflects the initial uncertainty of the state estimates, and the elements are selected a priori based upon the expected initial attitude uncertainty. There appeared to be little influence of the initial estimate for error covariance, but good design practice indicated selection of values larger than the actual expected initial attitude errors.

State noise arises principally from the gyro random drift, and the elements of the state noise covariance matrix are derived a priori based upon the estimated (measured) gyro noise statistics. The influence of state noise on performance was determined by evaluating the relative error as a function of state noise parameters. A value of the elements of the state noise covariance matrix can be determined which corresponds analytically to the value of gyro noise assuming a white noise gyro model. The tradeoffs indicate that a good design procedure is to utilize the analytically derived values for the state noise covariance matrix which correspond to a conservative estimate of gyro noise.

The elements of the measurement noise covariance matrix are based upon a priori estimates (measurements) of tracker noise. Tradeoffs were made for selection of elements of the measurement noise covariance matrix utilizing a parameter variation study employing various values of tracker noise and measurement noise covariance values. This tradeoff led to the indication that performance can be best achieved through selection of elements of the measurement noise covariance matrix which are, in fact, optimistic.

The PADS software is configured in a modular structure which will permit operational flexibility, capability for growth, and ease of modification. The software makes use of state-of-the-art techniques so far as possible, consistent with the capability of present generation spaceborne computer technology. The software is segmented into modules to be executed under control of the PADS executive according to a preassigned interactive

cycle. Individual program module interfaces have been allocated based upon cycle requirements of the main computation loops.

The following two sections explain those aspects of the PADS software which are peculiar to the strapdown and gimbal systems and their respective star trackers.

3.2.1 Strapdown System Test Associated Software

The sensor information provided by the Inertial Reference Unit (IRU) and the Strapdown Star Tracker (SST) are inputs to the strapdown algorithm, whose purpose is to establish system (spacecraft) attitude and estimate the IRU drift rates. A top level program flow diagram is illustrated in Figure 3-8. Its first task is to read Tape 1 which contains quantitative parameter values associated with the IRU and SST as well as initial estimates (and their statistics) associated with both attitude and gyro drift rates. Table 9-1 in Section 9 specifies a typical list of such inputs. Next a block of IRU and SST data is read into the computer via Tape 4, with successive blocks read thereafter as the data is utilized. For the PADS laboratory setup, the air bearing table angle is also input via Tape 4, as it establishes the reference star line-of-sight to be utilized by the SST. Next the attitude and drift state transition matrices are initialized, and a time tagged slice of sensor data read from the computer memory. If it is not time to terminate the run, the algorithm forms angular rate estimates, applying appropriate drift rate compensations. Next the actual attitude is estimated based upon the previous estimate and the intervening angular rates. The system state can then be printed on the output tape (Tape 2), if desired, and unless there is SST data associated with the present time slice, control returns to α for reading the next time tagged data entry.

When SST data does appear, a countdown begins until that data is actually utilized since the azimuth output of the SST becomes more accurate towards the center of its field of view. Once the data is utilized, the appropriate star is first identified, through use of the air bearing table angle, and the SST output corrected to compensate for nonlinearities off its boresight. The a priori estimate of expected SST output based upon the estimated rather than actual attitude is next formed, and subtracted from

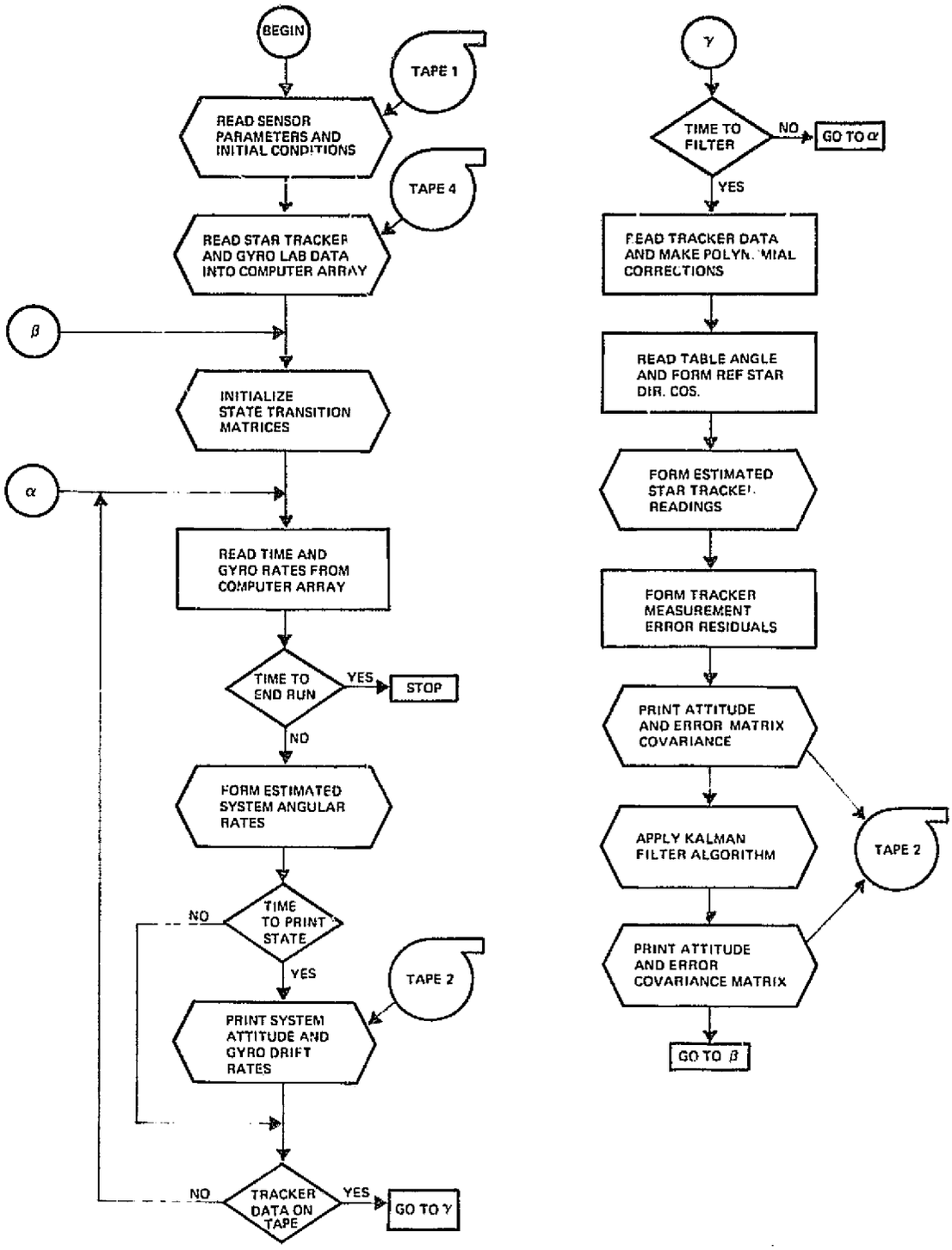

Figure 3-8. PADS Strapdown Software Flow Diagram

the actual readings to establish azimuth and elevation measurement residuals. The Kalman Filter algorithm is then applied resulting in both attitude and RGA drift rate updates. Also derived is an update of the state error covariance matrix, which establishes to what extent the algorithim believes its estimates. Control then returns to β for a new filter cycle. A detailed listing of this computer program appears in Appendix A.

3.2.2 Gimbal System Test Associated Software

The computer program associated with the GST version of PADS is almost identical to that associated with the SST version. The only significant difference involves the replacement of the SST subroutine forming estimated star tracker readings in Figure 3-8 by an equivalent GST subroutine. A detailed listing of the GST version is presented in Appendix B.

4. TEST CONFIGURATION AND ACCURACY

This section describes the laboratory test configuration in relationship to the simulated geosynchronous orbit environment. In addition the potential laboratory error sources are detailed.

4.1 SIMULATED ORBIT CONFIGURATION

The objective of the PADS system tests was to determine the performance capability of a PADS system in geosynchronous orbit through laboratory simulation. Two PADS systems were tested, one using a strapdown star tracker, the other using a single-axis gimbal star tracker. The simulated orbit conditions were the stellar optical stimuli and inertial angular rates which would be experienced on a three-axis stabilized, earth-pointed satellite in geosynchronous orbit.

Before hypothesizing the orbit configuration of both PADS systems, a number of practical test limitations had to be considered. The most important limitation was that only one strapdown star tracker could be developed under the scope of the program. Since practically no geometric leverage is obtained about the boresight of a 1^0 by 1^0 field of view, this meant that system performance would be achieved only about the two axes normal to the boresight: in essence, a two-axis test for the strapdown system.

Another limitation was the fact that it was technically impossible within the scope of the program to accurately simulate bright object interference to the performance of the star trackers. In view of this, the assumed orientations of the tracker fields of view in orbit were picked with the objective to make sensor errors as nearly as possible one-to-one with system errors.

With these considerations in mind the simulated orbit configurations which were arrived at are shown in Figure 4-1. It is seen that the strapdown system is a two-axis system consisting of one narrow field of view and two gyro input axes orthogonal to the field and to each other. For maximum star availability on the assumed uniformly distributed celestial sphere, the field of view points at the celestial equator. On the other hand, the gimbal system is a three-axis system since the 90 degree sweep of the tracker field of view does give adequate geometric leverage for three-axis tracker information, supplemented by the three orthogonal gyro axes. The center of the sweep is also pointed to the celestial equator for maximum star availability.

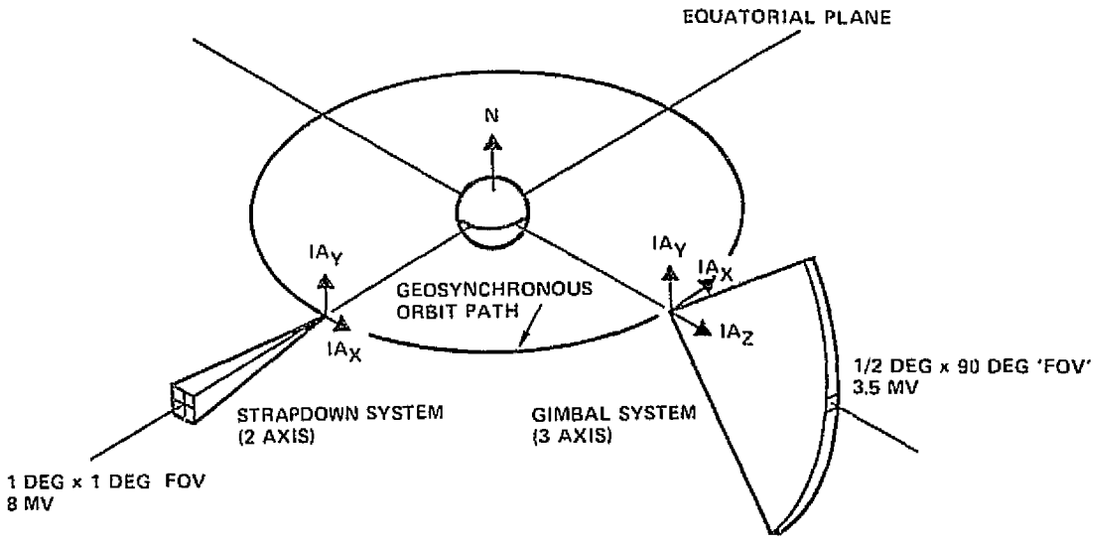

Figure 4-1. Simulated Orbit Configuration

The driving function for star update frequency is the random drift of the gyros. For the class of gyro considered on PADS a nominal update period of 20 minutes has been chosen in order to result in a total system accuracy of 0.001 degree. Using the equations developed in Volume I, Section 2.2, a 20 minute period in the case of the strapdown star tracker gives a probability of at least one star occurring in the field of view of:

$$p = 0.9963$$

For the gimbal star tracker a 20 minute period gives a probability of

$$p = 0.9736$$

To make the probability for the gimbal tracker equal to that of the strapdown tracker the update period must be extended to 32 minutes.

For the PADS testing the decision was made to make the star update period 20 minutes for both strapdown and gimbal cases. This is equivalent to acquiring a star every 5 degrees of right ascension in geosynchronous orbit. In the analysis of the test data a parametric analysis of the effect of update period was obtained by skipping updates. In this manner 20, 40, and 60 minute update periods were obtained. This approach was taken since

it simplified test procedures and avoided longer test runs in the case of the gimbal system. Comparison between the two systems was made on the basis of the parametric analyses.

Three different star declinations were used in the case of either system. For the strapdown system the purpose of multiple declinations was to exercise the accuracy of the tracker at more than one place in the field of view. The three declinations were:

- Star 1: 911.6 arc sec (0.3^{o})
- Star 2: 0.0 arc sec (0.0^{o})
- Star 3: -326.0 arc sec (-0.1^{o})

For the gimbal system the motivation for three declinations was to obtain three-axis star tracker information as well as to exercise the accuracy of the gimbal readout. Here the three declinations were:

- Star 1: 53814.9 arc sec (14.9^{o})
- Star 2: -14564.8 arc sec (-4.0^{o})
- Star 3: -82958.0 arc sec (-23.0^{o})

4.2 LABORATORY TEST CONFIGURATION

The key distinguishing feature of the laboratory test configurations for both the strapdown and gimbal system tests is that a ground-fixed test is implemented. The earth itself is used to simulate the inertial motion of an earth-pointed geosynchronous satellite. This is accomplished by mounting the PADS sensors stationary to the laboratory floor, which itself is a seismic pad isolated from building vibrations. The stellar optical stimuli are simulated by sweeping collimating star beams past the stationary PADS sensors. Ideally, the star beams, which are revolving at earth rate relative to the laboratory, are stationary in inertial coordinates since their rotation relative to the laboratory cancels the rotation of the laboratory, or the earth, relative to inertial space. In practice, since it was more practical to have the rotation axis of the stars vertical in the laboratory, and since the laboratory location was in Manhattan Beach, California, the star line-of-sights actually were rotating in inertial space. However, since the stars were revolved at earth rate

relative to the star trackers, the test configuration still satisfied the objective of the tests, namely, to evaluate the performance of the PADS systems.

Isometric representations of the strapdown and gimbal configurations are shown in Figures 4-2 and 4-3, respectively. Table 5-1 in Section 5 identifies the numbered equipment. Photographs of the actual configurations are shown in Figures 4-4 through 4-17. Figures 4-4 through 4-10 show details of the star stimulus of the strapdown star tracker. Stimulus of the gimbal star tracker is shown in Figures 4-11 through 4-16. The inertial reference assembly is shown in Figure 4-17.

The ground-fixed test provided two major advantages over the conventional approach of rotating the PADS on a rate table in the center of a room, and placing multiple star sources around the room which point at the rotating PADS. The first advantage is that the ground-fixed approach is compatible with the parallel beam star stimulus technique described in the following section. This technique is essential to providing laboratory instrumentation knowledge of star locations with one arc second accuracy. The technique is not compatible with the rate table and multiple stars approach. The second advantage is that the artificial subtraction of earth rate from the gyro outputs is not necessary in the ground-fixed approach. In fact, it becomes technically dubious in the rate table approach since a vector of the same magnitude as that produced by the rate table must be subtracted from the gyro outputs.

In the ground-fixed test approach, the PADS axes are identical to the laboratory axes. Both are physically defined by optical surfaces on the star trackers. The strapdown star tracker uses the normals to two faces of an optical cube to define the axes. The gimbal star tracker uses an orthogonal set of axes whose orientation is defined relative to three mirror surfaces on the tracker base. Star orientation relative to the laboratory (and PADS) axes is measured by laboratory instrumentation.

The PADS output is a continuous estimate throughout the length of the test run of the attitude of the PADS axes relative to their inertial attitude at the start of the test run. For performance evaluation this output is compared to the continuous inertial attitude of the physically defined

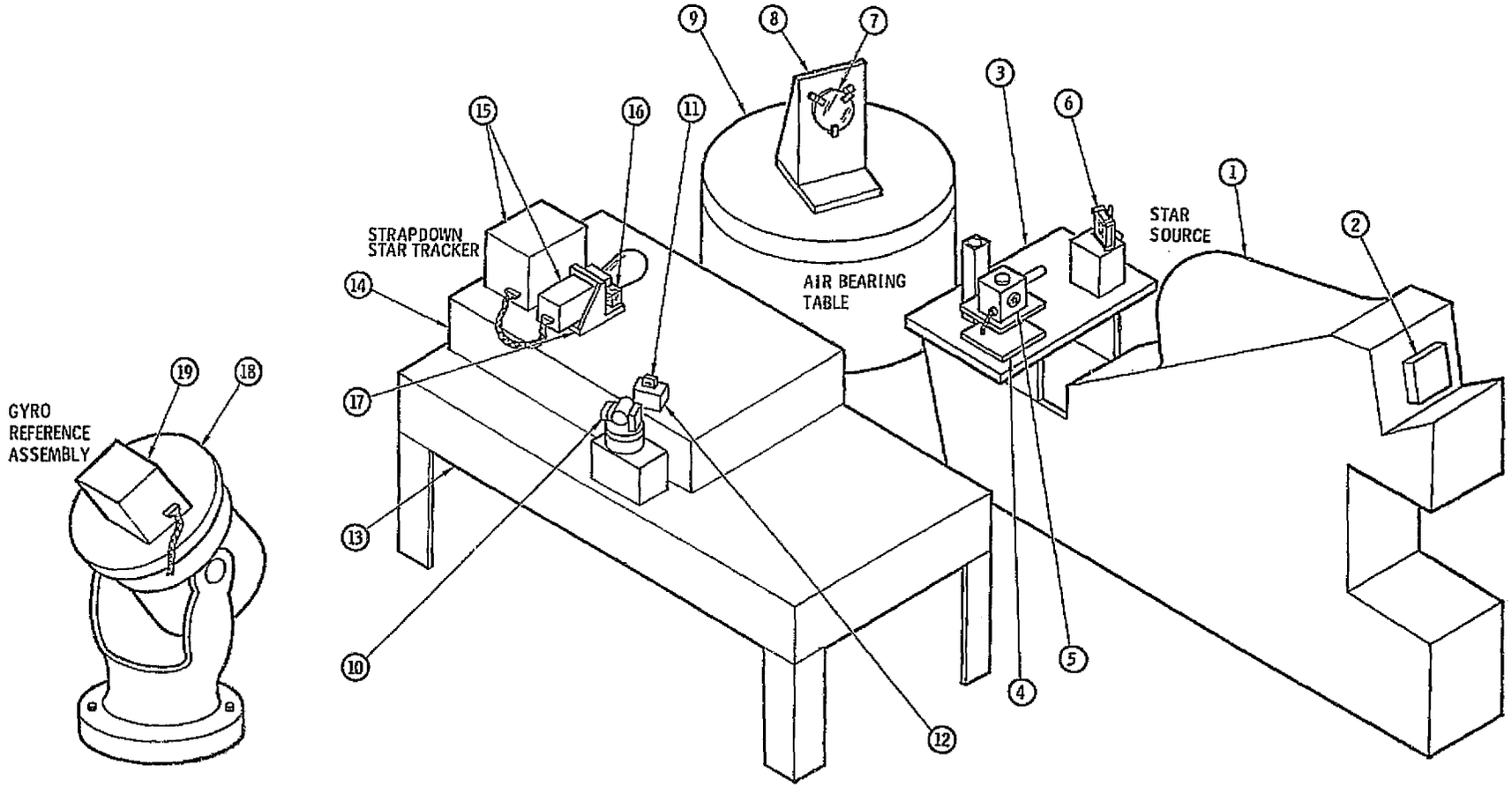

Figure 4-2. Strapdown Test Configuration

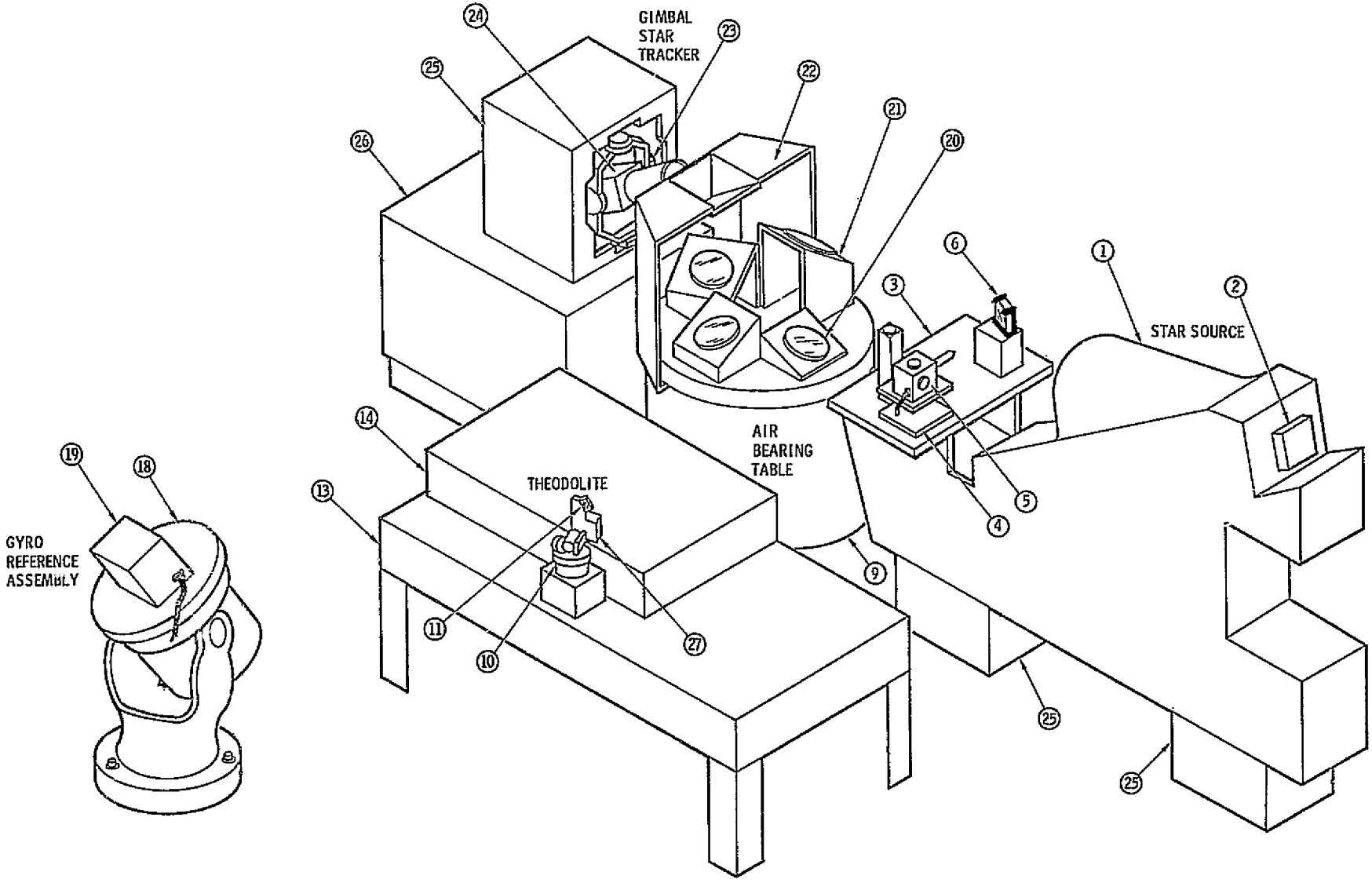

Figure 4-3. Gimbal Test Configuration

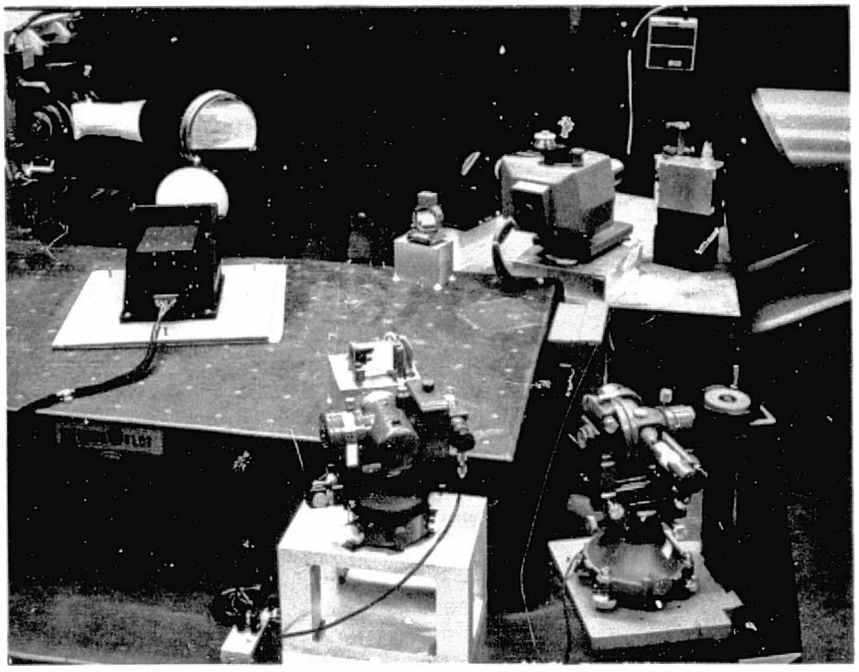

Figure 4-4. View of Strapdown Configuration

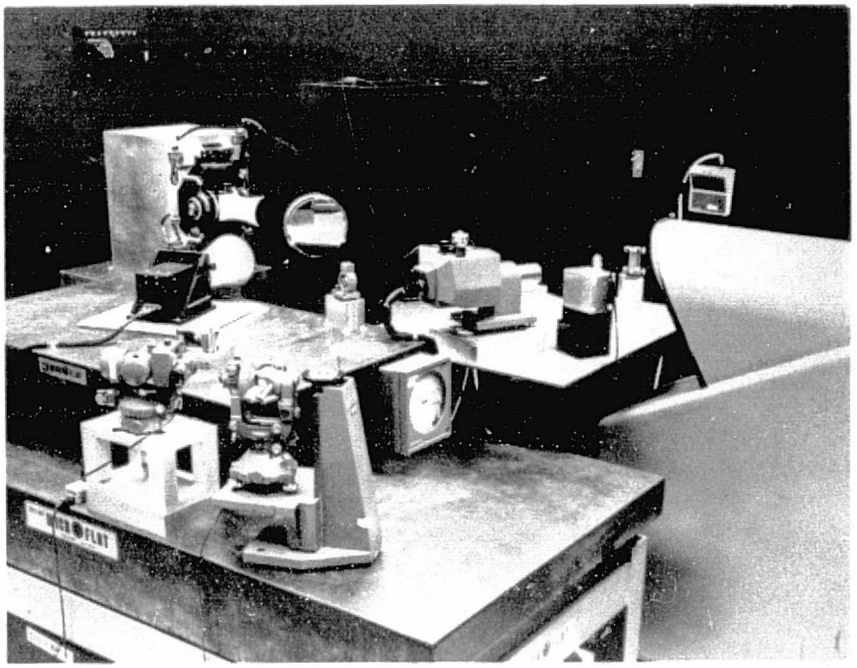

Figure 4-5. View of Strapdown Configuration From Back of Theodolite

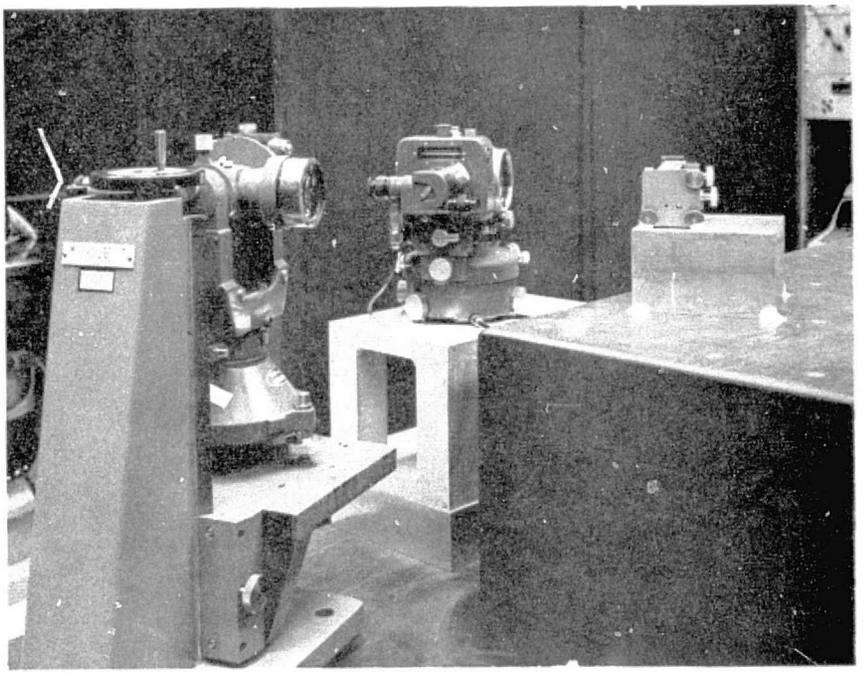

Figure 4-6. Front View of Theodolite

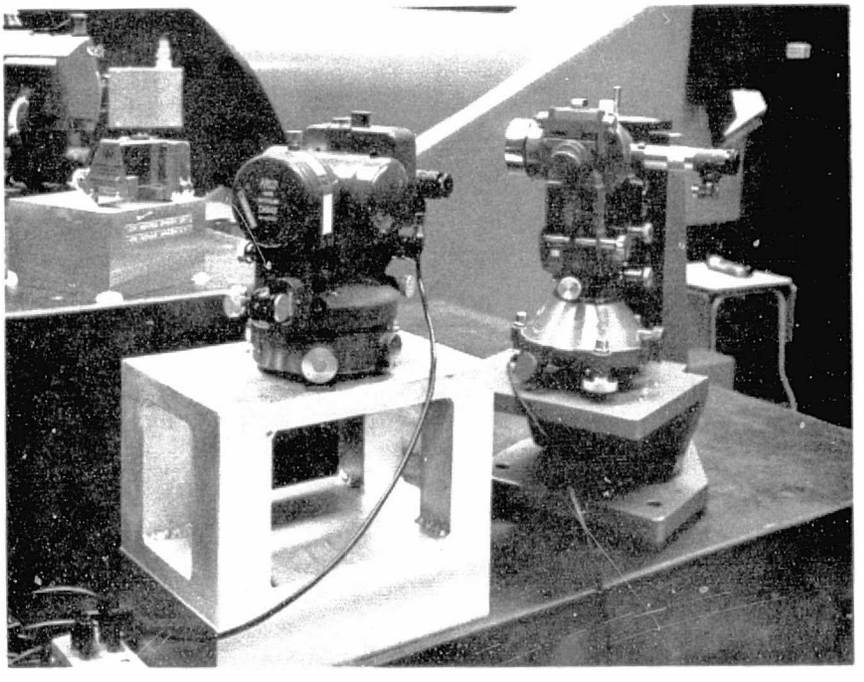

Figure 4-7. Back View of Theodolite

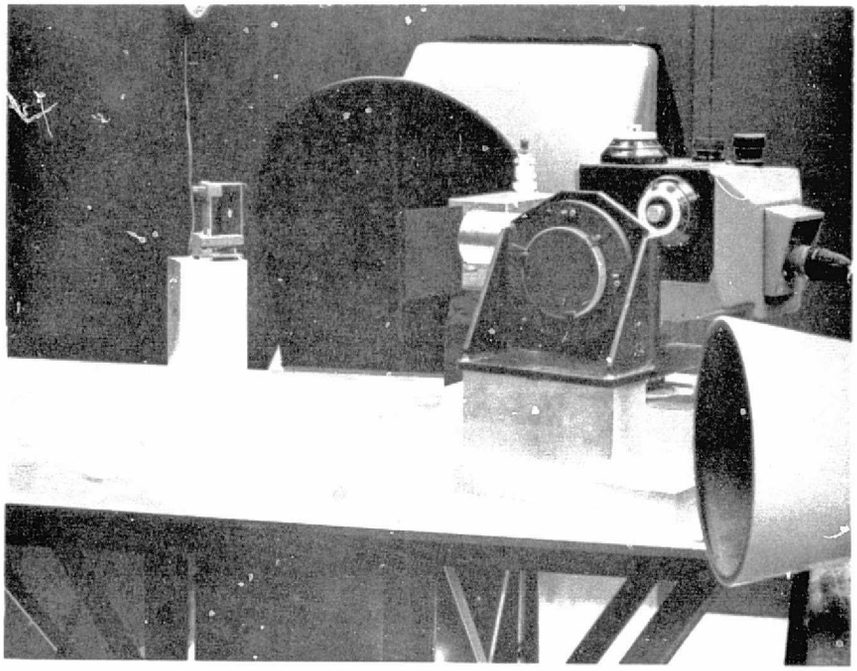

Figure 4-8. View of Automatic Autocollimator From Right of Star Source

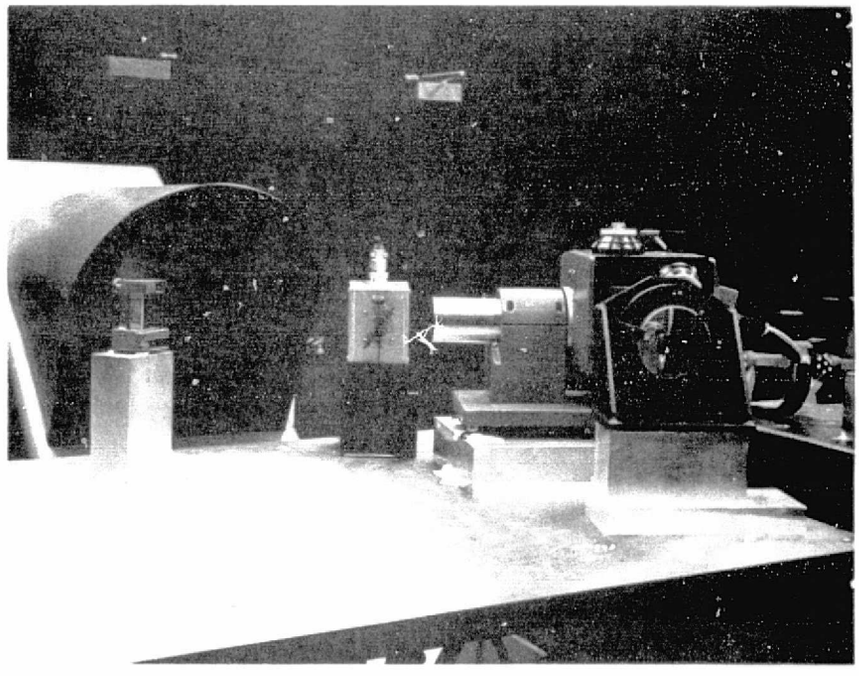

Figure 4-9. View of Automatic Autocollimator From Left of Star Source

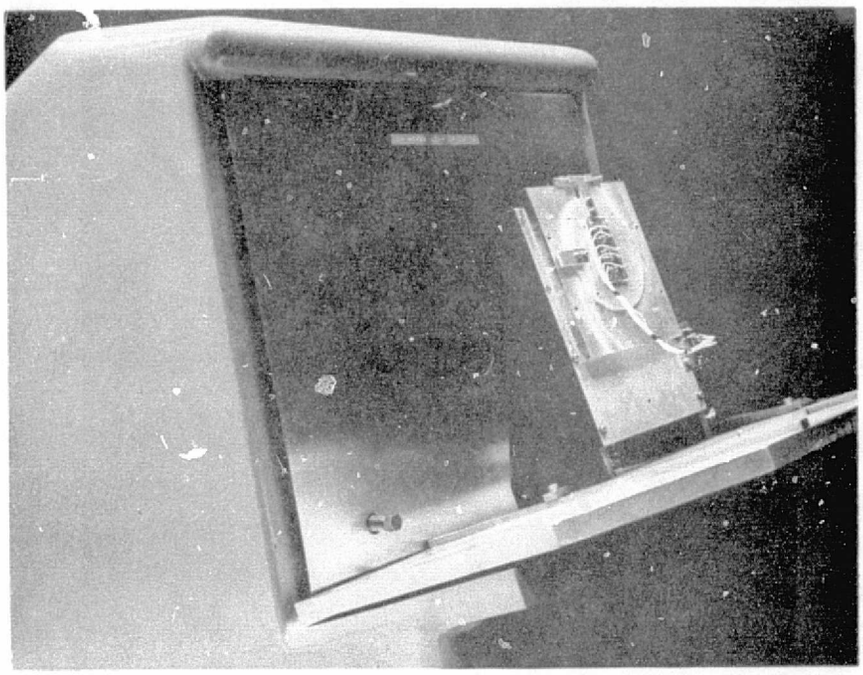

Figure 4-10. LED Assembly on Star Source

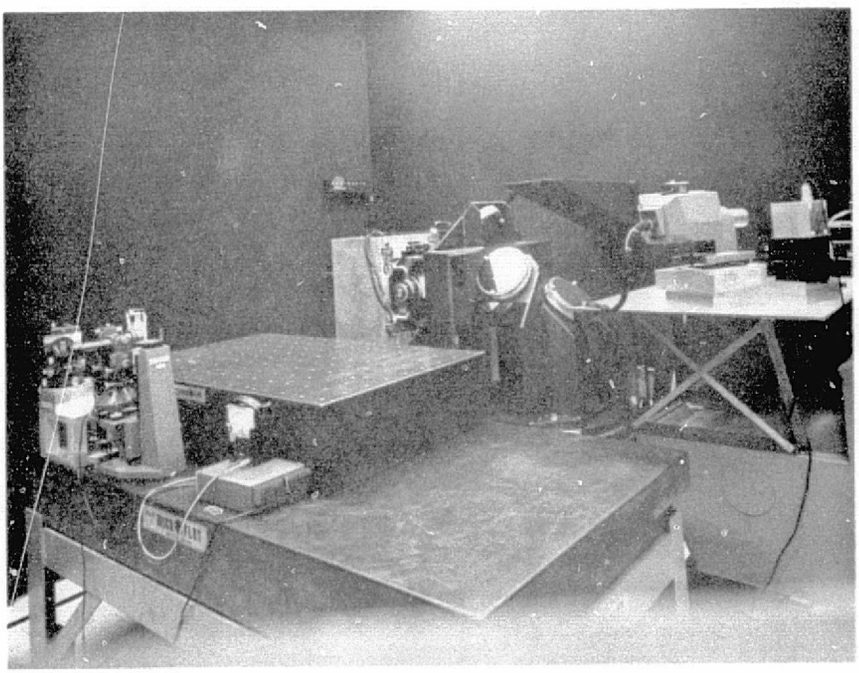

Figure 4-11. View of Gimbal Configuration

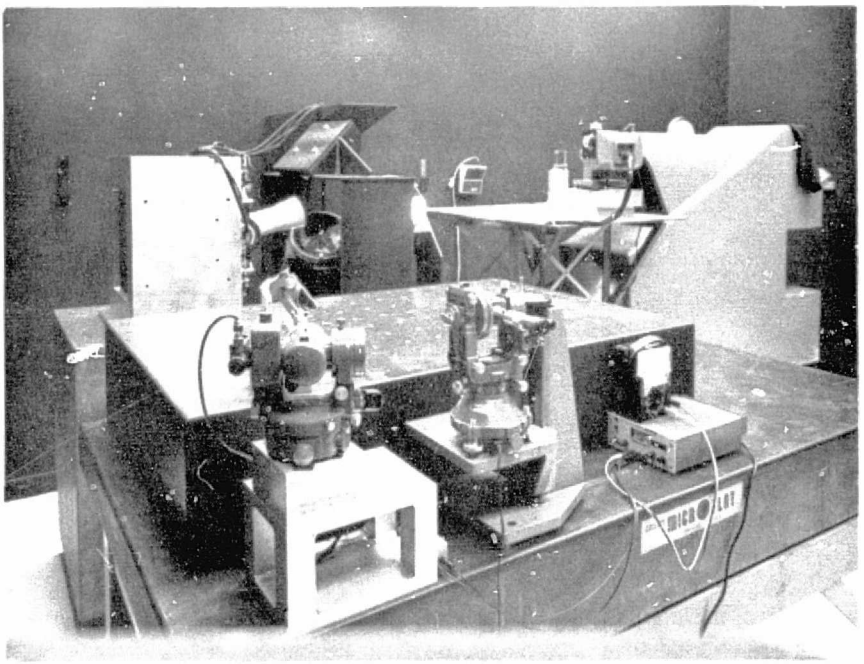

Figure 4-12. View of Gimbal Configuration From Back of Theodolite

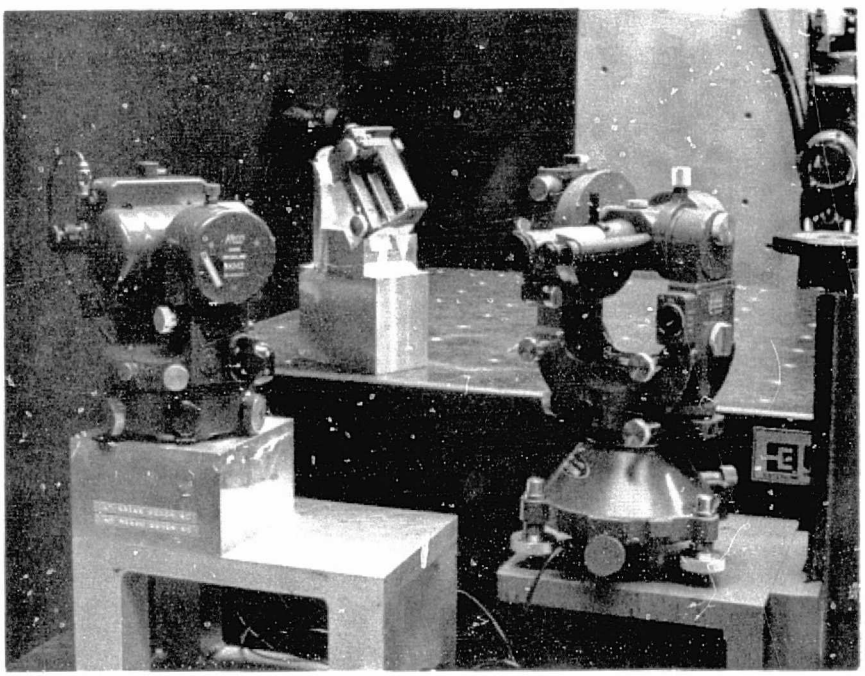

Figure 4-13. Side View of Theodolite and Double-Sided Mirror

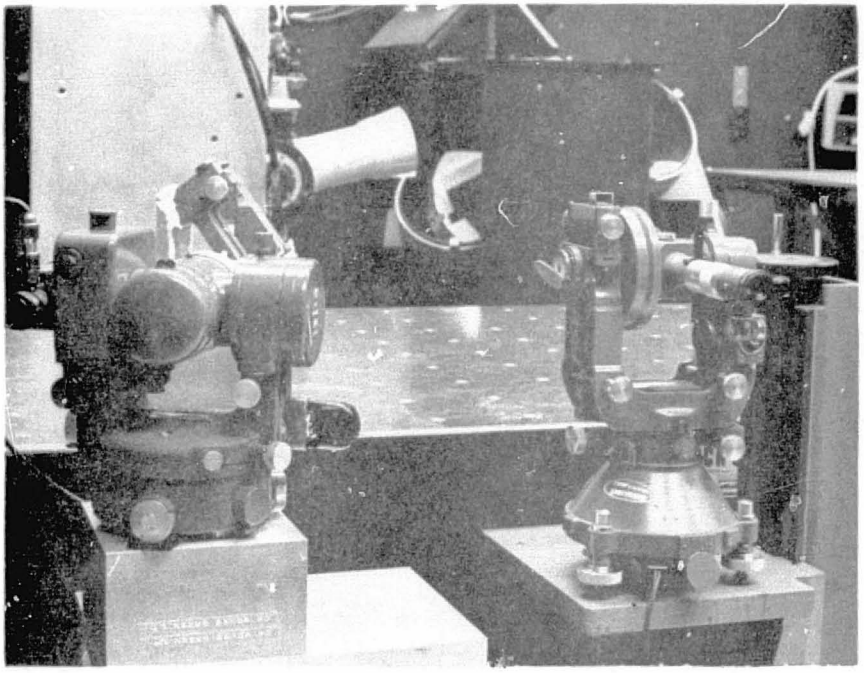

Figure 4-14. Theodolite View of Mirror Assembly in Reference Position

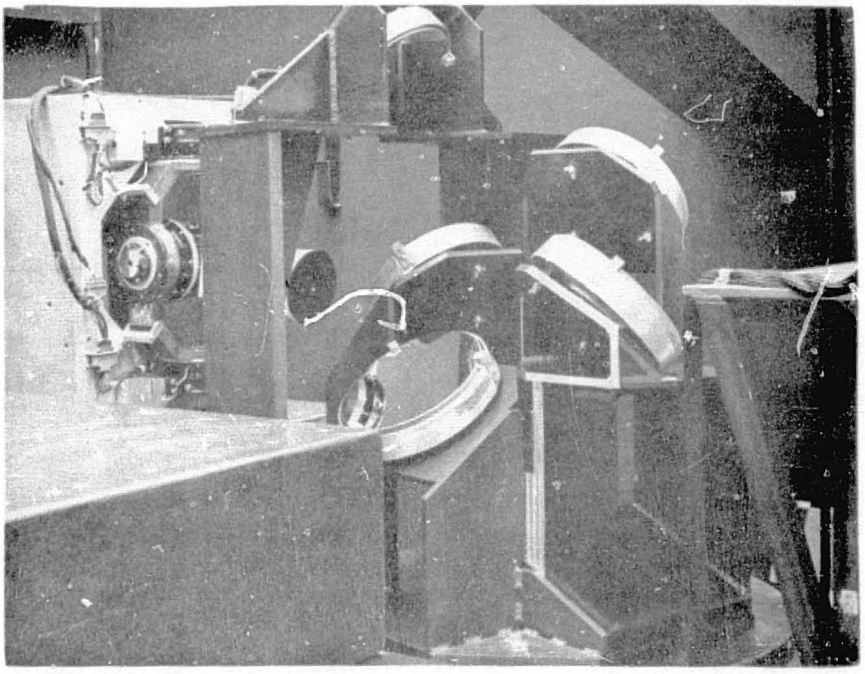

Figure 4-15. Stationary and Rotating Mirrors in Star 2 Position

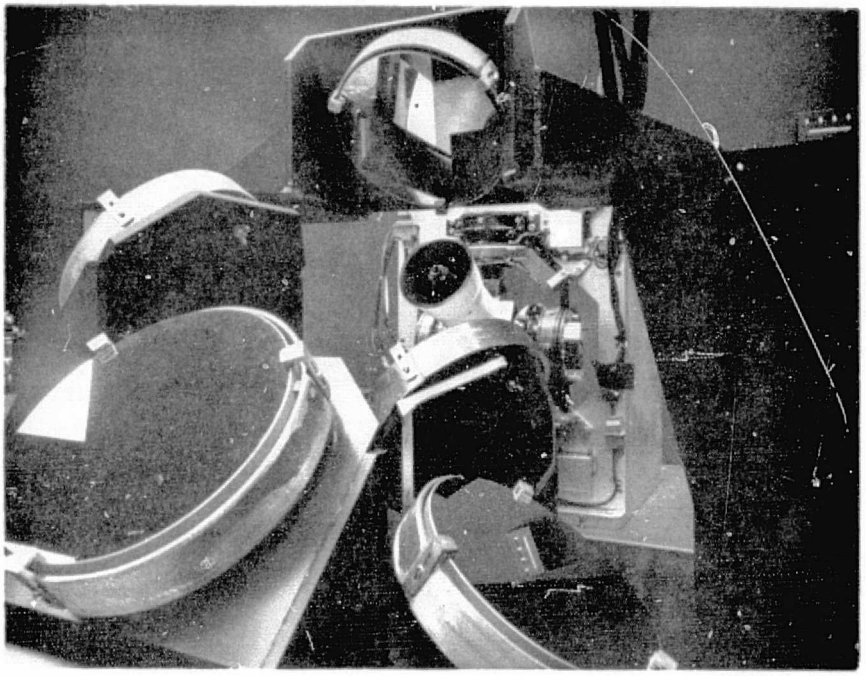

Figure 4-16. Stationary and Rotating Mirrors in Reference Position

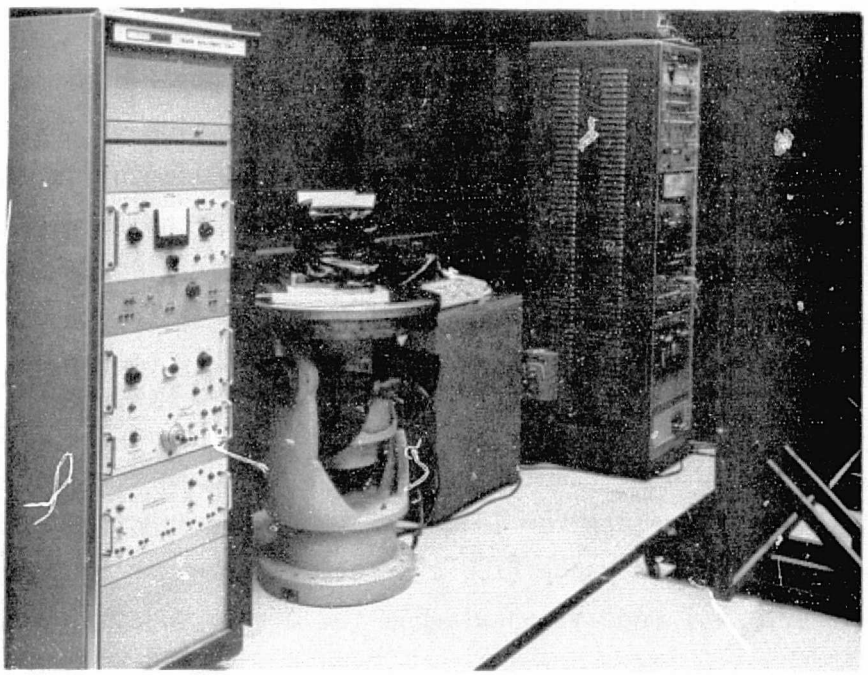

Figure 4-17. Inertial Reference Unit

PADS axes. This attitude is derived from the inertial attitude of the laboratory axes at the start of the test and from knowledge of the rate of the earth's rotation. The star orientation is measured relative to the laboratory axes. It is important that the star orientation in laboratory axes be known very accurately using laboratory instrumentation. An error in knowledge of the star position will result directly in an error in the performance evaluation of the PADS.

4.3 PARALLEL BEAM STAR STIMULUS TECHNIQUE

The key test configuration accuracy requirement is to know the orientation of the star line-of-sight relative to the laboratory axes, which in this case are also the PADS axes. Since the PADS performance requirement is 3.6 arc seconds per axes, knowledge of the star orientation must be significantly better than this value. By using a parallel beam star stimulus technique an accuracy approaching one arc second was obtained.

The parallel beam technique is perhaps best illustrated by the top view of the strapdown system test configuration shown in Figure 4-18. Functionally, the performance of a star transit (defined as a sweep of a star through the field of view of the tracker) is straightforward. The collimated star beam from the star source is reflected off the rotating mirror mounted on top of the air bearing table. The table is turned at half earth rate so that the reflected star beam sweeps past the star tracker at earth rate. In order to measure where the star beam is relative to the PADS axes, i.e., the optical cube on the right side of the star tracker, the collimated beam from an automatic autocollimator is transmitted parallel to the star beam. The normal to the front face of the cube is the defined boresight axis of the tracker. When the star beam (Star 2) is concident with the boresight axis, the autocollimator beam will be normal to the front face, and the horizontal and vertical output of the two-axis autocollimator will be zero.

This use of the automatic autocollimator is suitable for a static indication of the star orientation in a small region around the boresight axis. However, its limited range (±50 arc sec) and dynamic response (0.13 arc sec per arc sec/sec) make it unsuitable for a star sweeping through

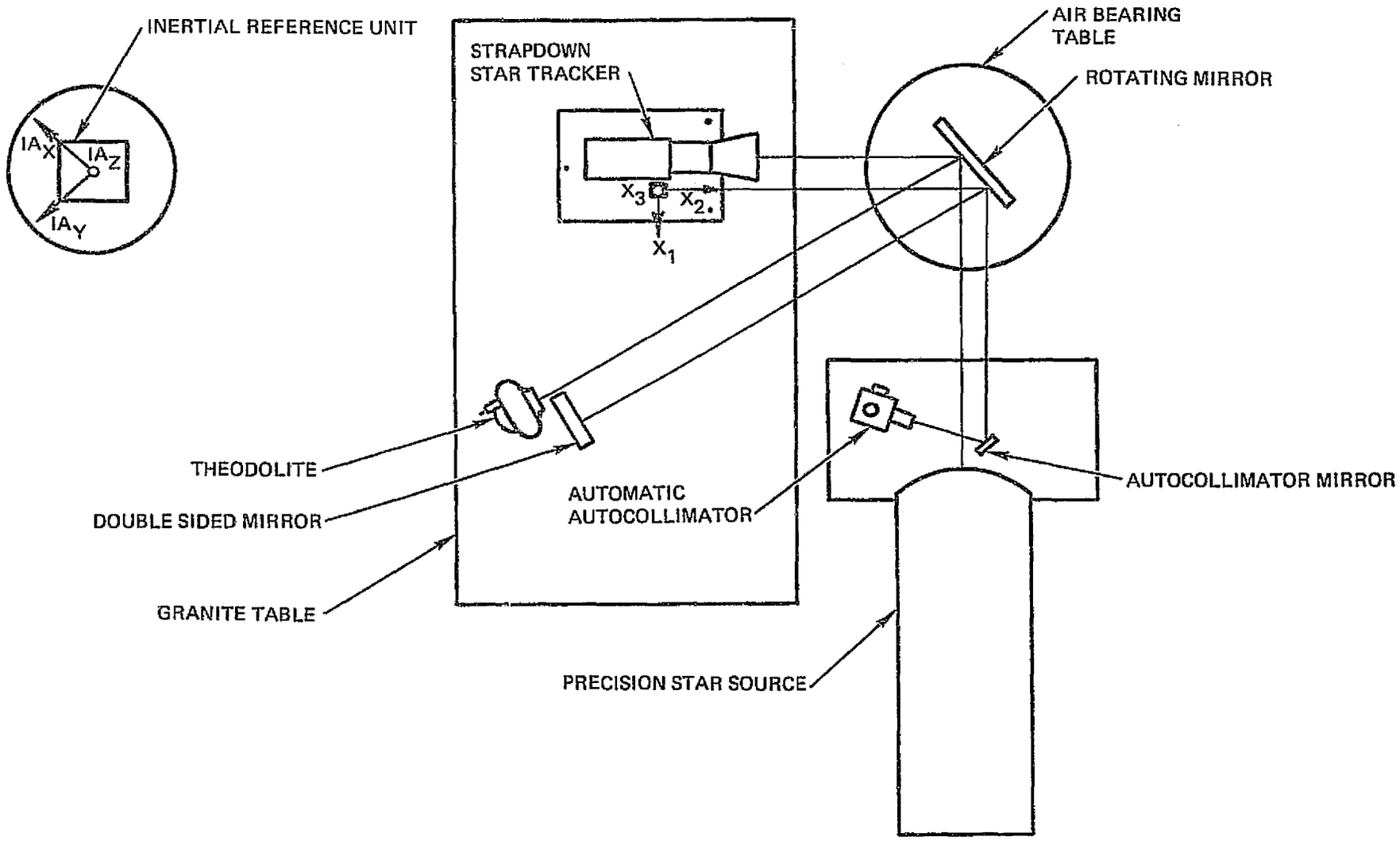

Figure 4-18. Strapdown , tem Test Configuration

the 1^{0} field of view at earth rate during a star transit. For this case the air bearing table readout is used. The zero reference for the readout is obtained by making a static table reading at the boresight position indicated by the automatic autocollimator.

So far the discourse has been limited to measuring the location of the center star (Star 2) relative to the PADS axes. By independently measuring the relative locations of the other two stars to the center star, their locations relative to the PADS axes can also be determined by the parallel beam technique. The independent measurements were made with a theodolite. The gravity vector was used as a reference for rotations about the boresight axis.

The key to the successful implementation of the parallel beam method is the ability to recalibrate as frequently as necessary the parallelism between the collimated center star and autocollimator beams. This is facilitated by use of the theodolite and double-sided mirror shown in Figure 4-18. The double-sided mirror is positioned half way in front of the aperture of the theodolite. The backside mirror is positioned perpendicular to the theodolite boresight by using the autocollimator feature of the theodolite. Since the frontside mirror is parallel to the backside mirror, the normal to the frontside is then parallel to the telescope boresight of the theodolite. Both can now be used to calibrate the parallelism between the two collimated beams. The air bearing table is rotated until the star beam is along the boresight of the theodolite. When this condition exists, the automatic autocollimator will adjust its beam normal to the frontside mirror. Any deviations from zero of the autocollimator horizontal and vertical outputs represent its null bias errors. The utility of this recalibration method is that it can be performed at any time during a test period.

The operational procedure which was developed during the test phase was to recalibrate in two stages. The strapdown or gimbal test consisted of four runs, four hours or longer in duration, which were performed over a ten day period. Since the star source beam would drift relative to the theodolite up to a couple of arc seconds per day, and since the air bearing table readout zero position would also shift from turn-on to turn-on, the

two collimated beams were realigned parallel at the start of each run. This was accomplished by driving the table to the reference (theodolite) position, adjusting the theodolite so that the center star was on boresight, adjusting the double-sided mirror face normal to the boresight, and then adjusting the autocollimator mirror to give zero horizontal and vertical output for the automatic autocollimator. The alignment of the star and double-sided mirror to the boresight was also checked at the end of each run to verify that no detectable misalignment occured. This was found to always be the case. During the four or five hour test run, however, the automatic autocollimator would drift up to three arc seconds. Therefore, before the start of each star transit (20 minutes apart), the table would be driven to the reference position and the autocollimator zero position recalibrated.

By using this operational procedure the only temporal stability requirements necessary for the entire test configuration were:

1) A four or five hour stability of the star source relative to the theodolite

2) Approximately a five minute stability of the autocollimator beam relative to the star beam. Stabilities better than one arc second were easily obtained by using a thermally passive star source and the Davidson Model 696 autocollimator.

4.4 LABORATORY ERROR SOURCES

The PADS system axes are defined by the optical cube. The computer axes are an analytical entity and represent the computed estimate of the orientation of the system axes relative to a set of reference axes. The computed estimate is derived from gyro and star tracker information. The reference axes are defined to be the inertial attitude of the system axes at the start of the test period.

The test purpose was to compare the attitude of the computer axes with that of the system axes, where both are expressed relative to the reference axes. The system attitude error is indicated by

$$\hat{A}_{XZ} \cdot A_{XZ}^{T}$$

where $\hat{A}_{XZ}$ and A_{XZ} are the direction cosine matrices of the computer and system axes, respectively, relative to the reference axes.

The matrix $\hat{A}_{XZ}$ is computed from the initial estimate of its orientation relative to the reference axes (which are also the system axes at test start), and from the output signals of the gyros and the star trackers. The matrix A_{XZ} is computed from knowledge of the initial orientation of the system axes at test start relative to the earth rate vector, and from time.

Figure 4-19 provides a useful representation of the coordinate axes and star vectors involved. Misalignment between computer and system axes is indicated at a star update time as the difference between:

1) Where the star should be in computer axes

2) Where the star is actually measured in system axes by the star sensor.

Where the star should be in computer axes is calculated as a function of:

1) The direction cosine matrix (or quaternion) relating the computer axes to the reference axes

2) A star catalog which describes where the star is in the reference axes.

This difference is then used (via a Kalman filter) to correct the direction cosine matrix. In between star update times, the incremental attitude change measured by the gyros is used to change the direction cosine matrix.

In the PADS laboratory test configuration the star catalog information is partly measured and partly analytical. The autocollimator directly measures where the star is in system axes, but the orientation of the system axes to the reference axes is an analytical relationship established by definition and the laboratory measurement of time.

Thus, laboratory measurement accuracies can be divided into two links:

1) The attitude of the system axes relative to reference axes

2) Star position relative to system axes.

The following sections describe the errors associated with both.

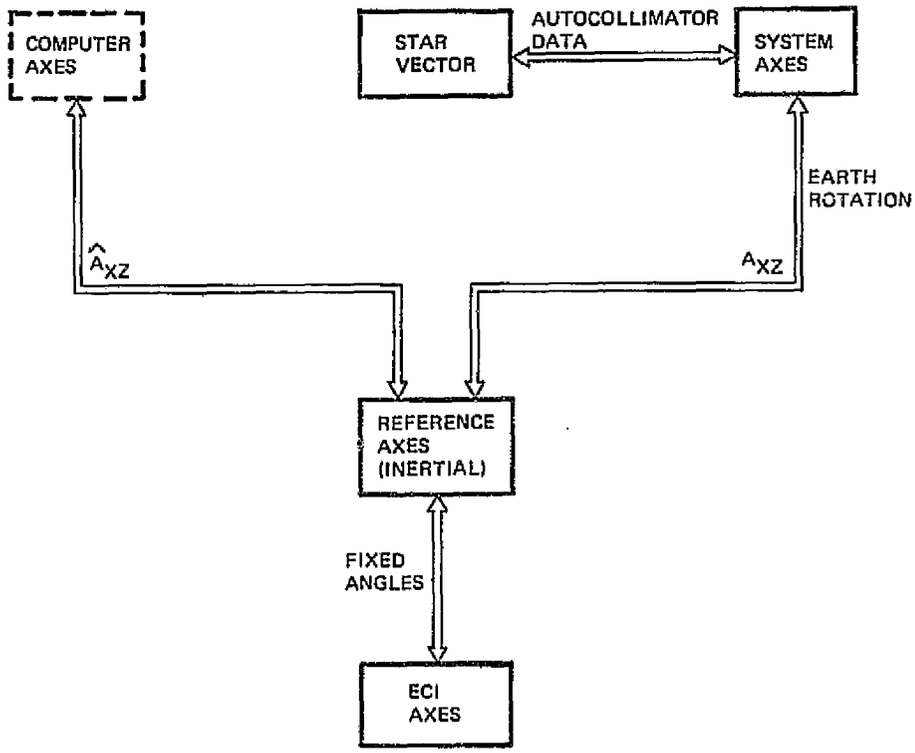

Figure 4-19. PADS Coordinate Systems

4.4.1 PADS System Attitude Uncertainties

Consider first an error in the matrix A_{XZ} at the start of the test due, for example, to incorrect knowledge of the latitude of the laboratory. This error will not evidence at a star update since A_{XZ} is used in both those quantities which are differenced and input to the Kalman filter. The error will cancel itself. On the other hand, it will appear initially in the gyro outputs. But, after a number of star updates, the filter will attribute the error to a gyro bias and thereafter compensate for it. Since the PADS system experiences a constant rate vector (earth rate) throughout the test, this error is indistinguishable from actual gyro bias error, scale factor errors, or input axis misalignments. However, separately identifying these error sources was not considered essential to the test objective of determining the PADS performance capability.

Seismic disturbances of the laboratory during a four or five hour test run will directly affect the laboratory evaluation of PADS. These disturbances will evidence as a random drift component in the gyro outputs.

However, from the measurements of the OAO/IRU performance both at GSFC and TRW it is clear that the gyro errors will completely predominate over possible seismic motions of the isolated laboratory floor.

Summarizing, neither static nor dynamic errors in describing the orientation of the PADS axes relative to inertial space significantly affect the laboratory evaluation of the PADS accuracy.

4.4.2 Star Position Measurement Errors

Determination of star position relative to the PADS system axes represents the major laboratory measurement error affecting the laboratory evaluation of the PADS accuracy. Since the PADS accuracy goal is 3.6 arc sec (1σ), the goal for this error source arbitrarily was selected to be 0.36 arc seconds (1σ), or 1.1 arc seconds (3σ). The ground rule was established that no attempt would be made to improve the measured PADS accuracy results by subtracting out either a statistical or deterministic measure of the laboratory errors.

Accuracy in knowledge of star line-of-sight position relative to the PADS axes is limited by three types of errors:

1) Absolute Errors. This term refers to systematic error sources which are present for all test runs.

2) Repeatability Errors. These are errors due to the realignment of the parallel beams prior to each test run. These errors are random from run to run, but constant for any one run.

3) Random Errors. These errors are random for any sequence of star measurements made either during a star transit or from transit to transit.

A further distinction which has been made is whether or not an error affects all three stars in the same manner, or if it is uncorrelated from one star to the next.

The error sources for the PADS test configurations are shown in Table 4-1. Since the purpose of the test program was to determine the performance capability of PADS, the systematic error of 3.3 arc seconds for all three stars, during all test runs, was not considered relevant. This error will not show up in the test results since both star trackers

Table 4-1. Star Measurement Errors

Error Source	Strapdown System Error -- Arc Sec		Gimbal System Error -- Arc Sec	
	All Stars (3σ)	Star to Star (3σ)	All Stars (3σ)	Star to Star (3σ)
1. Absolute Errors -- All Runs				
Star Position Measurement	0.0	0.6	0.0	1.2
Star Beam Collimation	0.0	0.0	0.0	0.0
Star Intensity Uniformity	3.0	3.0	3.0	0.0
Double-Sided Mirror Nonparallelism	1.0	0.0	1.0	0.0
Theodolite Boresight Alignments	0.7	0.0	0.7	0.0
Theodolite Spherical Aberrations	0.0	0.0	0.0	0.0
Theodolite Circle Accuracy	0.0	0.6	0.0	0.6
Theodolite Level Accuracy	0.0	0.0	--	--
Table Readout Accuracy	0.3	0.0	--	--
RSS	3.3[1]	3.1[2]	3.3[1]	1.3
2. Repeatability -- Run-to-Run				
Theodolite FOV Precision	0.6	0.0	0.6	0.0
3. Random -- During Run				
Autocollimator Noise	--	0.2	--	0.2
Autocollimator Drift	--	0.0	--	0.0
Autocollimator Scale Factor Error	--	0.3		0.3
Table Readout Quantization	--	0.6	--	0.5
RSS		0.7		0.6

1. Not relevant to PADS test.
2. Eliminated by field of view calibration and compensation.

are initially aligned using the same test configuration. It would surface, however, if the same PADS hardware, aligned using the laboratory configuration, were operated in orbit. The star to star absolute error of 3.1 arc seconds for the strapdown system also was eliminated by performing a strapdown star tracker field of view calibration and compensation using the same test configuration. As described in Volume I, Section 7, this was necessitated by inconsistencies discovered in the initial calibration data for the strapdown star tracker. All the remainder of the errors do affect the PADS performance results, and in combination (RSS) give 0.9 arc seconds (3σ) for the strapdown system and 1.6 arc seconds (3σ) for the gimbal system.

The most significant fact regarding the errors listed in Table 4-1 is that no significant error source due to temporal instabilities or drifts is present. As previously mentioned, this is a result of use of the parallel beam technique.

The following sections describe in detail the error sources listed in Table 4-1.

4.4.2.1 Star Source

The primary requirement for the star source was that it be stable to within an arc second throughout a four or five hour test run. This requirement was met by constructing a thermally passive source consisting of a Davidson (Model D-278) reflective bench and low power LED point sources. Since every part of the source was essentially at room temperature, no thermal deformations were possible.

The optics consist of a parabolic primary mirror with a focal length of 272 cm, and a flat secondary mirror. The aperture diameter is 40.6 cm with a center obscuration of less than 5.1 cm diameter.

The LED point sources are mounted in an aluminum plate which has a glass photographic plate bonded to its front side. The star images are formed by the photographic plate. Figure 4-20 illustrates the angular size and spacing of the three stars used in the strapdown system test. The vertical reference in the figure is the gravity vector with the plate in position for the strapdown test, and the stars as seen looking into the star source. The measurements were made with the Kern DKM3 theodolite.

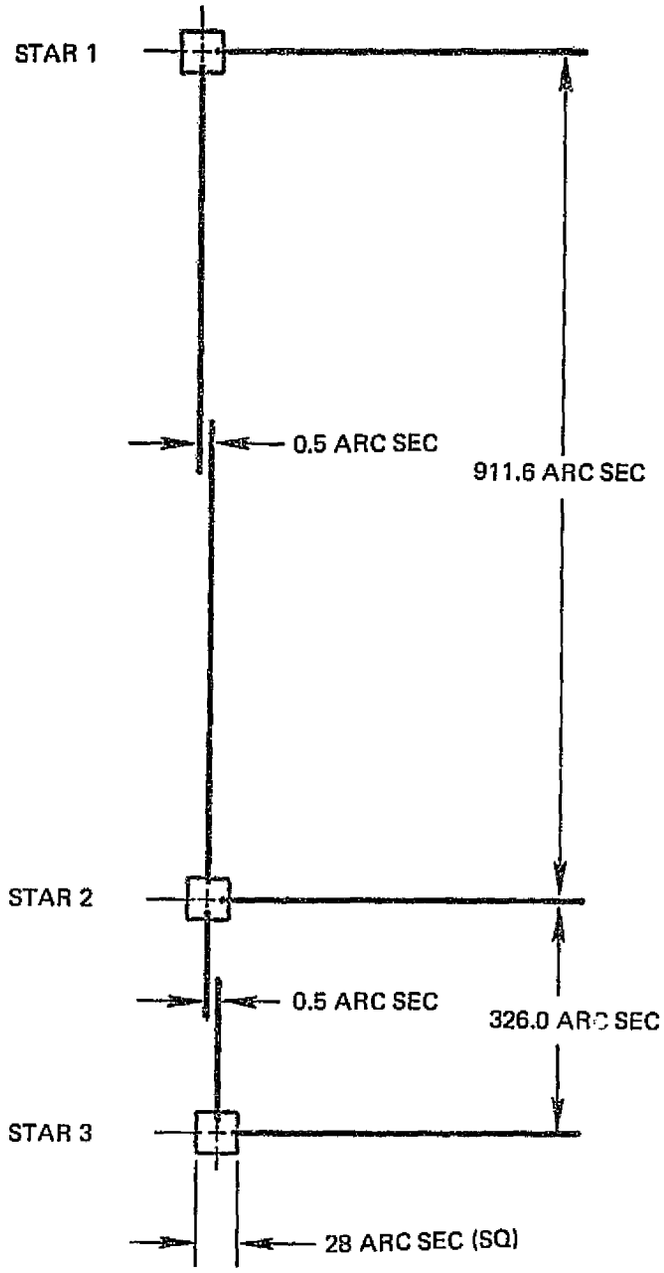

Figure 4-20. Angular Measurements of the LED Sources

The theodolite was placed in the same position in the collimated beam occupied by the strapdown star tracker. Each angle is the average of three measurements. Of the six angles the maximum standard deviation about the mean is 0.4 arc second; the peak deviation from the mean is 0.9 arc second. Using the maximum standard deviation, the standard deviation of the mean is 0.2 arc second.

For the gimbal test the center star was used together with a number of mirrors to produce the three different star elevations. A stationary mirror and three rotating mirrors were used to deflect the star beam. The mirrors were adjusted so that the star beam was normal to each of the three reference mirrors on the side of the gimbal star tracker base. This was accomplished by first adjusting the star beam parallel to the automatic autocollimator beam, and then adjusting the rotating mirrors so that the autocollimator beam was normal to each reference mirror face. Immediately following this adjustment, the tracker was removed, the theodolite inserted in its position, and the three star angles were measured. Figure 4-21 illustrates the measured angles. The reference axes are the gravity vector and an arbitrary azimuth. Each angle is the average of three measurements. The maximum standard deviation of the six angles is 0.7 arc second; the peak deviation from the mean is 1.0 arc second. Using the maximum standard deviation, the standard deviation of the mean is 0.4 arc second. The increase in measurement error over that obtained for the LED sources was due to two effects:

1) A drift trend in the measurements, probably due to motion of the deflection mirrors

2) Less precision in centering the theodolite crosshairs over the square star which was tilted for the gimbal tests.

The stars were made square to improve the repeatability of the field of view positioning of the theodolite. Figure 4-22 shows the vertical crosshairs of the DKM3 positioned over a star. The star was made large enough so that a strip approximately 2 arc seconds wide appeared outside of the crosshairs. The operator would position the instrument so that both strips appeared equal in width. A 0.5 arc second error in centering would produce an easily discernable 60 percent difference in strip widths.

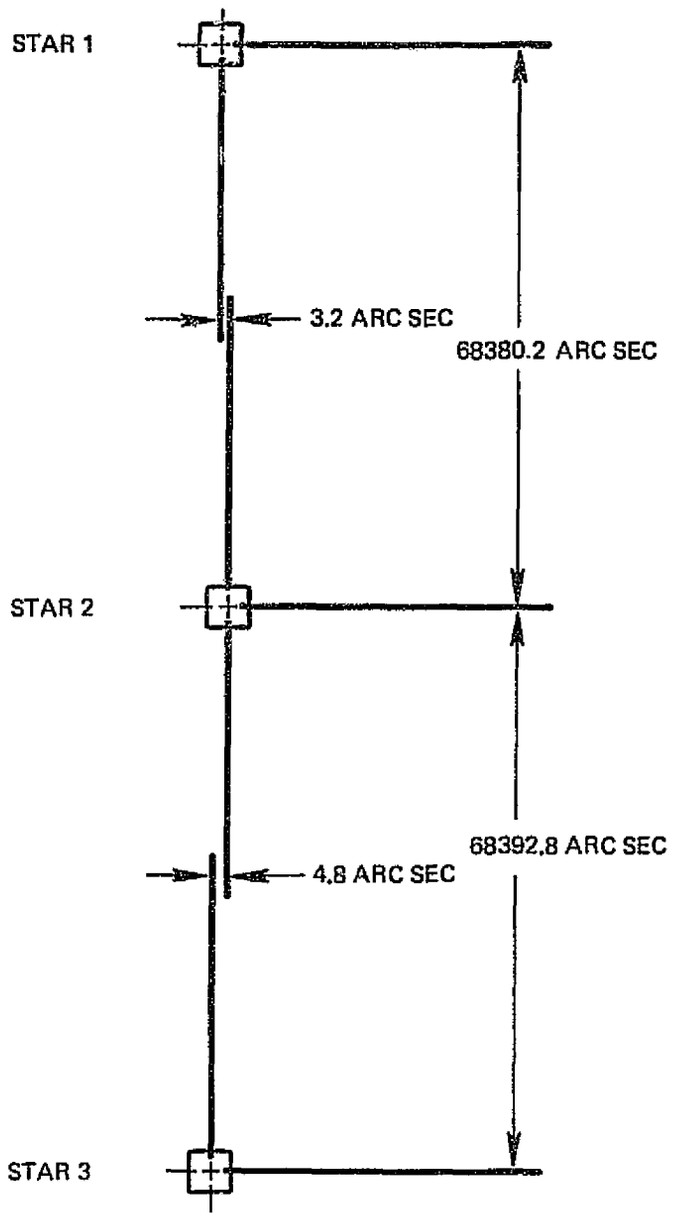

Figure 4-21. Angular Measurements of the Gimbal Star Sources

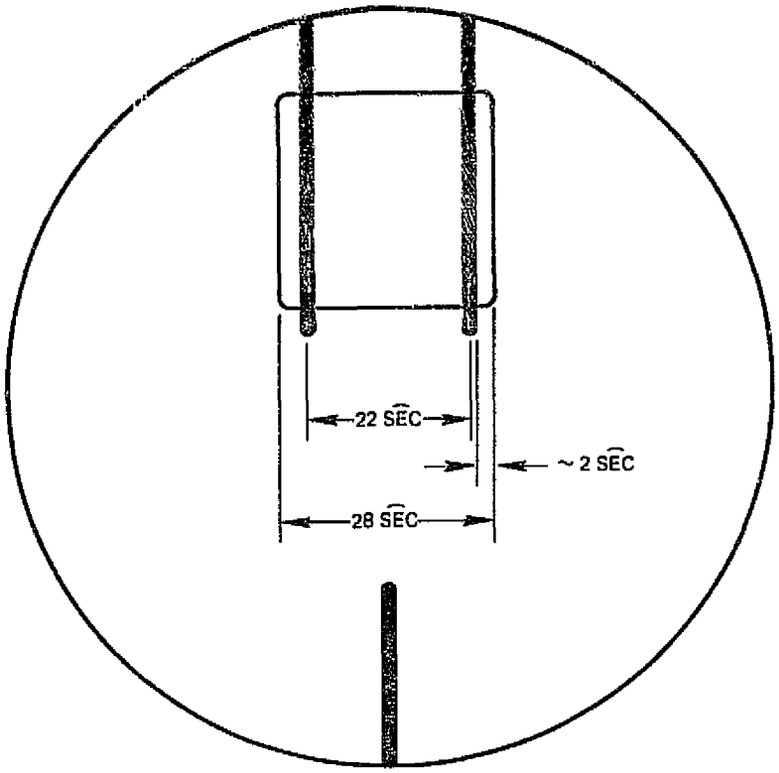

Figure 4-22. Theodolite Field of View Centering

The drawback in making such large stars is the susceptibility to non-unformities in the illumination within the 28 arc second star. Although the stars appeared uniform visually, there is no assurance that the centroid in the spectral bandwidth of the star tracker will be at the geometrical center of the star. Based on experience gained from the unit calibrations of the strapdown star tracker (Volume II, Section 7), a 4 percent error, 1.0 arc second (1σ), was attributed to this source. Although the error could be measured by noting the star tracker output before and after rotating the star 180 degrees, this was not done because of the irrelevance of the error to the PADS test results.

Again, because of the objective of the PADS tests, it was technically justifiable to use LED sources instead of light with a spectrum more nearly approaching that of starlight. The intensity of the LED was adjusted to give the same anode current from the image dissector in the star tracker that the convolution of starlight (G0, 6000^{o}K) with the nominal S20 photo-cathode response would produce. For the strapdown tracker, 8 M_v stars were

simulated; the gimbal tracker used 3.5 M_V stars. The tracker performance, and hence the PADS performance, is a function of the anode current, and is insensitive to the spectrum of the light producing the current, providing the intensity is such as to always produce the same current.

The collimation accuracy of the reflective bench is specified to be 2 arc seconds over the entire 40.6 cm aperture. Using the center star (on the focal axis), the collimation was checked around the area of the tracker and theodolite apertures shown in Figure 4-23. The theodolite together with a separate reference mirror mounted on the granite table was used. No collimation error, significant relative to the repeatability of the DKM3, was observed.

In the case of the strapdown test, a collimation error is caused by the top and bottom stars not being on the focal axis of the parabolic mirror. However, this did not cause a test error since the relative star positions were measured with the theodolite in the same position occupied by the star tracker.

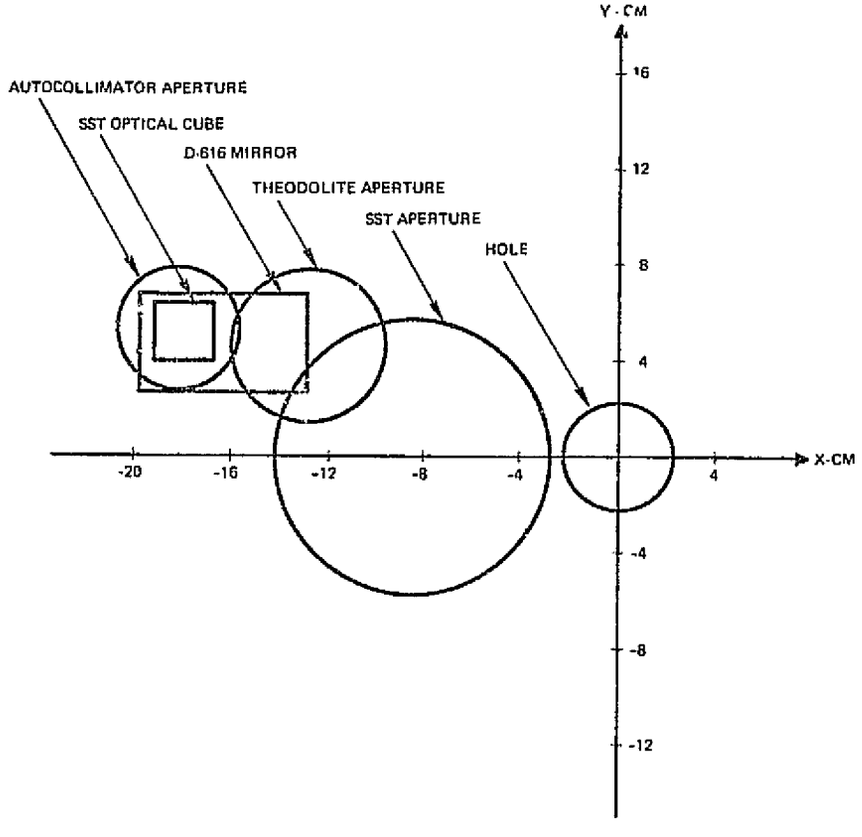

Figure 4-23. Aperture and Mirror Geometry

4.4.2.2 Double-Sided Mirror

The double-sided mirror is a Davidson (Model D-616) adjustable reference mirror. By manufacturer specification the two first-surface mirrors are parallel to within one arc second.

Non-parallelism between the two mirror surfaces will result in a one-to-one non-parallelism between the center star beam and the automatic autocollimator beam. This will appear as an absolute error common to all stars. Since this type of error is not relevant to determining the performance of the PADS systems, the parallelism was not checked in the laboratory.

4.4.2.3 Theodolite

The theodolite serves two functions:

1) Alignment of the center star and automatic autocollimator beams to a parallel condition

2) Measurement of the relative angles between the three stars used in both the strapdown and gimbal system tests.

These functions are the limiting factors in the accuracy of the laboratory instrumentation for the PADS tests. Consequently, the Kern Model DKM3 theodolite was used throughout the testing since it provides significantly better readout precision than other theodolites.(5)

Alignment of the star and autocollimator beams involves two steps:

1) Centering of the star in the telescope crosshairs

2) Adjustment of the double-sided mirror to center the autocollimating reticule return image in the crosshairs.

Although the micrometer readout was used to facilitate the first step, final verification of the alignment was through the telescope eyepiece and was independent of readout repeatability errors.

Repeatability in centering either the square star image or the reticule image in the crosshairs was measured indirectly by making two sets of measurements:

1) Sixteen micrometer readings wherein only the micrometer was moved after each reading

2) Sixteen micrometer reading wherein both the micrometer and the telescope were moved.

No statistically significant difference in the standard deviations of the two sets of readings was observed. The conclusion reached was that the centering repeatability is better than the readout repeatability. The latter falls within the range 0.2 to 0.4 arc second (1σ), depending on the ability and disposition of the observer. Arbitrarily, the centering repeatability was assigned the value 0.2 arc second (1σ).

A bias error in the alignment of the two beams can be introduced by the autocollimation technique used in the DKM3. A cube beamsplitter is used and the crosshair pattern and the autocollimating negative reticle are fixed to the sides of the cube. Coincidence of the telescope and autocollimating boresights was measured by first aligning the star and double-sided mirror, and ther plunging and reversing the theodolite and measuring any indicated deviation. The misalignment between boresights was found to be 0.7 arc seconds for the horizontal axis and negligible relative to the readout repeatability for the verticle axis.

A final error source which must be considered in the alignment of the two beams is the spherical abberation of the DKM3. This error arises because half the aperture of the telescope is covered by the double-sided mirror. It was minimized by adjusting the telescope focus so that no discernable star motion was observed with either a full aperture or half-covered aperture. Once set, the focus was not moved throughout the ten day system test.

Measurement of the angular position of the top and bottom stars relative to the center star is subject to three types of errors:

1) Micrometer readout repeatability

2) Horizontal and vertical circle accuracy

3) Horizontal axis runout (gimbal test only).

The first error can be minimized by repeated readings. No instrumentation was available to measure the second error. However, circle accuracy for the DKM3 instrument has previously been measured[6] as 0.2 to 0.3 arc second (1σ). Arbitrarily, 0.2 arc seconds (1σ) was assumed. Since the three stars for the gimbal system test are approximately 20 degrees apart, bearing runout in the horizontal axis of the theodolite is a factor. Unfortunately, no information is available for this error source.

Leveling of the theodolite can easily be accomplished within one or two arc second. In the case of the three stars for the strapdown system test, where the maximum star separation is 911 arc seconds, this is a negligible error source. For the three stars in the gimbal system test this error source is irrevalant since only the relative star positions are measured with the theodolite. Their absolute alignment relative to the gimbal star tracker axes is determined using the star sensor boresight as explained in Section 10.2.

4.4.2.4 Air Bearing Table Readout

The air bearing table and readout electronics are made by Fecker Systems Division, Owens-Illinois. The performance parameter critical to the PADS system tests is the stability of the angle readout. This readout is a 21 bit digital word with a scaling of $360^{o}/2^{21}$ counts, or approximately 0.6 arc second/count.

Following a four hour warmup period, the stability of the readout was checked by positioning the table so that an equal motion in either direction was required to change the readout by one bit. No change in the readout was noted thereafter for periods up to 24 hours.

For the strapdown system test the table readout is used over a $1/2^{o}$ interval to provide a laboratory measurement of the horizontal location of a star in the tracker 1^{o} by 1^{o} field of view. Consequently, the readout was calibrated over this range using two different makes of theodolites to provide independent references. A Kern DKM3 and a Wild T3 were the theodolites used in the calibration.

Five calibrations were made using the T3 over a period of 12 days. Two months later three calibrations were made with the DKM3. A different section of a theodolite circle was used for each calibration with that instrument.

The results of the T3 and DKM3 calibrations are shown in Figure 4-24. The agreement between theodolites is excellent. The temporal stability of the error is also high since the curves were taken two months apart.

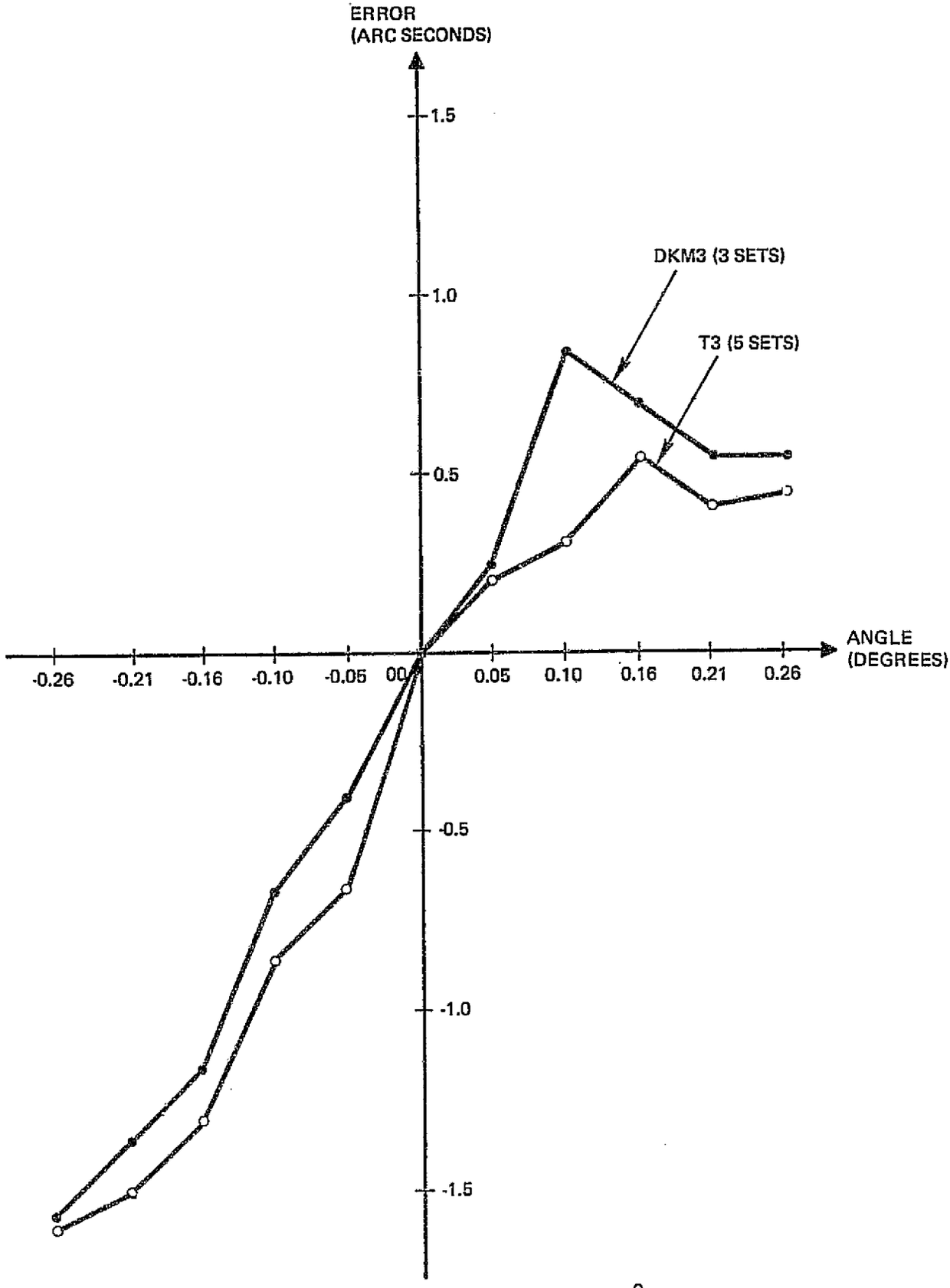

Figure 4-24. Data Results over $1/2^{0}$ Interval

A 256 cycle error is expected in the readout since a 512 pole Inductosyn is used. Consequently, the data in Figure 4-24 was modeled as

$$y_1 = x_1 + \left[\sin 2\pi \left(i - \frac{N+1}{2}\right)\frac{\Delta\theta}{\theta_p}\right] x_2 + \left[\cos 2\pi \left(i - \frac{N+1}{2}\right)\frac{\Delta\theta}{\theta_p}\right] x_3,\ i = 1, 2, \ldots 11$$

where

$N = 11$

$\Delta\theta = 188$ arc seconds

$\theta_p = 5062.5$ arc seconds

The observation equation for all data points representing the average of the two curves in Figure 4-24 is

$$y = Ax$$

The best fit in the least squares sense is

$$\hat{x} = (A^T A)^{-1} A^T y$$

Solution of this equation using a computer program gave the parameters

$$x_1 = -0.8$$

$$x_2 = 1.2$$

$$x_3 = 0.8$$

The standard deviation of the residues between the model and the 11 data points was 0.1 arc second.

In the case of the strapdown system test a total of three measurements in the field of view were made per star transit. Consequently, the optical angle (twice the table angle) quantization is

$$Q_S = \frac{3}{\sqrt{3}} \frac{2(0.6)}{\sqrt{12}}$$

$$Q_S = 0.6 \text{ arc second } (3\sigma)$$

For the gimbal system test a single measurement is taken per transit. In addition, the optical and table angles are the same. The quantization is then

$$Q_G = 3 \frac{0.6}{\sqrt{12}}$$

$$Q_G = 0.5 \text{ arc second } (3\sigma)$$

The response of the table readout to a constant rate is 1 arc sec per rad/sec. Since the maximum table rate during testing was 15 arc seconds/second, the lag in the angle readout is negligible.

4.4.2.5 Automatic Autocollimator

The two-axis autocollimator used in the PADS tests was a Davidson (Model 696) Automatic Autocollimator. The excitation of the output potentiometer was adjusted to give a scaling of 0.15 v/arc second.

For all of the test runs the output of either axis of the autocollimator never exceeded ten arc seconds. Since the excitation voltage was controlled to better than 1 percent, the scale factor error never exceeded 0.1 arc second. Of greater importance was a nonlinearity in the potentiometer output for the horizontal axis near null. This error amounted to 0.3 arc seconds deviation from an otherwise linear output.

The noise in the autocollimator output was filtered through a 20 second RC time constant mechanized in the digital computer. This reduced the noise level to 0.2 arc second (peak).

With the parallel beam star stimulus technique the bias drift of the autocollimator is calibrated before each star transit. This is accomplished by first directing the star and autocollimator beams at the theodolite and double-sided mirror and measuring the autocollimator bias. Next the beams are directed at the star tracker. A change in output between positions indicates the angle between the star beam and the normal to the reference mirror surface on the tracker.

The maximum drift of the autocollimator output observed during any of the eight test runs was 2 arc seconds for a four hour period. Since it took approximately 5 minutes of data to measure the steady-state output values at the reference and star positions, the effect of the drift was negligible.

5. TEST FACILITY DESCRIPTION

A general description of the PADS precision test facility is presented in this section. The facility layout, test equipment, and electronics are discussed.

5.1 FACILITY LAYOUT

The PADS precision test facility is located in TRW Building M5, Room 0222, Manhattan Beach, California. The test facility consists of four areas: 1) a laboratory, 2) a control platform, 3) a computer area, and 4) a work area. Figure 5-1 is a floor plan of the facility.

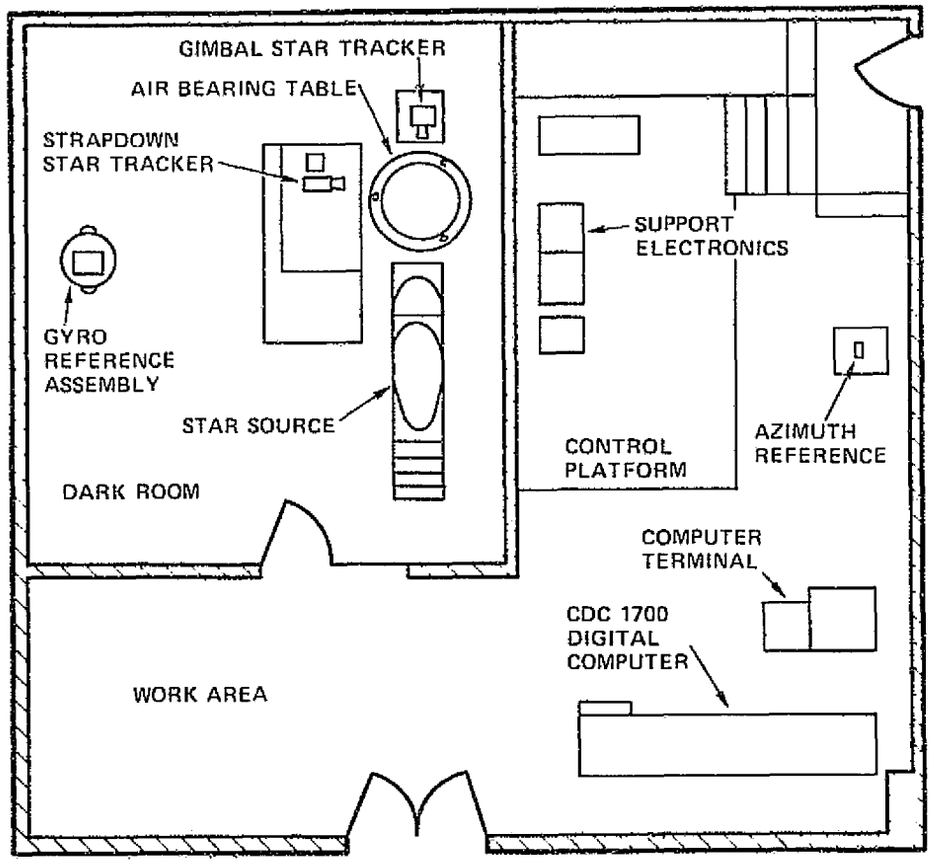

Figure 5-1. Test Facility Floor Plan

The laboratory is a dark room which is located on a seismic pad isolated from building vibrations. The pad rests on a sand base. The laboratory has its own air conditioning system which controls the air

temperature to 0.6°C. Whenever it was practical, all heat generating test equipment was located on the control platform to minimize thermal gradients within the laboratory. Equipment installation settling times greater than 60 days were allowed for both rotary tables, the granite tables, and the star source.

All electronic equipment necessary to monitor and control the system tests was located on the control platform. This area functioned as the center of activity throughout a test run.

The computer area contained the CDC 1700 digital computer and two computer control terminals. Although this computer implemented the control of various equipment during a test run, control of the computer itself was exercised from switches on the control platform. The terminals were used to initialize the program before a test run and for debugging.

A photographic montage of the facility is shown in Figure 1-3. The top photograph (a split photo) shows the inertial reference unit on the left together with its console and the rate table console. Since a ground-fixed test method was used, the rate table console was inoperative during all test runs. The star trackers and their associated test equipment are shown on the right. The test console shown on the rear wall is for unit testing of the strapdown star tracker and was also inoperative during the test runs. In addition to the two electronic consoles on the control paltform, two stripchart recorders were present to display quick look data, an oscilloscope for troubleshooting electronic failures, and a desk and bookcase for data storage.

5.2 LABORATORY TEST EQUIPMENT

The test equipment used in the laboratory for both the strapdown and gimbal system tests is listed in Table 5-1. The item numbers refer to the balloon numbers in Figures 4-2 and 4-3 which are isometric drawings of the laboratory configurations. Items 28 through 31 are not shown in the figures. Item 28 is a shutter to block the autocollimator light beam from entering the star tracker aperture. Items 29 through 31 were used for initial alignment of the laboratory equipment. Item 32 monitored the laboratory temperature.

Table 5-1. Laboratory Equipment

Item	Test		Name	Type	Relevant Specification
	Strap	Gim			
1	X	X	Star Source	Davidson Reflective Bench Model D-278	2 arc sec collimation accuracy
2	X	X	LED Point Sources	TRW	
3	X	X	Table	TRW	
4	X	X	Autocollimator Stand	TRW	
5	X	X	Automatic Autocollimator	Davidson Model D-696	0.1 arc sec resolution
6	X	X	Adjustable Mirror	Davidson Model D-616	1/8 wavelength flatness
7	X		Rotating Mirror	Ransom 10 in. diameter	1/10 wavelength flatness
8	X		Mirror Mount	TRW	
9	X	X	Air Bearing Table	Fecker Dwg 256-001	0.6 arc sec readout resolution
10	X	X	Theodolite	Kern Model DKM3	0.2 arc sec accuracy
11	X	X	Adjustable Mirror	Davidson Model D-616	1/8 wavelength flatness
12	X		Mirror Stand, Strapdown Test	TRW	
13	X	X	Granite Table	Collins Microflat	
14	X	X	Granite Slab	Collins Microflat	
15	X		Strapdown Star Tracker	TRW	
16	X		Optical Cube	Mark Optical	1/8 wavelength flatness
17	X		Star Tracker Stand	TRW	
18	X	X	Rate Table	Inland Model 712	
19	X	X	Inertial Reference Assembly	NASA/GSFC OAO	
20		X	Deflection Mirrors	Ransom 10 in. diameter	1/10 wavelength flatness
21		X	Rotating Mirror Fixture	TRW	
22		X	Stationary Mirror Fixture	TRW	
23		X	Reference Mirrors	Rolyn	1/8 wavelength flatness
24		X	Gimbal Star Tracker	TRW	
25		X	Granite Riser	Collins Microflat	
26		X	Granite Block	Collins Microflat	
27		X	Mirror Stand, Gimbal Test	TRW	
28	X	X	Shutter Assembly	TRW	
29	X	X	Theodolite	Wild T3	0.2 arc sec accuracy
30	X	X	Vertical Mirror	Farrand No. 88504	2 arc sec to vertical
31			Bubble Level	Starrett No. 199	1 arc sec resolution
32	X	X	Temperature and Humidity Gauge	Honeywell	

5.3 ELECTRONIC EQUIPMENT

The general approach to the design of the electronics was to provide redundancy and to avoid interdependence of equipment. The intent of both of these ground rules was to avoid delays during the equipment integration phase. Redundancy was provided for both the strapdown star tracker and the gyro readouts by having their unit test consoles on hand. This allowed their integration in the laboratory without dependence on the facility electronics. The facility electronics had the capability to duplicate the computer commands, thereby allowing operation of the laboratory equipment while the computer programs were being debugged. Operation of the equipment without either of the star trackers, or the gyros, was provided in order to avoid delays in the case of a malfunction of any of the units. Since it was a critical element, a backup automatic autocollimator was on hand. A complete supply of electronic components was maintained in the facility.

A block diagram of the electronic equipment in the PADS test facility is shown in Figure 5-2. An explanation of the acronyms used is given in Table 5-2. Figures 5-3 through 5-9 are photographs of the electronics located on the control platform. Functional descriptions of the panels in the two consoles are given in the following paragraphs.

AA/CP. This panel, supplied by Davidson Optronics, controls the automatic autocollimator unit in the laboratory. After intially setting the track loop gains, the panel was used only to indicate acquisition of an optical flat by the autocollimator.

ABP. This panel performs two functions: 1) it provides the servo electronics to drive the ABT, and 2) it supplies the excitation and buffer amplifiers for the AA/C potentiometers.

The computer supplies two analog voltage commands, position and rate, to the servo electronics. The electronics implements a proportional plus integral drive to the ABT power amplifiers. A potentiometer is available on the panel to sum a voltage in with the computer position command. This capability allows manual positioning of the table.

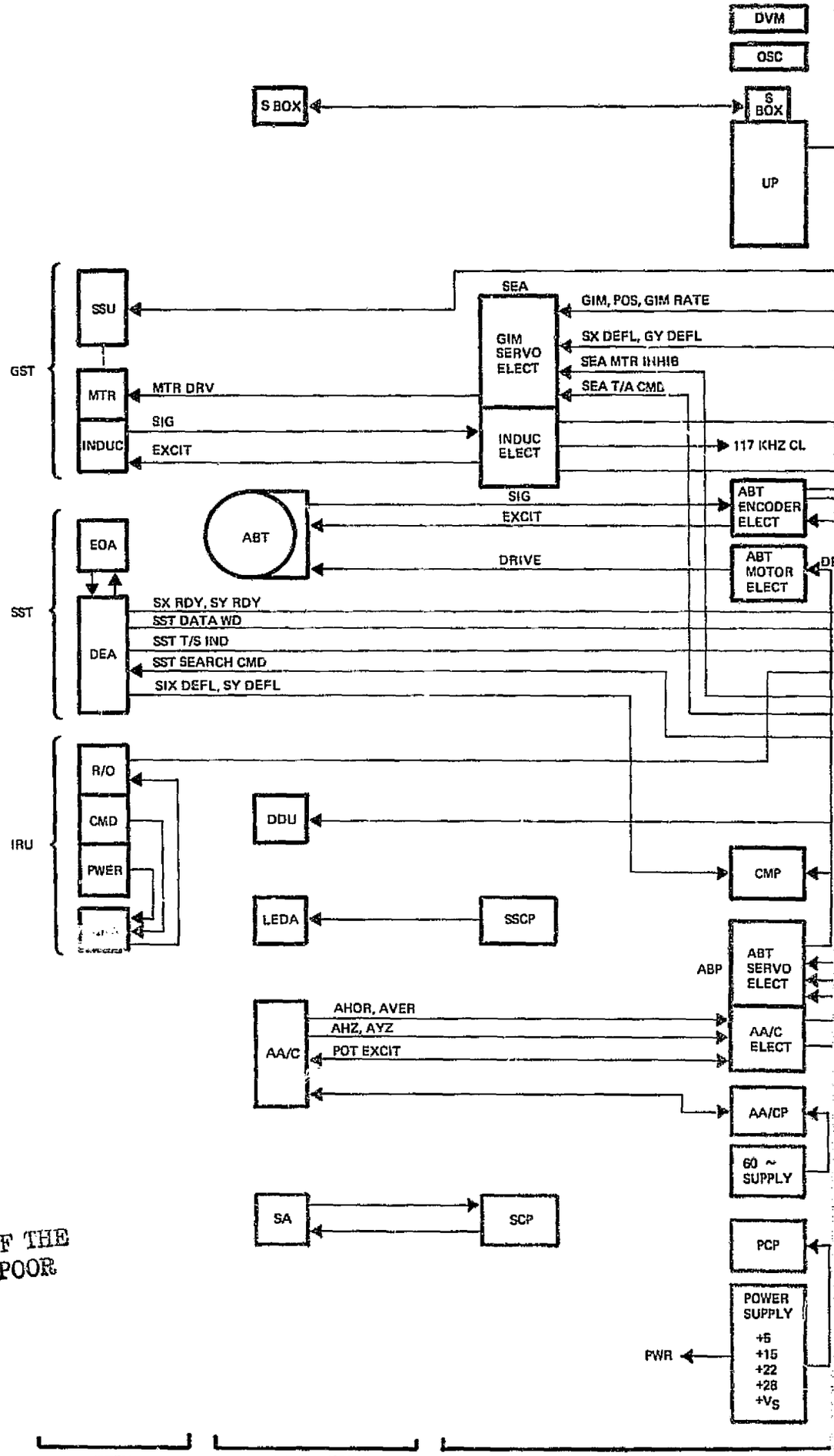

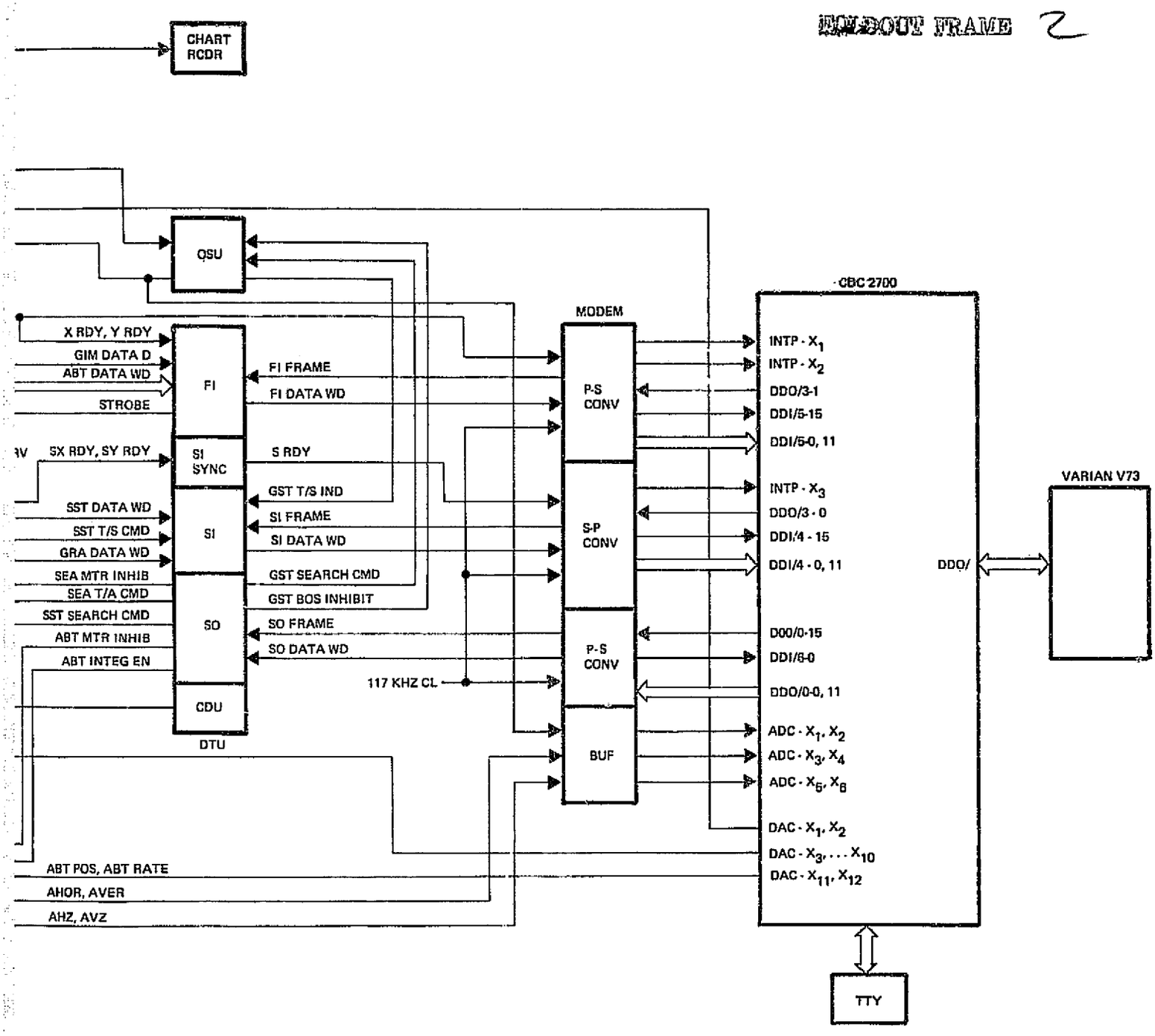

Figure 5-2. Electronic Interface Diagram

Table 5-2. Electronic Interface Acronyms

AA/C	Automatic Autocollimator	OSC	Oscilloscope
AA/CP	AA/C Control Panel	OSU	Optical Sensor Unit
ABP	Analog Buffer Panel	P-S	Parallel to Serial
ABT	Air Bearing Table	PCP	Power Control Panel
BUF	Buffer	PWR	Power
CDU	Control Room Display Unit	RCDR	Recorder
CMD	Command	R/O	Readout
CMP	Console Monitor Panel	RPP	Remote Patch Panel
DDU	Darkroom Display Unit	SA	Shutter Assembly
DEA	Digital Electronics Assembly	S Box	Speaker Box (Intercom)
DTU	Data Transfer Unit	SCP	Shutter Control Panel
DVM	Digital Voltmeter	S-P	Serial to Parallel
EOA	Electro-Optical Assembly	SEA	Sensor Electronics Assembly
FI	Fast Input	SI	Slow Input
GRA	Gyro Reference Assembly	SO	Slow Output
GST	Gimbal Star Tracker	SS	Star Source
INDUC	Inductosyn	SSCP	Star Source Control Panel
IRU	Inertial Reference Unit	SSU	Star Sensor Unit
LEDA	Light Emitting Diode Assembly	TTY	Teletypewriter
MTR	Motor	UP	Utility Panel

The excitation to the AA/C potentiometers is independently adjustable. A scale factor of 0.15 volt/arc second was used. The buffer amplifiers send the potentiometer outputs to the computer.

CMP. This panel monitors the gimbal motor current, the SST analog deflection signals, and eight DAC channels from the computer. The SST deflection signals were displayed on the oscilloscope. The DAC channels were displayed on the stripchart recorder via the UP.

UP. This panel provides direct connection to the two stripchart recorders. An eight channel and a six channel recorder are available. The eight channel was used for quick look information during a test run. The six channel was for long term monitoring of the gyro performance because it could be operated at a very slow chart rate.

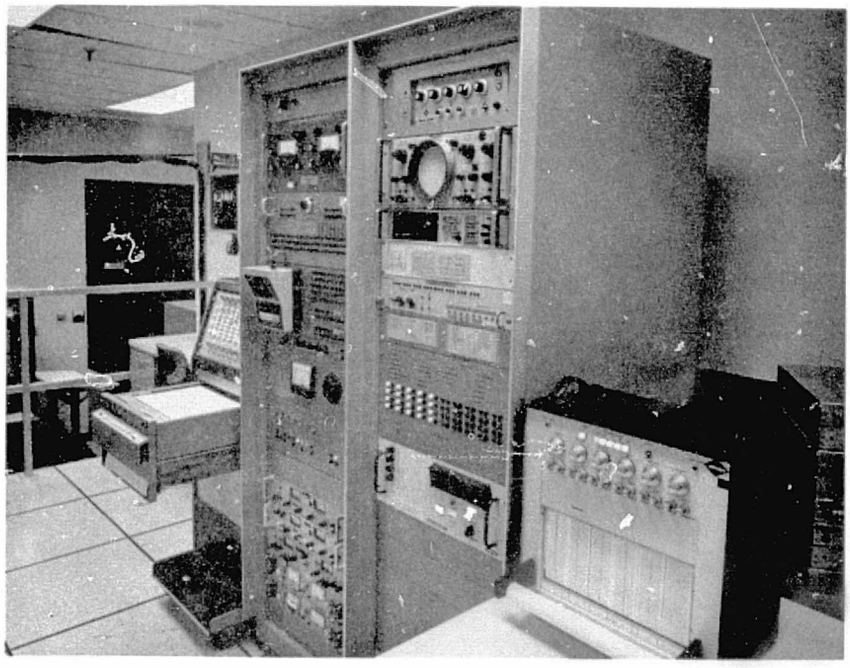

Figure 5-3. Control Platform View — Right

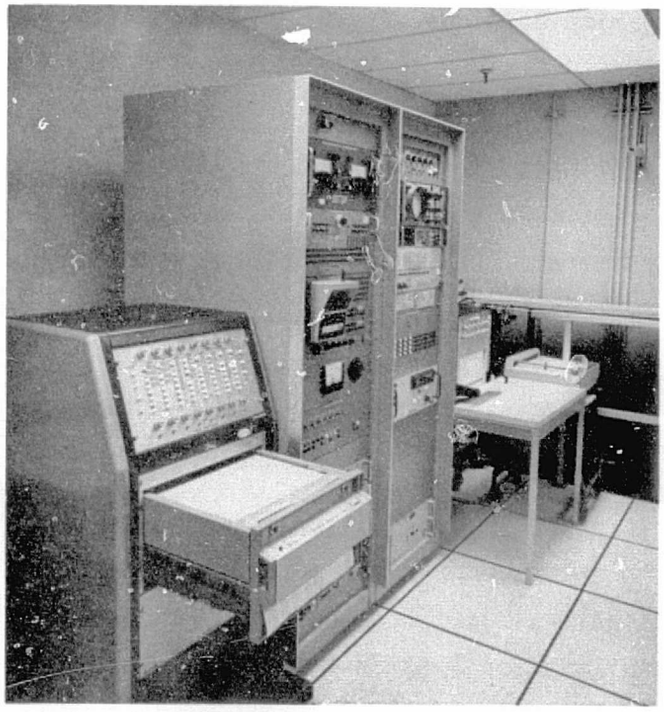

Figure 5-4. Control Platform View — Left

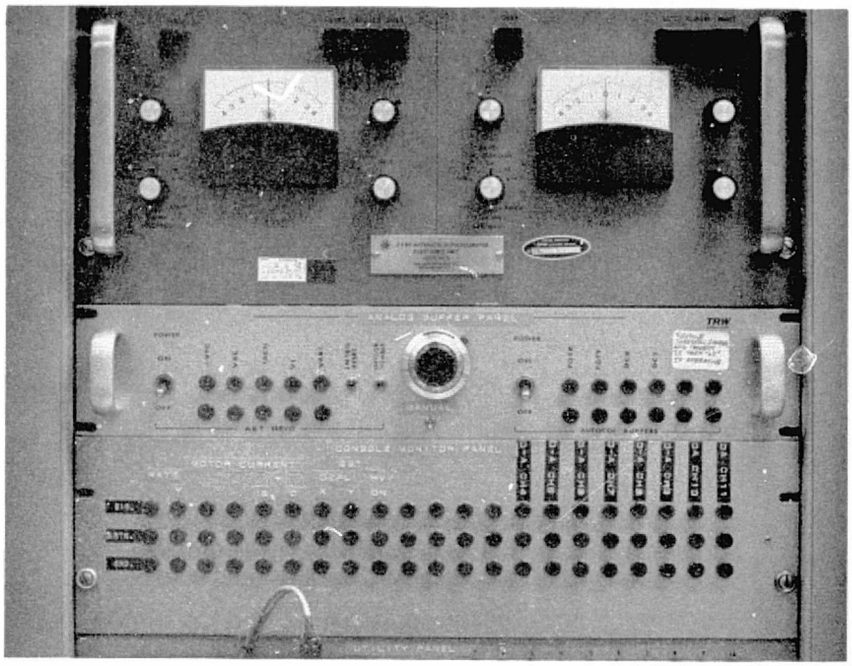

Figure 5-5. AA/CP to Up Panels

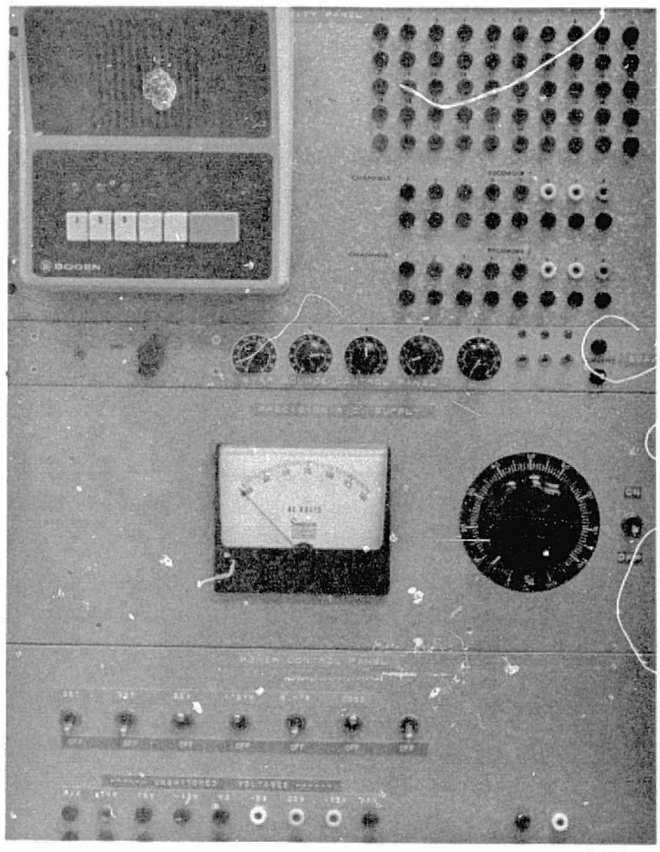

Figure 5-6. Up to PCP Panels

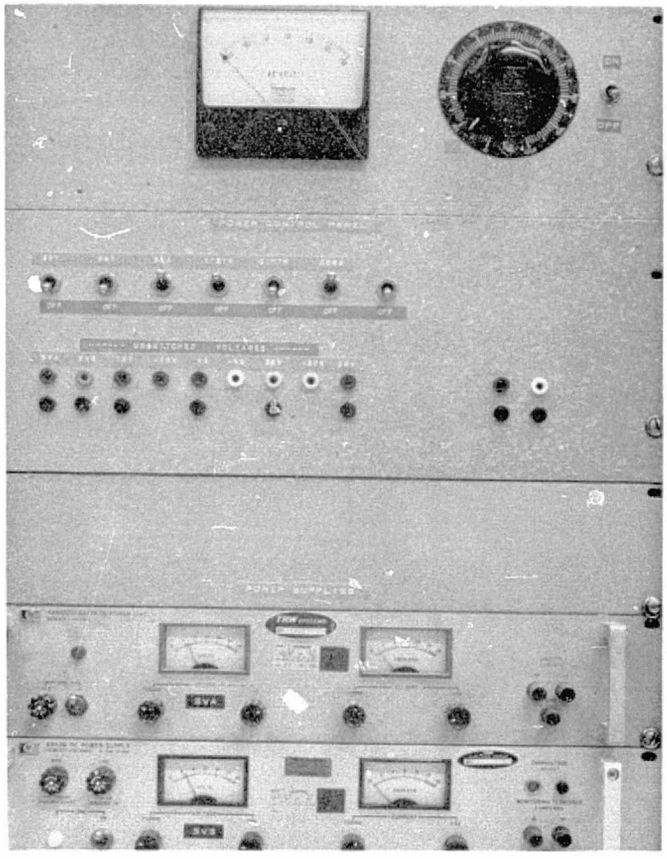

Figure 5-7. PCP Panel and Power Supplies

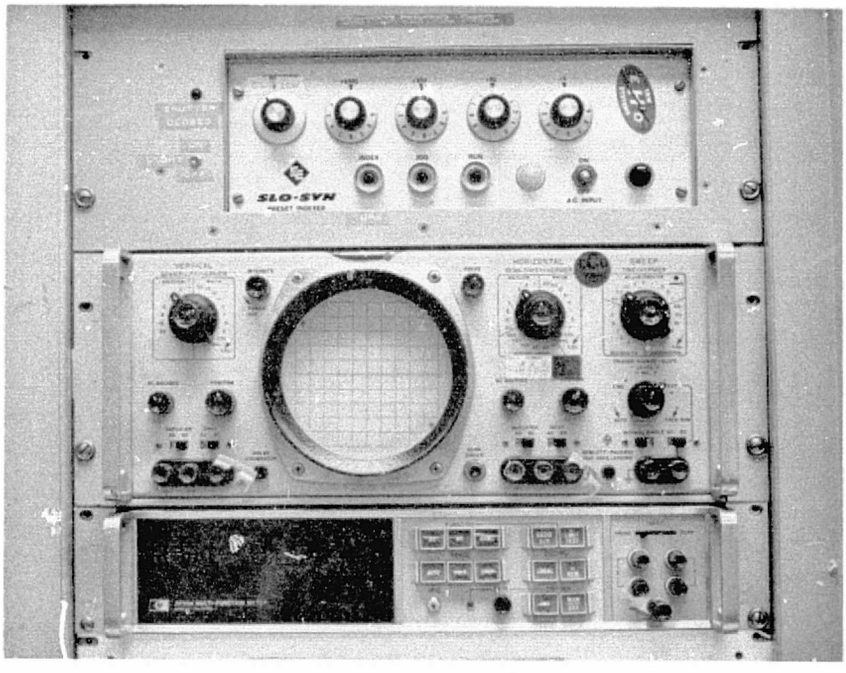

Figure 5-8. SCP to DTU Panels

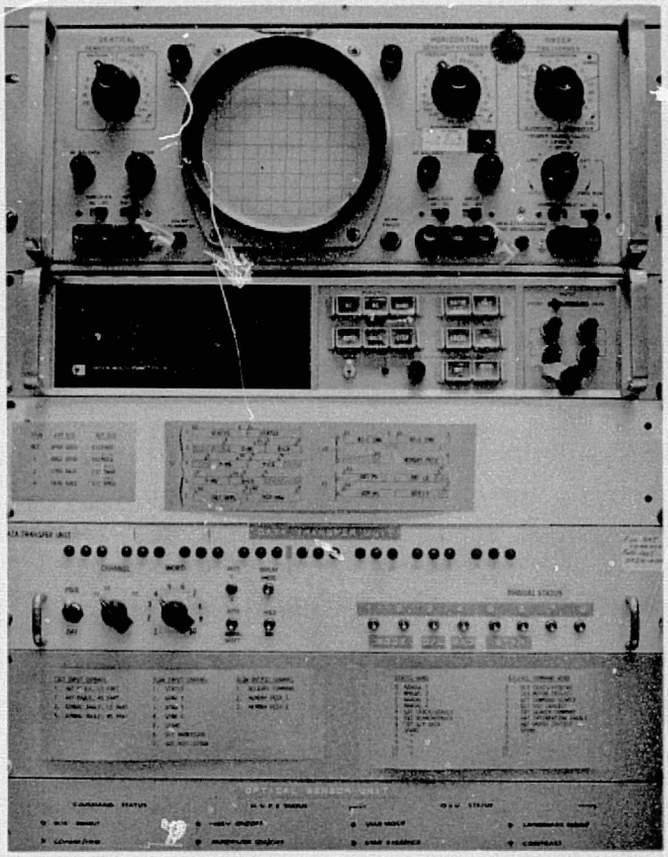

Figure 5-9. DTU and OSU Panels

PCP. This panel provides independent switching of the dc power supplies to the other panels and equipment. The purpose is to avoid power supply turn-on transients.

SCP. This panel operates the shutter in front of the AA/C. Since it was essential to avoid having the AA/C light beam enter the strapdown star tracker, a fail-safe light indicator is inserted in the panel to signal shutter closure.

DTU. This panel performs four functions: 1) it transfers all digital signals from the ABT, GST, SST, and IRU to the computer, and 2) it transfers digital signals from the computer to the ABT electronics, GST, and SST, 3) it displays digital information from the computer and from the ABT, GST, SST, and IRU, and 4) it provides commands to the computer program.

Digital data transfer into the computer is accomplished at two rates: 1) 6 msec/word (FI), and 2) 50 msec/word (SI). The ABT and GST gimbal angles are sent at the fast rate. SST deflection and magnitude, three gyro outputs, and a status word are sent at the slow rate.

Data transfer from the computer is accomplished on one channel (SO) at the rate of 50 msec/word. A command word and two memory peek words are transmitted. Individual bits of the command word are sent to the ABT electronics, the GST, and the SST. The memory peek words display program selected memory locations in the computer.

Any of the above digital words can be shown on the LED display on the panel by using the selector switches. This information can also be duplicated on a similar LED display in the laboratory.

In order to minimize operating personnel, the computer program was designed to be operated from the DTU by the test conductor. This is implemented from eight switches on the panel which set the state of eight bits in the status word sent on the SI channel.

An optional capability of the DTU is the ability to function without the computer. This allowed display of the ABT, GST, GRA, and SST signals while the computer was being used for other tasks.

OSU. This panel displays the status of the SSU. It also has a switch to enable the SSU high voltage supplies. The SSU analog deflection signals were displayed on the oscilloscope.

ABT ENCODER ELECTRONICS. This panel, supplied by Fecker, provides a visual display of the 21 bit digital word indicating the table angle. It also sends this word in parallel to the DTU.

ABT MOTOR ELECTRONICS. This panel functions as a power amplifier to drive the ABT motor.

In addition to the above described panels a MODEM panel in the CDC 1700 computer was designed. This panel functions both as a signal buffer and as a serial/parallel digital word converter.

The CDC 1700 computer has the capability of transmitting information to the Varian V73 computer. This capability was used to store the PADS test run data using the magnetic tape unit on the V73.

6. DATA HANDLING AND DISPLAY

Data was generated during the PADS system test from two sources: the PADS sensors and the laboratory instrumentation. This is illustrated in Figure 6-1. The data was collected for two purposes: 1) to provide the basis for the evaluation of the performance of the PADS system under test, and 2) to provide real time diagnostic data to indicate the validity of the test.

All data was transmitted to the CDC 1700 computer via the data transfer electronics. The data necessary for the evaluation of the PADS system was stored on magnetic tape. This data was transmitted to the V73 computer over data lines for storage on the tape since the CDC 1700 did not have a magnetic tape unit. The real time diagnostic data was displayed during a test run on an eight channel stripchart recorder via the test display electronics.

The following sections describe in detail the test performance and real time diagnostic data which was collected.

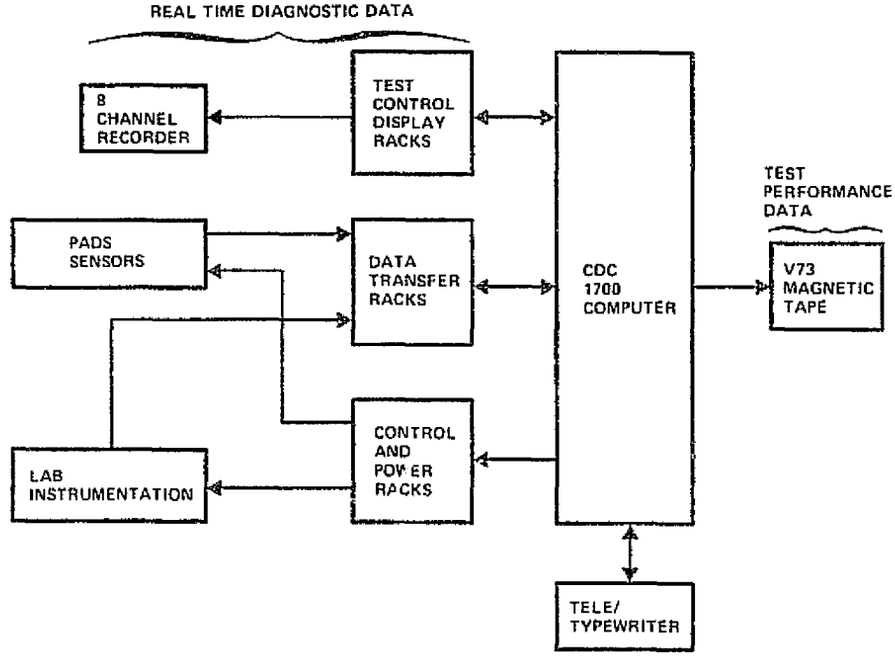

Figure 6-1. Data Handling and Display

6.1 TEST PERFORMANCE DATA

Three types of performance data were stored on magnetic tape for both the strapdown and gimbal system tests. These are listed in Table 6-1. PADS data consists of the gyro and star tracker signals. This information is used in the PADS algorithms to estimate the inertial attitude of the PADS axes. Lab data consists of the air bearing table angle and automatic autocollimator differences. This information, together with pretest measurements, identifies where the star is relative to the PADS axes, and, ultimately, the true inertial attitude of the PADS axes. Boresight data consists of filtered star tracker and automatic autocollimator signals. In essence it measures the static boresight stability of the tracker.

Table 6-1. Types of Performance

Data Word	PADS Data	Lab Data	Boresight Data
Strapdown System Test			
T	X	X	
GRAX	X		
GRAY	X		
GRAZ	X		
SSTX	X		
SSTY	X		
ABTA		X	
$\overline{\Delta AA/CX}$		X	X
$\overline{\Delta AA/CY}$		X	X
$\overline{SSTX}$			X
$\overline{SSTY}$			X
Gimbal System Test			
T	X	X	
GRAX	X	X	
GRAY	X		
GRAZ	X		
GSTX	X		
GSTY	X		
GSTA	X		
ABTA		X	
$\overline{\Delta AA/CX}$		X	X
$\overline{\Delta AA/CY}$		X	X
$\overline{GSTX}$			X
$\overline{GSTY}$			X
$\overline{GSTA}$			X

The first two data types provide the basis for the evaluation of the PADS performance; namely, the difference between the estimated PADS attitude from the sensor information and the true attitude from the laboratory instrumentation data. The third data type was included for two reasons: 1) to provide a check on the validity of the lab data accuracy, and 2) to measure the boresight stability of the star trackers throughout the test period.

Data was collected every second for both system tests. The word T is the time tag. The three-axis gyro information, GRAX, GRAY, and GRAZ, was collected continuously throughout the test run. Every 20 minutes, during a star transit, the star tracker information was collected. For the strapdown tracker the horizontal and vertical positions of the star in the field of view, SSTX and SSTY, were stored. The same signals for the gimbal star tracker, GSTY and GSTX, were collected, along with the gimbal angle, GSTA. The air bearing table angle, ABTA, was also collected during a star transit. The duration of the transit was approximately four minutes for the strapdown test and two minutes for the gimbal test. As described in Section 4.3 the autocollimator bias was calibrated prior to each star transit by pointing the parallel star and autocollimator beams at the theodolite and double-sided mirror. Following this calibration the static orientation of the star relative to the PADS axes was checked by pointing the parallel beams at the star tracker and its reference mirror surface. The star orientation was indicated by the autocollimator outputs, minus the bias errors, namely, $\overline{\Delta AA/CX}$ and $\overline{\Delta AA/CY}$. With the star pointed at the tracker, the output signals from the tracker were also collected: $\overline{SSTX}$ and $\overline{SSTY}$ for the strapdown tracker, and $\overline{GSTY}$, $\overline{GSTX}$, and $\overline{GSTA}$ for the gimbal tracker. The bar over these signals indicates that they are filtered to minimize their noise content. These filtered signals were stored once at the start of each star transit.

It is noted that the horizontal star position is indicated by the signals SSTX, GSTY, and $\Delta AA/CX$; the vertical by SSTY, GSTX, and $\Delta AA/CY$.

All data was converted into engineering units in the V73 computer before storage on the magnetic tape. Time was carried to a precision of 0.001 second, and all angles were carried out to 0.1 arc second. For a four hour run, with 12 star transits, the number of words stored on tape was approximately 78,000 for the strapdown system, and 69,000 for the gimbal system.

In the case of the gyro data the accumulated attitude was transmitted from the gyros and stored on tape. The advantage of this approach, compared to transmitting the incremental attitude, was that a random transmission error would not invalidate the long term knowledge of gyro attitude change.

6.2 REAL TIME DIAGNOSTIC DATA

The real time diagnostic data provided a continuous indication throughout a test run that the functional operation of the hardware was proper and that, with a high degree of probability, the test data being collected was valid in terms of indicating the PADS performance. This information was considered necessary in view of the length (4 to 5 hours) of the test runs. It eliminated any time which would have been wasted by continuing to run invalid tests.

The different types of diagnostic data that were used are listed in Table 6-2. All of the performance data signals listed in Table 6-1 were monitored by the stripchart recorder, the ABT readout, and the DTU LED display. The teletypewriter and the CRT display provided error messages indicating either a procedural error by the test conductor or a data transmission error.

Table 6-2. Types of Realtime Diagnostic Data

Stripchart Recorder

Channel	Strapdown Test	Gimbal Test
1	Δ GRAX	Δ GRAX
2	Δ GRAY	Δ GRAY
3	Δ GRAZ	Δ GRAZ
4	$\overline{\text{SSTX}}$	$\overline{\text{GSTX}}$
5	$\overline{\text{SSTY}}$	$\overline{\text{GSTY}}$
6	$\overline{\text{AA/CX}}$	$\overline{\text{AA/CX}}$
7	$\overline{\text{AA/CY}}$	$\overline{\text{AA/CY}}$
8	$\overline{\text{ERROR}}$	$\overline{\text{ERROR}}$

Air Bearing Table Readout

ABTA

DTU Led Display

$\overline{\text{GSTA}}$

CDC 1700 Teletypewriter

Operator Error Message

V73 CRT Display

Transmission Error Message

The stripchart recordings for the four strapdown system test runs and the four gimbal system test runs are included in Appendix D. The gyro signal, ΔGRA, is the attitude change over a 100 second time period. The filtered horizontal and vertical autocollimator signals are $\overline{AA/CX}$ and $\overline{AA/CY}$, respectively. The signal $\overline{ERROR}$ is the filtered difference between the star tracker horizontal axis signal and the air bearing table angle, biased to zero at the center of the tracker field of view. This signal occurred only during a star transit. The square wave discernible in the autocollimator signals reflects the two positions, one with the parallel beams pointed at the theodolite, the other with the beams pointed at the star tracker. The majority of the time between star transits was spent at the latter position. A peculiarity in the gyro data is that occasionally the digital to analog converter in the CDC 1700 will turn over if the signal is near ±10 volts. The result is a discrete change of 10 volts in the recorder output. This can be observed, for example, in the GRAZ signal in the first strapdown system test on 1 October 1975.

The air bearing table angle was observed during the test directly from the Fecker readout display. The gimbal angle was observed on the DTU LED display.

If the test operator followed an incorrect sequence in switching between program modes, the computer program printed an error message at the teletypewriter.

To provide a final data check before storage of the data on magnetic tape, the V73 computer program performed a check on the time word, T, to verify that one second occurred between successive words.

7. LABORATORY COMPUTER PROGRAMS

Two categories of computer programs were written for the CDC 1700 computer in the PADS test facility. The first provided for a step-by-step integration and checkout of the laboratory and system equipment. The second category consisted of the system test programs for the strapdown and gimbal system tests. These two programs are described in detail in this section since they are essential to a complete understanding of the tests.

The purpose of either system test program was twofold: 1) to provide star stimuli to the star tracker; and 2) to collect, store, and display the signals from the PADS sensors and the laboratory instrumentation. The star stimuli consisted of individual star transits in which a collimated star beam was moved past the field of view of the star tracker at earth rate. The frequency of the star transits as well as the length of the test were determined by the test conductor. All data was time-tagged and stored on magnetic tape. Separate programs were written for the strapdown and gimbal system tests due to the differences in operation of the star trackers. The programs were named SUE and GWEN, for the strapdown and gimbal tests, respectively.

Flow diagrams of the two programs appear in Appendix E.

7.1 STRAPDOWN SYSTEM TEST PROGRAM

The following sections describe the modes, data displays, and data collection capabilities of the strapdown system test program SUE.

7.1.1 Program Modes

There were three main program modes in SUE:

MODE 1 — REFERENCE POSITION. The star source (SS) and automatic autocollimator (AA/C) beams were pointed at the theodolite and reference mirror by the 1700 computer closing a servo loop about the ABT R/O to drive the ABT to a reference position, ABTO = 7710000. The difference between the readout, ABTA, and ABTO was output as a position signal, POS, to the servo electronics by a 1700 DAC channel every 3 milliseconds.

Expressed in equation form,

$$POS = ABTO-ABTA, \ |POS| \leq 2047 \text{ bits}$$

$$POS = 2047 \text{ sign } (POS), \ |POS| > 2047 \text{ bits}$$

where

1 bit = 0.617981 arc sec

Although a rate command channel was available, it was set to zero.

MODE 2 — ZERO POSITION. The SS and AA/C beams were pointed at the strapdown star tracker (SST) by the 1700 closing a servo loop around the ABT R/O to drive the ABT to 0010000. Position and rate were commanded as in MODE 1.

MODE 3 — STAR TRANSIT. The purpose of this mode was to drive the ABT at half earth rate to sweep a simulated star across the field of view of the star tracker. Before starting this sweep, the ABT was driven from the ZERO position of MODE 2 to the starting position which places the star outside the field of view. The complete ramp function generated in the 1700, using its clock as a time reference, is defined graphically in Figure 7-1. The ramp is continued until the mode is manually exited by the test conductor. The servo position command, computed and output every 3 milliseconds was:

$$POS = (RAMP + ZEROP)-ABTA$$

where

ZEROP is the ZERO position of MODE 2

and RAMP is the function in Figure 7-1.

There were two submodes in SUE:

RUNNING AVERAGES. This submode, when exercised, computed running averages of both AA/C outputs and, if the star tracker was in track, both SST digital outputs. This submode could only be entered from MODE 1 or MODE 2. When exited the last values of the running averages were stored in memory, one pair for each mode in the case of the AA/C. Since SST outputs were available only in MODE 2, only one pair was stored.

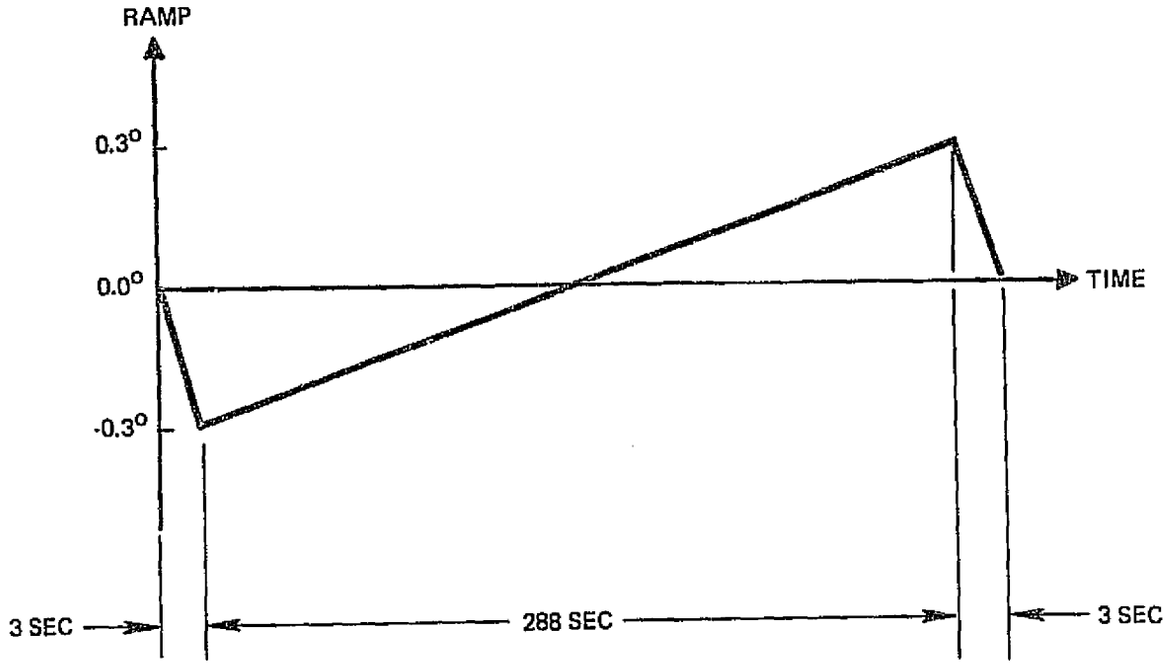

Figure 7-1. RAMP Function for the Strapdown Test

DATA COLLECTION. This submode sent data to the V73 computer to be stored on magnetic tape. It could be entered or exited from any of the three main modes. Its normal duration was four hours and constituted a "test run." Since a time base was required for the test run, the 1700 clock was initialized and started when the submode was entered and stopped when it was exited. Therefore the exercise of the clock dependent functions, the ramp and the one second period for some of the running averages, required this submode to be active.

7.1.2 Mode Control

The teletypewriter was used only to start and stop the program. All other control was from four manual switches on the DTU. The switch logic for mode control is shown in Table 7-1. Switch No. 3 controlled the RUNNING AVERAGES submode. Switch No. 4 controlled the DATA COLLECTION submode. The switch positions were transmitted to the 1700 computer via the lower order four bits of the slow input status word. A one corresponded to the "UP" switch position.

Table 7-1. SUE Mode Control

Mode	Description	Switch Number			
		No. 1* Bit 0	No. 2* Bit 1	No. 3* Bit 2	No. 4* Bit 3
1	Reference Position	0	0	--	--
2	Zero Position	0	1	--	--
3	Star Transit	1	1	--	--

*Slow input status word

7.1.3 Program Discrete Commands

The program set the discrete commands from the digital output channel to the states indicated in Table 7-2.

7.1.4 Real Time Diagnostic Data

Table 7-3 lists the parameters that were sent to the stripchart recorder through the DAC channels of the 1700 computer, for display during the test.

Table 7-2. Discrete Command States

Slow Output Bilevel Command Word Bit Number	Description	State
4	SST Search	0
5	ABT Integ Enable	0
6	ABT MTR Inhibit	0
All Others	Spares	0

Table 7-3. DAC Output Data

DAC	Data	Type	Update Period	Scaling
4	ΔGRAX	Incremental Count	100 sec	0.1 V/count
5	ΔGRAY	Incremental Count	100 sec	0.1 V/count
6	ΔGRAZ	Incremental Count	100 sec	0.1 V/count
7	$\overline{SSTX}$	Running Average	50 msec	0.5 V/count
8	$\overline{SSTY}$	Running Average	50 msec	0.5 V/count
9	$\overline{AA/CX}$	Running Average	1 sec	0.25 V/arc sec
10	$\overline{AA/CY}$	Running Average	1 sec	0.25 V/arc sec
11	$\overline{ERROR}$	Running Average	50 msec	0.5 V/count

An explanation of each data type is given below:

ΔGRA. These are the differences in the 16 bit gyro word at a 100 second interval. The scaling (1 meru = 0.015^{o}/hr) is:

0.05 meru = 1 count/100 sec

Since the maximum difference (at full earth rate) would be 20000 counts, less than half the capacity of a 16 bit word, differences could be taken without accounting for turnover of the gyro word. On the other hand, the DAC word, scaled for 0.1 V/count and limited to ±10 V, could turn over.

SST. These are the running averages of the 12-bit star tracker outputs. They are computed every 50 millisec by the equation:

$$\overline{SST}_{N+1} = (1 - e)\ \overline{SST}_{N} + e\ (SST_{N+1})$$

where

$e = 0.001$

These averages were computed only in MODE 2, and were stored upon exit of the RUNNING AVERAGE submode.

$\overline{AA/C}$. These are the running averages of the autocollimator outputs. They were computed every one second by the equation:

$$\overline{AA/C}_{N+1} = (1 - e)\ \overline{AA/C}_N + e\ (AA/C_{N+1})$$

where

$e = 0.05$

These averages were computed in MODE 1 and MODE 2, and were stored separately upon exit of the RUNNING AVERAGES submode.

$\overline{ERROR}$. This is the running average of the difference between the SST horizontal axis output and the ABT readout. It is computed every 50 millisec by the equations:

$$ERROR = SSTX - 1.236\ (ABTA)$$

$$\overline{ERROR}_{N+1} = (1 - e)\ \overline{ERROR}_N + e\ (SST_{N+1})$$

where

$e = 0.04$

This average was computed only in MODE 3 when the star tracker was in track.

7.1.5 Data Collection

Collection of data to be transmitted by the 1700 computer to the V73 is initiated by DTU switch 4 in the up position. There are three different data formats. Table 7-4 lists the data to be sent for each format.

Note that "Track" actually implies two conditions: 1) that the SST Search/Track signal indicates track, and 2) that the positive ramp in MODE 3 be present. "Start of track" is the first time the 1 sec counter changes after entry into track as defined above. "Non-track" is all the rest of the time.

Table 7-4. Data Stored on Magnetic Tape

Data	Nominal Scaling	Bits Required	Non-Track	Start of Track	Track
			1/Sec	Single	1/Sec
Time	1 msec/cnt	19	X	X	X
GRAX	0.075 $\widehat{\text{sec}}$/cnt	21	X	X	X
GRAY	0.075 $\widehat{\text{sec}}$/cnt	21	X	X	X
GRAZ	0.075 $\widehat{\text{sec}}$/cnt	21	X	X	X
SST X/Y Status	--	1		X	X
SSTX	1.0 $\widehat{\text{sec}}$/cnt	12		X	X
SSTY	1.0 $\widehat{\text{sec}}$/cnt	12		X	X
ABTA	0.618 $\widehat{\text{sec}}$/cnt	21		X	X
$\overline{\text{SSTX}}$	1.0 $\widehat{\text{sec}}$/cnt	12		X	
$\overline{\text{SSTY}}$	1.0 $\widehat{\text{sec}}$/cnt	12		X	
$\overline{\Delta\text{AA/CX}}$	0.15 $\widehat{\text{sec}}$/volt	12		X	
$\overline{\Delta\text{AA/CY}}$	0.15 $\widehat{\text{sec}}$/volt	12		X	

Comments regarding the data are:

- TIME AND STATUS. Time must have at least 21 bits to record 4 hours of data at 10 msec/count. Time will be zero at the start of data collection. The three status bits are:

  1) Search/Track (SI, Status, Bit 5)

  2) X/Y Data (SI, Status, Bit 6)

  3) Initial Track (True at start of track).

- ΔGRA. The gyro words were corrected for their own turnovers. At a maximum rate of 200 counts/sec, only 21 bits are actually needed.

- SST. The X and Y words were sent alternately every 50 msec to the 1700 computer. The data transmitted to the magnetic tape always included the X word corresponding to the nearest time-tag.

- ABTA. The range of the table movement in SUE required only 13 of the 21 bits available.

- $\overline{SST}$. These 2 words were the stored values from the last time the RUNNING AVERAGES submode was entered in MODE 2.
- $\overline{\Delta AA/C}$. These two words were computed as:

$$\overline{\Delta AA/C} = \overline{AA/C}_{\text{mode 3}} - \overline{AA/C}_{\text{mode 2}}$$

where

$\overline{AA/C}_{\text{mode 3}}$ = stored values from the last time the RUNNING AVERAGES submode was entered in MODE 2

$\overline{AA/C}_{\text{mode 2}}$ = stored values from the last time the RUNNING AVERAGES submode was entered in MODE 1.

7.2 GIMBAL SYSTEM TEST PROGRAM

The following sections describe the modes, data displays, and data collection capabilities of the gimbal system test program GWEN.

7.2.1 Program Modes

There were three main program modes in GWEN.

MODE 1 — REFERENCE POSITION. This mode positioned the ABT such that the SS and AA/C are pointed at the theodolite and reference mirror, respectively, and pointed the GST to a nominal angle. The mode was used:

1) To align the SS and reference mirror before the test
2) To define the AA/C boresight during the test
3) To measure any misalignment between the SS and the reference mirror after the test.

Servo loops were closed around the ABT and GST using their readouts. Constant angles, ABTO and GSTO, were commanded. The difference between the readouts and the command angles were output unscaled as position signals to the servo electronics. To hasten acquisition, rate signals were commanded whenever the corresponding position signal saturated. Expressed in equation form,

$$TPOS = ABTO - ABTA, \quad |TPOS| \leq 2047 \text{ bits}$$

$$TPOS = 2047 \cdot \text{sign}(TPOS), \quad |TPOS| > 2047 \text{ bits}$$

GPOS = GSTO-GSTA, |GPOS| $\leq$ 2047 bits

GPOS = 2047 sign (GPOS), |GPOS| > 2047 bits

and

TRATE = 0, |TPOS| < 2047 bits

TRATE = 2047 sign (TPOS), |TPOS| $\geq$ 2047 bits

GRATE = 0, |GPOS| < 2047 bits

GRATE = − sign (GPOS), |GPOS| $\geq$ 2047 bits (equivalent to 1^{o} sec)

These equations were updated every 3 msec.

MODE 2 − ZERO POSITION. This mode positioned the ABT such that the SS and AA/C are pointed at the GST via one of the three rotating mirrors on the ABT, and moved the GST gimbal to search for and lock on to the star. The mode was used immediately prior to each star transit to measure:

1) Small rotations of the GST with respect to the AA/C boresight which may occur during the test

2) Drifts in the GST static pointing angle during the test.

The same servo loops were closed about the ABT and, during search, about the GST as in MODE 1. When the star was acquired (track), upon command of the computer, the hardware switched to a second servo loop which drove the gimbal to null the OSU vertical deflection signal.

For the computer-closed loops, the same equations as in MODE 1 applied except that ABTO and GSTO were a function of the 3 star positions which were selected manually from two switches on the DTU. The servos were updated every 3 msec.

MODE 3 − STAR TRANSIT. This mode drove the ABT in a ramp at earth rate to sweep a simulated star across the field of view strip of the GST. The ramp described in Figure 7-2 was commanded to the ABT servo loop which was identical to the loops in MODES 1 and 2. The GST gimbal was driven in the same way as in MODE 2 to search and track the star. Exit from MODE 3 terminated the ABT ramp and also the GST search if a star had not been acquired. As in MODES 1 and 2 both servos were updated every 3 msec.

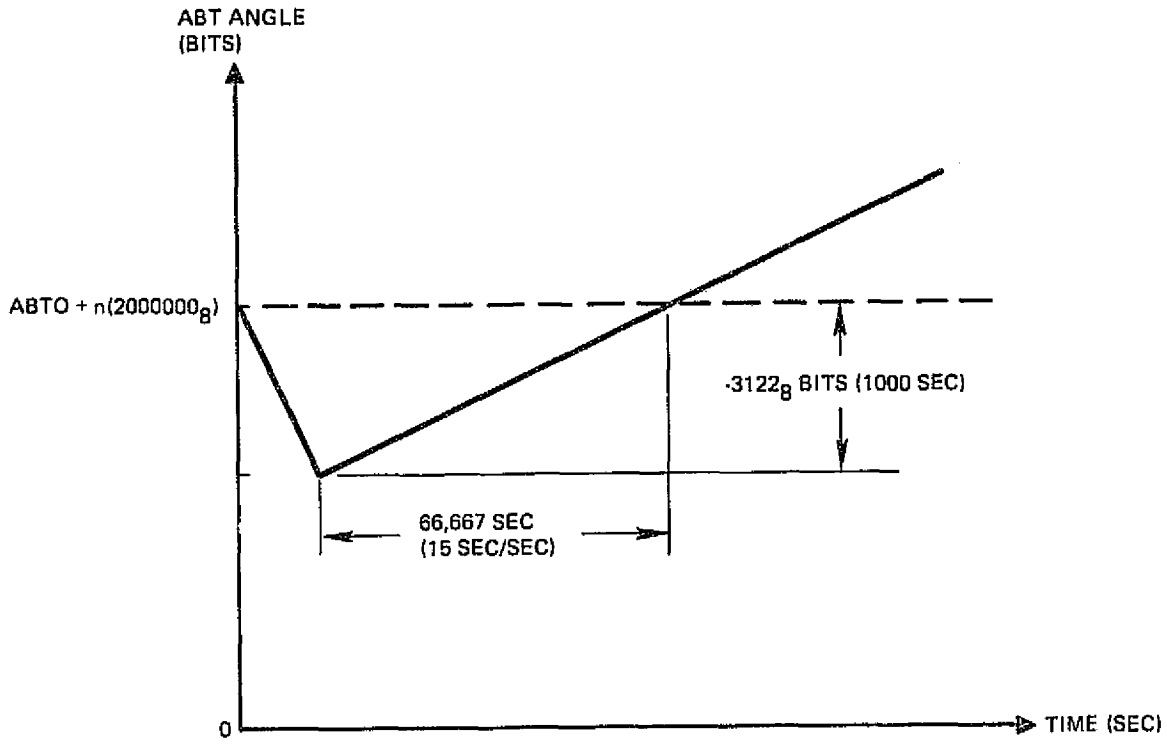

Figure 7-2. Ramp Function for the Gimbal Test

There were two submodes in GWEN:

RUNNING AVERAGES. This submode, when exercised, and depending on the main program mode, computed running averages of both AA/C axes, the gimbal readout, the GST x and y deflections, and the differences between the star tracker x deflection and table angle. The last computed running average for all but the latter signal, was stored for transmittal to magnetic tape upon exit from the submode. The running averages were each computed by the equation:

$$\bar{x}_{n+1} = (1 - e)\,\bar{x}_n + e\,y_{n+1}$$

where

$\bar{x}$ = running average

y = observation

e = weighting factor

The details for each running average including scaling, update interval and weighting constant are given in Table 7-8.

DATA COLLECTION. The remarks for the submode in SUE apply.

7.2.2 Mode Control

The teletypewriter was used only to start and stop the program. All other control was from six manual switches on the DTU. The switch logic for mode control is shown in Table 7-5. The logic for star selection is shown in Table 7-6. Switch No. 3 controlled the RUNNING AVERAGES submode, and switch No. 4 the DATA COLLECTION submode. For all switches "up" corresponded to a "one" state which in turn corresponded to the affirmative state of the switch function name.

Table 7-5. GWEN Mode Control Logic

Mode	Description	Switch	
		No. 1 Bit 0*	No. 2 Bit 1*
1	REF POS	0	0
2	ZERO POS	0	1
3	STAR TRANSIT	1	1

*Slow input channel, status word bits

Table 7-6. GWEN Star Selection Logic

Star	n Value	Switch	
		No. 5 Bit 10*	No. 6 Bit 9*
1	1	0	1
2	2	1	0
3	3	1	1

*Slow input channel, status word bits

7.2.3 Program Discrete Commands

The program sets the bits of the slow output channel, bilevel command word to the states indicated in Table 7-7. Bit 0, SEA TRACK/SEARCH commanded the GST to switch from the gimbal servo loop implemented about the gimbal readout and the computer to the loop using the star tracker vertical output signal. The former loop used the computer to supply a nominal star position and a summing junction; the latter was implemented entirely in the GST electronics. Since it was desired to switch to the tracker loop as soon as a star is acquired, bit 0 was made identical to bit 4 of the slow input channel status word, GST TRACK/SEARCH.

Table 7-7. GWEN Discrete Commands

Slow Output Channel Command Word		Mode		
Bit	Description	1	2	3
0	SEA TRACK/SEARCH	0	0,1	0,1
1	SEA MOTOR INHIBIT	0	0	0
2	GST SEARCH	0	0	0
3	GST BOS INHIBIT	0	0	0
4	SST SEARCH	0	0	0
5	ABT INTEGRATOR INHIBIT	0	0	0
6	ABT MOTOR INHIBIT	0	0	0
7 ↓ 15	SPARE ↓ SPARE	0	0	0

7.2.4 Real Time Diagnostic Data

Key signals were sent to the 8 channel stripchart recorder via the CDC 1700 DACs for display during the test. In addition the memory "peek," a LED display on the DTU of selected words in the 1700 memory, was used to display the running average of the gimbal readout angle. The

signals displayed are described in Table 7-8. The description of the DATA REAL TIME DISPLAY for SUE in the previous section applies to GWEN except for the weighting constants, e, and the equation for $\overline{\text{ERROR}}$ which, for GWEN, was:

$$\text{ERROR} = \frac{\text{GSTX}}{6.7} - (0.618)(\text{ABTA-ABTO})$$

where GSTX is the GST x deflection in millivolts and (ABTA-ABTO) is the difference between the ABT angle and its nominal angle for each star in counts.

Table 7-8. GWEN Real Time Display

	DAC Channel Mode			Update Interval	Scaling		Output Display Maximum	Running Average e
	1	2	3		Input Signal	Output Display		
GRAX	4	4	4	100 sec	Direct	0.1V/cnt	20,000 cnts	--
GRAY	5	5	5	100 sec	Direct	0.1V/cnt	20,000 cnts	--
GRAZ	6	6	6	100 sec	Direct	0.1V/cnt	20,000 cnts	--
$\overline{\text{GSTX}}$		7		50 msec	6.7 mV/$\widehat{\text{sec}}$	0.25V/$\widehat{\text{sec}}$	40 $\widehat{\text{sec}}$	0.0125
$\overline{\text{GSTY}}$		8		50 msec	6.7 mV/$\widehat{\text{sec}}$	0.25V/$\widehat{\text{sec}}$	40 $\widehat{\text{sec}}$	0.0125
$\overline{\text{AA/CX}}$	9	9		1 sec	0.15V/$\widehat{\text{sec}}$	0.25V/$\widehat{\text{sec}}$	40 $\widehat{\text{sec}}$	0.05
$\overline{\text{AA/CY}}$	10	10		1 sec	0.15V/$\widehat{\text{sec}}$	0.25V/$\widehat{\text{sec}}$	40 $\widehat{\text{sec}}$	0.05
$\overline{\text{ERROR}}$			11	50 msec	(see text)	0.25V/$\widehat{\text{sec}}$	200 $\widehat{\text{sec}}$	0.05
$\overline{\text{GSTA}}$	on DTU			50 msec	digital display		full	0.05

7.2.5 Data Collection

Collection of data on magnetic tape in the V73 computer was initiated and terminated by switch No. 4 on the DTU panel. There were three data formats:

1) Non-track
2) Start of track
3) Track.

Three conditions were necessary for the track state: 1) MODE 3; 2) a track signal from the GST (SI channel STATUS word, bit 4); and 3) a positive ramp be present. During the nontrack state three time-tagged gyro signals were stored on tape every one second:

GRAX = x gyro angle, arc seconds

GRAY = y gyro angle, arc seconds

GRAZ = z gyro angle, arc seconds.

At the start of track, running averages calculated and stored during MODE 1 and MODE 2 were stored on tape:

$\overline{GSTA}$ = Last average gimbal angle calculated in MODE 2 before switch No. 3 was turned off, arc seconds

$\overline{GSTX}$ = Last average star tracker horizontal angle calculated in MODE 2 before switch No. 3 was turned off, arc seconds

$\overline{GSTY}$ = (Same as GSTX, but for vertical angle)

$\overline{\Delta AA/CX}$ = Last average AA/C horizontal angle calculated in MODE 2 before switch No. 3 was turned off minus the last average AA/C horizontal angle calculated in MODE 1 before switch No. 3 was turned off, arc seconds

$\overline{\Delta AA/CY}$ = (Same as $\overline{AA/CX}$, but for vertical angle).

During track, time tagged information from the gyros, the GST, and the ABT were stored every one second:

GRAX = (see above)

GRAY = (see above)

GRAZ = (see above)

GSTA = Gimbal angle, arc second

GSTX = Star tracker horizontal angle, arc seconds

GSTY = Star tracker vertical angle, arc seconds

ABTA = ABT angle with zero corresponding to the GST horizontal boresight position, arc seconds.

Time tags were accurate to 1 msec. Scaling for the signals corresponded to Table 7-8. Angles in arc seconds were given to one significant place.

8. PADS PERFORMANCE EVALUATION PROGRAMS

The performance evaluation of the PADS test data was performed offline on a CDC 6500 digital computer via a timeshare terminal. The offline computer programs were coded in FORTRAN. Their input consisted of the magnetic tape data from the V73 computer and certain initialization and control parameters which were inserted from the timeshare terminal. Their output consisted of the three-axis attitude errors in the PADS estimate of its inertial attitude plus other data which facilitated interpretation of the attitude errors. Two offline programs were used: one for the strapdown tests, and one for the gimbal tests.

A functional block diagram applicable to either computer program is shown in Figure 8-1. The program is divided into two main sections: 1) the PADS algorithms, and 2) the laboratory algorithms. In the ground-fixed test configuration the PADS axes are identical to the laboratory axes, and are physically defined by the optical cube on the strapdown star tracker, or the three reference mirrors on the gimbal star tracker. The PADS algorithms estimate the attitude of the PADS axes relative to their inertial attitude at the start of the test run. In a four hour test, for example, the PADS axes will rotate 60^{o} due to the rotation of the earth. The orthogonal transformation matrix $\hat{A}$ will reflect the PADS estimation of the rotation given continuous gyro information and periodic star tracker transits. The laboratory algorithms compute the true inertial attitude of the laboratory, expressed by the matrix A, using the precisely known value of earth rate. The agreement between these two matrices is a direct measure of the PADS performance.

The PADS algorithms are identical to those described in Section 3.2 with the exception of the star catalog information. In the laboratory test the star catalog information is formed by the laboratory algorithms. These algorithms compute the orientation of the collimated star beams relative to the true laboratory or PADS axes.

In addition to the two main sections the computer programs also contain data formatting and attitude error generation algorithms. The latter determine the small angle three-axis attitude errors from the nondiagonal elements of the matrix product $\hat{A}\, A^{T}$.

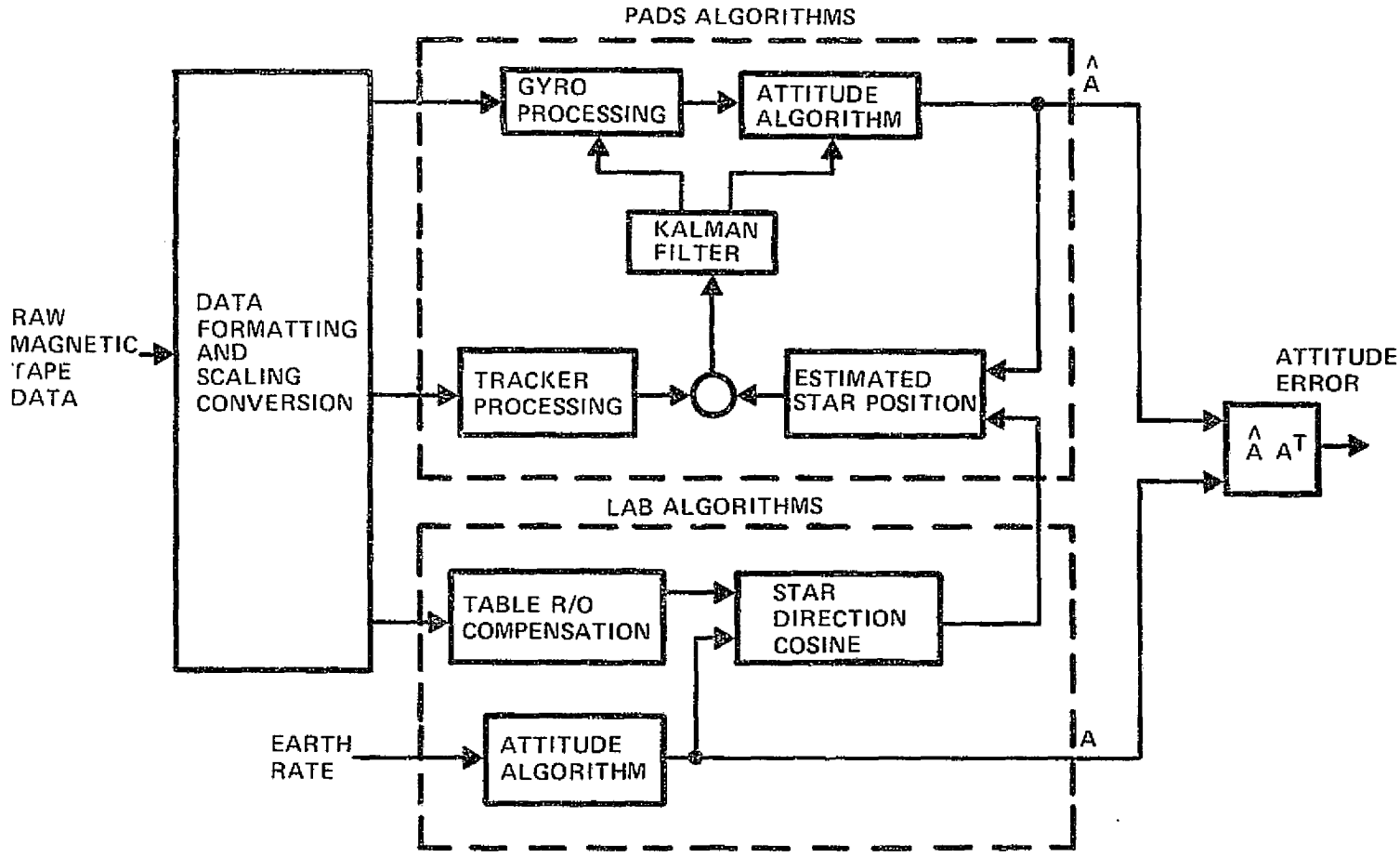

Figure 8-1. PADS Offline Data Evaluation Program

The derivation of the fundamental equations for the offline computer programs is given in Reference 7. Specific comments regarding the application of these equations to the PADS strapdown and gimbal system tests are given in the following sections.

8.1 STRAPDOWN SYSTEM DESCRIPTION

8.1.1 True Laboratory Attitude

The laboratory configuration of the PADS subsystem is illustrated in Figure 8-2. The SST optical cube defines both the PADS and the laboratory axes. The orientation of this optical cube can be described by a right-handed, orthogonal coordinate set (x_1, x_2, x_3) in which each axis is normal to a cube face as in Figure 8-2. To definitize this coordinate set $\bar{x}_3$ is taken to point opposite the gravity vector, and $\bar{x}_1$ is selected such that it experiences no component of the earth's angular velocity, $\bar{\omega}_e$, i.e., $\bar{\omega}_e \cdot \bar{x}_1 = 0$. The optical cube with its above defined coordinate set is thus taken to be the laboratory reference, and the term "laboratory attitude" will be taken to mean the orientation of the axes (x_1, x_2, x_3) relative to an inertial set (z_1, z_2, z_3). This latter set of axes will be taken to be identical to axes (x_1, x_2, x_3) at the start of any particular subsystem test run. The laboratory attitude at any subsequent run time is then given by

$$\begin{bmatrix} x_1 \\ x_2 \\ x_3 \end{bmatrix} = A_{xz}(t) \begin{bmatrix} z_1 \\ z_2 \\ z_3 \end{bmatrix} \tag{8-1}$$

where

$$A_{xz}(t) = \begin{bmatrix} 1 - \beta(\lambda_2^2 + \lambda_3^2) & \alpha\lambda_3 + \beta\lambda_1\lambda_2 & -\alpha\lambda_2 + \beta\lambda_1\lambda_3 \\ -\alpha\lambda_3 + \beta\lambda_1\lambda_2 & 1 - \beta(\lambda_1^2 + \lambda_3^2) & \alpha\lambda_1 + \beta\lambda_2\lambda_3 \\ \alpha\lambda_2 + \beta\lambda_1\lambda_2 & -\alpha\lambda_1 + \beta\lambda_2\lambda_3 & 1 - \beta(\lambda_1^2 + \lambda_2^2) \end{bmatrix} \tag{8-2}$$

$$\lambda_i = \frac{\bar{\omega}_e \cdot \bar{x}_i}{\omega_e} \quad i = 1, 2, 3 \tag{8-3}$$

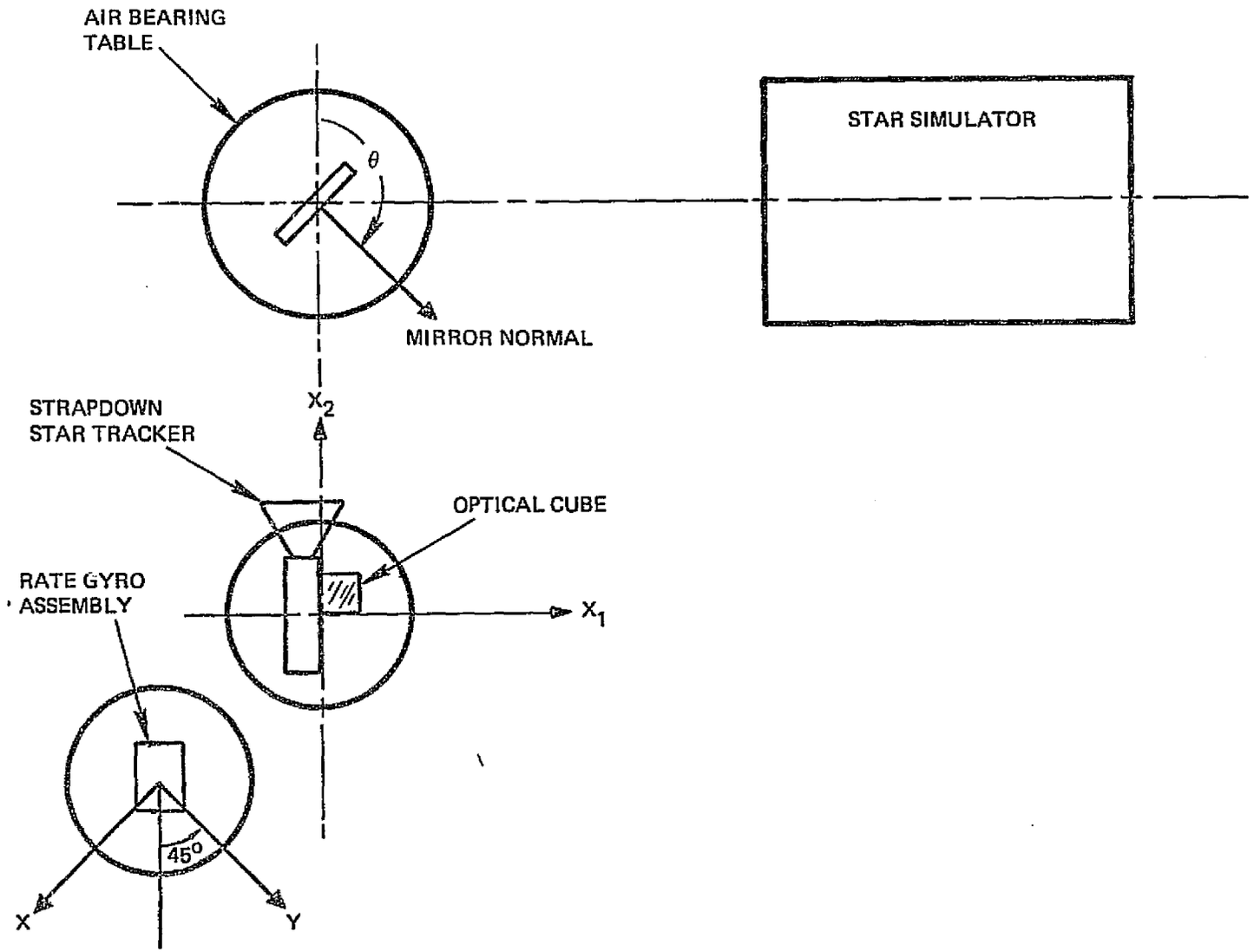

Figure 8-2. PADS Laboratory Setup

$$\alpha = \sin \omega_e t \quad ; \quad \omega_e = |\bar{\omega}_e| \tag{8-4}$$

$$\beta = 1-\cos \omega_e t \tag{8-5}$$

The λ_1 depend, of course, upon the orientation of the laboratory relative to the earth rate, $\bar{\omega}_e$. This is largely a function of its latitude, taken to be 33.90323 deg north. It should be mentioned that inaccuracies in this figure (or in the alignment of the optical cube), while influencing the true knowledge of $A_{xz}(t)$ will have no bearing upon the subsystem performance measure, as the estimated laboratory attitude provided by PADS will contain exactly the same effect. This will be discussed more fully in Section 8.1.2.

8.1.2 PADS Estimate of the Laboratory Attitude

The PADS subsystem must estimate the laboratory attitude without being privy to latitude and a priori earth rate information. The SST/optical cube alignment is such that the tracker's boresight lies along $\bar{x}_2$, with its azimuth and elevation outputs occurring, respectively, about x_3 and x_1. Now the actual orientation of (x_1, x_2, x_3) relative to (z_1, z_2, z_3) is unknown to the PADS subsystem, as this information can only be established through knowledge of ω_e, latitude, and run time, t. Thus PADS can only provide estimates of the x_i, say $\hat{x}_i$, by effective use of the SST and IRU. The PADS output is then an estimated laboratory attitude matrix, $A_{xz}(t)$, defined by

$$\begin{bmatrix} \hat{x}_1 \\ \hat{x}_2 \\ \hat{x}_3 \end{bmatrix} = \hat{A}_{xz}(t) \begin{bmatrix} z_1 \\ z_2 \\ z_3 \end{bmatrix} \tag{8-6}$$

Combining Equations (8-1) and (8-6)

$$\begin{bmatrix} \hat{x}_1 \\ \hat{x}_2 \\ \hat{x}_3 \end{bmatrix} = \hat{A}_{xz}(t)\, A^{-1}_{xz}(t) \begin{bmatrix} x_1 \\ x_2 \\ x_3 \end{bmatrix} \tag{8-7}$$

The degree to which $\hat{A}_{xz}\ A_{xz}^{-1}$ matches the identity matrix is a direct measure of the effectiveness of the PADS subsystem as an attitude estimator.

To be effective as a three-axis attitude estimator, the SST must be sensitive to attitude motions about each of its three axes. A single PADS tracker fails in this respect due to its extremely small field-of-view, and thus a complete PADS subsystem must employ two such trackers, with optical boresights separated by more than 30 deg or so. Since the laboratory test involved only a single tracker, the system prediction of attitude about the x_2 axis will be ignored, and performance measured solely upon its success in pointing the x_2 axis. In essence, the system will thus be treated as a two-axis estimator.

This two-axis estimator employs a three-axis gyro package, whose gyro input axes (x, y, z) are illustrated by Figure 8-2 and satisfy

$$\begin{bmatrix} x \\ y \\ z \end{bmatrix} = \begin{bmatrix} -.707 & -.707 & 0 \\ .707 & -.707 & 0 \\ 0 & 0 & 1 \end{bmatrix} \begin{bmatrix} x_1 \\ x_2 \\ x_3 \end{bmatrix} \qquad (8\text{-}8)$$

Unfortunately, the gyro whose input axis is z (or x_3) is much poorer in performance than the other two, and thus causes very pessimistic predictions of laboratory attitude about the x_3 axis. In fact, such results can be termed Worst Case. Best Case results would be obtained if the z gyro were aligned, instead, along the x_2 axis, whose attitude is not effectively estimated anyway. Thus two types of performance results will be presented in Section 9. Worst case results will deal with the actual laboratory gyro configuration given by Equation (8-8), and best case results will simply transform the actual gyro outputs to the values that they would have experienced had the z gyro been aligned along x_2. The only assumption made in this process is that the gyro errors are invarient to rotation, an assumption that is not really germane to the evaluation of the PADS.

8.1.3 The Star Catalog

The PADS estimation algorithm has been previously described in Section 3.2. Key to its operation is its usage of fixed star locations as

attitude benchmarks in an inertial reference frame. In analogy, the location of comparable stars in the inertial set (z_1, z_2, z_3) must be established. This effectively then becomes the estimator's star catalog.

Figure 8-2 illustrates the means whereby a star line of sight is formed using the star simulator and air bearing table mirror. A fixed separate light source for each of three stars is housed in the star simulator. The light emanating from the j^{th} such source is defined by

$$\bar{u}_s^{\,j} = \sum_{i=1}^{3} u_{si}^{j}\, \bar{x}_i \tag{8-9}$$

where the u_{si}^{j} are time invariant. The table mirror normal, on the other hand is defined by

$$\bar{n} = \sin\theta(t)\, \bar{x}_1 + \cos\theta(t)\, \bar{x}_2 \tag{8-10}$$

The input star line-of-sight to the SST is then given by

$$\bar{u}^{j} = \sum_{i=1}^{3} u_i^{\,j}\, \bar{x}_i = \bar{u}_s^{\,j} - 2\,\bar{n}\,(\bar{n} \cdot \bar{u}_s^{\,j}) \tag{8-11}$$

The inertial coordinates of this star at time t, namely the benchmark attitude reference used by PADS, are then given by the three direction cosines

$$a_i^{\,j} = \bar{u}^{j} \cdot \bar{z}_i \quad i = 1, 2, 3 \tag{8-12}$$

where clearly

$$\begin{bmatrix} a_1^{\,j} \\ a_2^{\,j} \\ a_3^{\,j} \end{bmatrix} = A_{xz}^{-1} \begin{bmatrix} u_1^{\,j} \\ u_2^{\,j} \\ u_3^{\,j} \end{bmatrix} \tag{8-13}$$

The method whereby PADS causes $\hat{A}_{xz}$ to converge toward A_{xz} is then basically dependent upon adjusting the attitude estimate until its estimate of the $u_i^{\,j}$, say $\hat{u}_i^{\,j}$, coincides with the $u_i^{\,j}$ as obtained by measurement. Clearly

$$\begin{bmatrix} \hat{u}_1^{\,j} \\ \hat{u}_2^{\,j} \\ \hat{u}_3^{\,j} \end{bmatrix} = \hat{A}_{xz} \begin{bmatrix} a_1^{\,j} \\ a_2^{\,j} \\ a_3^{\,j} \end{bmatrix} \tag{8-14}$$

As mentioned before, errors in providing exact truth model earth rate or latitude data will influence A_{xz}, but not the PADS performance measure $\hat{A}_{xz}\, A_{xz}^{-1}$. This is because the same error effect will appear in $\hat{A}_{xz}$ due to the fact that the inertial star direction cosines, $a_i^{\,j}$, are directly influenced by A_{xz} through Equation (8-13). Likewise, the apparent drift rates of the three gyros will shift slightly should inexact values of ω_e or latitude be used. A similar comment can be made should the gyros not precisely satisfy the transformation of Equation (8-8). In neither event is the performance measure of PADS degraded.

8.2 GIMBAL SYSTEM TEST

In parallel to the system test employing a body fixed tracker, the purpose of the gimbaled system test is to establish the performance of the gimbaled star tracker (SST) and the gyro assembly when combined with a suitable data reduction algorithm as an attitude estimation subsystem. This subsystem will be used to estimate the attitude of the laboratory relative to an inertial set of coordinates. As before, the true attitude of this earth-fixed laboratory is essentially known as a function of time, providing a direct means of evaluating system performance.

8.2.1 True Laboratory Attitude

The laboratory configuration of the PADS subsystem is illustrated in Figure 8-3. The laboratory fixed axes are defined as in Section 8.1; a right-handed, orthogonal, coordinate set for which x_3 is taken to point opposite the gravity vector, and x_1 is selected such that it experiences no component of the earth's angular velocity, $\bar{\omega}_e$, i.e., $\bar{\omega}_e \cdot \bar{x}_i = 0$. The term "laboratory attitude" will be taken to mean the orientation of the axes (x_1, x_2, x_3) relative to an inertial set (z_1, z_2, z_3). This latter set of axes will be taken to be identical to axes (x_1, x_2, x_3) at the start of any particular subsystem test run. The laboratory attitude at any subsequent time is then given by Equations (8-1) to (8-5).

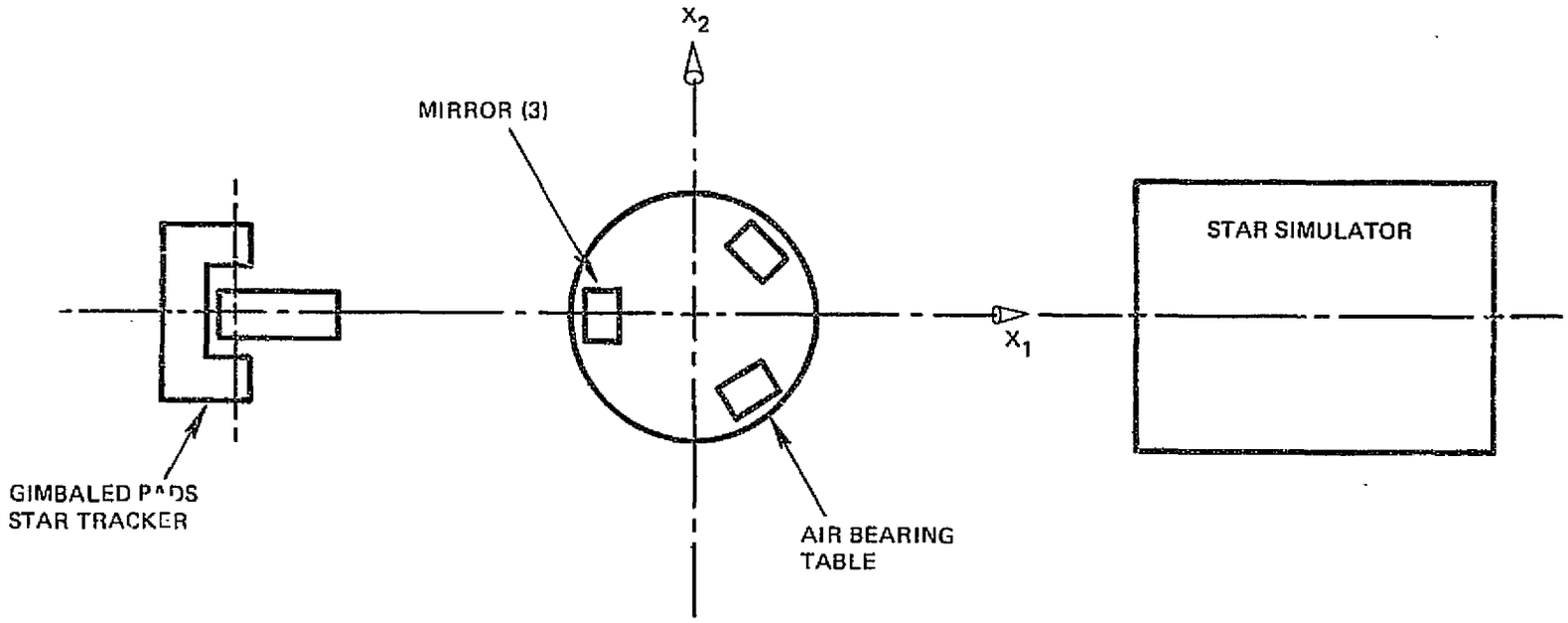

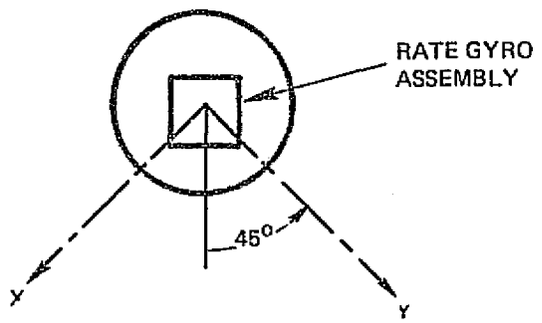

Figure 8-3. Gimballed PADS Laboratory Setup

8.2.2 Gimbal PADS Estimate of the Laboratory Attitude

The PADS subsystem must estimate the laboratory attitude without being privy to latitude and a priori earth rate information.

Consequently, the actual orientation of (x_1, x_2, x_3) relative to (z_1, z_2, z_3) cannot be established by the PADS subsystem, as this information can only be obtained through knowledge of ω_e, latitude, and time, t. Thus PADS can only provide estimates of the x_i, say $\hat{x}_i$, by effective use of the GST and IRU data. The PADS output is then an estimated laboratory attitude matrix, $\hat{A}_{xz}(t)$, defined by Equation (8-6), with Equation (8-7) again providing a measure of the system's effectiveness.

Unlike the body fixed tracker, the gimbal star tracker provides attitude estimates about all three axes (rather than two axes). However, since the gimbal motion between the two outer laboratory "stars" is only about 38 deg, the anticipated accuracy about the x_1 axis is less than that about either x_1 or x_3. Thus the results will be presented in two ways: as a full three-axis estimator, and as a two-axis estimator which ignores errors about x_1. This latter figure of merit will provide a more direct comparison to the results obtained for the body fixed tracker. Also, since three-axis estimates are the primary goal of this test, there is no great advantage in any particular alignment of the IRU. Thus, the actual laboratory orientation of this unit given by Equation (8-8) will be assumed throughout the test runs.

8.2.3 The Star Catalog

The gimbal PADS estimation algorithm has been previously described in Section 3.2. Key to its operation is its usage of fixed star locations as attitude benchmarks in an inertial reference frame. In analogy, the location of comparable stars in the inertial set (z_1, z_2, z_3) must be established. This effectively then becomes the estimator's star catolog.

Figure 8-4 illustrates the means whereby a star line of sight is formed using the star simulator and air bearing table mirror. A single fixed light source emanates from the star simulator and is deflected downward along $-x_3$ by a fixed mirror mounted above the air bearing table. A tilted mirror mounted to the table top then deflects this light beam (when the table top is in position) toward the tracker. By utilizing the table mirrors, three such stars of differing elevation angles can be simulated. This establishes the direction cosines (in lab axes) of each star, and its equivalent inertial coordinates are then given, as before, by Equations (8-12) and (8-13). Likewise, estimates of the star direction cosines (in estimated lab axes) are given by Equation (8-14), and the comments following this equation apply here as well.

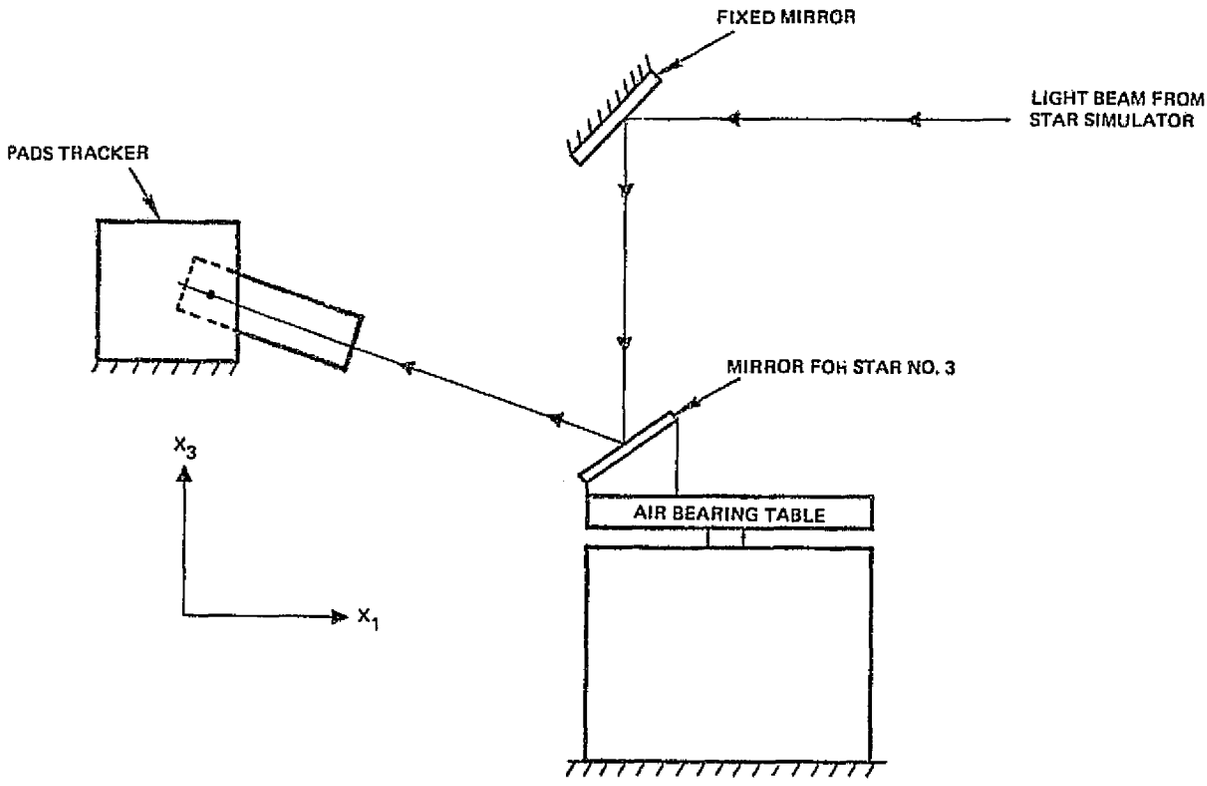

Figure 8-4. Establishing Star Line of Sights for the Gimballed Star Tracker

9. STRAPDOWN SYSTEM TEST

This section describes the strapdown system test which was run from 1 October 1975 to 10 October 1975. The orbit scenario on which the test was based is described along with comments regarding initial alignment of the PADS axes. All of the four test runs which were conducted during the ten day test period are analyzed using several performance measures. Two of the test runs were selected for detailed analysis to illustrate the effect of individual error sources on the PADS attitude estimates. A parametric analysis is made to evaluate the effect of star update interval on the PADS accuracy. Lastly, a summary of the PADS accuracy is presented.

9.1 TEST DESCRIPTION

The spacecraft configuration postulated for the PADS system test is that of a three-axis stabilized , earth-pointed satellite in geosynchronous orbit. An experiment on board, a telescope, for example, requires precise information regarding the inertial attitude of its sensitive axis or axes. The PADS is used to provide this information.

A calibration of the PADS star tracker boresight axis relative to the experiment axes is allowed once every ten days. Following a calibration the experiment may require the PADS attitude information for any length of time, for any number of times, during the next ten days.

By way of configuring a practical laboratory test, four test runs, nearly evenly spaced in time, were conducted during a ten day test period. Each run was four hours in duration. During each run a star update was made every 20 minutes. This corresponded to a star being available every 5^{o} in right ascension. Three different star declinations were used. All stars were 8 M_{v} G0 (6000^{o}K).

The test period was limited to ten days by the scope of the PADS contract and not by any limitation in the stability of the star tracker. Four runs during the ten day period were adequate to measure the day-to-day stability of the tracker, while a four hour run was sufficient to ensure steady-state behavior for star updates up to 60 minutes apart. The minimum star update time of 20 minutes was determined by the gyro performance (see Section 4.1). Three star declinations were considered adequate to exercise

the tracker field of view linearity accuracy. Making all stars 8 M_v presented a worst case situation in terms of tracker noise and simplified test equipment design.

9.2 INITIAL ALIGNMENT/CALIBRATION

The PADS reference axes were defined physically by the optical cube on the strapdown star tracker. The PADS experienced a fixed input rate, i.e., earth rate, during a test run. Consequently, no effort was made to precisely determine the gyro input axes orientations relative to the cube since an axis misalignment would be indistinguishable from a fixed drift rate error.

The original intent was to align the tracker electro-optical boresight to the normal to the front face of the optical cube, and to adjust the field of view alignment about the boresight so that a zero vertical output resulted for a star on the negative x axis at the edge of the field of view. The field of view nonlinearities were to be calibrated from a component test performed in a separate facility from that of the system test.

Unfortunately, the calibration data from the star tracker component test contained unacceptable errors which were not recognized at the time the data was collected. These errors are described in Volume I, Section 7. As a result it was necessary to recalibrate the field of view using the three stars in the system test configuration. This recalibration took place immediately prior to the ten day system test. The overall result was the invalidation of the independent measure of the accuracy of the field of view linearity. The recalibration did not affect the basis for the alignment, albeit indirect, of the boresight to the optical cube, namely, the ground-rule that the boresight would be calibrated relative to the experiment axes every ten days.

9.3 SYSTEM TEST RESULTS

The following system test results were obtained using the computer performance evaluation programs described in Section 8.

9.3.1 Pass Parameters

Four test runs, each of approximately four hours in duration, were conducted between 1 October 1975 and 10 October 1975. This time tagged sensor data was then utilized by the Estimation Algorithm to predict both laboratory attitude and the gyro drift rates. Aside from the time tagged sensor data, the algorithm requires a number of additional inputs dealing primarily with statistical quantities that describe initial uncertainties in both attitude and gyro drift rates, as well as uncertainties in both gyro and star tracker noise parameters. In general, the attitude estimation performance of the Estimation Algorithm is dependent upon the values of assumed noise. Also of significance is the degree of filtering applied to the output of the tracker, as longer time constants tend to reduce the impact of tracker noise. Taking such parameter variations into account, a total of 31 attitude estimation computer passes were made based upon the four test runs previously mentioned. Table 9-1 lists the conditions for these 31 passes.

9.3.2 Performance Measures

The effectiveness of the Attitude Estimator is based primarily upon three things:

1) The degree to which the estimator accurately predicts the attitude of the x_2 axis. If θ_1 and θ_3 represent the estimation errors about, respectively, the x_1 and x_3 axis, then the boresight (x_2) attitude error is given by

$$\theta = \sqrt{\theta_1^2 + \theta_3^2} \qquad (9\text{-}1)$$

2) The degree to which the boresight attitude error, which of course is unknown operationally, is reflected by the estimator's error covariance prediction. Observation of the latter should give a strong indication of the actual errors. Comparing the attitude error covariance prediction with the SST measurement residuals will check estimator "consistency."

3) The speed with which the attitude estimates converge from sizeable initial estimation errors (e.g., 100 sec) to errors that are close to "steady state."

Table 9-1. Conditions and Parameters of Computer Passes

Pass Conditions

Run Duration - 14800 sec

Star Update Interval - 20 min/40 min/60 min*

Each star utilized 3 times at 55 sec intervals

Gyro Orientation - Best Case/Worst Case*

Initial Conditions

Initial Attitude Estimate - 100 $\widehat{\text{sec}}$ error about x_1 and x_3

Initial Attitude Uncertainty (1σ) 100 sec about x_1 and x_3; 10 $\widehat{\text{sec}}$ about x_2

Initial gyro drift rate uncertainty - .02 $\widehat{\text{sec}}$/sec

Sensor Parameters

Gyro:

Estimated Drift Rates. Gyro x -.833 $\widehat{\text{sec}}$/sec
y -.478 $\widehat{\text{sec}}$/sec
z -1.055 $\widehat{\text{sec}}$/sec

Gyro noise σ_v - .02 to .08 $\widehat{\text{sec}}/(\text{sec})^{1/2}$*

Gyro noise σ_u - $.2 \times 10^{-4}$ to $.6 \times 10^{-4}$ sec/$(\widehat{\text{sec}})^{3/2}$*

Gyro noise σ_e - 0.1 $\widehat{\text{sec}}$

Star Tracker:

Calibration coefficients as specified in Volume I, Section 7

Time constant (both axes) - .0466 sec

Digital output filter (both axes) - 0 to 3 sec*

Output noise (both axes) - 1.5 to 3 $\widehat{\text{sec}}$*

*Specified in Test Run

Items 1) and 2) are time variant and require additional qualification if clear figures of merit are to be adopted. Figure 9-1 illustrates a typical sequence of θ values, a value being plotted every 300 sec and also at times just prior and just subsequent to an attitude update.

For the merit figures, the discrete points are connected by straight lines. The mean pointing error and its standard deviation are then computed as

$$\mu_\theta = \frac{1}{(t_N - t_n)} \sum_{i=n}^{N} \frac{1}{2} (\check{\theta}_{i+1} + \tilde{\theta}_i) (t_{i+1} - t_i) \tag{9-2}$$

$$\sigma_\theta = \left\{ \frac{1}{(t_N - t_n)} \sum_{i=n}^{N} \frac{1}{3} \left[\tilde{\theta}^2_{i+1} + \check{\theta}_i^{\,2} + \tilde{\theta}_{i+1} \check{\theta}_i \right] (t_{i+1} - t_i) \right\}^{1/2} \tag{9-3}$$

where

$$\tilde{\theta}_i = \theta\ (t_i +) \tag{9-4}$$

$$\check{\theta}_i = \theta\ (t_i -) \tag{9-5}$$

with t_N and t_n representing, respectively, the final time and time at which the effect of initial estimates have disappeared. A similar appraoch is also used in computing the mean and standard deviation, $\mu_{\hat{\theta}}$ and $\sigma_{\hat{\theta}}$, of the attitude estimator's guess (based upon its covariance matrix) as to the reliability of its output. Lastly, μ_y and σ_y have similar interpretations regarding the measurement residual. The six merit figures will be used extensively in what follows.

9.3.3 Detailed Analyses of Passes No. 8 and No. 9

Pass No. 8 met the general conditions of Table 9-1 under the additional specifications:

Tracker noise (1σ) - 1.5 $\widehat{\text{sec}}$
Tracker output filter time constant - 3 sec
Tracker update interval - 20 min
Gyro noise σ_v - .04 $\widehat{\text{sec}}/\text{sec}^{1/2}$ in x and y; .08 in z
σ_u - $.6 \times 10^{-4}$ $\widehat{\text{sec}}/\text{sec}^{3/2}$ in x, y, and z
Gyro Orientation - Best Case

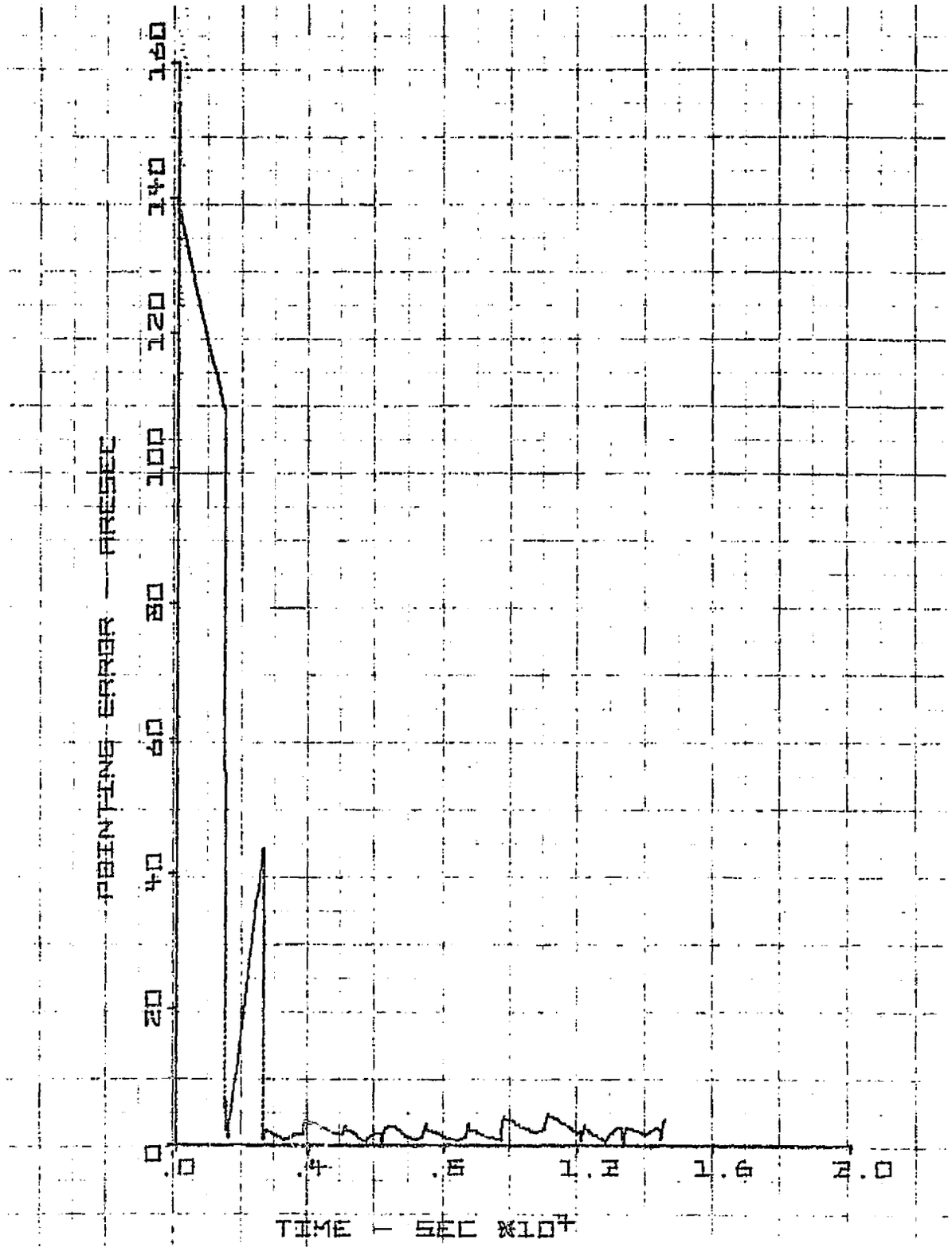

Figure 9-1. Pass No. 8

Figure 9-1 illustrates the convergence of the estimation error, θ, of the boresight (x_2) attitude. A dramatic correction in attitude estimation error is made after just one star sighting. However, the gyro drift rates retain sufficient error to cause considerable divergence until the second star sighting at about 2600 sec. The drift rates are then also corrected and fairly benign performance (which we shall call "steady state") occurs thereafter. Figure 9-2 illustrates, on a larger scale, the estimation error from about 5000 sec onward. An average pointing error of about 2 $\widehat{\text{sec}}$ is experienced, which corresponds to a 1.4 $\widehat{\text{sec}}$ error per axis.

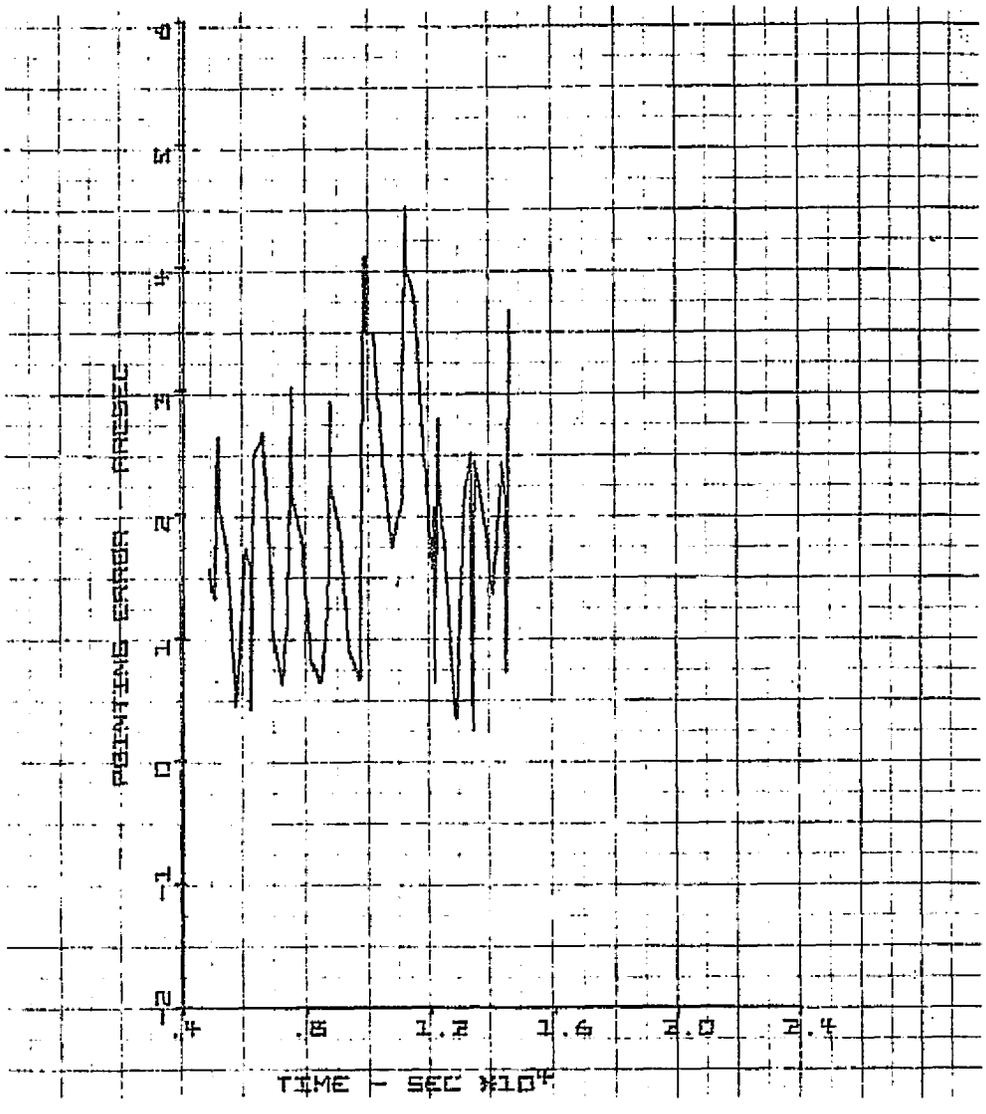

Figure 9-2. Pass No. 8 Expanded

When the conditions of Pass No. 8 are altered by assuming a worst case rather than best case gyro orientation, the convergence of θ remains about the same. Steady state behavior is considerably degraded, however, as Pass No. 9 in Figure 9-3 clearly shows. In this case an average pointing error of about 3.2 $\widehat{sec}$ is evident, corresponding to 2.3 $\widehat{sec}$ per axis. This is clearly a result of the z gyro drift rate fluctuation, which now directly influences the pointing estimate. If $\omega_g(t)$ represents a gyro's rate output, then Figure 9-4 presents the rate variation $\omega_g'(t)$ for each of the three gyros over the run duration [0,T] where T = 14800 sec. $\omega_g'(t)$ is of the form

$$\omega_g'(t) = \omega_g(t) - \bar{\omega}_g(t) \qquad (9\text{-}6)$$

where

$\bar{\omega}_g(t)$ is the average drift rate for the run duration.

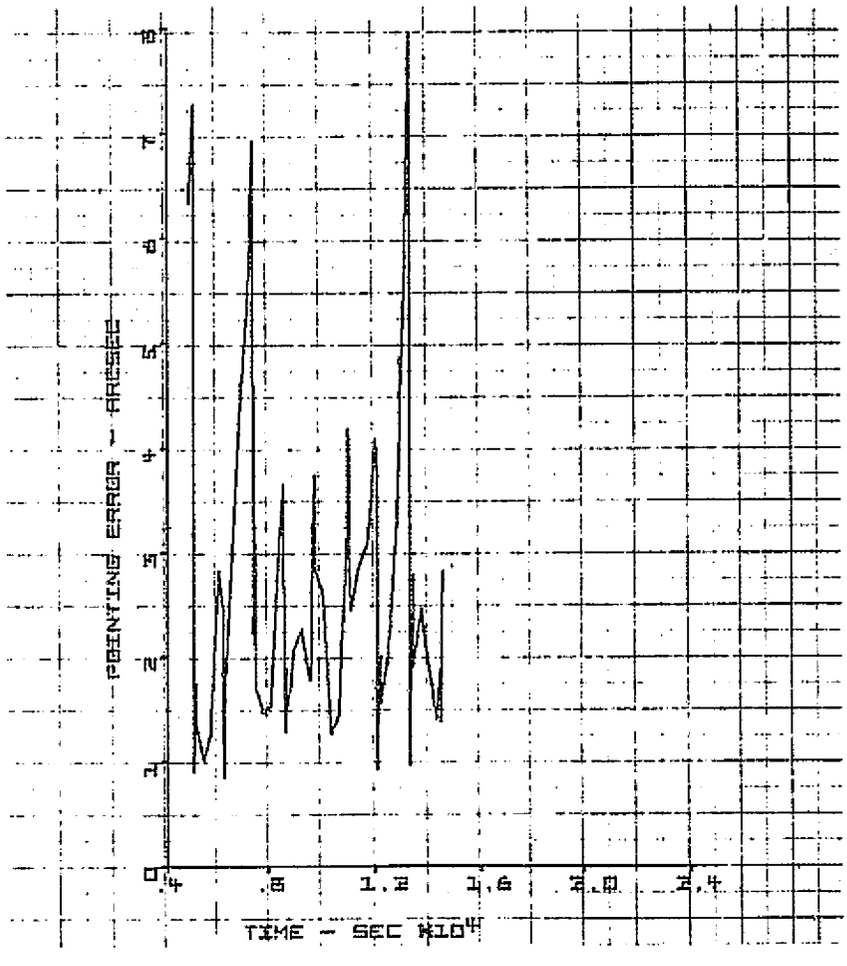

Figure 9-3. Pass No. 9

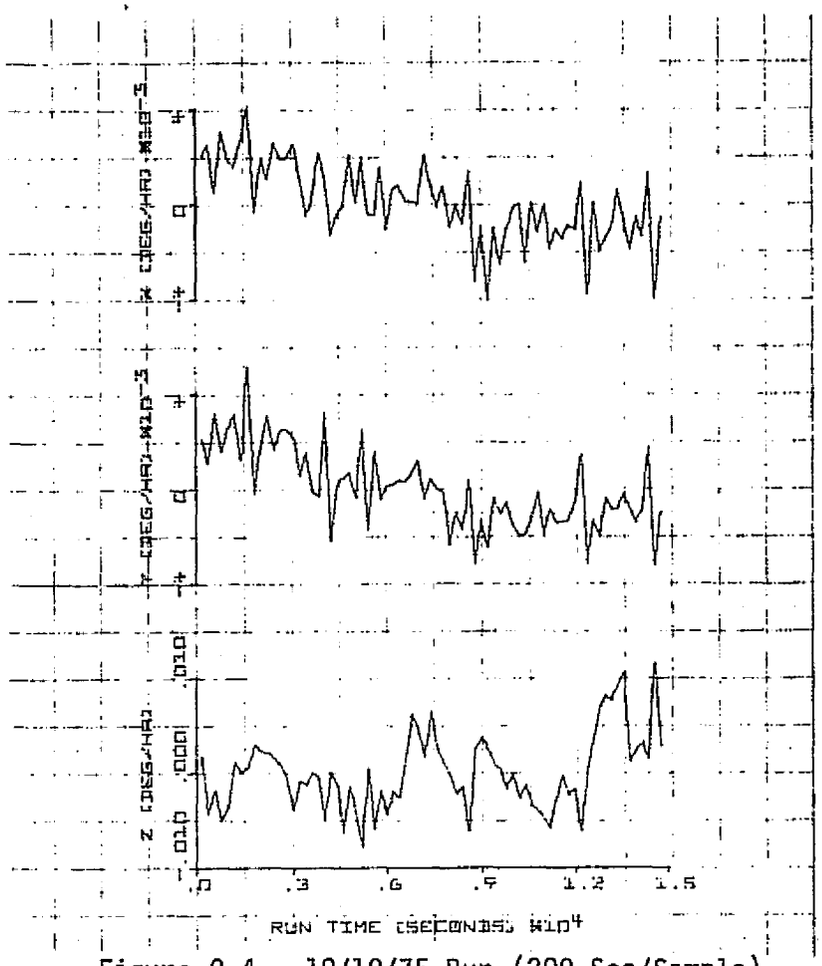

Figure 9-4. 10/10/75 Run (200 Sec/Sample)

It is clear that the z gyro experiences severe drift rate changes at both 6100 sec and 12730 sec. This is consistent with the results of Figure 9-3, which shows the start of a severe fluctuation in the attitude estimate at about these times.

9.3.4 PADS Steady State Parametric Test Results

The results for all four test runs are shown in Figure 9-5, in terms of the previously defined performance criteria μ_θ, σ_θ, $\mu_{\hat{\theta}}$, $\sigma_{\hat{\theta}}$, μ_y, σ_y. In general, the system results are excellent, with the following conclusions evident

- All of the 13 passes indicate an RMS pointing error, σ_θ, of better than 4 $\widehat{\text{sec}}$. In fact, the average σ_θ over the 13 passes is 3.08 $\widehat{\text{sec}}$ for a per axis error of 2.2 sec.
- The performance of the best gyro orientation exceeds that for the worst orientation by 0.4 - 1.0 $\widehat{\text{sec}}$.
- Filtering the tracker output through a 3 sec time constant filter shows significant improvement over a 1 sec filter.

- Gyro data base B results in filter covariance estimates that agree more closely than A with actual performance.
- Passes 5, 6, 8, 17, 23, and 18 show excellent agreement between actual performance, filter predicted performance, and the actual measurement residuals.
- Passes 1, 7, 28, and 16 indicate poorer agreement. In Passes 1 and 7 too high a value of tracker noise was assumed. Pass 28 is plagued by tracker bias, which was independently established. Pass 16 is also somewhat plagued by such bias, but in addition is optimistic in its assessment of gyro noise.

Figure 9-5. PADS Test Results – 20 Min. Updates

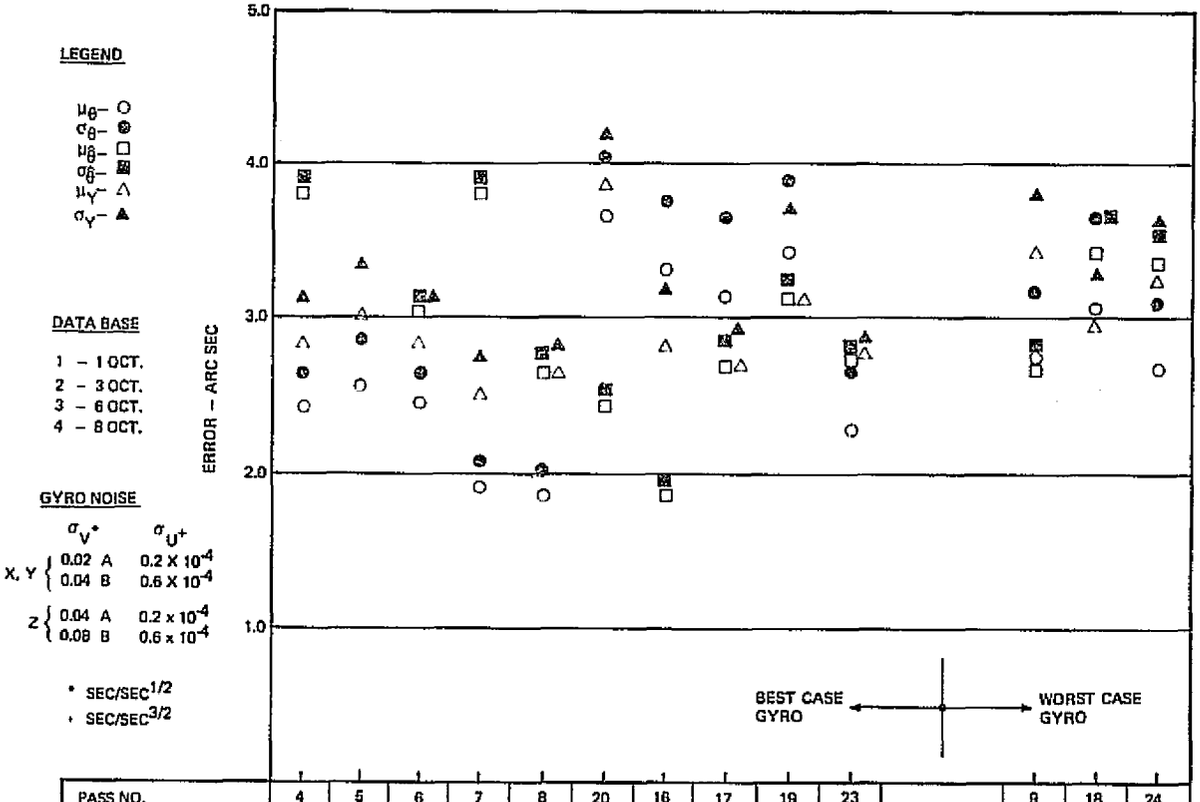

PASS NO.	4	5	6	7	8	20	16	17	19	23		9	18	24
FILTER TIME CONST.	1	1	1	3	3	3	3	3	1	3		3	3	3
GYRO NOISE	B	A	B	B	B	B	A	B	B	B		B	B	B
SST NOISE	3	3	2	3	1.5	1.5	1.5	1.5	2	1.5		1.5	2	1.5
TEST RUN	1	1	1	1	1	2	3	3	3	4		1	3	4

Figure 9-5. PADS Test Results – 20 Minute Updates

Additional examples of steady state performance are shown in Figure 9-6 to 9-10.

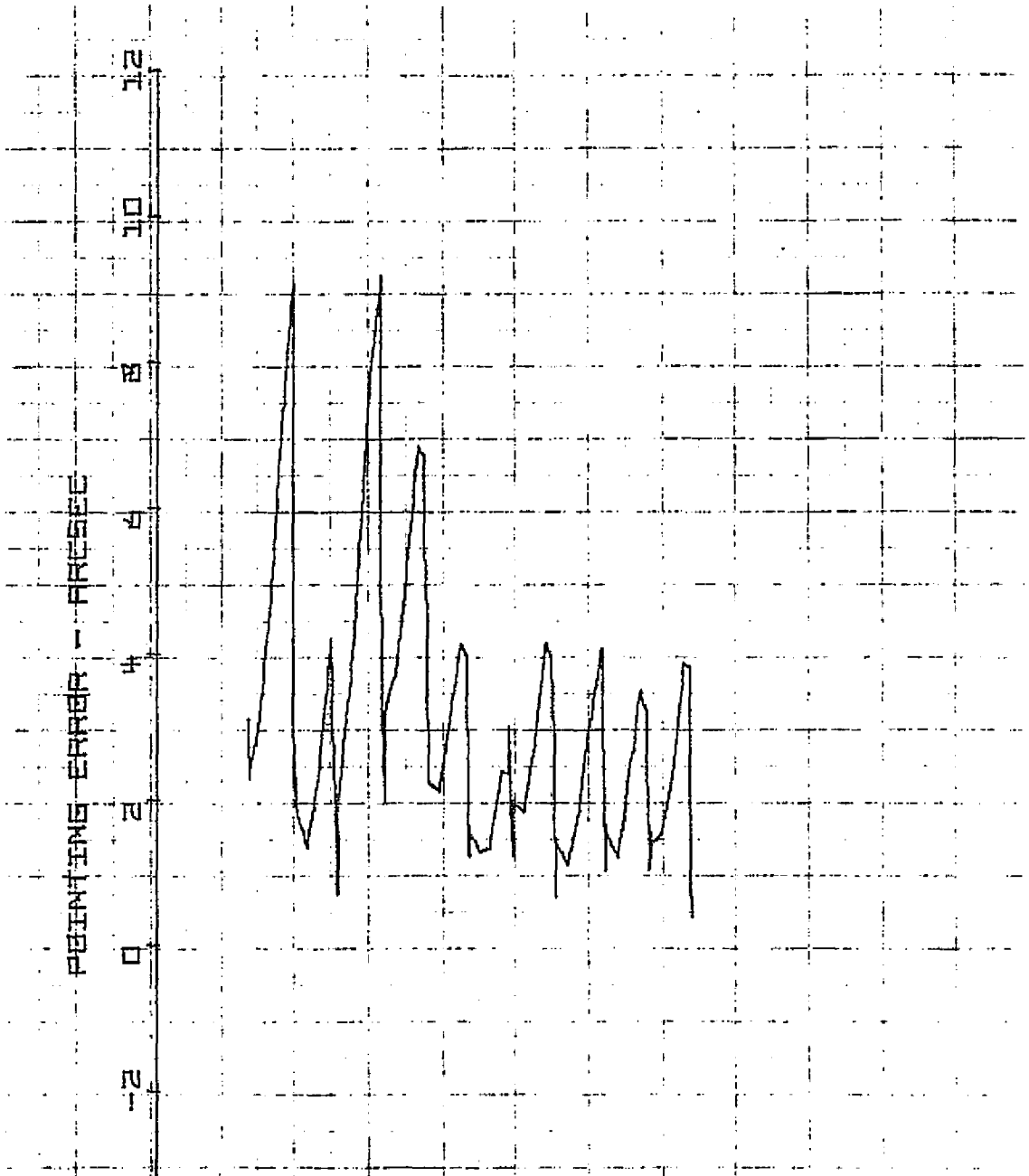

Figure 9-6. Pass No. 17

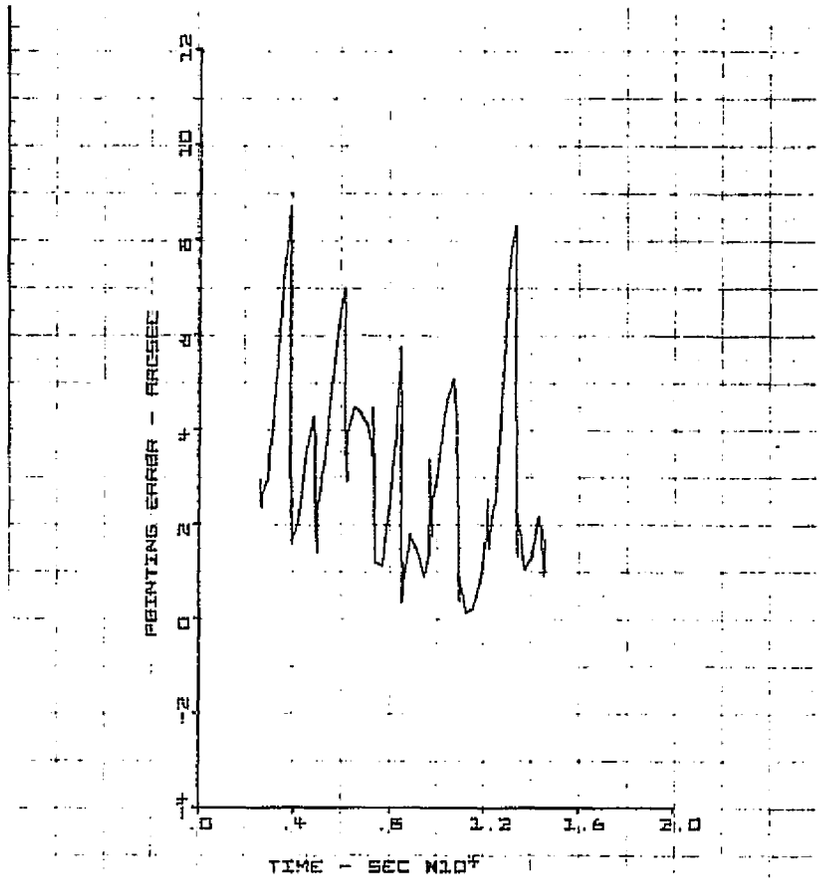

Figure 9-7. Pass No. 18

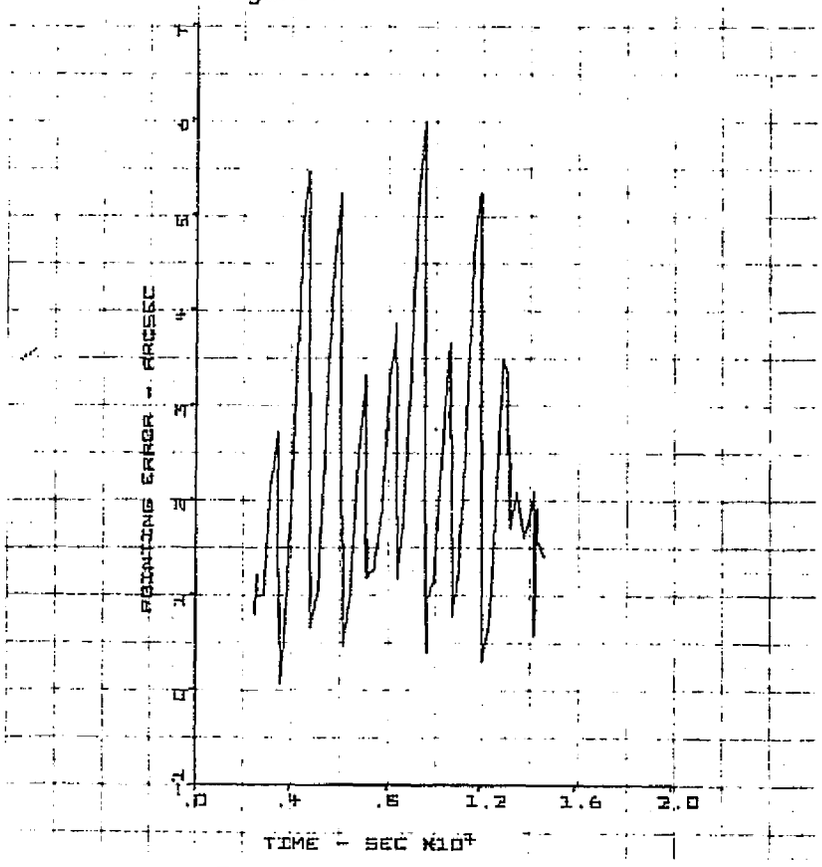

Figure 9-8. Pass No. 28

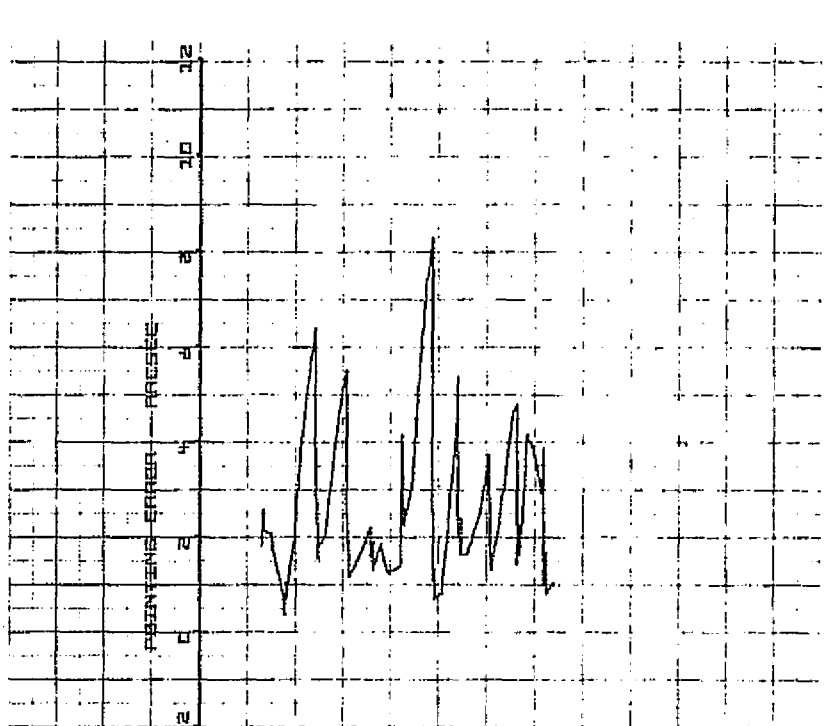

Figure 9-9. Pass No. 24

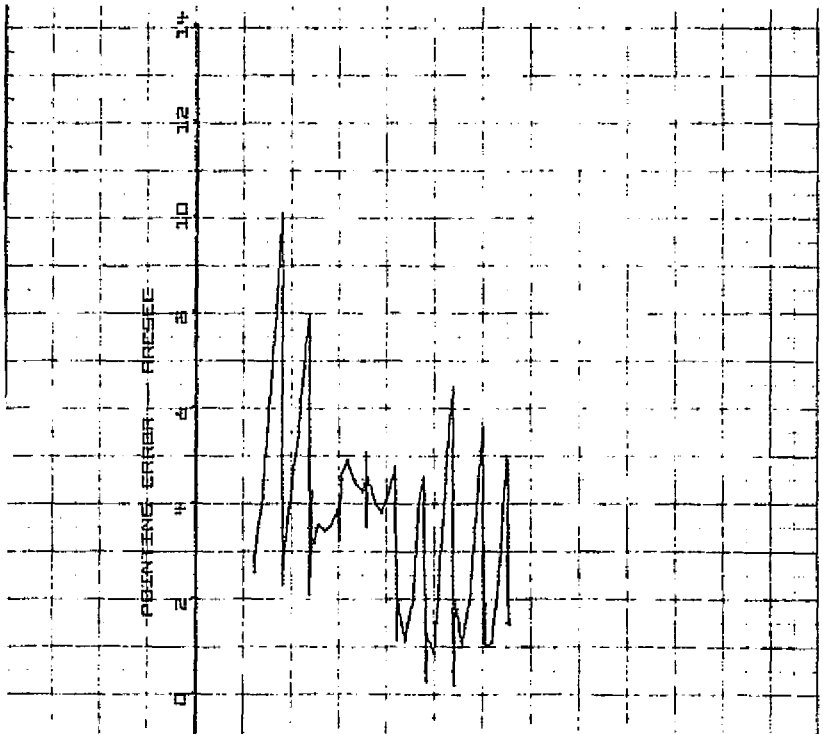

Figure 9-10. Pass No. 28

Figure 9-11 presents results similar to Figure 9-5, but for systems with less frequent star updates. In each case rapid initial convergence was obtained as the first two star updates were taken 20 min apart. Thereafter, the update interval was as noted, either 40 or 60 minutes. As anticipated, these results are somewhat poorer. Specifically:

- The peak 40 min RMS error, σ_θ, is 7 sec, with the average σ_θ given by 4.32 sec, or 3.06 sec, per axis.
- The peak 60 min RMS error, σ_θ is 13 sec, with the average σ_θ given by 7.72 sec, or 5.46 sec, per axis.
- The influence of worst case over best case gyro alignment is now much more severe, as much longer time intervals exist between gyro bias corrections.
- Test runs 1 and 4 indicate much better results than either 2 or 3. Test run 2 is particularly poor due to the aforementioned tracker bias.
- Passes 11, 13, 25, 26, 14, and 15 show fairly good agreement between actual and filter predicted performance.
- Passes 10, 30, and 31 show quite a difference between actual and predicted results. The latter two are influenced by the unobservable tracker bias, whereas Pass 10 uses gyro noise parameters which are pessimistic for these longer filtering durations. In practice, when the update intervals vary, the gyro noise parameters must assume some compromise values.

Figures 9-12 to 9-15 illustrate typical steady state behavior patterns for these increased update duration runs.

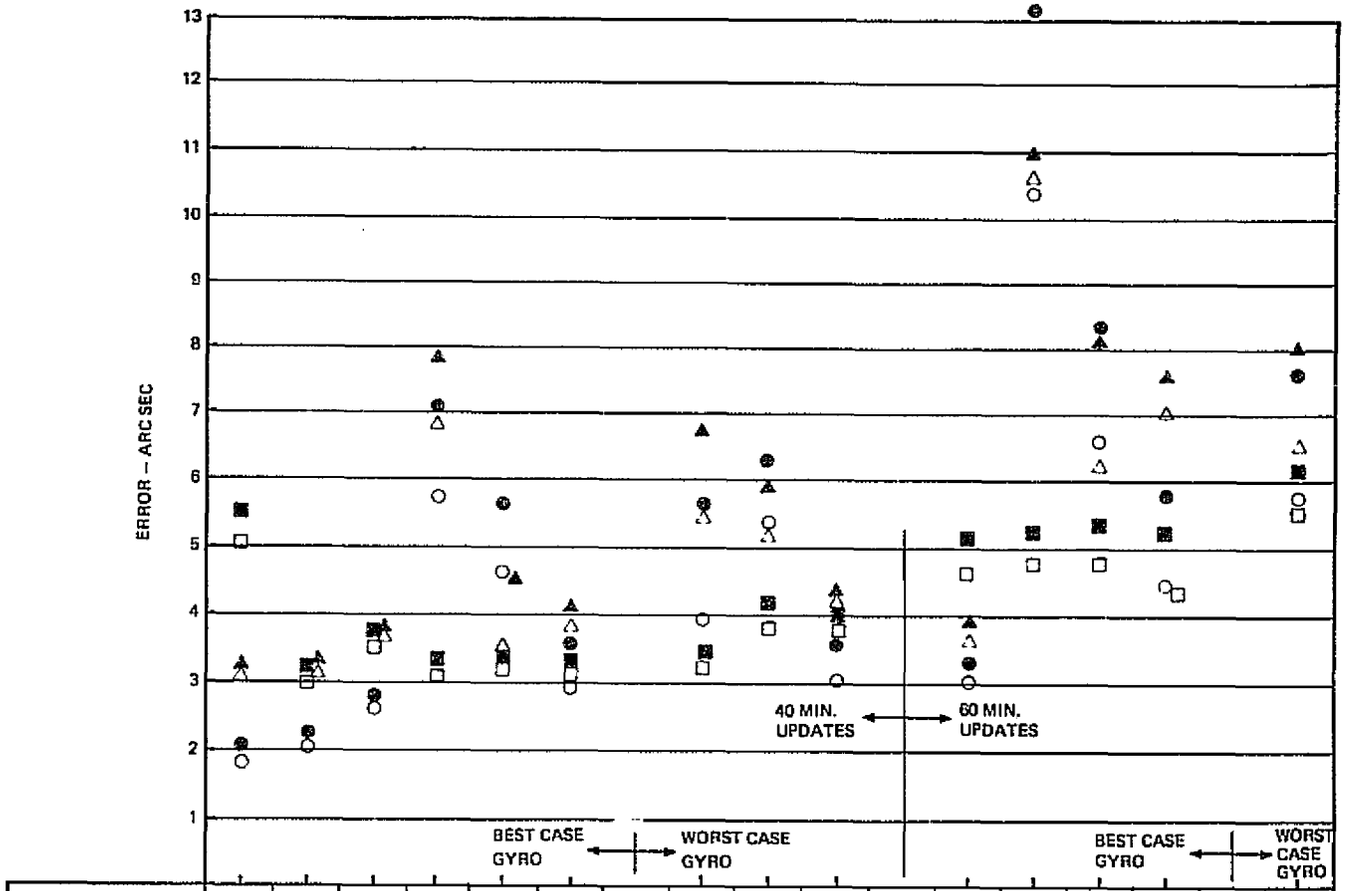

PASS NO.	10	11	13	30	20	25		12	21	26		14	31	22	27		15
FILTER TIME CONST.	3	3	1	3	3	3		3	3	3		3	3	3	3		3
GYRO NOISE	B	A	A	A	A	A		A	A	A		A	A	A	A		A
SST NOISE	1.5	1.5	2	1.5	1.5	1.5		1.5	2	2		1.5	1.5	1.5	2.5		2
DATA BASE	1	1	1	2	3			1	3	4		1	2	3	4		1

Figure 9-11. PADS Test Results - 40 and 60 Minute Updates.

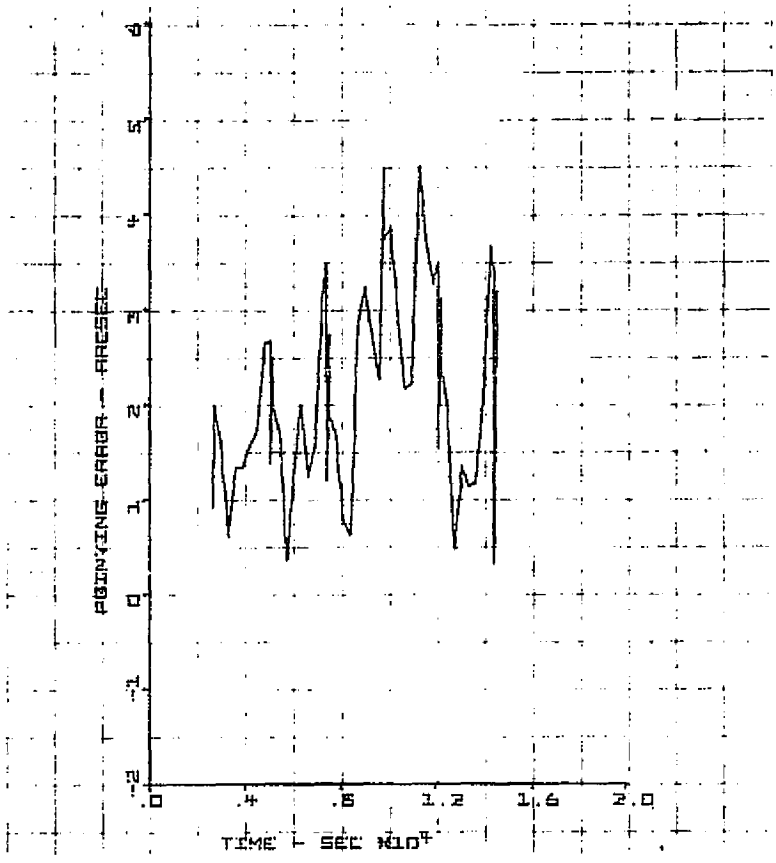

Figure 9-12. Pass No. 11

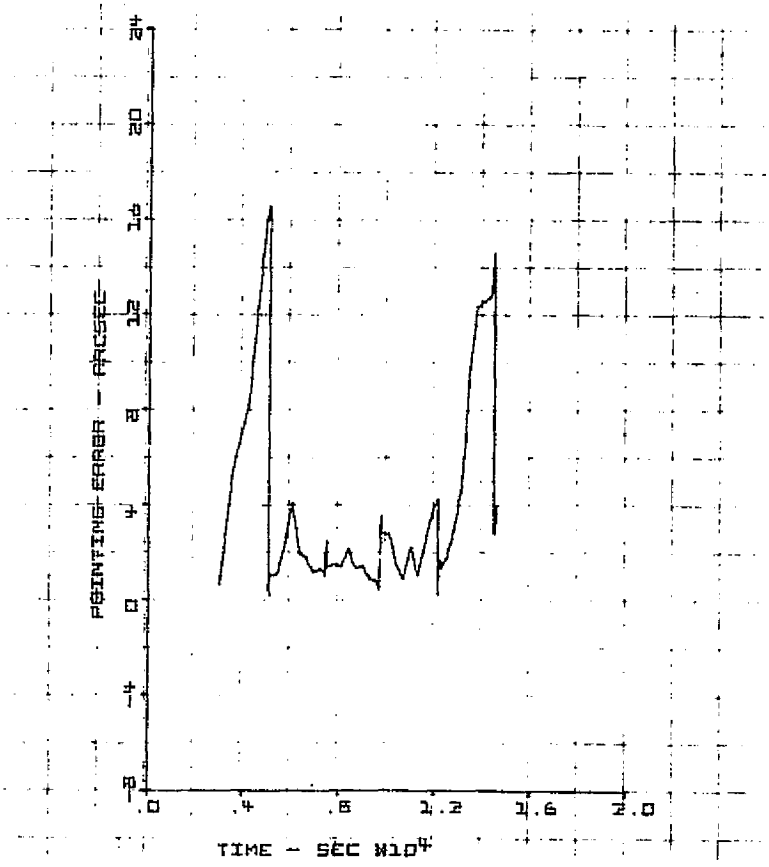

Figure 9-13. Pass No. 12

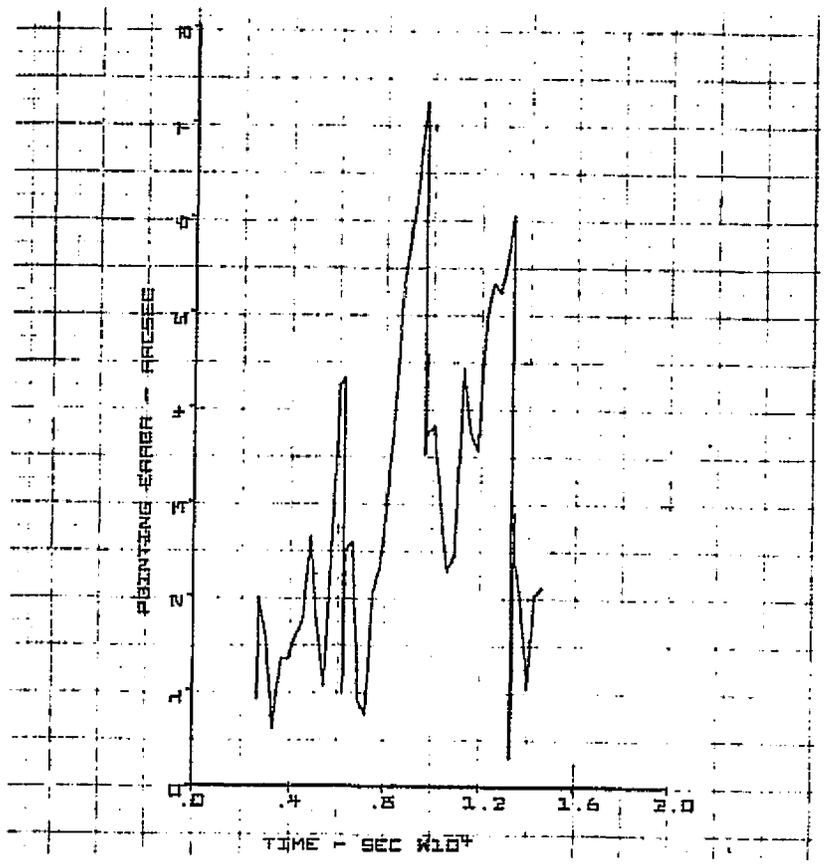

Figure 9-14. Pass No. 14

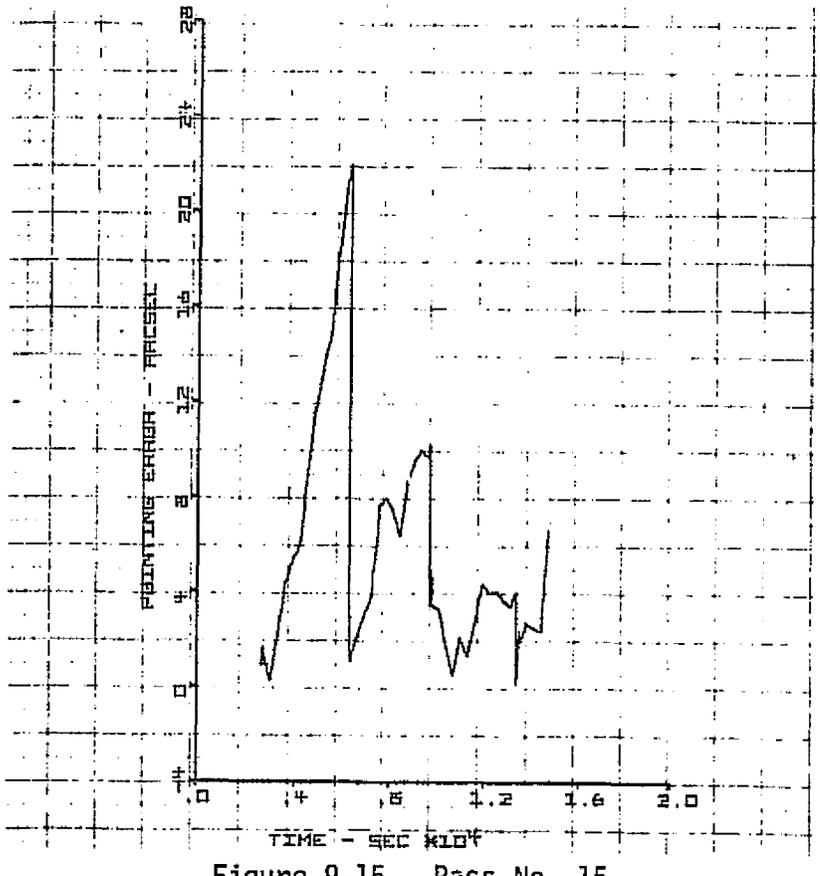

Figure 9-15. Pass No. 15

9.3.5 PADS Accuracy

The criteria for the accuracy of the PADS is the RMS of the difference between the PADS estimate of the inertial attitude of its reference axes and the true attitude of these axes as indicated by:

1) Laboratory instrumentation

2) A priori knowledge of earth rate and the inertial attitude of the laboratory at the start of a test run.

This criteria is designated σ_θ in Figures 9-5 and 9-11.

The parameters selected for the nominal PADS algorithm for the 20 minute updates are:

1) Filter time constant: 3 sec

2) Gyro noise (x and y gyros): $\sigma_v = 0.04$ arc sec/sec$^{1/2}$
$\sigma_u = 0.6 \times 10^{-4}$ arc sec/sec$^{3/2}$

3) SST noise: 1.5 arc sec.

The parameters for the 40 and 60 minute updates were the same except for the gyro noise sigmas which were reduced by 1/2 and 1/3 for σ_v and σ_u, respectively. The passes representative of the values in Figure 9-5 are numbers 8, 28, 17, and 23, or test runs 1, 2, 3, and 4, respectively. In Figure 9-11 the 40 minute update representative passes are numbers 11, 30, 20, and 25, or test runs 1, 2, 3, and 4, respectively. The 60 minute update representative passes are numbers 14, 31, 22, and 27, or test runs 1, 2, 3, and 4, respectively.

Table 9-2 summarizes the value of σ_θ for the nominal PADS algorithm with the best gyro orientation. Values from all four test runs are available for each update interval. The rms of the values for the four runs is the PADS two-axis error for a given update interval. This rms, divided by $\sqrt{2}$, is the PADS single-axis error.

The PADS design goal is 3.6 arc seconds (1σ) per axis for 20 minute star updates. The measured error of 2.3 arc seconds is well within the design goal.

Table 9-2. PADS RMS Error

Test Run	20 Minute Updates	40 Minute Updates	60 Minute Updates
1	2.0	2.3	3.3
2	4.0	7.1	13.5
3	3.7	5.7	8.3
4	2.7	3.6	5.8
rms (2-axis)	3.2	5.0	8.6
rms (1-axis)	2.3 arc sec	3.6 arc sec	6.1 arc sec

The increase in measured error with increased update interval is also indicated in Table 9-2. Although the increase appears well behaved, examination of the individual test runs reveals a large variation in values, indicating caution should be applied in generalizing these results.

10. GIMBAL SYSTEM TEST

This section describes the gimbal system test which was run from 6 February 1976 to 16 February 1976. The orbit scenario on which the test was based is described along with comments regarding initial alignment of the PADS axes. All of the four test runs which were conducted during the ten day test period are analyzed using several performance measures. Two of the test runs were selected for detailed analysis to illustrate the effect of individual error sources on the PADS attitude estimates. A parametric analysis is made to evaluate the effect of star update interval on the PADS accuracy. Lastly, a summary of the PADS accuracy is presented.

10.1 TEST DESCRIPTION

The spacecraft configuration postulated for the PADS system test is that of a three-axis stabilized, earth-pointed satellite in geosynchronous orbit. An experiment on board, a telescope, for example, requires precise information regarding the inertial attitude of its sensitive axis or axes. The PADS is used to provide this information.

A calibration of the PADS gimbal star tracker axes relative to the experiment axes is allowed once every ten days. Following a calibration the experiment may require the PADS attitude information for any length of time, for any number of times, during the next ten days.

By way of configuring a practical laboratory test, four test runs, nearly evenly spaced in time, were conducted during a ten day test period. The first three runs were four hours in duration, the last was five hours. During each run a star update was made every 20 minutes. This corresponded to a star being available every 5^{o} in right ascension. Three different star declinations over approximately a 40^{o} span were used. All stars were 3.5 M_{V} G0 (6000^{o}K).

The test period was limited to ten days by the scope of the PADS contract and not by an assumed limitation in the stability of the star tracker. Four runs during the ten day period were adequate to measure the day-to-day stability of the tracker. Four hour runs were sufficient to ensure steady-state behavior for star updates up to 40 minutes apart. The five hour run was made to provide data for star updates 60 minutes apart. The minimum

star update time of 20 minutes was determined by the gyro performance (see Section 4.1). The maximum star separation in declination of 40^{o} was considered adequate to provide three-axis information with the single star tracker. Making all stars 3.5 M_v presented a worst case situation in terms of tracker noise and simplified test equipment design.

10.2 INITIAL ALIGNMENT

Alignment of the gimbal star tracker presented considerably more complexity than that encountered with the strapdown star tracker. In the case of either tracker the objective was to determine the alignment of the electro-optical (EO) axes relative to optical surfaces on the tracker base. For the strapdown tracker the only critical EO axis was the EO boresight, i.e., that position in the field of view at which a star produced zero electronic output in two axes. Using the parallel beam star stimulus approach, it was an easy task to align the boresight normal to the front face of the optical cube within an arc second. However, the gimbal tracker has two EO axis which are critical: 1) the EO boresight zero position, defined as that position of a star wherein both optical sensor field of view outputs are zero, and the gimbal angle readout is also zero, and 2) the normal to that plane for which the angle of incidence between the plane and the EO boresight remains constant for all gimbal angles. The second axis is the effective gimbal axis, purposely defined in an electro-optical rather than a mechanical sense. The obliqueness of the definition is necessary to account for a possible nonorthogonality between the EO boresight and the effective gimbal axis. Determining the orientation of both these EO axes relative to the three mirrors attached to the base of the tracker to within one arc second entailed a significant activity.

The first step undertaken was identification of the effective gimbal axis. Ideally this should have been accomplished electro-optically, but no practical technique was available to do this with an arc second accuracy. Consequently, recourse was made to an optical-mechanical technique. This consisted of mounting a mirror on the end of the gimbal axis with its surface normal to the gimbal axis. Normality was observed by autocollimating off the mirror with a theodolite and adjusting the mirror orientation until no deflection was observed with the theodolite as the gimbal and attached

mirror were rotated. Performance of this task led to two observations: 1) the gimbal axis sagged such that the mirror on the end of the axis tilted 34 arc seconds from the effective gimbal axis, and 2) the rate of change of this sag was 4 arc seconds for a gimbal motion of 30^{o}. Both of these effects are shown in Figure 10-1. The sag was determined by leveling the gimbal axis using the optical cube on the optical sensor. With the theodolite viewing the back face (negative boresight axis) of the cube, the tracker base fixture was shimmed until no horizontal deflection was measured as the gimbal was turned through 20^{o}. In view of the method used, the accuracy of the measured sag is probably no better than 5 arc seconds. On the other hand, the relative change of the sag with gimbal angle was measured directly with the theodolite, and its accuracy is better than one arc second.

The gimbal axis sag theoretically should have no significant effect on the performance of the star tracker. However, it did invalidate accurate determination of the vertical alignment of the effective gimbal axis through optical-mechanical techniques. In view of the symmetry of the curve in Figure 10-1 about the ordinate, and the mechanical symmetry of the plus and minus 30^{o} gimbal positions relative to the gravity vector, it was assumed that the horizontal component of the mirror normal was within an arc second of the effective gimbal axis.

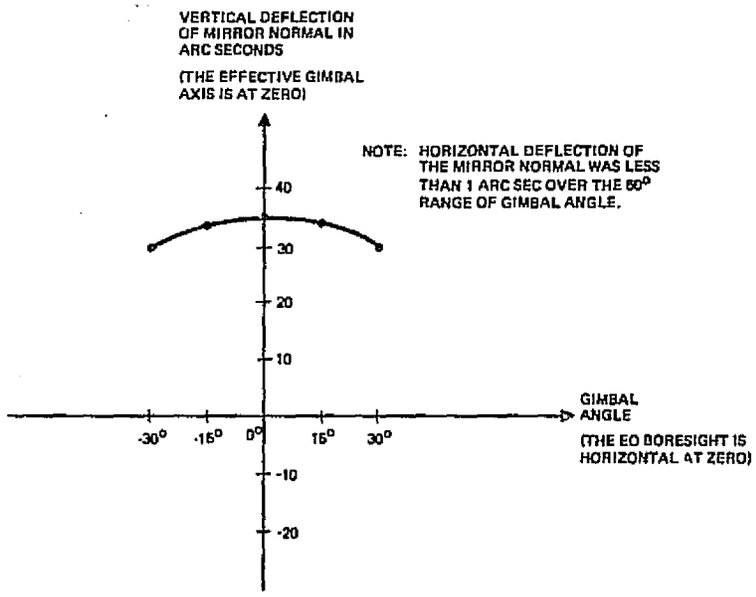

Figure 10-1. Gimbal Axis Sag

The next step in the alignment procedure was to adjust the EO boresight normal to the effective gimbal axis. This was accomplished using two theodolites as shown in Figure 10-2. The tracker base was turned until the sum of the two angles indicated in the figure was 90^{o}. The optical sensor was then rotated in the gimbal until zero horizontal output was obtained. Using both theodolites in this manner gave an accuracy of one or two arc seconds for this step.

With the EO boresight now aligned normal to the effective gimbal axis, the relative orientations of the three reference mirrors were determined through the use of the parallel beam star stimulus technique. With the tracker in place the stars were adjusted via the rotating mirror assembly so that the three star beams were normal to the three tracker reference mirrors. Immediately following this the star tracker was removed and the theodolite inserted in its place. The theodolite was then used to measure the relative orientations of the star beams. The results were previously shown in Figure 4-21 and are repeated in Table 10-1.

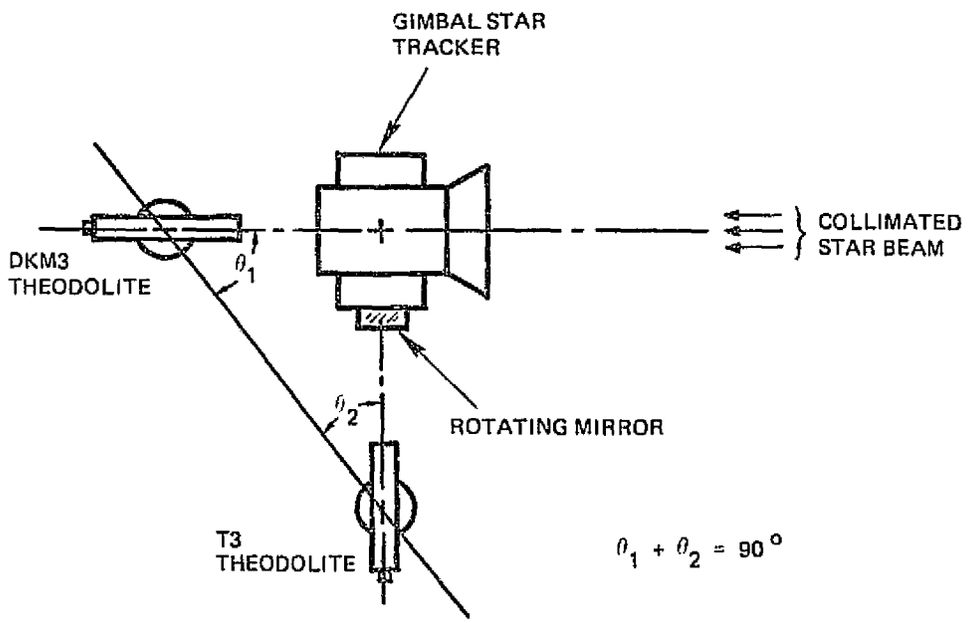

Figure 10-2. Alignment of the EO Boresight to the Effective Gimbal Axis

Table 10-1. Relative Reference Mirror Orientations

Mirror No.	Vertical (arc sec)	Horizontal (arc sec)
1	+68380.2	-3.2
2	0.0	0.0
3	-68392.8	-4.8

The last alignment step was to determine the orientation of the three mirror normals relative to the tracker axes. Immediately prior to the system test, with the tracker in place, the orientation of the tracker axes relative to the stars was measured using the tracker outputs, and the orientation of the stars relative to the mirror normals was measured using the parallel beam technique and the automatic autocollimator outputs. Combining the two sets of measurements gave the results shown in Table 10-2. The numbers in parenthesis are the relative orientations.

Table 10-2. Reference Mirror Positions in Tracker Axes

Mirror No.	Vertical (arc sec)	Horizontal (arc sec)
1	53814.9 (68379.9)	-9.6 (-5.2)
2	-14564.8 (0.0)	-4.4 (0.0)
3	-82958.0 (-68393.2)	-8.2 (-3.9)

Comparison between Tables 10-1 and 10-2 leads to two observations. First, if the coordinates in Table 10-1 are rotated 4.5 degrees as shown in Figure 10-3, then the agreement between the relative horizontal measurements from the two tables is within 0.5 arc second. This indicates that: 1) the boresight axis was accurately aligned normal to the effective gimbal axis, and 2) the angles between the mirror normals and plane orthogonal to the gimbal axis are accurately known. Secondly, the agreement between the relative vertical measurements indicates that the gimbal readout, at least for the three positions measured, does not have to be calibrated.

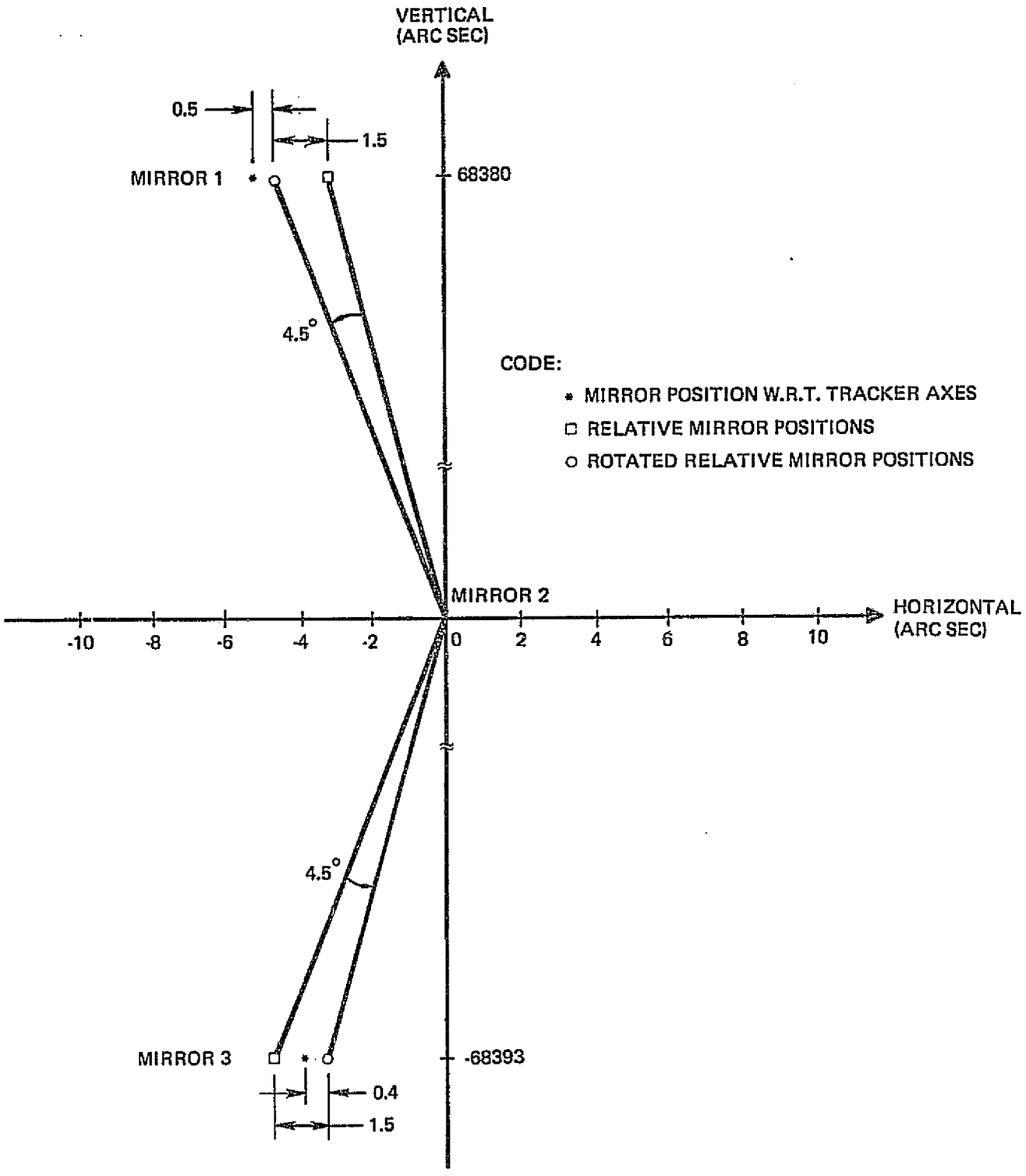

Figure 10-3. Relative Locations of Mirror Normals

10.3 SYSTEM TEST RESULTS

The following system test results were obtained using the computer performance evaluation programs described in Section 8.

10.3.1 Pass Parameters

Four test runs, each of approximately four hours in duration, were conducted between 6 February 1976 and 16 February 1976. The time-tagged sensor data was then utilized by the Estimation Algorithm to predict both laboratory attitude and the gyro drift rates. As before, the algorithm requires a number of additional inputs dealing primarily with statistical quantities that describe initial uncertainties in both attitude and gyro drift rates, as well as uncertainties in both gyro and GST noise parameters. These parameters are listed in Table 10-3. Varying these parameters, a total of 31 attitude estimations passes were made based upon the four test runs mentioned above.

10.3.2 Performance Measures

The effectiveness of the Attitude Estimator as a three axis device is based primarily upon three things:

1) The degree to which the estimator accurately predicts the attitude of the laboratory. If θ_1, θ_2, and θ_3 represent the estimation errors about, respectively, the x_1, x_2, and x_3 axes, then the attitude error is defined by

$$\theta = \sqrt{\theta_1^2 + \theta_2^2 + \theta_3^2} \qquad (10\text{-}1)$$

2) The degree to which the laboratory attitude error, which of course is unknown operationally, is reflected by the estimator's error covariance prediction. Observation of the latter should give a strong indication of the actual errors. In practice, the operator will compare the attitude error covariance prediction with the GST measurement residuals in order to check estimator "consistency."

3) The speed with which the attitude estimates converge from sizeable initial estimation errors (e.g., 100 sec), to errors that are close to "steady state."

Items 1) and 2) are time variant and require additional quantification if clear figures of merit are to be adopted. In this regard, the per axis mean pointing error and its standard deviation are computed as described in Section 9.3.2.

Table 10-3. Conditions and Parameters of Computer Passes

Pass Conditions

Run Duration - 14500 to 18370 sec

Star Update Interval - 20 min/40 min/60 min*

Each star utilized once near the azimuth center of the GST field of view

Initial Conditions

Initial Attitude Estimate - 100 $\widehat{\text{sec}}$ error about x_1, x_2, and x_3

Initial Attitude Uncertainty (1σ) 100 sec about x_1, x_2, and x_3

Initial gyro drift rate uncertainty - 0.02 $\widehat{\text{sec}}$/sec

Sensor Parameters

Gyros:

Estimated Drift rates. Gyro x -0.840 $\widehat{\text{sec}}$/sec

y -0.422 $\widehat{\text{sec}}$/sec

z -1.165 $\widehat{\text{sec}}$/sec

Gyro noise $_v$ - 0.02 to 0.08 $\widehat{\text{sec}}/(\text{sec})^{1/2}$*

Gyro noise $_u$ - 0.2×10^{-4} to 0.6×10^{-4} $\widehat{\text{sec}}/(\text{sec})^{3/2}$*

Gyro noise $_e$ - 0.1 $\widehat{\text{sec}}$

Gimbal Tracker:

Time constant (both axes) - 0.0466 sec

Digital Output filter (both axes) - 3 sec

Output noise (both axes) - 1.5 $\widehat{\text{sec}}$

*Specified in Test Run

10.3.3 Detailed Analyses of Passes No. 11 and No. 21

Pass No. 11 corresponds to the general conditions of Table 10-3 and utilizes the PADS data of 9 February, the gyro being updated every 20 minutes by the gimbaled star tracker. Figures 10-4 and 10-5 show, respectively, the corresponding two and three axis convergence of the laboratory attitude estimation errors. A total of 12 star updates are employed, in the order

Star Number: 1,3,3,3,1,3,2,1,3,1,2,3,3 (A)

where, noting Figure 8-4, the tracker input star line-of-sight has a large negative projection on x_3 for star No. 1, a slight positive projection for star No. 2, and a large positive projection for star No. 3. The particular sequence noted above was chosen to insure the differing geometric conditions inherent in sighting different stars for the more demanding convergence conditions associated with 40 and 60 minute updates. Thus when 40 minute update passes are made, the star sequence is

Star Number: 1,3,1,2,3,2,3 (B)

and for 60 minute updates passes

Star Number: 1,3,2,1,3 (C)

The sequence (A) is not optimally beneficial in assuring rapid convergence for 20 minute update passes, as star No. 3 is used 3 successive times. This is the price paid for better results when the updates are less frequent.

For Pass No. 11, the first five updates occur at times 329, 1365, 2649, 3850, and 5044 sec, corresponding to stars 1,3,3,3,1 respectively. As the results of Figures 10-4 and 10-5 indicate, the first two updates (providing 4 pieces of independent azimuth-elevation star data) considerably reduce the initial error, but are not adequate to establish the six unknowns defined by the three attitude and three gyro drift rates. Additional updates by star No. 3 at 2649 and 3850 sec provide only slight improvement as the geometric conditions are not much different than at 1365 sec. Once star No. 1 is again used (at 5044 sec) a dramatic improvement occurs, and the filter can subsequently be considered to be close to its "steady state" operation. The reuse of star No. 1 proved geometrically beneficial as its previous use occurred sufficiently far in the past. This same convergence pattern appeared in all of the 20 minute update passes, regardless of which PADS test run was used.

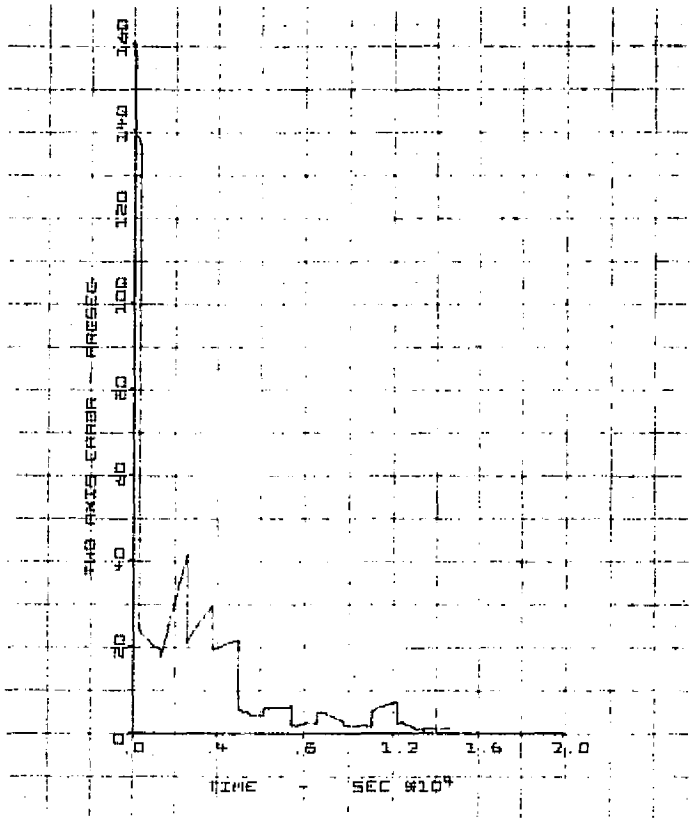

Figure 10-4. Pass No. 11 - Two Axis

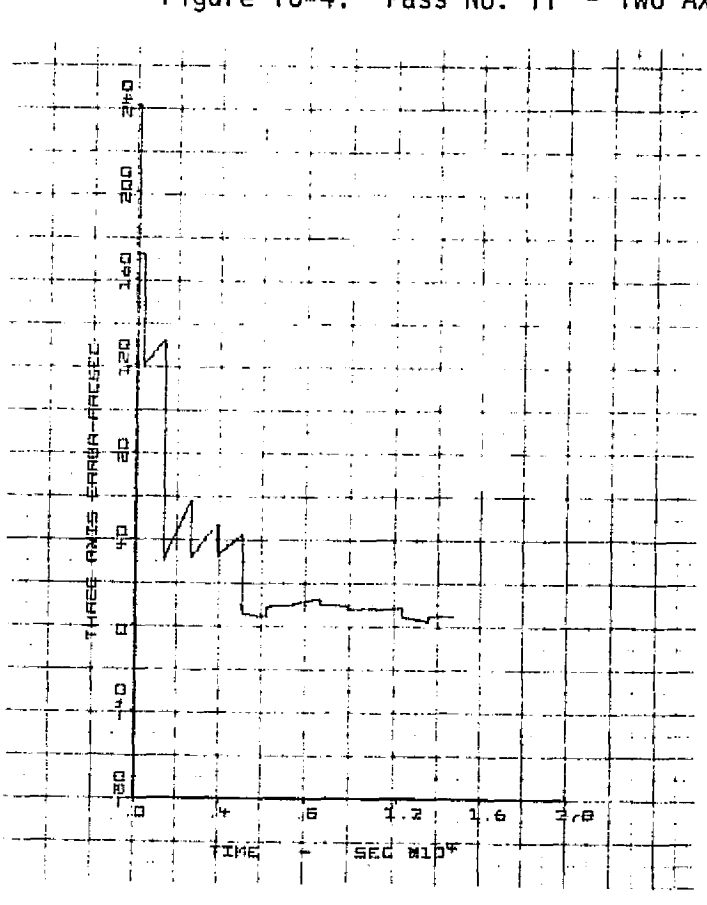

Figure 10-5. Pass No. 11 - Three Axis

Figure 10-6 shows a comparable three-axis run for the test data of 6 February. Convergence behavior is essentially the same as described above, but there appears a dramatic temporary degradation in the attitude estimates at about 8000 sec, long after the filter has supposedly reached "steady state." This is caused by a severe shift in the z gyro drift rate at about the same time, as indicated by the gyro data of Figure 10-7. Of significance is the fact that the filter is only temporarily confused by this event, providing better and better estimates of the new z gyro drift rates as additional star updates appear.

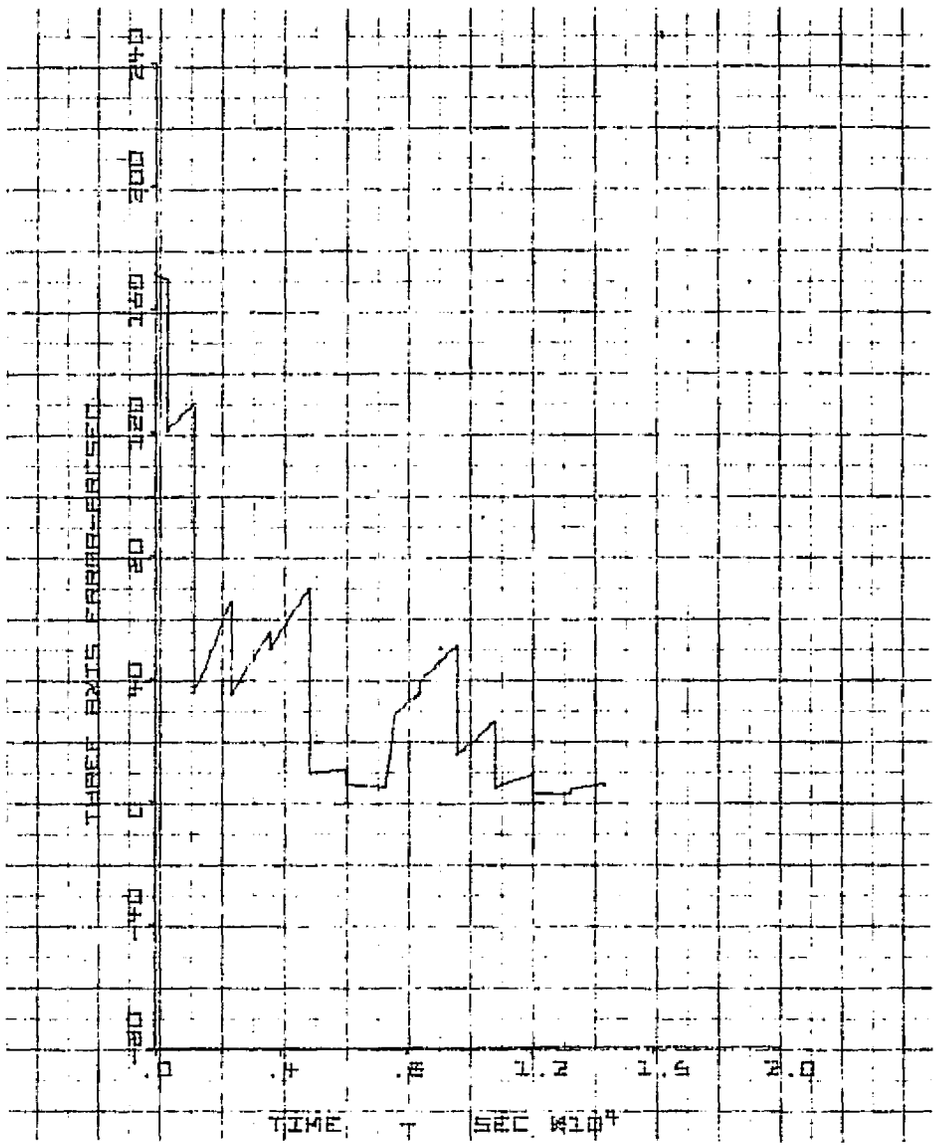

Figure 10-6. Pass No. 21 - Three Axis

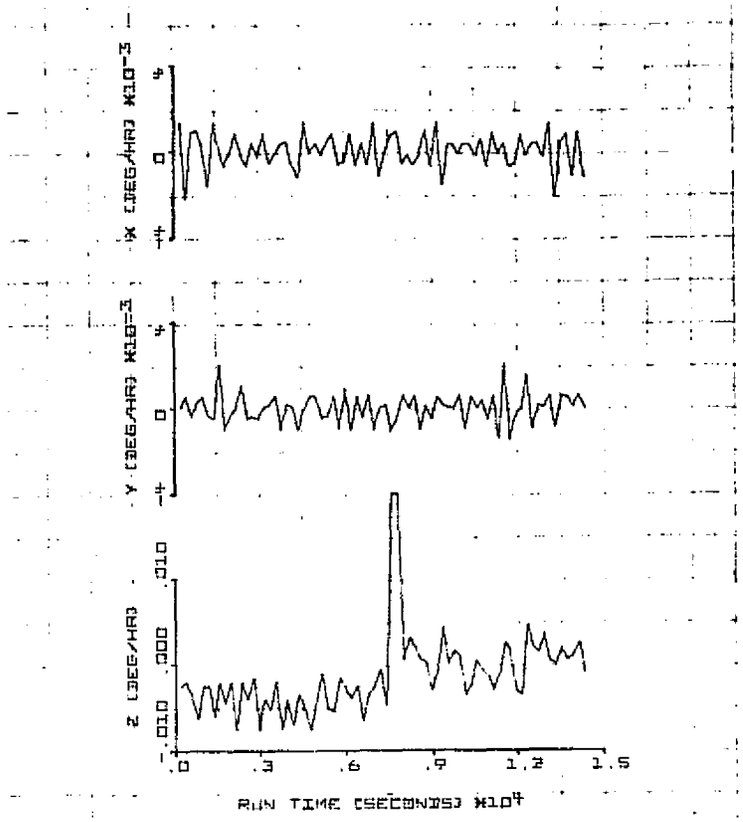

Figure 10-7. 02/06/76 Run (200 Sec/Sample)

10.3.4 PADS Steady State Parametric Test Results

The results for the runs taken on the 9th, 11th, and 16th of February are shown in Figure 10-8, for 20 minute updates. The statistics presented in each case cover the time interval subsequent to the fifth star update to the end of the run. The results of the PADS data taken on 6 February are not included as the severe jump in the z gyro drift rate provides untypically pessimistic answers. The following conclusions are evident from Figure 10-8.

- Passes 11 and 13 provide two-axis estimates between 3 and 4 $\widehat{sec}$ and show good agreement to both the corresponding filter estimates and the measurement residuals.

- Pass 12 indicates poorer results than either 11 or 13. This can be traced to anomalous drift rate behavior of both the x and y gyros as each gyro's drift rate suddenly shifts by 0.0014 deg/hr at one point in the run. The effect is not major, but has sufficient impact to negatively influence a short test run of only 4 hours.

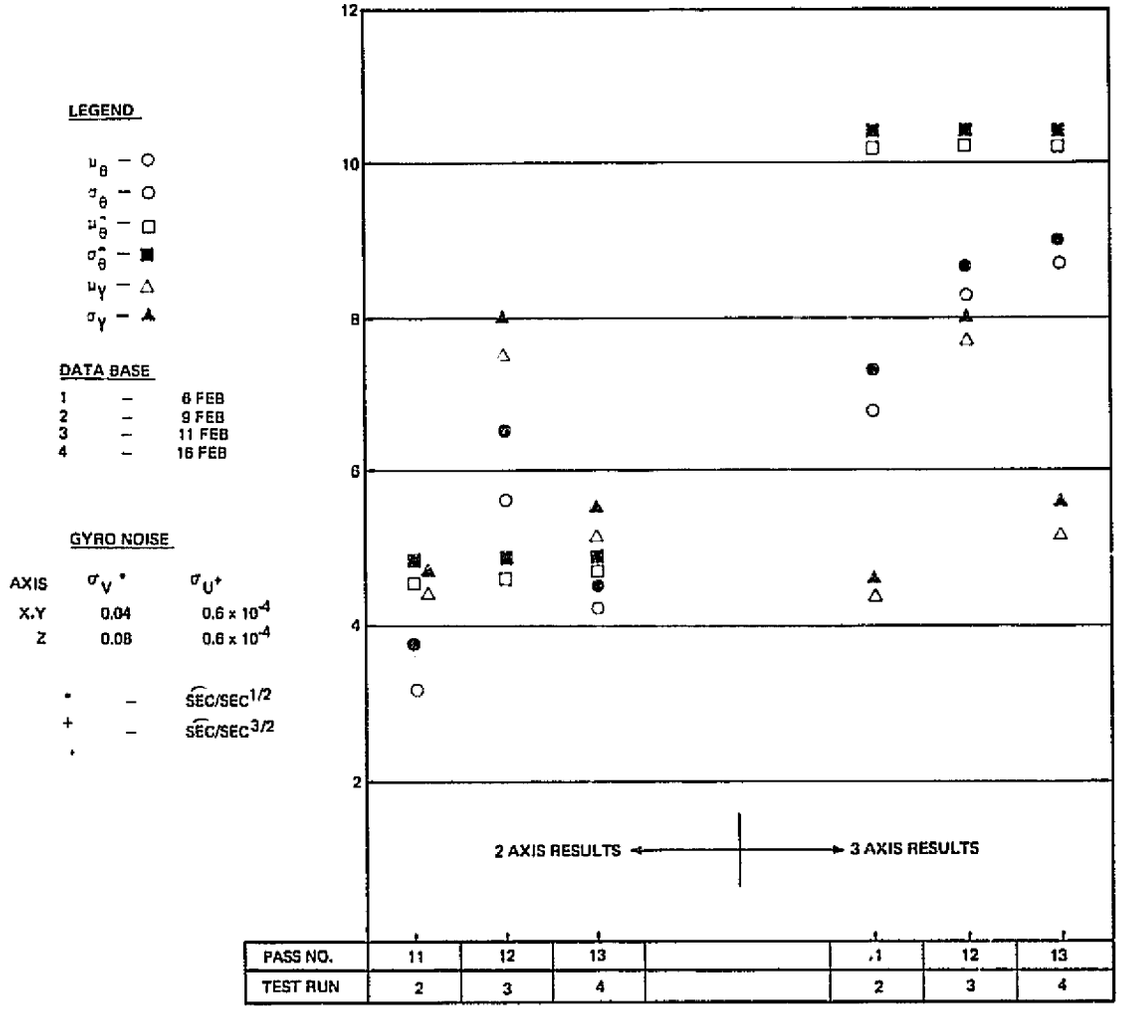

Figure 10-8 Gimbaled PADS Test Results (20 Minute Updates)

Figures 10-9 to 10-12 show typical convergence responses of the 20 minute update results.

Figure 10-13 shows results for 40 and 60 minute update intervals. Only test run 4 is shown for the latter, as this somewhat lengthened run alone allows an adequate number of updates necessary for "steady state" behavior. Even at that only the two axis results of Pass 18 have reached what can be considered final values. Errors about x_2 would have continued to reduce had the run time been longer.

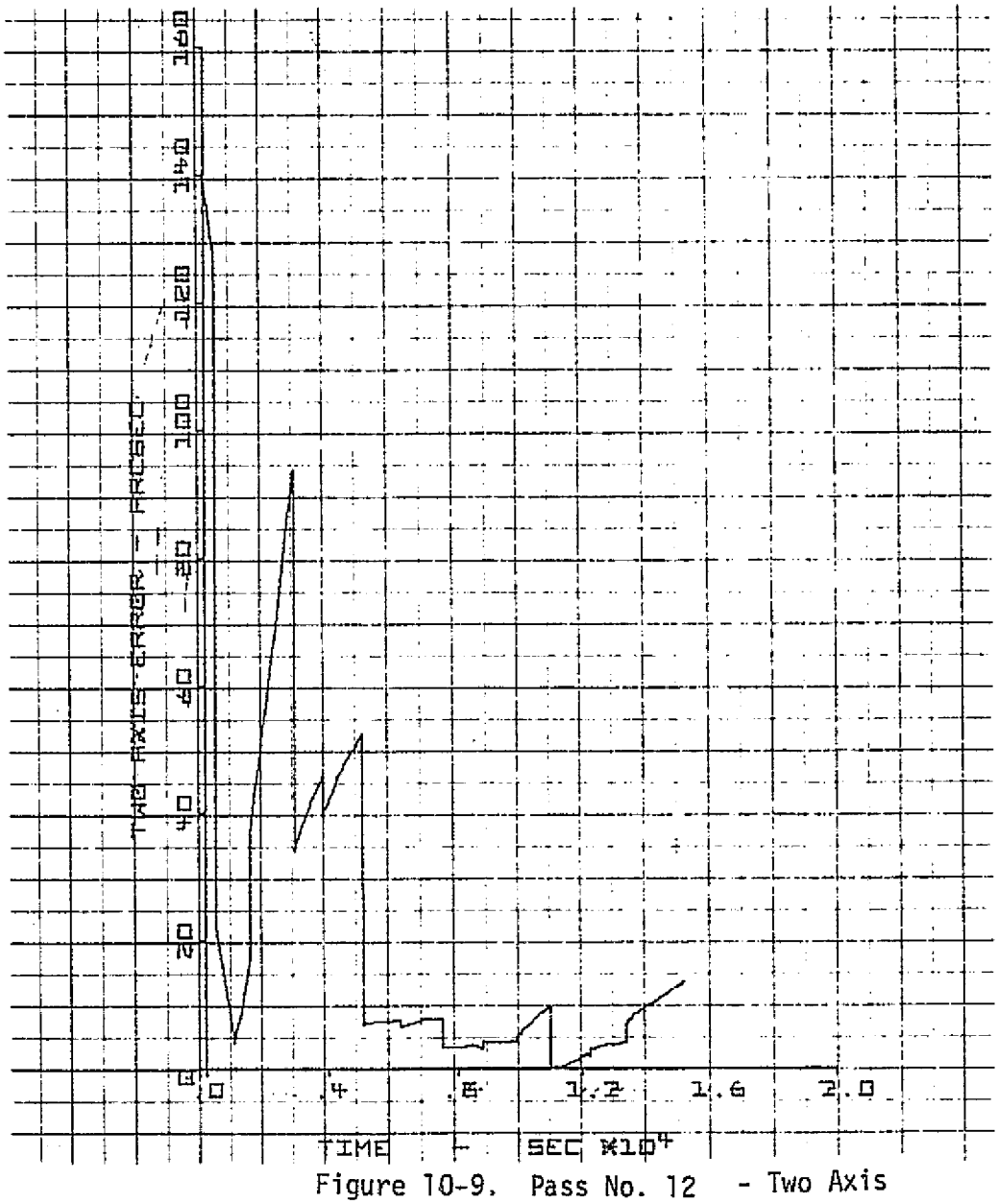

Figure 10-9. Pass No. 12 - Two Axis

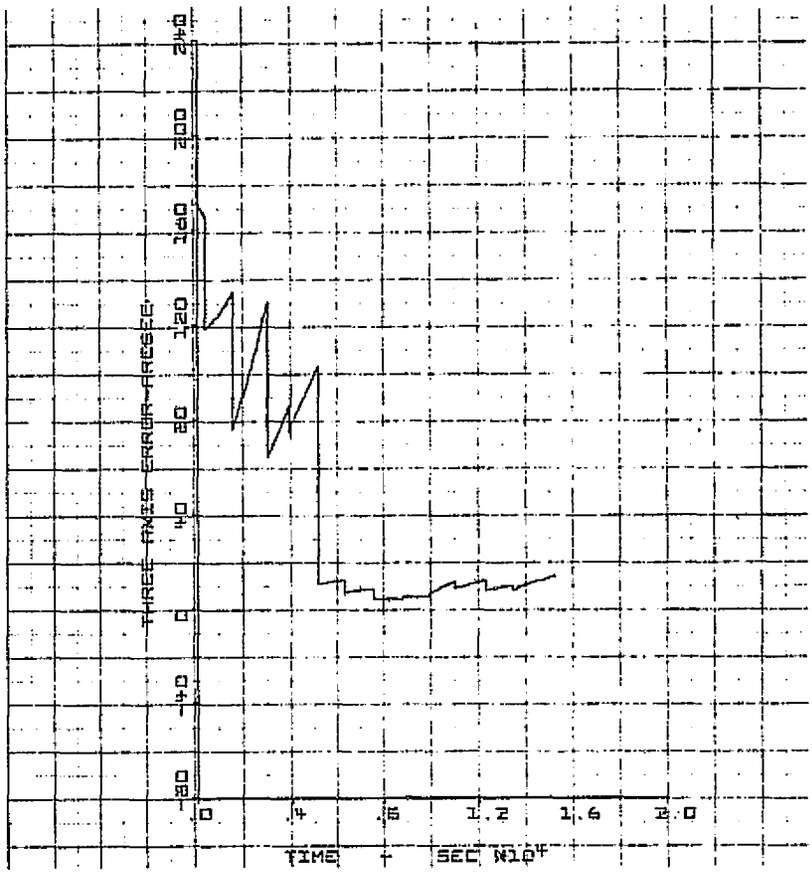

Figure 10-10. Pass No. 12 - Three Axis

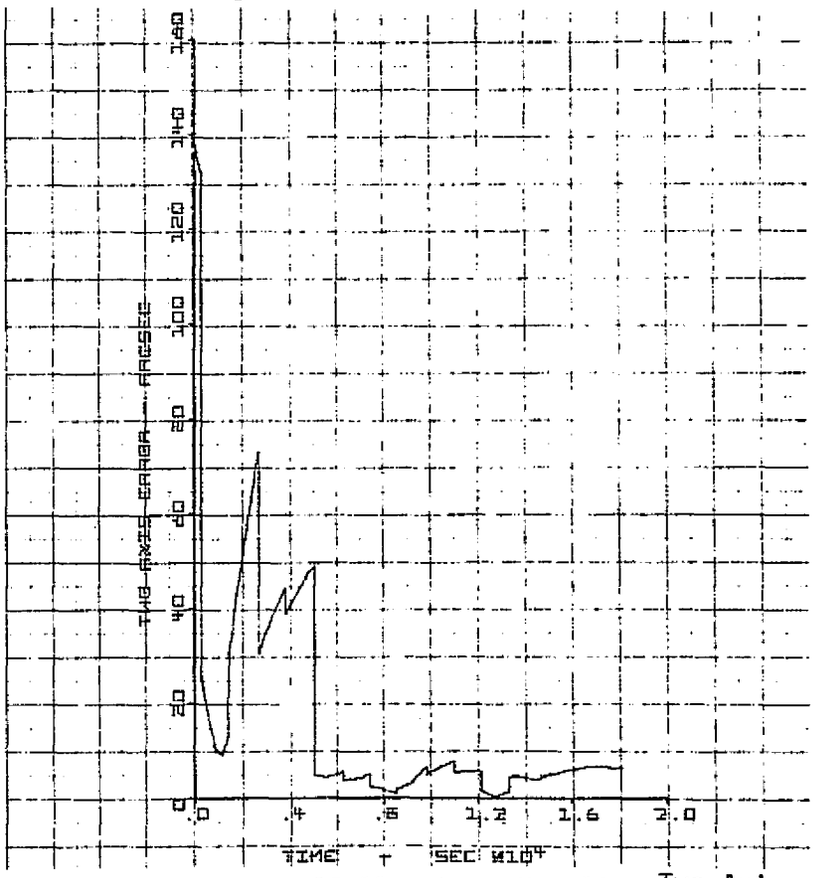

Figure 10-11. Pass No. 13 - Two Axis

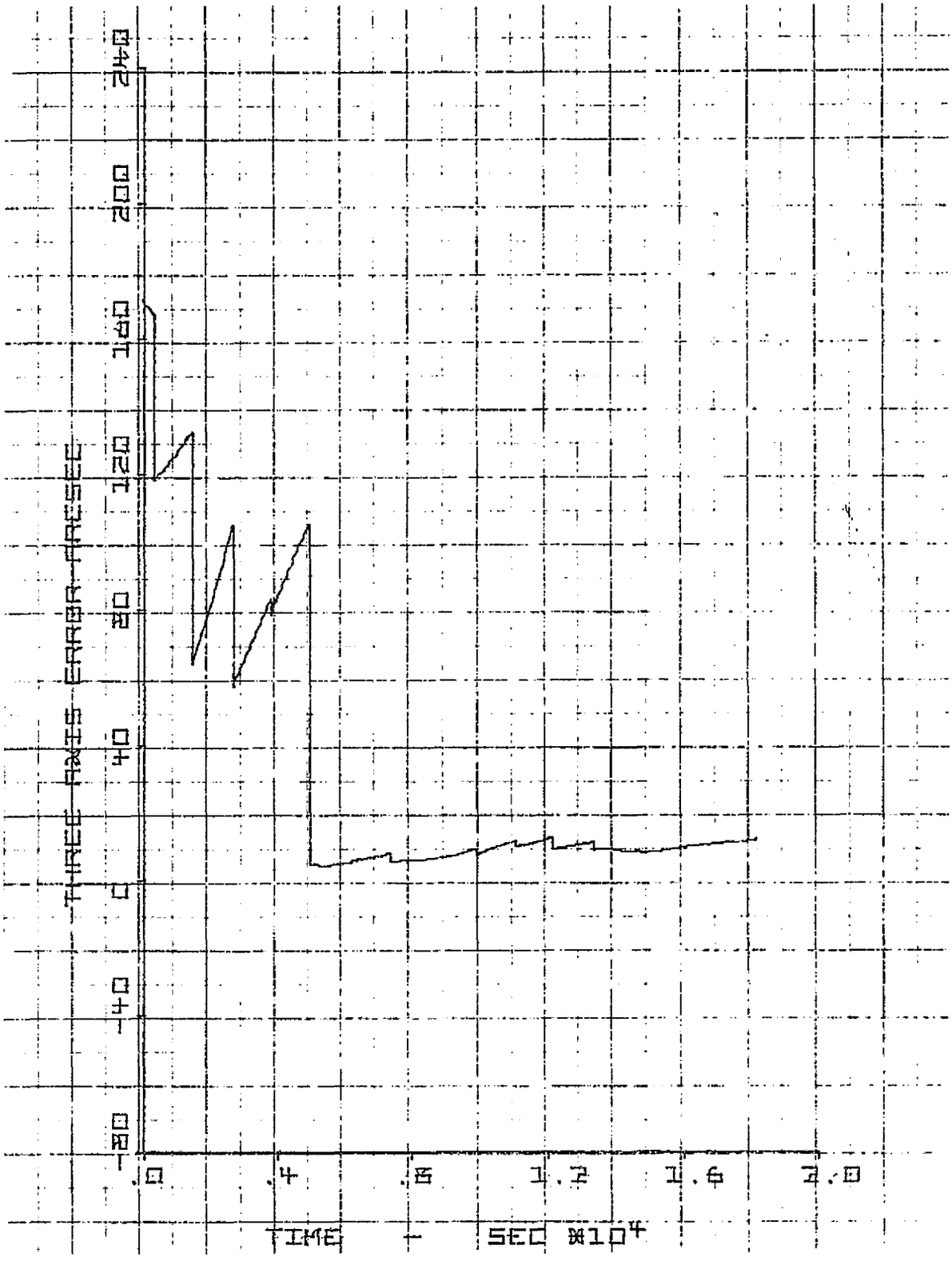

Figure 10-12. Pass No. 13 - Three Axis

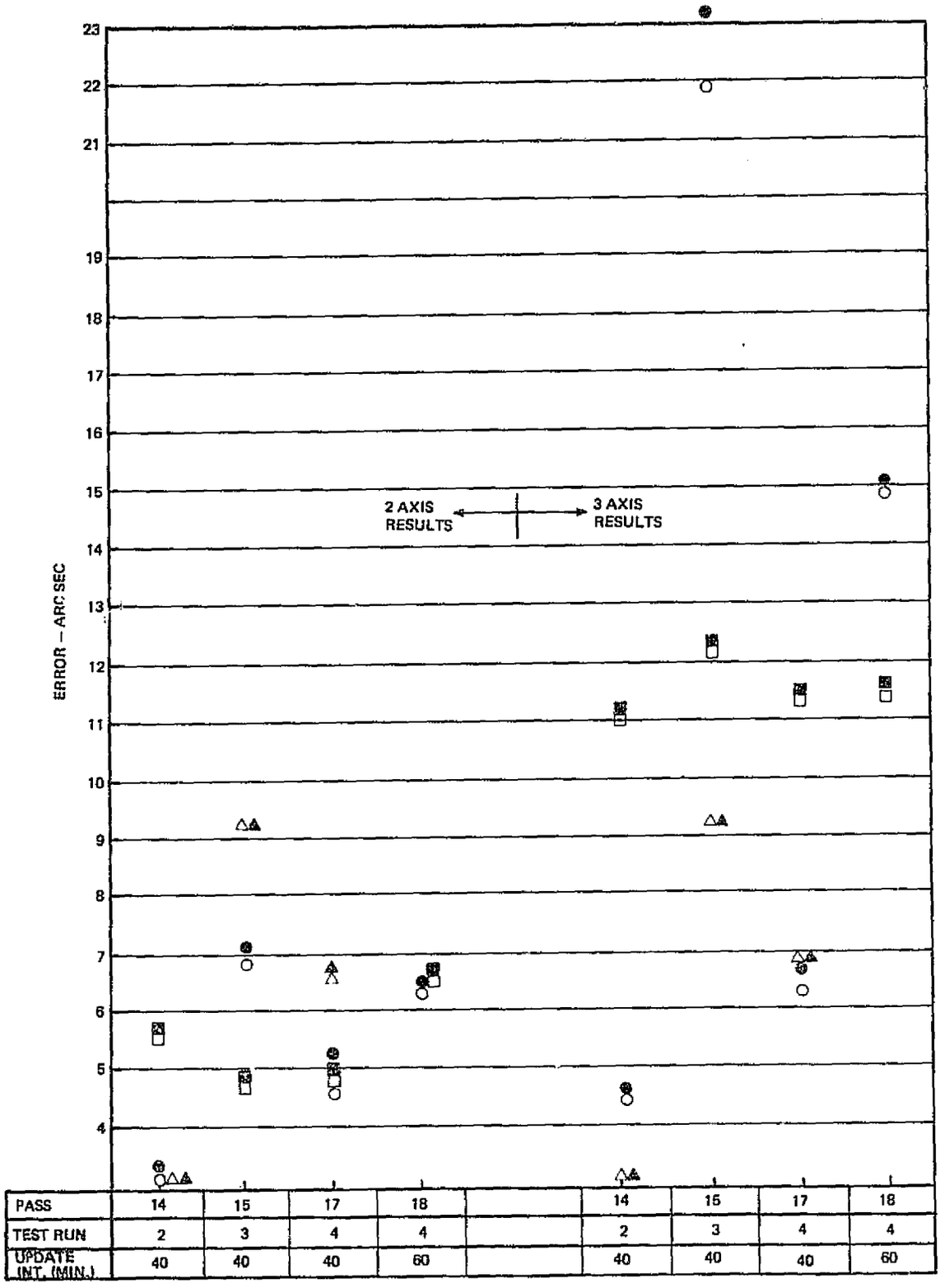

Figure 10-13. Gimbaled PADS Test Results - 40 and 60 Min. Updates

Of the 40 minute update passes, Passes 15 and 17 perform very well, although the three-axis filter confidence has clearly not settled to its final value as errors about x_1 inherently require more star data. The performance of Pass 15 is somewhat worse, again being plagued by the drift rate change of the x and y gyros noted before. Figures 10-14 to 10-17 illustrate these 40 and 60 minute updating runs.

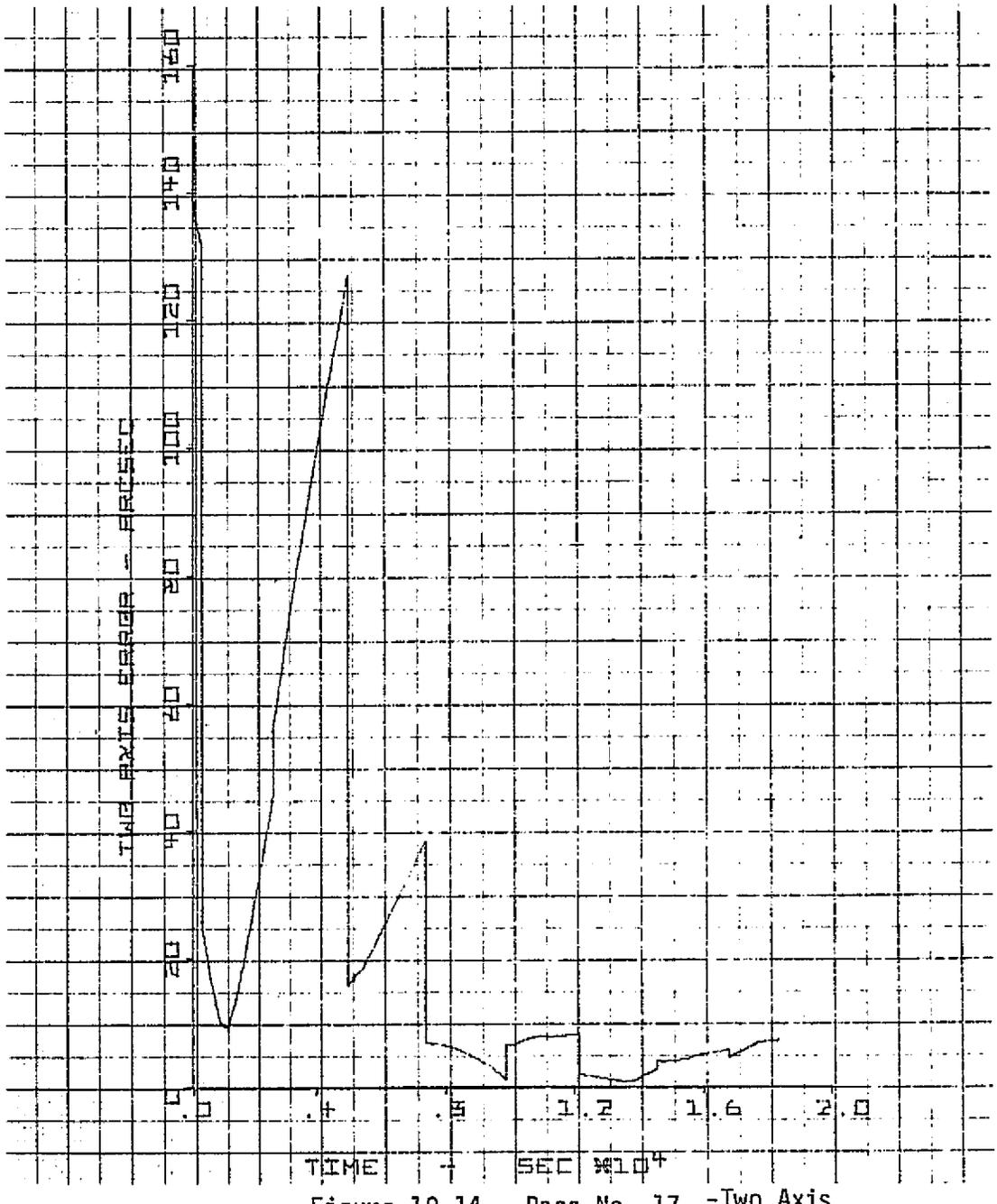

Figure 10-14. Pass No. 17 -Two Axis

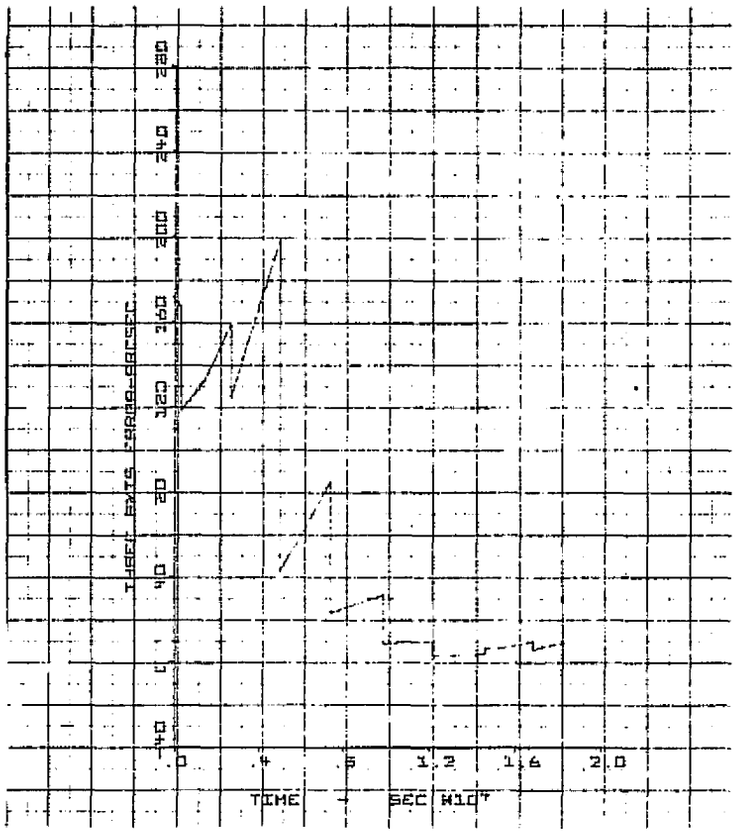

Figure 10-15. Pass No. 17 - Three Axis

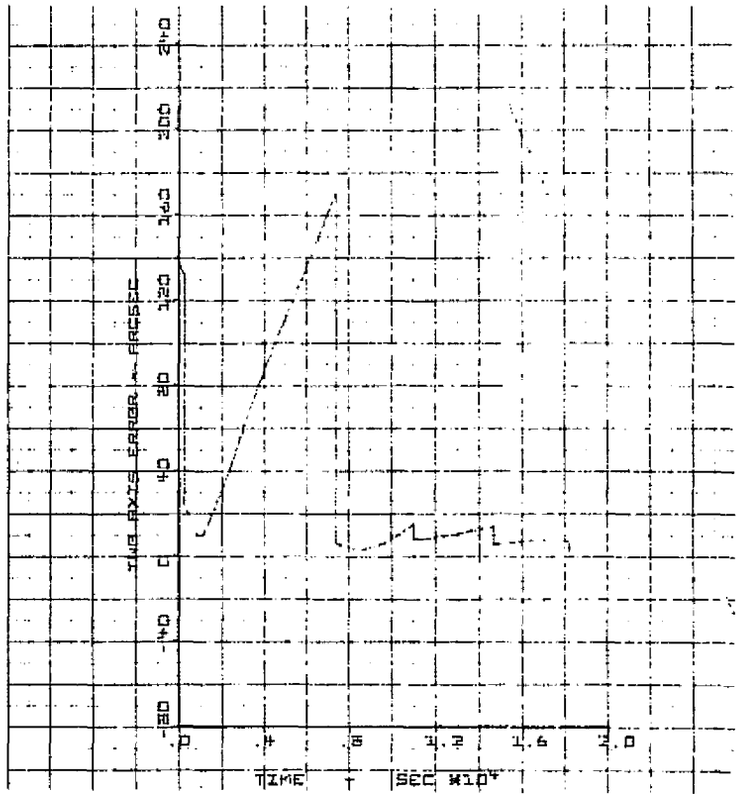

Figure 10-16. Pass No. 18 - Two Axis

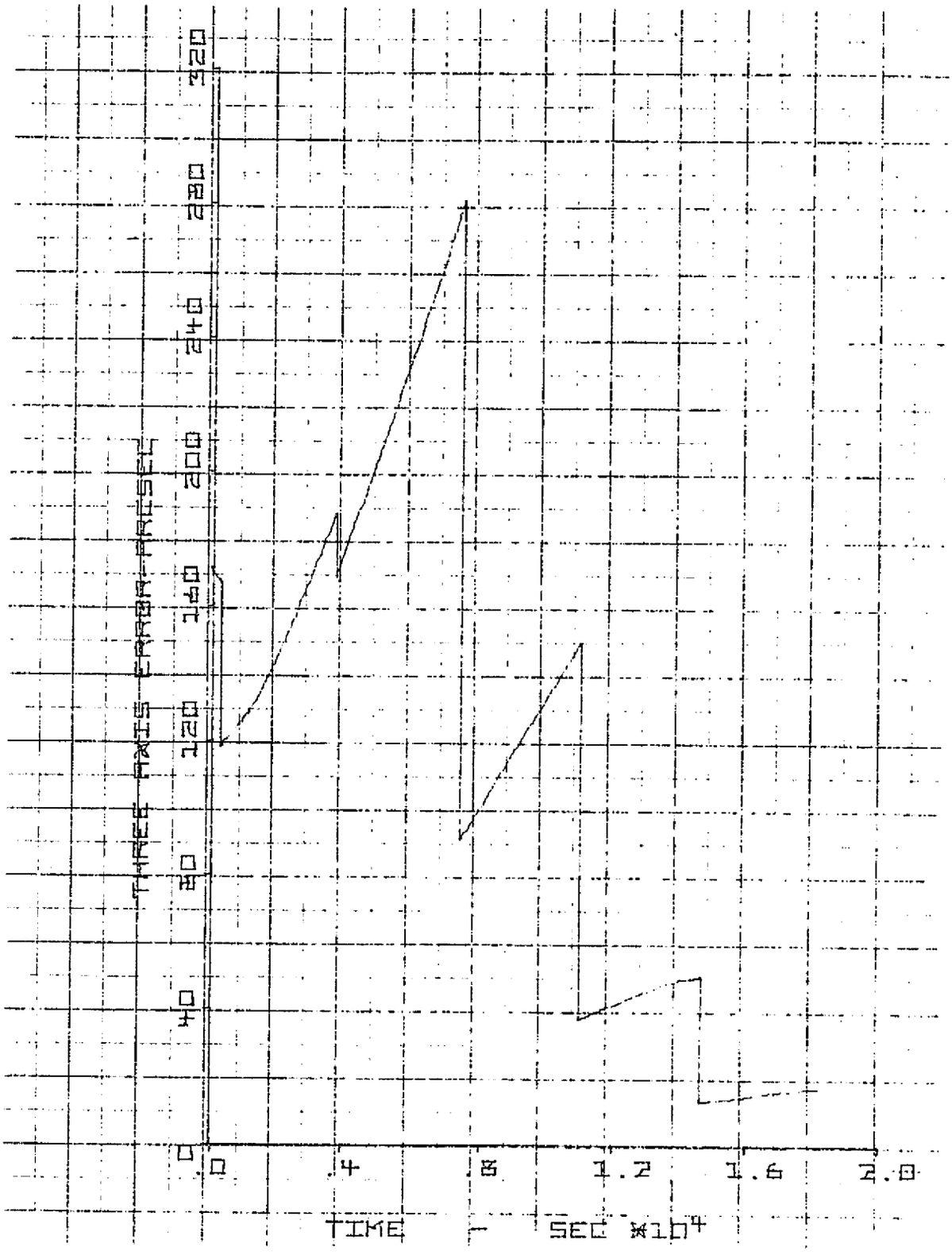

Figure 10-17. Pass No. 18 - Three Axis

10.3.5 PADS Accuracy

The criteria for the accuracy of the PADS is the mean difference between the PADS estimate of the inertial attitude of its reference axes and the true attitude of these axes as indicated by the laboratory instrumentation, and a priori knowledge of earth rate and the inertial attitude of the laboratory at the start of a test run. This criteria is designated σ_θ in Figures 10-8 and 10-13.

Tables 10-4 and 10-5 summarize the values of σ_θ for the two-axis and three-axis results. As mentioned previously, the first test run contained a z gyro malfunction and was not used. Also, only the fourth run was long enough to obtain a steady-state result for 60 minute updates. The n-axis RMS erro divided by $\sqrt{n}$, is the PADS single-axis error.

The PADS design goal is 3.6 arc seconds (1σ) per axis for 20 minute star updates. The value of 3.6 arc seconds calculated from the two-axis results meets this goal, but the corresponding value of 4.8 arc seconds from the three-axis results does not. The poorer accuracy from the three-axis results is expected since the maximum angle between the three available stars was only 38 degree as compared to the optimum of 90 degrees. For the purpose of a comparison with the strapdown PADS, which did not have such a geometry constraint, the errors from the gimbal two-axis results will be used.

The two tables also show the increase in measured error with increased update interval. The inconsistency between the two-axis and three-axis trends is probably due to insufficient data points. The 23.3 arc seconds in Table 10-5 is definitely an anomalous point. No generalizations are apparent.

Table 10-4. PADS RMS Error μ_θ for Two-Axis Results

Test Run	20 Minute Updates	40 Minute Updates	60 Minute Updates
1	—	—	—
2	3.8	3.2	—
3	6.6	7.1	—
4	4.5	5.3	6.5
rms (2-axis)	5.1	5.4	6.5
rms (1-axis)	3.6 arc sec	3.8 arc sec	4.6 arc sec

Table 10-5. PADS RMS Error μ_θ for Three-Axis Results

Test Run	20 Minute Updates	40 Minute Updates	60 Minute Updates
1	—	—	—
2	7.3	4.6	—
3	8.6	23.3	—
4	8.9	6.6	15.0
rms (3-axis)	8.3	14.2	15.0
rms (1-axis)	4.8 arc sec	8.2 arc sec	8.7 arc sec

11. COMPONENT ACCURACIES

As a by-product of the system tests certain measurements of the performance of the individual star trackers and gyros were obtained. These measurements are presented in this section.

11.1 STRAPDOWN STAR TRACKER

As described in Section 4.3 the automatic autocollimator null bias was calibrated immediately before each star transit during a test run for the strapdown system test. This was accomplished by first pointing the parallel star and autocollimator beams at the theodolite, and then pointing them at the star tracker. While in the latter position, the tracker outputs as well as the autocollimator signals were stored on magnetic tape. Thus a measure of the boresight stability of the tracker was obtained before each star transit, i.e., every 20 minutes. Figure 11-1 is a plot of these measurements for the 12 star transits in the 1 October 1975 test run. Figure 11-2 is a plot of the mean of a run's measurements for the four runs made during the ten day test period. The fifth measurement in the plot was obtained from the initial data of a test run on 10 October 1975. This run was aborted due to an electronics failure in the data transmission equipment. The error shown in Figure 11-1 is probably due to the laboratory instrumentation errors. However, the error shown in Figure 11-2 does reflect the drift of the boresight over a ten day period since the run-to-run repeatability of the laboratory instrumentation is 0.6 arc second (3σ) (see Table 4-1).

In addition to the static boresight measurements, dynamic measurements of the star tracker accuracy were obtained for each star transit. The magnetic tape data from a test run was processed in an offline timeshare computer program. This program compared the compensated tracker outputs with the air bearing table compensated readout and prior knowledge of the star positions. The resulting error signal was passed through an RC filter with a 20 second time constant in order to smooth the tracker noise. Figure 11-3 through 11-14 are plots of the error signal for the 12 star transits of the 1 October 1975 test run. The beginning of the transit occurred on the right side of a plot, and the signal moved from right to left. This is evident in the vertical axis error signal of Figure 11-6 which shows two

sudden jumps in the data and their subsequent decays. The dynamic lag of the star tracker track loop is apparent in the horizontal axis error signal for all of the transits. The analytical calculation of this lag (Volume I) was 0.8 arc second, which is in good agreement with the plots. The star sequence for the 12 transits was 1,2,3,1,2,3, etc. Examination of the four plots for any particular star does not reveal a clear indication of a systematic error resulting from the polynomial compensation of the tracker output. This error is indistinguishable from the filtered tracker noise.

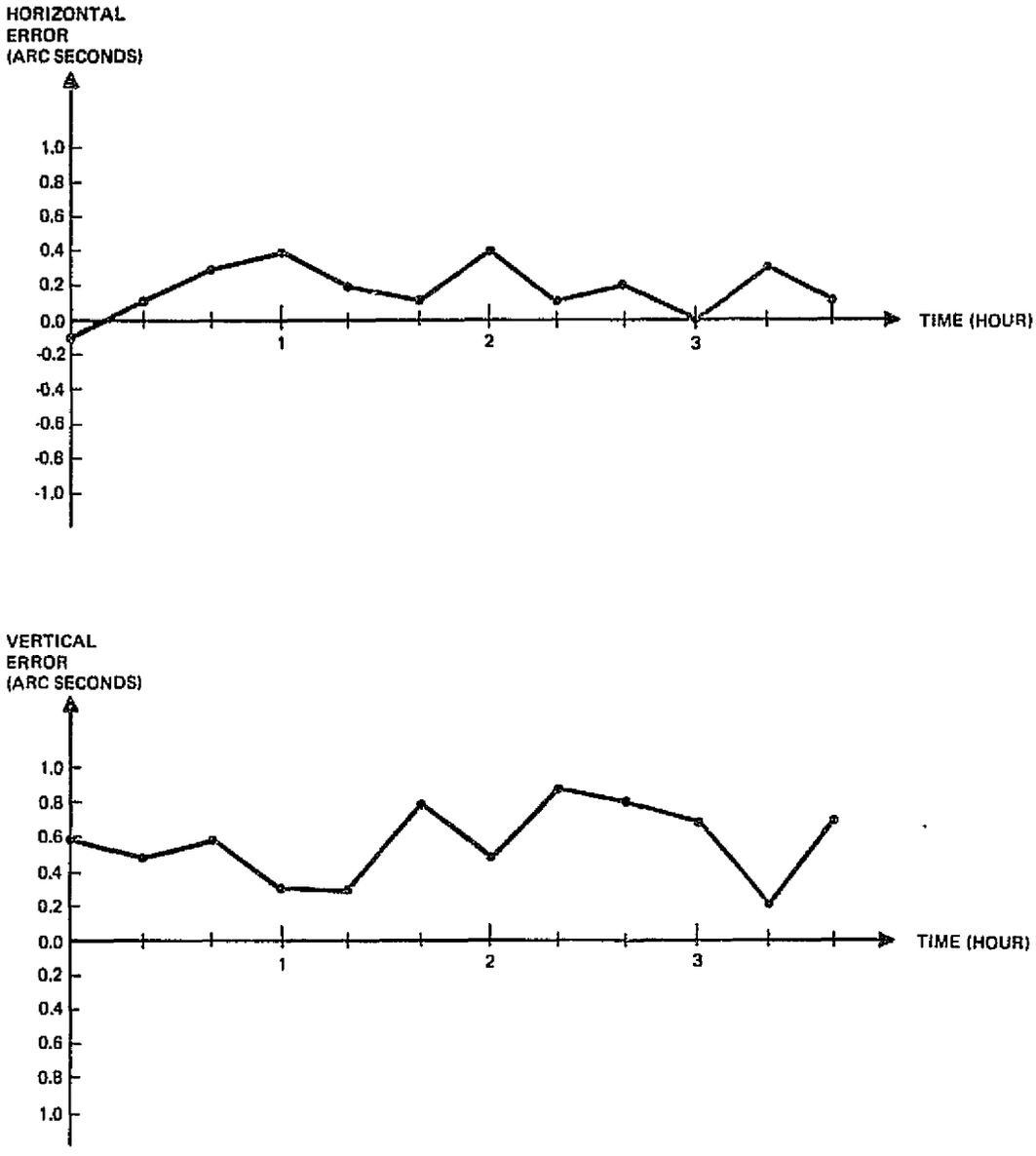

Figure 11-1. Static Boresight Error for 1 October 1975 Test Run

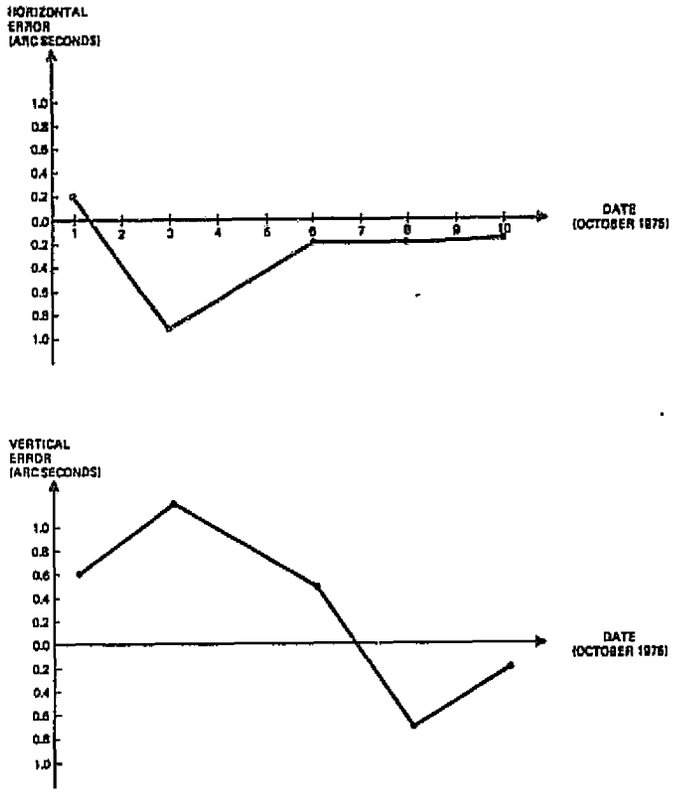

Figure 11-2. Mean Boresight Errors for Strapdown System Test

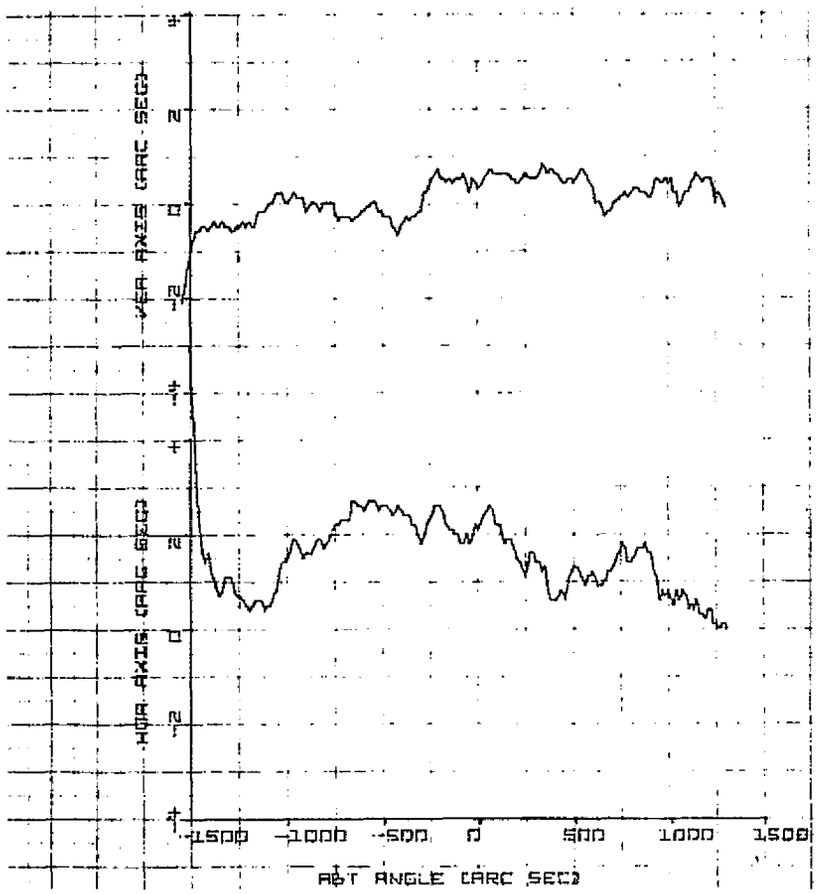

Figure 11-3. Star Transit Number 1

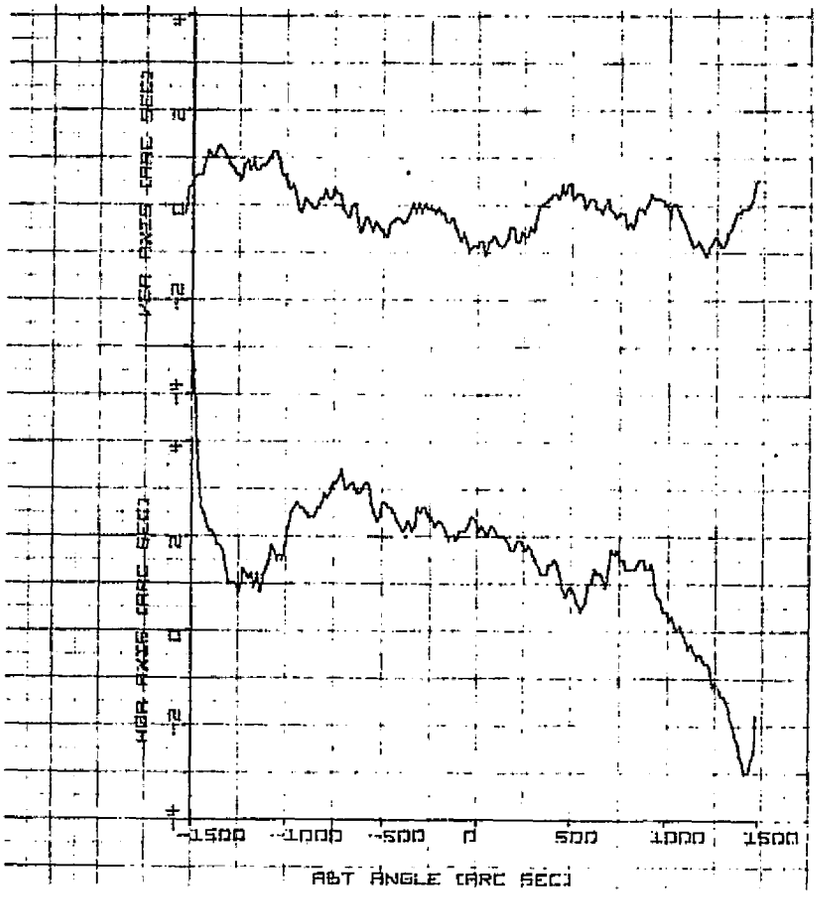

Figure 11-4. Star Transit Number 2

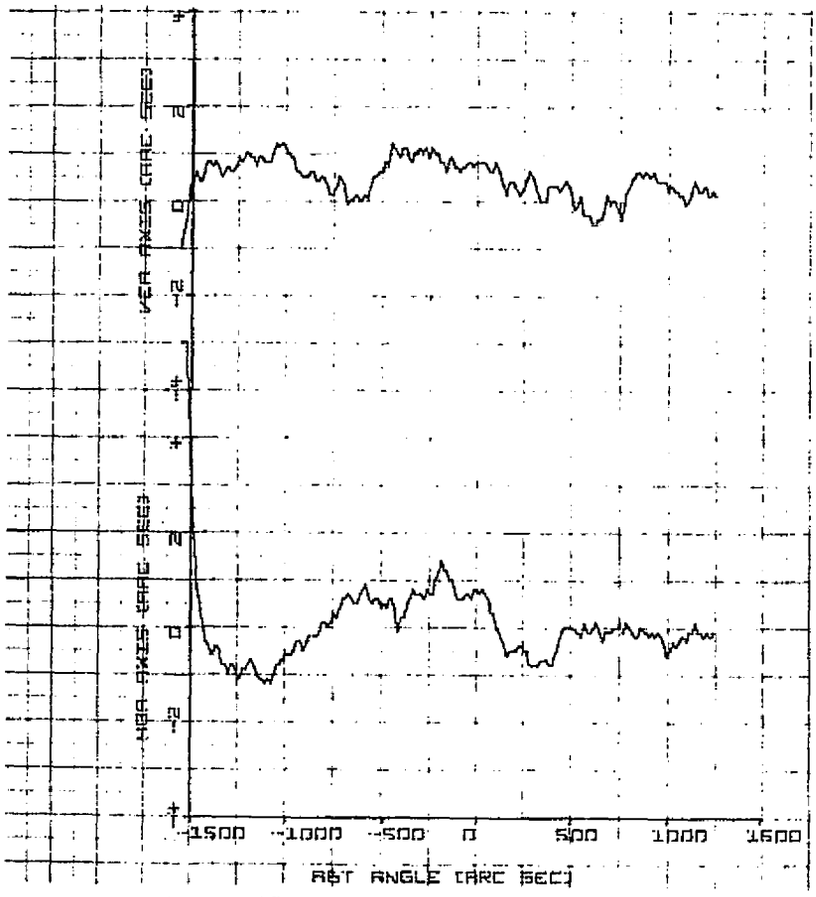

Figure 11-5. Star Transit Number 3

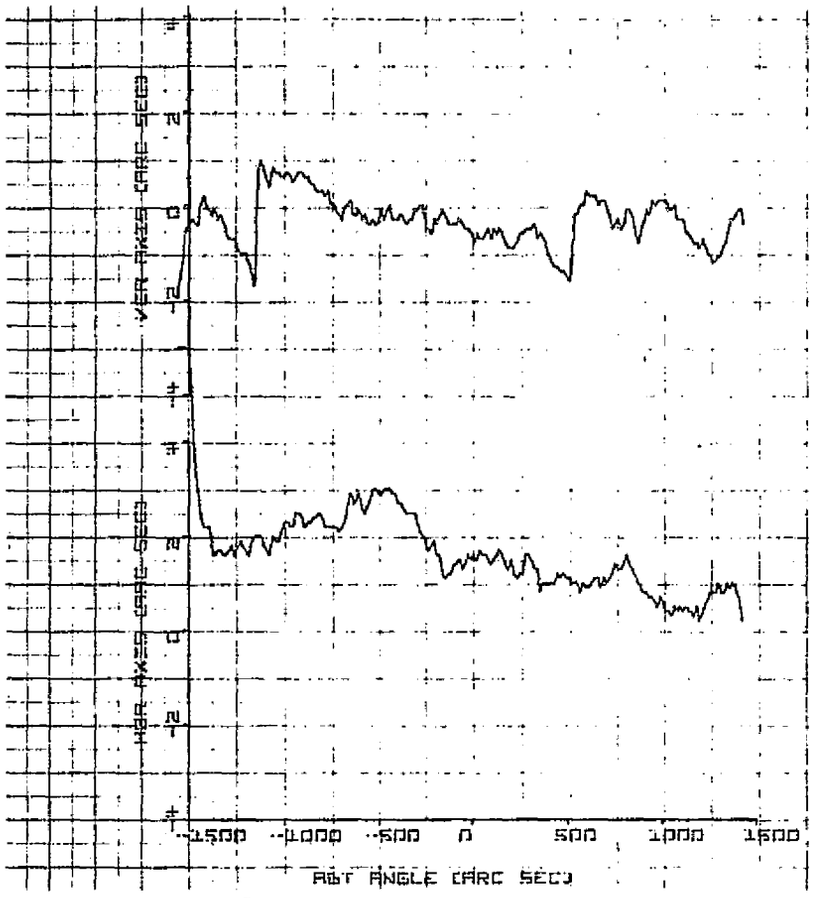

Figure 11-6. Star Transit Number 4

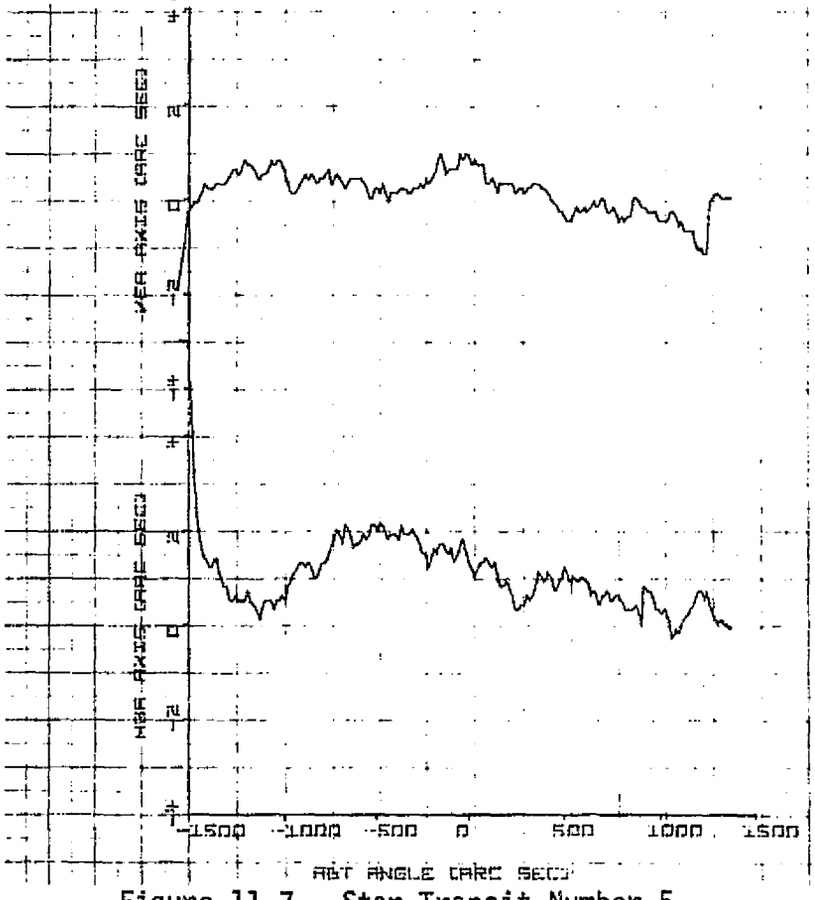

Figure 11-7. Star Transit Number 5

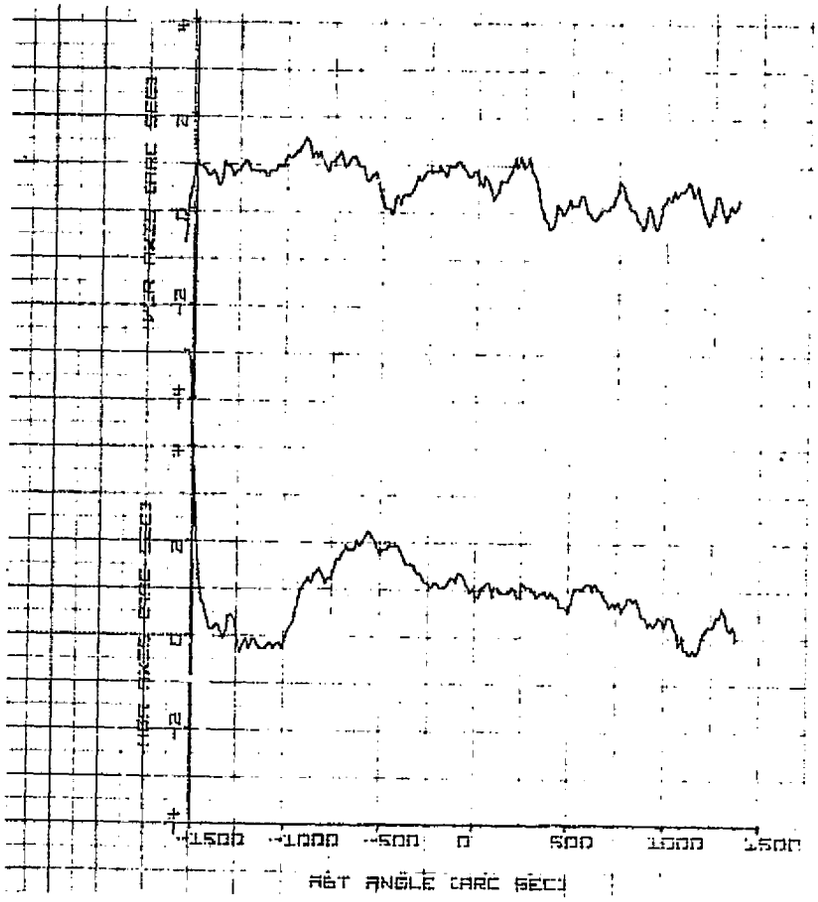

Figure 11-8. Star Transit Number 6

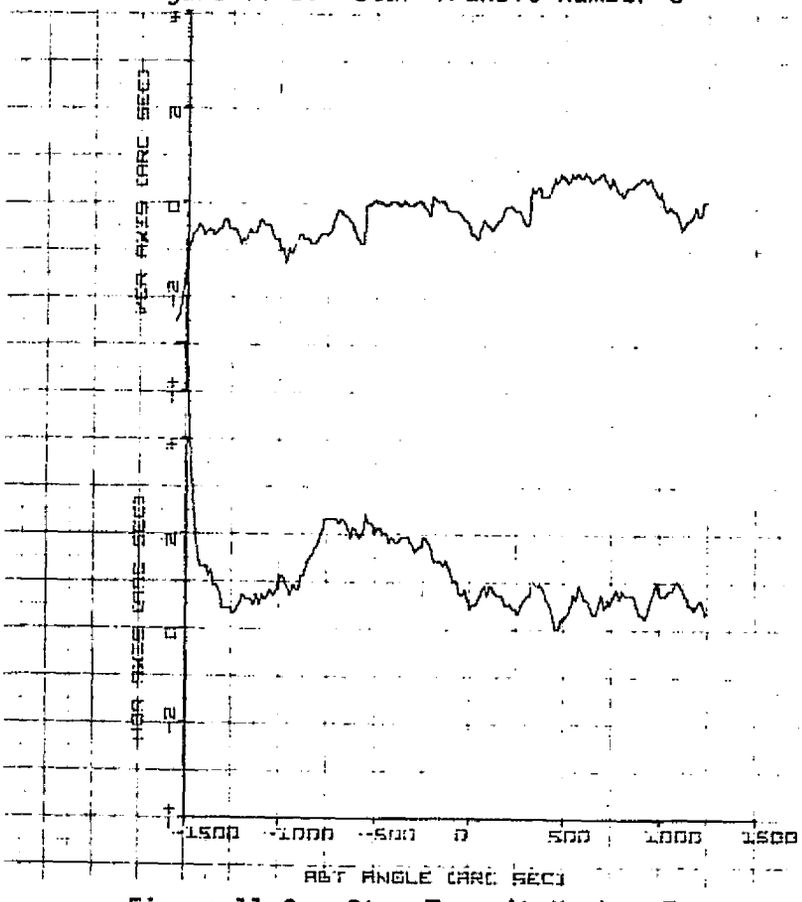

Figure 11-9. Star Transit Number 7

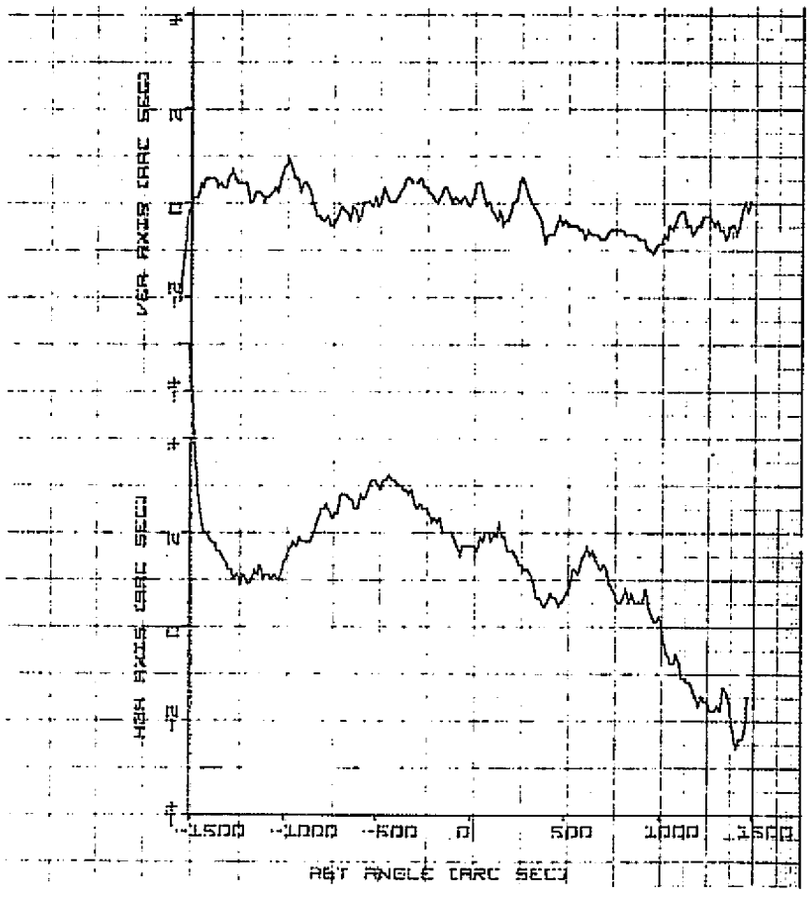

Figure 11-10. Star Transit Number 8

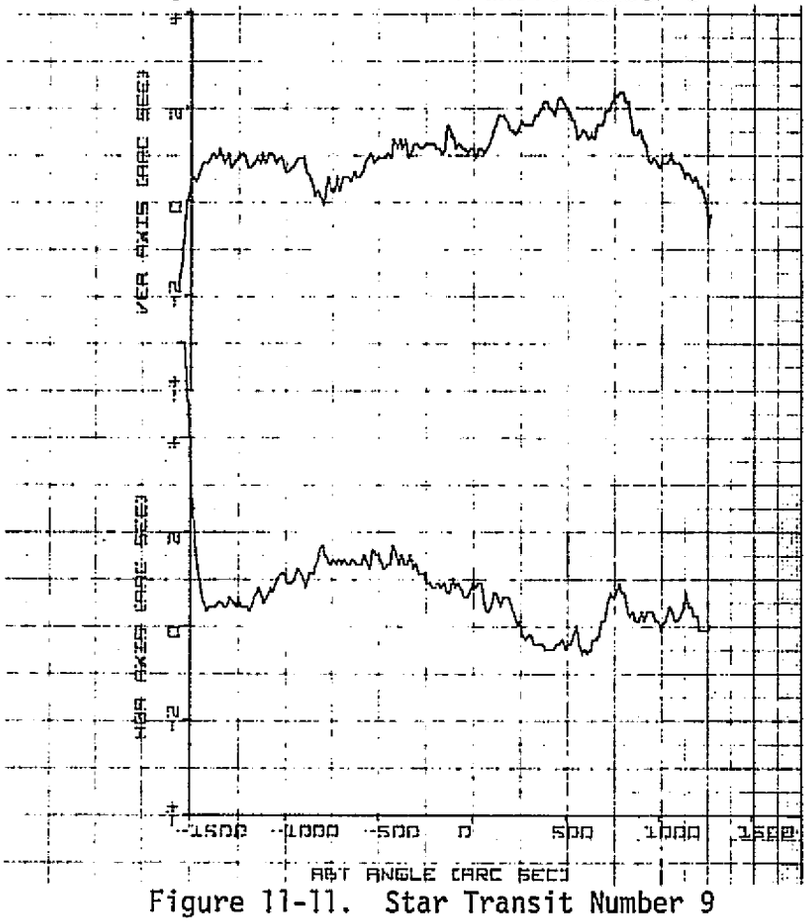

Figure 11-11. Star Transit Number 9

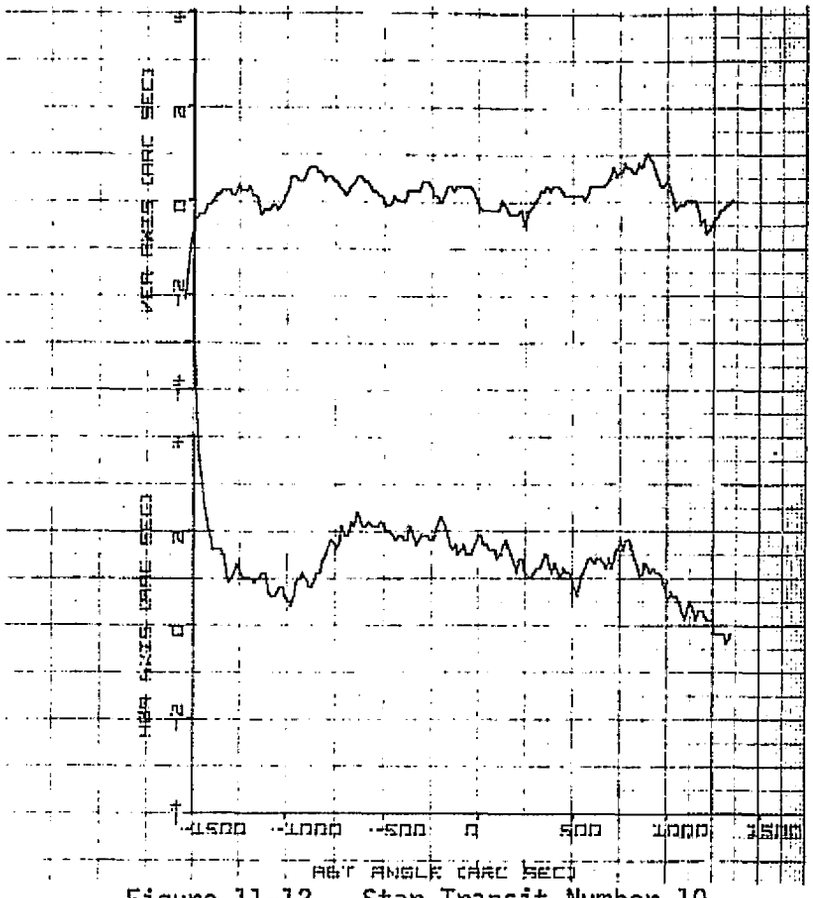

Figure 11-12. Star Transit Number 10

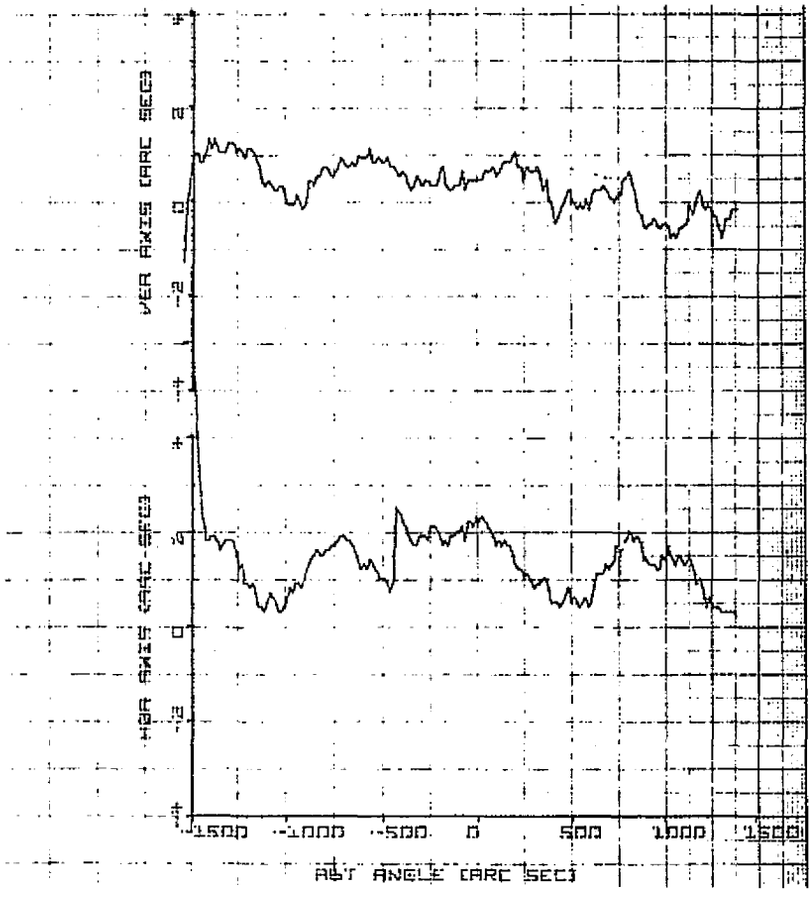

Figure 11-13. Star Transit Number 11

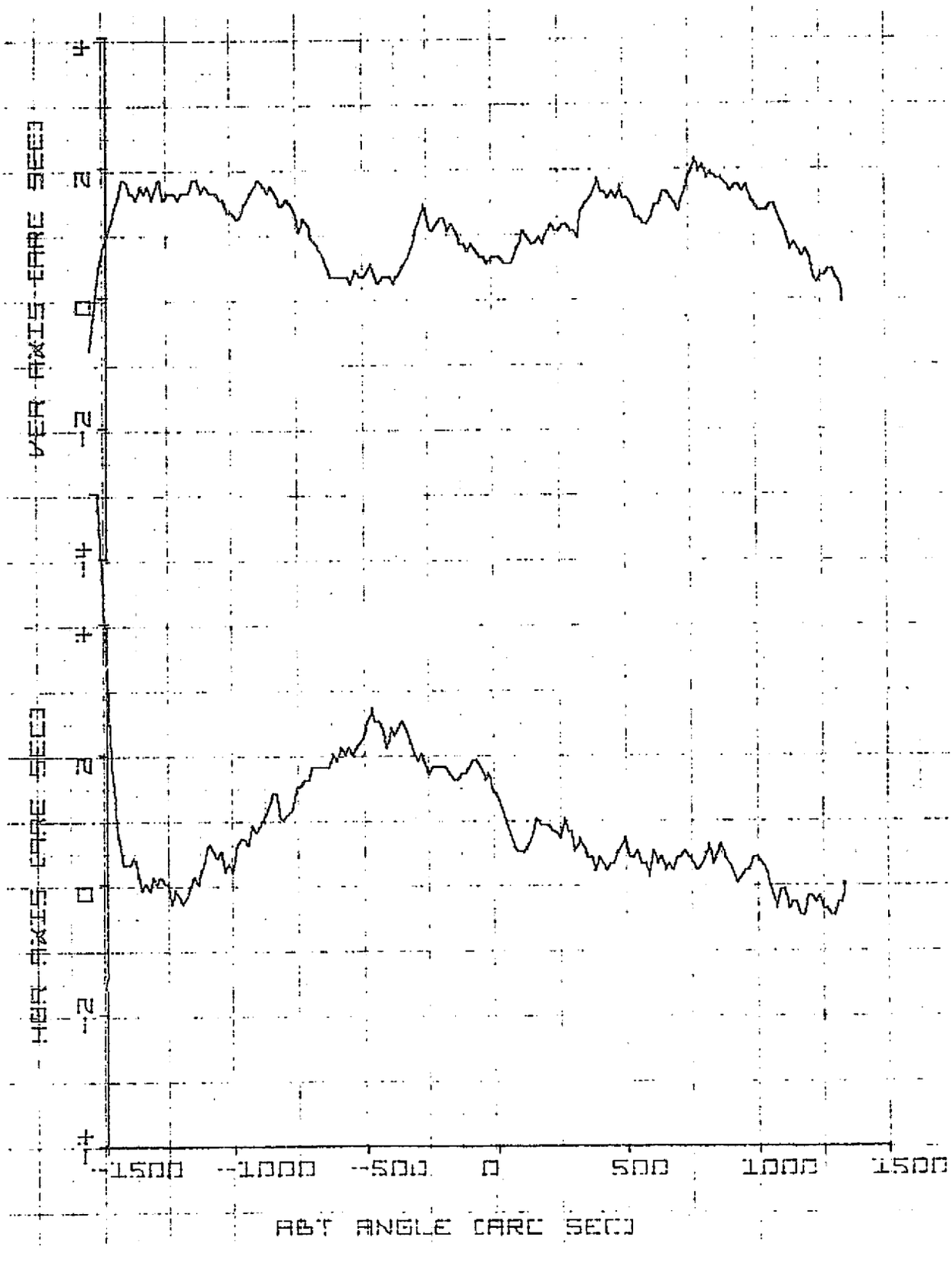

Figure 11-14. Star Transit Number 12

11.2 GIMBAL STAR TRACKER

The static boresight measurements recorded during the gimbal system test differed from those of the strapdown test in that each measurement was for one of the three different stars, not all for the middle star. The measured star positions immediately prior to the ten day system test are given in Section 4.1. The average deviations throughout a test run from these values are shown in Table 11-1 under the column absolute error. The table also lists the errors in the locations of the upper and lower stars relative to the center star.

Table 11-1. Static Boresight Errors for the Gimbal System Test

Test Run	Star	Absolute Error		Relative Error	
		AZ	EL	AZ	EL
8 Feb 76	1	-0.5	0.1	-0.4	0.0
	2	0.1	0.1	0.0	0.0
	3	0.4	-0.2	0.5	-0.3
9 Feb 76	1	1.8	-1.2	0.4	-0.4
	2	1.4	-0.8	0.0	0.0
	3	3.9	-0.9	2.5	-0.1
11 Feb 76	1	2.5	-0.1	0.2	-0.1
	2	2.3	0.0	0.0	0.0
	3	3.2	-0.5	0.9	-0.5
16 Feb 76	1	1.0	-0.4	-0.3	0.3
	2	1.3	-0.7	0.0	0.0
	3	1.9	-1.6	-0.6	-0.9

The relative errors are presented to indicate the accuracy of the laboratory instrumentation. These errors will be independent of bias shifts in either the optical sensor or the gimbal readout. With one exception, these errors support the accuracy assumed for the laboratory instrumentation. The exception is for star 3 azimuth during the 9 February 1976 run. Both the absolute and the relative errors appear off by 2.5 arc seconds. No explanation for this discrepancy was found. In general the absolute elevation

errors are small, while the azimuth errors are in the region of one to two arc seconds. These errors are believed to be indicative of the boresight stability of the tracker.

11.3 GYROS

The magnetic tape data for all eight test runs of both system tests was processed to indicate the drift stability of the gyros throughout a particular test run. Figures 11-15 through 11-22 show the attitude output stability of the three gyro axes for the eight test runs. The actual gyro output was a ramp function when plotted against time. In order to clearly show the ramp irregularities, the figures plot the output minus the ramp defined by the start and end points of the data.

In general the plots verify the performance measured previously for the gyros and presented in Appendix C. An exception, however, was the performance of the z gyro for the last three runs of the gimbal system test. Unexplanably, but fortuitiously in view of the three-axis requirement of the test, the performance was much improved.

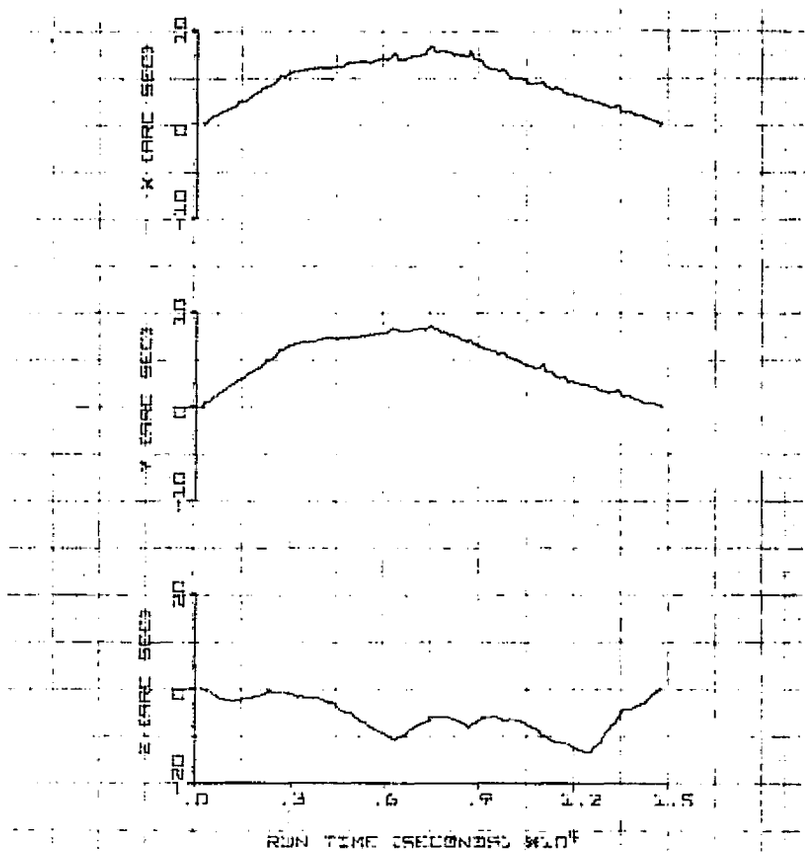

Figure 11-15. 10/01/75 Run

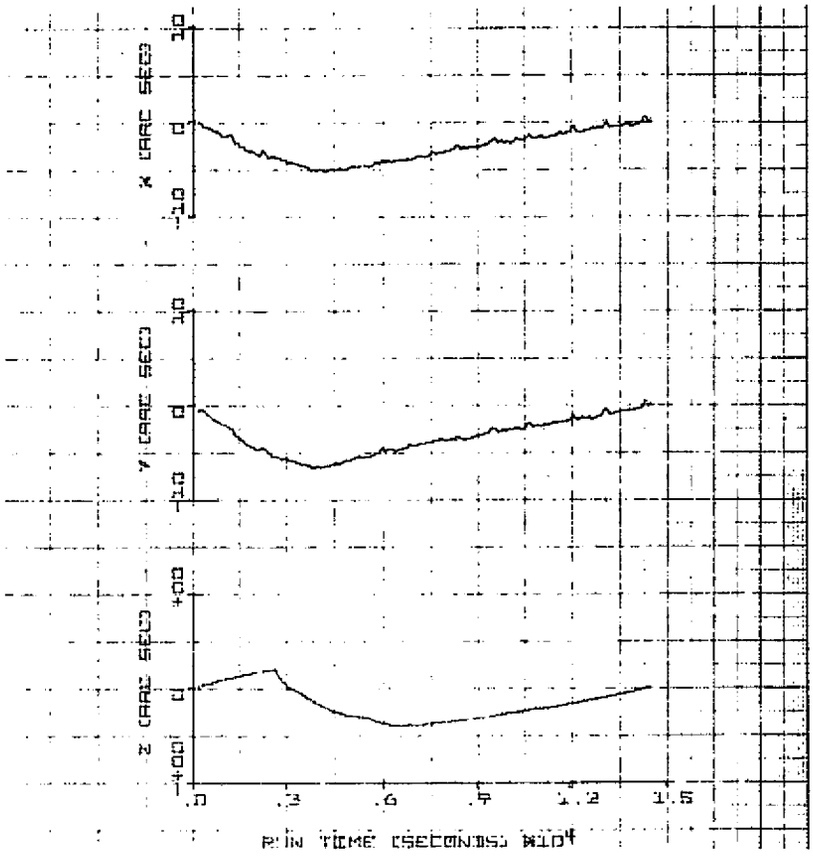

Figure 11-16. 10/03/75 Run

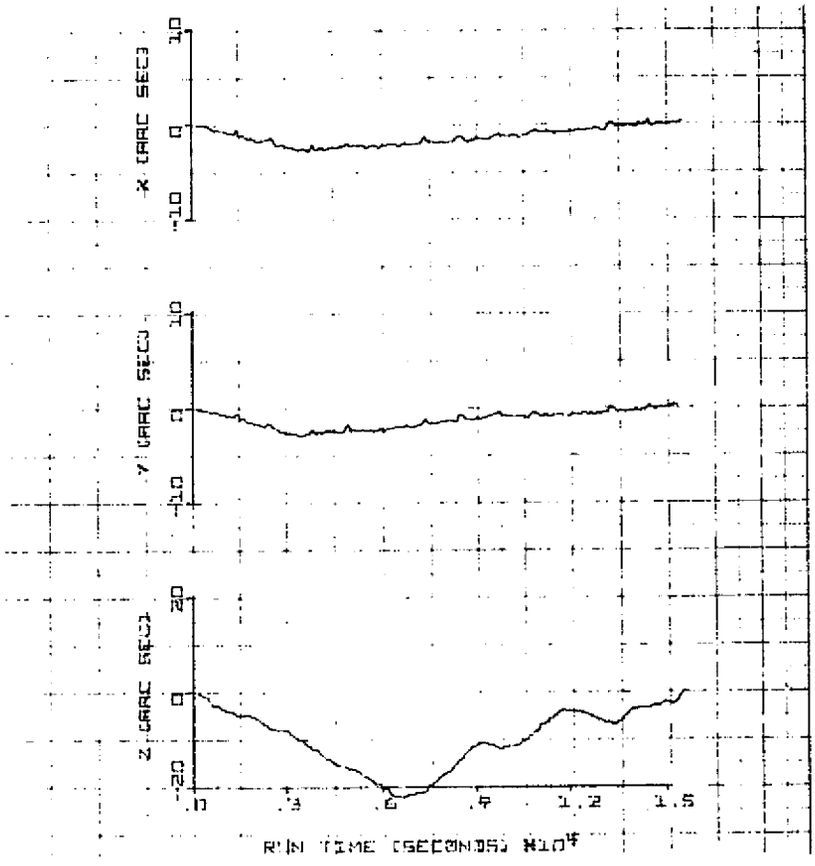

Figure 11-17. 10/06/75 Run

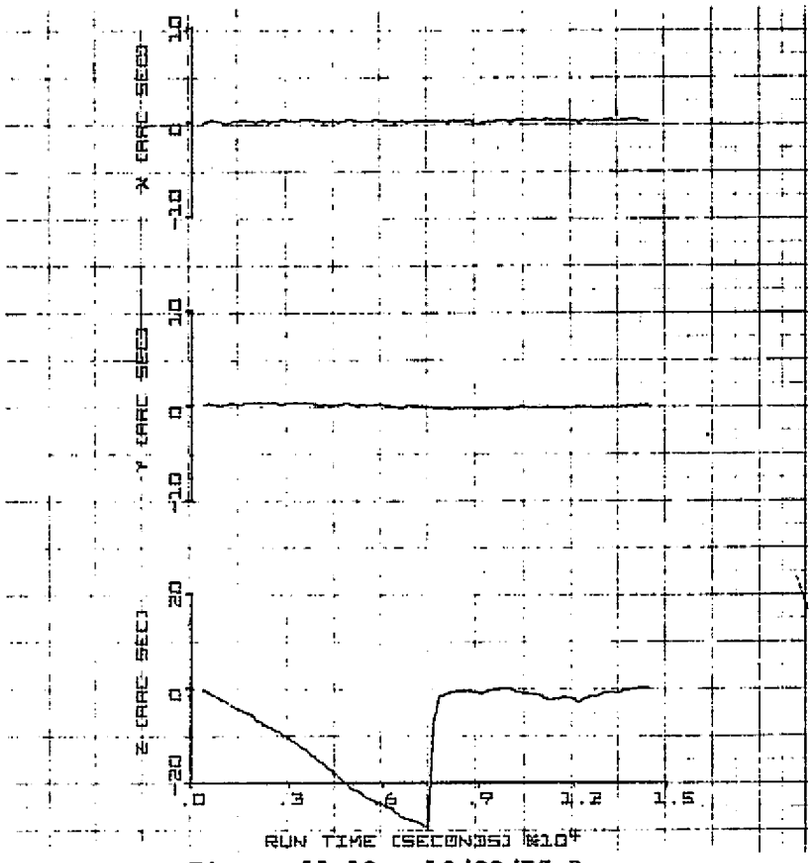

Figure 11-18. 10/08/75 Run

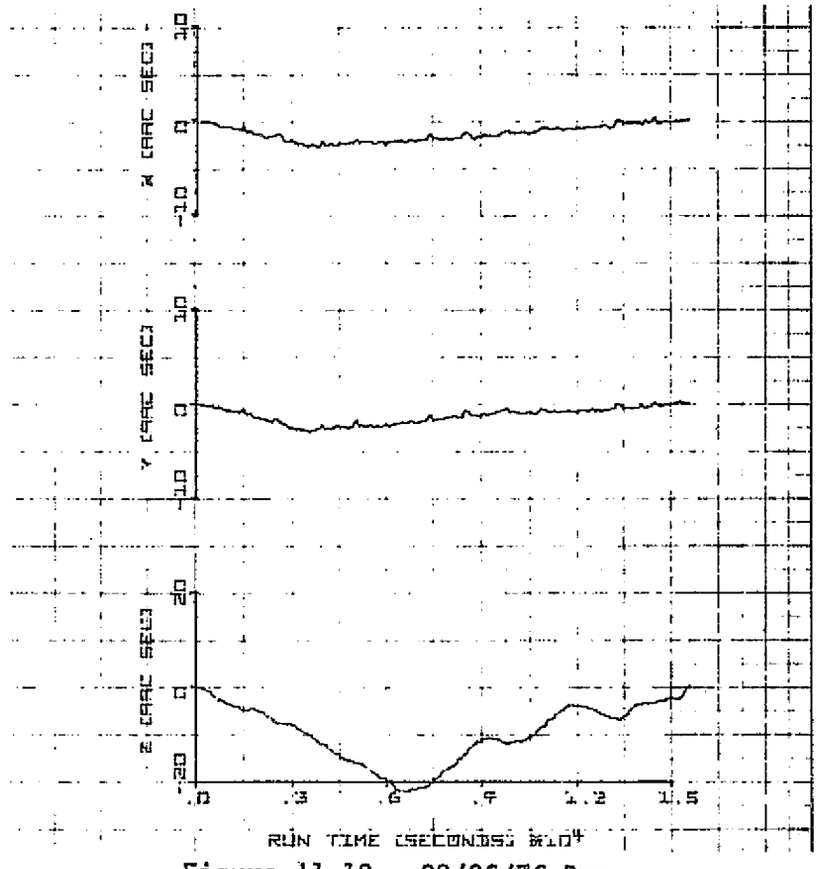

Figure 11-19. 02/06/76 Run

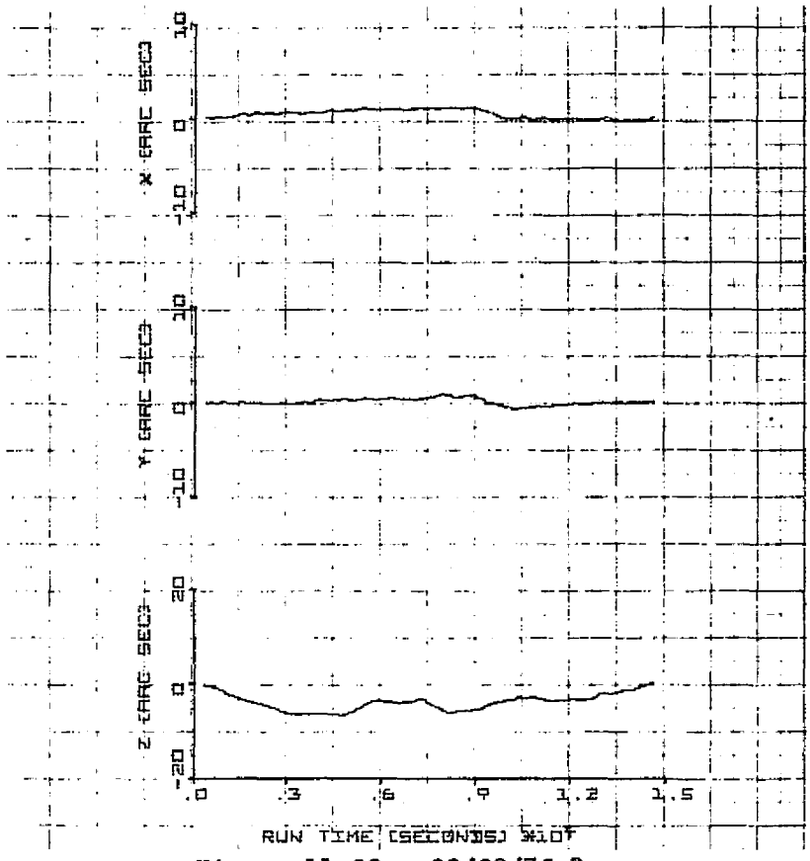

Figure 11-20. 02/09/76 Run

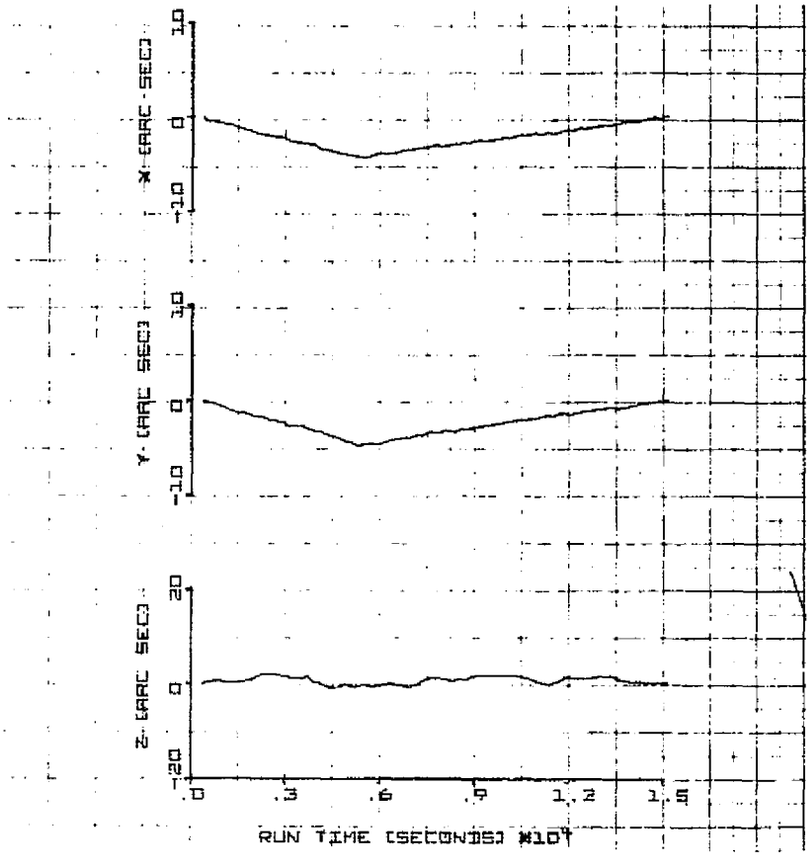

Figure 11-21. 02/11/76 Run

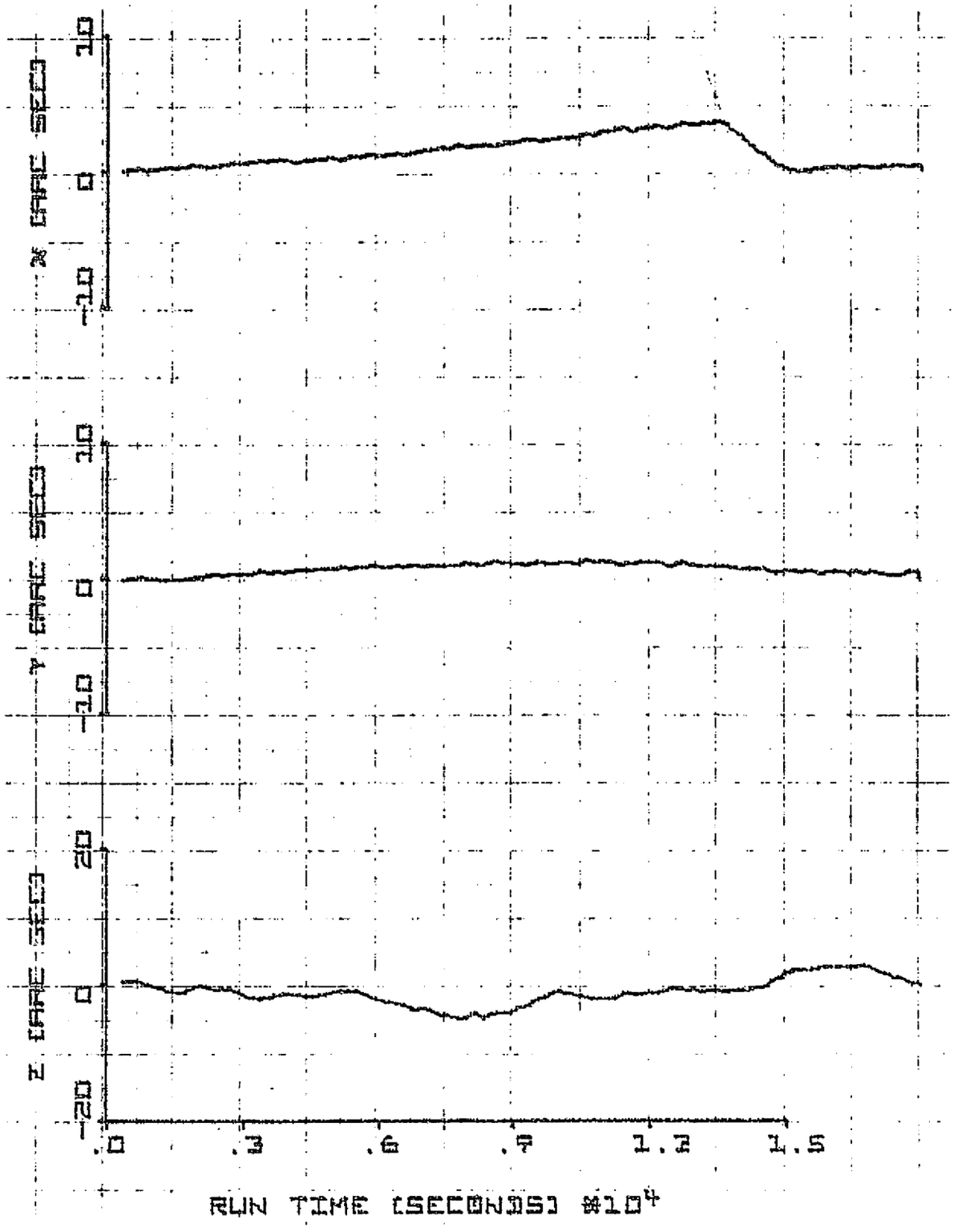

Figure 11-22. 02/16/76 Run

12. CONCLUSION

Both the strapdown and gimbal PADS met the accuracy goal of 3.6 arc seconds (1σ) per axis as demonstrated by the laboratory tests. The strapdown PADS accuracy of 2.3 arc second actually exceeded the goal by a convincing margin. The gimbal PADS accuracy of 3.6 just equaled the goal. It is noted that the gimbal accuracy was derived from the gimbal two-axis results which did not include the detrimental effect of the limited 38^{o} separation between stars.

The laboratory tests have demonstrated that either system, under laboratory controlled temperature and vibration environments, will meet the design goal.

In a comparative sense, the performance of the strapdown system exceeds that of the gimbal system even more than the 20 minute update accuracies indicate. As pointed out in Section 4.1, for equal probabilities of star acquisition the gimbal tracker update interval should be 32 minutes if the strapdown tracker interval is 20 minutes. Although the quantitative effect of the longer update is not clear from the parametric results in Section 10.3.4, it is certain that the accuracy of the gimbal system will be even less for the longer update.

Also in a comparative manner, the alignment complexities associated with a test evaluation of the gimbal system, specifically the gimbal star tracker, are more numerous than those of a comparable strapdown system with two star trackers. These complexities arise primarily from the inability to directly identify the gimbal axis with an optical flat in the presence of a 1 g field. In another aspect, the hardware connected difficulties encountered with the gimbal star tracker provided a reminder of the comparative complexity of that unit relative to the strapdown star tracker.

The substitution of the OAO gyros for the originally intended Bendix gyros turned out well in that the anomalous behavior of the normally higher performance OAO gyros made their random drift rates comparable to those expected from the Bendix gyros. On the other hand, the drift rate variations of the x and y gyros were decidedly deterministic, displaying a

squarewave variation in rate which did not fit the assumed statistical models. Also, the performance of the z gyro was much poorer than either the z or y gyros, necessitating an artificial rotation of the gyro axes in the strapdown test to eliminate its effect from the two-axis results. It also invalidated one of the four gimbal test runs.

The attitude error convergence plots for both systems indicate that the limiting factor for the 20 minute update intervals is the star tracker error. The independent evaluations of the tracker noise and bias errors led to the conclusion that the software algorithms, and the Kalman filter in specific, did not add significantly to the total error. In this area the primary emphasis of the laboratory evaluations, namely, the star trackers and the algorithms, was fulfilled. However, the 40 and 60 minute update intervals presented a different case. Here the anomalous behavior of the gyros became dominant, and the Kalman filter understandably was unable to compensate for the sudden drift rate changes between star updates.

In terms of development status then, both star trackers have proven their performance capabilities and appear ready to proceed to flight level designs and environmental testing. The one reservation, however, involves the strapdown star tracker hysteresis described in Volume I. In many applications this effect is undesirable, and efforts are now underway to identity and eliminate it.

The results obtained in the area of minimizing the laboratory instrumentation errors justify the ground-fixed test configuration chosen for the system tests. The predicted instrumentation errors of 0.9 and 1.6 arc seconds for the strapdown and gimbal tests, respectively, most probably were achieved in view of the overall test results. The advantage of presenting PADS attitude errors as computed, without qualifications for hypothesized instrumentation errors, outweighs the subtle aspects involved with the ground-fixed configuration.

While the ground-fixed test configuration did minimize the instrumentation errors, it also made clear that the limit in test accuracy for star trackers and attitude determination systems was reached using commercially-available instrumentation. The most obvious limitation was the theodolite.

While the Kern DKM3 is one of the best, if not the best, such instrument available, obtaining better than 0.5 arc second accuracy with the instrument is doubtful. Another limitation is the parallelism and perpendicularity accuracies of mirror surfaces. Procurement of such mirrors with specifications below one arc second is not only costly but often beyond the capabilities of most optical suppliers. Stability and collimation accuracy of star sources is another limitation. Even with the thermally passive approach used in this program, material creep and long-term deformations will often require months of settling time after initial installation to achieve better than 1 arc second stability.

It seems clear that if star trackers or attitude determination systems with sub-arc second accuracies are developed, a significant increase in the cost of testing such units or systems will be experienced. A large part of the test cost will be the development and certification of the precision test instrumentation required.

REFERENCES

1. "Autonomous Navigation Technology — Phase I Final Report," TRW Report 23850-6023-TU-00, AF SAMSO, Contract No. F04701-73-C-0222, August 1974.

2. "PADS System Design and Analysis (Single-Axis Gimbal Star Tracker)," TRW Report 13900-6016-RU-00, NASA/GSFC, Contract No. NAS 5-2111, 1 July 1974.

3. "IRU (OAO) Systems Handbook," Charles Stark Draper Laboratory Report, Contract No. NAS 5-11002, May 1970.

4. Bendett, R.M., et al, "Test Evaluation of a High Performance Pulse Rebalanced Gyro for Strapdown IMU Applications," presented at The National Aerospace Meeting of the Institute of Navigation, 12 May 1975.

5. Popelka, M.F., and Ferren, F.R., "Astro-Azimuth Comparative Studies with Wild T3, Wild T4, and Kern DKM3 Theodolites," AIAA Paper No. 72-842, 14-16 August 1972.

6. Fondelli, M., "Examination of the Precision of Kern DKM3 Theodolites," Military Geographic Institute, Florence, Italy.

7. Farrenkopf, R.L., "Attitude Determination Software for HEAO," TRW Report HEAO-75-460-177, 10 April 1975.

APPENDIX A

DATA ANALYSIS PROGRAM LISTING FOR THE STRAPDOWN SYSTEM TEST

```
00100       PROGRAM PADS(INPUT,OUTPUT,TAPE1,TAPE2,TAPE4,TAPE5)
00110       COMMON/1/NG,NDELP,NN1
00120       COMMON/2/TIME,TO,TF,DELT,KDELT,X1(4),X1L(4),KSKP
00130       COMMON/3/PIMU(12),TAU(3,6),WM(6),DRFT(6),GY(9,6)
00140       COMMON/4/PHI1(4,4),PHI2(4,3),Q(7,7),QO(4,6),WR(3,2),RP(4,4)
00150       COMMON/5/SSV(27,2),PP(3),B(3,3,3)
00160       COMMON/6/NTP,ICAT,NO,YL(2,2)
00170       COMMON/7/YD(2,2),Y(2,2),U(15),AST(3,3,2),STR(3,2)
00180       COMMON/8/P(7,7),K(2,2),AK(8,2),HMAT(2,7)
00190       DIMENSION GYDAT(500,12),GX1(12),GX2(12),MSTR(12)
00192 C     KTYP=0 - REAL LAB ;KTYP=1 - GYROS REORIENTED;
00194 C     KTYP=2 - IDEAL GYROS
00200       DATA KTYP/1/
00203 C     MSTR(I) DENOTES WHETHER THE I TH VISIBLE STAR WILL BE USED
00204 C     FOR FILTERING; IF SO, MSTR(I)=1
00205       DATA (MSTR(I),I=1,12)/1,1,1,1,1,1,1,1,1,1,1,1/
00206     5 FORMAT(X,7HKTYP = ,I1/)
00210     1 CONTINUE
00212       N7=3
00220 C     REWIND TAPES
00230       REWIND 1
00240       REWIND 2
00250       REWIND 4
00255       REWIND 5
00256       WRITE(2,5) KTYP
00260 C     EFFECTIVELY ELIMINATE THE FIRST DATA LINE
00280       READ(4,2) (GYDAT(1,J),J=1,12)
00310       NN1=3
00320 C     READ IN AND PRINT OUT INITIAL VALUES, SYSTEM PARAMETERS AND RUN
00330 C     CONTROL CONSTANTS
00340       CALL INPUT
00350 C     INITIALIZE COUNTERS AND FLAGS
00360       NXC=KPR=NF=0
00370       IGY=500
00375       MT=0
00380       NO=1
00390       READ(4,2) (GX1(J),J=1,12)
00400 C     BEGINNING OF FILTER LOOP
00410 C     INITIALIZE STATE TRANSITION MATRICES PHI1 AND PHI2
00420    15 CONTINUE
00440       CALL ZERO
00460    20 CONTINUE
```

REPRODUCIBILITY OF THE ORIGINAL PAGE IS POOR

```
00490 C      INDEX, THEN TEST FOR WHETHER NEW FLIGHT GYRO DATA SHOULD BE READ
00500        IGY=IGY+1
00510        IF(IGY.LE.500) GO TO 23
00520        IGY=1
00530        DO 24 I=1,500
00540        READ(4,2) (GX2(J),J=1,12)
00550        DLT=GX2(1)-GX1(1)
00560        GYDAT(I,1)=GX1(1)
00570        DO 17 K=2,4
00580    17  GYDAT(I,K)=(GX2(K)-GX1(K))/DLT*4.8481368E-6
00590        IF(KTYP.EQ.0) GO TO 25
00592        IF(KTYP.EQ.1) GO TO 26
00600        GYDAT(I,2)=-4.68164026E-5
00610        GYDAT(I,3)=-4.49498700E-5
00620        GYDAT(I,4)=4.57512760E-5
00622        GO TO 25
00623    26  CONTINUE
00624        GYDAT(I,2)=GYDAT(I,2)+4.26794875E-5
00625        GYDAT(I,3)=GYDAT(I,3)+2.11571588E-6
00626        GYDAT(I,4)=GYDAT(I,4)+1.97941384E-5
00630    25  CONTINUE
00640        DO 18 K=5,12
00650     18 GYDAT(I,K)=GX1(K)
00660        DO 19 K=1,12
00670    19  GX1(K)=GX2(K)
00680        IF(EOF,4) 23,24
00690    24  CONTINUE
00700 C      FORMAT 2 IS BELSKYS TAPE FORMAT
00710     2  FORMAT(X,F10.3,3(F12.1),F3,X,3(F7.1,X),4(F5.1,X))
00720 C      FORM TIME AND INTEGRATION STEP
00730    23  CONTINUE
00740        DELT=GYDAT(IGY,1)-TIME
00750        TIME=GYDAT(IGY,1)
00760        DO 33 I=1,NG
00770    33  WM(I)=GYDAT(IGY,I+1)
00890 C      TEST FOR END OF RUN
00900        IF(TIME.LT.TF) GO TO 43
00910        STOP
00920    43  CONTINUE
00930 C      ADVANCE STATE PRINT COUNTER
00940        NXC=NXC+1
00950 C      COMPUTE ESTIMATED SPACECRAFT BODY ANGULAR RATES
```

```
00960         CALL GYPCK
00970 C       COMPUTE ESTIMATED SPACECRAFT ATTITUDE
00980         CALL ATT
00990 C       TIME TO PRINT STATE
01000         IF(NXC.LT.NDELP) 44,81
01010    81   CONTINUE
01020 C       FORM ESTIMATED SPACECRAFT ATTITUDE DIRECTION COSINE MATRIX
01030         CALL TRNS
01060 C       PRINT ESTIMATED STATE
01070         CALL Y1PRNT
01140         NXC=0
01150 C       IF KPR=1,THIS PRINT FOLLOWED A FILTER OPERATION
01160         IF(KPR.EQ.1) 48,44
01170    48   KPR=0
01180         GO TO 15
01190    44   CONTINUE
01230 C       TEST IF TRACKER DATA IS PRESENT
01240         IF(GYDAT(IGY,5).GT.0.5) 60,52
01250    52   NF=-KSKP
01260         GO TO 20
01300    60   CONTINUE
01310         IF(GYDAT(IGY,5).LT.1.5) GO TO 601
01312         MT=MT+1
01320         DV1=GYDAT(IGY,11)
01330         DV2=GYDAT(IGY,12)
01340    601  CONTINUE
01350         NF=NF+1
01360         IF(NF.LT.1) GO TO 20
01362 C       TEST WHETHER THIS STAR IS ACCEPTABLE
01364         IF(MSTR(MT).NE.1) GO TO 52
01370         TU=GYDAT(IGY,6)-DV1
01380         TV=GYDAT(IGY,7)-DV2
01390         TAZ=-.0329266874+SSV(4,1)*TU  +SSV(5,1)*TU*TU  +SSV(6,1)*TU**3
01400        1+SSV(7,1)  *TV+SSV(8,1)*TV*TV  +SSV(9,1)*TV**3
01410        2+SSV(10,1)*TU*TV  +SSV(11,1)  *TU*TU*TV+SSV(12,1)  *TU*TV**2
01420         TEL=-.40269706+SSV(13,1)  *TV+SSV(14,1)  *TV*TV+SSV(15,1)
01430        1*TV**3+SSV(16,1)  *TU+SSV(17,1)  *TU*TU+SSV(18,1)  *TU**3
01440        2+SSV(19,1)  *TV*TU+SSV(20,1)  *TU*TV**2+SSV(21,1)  *TV*TU**2
01450         YL(1,2)=Y(1,2)
01460         YL(2,2)=Y(2,2)
01470         Y(1,2) =-TAZ*4.848136681E-6
01480         Y(2,2) =TEL*4.848136681E-6
```

```
01490 C      AIR BEARING TABLE ANGLE COMPUTATION
01500        TD=6.28561512E-4*GYDAT(IGY,8)
01510        ER1=-0.8+1.2*SIN(TD)+0.8*COS(TD)
01520        TBL=-(GYDAT(IGY,8)/2.-ER1)*4.84813681E-6-2.39619449
01530        IF(NF.EQ.1) 62,61
01540    62  CALL STRCHK(IBL)
01550    61  CONTINUE
01560 C      COMPUTE INERTIAL STAR DIR. COS.
01570        CALL STARDC(STR(1,1),ICAT,IBL)
01580 C      COMPUTE EST. TRACKER OUTPUT
01590        CALL TRAC
01600        CALL TRCFLT
01610        IF(NF.LT.10) GO TO 20
01620 C      START FILTERING
01630 C      COMPUTE TRACKER MEASURMENT RESIDUAL NO M
01640        W1=SQRT((YD(1,2)-YD(1,1))**2+(YD(2,2)-YD(2,1))**2)
01650 C      DOES IT FALL WITHIN AN ALLOWABLE ERROR
01660        IF(W1.LT..1) GO TO 70
01670    72  PRINT 3,W1
01680     3  FORMAT(20HMEASUREMENT ERROR IS,2X,E13.6,6H, PUNT)
01690        STOP
01700    70  CONTINUE
01705        WRITE(5,4) TIME,W1,N7
01706    4   FORMAT(2(2X,E13.6),2X,I1)
01710        CALL X1PRNT
01720        NF=-KSKP
01730 C      FORM STATE NOISE ERROR COVARIANCE MATRIX
01740        CALL QMAT
01750 C      ALTER STATE TRANSITION MATRIX TO DEAL WITH 3 RATHER THAN 4
01760 C      ATTITUDE VARIABLES
01770        CALL PRFIL
01780 C      PROPAGATE STATE ERROR COVARIANCE MATRIX
01790        CALL FILT
01795        CALL PRNT(1)
01800 C      FORM MEASURMENT MATRIX
01810        CALL HMTRX
01820 C      FORM MEASUREMENT NOISE COVARIANCE MATRIX
01830        CALL RMAT
01840 C      APPLY KALMAN ALGORITHM
01850        CALL EFILT
01860 C      UPDATE STATE
01870        CALL PDFTL
```

```
      ADVANCE FILTER COUNTER
      NPC=NPC+1
C     TIME TO PRINT STATE ERROR COVARIANCE MATRIX
      IF(NPC-NPP) 15,60,80
   80 CONTINUE
      CALL PRNT(1)
      KPR=1
      GO TO 81
      END
C
C
      SUBROUTINE TRNS
C     COMPUTE DIRECTION COSINES OF SPACECRAFT ATTITUDE RELATIVE TO
C     ATTITUDE REFERENCE AXES(ECI COORDINATES)
      COMMON/2/TIME,TO,TF,DELT,KDELT,X1(4),X1L(4)
      COMMON/5/SSV(27,2),PP(3),B(3,3,2)
      DIMENSION T(4,4)
C     TRANSFORM EULER SYMMETRIC PARAMETERS TO DIRECTION COSINES RELATIVE
C     TO ECI AXES
      DO 10 I = 1,3
      T(I,I) = X1(4)
   10 CONTINUE
      T(1,2)=X1(3)
      T(1,3)=-X1(2)
      T(1,4)=X1(1)
      T(2,3)=X1(1)
      T(2,4)=X1(2)
      T(3,4)=X1(3)
      T(2,1) = -T(1,2)
      T(3,1) = -T(1,3)
      T(3,2) = -T(2,3)
      T(4,1) = T(1,4)
      T(4,2) = T(2,4)
      T(4,3) = T(3,4)
      T(4,4) = -X1(4)
      DO 40 I=1,3
      DO 40 J=1,3
      B(I,J,1)=0.
      DO 40 K=1,4
      B(I,J,1)=   B(I,J,1 )+T(I,K)*T(K,J)
   40 CONTINUE
      RETURN
```

```
02300       END
02310 C
02320 C
03100       SUBROUTINE X1PRNT
03110 C     PRINTS ESTIMATED STATE VECTOR AND S/C ATTITUDE MATRIX
03120       COMMON/1/NG,NDELP,NN1
03130       COMMON/2/TIME,TO,TF,DELT,KDELT,X1(4),X1L(4)
03140       COMMON/3/PIMU(12),TAU(3,6),WM(6),DRFT(6),GY(9,6)
03150       COMMON/5/SSV(27,2),PP(3),B(3,3,2)
03160       DIMENSION C(3,3),D(4)
03170       CA=206264.81
03175       N7=1
03180 C     PRINT HEADING AND TIME
03190       WRITE(2,30) TIME
03200       CALL LABATT
03210       DO 60 I=1,3
03220       DO 60 J=1,3
03230       C(I,J)=0.
03240       DO 60 K=1,3
03250    60 C(I,J)=C(I,J)+B(I,K,1)*B(J,K,2)
03260       D(1)=CA*C(2,3)
03270       D(2)=CA*C(3,1)
03280       D(3)=CA*C(1,2)
03290       D(4)=SQRT(D(1)**2+D(3)**2)
03300 C     PRINT ESTIMATED EULER PARAMETERS AND S/C AND LAB ATTITUDE MATRIX
03310       WRITE(2,20) (I,X1(I),B(I,1,1)  ,B(I,2,1),B(I,3,1),
03320      1B(I,1,2),B(I,2,2),B(I,3,2),D(I),I=1,3)
03330       WRITE(2,22) X1(4)  ,D(4)
03340       WRITE(5,23) TIME,D(4),N7
03350    23 FORMAT(2(2X,E13.6),2X,I1)
03390 C     PRINT HEADING
03400       WRITE(2,50)
03420       DO 45 I=1,NN1
03520       PIMU1A=CA*PIMU(I)
03530       WRITE(2,21) I,PIMU1A
03570    45 CONTINUE
03590    30 FORMAT(X///8H TIME = ,E16.9//30X,
03600      150HESTIMATED SPACECRAFT ATTITUDE RELATIVE TO ECI AXES//X,
03610      234HNO.,X,11HEULER PARAM,12X,17HATTITUDE ESTIMATE,27X,
03620      312HLAB ATTITUDE,12X,12HR,P,Y,RSS ER//)
03630    20 FORMAT(X,I1,2X,F12.9,X,3(X,F12.9),2X,3(X,F12.9),2X,F9.2)
03640    22 FORMAT(X,1H4,2X,F12.9,83X,F9.2)
```

```
03650    50  FORMAT(X/14X,26HESTIMATED GYRO BIAS VECTOR/)
03660    21  FORMAT(15X,I1,4X,E12.5)
03670        RETURN
03680        END
03690 C
03700 C
03710        SUBROUTINE PRNT(K1)
03720        COMMON/1/NG,NDELP,NN1
03730        COMMON/2/TIME,TO,TF,DELT,KDELT,X1(4),X1L(4)
03740        COMMON/6/NTP,ICAT,NG,YL(2,2)
03750        COMMON/7/YD(2,2),Y(2,2),U(15),AST(3,3,2),STR(3,2)
03760        COMMON/8/P(7,7),R(2,2),AK(8,2),HMAT(2,7)
03770        DIMENSION PT(3,3),F(3,3),TP(3,3)
03775        N7=7
03780 C      PRINTS THE ERROR COVARIANCE MATRIX,UPPER LEFT 3 BY 3 IN
03790 C      SMALL ANGLE FORM
03800 C      SAVE UPPER 3 BY 3
03810        DO 40 I=1,3
03820        DO 40 J=1,3
03830    40  PT(I,J)=P(I,J)
03840 C      CONVERT UPPER 3 BY 3 OF P MATRIX TO SMALL ANGLE FORM
03850        F(1,1)=2.*(X1(4) +X1(1)**2/X1(4))
03860        F(1,2)=2.*(X1(3)+X1(1)*X1(2)/X1(4))
03870        F(1,3)=-2.*(X1(2)-X1(1)*X1(3)/X1(4))
03880        F(2,1)=-2.*(X1(3)-X1(2)*X1(1)/X1(4))
03890        F(2,2)=2.*(X1(4) +X1(2)**2/X1(4))
03900        F(2,3)=2.*(X1(1)+X1(2)*X1(3)/X1(4))
03910        F(3,1)=2.*(X1(2)+X1(1)*X1(3)/X1(4))
03920        F(3,2)=-2.*(X1(1)-X1(2)*X1(3)/X1(4))
03930        F(3,3)=2.*(X1(4) +X1(3)**2/X1(4))
03940        DO 70 I=1,3
03950        DO 70 J=1,3
03960        TP(I,J)=0.
03970        DO 70 K=1,3
03980    70  TP(I,J)=TP(I,J)+P(I,K)*F(J,K)
03990        DO 75 I=1,3
04000        DO 75 J=1,3
04010        P(I,J)=0.
04020        DO 75 K=1,3
04030    75  P(I,J)=P(I,J)+F(I,K)*TP(K,J)
04070        NA = NN1+3
04100 C      PRINT HEADING
```

```
04110     10 WRITE(2,1)
04120      1 FORMAT(1H1,50X,6HP MATRIX)
04130        DO 20 I=1,NA
04140        WRITE(2,3) I
04150      3 FORMAT(/8X,4HROW ,I2/)
04160 C      PRINT P MATRIX
04170     20 WRITE(2,30) (P(I,J),J=1,NA)
04180 30     FORMAT(3X,6E17.6)
04190        IF(K1.EQ.0) GO TO 44
04200 C      PRINT STAR NUMBER
04210     50 WRITE(2,45) ICAT
04220     45 FORMAT( /  7X,14HSTAR NUMBER = ,I3)
04230        TST2=ATAN2(YD(2,2),1.)
04240        TST1=ATAN2(YD(1,2)*COS(TST2),1.)
04250        TT=ATAN2(YD(2,1),1.)
04260        DEL2=(TST2-TT)*206264.81
04270        DEL1=(TST1-ATAN2(YD(1,1)*COS(TT),1.))*206264.81
04280        WRITE(2,60) TST1,DEL1,TST2,DEL2
04290     60 FORMAT(3X,37HTRACKER OUTPUT ANGLES AND MEAS. ERROR/
04300       15X,7HAZIMUTH,2X,E11.4,5H RAD.,3X,F10.3,
04310       27H ARCSEC/6X,5HELEV ,3X,E11.4,5H RAD.,3X,F10.3,
04320       37H ARCSEC)
04330    44  CONTINUE
04340        AT=SQRT(P(1,1)        +P(3,3))*206264.81
04350        WRITE(2,39) AT
04360     39 FORMAT(26H SQRT OF POINTING TRACE = ,F10.3,9H ARC SEC.)
04365        WRITE(5,8) TIME,AT,N7
04366    8   FORMAT(2(2X,E13.6),2X,I1)
04370        DISPLAY AT
04380 C      RESTORE P MATRIX
04390        DO 43 I=1,3
04400        DO 43 J=1,3
04410    43  P(I,J)=PT(I,J)
04420        RETURN
04430        END
04440 C
04450 C
04930        SUBROUTINE INPUT
04940 C      READS IN AND PRINTS INITIAL VALUES, SYSTEM PARAMETERS,RUN CONTROL
04950 C      CONSTANTS, AND CONVERTS SPECIFIED ANGLES TO RADIANS
04960        COMMON/1/NG,NDELP,NN1
04970        COMMON/2/TIME,TC,TF,DELT,KDELT,X1(4),X1L(4),KSKP
```

```
04980         COMMON/3/PIMU(12),TAU(3,6),WM(6),DRFT(6),GY(9,6)
04990         COMMON/4/PHI1(4,4),PHI2(4,3),Q(7,7),QQ(4,6),WR(3,2),RP(4,4)
05000         COMMON/5/SSV(27,2),PP(3),B(3,3,2)
05010         COMMON/6/NTR,ICAT,NG,YL(2,2)
05020         COMMON/7/YD(2,2),Y(2,2),U(15),AST(3,3,2),STR(3,2)
05030         COMMON/8/P(7,7),R(2,2),AK(8,2),HMAT(2,7)
05040         DIMENSION MSV(4,32),C(3,3),T(3)
05050         NN=NN1+3
05060         DO 112 I=1,NN
05070         DO 112 J=1,NN
05080   112   P(I,J)=Q(I,J)=0.
05090 C       READ INPUT FLAGS DEFINING TYPE OF RUN AAND PRINT OPTIONS
05100         READ(1,2) NTR,NG
05110     2   FORMAT(I1)
05120         READ(1,3) NDELP,KSKP
05130     3   FORMAT(I3)
05150 C       READ NOMINAL STAR TRACKER TRANSFORMATION MATRIX
05160         DO 20 K=1,NTR
05170    20   READ(1,4) ((AST(I,J,K),J=1,3),I=1,3)
05180     4   FORMAT(F9.6)
05200 C       READ STAR SENSOR PARAMETERS
05210         DO 24 J=1,NTR
05220         READ(1,6) (SSV(I,J),I=1,21)
05230    24   READ(1,5) (SSV(I,J),I=22,27)
05240     5   FORMAT(F9.3)
05250 C       READ GYRO PARAMETERS
05260         DO 25 J=1,NG
05270    25   READ(1,6) (GY(I,J),I=1,9)
05280 C       READ ESTIMATED INITIAL RATES
05300         DO 27 I=1,3
05310    27   READ(1,6) PP(I)
05330     6   FORMAT(F12.6)
05340 C       READ INITIAL 4 PARAMETER ATTITUDE
05350         READ(1,4) (X1(I),I=1,4)
05360    22   CONTINUE
05370 C       READ INITIAL AND FINAL TIMES AND INTEGRATION STEP SIZE
05380         READ(1,6) T0,TF,DELT
05390 C       READ ERROR COVARIANCE INITIAL DIAGONAL ELEMENTS
05400 C       UNITS ARE RAD.,SEC
05410         DO 28 I=1,NN
05420    28   READ(1,6) P(I,I)
05470 C
```

```
05490 C      TEMPORARY INPUT PRINT ROUTINE
05500        WRITE(2,12)
05510    12  FORMAT(1H1)
05520        WRITE(2,7) NTR,NG,NDELP
05540     7  FORMAT( 3(X,I3)//)
05560        DO 31 J=1,NG
05570    31  WRITE(2,8) (GY(I,J),I=1,9)
05580    8   FORMAT(9(X,F10.3))
05590        WRITE(2,10)
05600    10  FORMAT(/)
05610        DO 32 K=1,NTR
05620    32  WRITE(2,9)((AST(I,J,K),J=1,3),I=1,3)
05630     9  FORMAT(9(X,F9.6))
05640        WRITE(2,10)
05650        DO 34 J=1,NTK
05670    34  WRITE(2,11) (SSV(I,J),I=1,27)
05680    11  FORMAT(9(X,F10.3))
05690        WRITE(2,10)
05700        DO 35 J=1,3
05720    35  WRITE(2,8) PP(J)
05730    41  CONTINUE
05740        WRITE(2,10)
05760        WRITE(2,8) (X1(I),I=1,4)
05770        WRITE(2,10)
05780        DO 37 K=1,NN
05790    37  WRITE(2,9) P(K,K)
05800        WRITE(2,10)
05810        WRITE(2,8) TO,TF,DELT
05820        WRITE(2,10)
05880 C
05890 C      INITIALIZE PROBLEM TIME
05900        TIME = TO
05910     15 FORMAT(1H1)
05920        WRITE(2,15)
05930 C      CONVERT ANGLES TO RADIANS
05940        CF = 4.848136E-06
05950        CFSQ = CF*CF
05970        DO 130 J=1,NTR
05980        SSV(24,J)=SSV(24,J)*CF
05990        SSV(25,J)=SSV(25,J)*CF
06000    130 CONTINUE
06020        DO 135 J=1,NG
```

```
06030        GY(1,J)=GY(1,J)*CF
06040        DO 135 I=7,9
06050        GY(I,J)=GY(I,J)*CF
06060    135 CONTINUE
06070        CALL INITIAL
06080 C      PRINT ERROR COVARIANCE MATRIX
06090        CALL PRNT(0)
06100 C      PRINT INITIAL STATE VECTOR
06110        CALL TRNS
06130        CALL XIPRNT
06180        RETURN
06190        END
06200 C
06210 C
06220        SUBROUTINE ZERO
06230 C      INITIALIZES STATE TRANSITION MATRICES PHI1 AND PHI2 AFTER EACH
06240 C      FILTER UPDATE
06250        COMMON/1/NG,NDELP,NN1
06260        COMMON/2/TIME,TO,TF,DELT,KDELT,X1(4),X1L(4)
06270        COMMON/4/PHI1(4,4),PHI2(4,3),Q(7,7),QO(4,6),WR(3,2),RP(4,4)
06280 C      RETAIN FILTER UPDATED VALUES OF EULER PARAMETERS FOR NEXT FILTER
06290 C      OPERATION
06300        DO 21 I=1,4
06310        X1L(I)=X1(I)
06320 C      SET PHI1 ELEMENTS EQUAL TO ZERO
06330        DO 22 J=1,4
06340        PHI1(I,J)=0.
06350     22 CONTINUE
06360 C      SET PHI2 ELEMENTS EQUAL TO ZERO
06370        DO 23 J=1,NN1
06380        PHI2(I,J)=0.
06390     23 CONTINUE
06400 C      SET PHI1 DIAGONAL ELEMENTS EQUAL TO ONE
06410        PHI1(I,I)=1.
06420     21 CONTINUE
06430 C      SET Q MATRIX COMPUTATION INTERVAL COUNTER TO ZERO
06440        KDELT=0
06450 C      SET Q MATRIX ELEMENTS TO ZERO
06460        DO 10 I=1,7
06470        DO 10 J=1,7
06480    10  Q(I,J)=0.
06490        RETURN
```

```
      END
C
C
      SUBROUTINE INITIAL
      COMMON/1/NG,NDELP,NN1
      COMMON/2/TIME,TO,TF,DEL1,KDELT,X1(4),X1L(4)
      COMMON/3/PIMU(12),TAU(3,6),WM(6),DRFT(6),GY(9,6)
      COMMON/4/PHI1(4,4),PHI2(4,3),Q(7,7),QO(4,6),WR(3,2),RP(4,4)
      COMMON/5/SSV(27,2),PP(3),B(3,3,2)
      COMMON/6/NTR,ICAT,NO,YL(2,2)
      COMMON/8/P(7,7),R(2,2),AK(8,2),HMAT(2,7)
      DIMENSION TP1(3,3),TP2(3,3),TP(3,12),TP4(6,3)
C     COMPUTE GYRO WEIGHTING MATRIX, TAU
      DO 12 I=1,NG
      DO 12 J=1,3
   12 TP4(I,J)=(1.+GY(2,I))*GY(3+J,I)
      DO 10 I=1,3
      DO 10 J=1,3
      TP1(I,J)=0.
      DO 10 K=1,NG
      TP1(I,J)=TP1(I,J)+TP4(K,I)*TP4(K,J)
   10 CONTINUE
      DEL=TP1(1,1)*TP1(2,2)*TP1(3,3)+TP1(1,2)*TP1(2,3)*TP1(3,1)
     1+TP1(1,3)*TP1(2,1)*TP1(3,2)-TP1(1,3)*TP1(2,2)*TP1(3,1)
     2-TP1(1,1)*TP1(2,3)*TP1(3,2)-TP1(1,2)*TP1(2,1)*TP1(3,3)
      DL=1./DEL
      TP2(1,1)=(TP1(2,2)*TP1(3,3)-TP1(3,2)*TP1(2,3))*DL
      TP2(1,2)=(TP1(3,2)*TP1(1,3)-TP1(1,2)*TP1(3,3))*DL
      TP2(1,3)=(TP1(1,2)*TP1(2,3)-TP1(2,2)*TP1(1,3))*DL
      TP2(2,1)=(TP1(3,1)*TP1(2,3)-TP1(2,1)*TP1(3,3))*DL
      TP2(2,2)=(TP1(1,1)*TP1(3,3)-TP1(1,3)*TP1(3,1))*DL
      TP2(2,3)=(TP1(2,1)*TP1(1,3)-TP1(1,1)*TP1(2,3))*DL
      TP2(3,1)=(TP1(2,1)*TP1(3,2)-TP1(3,1)*TP1(2,2))*DL
      TP2(3,2)=(TP1(3,1)*TP1(1,2)-TP1(1,1)*TP1(3,2))*DL
      TP2(3,3)=(TP1(1,1)*TP1(2,2)-TP1(2,1)*TP1(1,2))*DL
      DO 15 I=1,3
      DO 15 J=1,NG
      TAU(I,J)=0.
      DO 15 K=1,3
      TAU(I,J)=TAU(I,J)+TP2(I,K)*TP4(J,K)
   15 CONTINUE
C     INITIALIZE PAST DATA
```

```
06930          DO 20 I=1,NG
06940          DO 20 J=1,2
06950    20    OPRT(I)=GY(1,I)
06960          DO 30 I=1,3
06980    30    WP(I,1)=WP(I,2)=PP(I)
06990 C        COMPUTE INITIAL GYROPACK PARAMETERS, PIMU
07010          DO 40 I=1,3
07020          PIMU(I)=0.
07030          DO 40 J=1,NG
07040          PIMU(I)=PIMU(I)+TAU(I,J)*(1.+GY(2,J))*GY(1,J)
07050    40    CONTINUE
07070          L=3
07080          DO 50 I=1,3
07090          DO 60 J=1,3
07100          L=L+1
07110          PIMU(L)=0.
07120          DO 60 K1=1,NG
07130          PIMU(L)=PIMU(L)+TAU(I,K1)*(1.+GY(2,K1))*GY(3+J,K1)
07140    60    CONTINUE
07150          PIMU(4*I)=PIMU(4*I)-1.
07160    50    CONTINUE
07170 C        COMPUTE TAU*TAU-T*SIG-SQ FOR USE IN Q
07180          DO 65 J=1,NG
07190          TP3=SQRT(GY(7,J)**2*100.00*DELT+GY(9,J)**2)  /100./DELT
07200          DO 65 I=1,3
07210          TP(I,J+6)=TAU(I,J)*GY(8,J)  *SQRT(100.*DELT)
07220    65    TP(I,J)=TAU(I,J)*TP3
07230          DO 70 I=1,3
07240          DO 70 J=1,3
07250          QQ(I,J)=0.
07260          QQ(I,J+3)=0.
07270          DO 70 K=1,NG
07280          QQ(I,J+3)=QQ(I,J+3)+TP(I,K+6)*TP(J,K+6)
07290    70    QQ(I,J)=QQ(I,J)+TP(I,K)*TP(J,K)*2500.*DELT*DELT
07370 C        CONVERT UPPER LEFT 3 BY 3 OF P MATRIX TO EULER SYMMETRIC
07380 C        PARAMETER FORM. ORIGINAL P ASSUMED DIAGONAL.
07390          Z1=P(1,1)
07400          Z2=P(2,2)
07410          Z3=P(3,3)
07420          P(1,1)=.25*(Z1*X1(4)**2+Z2*X1(3)**2+Z3*X1(2)**2)
07430          P(1,2)=P(2,1)=.25*((Z1-Z2)*X1(4)*X1(3)-Z3*X1(1)*X1(2))
07440          P(1,3)=P(3,1)=.25*((Z3-Z1)*X1(4)*X1(2)-Z2*X1(1)*X1(3))
```

```
07450         P(2,2)=.25*(Z1*X1(3)**2+Z2*X1(4)**2+Z3*X1(1)**2)
07460         P(2,3)=P(3,2)=.25*((Z2-Z3)*X1(1)*X1(4)-Z1*X1(2)*X1(3))
07470         P(3,3)=.25*(Z1*X1(2)**2+Z2*X1(1)**2+Z3*X1(4)**2)
07600         RETURN
07610         END
07620 C
07630 C
07640         SUBROUTINE STRCHK(TBL)
07650         COMMON/1/NG,NDELP,NN1
07660         COMMON/2/TIME,TO,TF,DELT,KDELT,X1(4),X1L(4)
07670         COMMON/5/SSV(27,2),PP(3),B(3,3,2)
07680         COMMON/6/NTR,ICAT,NO,YL(2,2)
07690         COMMON/7/YD(2,2),Y(2,2),U(15),AST(3,3,2),STR(3,2)
07700         DIMENSION TP(3),A(3,3)
07710         I=0
07720         CR=10.
07730    40   I=I+1
07740         IF(I.GT.3) GO TO 100
07750 C       FORM STAR I INERTIAL DIR.COS.
07760         CALL STARDC(STR(1,1),I,TBL)
07770 C       FORM STAR DIR. COS. IN STA AXES
07780         DO 50 K=1,3
07790         U(K)=0.
07800         DO 50 J=1,3
07810    50   U(K)=U(K)+B(K,J,1)*STR(J,1)
07820 C       FORM MEAS. RESIDUAL
07830         RR=(Y(1,2) +U(1)/U(2))**2+(Y(2,2) -U(3)/U(2))**2
07840         IF(RR.GT.CR) GO TO 40
07850         CR=RR
07860         ICAT=I
07870         GO TO 40
07880   100   CONTINUE
07890         YL(1,1)=YL(1,2)=Y(1,1)=YD(1,1)=YD(1,2)=Y(1,2)
07900         YL(2,1)=YL(2,2)=Y(2,1)=YD(2,1)=YD(2,2)=Y(2,2)
07910         RETURN
07920         END
07930 C
07940 C
07950         SUBROUTINE STARDC(C,ISTR,TBL)
07960         COMMON/2/TIME,TO,TF,DELT,KDELT,X1(4),X1L(4)
07970         COMMON/5/SSV(27,2),PP(3),B(3,3,2)
07980         DIMENSION C(3),TP(3,3),RN(3),D(3)
```

C-3

```
07990 C      DEFINE STAR DIR. COS. IN LAB(STA) AXES
08000        TP(1,1)=1.
08010        TP(1,2)=TP(1,3)=0.
08020        TP(2,1)=.9999902
08030        TP(2,2)=2.424E-6
08040        TP(2,3)=4.41956E-3
08050        TP(3,1)=.9999986
08060        TP(3,2)=-2.424E-6
08070        TP(3,3)=-1.580493E-3
08080        CALL TPMS
08090 C      FORM MIRROR OUTWARD NORMAL
08100 C      TBL=0 ASSUMES NORMAL ALONG X2
08110        RN(1)=-SIN(TBL)
08120        RN(2)=COS(TBL)
08130        RN(3)=0.
08140 C      FORM INPUT TO STA IN LAB AXES USING REFLECTION FORMULA
08150        T1=RN(1)*TP(ISTR,1)+RN(2)*TP(ISTR,2)+RN(3)*TP(ISTR,3)
08160        DO 10 I=1,3
08170   10   D(I)=TP(ISTR,I)-2.*T1*RN(I)
08180 C      FORM LAB INERTIAL ATTITUDE
08190        CALL LABATT
08200 C      CONVERT TO INERTIAL COORD.
08210        DO 20 I=1,3
08220        C(I)=0.
08230        DO 20 J=1,3
08240   20   C(I)=C(I)+B(J,I,2)*D(J)
08250        RETURN
08260        END
08270 C
08280 C
08290        SUBROUTINE LABATT
08300        COMMON/2/TIME,T0,TF,DELT,KDELT,X1(4),X1L(4)
08310        COMMON/5/SSV(27,2),PP(3),B(3,3,2)
08320        BTA=1.-COS(7.27220522E-5*TIME)
08330        R1=0.
08340        R2=0.829980841
08350        R3=0.557791899
08360        AL=SIN(7.27220522E-5*TIME)
08370        B(1,1,2)=1.-BTA*(R2**2+R3**2)
08380        B(1,2,2)=AL*R3+BTA*R1*R2
08390        B(1,3,2)=-AL*R2+BTA*R1*R3
08400        B(2,1,2)=-AL*R3+BTA*R1*R2
```

```
      R(2,2,2)=1.-BTA*(R1**2+R3**2)
      R(2,3,2)=AL*R1+BTA*R2*R3
      R(3,1,2)=AL*R2+BTA*R1*R3
      R(3,2,2)=-AL*R1+BTA*R2*R3
      R(3,3,2)=1.-BTA*(R1**2+R2**2)
      RETURN
      END
C
C
      SUBROUTINE GYPCK
      COMMON/1/NG,NDELP,NN1
      COMMON/3/PIMU(12),TAU(3,6),WM(6),DRFT(6),GY(9,6)
      COMMON/4/PHI1(4,4),PHI2(4,3),Q(7,7),QQ(4,6),WR(3,2),RP(4,4)
      DIMENSION TP(3)
C     PROVIDES ESTIMATED S/C RATES BASED UPON COMPENSATED GYROS.
      DO 10 I=1,3
C     SHIFT PREVIOUS RATE DATA BACK ONE STEP
      WR(I,2)=WR(I,1)
C     COMPUTE NEW GYRO PACKAGE RATE ESTIMATE
      TP(I)=-PIMU(I)
      DO 10 J=1,NG
      TP(I)=TP(I)+TAU(I,J)*WM(J)
   10 CONTINUE
      L=3
      DO 20 I=1,3
      WR(I,1)=TP(I)
      DO 20 J=1,3
      L=L+1
      WR(I,1)=WR(I,1)-PIMU(L)*TP(J)
   20 CONTINUE
      RETURN
      END
C
C
      SUBROUTINE ATT
C     PERFORMS NUMERICAL INTEGRATION TO DETERMINE SPACECRAFT ATTITUDE
C     AS REPRESENTED BY EULER SYMMETRIC PARAMETERS
      COMMON/2/TIME,TO,TF,DELT,KDELT,X1(4),X1L(4)
      COMMON/4/PHI1(4,4),PHI2(4,3),Q(7,7),QQ(4,6),WR(3,2),RP(4,4)
      DIMENSION T(5),TP(3)
      DO 20 I=1,3
   20 TP(I)=.5*(WR(I,1)+WR(I,2))
```

```
09300 C      COMPUTE S(0) FOR USE IN RP MATRIX
09310        T(2)=(TP(1)**2+TP(2)**2+TP(3)**2)*DELT**2/4.
09320        T(1) = SQRT(T(2))
09330        T(2) = COS(T(1))
09340        T(3)=.5
09350        IF(ABS(T(1)).LE.1.E-20) GO TO 6
09360        T(3) = SIN(T(1))
09370        T(3)=T(3)/(2.*T(1))
09380      6 CONTINUE
09390 C      FORM RP MATRIX FOR PROPAGATING EULER PARAMETERS
09400        RP(1,2)=T(3)*TP(3)*DELT
09410        RP(1,3)=-T(3)*TP(2)*DELT
09420        RP(1,4)=T(3)*TP(1)*DELT
09430        RP(2,3)=RP(1,4)
09440        RP(2,4)=-RP(1,3)
09450        RP(3,4)=RP(1,2)
09460        DO 10 I=1,4
09470        RP(I,I)=-T(2)
09480        DO 10 J=1,I
09490        RP(I,J)=-RP(J,I)
09500     10 CONTINUE
09530        CALL PHI
09550 C      PROPAGATE EULER PARAMETERS
09560        DO 12 I=1,4
09570        T(I)=0.
09580        DO 12 J=1,4
09590        T(I)=T(I)+RP(I,J)*X1(J)
09600     12 CONTINUE
09610 C      NORMALIZE EULER PARAMETERS
09620        T(5) = SQRT(T(1)**2+T(2)**2+T(3)**2+T(4)**2)
09630        DO 14 I=1,4
09640        X1(I)=T(I)/T(5)
09650     14 CONTINUE
09660        RETURN
09670        END
09680 C
09690 C
09700        SUBROUTINE PHI
09710 C      COMPUTES THE STATE TRANSITION MATRICES PHI1 AND PHI2
09720        COMMON/1/NG,NDELP,NN1
09730        COMMON/2/TIME,TO,TF,DELT,KDELT,X1(4),X1L(4)
09740        COMMON/4/PHI1(4,4),PHI2(4,3),G(7,7),QQ(4,6),WR(3,2),RP(4,4)
```

```
      DIMENSION W(4),T1(3,12),PK(4,3),PHI2T(4,12),TP1(7,7),TP2(7,7)
      DIMENSION RP(7,7)
C     COMPUTE PHI1
      DO 10 J=1,4
      DO 11 I=1,4
      W(I)=0.
      DO 11 K=1,4
      W(I)=W(I)+RP(I,K)*PHI1(K,J)
   11 CONTINUE
      DO 10 I=1,4
      PHI1(I,J)=W(I)
   10 CONTINUE
C     COMPUTE PHI2
      DO 42 I=1,4
      DO 42 J=1,NN1
      PHI2T(I,J)=0.
      DO 42 K=1,4
   42 PHI2T(I,J)=PHI2T(I,J)+RP(I,K)*PHI2(K,J)
      DO 14 I=1,3
      PK(I,I)=X1(4)
   14 CONTINUE
      PK(1,2)=-X1(3)
      PK(1,3)=X1(2)
      PK(2,3)=-X1(1)
      PK(2,1)=X1(3)
      PK(3,1)=-X1(2)
      PK(3,2)=X1(1)
      PK(4,1)=-X1(1)
      PK(4,2) = -X1(2)
      PK(4,3)=-X1(3)
      DO 30 I=1,3
      DO 31 J=1,3
   31 T1(I,J)=0.
   30 T1(I,I)=-1.
      J1=1
      DO 19 J = 1,3
      DO 22 I=1,4
      TZ = 0.
      DO 23 K=1,3
      TZ = TZ+PK(I,K)*T1(K,J)
   23 CONTINUE
      PHI2(I,J1) = PHI2T(I,J1)+TZ
```

```
10310     22 CONTINUE
10320        J1=J1+1
10330     19 CONTINUE
10350 C      UPDATE Q IF TIME IS APPROPRIATE
10360        KDELT=KDELT+1
10370        IF(KDELT.LT.100) GO TO 50
10380        KDELT=0
10390        DO 55 I=1,4
10400        DO 55 J=1,3
10410        TP2(I,J)=0.
10420        DO 55 K=1,3
10430     55 TP2(I,J)=TP2(I,J)+PK(I,K)*QQ(K,J)
10440        DO 60 I=1,4
10450        DO 60 J=1,4
10460        TP1(I,J)=0.
10470        DO 60 K=1,3
10480     60 TP1(I,J)=TP1(I,J)+TP2(I,K)*PK(J,K)
10490        DO 61 I=5,7
10500        DO 61 J=1,4
10510     61 TP1(I,J)=TP1(J,1)=0.
10520        DO 62 I=5,7
10530        DO 62 J=5,7
10540     62 TP1(I,J)=QQ(I-4,J-1)
10550        T9=PP(2,1)**2+PP(3,1)**2+PP(4,1)**2
10560        T9=SQRT(1.-10000.*T9)
10570        DO 63 I=1,4
10580        DO 64 J=1,4
10590        RQ(I,J)=PP(I,J)*100.
10600     64 RQ(I+3,J)=0.
10610        DO 65 J=1,3
10620        RQ(I,J+4)=-DELT*PK(I,J)*50.
10630     65 RQ(I+3,J+4)=0.
10640        RQ(I+3,I+3)=1.
10650        RQ(I,I)=T9
10660     63 CONTINUE
10670        DO 66 I=1,7
10680        DO 66 J=1,7
10690        TP2(I,J)=0.
10700        DO 66 K=1,7
10710     66 TP2(I,J)=TP2(I,J)+Q(I,K)*RC(J,K)
10720        DO 67 I=1,7
10730        DO 67 J=1,7
```

```
10740          Q(I,J)=TP1(I,J)
10750          DO 67 K=1,7
10760     67   Q(I,J)=Q(I,J)+RC(I,K)*TP2(K,J)
10770     50   CONTINUE
10780  C       PHI2 MUST STILL BE MULTIPLIED BY DELT/2 IN PRFIL
10790          RETURN
10800          END
10810  C
10820  C
10830          SUBROUTINE QMAT
10840  C       FORM THE STATE NOISE COVARIANCE MATRIX
10850          COMMON/1/NG,NDELP,NN1
10860          COMMON/4/PHI1(4,4),PHI2(4,3),Q(7,7),QQ(4,6),WR(3,2),RP(4,4)
10870          DIMENSION TP1(7,7)
10880  C       PROPERLY PACK Q MATRIX
10890          DO 10 I=1,7
10900          DO 10 J=1,7
10910     10   TP1(I,J)=Q(I,J)
10920          J3=3
10930          DO 15 I=1,3
10940          J1=3
10950          DO 17 J=1,3
10970          J1=J1+1
10980          Q(I,J1)=Q(J1,I)=TP1(I,J+4)
10990     17   CONTINUE
11010          J3=J3+1
11020          J2=3
11030          DO 16 J=1,3
11050          J2=J2+1
11060          Q(J3,J2)=TP1(I+4,J+4)
11070     16   CONTINUE
11080     15   CONTINUE
11160          RETURN
11170          END
11180  C
11190  C
11200          SUBROUTINE TRAC
11210  C       COMPUTES TRACKER OUTPUT ANGLES FROM ATTITUDE AND
11220  C       TRACKER IDENTIFICATION NUMBER
11230          COMMON/2/TIME,TO,TF,DELT,KDELT,X1(4),X1L(4)
11240          COMMON/5/SSV(27,2),PP(3),B(3,3,2)
11250          COMMON/6/NTP,ICAT,NO,YL(2,2)
```

```
11260         COMMON/7/YD(2,2),Y(2,2),U(15),AST(3,3,2),STR(3,2)
11270         DIMENSION T(6),C(3,3),TT(3)
11280         YL(1,1)=Y(1,1)
11290         YL(2,1)=Y(2,1)
11300         CALL TRNS
11400 C       COMPUTE TRACKER TRANSFORMATION RELATIVE TO ECI
11410         DO 80 I=1,3
11420         DO 80 J=1,3
11430         C(I,J)=0.
11440         DO 80 K=1,3
11450         C(I,J) =C(I,J)+AST(I,K,NO)*B(K,J,1)
11460      80 CONTINUE
11470 C       COMPUTE STAR DIRECTION COSINES IN TRACKER AXES
11480         DO 90 I=1,3
11490         U(I) = C(I,1)*STR(1,1)+C(I,2)*STR(2,1)+C(I,3)*STR(3,1)
11500      90 CONTINUE
11620         U(4)=U(1)/U(2)
11630         U(5)=U(3)/U(2)
11640         U(6)=U(4)*U(5)
11650         U(7)=U(4)**2
11660         U(8)=U(5)**2
11820 C       COMPUTE TRACKER OUTPUT IF IT HAD INFINITE BANDWIDTH (INTERVAL AVE.)
11830         Y(1,1 )=(-U(4)+     U(6)*SSV(1,NO)   +U(5)*SSV(2,NO)
11840        1-(1.+U(7))*SSV(3,NO))
11850         Y(2,1 )=(U(5)     -(1.+U(8))*SSV(1,NO)  )+U(4)*SSV(2,NO)
11860        1+U(6)*SSV(3,NO)
11870 C       INCLUDE TRACKER DYNAMIC EFFECTS (HI Bw TRACKER)
11880         Y(1,1 ) =Y(1,1 )-SSV( 22 ,NO)   *7.272205E-5
11890     100 RETURN
11900         END
11910 C
11920 C
11930         SUBROUTINE TRCFLT
11940         COMMON/2/TIME,TO,TF,DELT,KDELT,X1(4),X1L(4)
11950         COMMON/5/SSV(27,2),PP(3),B(3,3,2)
11960         COMMON/6/NTR,ICAT,NO,YL(2,2)
11970         COMMON/7/YD(2,2),Y(2,2),U(15),AST(3,3,2),STR(3,2)
11980         DIMENSION C(2),R(2)
11990 C       PROVIDES FILTERED TRACKER OUTPUT
12000         C(1)=SSV(26,NO)/DELT
12010         C(2)=SSV(27,NO)/DELT
12020         R(1)=EXP(-1./C(1))
```

```
12030        R(2)=EXP(-1./C(2))
12040        DO 10 K=1,2
12050        DO 10 I=1,2
12060     10 YD(I,K)=YD(I,K)*R(I)+(1.-C(I)*(1.-R(I)))*Y(I,K)
12070       1+(C(I)*(1.-R(I))-R(I))*YL(I,K)
12080        RETURN
12090        END
12100 C
12110 C
12120        SUBROUTINE PREIL
12130 C      CONVERTS 4-PARAMETER ATTITUDE SYSTEM TO 3 PARAMETERS AND MODIFIES
12140 C      STATE TRANSITION MATRIX
12150        COMMON/1/NG,NDELP,NN1
12160        COMMON/2/TIME,TO,TF,DELT,KDELT,X1(4),X1L(4)
12170        COMMON/3/PTMU(12),TAU(3,6),WM(6),DRFT(6),GY(9,6)
12180        COMMON/4/PHI1(4,4),PHI2(4,3),Q(7,7),QQ(4,6),WR(3,2),RP(4,4)
12190        COMMON/5/SSV(27,2),PP(3),B(3,3,2)
12200        COMMON/6/NTR,ICAT,NO,YL(2,2)
12210        COMMON/7/YD(2,2),Y(2,2),U(15),AST(3,3,2),STR(3,2)
12220        COMMON/8/P(7,7),R(2,2),AK(8,2),HMAT(2,7)
12230        DIMENSION W(3)
12240        W(1)=X1L(1)/X1L(4)
12250        W(2)=X1L(2)/X1L(4)
12260        W(3)=X1L(3)/X1L(4)
12270        DO 10 I=1,3
12280        DO 10 J=1,3
12290        PHI1(I,J)=PHI1(I,J)-PHI1(I,4)*W(J)
12300     10 CONTINUE
12310        DO 12 I=1,3
12320        DO 12 J=1,NN1
12330        PHI2(I,J)=PHI2(I,J)*DELT/2.
12340     12 CONTINUE
12350        RETURN
12360        END
12370 C
12380 C
12390        SUBROUTINE HMTRX
12400 C      COMPUTES MEASUREMENT MATRIX
12410        COMMON/1/NG,NDELP,NN1
12420        COMMON/2/TIME,TO,TF,DELT,KDELT,X1(4),X1L(4)
12430        COMMON/6/NTR,ICAT,NO,YL(2,2)
12440        COMMON/7/YD(2,2),Y(2,2),U(15),AST(3,3,2),STR(3,2)
```

```
      COMMON/P/P(7,7),R(2,2),AK(6,2),HMAT(2,7)
      DIMENSION T(3),TT(4,4),T1(3,4)
      DIMENSION TA(2,4)
      DO 130 I=1,4
      TT(I,I)=0.
  130 CONTINUE
      TT(1,2) = -STR(3,1)
      TT(1,3) = STR(2,1)
      TT(1,4) = STR(1,1)
      TT(2,3) = -STR(1,1)
      TT(2,4) = STR(2,1)
      TT(3,4) = STR(3,1)
      TT(2,1) = -TT(1,2)
      TT(3,1) = -TT(1,3)
      TT(3,2) = -TT(2,3)
      TT(4,1) = TT(1,4)
      TT(4,2) = TT(2,4)
      TT(4,3) = TT(3,4)
      T(1) = -X1(1)/X1(4)
      T(2) = -X1(2)/X1(4)
      T(3) = -X1(3)/X1(4)
      DO 160 I=1,3
      DO 160 J=1,3
      TT(I,J) = TT(I,J)+STR(I,1)*T(J)
  160 CONTINUE
      DO 165 I=1,3
      T1(I,1) = (-AST(1,1,NO)*X1(4)+AST(I,2,NO)*X1(3)
     1-AST(I,3,NO)*X1(2))*2.
      T1(I,2) = (-AST(I,1,NO)*X1(3)-AST(I,2,NO)*X1(4)
     1+AST(I,3,NO)*X1(1))*2.
      T1(I,3) =(AST(I,1,NO)*X1(2)-AST(I,2,NO)*X1(1)
     1-AST(I,3,NO)*X1(4))*2.
      T1(I,4) = (-AST(I,1,NO)*X1(1)-AST(I,2,NO)*X1(2)
     1-AST(I,3,NO)*X1(3))*2.
  165 CONTINUE
      DO 166 K=1,4
      TA(1,K)=T1(1,K)/U(2)-T1(2,K)*U(1)/U(2)**2
      TA(2,K)=T1(2,K)*U(3)/U(2)**2-T1(3,K)/U(2)
  166 CONTINUE
      DO 180 J=1,3
      HMAT(1,J)=0.
      HMAT(2,J)=0.
```

```
      DO 180 K=1,4
      HMAT(1,J)=HMAT(1,J)+TA(1,K)*TT(K,J)
      HMAT(2,J)=HMAT(2,J)+TA(2,K)*TT(K,J)
  180 CONTINUE
      RETURN
      END
C
C
      SUBROUTINE RMAT
C     FORMS MEASUREMENT NOISE COVARIANCE MATRIX
      COMMON/5/SSV(27,2),PP(3),B(3,3,2)
      COMMON/F/NTR,ICAT,NO,YL(2,2)
      COMMON/8/P(7,7),R(2,2),AK(8,2),HMAT(2,7)
      P(1,2)=P(2,1)=0.
      R(1,1)=SSV(24,NO)**2
      R(2,2)=SSV(25,NO)**2
      RETURN
      END
C
C
      SUBROUTINE FILT
C     USING KALMAN FILTER EQS., COMPUTES FILTER GAINS,AK, AND PROPAGATES
C     ERROR COVARIANCE MATRIX,P
      COMMON/1/NG,NDELP,NN1
      COMMON/3/PTMU(12),TAU(3,6),WM(6),DRFT(6),GY(9,6)
      COMMON/4/PHI1(4,4),PHI2(4,3),Q(7,7),QQ(4,6),WR(3,2),RP(4,4)
      COMMON/5/SSV(27,2),PP(3),B(3,3,2)
      COMMON/8/P(7,7),R(2,2),AK(8,2),HMAT(2,7)
      DIMENSION TA(7,7),TB(7)
C     COMPUTE ADDITIONAL CONSTANTS FOR PARTITIONING MATRICES
      NN2=NN1
      NN3=NN1-NN2
      N=NN1+3
      M=2
      CALL SRMMUL(PHI1,1,1,3,3,P,1,1,3,TA,1,1,4,7,7)
      CALL SRMMUL(PHI2,1,1,3,NN2,P,4,1,3,P,1,1,4,7,7)
      CALL SRMADD(TA,1,1,P,1,1,TA,1,1,3,3,7,7,7)
      CALL SRMMUL(PHI1,1,1,3,3,P,1,4,NN2,TA,1,4,4,7,7)
      CALL SRMMUL(PHI2,1,1,3,NN2,P,4,4,NN2,P,1,4,4,7,7)
      CALL SRMADD(TA,1,4,P,1,4,P,1,4,3,NN2,7,7,7)
      CALL SRMMUL(PHI1,1,1,3,3,P,1,4+NN2,NN3,TA,1,4+NN2,4,7,7)
      CALL SRMMUL(PHI2,1,1,3,NN2,P,4,4+NN2,NN3,P,1,4+NN2,4,7,7)
```

```
      I1=4+NN2
      CALL SRMADD(TA,1,I1,P,1,I1,P,1,I1,3,NN3,7,7,7)
      DO 15 I=1,3
      DO 15 K=1,3
      P(I,K)=0.
      DO 15 J=1,3
   15 P(I,K)=P(I,K)+TA(I,J)*PHI1(K,J)
      DO 20 I=1,3
      DO 20 K=1,3
      TA(I,K)=0.
      DO 20 J=1,NN2
   20 TA(I,K)=TA(I,K)+P(I,J+3)*PHI2(K,J)
      CALL SRMADD(P,1,1,TA,1,1,P,1,1,3,3,7,7,7)
      CALL SRMTRA(P,1,4,3,NN2,P,4,1,7,7)
      CALL SRMTRA(P,1,4+NN2,3,NN3,P,4+NN2,1,7,7)
C     P=PHI P PHI-TRANSPOSE HAS BEEN COMPUTED
      CALL SRMADD(P,1,1,Q,1,1,P,1,1,N,N,7,7,7)
      RETURN
      ENTRY FFILT
      CALL SRMMUL(HMAT,1,1,M,N,P,1,1,N,TA,1,1,2,7,7)
      CALL SRMTRA(HMAT,1,1,M,N,AK,1,1,2,8)
      CALL SRMMUL(TA,1,1,M,N,AK,1,1,M,TA,M+1,1,7,8,7)
      CALL SRMADD(TA,M+1,1,R,1,1,TA,1,1,M,M,7,2,7)
C     INVERSE ROUTINE FOLLOWS
      DET=TA(1,1)*TA(2,2)-TA(2,1)*TA(1,2)
      TA(1,M+1)=TA(2,2)/DET
      TA(1,M+2)=-TA(1,2)/DET
      TA(2,M+1)=-TA(2,1)/DET
      TA(2,M+2)=TA(1,1)/DET
C     END OF INVERSE ROUTINE
      CALL SRMMUL(AK,1,1,N,M,TA,1,M+1,M,TA,1,1,8,7,7)
      CALL SRMMUL(P,1,1,N,N,TA,1,1,M,AK,1,1,7,7,8)
C     AK HAS BEEN COMPUTED
      DO 45 I=1,M
      DO 45 K=1,N
      TA(I,K)=0.
      DO 40 J=1,M
   40 TA(I,K) = TA(I,K)-AK(I,J)*HMAT(J,K)
      IF (I.NE.K) GO TO 45
      TA(I,K) = 1.+TA(I,K)
   45 CONTINUE
      DO 55 I=1,N
```

```
14000         DO 50 K=1,N
14010         TB(K)=0.
14020         DO 50 J=1,N
14030      50 TB(K)=TB(K)+TA(I,J)*P(J,K)
14040         DO 55 K=1,N
14050      55 TA(I,K)=TB(K)
14060  C      SYMMETRIZE ERROR COVARIANCE MATRIX
14070         DO 60 I=1,N
14080         DO 60 J=1,N
14090      60 P(I,J)=0.5*(TA(I,J)+TA(J,I))
14100  C      P(K+1) HAS BEEN COMPUTED
14110         RETURN
14120         END
14130  C
14140  C
14150         SUBROUTINE SRMMUL(A,IMA,INA,MA,NA,B,IMB,INB,NB,C,IMC,INC,IRA,IRB,
14160        1IRC)
14170  C      C=A*B WITH INIT. ARRAY ELEMENTS SPECIFIED
14180         DIMENSION A(49),B(49),C(49)
14190         DO 5 I=1,MA
14200         IPIMC = I+IMC
14210         IPIMA = I+IMA
14220         IF (NB.LT.1) GO TO 6
14230         DO 5 K=1,NB
14240         KPINC = K+INC
14250         KPINB = K+INB
14260         IC = IPIMC-1+(KPINC-2)*IRC
14270         C(IC) = 0.
14280         IF (NA.LT.1) GO TO 6
14290         DO 5 J=1,NA
14300         JPINA = J+INA
14310         JPIMB = J+IMB
14320         IA = IPIMA-1+(JPINA-2)*IRA
14330         IB = JPIMB-1+(KPINB-2)*IRB
14340       5 C(IC) = C(IC)+A(IA)*B(IB)
14350       6 RETURN
14360         END
14370  C
14380  C
14390         SUBROUTINE SRMALO(A,IMA,INA,B,IMB,INB,C,IMC,INC,M,N,IRA,IRB,IRC)
14400  C      C=A+B WITH INIT. ARRAY ELEMENTS SPECIFIED
14410         DIMENSION A(49),B(49),C(49)
```

```
      DO 5 I=1,M
      IF (N.LT.1) GO TO 6
      DO 5 J=1,N
      IPIMC = I+IMC
      JPINC = J+INC
      IPIMA = I+IMA
      JPINA = J+INA
      IPIMB = I+IMB
      JPINB = J+INB
      IA = IPIMA-1+(JPINA-2)*IRA
      IB = IPIMB-1+(JPINB-2)*IRB
      IC = IPIMC-1+(JPINC-2)*IRC
    5 C(IC) = A(IA)+B(IB)
    6 RETURN
      END
C
C
      SUBROUTINE SBMTRA(A,IMA,INA,M,N,B,IMB,INB,IRA,IRB)
      DIMENSION A(49),B(49)
C     B=A-TRANSPOSE WITH INIT. ARRAY ELEMENTS SPECIFIED
      IF (N.LT.1) GO TO 6
      DO 5 I=1,N
      DO 5 J=1,M
      IPIMB = I+IMB
      JPINB = J+INB
      JPIMA = J+IMA
      IPINA = I+INA
      IA = JPIMA-1+(IPINA-2)*IRA
      IB = IPIMB-1+(JPINB-2)*IRB
    5 B(IB)=A(IA)
    6 RETURN
      END
C
C
      SUBROUTINE PCFIL
C     UPDATES ATTITUDE VARIABLES AND OTHER SYSTEM ELEMENTS OF THE
C     STATE VECTOR
      COMMON/1/NG,NDELP,NN1
      COMMON/2/TIME,TO,TF,DELT,KDELT,X1(4),X1L(4)
      COMMON/3/PIMO(12),TAU(3,6),WM(6),DRFT(6),GY(9,6)
      COMMON/5/SSV(27,2),PP(3),R(3,3,2)
      COMMON/7/YD(2,2),Y(2,2),U(15),ASI(3,3,2),STR(3,2)
```

```
14840         COMMON/B/P(7,7),R(2,2),AK(6,2),HMAT(2,7)
14850         DIMENSION W(3),T(3)
14860         W(1)=YD(1,2)-YD(1,1)
14870         W(2)=YD(2,2)-YD(2,1)
14900 C       COMPUTE CORRECTION FOR EACH SYSTEM PARAMETER OF STATE VECTOR
14910         DO 11 I=1,NN1
14920         W(3) = AK(I+3,1)*W(1)+AK(I+3,2)*W(2)
15020         PIMU(I)=PIMU(I)+W(3)
15060      11 CONTINUE
15080 C       COMPUTE CORRECTIONS FOR EACH ATTITUDE VARIABLE
15090         DO 9 I=1,3
15100         T(I) = AK(I,1)*W(1)+AK(I,2)*W(2)
15110       9 CONTINUE
15120 C       UPDATE ATTITUDE VARIABLES
15130         X1(4)=X1(4)-(X1(1)*T(1)+X1(2)*T(2)+X1(3)*T(3))/X1(4)
15140         DO 10 I=1,3
15150         X1(I)=X1(I)+T(I)
15160      10 CONTINUE
15170         RETURN
15180         END
15190 C
15200 C
```

APPENDIX B

DATA ANALYSIS PROGRAM LISTING FOR THE GIMBAL SYSTEM TEST

```
00100       PROGRAM PADS(INPUT,OUTPUT,TAPE1,TAPE2,TAPE4,TAPE5)
00110       COMMON/1/NG,NDELP,NN1
00120       COMMON/2/TIME,TO,TF,DELT,KDELT,X1(4),X1L(4),KSKP
00130       COMMON/3/PTMU(12),TAU(3,6),WM(6),DRFT(6),GY(9,6)
00140       COMMON/4/PHI1(4,4),PHI2(4,3),Q(7,7),QO(4,6),WR(3,2),RP(4,4)
00150       COMMON/5/SSV(27,2),PP(3),B(3,3,2)
00160       COMMON/6/NTR,ICAT,NO,YL(2,2)
00170       COMMON/7/YP(2,2),Y(2,2),U(15),AST(3,3,2),STR(3,2)
00180       COMMON/8/P(7,7),R(2,2),AK(6,2),HMAT(2,7)
00190       DIMENSION GYDAT(500,14),GX1(14),GX2(14),MSTR(20)
00192 C     KTYP=0 - PEAL LAB ;KTYP=1 - GYROS REORIENTED;
00194 C     KTYP=2 - IDEAL GYROS
00200       DATA KTYP/0/
00203 C     MSTR(I) DENOTES WHETHER THE I TH VISIBLE STAR WILL BE USED
00204 C     FOR FILTERING; IF SO, MSTR(I)=1
00205       DATA (MSTR(I),I=1,17)/1,1,1,1,1,1,1,1,1,1,1,1,1,1,1,1,1/
00206     5 FORMAT(X,7HKTYP = ,I1/)
00210       1 CONTINUE
00212       N7=3
00220 C     REWIND TAPES
00230       REWIND 1
00240       REWIND 2
00250       REWIND 4
00255       REWIND 5
00256       WRITE(2,5) KTYP
00260 C     EFFECTIVELY ELIMINATE THE FIRST DATA LINE
00280       READ(4,2) (GYDAT(1,J),J=1,14)
00310       NN1=3
00320 C     READ IN AND PRINT OUT INITIAL VALUES, SYSTEM PARAMETERS AND RUN
00330 C     CONTROL CONSTANTS
00340       CALL INPUT
00350 C     INITIALIZE COUNTERS AND FLAGS
00360       NXC=KPP=NF=0
00370       IGY=500
00375       MT=KKF=0
00380       NO=1
00390       READ(4,2) (GX1(J),J=1,14)
00400 C     BEGINNING OF FILTER LOOP
00410 C     INITIALIZE STATE TRANSITION MATRICES PHI1 AND PHI2
00420    15 CONTINUE
00440       CALL ZERO
00460    20 CONTINUE
```

```
00490 C      INDEX,THEN TEST FOR WHETHER NEW FLIGHT GYRO DATA SHOULD BE READ
00500        IGY=IGY+1
00510        IF(IGY.LE.500) GO TO 23
00520        IGY=1
00530        DO 24 I=1,500
00540        READ(4,2) (GX2(J),J=1,14)
00550        DLT=GX2(1)-GX1(1)
00560        GYDAT(I,1)=GX1(1)
00570        DO 17 K=2,4
00580     17 GYDAT(I,K)=(GX2(K)-GX1(K))/DLT*4.8481368E-6
00590        IF(KTYP.EQ.0) GO TO 25
00592        IF(KTYP.EQ.1) GO TO 26
00600        GYDAT(I,2)=-4.66164026E-5
00610        GYDAT(I,3)=-4.49498700E-5
00620        GYDAT(I,4)=4.57512760E-5
00622        GO TO 25
00623     26 CONTINUE
00624        GYDAT(I,2)=GYDAT(I,2)+4.26794875E-5
00625        GYDAT(I,3)=GYDAT(1,3)+2.11571588E-6
00626        GYDAT(I,4)=GYDAT(1,4)+1.97941384E-5
00630     25 CONTINUE
00640        DO 18 K=5,14
00650     18 GYDAT(I,K)=GX1(K)
00660        DO 19 K=1,14
00670     19 GX1(K)=GX2(K)
00680        IF(EOF,4) 23,24
00690     24 CONTINUE
00700 C      FORMAT 2 IS BELSKYS TAPE FORMAT
00710      2 FORMAT(X,F10.3,3(F12.1),F3,X,F11.1,X,2(F7.1,X),2(F11.1,X),
00711       14(F5.1,X))
00720 C      FORM TIME AND INTEGRATION STEP
00730     23 CONTINUE
00740        DELT=GYDAT(IGY,1)-TIME
00750        TIME=GYDAT(IGY,1)
00760        DO 33 I=1,NC
00770     33 WM(I)=GYDAT(IGY,I+1)
00890 C      TEST FOR END OF RUN
00900        IF(TIME.LT.TF) GO TO 43
00910        STOP
00920     43 CONTINUE
00930 C      ADVANCE STATE PRINT COUNTER
00940        NXC=NXC+1
```

```
00950 C      COMPUTE ESTIMATED SPACECRAFT BODY ANGULAR RATES
00960        CALL GYPCK
00970 C      COMPUTE ESTIMATED SPACECRAFT ATTITUDE
00980        CALL ATT
00990 C      TIME TO PRINT STATE
01000        IF(NXC.LT.NDELP) 44,81
01010    81  CONTINUE
01020 C      FORM ESTIMATED SPACECRAFT ATTITUDE DIRECTION COSINE MATRIX
01030        CALL TRNS
01060 C      PRINT ESTIMATED STATE
01070        CALL X1PRNT
01140        NXC=0
01150 C      IF KPP=1,THIS PRINT FOLLOWED A FILTER OPERATION
01160        IF(KPP.EQ.1) 46,44
01170    48  KPP=0
01180        GO TO 15
01190    44  CONTINUE
01230 C      TEST IF TRACKER DATA IS PRESENT
01240        IF(GYDAT(IGY,5).GT.0.5) 60,52
01250    52  NF=-KSKP
01255        KKF=0
01260        GO TO 20
01300    60  CONTINUE
01305        IF(KKF.EQ.1) GO TO 20
01310        IF(GYDAT(IGY,5).GT.1.5) GO TO 601
01312        MT=MT+1
01320        DV1=GYDAT(IGY,13)
01330        DV2=GYDAT(IGY,14)
01340    601 CONTINUE
01350        NF=NF+1
01360        IF(NF.LT.1) GO TO 20
01362 C      TEST WHETHER THIS STAR IS ACCEPTABLE
01364        IF(MSTR(MT).NE.1) GO TO 52
01370        TU=GYDAT(IGY,7)+DV2
01380        TV=GYDAT(IGY,8)+DV1
01450        YL(1,2)=Y(1,2)
01460        YL(2,2)=Y(2,2)
01470        Y(1,2) =- TU*4.84c136e1E-6
01480        Y(2,2) = TV*4.84c136e1E-6
01482        YG= GYDAT(IGY,6)*4.c48136E1E-6
01490 C      AIR BEARING TABLE ANGLE COMPUTATION
01520        TRL= GYDAT(IGY,9)*4.848136E1E-6
```

```
01530         IF(NF.EQ.1) 62,61
01540    62   CALL STRCHK(YG)
01550    61   CONTINUE
01560 C       COMPUTE INERTIAL STAR DIR. COS.
01570         CALL STARDC(STR(1,1),ICAT,TBL)
01580 C       COMPUTE EST. TRACKER OUTPUT
01590         CALL TRAC(YG)
01600         CALL TRFLT
01610         IF(NF.LT.10) GO TO 20
01615         KKF=1
01620 C       START FILTERING
01630 C       COMPUTE TRACKER MEASURMENT RESIDUAL NORM
01640         W1=SQRT((YD(1,2)-YD(1,1))**2+(YD(2,2)-YD(2,1))**2)
01650 C       DOES IT FALL WITHIN AN ALLOWABLE ERROR
01660         IF(W1.LT..1) GO TO 70
01670    72   PRINT 3,W1
01680     3   FORMAT(20HMEASUREMENT ERROR IS,2X,E13.6,6H, PUNT)
01690         STOP
01700    70   CONTINUE
01701         X09=0.
01705         WRITE(5,4) TIME,W1,X09,N7
01706    4    FORMAT(3(2X,E13.6),2X,I1)
01710         CALL X1PRNT
01720         NF=-KSKP
01730 C       FORM STATE NOISE ERROR COVARIANCE MATRIX
01740         CALL QMAT
01750 C       ALTER STATE TRANSITION MATRIX TO DEAL WITH 3 RATHER THAN 4
01760 C       ATTITUDE VARIABLES
01770         CALL PREFIL
01780 C       PROPAGATE STATE ERROR COVARIANCE MATRIX
01790         CALL FILT
01795         CALL PRNT(1)
01800 C       FORM MEASURMENT MATRIX
01810         CALL HMTRX
01820 C       FORM MEASUREMENT NOISE COVARIANCE MATRIX
01830         CALL RMAT
01840 C       APPLY KALMAN ALGORITHM
01850         CALL FFILT
01860 C       UPDATE STATE
01870         CALL POFIL
01880 C       ADVANCE FILTER COUNTER
01890         NPC=NPC+1
```

```
01900 C      TIME TO PRINT STATE ERROR COVARIANCE MATRIX
01910        IF(NPC-NFP) 15,60,80
01920    60  CONTINUE
01930        CALL PRNT(1)
01940        KPR=1
01950        GO TO 81
01960        END
01970 C
01980 C
01990        SUBROUTINE TRNS
02000 C      COMPUTE DIRECTION COSINES OF SPACECRAFT ATTITUDE RELATIVE TO
02010 C      ATTITUDE REFERENCE AXES(ECI COORDINATES)
02020        COMMON/2/TIME,TO,TF,DELT,KDELT,X1(4),X1L(4)
02030        COMMON/5/SSV(27,2),PP(3),B(3,3,2)
02040        DIMENSION T(4,4)
02050 C      TRANSFORM EULER SYMMETRIC PARAMETERS TO DIRECTION COSINES RELATIVE
02060 C      TO ECI AXES
02070        DO 10 I = 1,3
02080        T(I,I) = X1(4)
02090    10 CONTINUE
02100        T(1,2)=X1(3)
02110        T(1,3)=-X1(2)
02120        T(1,4)=X1(1)
02130        T(2,3)=X1(1)
02140        T(2,4)=X1(2)
02150        T(3,4)=X1(3)
02160        T(2,1) = -T(1,2)
02170        T(3,1) = -T(1,3)
02180        T(3,2) = -T(2,3)
02190        T(4,1) = T(1,4)
02200        T(4,2) = T(2,4)
02210        T(4,3) = T(3,4)
02220        T(4,4) = -X1(4)
02230        DO 40 I=1,3
02240        DO 40 J=1,3
02250        B(I,J,1)=0.
02260        DO 40 K=1,4
02270        B(I,J,1)=   B(I,J,1 )+T(I,K)*T(K,J)
02280    40 CONTINUE
02290        RETURN
02300        END
02310 C
```

```
02320 C
03100       SUBROUTINE XLPRNT
03110 C     PRINTS ESTIMATED STATE VECTOR AND S/C ATTITUDE MATRIX
03120       COMMON/1/NG,NDELP,NN1
03130       COMMON/2/TIME,TO,TF,DELT,KDELT,X1(4),X1L(4)
03140       COMMON/3/PIMU(12),TAU(3,6),WM(6),DRFT(6),GY(9,6)
03150       COMMON/5/SSV(27,2),PP(3),B(3,3,2)
03160       DIMENSION C(3,3),D(4)
03170       CA=206264.81
03175       N7=1
03180 C     PRINT HEADING AND TIME
03190       WRITE(2,30) TIME
03200       CALL LABATT
03210       DO 60 I=1,3
03220       DO 60 J=1,3
03230       C(I,J)=0.
03240       DO 60 K=1,3
03250    60 C(I,J)=C(I,J)+B(I,K,1)*B(J,K,2)
03260       D(1)=CA*C(2,3)
03270       D(2)=CA*C(3,1)
03280       D(3)=CA*C(1,2)
03290       D(4)=SQRT(D(2)**2+D(3)**2)
03291       DISPLAY TIME,D(4),D(1)
03300 C     PRINT ESTIMATED EULER PARAMETERS AND S/C AND LAB ATTITUDE MATRIX
03310       WRITE(2,20) (I,X1(I),B(I,1,1)  ,B(I,2,1),B(I,3,1),
03320      1B(I,1,2),B(I,2,2),B(I,3,2),D(I),I=1,3)
03330       WRITE(2,22) X1(4)  ,D(4)
03340       WRITE(5,23) TIME,D(4),D(1),N7
03350    23 FORMAT(3(2X,E13.6),2X,I1)
03390 C     PRINT HEADING
03400       WRITE(2,50)
03420       DO 45 I=1,NN1
03520       PIMU1A=CA*PIMU(I)
03530       WRITE(2,21) I,PIMU1A
03570    45 CONTINUE
03590    30 FORMAT(X///8H TIME = ,E16.9//30X,
03600      150HESTIMATED SPACECRAFT ATTITUDE RELATIVE TO EC1 AXES//X,
03610      23HNO.,X,11HEULER PARAM,12X,17HATTITUDE ESTIMATE,27X,
03620      312HLAB ATTITUDE,12X,12HR,P,Y,RSS ER//)
03630    20 FORMAT(X,I1,2X,F12.9,X,3(X,F12.9),2X,3(X,F12.9),2X,F9.2)
03640    22 FORMAT(X,1H4,2X,F12.9,83X,F9.2)
03650    50 FORMAT(X/14X,26HESTIMATED GYRO BIAS VECTOR/)
```

```
03660    21  FORMAT(15X,I1,4X,E12.5)
03670        RETURN
03680        END
03690 C
03700 C
03710        SUBROUTINE PRNT(K1)
03720        COMMON/1/NG,NDELP,NN1
03730        COMMON/2/TIME,TO,TF,DELT,KDELT,X1(4),X1L(4)
03740        COMMON/6/NTP,ICAT,NO,YL(2,2)
03750        COMMON/7/YD(2,2),Y(2,2),U(15),AST(3,3,2),STR(3,2)
03760        COMMON/8/P(7,7),R(2,2),AK(8,2),HMAT(2,7)
03770        DIMENSION PT(3,3),F(3,3),TP(3,3)
03775        N2=2
03780 C      PRINTS THE ERROR COVARIANCE MATRIX,UPPER LEFT 3 BY 3 IN
03790 C      SMALL ANGLE FORM
03800 C      SAVE UPPER 3 BY 3
03810        DO 40 I=1,3
03820        DO 40 J=1,3
03830    40  PT(I,J)=P(I,J)
03840 C      CONVERT UPPER 3 BY 3 OF P MATRIX TO SMALL ANGLE FORM
03850        F(1,1)=2.*(X1(4) +X1(1)**2/X1(4))
03860        F(1,2)=2.*(X1(3)+X1(1)*X1(2)/X1(4))
03870        F(1,3)=-2.*(X1(2)-X1(1)*X1(3)/X1(4))
03880        F(2,1)=-2.*(X1(3)-X1(2)*X1(1)/X1(4))
03890        F(2,2)=2.*(X1(4) +X1(2)**2/X1(4))
03900        F(2,3)=2.*(X1(1)+X1(2)*X1(3)/X1(4))
03910        F(3,1)=2.*(X1(2)+X1(1)*X1(3)/X1(4))
03920        F(3,2)=-2.*(X1(1)-X1(2)*X1(3)/X1(4))
03930        F(3,3)=2.*(X1(4) +X1(3)**2/X1(4))
03940        DO 70 I=1,3
03950        DO 70 J=1,3
03960        TP(I,J)=0.
03970        DO 70 K=1,3
03980    70  TP(I,J)=TP(I,J)+P(I,K)*F(J,K)
03990        DO 75 I=1,3
04000        DO 75 J=1,3
04010        P(I,J)=0.
04020        DO 75 K=1,3
04030    75  P(I,J)=P(I,J)+F(I,K)*TP(K,J)
04070        NA = NN1+3
04100 C      PRINT HEADING
04110    10  WRITE(2,1)
```

```
04120      1 FORMAT(1H1,50X,6HP MATRIX)
04130        DO 20 I=1,NA
04140        WRITE(2,3) I
04150      3 FORMAT(/2X,4HROW ,I2/)
04160 C      PRINT P MATRIX
04170     20 WRITE(2,30) (P(I,J),J=1,NA)
04180 30     FORMAT(3X,6E17.6)
04190        IF(K1.EQ.0) GO TO 44
04200 C      PRINT STAR NUMBER
04210     50 WRITE(2,45) ICAT
04220     45 FORMAT( /  7X,14HSTAR NUMBER = ,I3)
04230        TST1=YD(2,2)
04240        TST2=YD(1,2)
04250        DEL1=(TST1-YD(2,1))*206264.81
04260        DEL2=(TST2-YD(1,1))*206264.81
04280        WRITE(2,60) TST1,DEL1,TST2,DEL2
04290     60 FORMAT(3X,37HTRACKER OUTPUT ANGLES AND MEAS. ERROR/
04300       15X,7HAZIMUTH,2X,E11.4,5H RAD.,3X,F10.3,
04310       27H ARCSEC/6X,5HELEV ,3X,E11.4,5H RAD.,3X,F10.3,
04320       37H ARCSEC)
04330    44   CONTINUE
04340        AT=SQRT(P(2,2)       +P(3,3))*206264.81
04350        WRITE(2,39) AT
04360     39 FORMAT(26H SQRT OF POINTING TRACE = ,F10.3,9H ARC SEC.)
04361        AT1=SQRT(P(1,1))*206264.81
04362        WRITE(2,391) AT1
04363   391  FORMAT(X,17HBORESIGHT ERROR = ,F10.3,9H ARC SEC.)
04365        WRITE(5,8) TIME,AT,AT1,N7
04366    8   FORMAT(3(2X,E13.6),2X,I1)
04370        DISPLAY AT,AT1
04380 C      RESTORE P MATRIX
04390        DO 43 I=1,3
04400        DO 43 J=1,3
04410    43  P(I,J)=PT(I,J)
04420        RETURN
04430        END
04440 C
04450 C
04930        SUBROUTINE INPUT
04940 C      READS IN AND PRINTS INITIAL VALUES, SYSTEM PARAMETERS,RUN CONTROL
04950 C      CONSTANTS, AND CONVERTS SPECIFIED ANGLES TO RADIANS
04960        COMMON/1/NC,NDELP,NN1
```

```
04970          COMMON/2/TIME,TO,TF,DELT,KDELT,X1(4),X1L(4),KSKP
04980          COMMON/3/PTMU(12),TAU(3,6),WM(6),DRFT(6),GY(9,6)
04990          COMMON/4/PHI1(4,4),PHI2(4,3),Q(7,7),QQ(4,6),WR(3,2),RP(4,4)
05000          COMMON/5/SSV(27,2),PP(3),B(3,3,2)
05010          COMMON/6/NTR,ICAT,NG,YL(2,2)
05020          COMMON/7/YD(2,2),Y(2,2),U(15),AST(3,3,2),STR(3,2)
05030          COMMON/8/P(7,7),R(2,2),AK(8,2),HMAT(2,7)
05040          DIMENSION NSV(4,32),C(3,3),T(3)
05050          NN=NN1+3
05060          DO 112 I=1,NN
05070          DO 112 J=1,NN
05080   112    P(I,J)=Q(I,J)=0.
05090 C        READ INPUT FLAGS DEFINING TYPE OF RUN AND PRINT OPTIONS
05100          READ(1,2) NTR,NG
05110      2   FORMAT(I1)
05120          READ(1,3) NDELP,KSKP
05130      3   FORMAT(I3)
05150 C        READ NOMINAL STAR TRACKER TRANSFORMATION MATRIX
05160          DO 20 K=1,NTR
05170     20   READ(1,4) ((AST(I,J,K),J=1,3),I=1,3)
05180      4   FORMAT(F9.6)
05200 C        READ STAR SENSOR PARAMETERS
05210          DO 24 J=1,NTR
05230     24   READ(1,5) (SSV(I,J),I=1,9)
05240      5   FORMAT(F9.3)
05250 C        READ GYRO PARAMETERS
05260          DO 25 J=1,NG
05270     25   READ(1,6) (GY(I,J),I=1,9)
05280 C        READ ESTIMATED INITIAL RATES
05300          DO 27 I=1,3
05310     27   READ(1,6) PP(I)
05330      6   FORMAT(F12.6)
05340 C        READ INITIAL 4 PARAMETER ATTITUDE
05350          READ(1,4) (X1(I),I=1,4)
05360     22   CONTINUE
05370 C        READ INITIAL AND FINAL TIMES AND INTEGRATION STEP SIZE
05380          READ(1,6) TO,TF,DELT
05390 C        READ ERROR COVARIANCE INITIAL DIAGONAL ELEMENTS
05400 C        UNITS ARE RAD.,SEC
05410          DO 28 I=1,NN
05420     28   READ(1,6) P(I,I)
05470 C
```

```
05490 C      TEMPORARY INPUT PRINT ROUTINE
05500        WRITE(2,12)
05510    12  FORMAT(1H1)
05520        WRITE(2,7) NTR,NG,NDELP
05540     7  FORMAT( 3(X,I3)/)
05560        DO 31 J=1,NG
05570    31  WRITE(2,8) (GY(I,J),I=1,9)
05580    8   FORMAT(9(X,F10.3))
05590        WRITE(2,10)
05600    10  FORMAT(/)
05610        DO 32 K=1,NTR
05620    32  WRITE(2,9)((AST(I,J,K),J=1,3),I=1,3)
05630     9  FORMAT(9(X,E9.6))
05640        WRITE(2,10)
05650        DO 34 J=1,NTR
05670    34  WRITE(2,11) (SSV(I,J),I=1,9)
05680    11  FORMAT(9(X,F10.3))
05690        WRITE(2,10)
05700        DO 35 J=1,3
05720    35  WRITE(2,9) PP(J)
05730    41  CONTINUE
05740        WRITE(2,10)
05760        WRITE(2,8) (X1(I),I=1,4)
05770        WRITE(2,10)
05780        DO 37 K=1,NN
05790    37  WRITE(2,8) P(K,K)
05800        WRITE(2,10)
05810        WRITE(2,9) TO,TF,DELT
05820        WRITE(2,10)
05880 C
05890 C      INITIALIZE PROBLEM TIME
05900        TIME = TO
05910     15 FORMAT(1H1)
05920        WRITE(2,15)
05930 C      CONVERT ANGLES TO RADIANS
05940        CF = 4.8481368E-06
05950        CFSQ = CF*CF
05970        DO  30 J=1,NTR
05980        DO 131 I=1,7
05990    131 SSV(I,J)=CF*SSV(I,J)
06000    130 CONTINUE
06020        DO 135 J=1,NG
```

```
06030        GY(1,J)=GY(1,J)*CF
06040        DO 135 I=7,9
06050        GY(I,J)=GY(I,J)*CF
06060    135 CONTINUE
06070        CALL INITIAL
06080  C     PRINT ERROR COVARIANCE MATRIX
06090        CALL PRNT(0)
06100  C     PRINT INITIAL STATE VECTOR
06110        CALL TRNS
06130        CALL X1PRNT
06160        RETURN
06190        END
06200  C
06210  C
06220        SUBROUTINE ZERO
06230  C     INITIALIZES STATE TRANSITION MATRICES PHI1 AND PHI2 AFTER EACH
06240  C     FILTER UPDATE
06250        COMMON/1/NG,NDELP,NN1
06260        COMMON/2/TIME,TO,TF,DELT,KDELT,X1(4),X1L(4)
06270        COMMON/4/PHI1(4,4),PHI2(4,3),Q(7,7),QQ(4,6),WR(3,2),RP(4,4)
06280  C     RETAIN FILTER UPDATED VALUES OF EULER PARAMETERS FOR NEXT FILTER
06290  C     OPERATION
06300        DO 21 I=1,4
06310        X1L(I)=X1(I)
06320  C     SET PHI1 ELEMENTS EQUAL TO ZERO
06330        DO 22 J=1,4
06340        PHI1(I,J)=0.
06350    22 CONTINUE
06360  C     SET PHI2 ELEMENTS EQUAL TO ZERO
06370        DO 23 J=1,NN1
06380        PHI2(I,J)=0.
06390    23 CONTINUE
06400  C     SET PHI1 DIAGONAL ELEMENTS EQUAL TO ONE
06410        PHI1(I,I)=1.
06420    21 CONTINUE
06430  C     SET Q MATRIX COMPUTATION INTERVAL COUNTER TO ZERO
06440        KDELT=0
06450  C     SET Q MATRIX ELEMENTS TO ZERO
06460        DO 10 I=1,7
06470        DO 10 J=1,7
06480    10  Q(I,J)=0.
06490        RETURN
```

```
      END
C
C
      SUBROUTINE INITIAL
      COMMON/1/NG,NDELP,NN1
      COMMON/2/TIME,TG,TF,DELT,KDELT,X1(4),X1L(4)
      COMMON/3/PIMU(12),TAU(3,6),WM(6),DRFT(6),GY(9,6)
      COMMON/4/PHI1(4,4),PHI2(4,3),Q(7,7),QO(4,6),WK(3,2),RP(4,4)
      COMMON/5/SSV(27,2),PP(3),B(3,3,2)
      COMMON/6/NTP,ICAT,NO,YL(2,2)
      COMMON/8/P(7,7),K(2,2),AK(8,2),HMAT(2,7)
      DIMENSION TP1(3,3),TP2(3,3),TP(3,12),TP4(6,3)
C     COMPUTE GYRO WEIGHTING MATRIX, TAU
      DO 12 I=1,NG
      DO 12 J=1,3
   12 TP4(I,J)=(1.+GY(2,I))*GY(3+J,I)
      DO 10 I=1,3
      DO 10 J=1,3
      TP1(I,J)=0.
      DO 10 K=1,NG
      TP1(I,J)=TP1(I,J)+TP4(K,I)*TP4(K,J)
   10 CONTINUE
      DEL=TP1(1,1)*TP1(2,2)*TP1(3,3)+TP1(1,2)*TP1(2,3)*TP1(3,1)
     1+TP1(1,3)*TP1(2,1)*TP1(3,2)-TP1(1,3)*TP1(2,2)*TP1(3,1)
     2-TP1(1,1)*TP1(2,3)*TP1(3,2)-TP1(1,2)*TP1(2,1)*TP1(3,3)
      DL=1./DEL
      TP2(1,1)=(TP1(2,2)*TP1(3,3)-TP1(3,2)*TP1(2,3))*DL
      TP2(1,2)=(TP1(3,2)*TP1(1,3)-TP1(1,2)*TP1(3,3))*DL
      TP2(1,3)=(TP1(1,2)*TP1(2,3)-TP1(2,2)*TP1(1,3))*DL
      TP2(2,1)=(TP1(3,1)*TP1(2,3)-TP1(2,1)*TP1(3,3))*DL
      TP2(2,2)=(TP1(1,1)*TP1(3,3)-TP1(1,3)*TP1(3,1))*DL
      TP2(2,3)=(TP1(2,1)*TP1(1,3)-TP1(1,1)*TP1(2,3))*DL
      TP2(3,1)=(TP1(2,1)*TP1(3,2)-TP1(3,1)*TP1(2,2))*DL
      TP2(3,2)=(TP1(3,1)*TP1(1,2)-TP1(1,1)*TP1(3,2))*DL
      TP2(3,3)=(TP1(1,1)*TP1(2,2)-TP1(2,1)*TP1(1,2))*DL
      DO 15 I=1,3
      DO 15 J=1,NG
      TAU(I,J)=0.
      DO 15 K=1,3
      TAU(I,J)=TAU(I,J)+TP2(I,K)*TP4(J,K)
   15 CONTINUE
C     INITIALIZE PAST DATA
```

```
06930          DO 20 I=1,NG
06950     20   DRET(I)=GY(1,I)
06960          DO 30 I=1,3
06980     30   WP(I,1)=WP(I,2)=PP(I)
06990 C        COMPUTE INITIAL GYROPACK PARAMETERS, PIMU
07010          DO 40 I=1,3
07020          PIMU(I)=0.
07030          DO 40 J=1,NG
07040          PIMU(I)=PIMU(I)+TAU(I,J)*(1.+GY(2,J))*GY(1,J)
07050     40   CONTINUE
07070          L=3
07080          DO 50 I=1,3
07090          DO 60 J=1,3
07100          L=L+1
07110          PIMU(L)=0.
07120          DO 60 K1=1,NG
07130          PIMU(L)=PIMU(L)+TAU(I,K1)*(1.+GY(2,K1))*GY(3+J,K1)
07140     60   CONTINUE
07150          PIMU(4*I)=PIMU(4*I)-1.
07160     50   CONTINUE
07170 C        COMPUTE TAU*TAU-T*SIG-SQ FOR USE IN Q
07180          DO 65 J=1,NG
07190          TP3=SQRT(GY(7,J)**2*100.00*DELT+GY(9,J)**2)  /100./DELT
07200          DO 65 I=1,3
07210          TP(I,J+6)=TAU(I,J)*GY(8,J)  *SQRT(100.*DELT)
07220     65   TP(I,J)=TAU(I,J)*TP3
07230          DO 70 I=1,3
07240          DO 70 J=1,3
07250          QQ(I,J)=0.
07260          QQ(I,J+3)=0.
07270          DO 70 K=1,NG
07280          QQ(I,J+3)=QQ(I,J+3)+TP(I,K+6)*TP(J,K+6)
07290     70   QQ(I,J)=QQ(I,J)+TP(I,K)*TP(J,K)*2500.*DELT*DELT
07370 C        CONVERT UPPER LEFT 3 BY 3 OF P MATRIX TO EULER SYMMETRIC
07380 C        PARAMETER FORM. ORIGINAL P ASSUMED DIAGONAL.
07390          Z1=P(1,1)
07400          Z2=P(2,2)
07410          Z3=P(3,3)
07420          P(1,1)=.25*(Z1*X1(4)**2+Z2*X1(3)**2+Z3*X1(2)**2)
07430          P(1,2)=P(2,1)=.25*((Z1-Z2)*X1(4)*X1(3)-Z3*X1(1)*X1(2))
07440          P(1,3)=P(3,1)=.25*((Z3-Z1)*X1(4)*X1(2)-Z2*X1(1)*X1(3))
07450          P(2,2)=.25*(Z1*X1(3)**2+Z2*X1(4)**2+Z3*X1(1)**2)
```

```
07460          P(2,3)=P(3,2)=.25*((Z2-Z3)*X1(1)*X1(4)-Z1*X1(2)*X1(3))
07470          P(3,3)=.25*(Z1*X1(2)**2+Z2*X1(1)**2+Z3*X1(4)**2)
07600          RETURN
07610          END
07620  C
07630  C
07640          SUBROUTINE STRCHK(YG)
07650          COMMON/1/NG,NDELP,NN1
07660          COMMON/2/TIME,TO,TF,DELT,KDELT,X1(4),X1L(4)
07670          COMMON/5/SSV(27,2),PP(3),B(3,3,2)
07680          COMMON/6/NTR,ICAT,NO,YL(2,2)
07690          COMMON/7/YD(2,2),Y(2,2),U(15),AST(3,3,2),STR(3,2)
07700          ICAT=2
07710          IF(YG.GT..1) ICAT=1
07720          IF(YG.LT.-.1) ICAT=3
07880   100    CONTINUE
07890          YL(1,1)=YL(1,2)=Y(1,1)=YD(1,1)=YD(1,2)=Y(1,2)
07900          YL(2,1)=YL(2,2)=Y(2,1)=YD(2,1)=YD(2,2)=Y(2,2)
07910          RETURN
07920          END
07930  C
07940  C
07950          SUBROUTINE STARDC(C,ISTR,TBL)
07960          COMMON/2/TIME,TO,TF,DELT,KDELT,X1(4),X1L(4)
07970          COMMON/5/SSV(27,2),PP(3),B(3,3,2)
07980          DIMENSION C(3),TP(3,3),RN(3),D(3)
07990  C       DEFINE STAR DIR. COS. IN LAB AXES
08000          TP(1,1)=-.6886902
08010          TP(1,2)= 4.7424E-5
08020          TP(2,1)=-.8544475
08030          TP(2,2)=2.153E-5
08050          TP(3,1)=-1.020237
08060          TP(3,2)= 4.512E-5
08080          CALL TRNS
08082          TT=2.*TP(ISTR,1)
08084          TW=TP(ISTR,2)+TBL
08086          D(1)=-SIN(TT)*COS(TW)
08086          D(2)=SIN(TT)*SIN(TW)
08090          D(3)=COS(TT)
08180  C       FORM LAB INERTIAL ATTITUDE
08190          CALL LABATT
08200  C       CONVERT TO INERTIAL COORD.
```

```
      DO 20 I=1,3
      C(I)=0.
      DO 20 J=1,3
   20 C(I)=C(I)+B(J,I,2)*D(J)
      RETURN
      END
C
C
      SUBROUTINE LABATT
      COMMON/2/TIME,TO,TF,DELT,KDELT,X1(4),X1L(4)
      COMMON/5/SSV(27,2),PP(3),B(3,3,2)
      BTA=1.-COS(7.27220522E-5*TIME)
      R1=0.
      R2=0.829080841
      R3=0.557791849
      AL=SIN(7.27220522E-5*TIME)
      B(1,1,2)=1.-BTA*(R2**2+R3**2)
      B(1,2,2)=AL*R3+BTA*R1*R2
      B(1,3,2)=-AL*R2+BTA*R1*R3
      B(2,1,2)=-AL*R3+BTA*R1*R2
      B(2,2,2)=1.-BTA*(R1**2+R3**2)
      B(2,3,2)=AL*R1+BTA*R2*R3
      B(3,1,2)=AL*R2+BTA*R1*R3
      B(3,2,2)=-AL*R1+BTA*R2*R3
      B(3,3,2)=1.-BTA*(R1**2+R2**2)
      RETURN
      END
C
C
      SUBROUTINE GYPCK
      COMMON/1/NG,NDELP,NN1
      COMMON/3/PTMU(12),TAU(3,6),WM(6),DRFT(6),GY(9,6)
      COMMON/4/PHI1(4,4),PHI2(4,3),Q(7,7),QQ(4,6),WK(3,2),RP(4,4)
      DIMENSION TP(3)
C     PROVIDES ESTIMATED S/C RATES BASED UPON COMPENSATED GYROS.
      DO 10 I=1,3
C     SHIFT PREVIOUS RATE DATA BACK ONE STEP
      WP(I,2)=WP(I,1)
C     COMPUTE NEW GYRO PACKAGE RATE ESTIMATE
      TP(I)=-PTMU(I)
      DO 10 J=1,NG
      TP(I)=TP(I)+TAU(I,J)*WM(J)
```

```
06780    10  CONTINUE
08790        L=3
08800        DO 20 I=1,3
08810        WR(I,1)=TP(I)
08820        DO 20 J=1,3
08830        L=L+1
08840        WR(I,1)=WR(I,1)-PINU(L)*TP(J)
08850    20  CONTINUE
08860        RETURN
08870        END
08880 C
08890 C
09220        SUBROUTINE ATT
09230 C      PERFORMS NUMERICAL INTEGRATION TO DETERMINE SPACECRAFT ATTITUDE
09240 C      AS REPRESENTED BY EULER SYMMETRIC PARAMETERS
09250        COMMON/2/TIME,TO,TF,DELT,KDEL1,X1(4),X1L(4)
09260        COMMON/4/PHI1(4,4),PHI2(4,3),Q(7,7),QQ(4,6),WR(3,2),RP(4,4)
09270        DIMENSION T(5),TP(3)
09280        DO 20 I=1,3
09290    20  TP(I)=.5*(WR(I,1)+WR(I,2))
09300 C      COMPUTE S(0) FOR USE IN RP MATRIX
09310        T(2)=(TP(1)**2+TP(2)**2+TP(3)**2)*DELT**2/4.
09320        T(1) = SQRT(T(2))
09330        T(2) = COS(T(1))
09340        T(3)=.5
09350        IF(ABS(T(1)).LE.1.E-20) GO TO 6
09360        T(3) = SIN(T(1))
09370        T(3)=T(3)/(2.*T(1))
09380     6  CONTINUE
09390 C      FORM RP MATRIX FOR PROPAGATING EULER PARAMETERS
09400        RP(1,2)=T(3)*TP(3)*DELT
09410        RP(1,3)=-T(3)*TP(2)*DELT
09420        RP(1,4)=T(3)*TP(1)*DELT
09430        RP(2,3)=RP(1,4)
09440        RP(2,4)=-RP(1,3)
09450        RP(3,4)=RP(1,2)
09460        DO 10 I=1,4
09470        RP(I,I)=-T(2)
09480        DO 10 J=1,I
09490        RP(I,J)=-RP(J,I)
09500    10  CONTINUE
09530        CALL PHI
```

```
09550 C      PROPAGATE EULER PARAMETERS
09560        DO 12 I=1,4
09570        T(I)=0.
09580        DO 12 J=1,4
09590        T(I)=T(I)+RP(I,J)*X1(J)
09600     12 CONTINUE
09610 C      NORMALIZE EULER PARAMETERS
09620        T(5) = SQRT(T(1)**2+T(2)**2+T(3)**2+T(4)**2)
09630        DO 14 I=1,4
09640        X1(I)=T(I)/T(5)
09650     14 CONTINUE
09660        RETURN
09670        END
09680 C
09690 C
09700        SUBROUTINE PHI
09710 C      COMPUTES THE STATE TRANSITION MATRICES PHI1 AND PHI2
09720        COMMON/1/NG,NDELP,NN1
09730        COMMON/2/TIME,TO,TF,DELT,KDELT,X1(4),X1L(4)
09740        COMMON/4/PHI1(4,4),PHI2(4,3),Q(7,7),QQ(4,6),WR(3,2),RP(4,4)
09750        DIMENSION W(4),T1(3,12),PK(4,3),PHI2T(4,12),TP1(7,7),TP2(7,7)
09760        DIMENSION PQ(7,7)
09770 C      COMPUTE PHI1
09780        DO 10 J=1,4
09790        DO 11 I=1,4
09800        W(I)=0.
09810        DO 11 K=1,4
09820        W(I)=W(I)+RP(I,K)*PHI1(K,J)
09830     11 CONTINUE
09840        DO 10 I=1,4
09850        PHI1(I,J)=W(I)
09860     10 CONTINUE
09880 C      COMPUTE PHI2
09890        DO 42 I=1,4
09900        DO 42 J=1,NN1
09910        PHI2T(I,J)=0.
09920        DO 42 K=1,4
09930     42 PHI2T(I,J)=PHI2T(I,J)+RP(I,K)*PHI2(K,J)
09940        DO 14 I=1,3
09950        PK(I,I)=X1(4)
09960     14 CONTINUE
09970        PK(1,2)=-X1(3)
```

```
09960          PK(1,3)=X1(2)
09990          PK(2,3)=-X1(1)
10000          PK(2,1)=X1(3)
10010          PK(3,1)=-X1(2)
10020          PK(3,2)=X1(1)
10030          PK(4,1)=-X1(1)
10040          PK(4,2) = -X1(2)
10050          PK(4,3)=-X1(3)
10060          DO 30 I=1,3
10070          DO 31 J=1,3
10080    31    T1(I,J)=0.
10090    30    T1(I,I)=-1.
10210          J1=1
10220          DO 19 J = 1,3
10250          DO 22 I=1,4
10260          TZ = 0.
10270          DO 23 K=1,3
10280          TZ = TZ+PK(I,K)*T1(K,J)
10290       23 CONTINUE
10300          PHI2(I,J1) = PHI2T(I,J1)+TZ
10310       22 CONTINUE
10320          J1=J1+1
10330       19 CONTINUE
10350 C        UPDATE Q IF TIME IS APPROPRIATE
10360          KDELT=KDELT+1
10370          IF(KDELT.LT.100) GO TO 50
10380          KDELT=0
10390          DO 55 I=1,4
10400          DO 55 J=1,3
10410          TP2(I,J)=0.
10420          DO 55 K=1,3
10430    55    TP2(I,J)=TP2(I,J)+PK(I,K)*Q0(K,J)
10440          DO 60 I=1,4
10450          DO 60 J=1,4
10460          TP1(I,J)=0.
10470          DO 60 K=1,3
10480    60    TP1(I,J)=TP1(I,J)+TP2(I,K)*PK(J,K)
10490          DO 61 I=5,7
10500          DO 61 J=1,4
10510    61    TP1(I,J)=TP1(J,I)=0.
10520          DO 62 I=5,7
10530          DO 62 J=5,7
```

```
10540    62  TP1(I,J)=QQ(I-4,J-1)
10550        T9=RP(2,1)**2+RP(3,1)**2+RP(4,1)**2
10560        T9=SQRT(1.-10000.*T9)
10570        DO 63 I=1,4
10580        DO 64 J=1,4
10590        RQ(I,J)=RP(I,J)*100.
10600    64  RQ(I+3,J)=0.
10610        DO 65 J=1,3
10620        RQ(I,J+4)=-DELT*PR(I,J)*50.
10630    65  RQ(I+3,J+4)=0.
10640        RQ(I+3,I+3)=1.
10650        RQ(I,I)=T9
10660    63  CONTINUE
10670        DO 66 I=1,7
10680        DO 66 J=1,7
10690        TP2(I,J)=0.
10700        DO 66 K=1,7
10710    66  TP2(I,J)=TP2(I,J)+Q(I,K)*RQ(J,K)
10720        DO 67 I=1,7
10730        DO 67 J=1,7
10740        Q(I,J)=TP1(I,J)
10750        DO 67 K=1,7
10760    67  Q(I,J)=Q(I,J)+RQ(I,K)*TP2(K,J)
10770    50  CONTINUE
10780 C      PHI2 MUST STILL BE MULTIPLIED BY DELT/2 IN PRFIL
10790        RETURN
10800        END
10810 C
10820 C
10830        SUBROUTINE QMAT
10840 C      FORM THE STATE NOISE COVARIANCE MATRIX
10850        COMMON/1/NG,NDELP,NN1
10860        COMMON/4/PHI1(4,4),PHI2(4,3),Q(7,7),QQ(4,6),WR(3,2),RP(4,4)
10870        DIMENSION TP1(7,7)
10880 C      PROPERLY PACK Q MATRIX
10890        DO 10 I=1,7
10900        DO 10 J=1,7
10910    10  TP1(I,J)=Q(I,J)
10920        J3=3
10930        DO 15 I=1,3
10940        J1=3
10950        DO 17 J=1,3
```

```
10970         J1=J1+1
10980         Q(I,J1)=Q(J1,I)=TP1(I,J+4)
10990      17 CONTINUE
11010         J3=J3+1
11020         J2=3
11030         DO 16 J=1,3
11050         J2=J2+1
11060         Q(J3,J2)=TP1(I+4,J+4)
11070      16 CONTINUE
11080      15 CONTINUE
11160         RETURN
11170         END
11180 C
11190 C
11200         SUBROUTINE TRAC(YG)
11210 C       COMPUTES TRACKER OUTPUT ANGLES FROM ATTITUDE AND
11220 C       TRACKER IDENTIFICATION NUMBER
11230         COMMON/2/TIME,TO,TF,DELT,KDELT,X1(4),X1L(4)
11240         COMMON/5/SSV(27,2),PP(3),B(3,3,2)
11250         COMMON/6/NTR,ICAT,NO,YL(2,2)
11260         COMMON/7/YD(2,2),Y(2,2),U(15),AST(3,3,2),STR(3,2)
11270         DIMENSION T(6),C(3,3),TT(3)
11280         YL(1,1)=Y(1,1)
11290         YL(2,1)=Y(2,1)
11300         CALL TRNS
11400 C       COMPUTE TRACKER TRANSFORMATION RELATIVE TO INERTIAL COORD
11410         DO 80 I=1,3
11420         DO 80 J=1,3
11430         C(I,J)=0.
11440         DO 80 K=1,3
11450         C(I,J) =C(I,J)+AST(I,K,NO)*B(K,J,1)
11460      80 CONTINUE
11470 C       COMPUTE STAR DIRECTION COSINES IN TRACKER AXES
11480         DO 90 I=1,3
11490         U(I) = C(I,1)*STR(1,1)+C(I,2)*STR(2,1)+C(I,3)*STR(3,1)
11500      90 CONTINUE
11630         U(5)=SQRT(1.-U(1)**2)
11820 C       COMPUTE TRACKER OUTPUT IF IT HAD INFINITE BANDWIDTH (INTERVAL AVE.)
11830         Y(1,1)=-(U(1)+SIN(YG))/U(5)-(SSV(4,1)+SSV(5,1))
11840         Y(2,1)=U(3)-(SSV(3,1)+U(5)*SSV(1,1)-U(1)*SSV(2,1))

11890    100 RETURN
```

```
      END
C
C
      SUBROUTINE TRCFLT
      COMMON/2/TTME,TO,TF,DELT,KDELT,X1(4),X1L(4)
      COMMON/5/SSV(27,2),PP(3),B(3,3,2)
      COMMON/6/NTR,ICAT,NO,YL(2,2)
      COMMON/7/YD(2,2),Y(2,2),U(15),AST(3,3,2),STR(3,2)
      DIMENSION C(2),R(2)
C     PROVIDES FILTERED TRACKER OUTPUT
      C(1)=SSV( 8,NO)/DELT
      C(2)=SSV( 9,NO)/DELT
      R(1)=EXP(-1./C(1))
      R(2)=EXP(-1./C(2))
      DO 10 K=1,2
      DO 10 I=1,2
   10 YD(I,K)=YD(I,K)*R(I)+(1.-C(I)*(1.-R(I)))*Y(I,K)
     1+(C(I)*(1.-R(I))-R(I))*YL(I,K)
      RETURN
      END
C
C
      SUBROUTINE PRFIL
C     CONVERTS 4-PARAMETER ATTITUDE SYSTEM TO 3 PARAMETERS AND MODIFIES
C     STATE TRANSITION MATRIX
      COMMON/1/NG,NOELP,NN1
      COMMON/2/TTME,TO,TF,DELT,KDELT,X1(4),X1L(4)
      COMMON/3/PHI0(12),TAU(3,6),WM(6),DRFT(6),GY(9,6)
      COMMON/4/PHI1(4,4),PHI2(4,3),Q(7,7),QQ(4,6),WR(3,2),RP(4,4)
      COMMON/5/SSV(27,2),PP(3),B(3,3,2)
      COMMON/6/NTR,ICAT,NO,YL(2,2)
      COMMON/7/YD(2,2),Y(2,2),U(15),AST(3,3,2),STR(3,2)
      COMMON/8/P(7,7),R(2,2),AK(9,2),HMAT(2,7)
      DIMENSION W(3)
      W(1)=X1L(1)/X1L(4)
      W(2)=X1L(2)/X1L(4)
      W(3)=X1L(3)/X1L(4)
      DO 10 I=1,3
      DO 10 J=1,3
      PHI1(I,J)=PHI1(I,J)-PHI1(I,4)*W(J)
   10 CONTINUE
      DO 12 I=1,3
```

```
      DO 12 J=1,NN1
      PHI2(I,J)=PH12(I,J)*DELT/2.
   12 CONTINUE
      RETURN
      END
C
C
      SUBROUTINE HMTRX
C     COMPUTES MEASUREMENT MATRIX
      COMMON/1/NG,NDELP,NN1
      COMMON/2/TIME,TO,TF,DELT,KDELT,X1(4),X1L(4)
      COMMON/6/NTR,ICAT,NO,YL(2,2)
      COMMON/7/YD(2,2),Y(2,2),U(15),AST(3,3,2),STR(3,2)
      COMMON/8/P(7,7),R(2,2),AK(8,2),HMAT(2,7)
      DIMENSION T(3),TT(4,4),T1(3,4)
      DIMENSION TA(2,4)
      DO 130 I=1,4
      TT(I,I)=0.
  130 CONTINUE
      TT(1,2) = -STR(3,1)
      TT(1,3) = STR(2,1)
      TT(1,4) = STR(1,1)
      TT(2,3) = -STR(1,1)
      TT(2,4) = STR(2,1)
      TT(3,4) = STR(3,1)
      TT(2,1) = -TT(1,2)
      TT(3,1) = -TT(1,3)
      TT(3,2) = -TT(2,3)
      TT(4,1) = TT(1,4)
      TT(4,2) = TT(2,4)
      TT(4,3) = TT(3,4)
      T(1) = -X1(1)/X1(4)
      T(2) = -X1(2)/X1(4)
      T(3) = -X1(3)/X1(4)
      DO 160 I=1,3
      DO 160 J=1,3
      TT(I,J) = TT(I,J)+STR(I,1)*T(J)
  160 CONTINUE
      DO 165 I=1,2
      T1(I,1) = (-AST(1,1,NO)*X1(4)+AST(I,2,NO)*X1(3)
     1-AST(I,3,NO)*X1(2))*2.
      T1(I,2) = (-AST(I,1,NO)*X1(3)-AST(I,2,NO)*X1(4)
```

```
      1+AST(I,3,NO)*X1(1))*2.
       T1(I,3) =(AST(I,1,NO)*X1(2)-AST(I,2,NO)*X1(1)
      1-AST(I,3,NO)*X1(4))*2.
       T1(I,4) = (-AST(I,1,NO)*X1(1)-AST(I,2,NO)*X1(2)
      1-AST(I,3,NO)*X1(3))*2.
  165 CONTINUE
      DO 166 K=1,4
      TA(1,K)=T1(1,K)/SQRT(1.-U(1)**2)
      TA(2,K)=-T1(3,K)
  166 CONTINUE
      DO 180 J=1,3
      HMAT(1,J)=0.
      HMAT(2,J)=0.
      DO 180 K=1,4
      HMAT(1,J)=HMAT(1,J)+TA(1,K)*TT(K,J)
      HMAT(2,J)=HMAT(2,J)+TA(2,K)*TT(K,J)
  180 CONTINUE
      RETURN
      END
C
C
      SUBROUTINE RMAT
C     FORMS MEASUREMENT NOISE COVARIANCE MATRIX
      COMMON/5/SSV(27,2),PP(3),B(3,3,2)
      COMMON/6/NTP,ICAT,NO,YL(2,2)
      COMMON/8/P(7,7),R(2,2),AK(8,2),HMAT(2,7)
      R(1,2)=R(2,1)=0.
      R(1,1)=SSV( 6,NO)**2
      R(2,2)=SSV( 7,NO)**2
      RETURN
      END
C
C
      SUBROUTINE FILT
C     USING KALMAN FILTER EQS., COMPUTES FILTER GAINS,AK, AND PROPAGATES
C     ERROR COVARIANCE MATRIX,P
      COMMON/1/NG,NDELP,NN1
      COMMON/3/PTMU(12),TAU(3,6),WM(6),DRFT(6),GY(9,6)
      COMMON/4/PHI1(4,4),PHI2(4,3),Q(7,7),QQ(4,6),WR(3,2),RP(4,4)
      COMMON/5/SSV(27,2),PP(3),B(3,3,2)
      COMMON/8/P(7,7),R(2,2),AK(8,2),HMAT(2,7)
      DIMENSION TA(7,7),TB(7)
```

```
C      COMPUTE ADDITIONAL CONSTANTS FOR PARTITIONING MATRICES
       NN2=NN1
       NN3=NN1-NN2
       N=NN1+3
       M=2
       CALL SPMMUL(PHI1,1,1,3,3,P,1,1,3,TA,1,1,4,7,7)
       CALL SPMMUL(PHI2,1,1,3,NN2,P,4,1,3,P,1,1,4,7,7)
       CALL SPMADD(TA,1,1,P,1,1,TA,1,1,3,3,7,7,7)
       CALL SPMMUL(PHI1,1,1,3,3,P,1,4,NN2,TA,1,4,4,7,7)
       CALL SPMMUL(PHI2,1,1,3,NN2,P,4,4,NN2,P,1,4,4,7,7)
       CALL SPMADD(TA,1,4,P,1,4,P,1,4,3,NN2,7,7,7)
       CALL SPMMUL(PHI1,1,1,3,3,P,1,4+NN2,NN3,TA,1,4+NN2,4,7,7)
       CALL SPMMUL(PHI2,1,1,3,NN2,P,4,4+NN2,NN3,P,1,4+NN2,4,7,7)
       I1=4+NN2
       CALL SPMADD(TA,1,I1,P,1,I1,P,1,I1,3,NN3,7,7,7)
       DO 15 I=1,3
       DO 15 K=1,3
       P(I,K)=0.
       DO 15 J=1,3
   15  P(I,K)=P(I,K)+TA(I,J)*PHI1(K,J)
       DO 20 I=1,3
       DO 20 K=1,3
       TA(I,K)=0.
       DO 20 J=1,NN2
   20  TA(I,K)=TA(I,K)+P(I,J+3)*PHI2(K,J)
       CALL SPMADD(P,1,1,TA,1,1,P,1,1,3,3,7,7,7)
       CALL SPMTRA(P,1,4,3,NN2,P,4,1,7,7)
       CALL SPMTRA(P,1,4+NN2,3,NN3,P,4+NN2,1,7,7)
C      P=PHI P PHI-TRANSPOSE HAS BEEN COMPUTED
       CALL SPMADD(P,1,1,Q,1,1,P,1,1,N,N,7,7,7)
       RETURN
       ENTRY FFILT
       CALL SPMMUL(HMAT,1,1,M,N,P,1,1,N,TA,1,1,2,7,7)
       CALL SPMTRA(HMAT,1,1,M,N,AK,1,1,2,8)
       CALL SPMMUL(TA,1,1,M,N,AK,1,1,M,TA,M+1,1,7,8,7)
       CALL SPMADD(TA,M+1,1,R,1,1,TA,1,1,M,M,7,2,7)
C      INVERSE ROUTINE FOLLOWS
       DET=TA(1,1)*TA(2,2)-TA(2,1)*TA(1,2)
       TA(1,M+1)=TA(2,2)/DET
       TA(1,M+2)=-TA(1,2)/DET
       TA(2,M+1)=-TA(2,1)/DET
       TA(2,M+2)=TA(1,1)/DET
```

```
C      END OF INVERSE ROUTINE
       CALL SRMMUL(AK,1,1,N,M,TA,1,M+1,M,TA,1,1,8,7,7)
       CALL SRMMUL(P,1,1,N,N,TA,1,1,M,AK,1,1,7,7,8)
C      AK HAS BEEN COMPUTED
       DO 45 I=1,N
       DO 45 K=1,N
       TA(I,K)=0.
       DO 40 J=1,M
   40  TA(I,K) = TA(I,K)-AK(I,J)*HMAT(J,K)
       IF (I.NE.K) GO TO 45
       TA(I,K) = 1.+TA(I,K)
   45  CONTINUE
       DO 55 I=1,N
       DO 50 K=1,N
       TB(K)=0.
       DO 50 J=1,N
   50  TB(K)=TB(K)+TA(I,J)*P(J,K)
       DO 55 K=1,N
   55  TA(I,K)=TB(K)
C      SYMMETRIZE ERROR COVARIANCE MATRIX
       DO 60 I=1,N
       DO 60 J=1,N
   60  P(I,J)=0.5*(TA(I,J)+TA(J,I))
C      P(K+1) HAS BEEN COMPUTED
       RETURN
       END
C
C
       SUBROUTINE SRMMUL(A,IMA,INA,MA,NA,B,IMB,INB,NB,C,IMC,INC,IRA,IRB,
      1IPC)
C      C=A*B WITH INIT. ARRAY ELEMENTS SPECIFIED
       DIMENSION A(49),B(49),C(49)
       DO 5 I=1,MA
       IPIMC = I+IMC
       IPIMA = I+IMA
       IF (NB.LT.1) GO TO 6
       DO 5 K=1,NB
       KPINC = K+INC
       KPINB = K+INB
       IC = IPIMC-1+(KPINC-2)*IRC
       C(IC) = 0.
       IF (NA.LT.1) GO TO 5
```

```
      DO 5 J=1,NA
      JPINA = J+INA
      JPIMB = J+IMB
      IA = IPIMA-1+(JPINA-2)*IRA
      IB = JPIMB-1+(KPINB-2)*IRB
    5 C(IC) = C(IC)+A(IA)*B(IB)
    6 RETURN
      END
C
C
      SUBROUTINE SRMADD(A,IMA,INA,B,IMB,INB,C,IMC,INC,M,N,IRA,IRB,IRC)
C     C=A+B WITH INIT. ARRAY ELEMENTS SPECIFIED
      DIMENSION A(49),B(49),C(49)
      DO 5 I=1,M
      IF (N.LT.1) GO TO 6
      DO 5 J=1,N
      IPIMC = I+IMC
      JPINC = J+INC
      IPIMA = I+IMA
      JPINA = J+INA
      IPIMB = I+IMB
      JPINB = J+INB
      IA = IPIMA-1+(JPINA-2)*IRA
      IB = IPIMB-1+(JPINB-2)*IRB
      IC = IPIMC-1+(JPINC-2)*IRC
    5 C(IC) = A(IA)+B(IB)
    6 RETURN
      END
C
C
      SUBROUTINE SRMTRA(A,IMA,INA,M,N,B,IMB,INB,IRA,IRB)
      DIMENSION A(49),B(49)
C     B=A-TRANSPOSE WITH INIT. ARRAY ELEMENTS SPECIFIED
      IF (N.LT.1) GO TO 6
      DO 5 I=1,N
      DO 5 J=1,M
      IPIMB = I+IMB
      JPINB = J+INB
      JPIMA = J+IMA
      IPINA = I+INA
      IA = JPIMA-1+(IPINA-2)*IRA
      IB = IPIMB-1+(JPINB-2)*IRB
```

```
14710      5 B(IB)=A(IA)
14720      6 RETURN
14730        END
14740  C
14750  C
14760        SUBROUTINE POFIL
14770  C     UPDATES ATTITUDE VARIABLES AND OTHER SYSTEM ELEMENTS OF THE
14780  C     STATE VECTOR
14790        COMMON/1/NG,NDELP,NN1
14800        COMMON/2/TIME,TO,TE,DELT,KDELT,X1(4),X1L(4)
14810        COMMON/3/PIMU(12),TAU(3,6),WM(6),DRFT(6),GY(9,6)
14820        COMMON/5/SSV(27,2),PP(3),B(3,3,2)
14830        COMMON/7/YD(2,2),Y(2,2),U(15),AST(3,3,2),STR(3,2)
14840        COMMON/8/P(7,7),R(2,2),AK(8,2),HMAT(2,7)
14850        DIMENSION W(3),T(3)
14860        W(1)=YD(1,2)-YD(1,1)
14870        W(2)=YD(2,2)-YD(2,1)
14900  C     COMPUTE CORRECTION FOR EACH SYSTEM PARAMETER OF STATE VECTOR
14910        DO 11 I=1,NN1
14920        W(3) = AK(I+3,1)*W(1)+AK(I+3,2)*W(2)
15020        PIMU(I)=PIMU(I)+W(3)
15060     11 CONTINUE
15080  C     COMPUTE CORRECTIONS FOR EACH ATTITUDE VARIABLE
15090        DO 9 I=1,3
15100        T(I) = AK(I,1)*W(1)+AK(I,2)*W(2)
15110      9 CONTINUE
15120  C     UPDATE ATTITUDE VARIABLES
15130        X1(4)=X1(4)-(X1(1)*T(1)+X1(2)*T(2)+X1(3)*T(3))/X1(4)
15140        DO 10 I=1,3
15150        X1(I)=X1(I)+T(I)
15160     10 CONTINUE
15170        RETURN
15180        END
15190  C
15200  C
```

```
00100       PROGRAM DTAPED(INPUT,OUTPUT,TAPE1)
00110       COMMON A(300,3),N(300),LFILE
00120       DIMENSION B(3)
00125       REWIND 1
00130       I=0
00140    10 I=I+1
00150       READ(1,6) A(I,1),A(I,2),A(I,3),N(I)
00155       A(I,3)=SQRT(A(I,2)**2+A(I,3)**2)
00160    6  FORMAT(3(2X,E13.6),2X,I1)
00170       IF(EOF,1) 20,10
00180    20 CONTINUE
00190       LFILE=I-1
00200       ACCEPT N1
00210       PRINT 2,N1
00220    2  FORMAT(X,8HRUN NO. ,I2)
00221       DO 100 L1=2,3
00222       PRINT 7,L1
00223    7  FORMAT(//X,I1,X,12HAXIS RESULTS/
00224      122X,3HAV.,5X,3HRSS,4X,4HPEAK/)
00230       CALL ANAL(B,1,L1)
00240       PRINT 3,(B(I),I=1,3)
00250    3  FORMAT(16HESTIMATION ERROR,5X,3(F5.2,3X))
00260       CALL ANAL(B,2,L1)
00270       PRINT 4,(B(I),I=1,3)
00280    4  FORMAT(17HFILTER CONFIDENCE,4X,3(F5.2,3X))
00290       CALL ANAL(B,3,L1)
00292       DO 30 I=1,3
00294    30 B(I)=B(I)/4.648E-6
00300       PRINT 5,(B(I),I=1,3)
00310    5  FORMAT(14HMEAS. RESIDUAL,7X,3(F5.2,3X))
00315    100 CONTINUE
00320       END
00330 C
00340 C
00350       SUBROUTINE ANAL(B,K,L1)
00360       COMMON A(300,3),N(300),LFILE
00370       DIMENSION B(3),C(200,2)
00380       I=0
00390       DO 50 J=1,LFILE
00400       IF(N(J).NE.K) GO TO 50
00410       I=I+1
00420       C(I,1)=A(J,1)
```

```
00430         C(I,2)=A(J,L1)
00440      50 CONTINUE
00450         I1=I-1
00460         S=SM=0.
00470         T0=C(I,1)-C(1,1)
00480         SMX=C(1,2)
00490         DO 30 J=1,I1
00500         T=C(J+1,1)-C(J,1)
00510         X2=C(J+1,2)
00520         X1=C(J,2)
00530         S=S+(X1**2+X2**2+X1*X2)*T/3.
00540         SM=SM+T*(X1+X2)/2.
00550         IF(X2.LT.SMX) GO TO 30
00560         SMX=X2
00570      30 CONTINUE
00580         B(1)=SM/T0
00590         B(2)=SQRT(S/T0)
00600         B(3)=SMX
00610         RETURN
00620         END
```

APPENDIX C

CSDL GYRO REPORTS

C-4441

OAO-IRU ENGINEERING MODEL DATA AT GODDARD SPACE FLIGHT CENTER

May 1975

by

R. CARSON

R. HARRIS

ACKNOWLEDGEMENT

The authors wish to thank F. J. Kull and Terrance P. O'Neil of Goddard Space Flight Center for their invaluable support and assistance in obtaining data from the OAO-IRU Engineering Model.

This report was prepared under DSR Project 55-67800 sponsored by the Goddard Space Flight Center of the National Aeronautics and Space Administration. (P.O. S-11566B).

TABLE OF CONTENTS

1.0 INTRODUCTION

The IRU(OAO) is a three-axis strap-down inertial reference unit that was designed and built by the Charles Stark Draper Laboratory (CSDL) under contract with NASA's Goddard Space Flight Center (GSFC) for their Orbiting Astronomical Observatory. The IRU(OAO) Engineering Model was built in 1968, went through qualification testing in 1969 and was delivered to GSFC in March 1970. Since then it has been modified and used by GSFC to demonstrate various concepts.

Early in 1975 consideration was given to using the Engineering Model in a concept evaluation program to be conducted with the TRW Precision Attitude Determination System (PADS). In mid-April 1975, GSFC contracted with CSDL for the following efforts:

1. to evaluate the current performance and operating characteristics of the Engineering Model

2. to assist with the integration of the unit with the PADS if the first item shows the Engineering Model to be in satisfactory operating condition.

This report describes the first effort. Two trips were made to GSFC in support of the first item. The first trip was made from 7-10 April 1975 to investigate the modifications made by GSFC to the Engineering Model. The second trip was made from 20-23 May 1975 to take data from the system. A brief summary of both trips is included in Section 3. Section 4 contains a summary of the result for data accumulated from 20-28 May 1975. The conclusion and recommendations are reported in section 2.

2.0 CONCLUSION AND RECOMMENDATIONS

The Engineering Model of the OAO-IRU is not operating properly. This is apparent from several system malfunctions during testing and the results of the data accumulated. Assuming, however, that the system does not degrade further, the following performance capabilities are feasible if the system is continually updated at 30 minute intervals or less.

1. Roll Axis - One sigma angle uncertainty
   < 1 arc-second.

2. Pitch Axis - One sigma angle uncertainty
   < 2 arc-seconds.

3. Yaw Axis - One sigma angle uncertainty
   < 10 arc-seconds.

Because of abnormalities in the system data obtained (especially for the yaw axis gyro), history of system malfunctions, and the possibility of future malfunctions or failures, CSDL recommends that GSFC does not send the OAO-IRU Engineering Mdoel to TRW for integration with the PADS system. It is believed that there is an intermittant failure either in the Precision Power Supply or Wheel Power Supply within the Electronics Package. However, identifying and correcting such a problem could be quite time consuming and unfortunately is beyond the scope of this contract.

3.0 SUMMARY OF EVENTS

The first trip was made to GSFC from 7-10 April 1975. The purpose of this trip was to investigate a possible module failure and become familiar with the modifications made by GSFC to the OAO-IRU Engineering Model. The suspect module was an MH-7 type which supplies the gyro's signal generator excitation. This module was found to be defective and was subsequently repaired by externally wiring a set of transistors to replace the defective ones within the module. This same procedure was previously used on an MH-3 type module that provides the suspension excitation. There was no apparent reason for either of these modules' demise. It is known however that the MH-3 module will self-destruct if it loses a reference frequency from the precision power supply in the electronics package. Another possible malfunction in an MD-10 type module was also noted (R-Term Pulse Generator). However, since this failure should not affect PADS testing it was not pursued. All repairs were made by GSFC technicians.

After the above repairs were made to the system, a second trip (20-23 May 1975) was made to obtain data from the IRU. The system was turned on and data acquisition was started at approximately 9 pm on 20 May 1975. At approximately 6 am on 21 May 1975 the system went into the ISTAB mode with a continuous-angle-reset commanded. This is symptomatic of a momentary loss of power. The system was reset at approximately 9 am and ran for approximately 8 hours before the same thing happened again. The power supply in the Ground Support Equipment which supplies the prime power to the IRU was then replaced and data was accumulated from Wednesday night until Thursday morning (21-22 May). No problems occurred during that period.

During Thursday the system was shut down for modifications to the IRU-PADS data interface. After those modifications were completed, the system was turned on with the IP-load panel (gyro package simulator) and the electronics package checked out. Once, while in this configuration the system went into the ISTAB mode with a continuous angle reset commanded. Also while in this mode a second anomalous behavior was observed. When the dummy wheel load was cycled on and off, the system power would frequently (approximately 50% of the time) increase by 60 watts. When this happened, the only noticeable effect was a 3 to 4 volt drop in the 45 volts which is used for the gyro torque loops. On Thursday pm (22 May) the IRU was again turned on with the Inertial Package and data was accumulated until 2:30 pm on 28 May 1975 without any further visible abnormalities.

4.0 SUMMARY OF RESULTS

Two types of data were accumulated during the period from 20-28 May 1975.

(1) Long Term Stability data where the net number of rebalance torque pulses were calculated and recorded every 2.56 or 20.48 seconds.

(2) Noise Equivalent Angle data where each 5 millisecond rebalance pulse was recorded.

4.1 Long Term Stability Data

Three sets of long term data were recorded for each gyro. The periods over which each set of data was taken are listed below.

(1) Set 1 9 pm 20 May to 9 am 21 May 1975.

(2) Set 2 9 pm 21 May to 9 am 22 May 1975.

(3) Set 3 11 pm 22 May to 2:30 pm 28 May 1975.

Figures 1 through 3 show the results of set 1 for the roll, pitch, and yaw axis respectively. This data was processed by calculating the average rate every 71.68 seconds. Figure 4 is the output of a tiltmeter whose sensitive axis was about a NW-SE line.

These plots reveal the following:

(1)* Rate impulses in the roll axis output that occur every 1/2 to 1 hour and have a magnitude of 0.2 to 0.3 meru.

(2) Several small changes in level (0.1 to 0.2 meru) and one large change of about 0.5 meru in the pitch axis.

(3) Very erratic behavior of the yaw axis with peak-to-peak changes of 1.5 meru.

(4) The tiltmeter data is quiet and well behaved thus eliminating base motion as a source of the gyros' behavior.

Figures 5 through 8 are the results of data set 2 and were processed as set 1. Again each instrument has its own unique behavior. Figure 9 through 11 are the results of data set 3. This data is a graphical presentation of the average

* This data without the presence of the rate impulses is characteristic of the performance of each instrument when the IRU is operating properly.

rate over every 675.84 seconds. The spikes in fig 10 (pitch axis) are a result of a data acquisition malfunction. This data again is consistent with that previously obtained even though no visible system malfunctions occurred. Data set 3 also shows the following long term characteristics of each instrument.

(1) The roll gyro is fairly well behaved except for the existence of rate impulses (.2 to .3 meru) occurring every 1/2 to 1 hour.

(2) The pitch gyro exhibits discrete changes in the rate output with a peak amplitude of 1 meru. These changes are very regular and have a periodicity of ~ 16 hours.

(3) The yaw gyro is extremely erratic with peak to peak changes in rate of approximately 7.5 meru.

4.2 Noise Equivalent Data

As mentioned above, this data was recorded every .005 seconds. To fulfill contractual requirements, 40 samples were summed to yield .200 second samples. This data was then processed to determine the best fit (least squares) attitude for each 30 minute segment of the data. Tables 1-3 show the peak and one sigma deviation of the .200 sec data samples from the best fit data for each 30 minute segment of the roll, pitch any yaw axis gyros respectively. These data are consistent with Long Term data; especially the erratic behavior of yaw gyro. The deviations for each 30 minute segment are graphically shown in figures 12 through 14. This data was plotted by sampling the deviation from the best fit every 36 seconds.

MINI-MIDRC ORD IRU TEST CHANNEL M1 TWX
MAY 20 TO MAY 21, 1975 RUN 055

ROLL AXIS

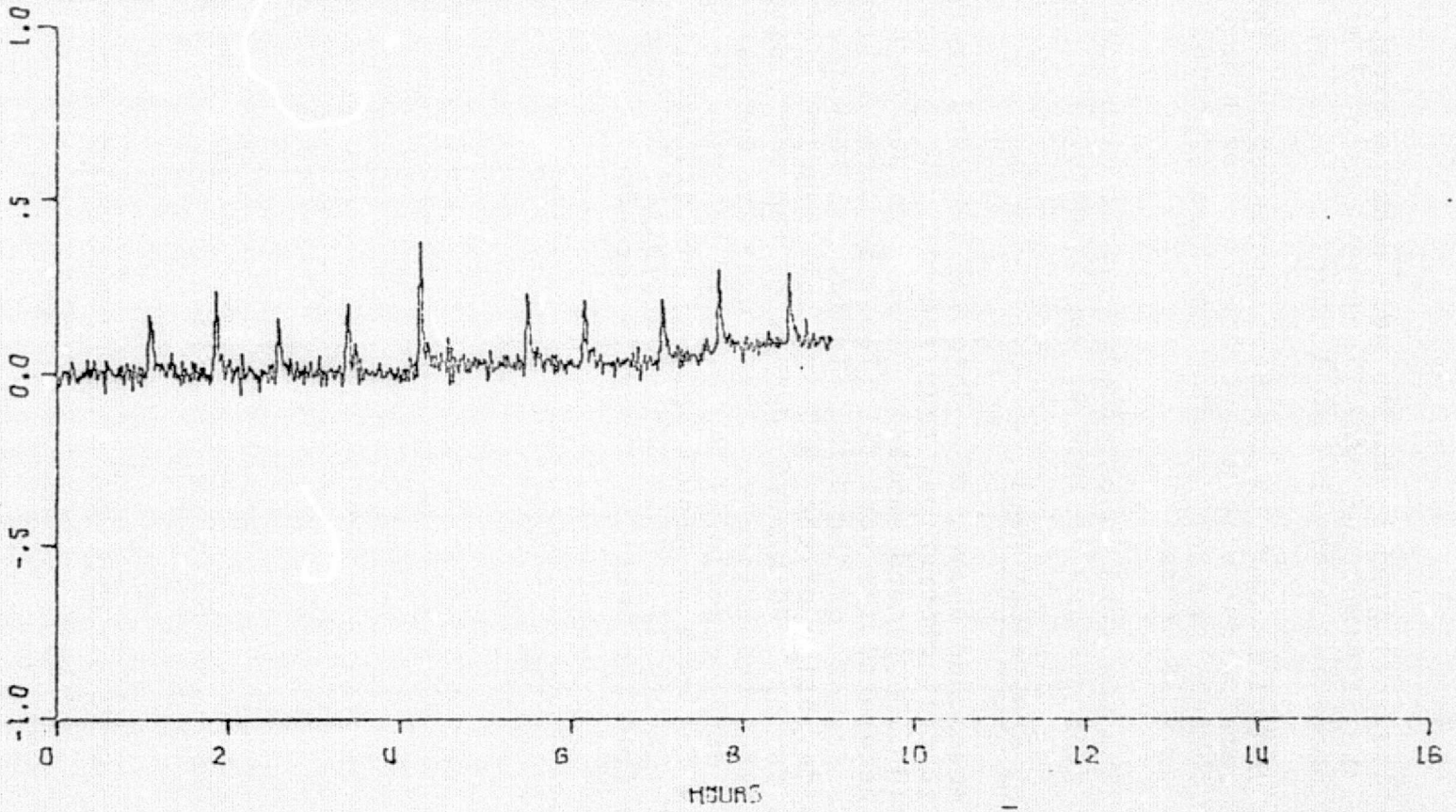

C-12

REFERENCE VALUE	53.700000	MERU
MEAN	53.734668	MERU
SIGMA	.05359	MERU
TREND	.01104	MERU /HOURS
SIGMA/TREND	.04582	MERU
AVERAGING PERIOD	71.68	SECONDS
REJECTED POINTS 198	OUT OF 652	SAMPLES

MINI 055M 1

Fig 1

THE ABOVE DATA WERE PROCESSED BY SLIDING AN AVERAGING [illegible] SECOND CONTINUOUS DATA SAMPLES. THE APPROXIMATE FILTER CHARACTERISTICS DERIVED ARE:

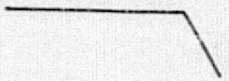

(-2) Effective Bandwidth
rad/s

SKIPPER K TEST LABORATORY/BEDFORD FLIGHT FACILITY
SMS TEST LAB [illegible] 5/27/75 BY

MINI-MIDAC ORD IRU TEST CHANNEL M1 TWX
MAY 20 TO MAY 21, 1975 RUN 055

ROLL AXIS

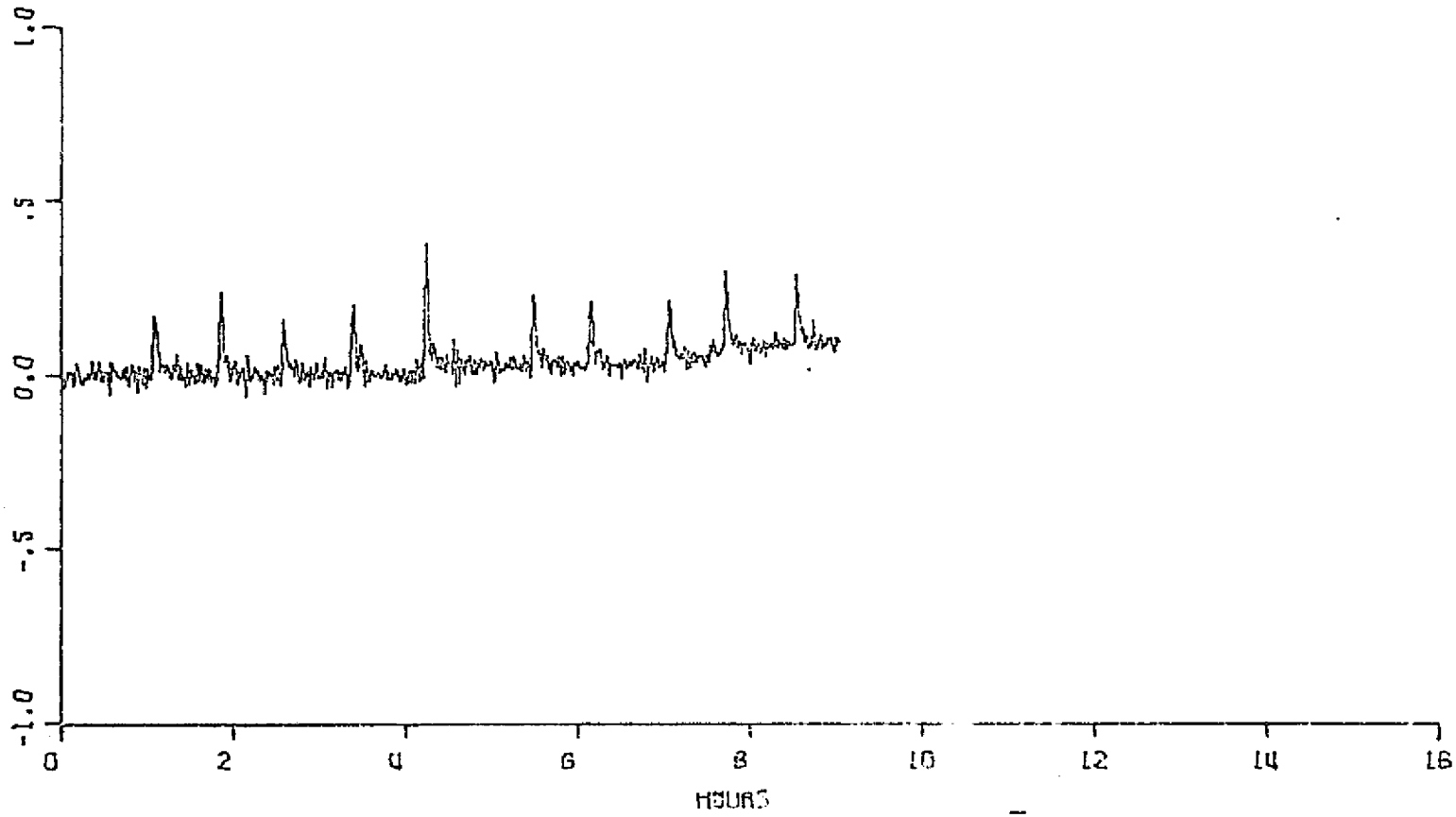

REFERENCE VALUE	53.700000	MEAN
MEAN	53.734668	MEAN
SIGMA	.05359	MEAN
TREND	.01104	MEAN /HOURS
SIGMA/TREND	.04862	MEAN
AVERAGING PERIOD	71.68	SECONDS
REJECTED POINTS 198	OUT OF 657	SAMPLES
MINI 055M 1		

Fig 1

THE ABOVE DATA WERE PROCESSED BY SLIDING AN AVERAGING [illegible] SECOND CONTINUOUS DATA SAMPLES. THE APPROXIMATE FILTER CHARACTERISTICS DERIVED ARE:

(-2) Effective Bandwidth
rad/s

SKIPPER K TEST LABORATORY/REDSTONE FLIGHT FACILITY
[illegible]

MINI-MIORC ORD IRU TEST CHANNEL M2 TWY
MAY 20 TO MAY 21, 1975 RUN 055

PITCH AXIS

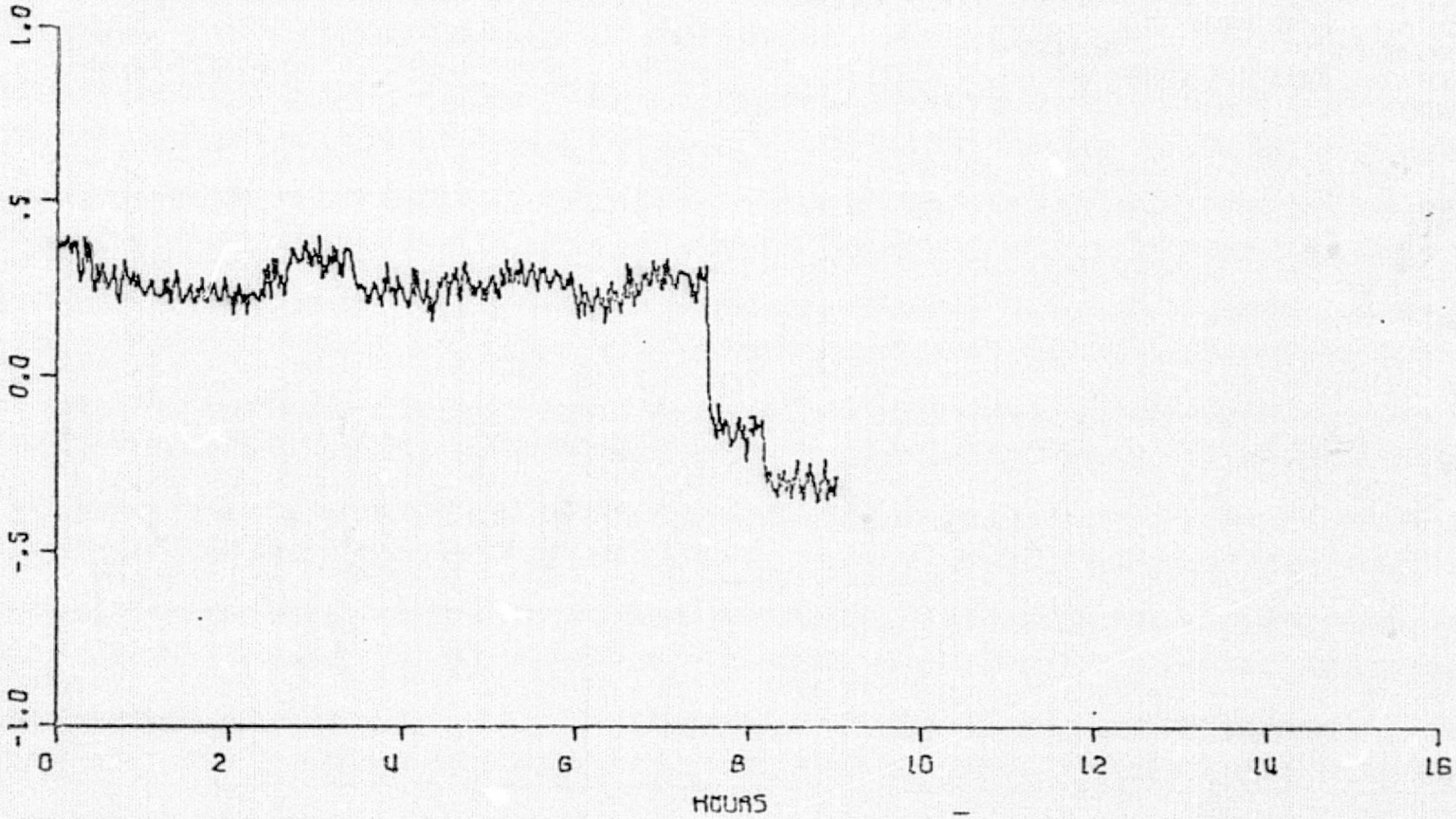

REFERENCE VALUE	-780.00000	MERU
MEAN	-779.81608	MERU
SIGMA	.1966	MERU
TREND	-.04614	MERU /HOURS
SIGMA/TREND	.1545	MERU
AVERAGING PERIOD	71.68	SECONDS
REJECTED POINTS 198	OUT OF 652	SAMPLES

MINNY 055M 2

Fig 2

THE ABOVE DATA WERE PROCESSED BY SLIDING AND AVERAGING [illegible] SECOND CONTINUOUS DATA SAMPLES. THE APPROXIMATE FILTER CHARACTERISTICS DERIVED ARE:

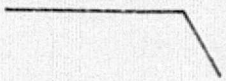

(-2) Effective Bandwidth
[illegible] rad/s

SKIPPER K TEST LABORATORY/BEDFORD FLIGHT FACILITY
SDS TEST LAB LSK 5/27/75 BV

MINI-MIDAC GRO IMU TEST CHANNEL M2 TWY
MAY 20 TO MAY 21, 1975 RUN 055

PITCH AXIS

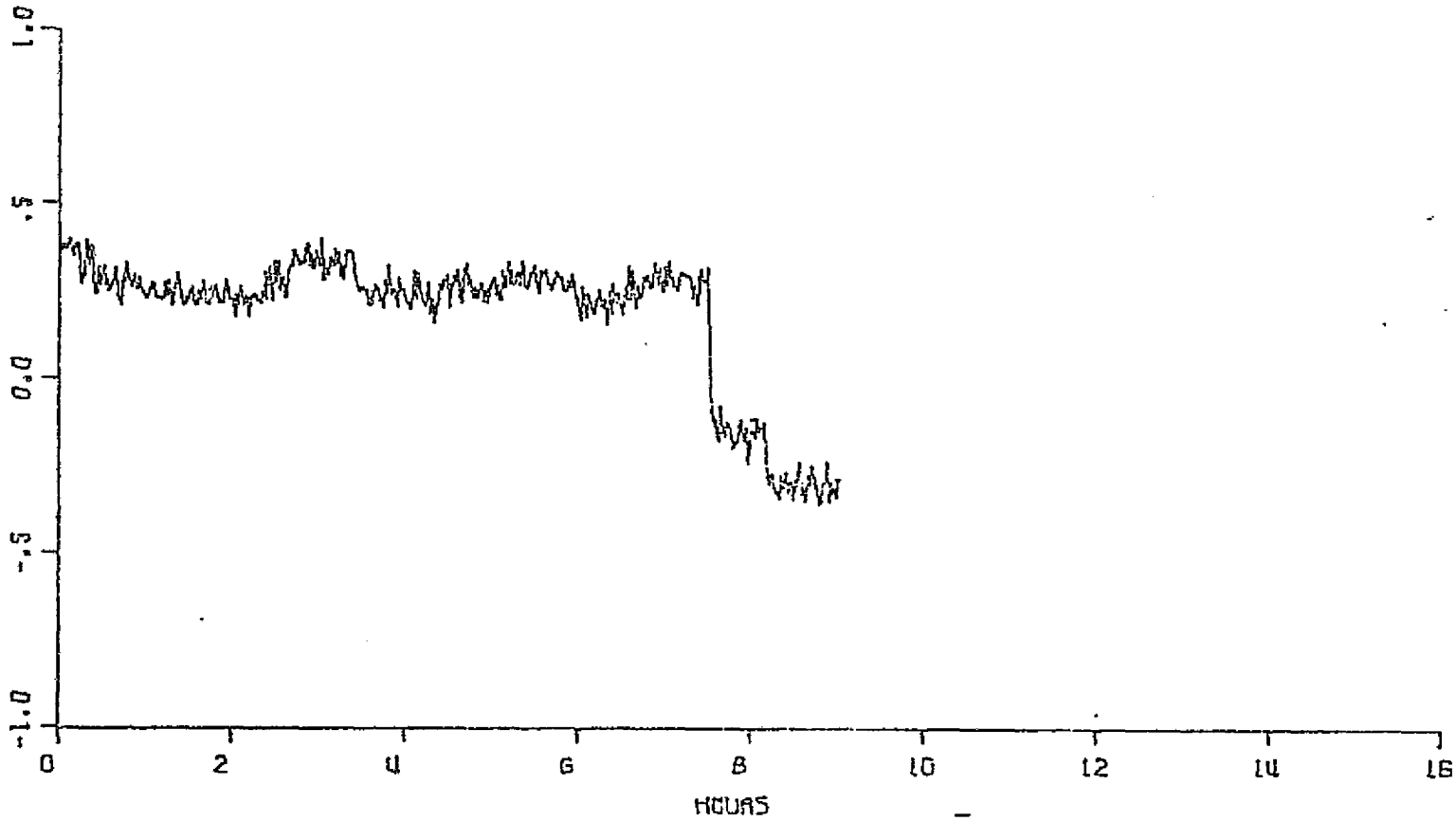

REFERENCE VALUE	-780.00000	MERU
MEAN	-779.81608	MERU
SIGMA	.1966	MERU
TREND	-.04614	MERU / HOURS
SIGMA/TREND	.1545	MERU
AVERAGING PERIOD	71.68	SECONDS
REJECTED POINTS 198	OUT OF 652	SAMPLES
MINNY 055M 2		

Fig 2

THE ABOVE DATA WERE PROCESSED BY SLIDING AND AVERAGING [illegible] SECOND CONTINUOUS DATA SAMPLES. THE APPROXIMATE FILTER CHARACTERISTICS DERIVED ARE:

(-2) Effective Bandwidth
[illegible] rad/s

SKIPPER K TEST LABORATORY/BEDFORD FLIGHT FACILITY
SRS TEST LAB LEK 5/27/75 GV

MINI-MIORC ORO IRU TEST CHANNEL M3 TWZ
MAY 20 TO MAY 21, 1975 RUN 055

YAW AXIS

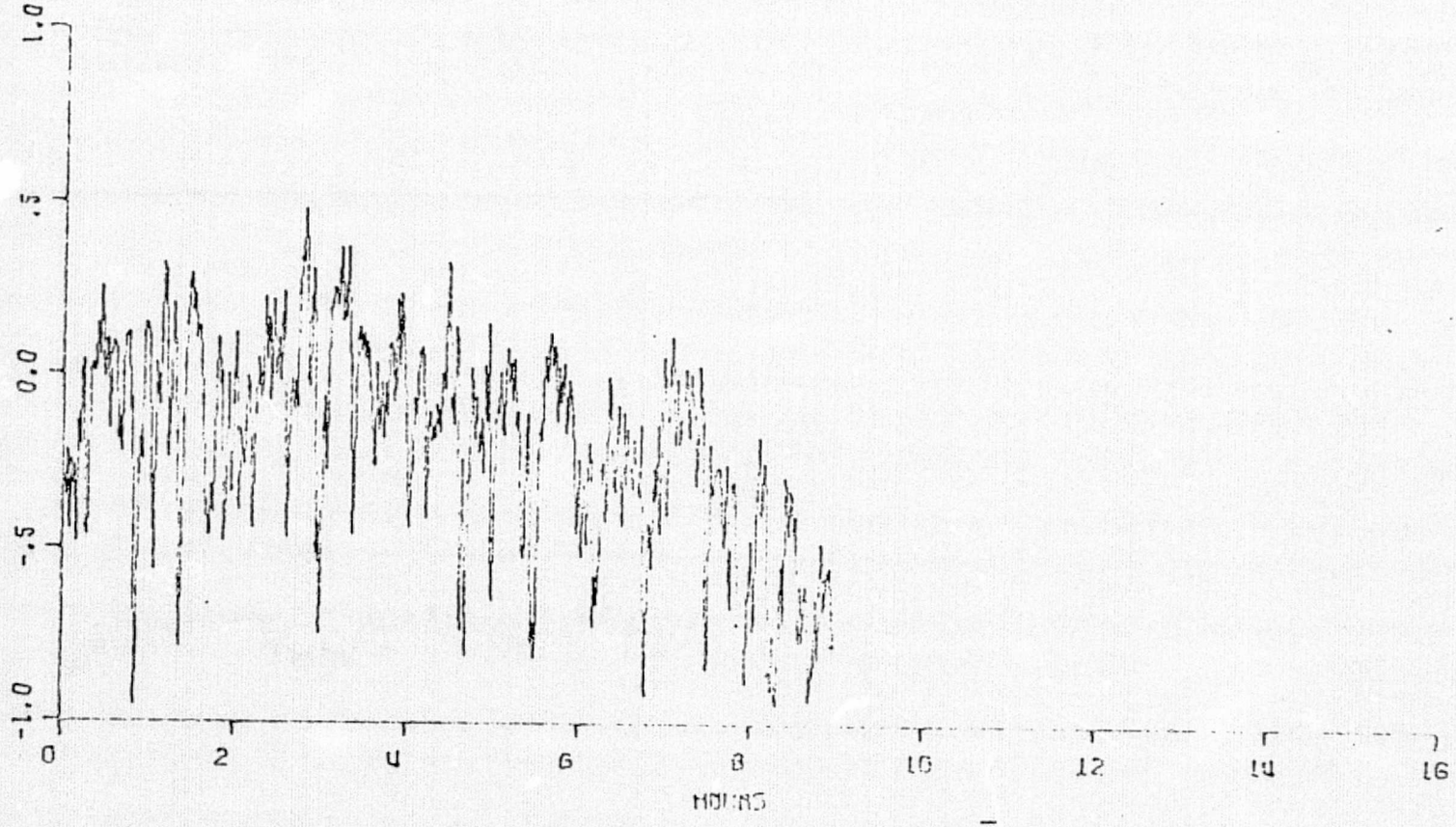

REFERENCE VALUE	-718.69999	MERU
MEAN	-718.90233	MERU
SIGMA	.2899	MERU
TREND	-.05416	MERU /HOURS
SIGMA/TREND	.2541	MERU
AVERAGING PERIOD	71.68	SECONDS
REJECTED POINTS 207	OUT OF 652	SAMPLES
MINNY OSSM 3		

Fig 3

THE ABOVE DATA WERE PROCESSED BY SLIDING AND AVERAGING [illegible] SECOND CONTINUOUS DATA SAMPLES. THE APPROXIMATE FILTER CHARACTERISTICS DERIVED ARE:

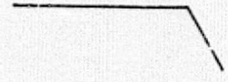

SKIPPER K TEST LABORATORY/REDSTONE FLIGHT FACILITY
[illegible]

MINI-MIDRC GRD IRU TEST CHANNEL M3 TWZ
MAY 20 TO MAY 21, 1975 RUN 055

YAW AXIS

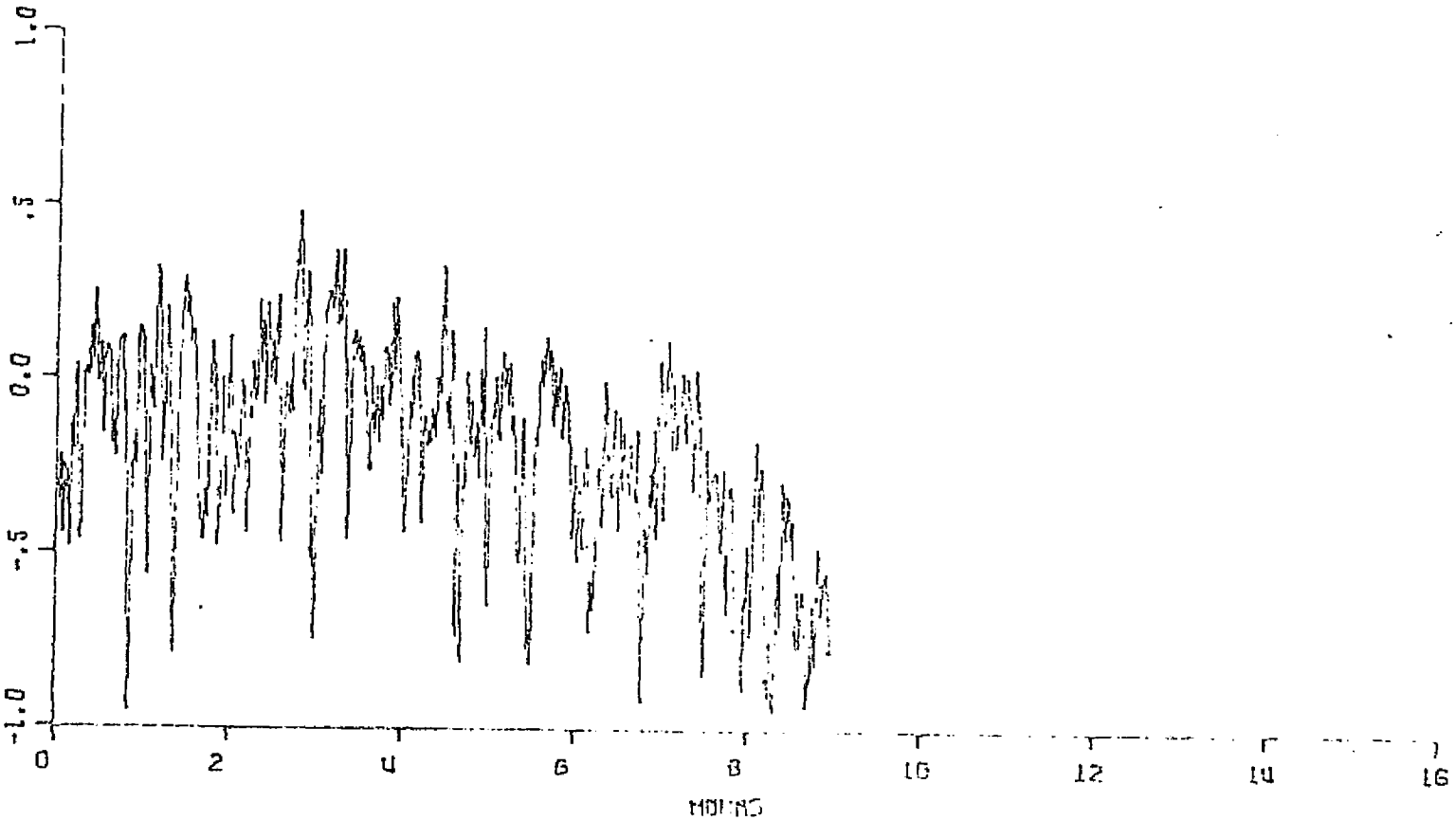

REFERENCE VALUE	-718.69999	MERU
MEAN	-718.90233	MERU
SIGMA	.2899	MERU
TREND	-.05416	MERU /MINS
SIGMA/TREND	.2541	MINS
AVERAGING PERIOD	71.68	SECONDS
REJECTED POINTS 207	OUT OF 652	SAMPLES

MINNY 055M 3

Fig. 3

THE ABOVE DATA WERE PROCESSED BY SLIDING AND AVERAGING [illegible] SECOND CONTINUOUS DATA SAMPLES. THE APPROXIMATE FILTER CHARACTERISTICS DERIVED ARE:

(-2) Effective Bandwidth
rad/s

SKIPPER K TEST LABORATORY/RED STONE FLIGHT FACILITY
[illegible]

MINI-MIORC ORD IMU TEST CHANNEL M4 TILT METER
MAY 20 TO MAY 21, 1975 RUN 055

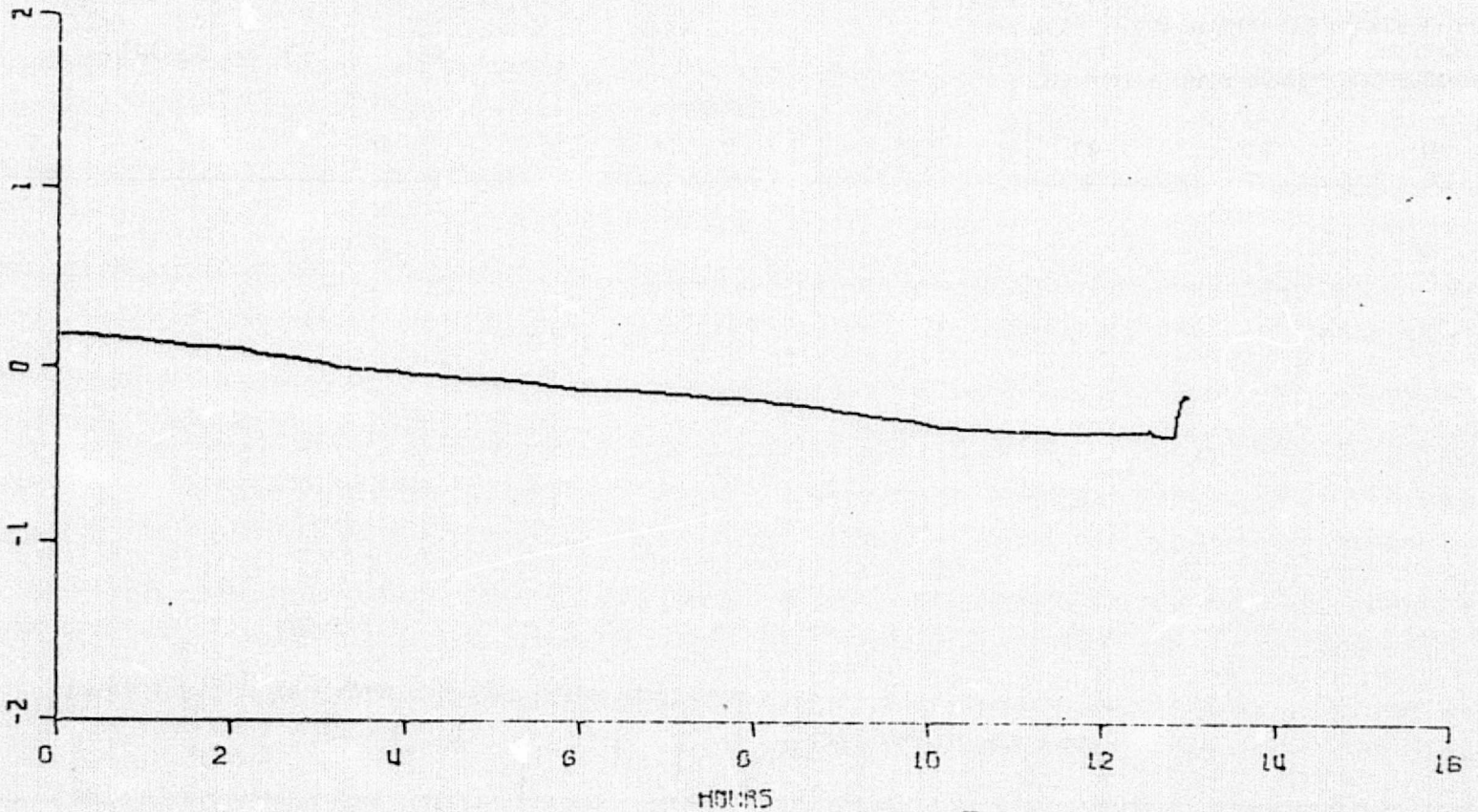

REFERENCE VALUE	1.8390000	ARC SEC
MEAN	1.7107270	ARC SEC
SIGMA	.1660	ARC SEC
TREND	-.04345	ARC SEC/HOURS
SIGMA/TREND	.03156	ARC SEC
AVERAGING PERIOD	71.68	SECONDS
REJECTED POINTS 0	OUT OF 652	SAMPLES

MINNY 055M V

THE ABOVE DATA WERE PROCESSED BY SLIDING AND AVERAGING [illegible] SECOND CONTINUOUS DATA SAMPLES. THE APPROXIMATE FILTER CHARACTERISTICS DERIVED ARE:

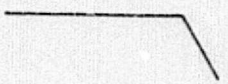

SKIPPER K TEST LABORATORY/BEDFORD FLIGHT FACILITY
SDS TEST LAB LOG 3279/75 EV

Fig. 4

MINI-MIDRC ORD IRU TEST CHANNEL M4 TILT METER
MAY 20 TO MAY 21, 1975 RUN 055

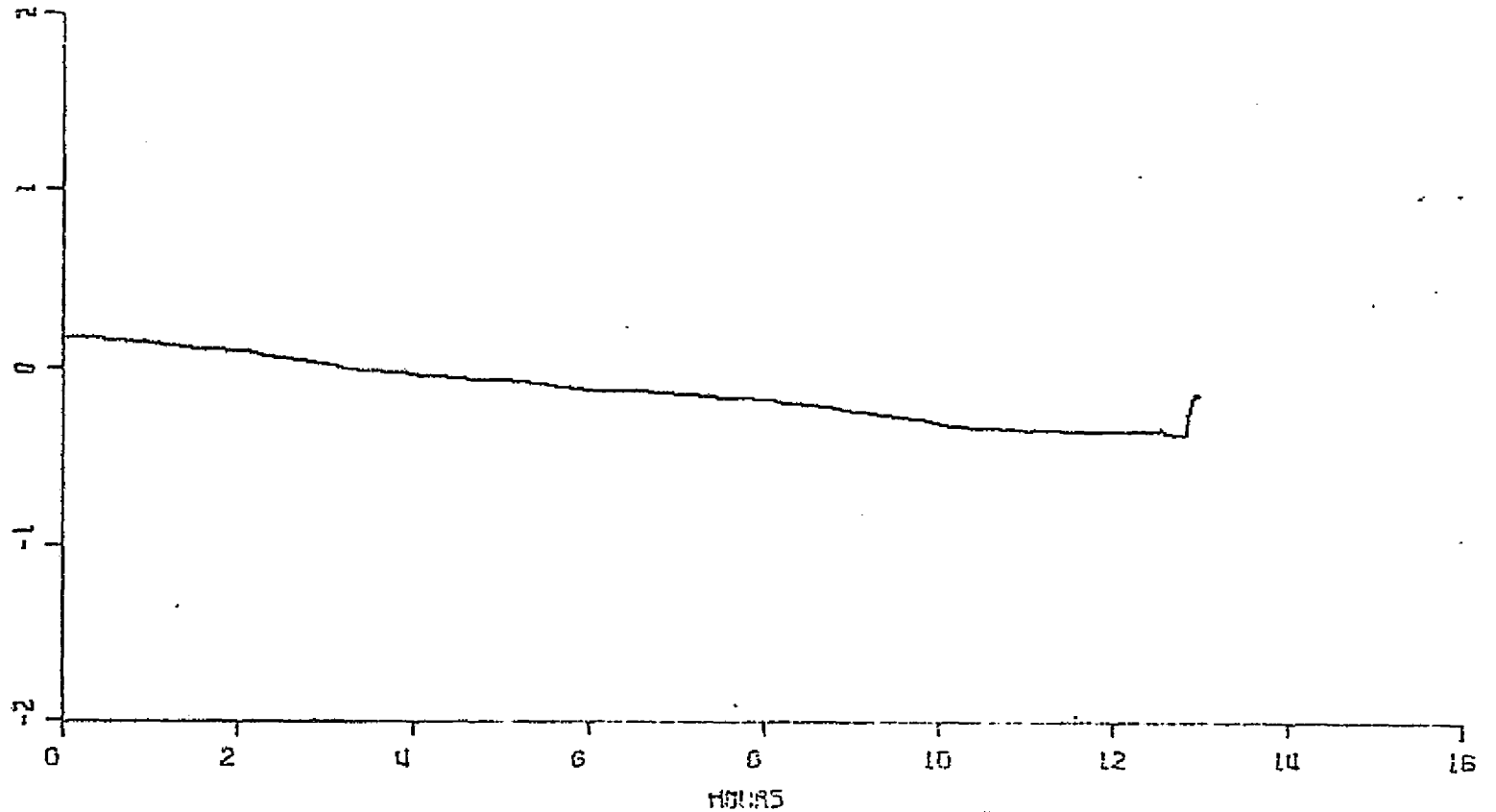

REFERENCE VALUE	1.8390000	ARC SEC
MEAN	1.7107270	ARC SEC
SIGMA	.1660	ARC SEC
TREND	-.04345	ARC SEC/HOURS
SIGMA/TREND	.03156	ARC SEC
AVERAGING PERIOD	71.68	SECONDS
REJECTED POINTS 0	OUT OF 65?	SAMPLES
MINNY 055M 4		

Fig. 4

THE ABOVE DATA WERE PROCESSED BY SLIDING AND AVERAGING [illegible] SECOND CONTINUOUS DATA SAMPLES. THE APPROXIMATE FILTER CHARACTERISTICS DERIVED ARE:

(-2) Effective Bandwidth
rad/s

SKIPPER K TEST LABORATORY/BEDFORD FLIGHT FACILITY
[illegible]

MINI-MIORC ORO IRU TEST CHANNEL M1 TWY
MAY 21 TO MAY 22. 1975 RUN 056

ROLL AXIS

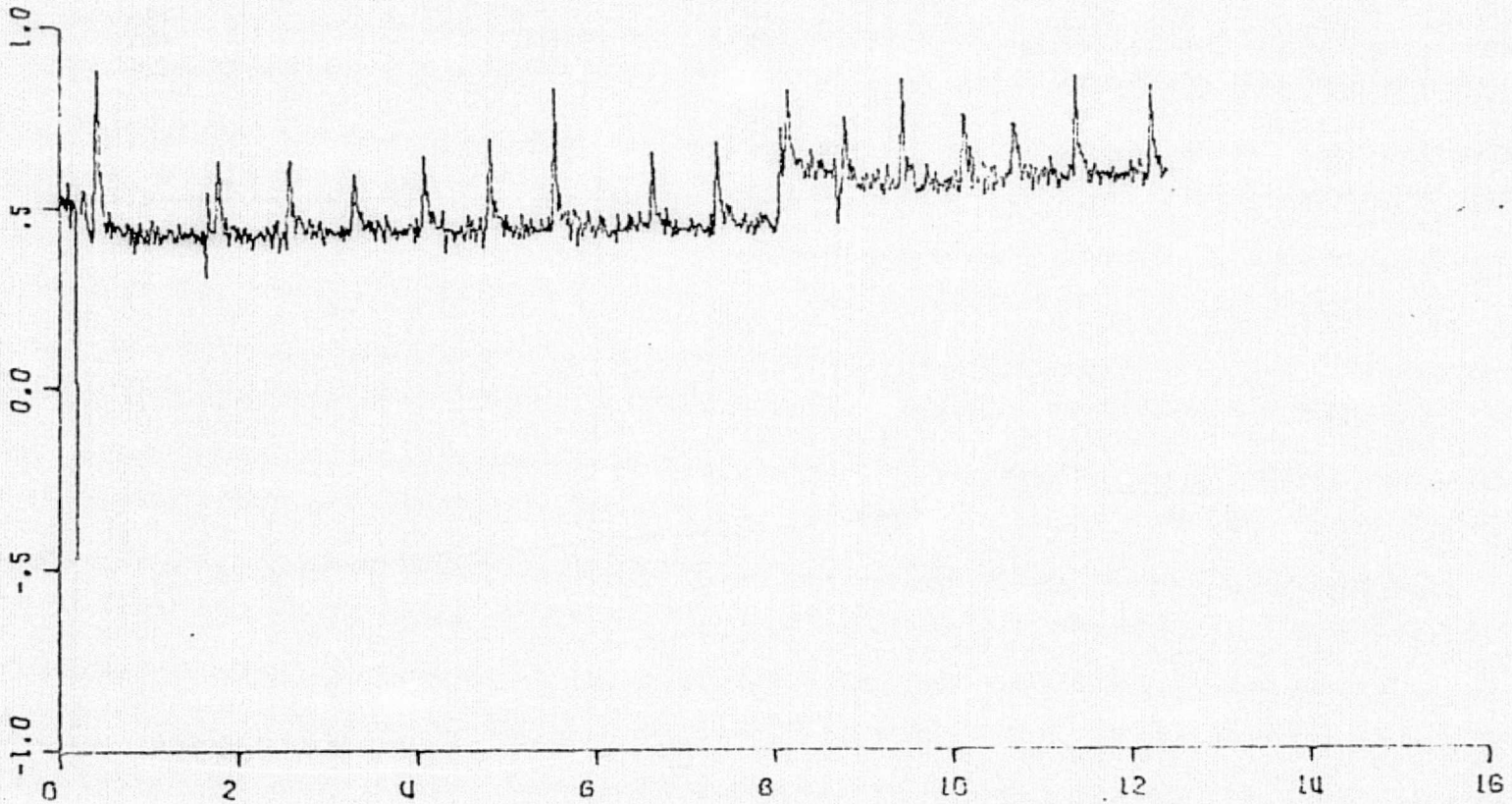

REFERENCE VALUE	53.700000	MERU
MEAN	54.200475	MERU
SIGMA	.09771	MERU
TREND	.01735	MERU /HOURS
SIGMA/TREND	.07545	MERU SECONDS
AVERAGING PERIOD	71.68	SAMPLES
REJECTED POINTS 1	OUT OF 623	
MINNY 056M 1		

Fig. 5

THE ABOVE DATA WERE PROCESSED BY SLIDING AND AVERAGING 2[illegible] , 2.5[illegible] SECOND CONTINUOUS DATA SAMPLES. THE APPROXIMATE FILTER CHARACTERISTICS DERIVED ARE:

(-2) Effective Bandwidth
[illegible] rad/s

SKIPPER K TEST LABORATORY/BEDFORD FLIGHT FACILITY
SKS TEST [illegible]

MINI-MIDRC DRO IRU TEST CHANNEL M1 TNY
MAY 21 TO MAY 22, 1975 RUN 056

ROLL AXIS

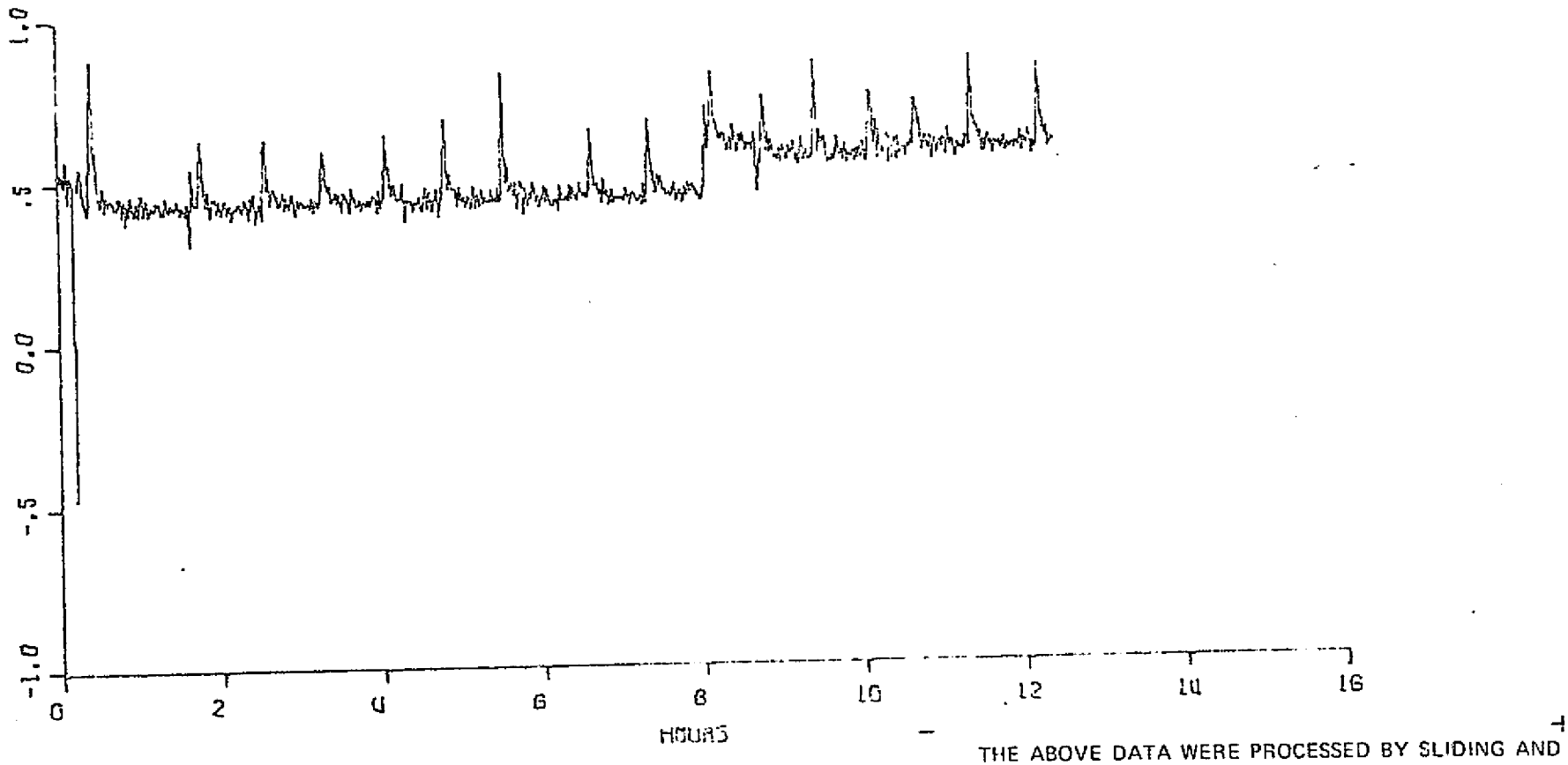

REFERENCE VALUE	53.700000	MERU
MEAN	54.250475	MERU
SIGMA	.09771	MERU
TREND	.01735	MERU /HOURS
SIGMA/TREND	.07545	MERU
AVERAGING PERIOD	71.68	SECONDS
REJECTED POINTS 1	OUT OF 623	SAMPLES

MINNY 056M 1

Fig 5

THE ABOVE DATA WERE PROCESSED BY SLIDING AND AVERAGING [illegible] SECOND CONTINUOUS DATA SAMPLES. THE APPROXIMATE FILTER CHARACTERISTICS DERIVED ARE:

(-2) Effective Bandwidth
[illegible] rad/s

SKIPPER K TEST LABORATORY/BEDFORD FLIGHT FACILITY
[illegible]

MINI-MIDAC ORD IRU TEST CHANNEL M2 TWT
MAY 21 TO MAY 22, 1975 RUN 056

PITCH AXIS

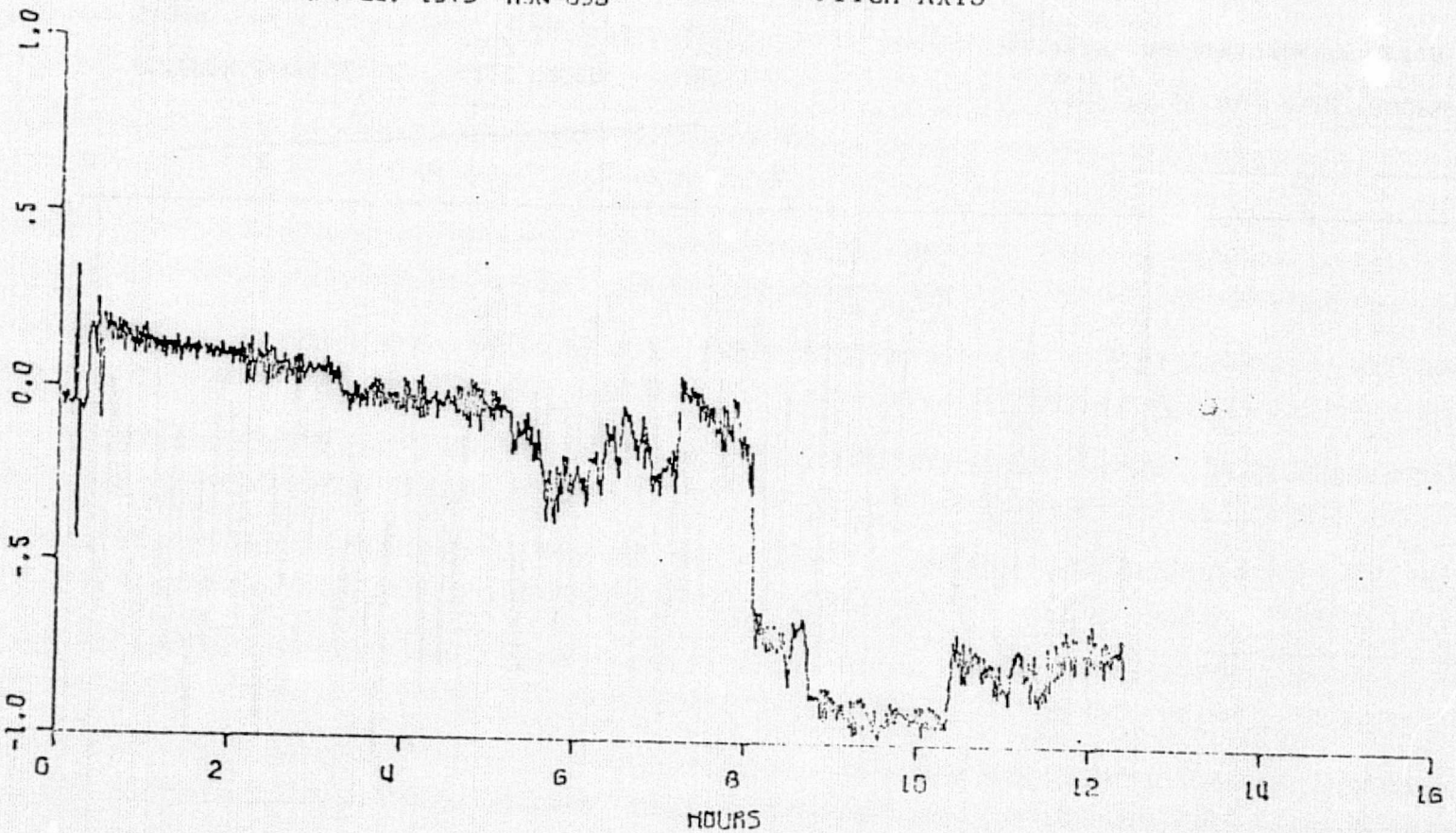

REFERENCE VALUE	-781.00000	MEAN
MEAN	-781.30637	MEAN
SIGMA	.3892	MEAN
TREND	-.09595	MEAN , HOURS
SIGMA/TREND	.1831	MEAN
AVERAGING PERIOD	71.68	SECONDS
REJECTED POINTS 2	OUT OF 623	SAMPLES
MINNY OSGM 2		

THE ABOVE DATA WERE PROCESSED BY SLIDING AND AVERAGING [illegible] SECOND CONTINUOUS DATA SAMPLES. THE APPROXIMATE FILTER CHARACTERISTICS DERIVED ARE:

(-2) Effective Bandwidth
rad/s

SKIPPER K TEST LABORATORY/BEDFORD FLIGHT FACILITY

[illegible] TEST LAB USK [illegible] BY

Fig 6

MINI-MIORC ORD IRU TEST CHANNEL M2 TWT
MAY 21 TO MAY 22, 1975 RUN 056

PITCH AXIS

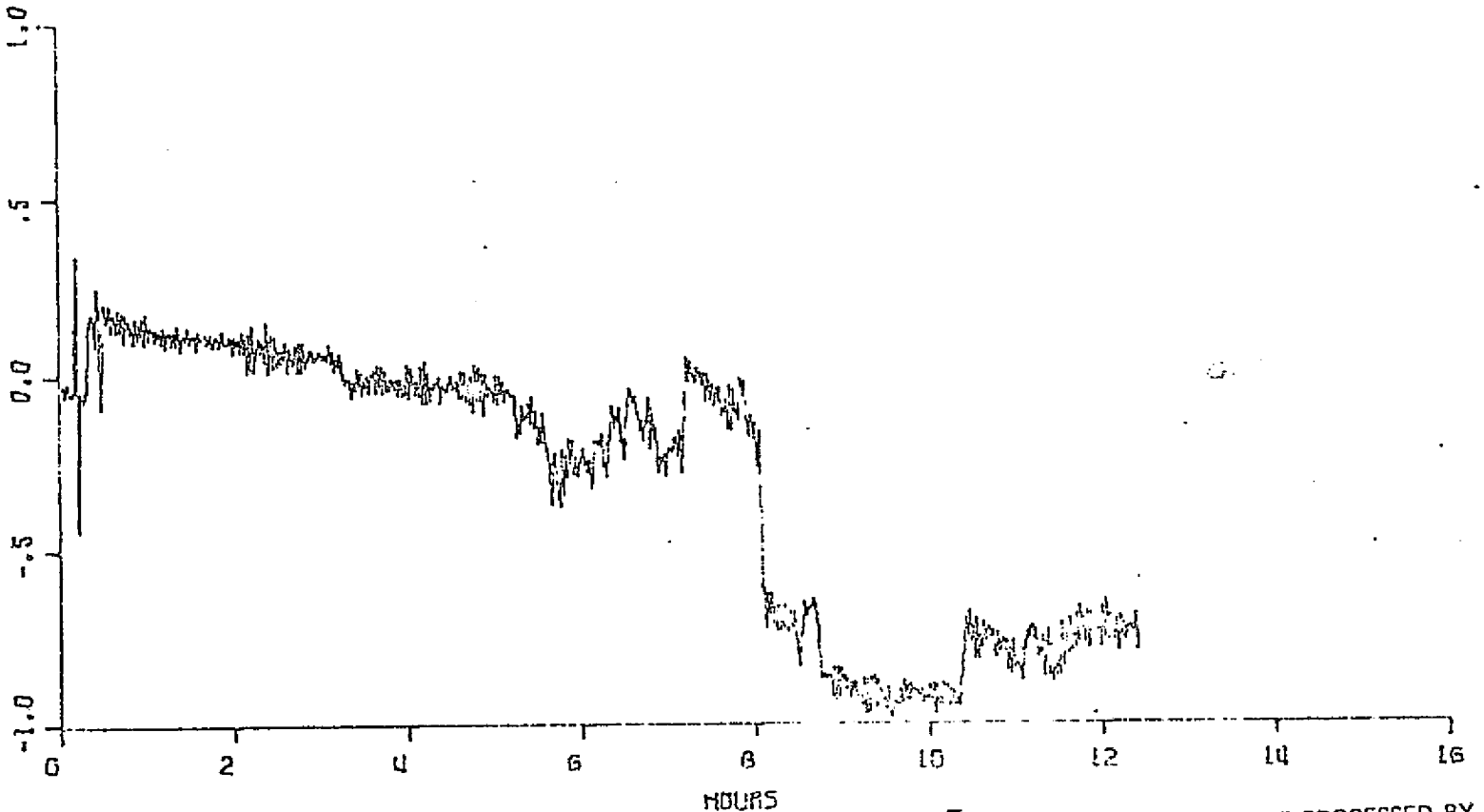

REFERENCE VALUE	-781.00000	MERU
MEAN	-781.30637	MERU
SIGMA	.3892	MERU
TREND	-.09595	MERU / HOURS
SIGMA/TREND	.1031	HOURS
AVERAGING PERIOD	71.68	SECONDS
REJECTED POINTS 2	OUT OF 673	SAMPLES
MINNY OSGM 2		

THE ABOVE DATA WERE PROCESSED BY SLIDING AND AVERAGING [illegible] SECOND CONTINUOUS DATA SAMPLES. THE APPROXIMATE FILTER CHARACTERISTICS DERIVED ARE:

(-2) Effective Bandwidth
rad/s

SKIPPER K TEST LABORATORY/BEDFORD FLIGHT FACILITY

Fig 6

MINI-MIORC ORD IRU TEST CHANNEL M3 TWZ
MAY 21 TO MAY 22, 1975 RUN 056

YAW AXIS

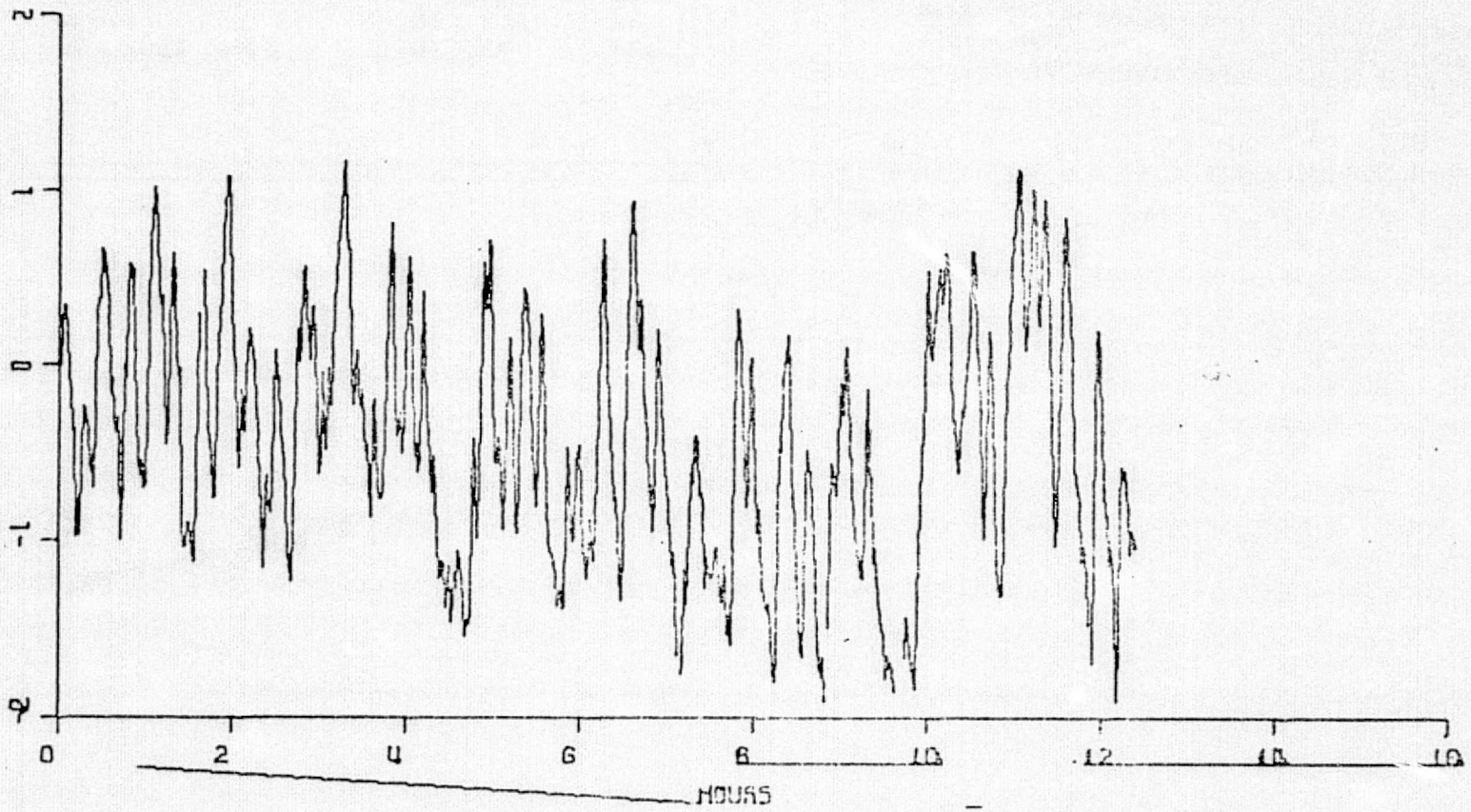

REFERENCE VALUE	-720.00000	MERU
MEAN	-720.41500	MERU
SIGMA	.6661	MERU
TREND	-.0[illegible]46	MERU /HOURS
SIGMA/TREND	.6709	MERU
AVERAGING PERIOD	71.68	SECONDS
ADJUSTED POINTS 10	OUT OF 603	SAMPLES
MINAY 056M 3		

Fig 7

THE ABOVE DATA WERE PROCESSED BY SLIDING AND AVERAGING [illegible] SECOND CONTINUOUS DATA SAMPLES. THE APPROXIMATE FILTER CHARACTERISTICS DERIVED ARE:

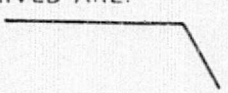

SKIPPER K TEST LABORATORY/BEDFORD FLIGHT FACILITY
SCS TEST LAB LFK 5/27/75 BV

MINI-MIDAC ORD IRU TEST CHANNEL M3 THZ
MAY 21 TO MAY 22, 1975 RUN 056

YAW AXIS

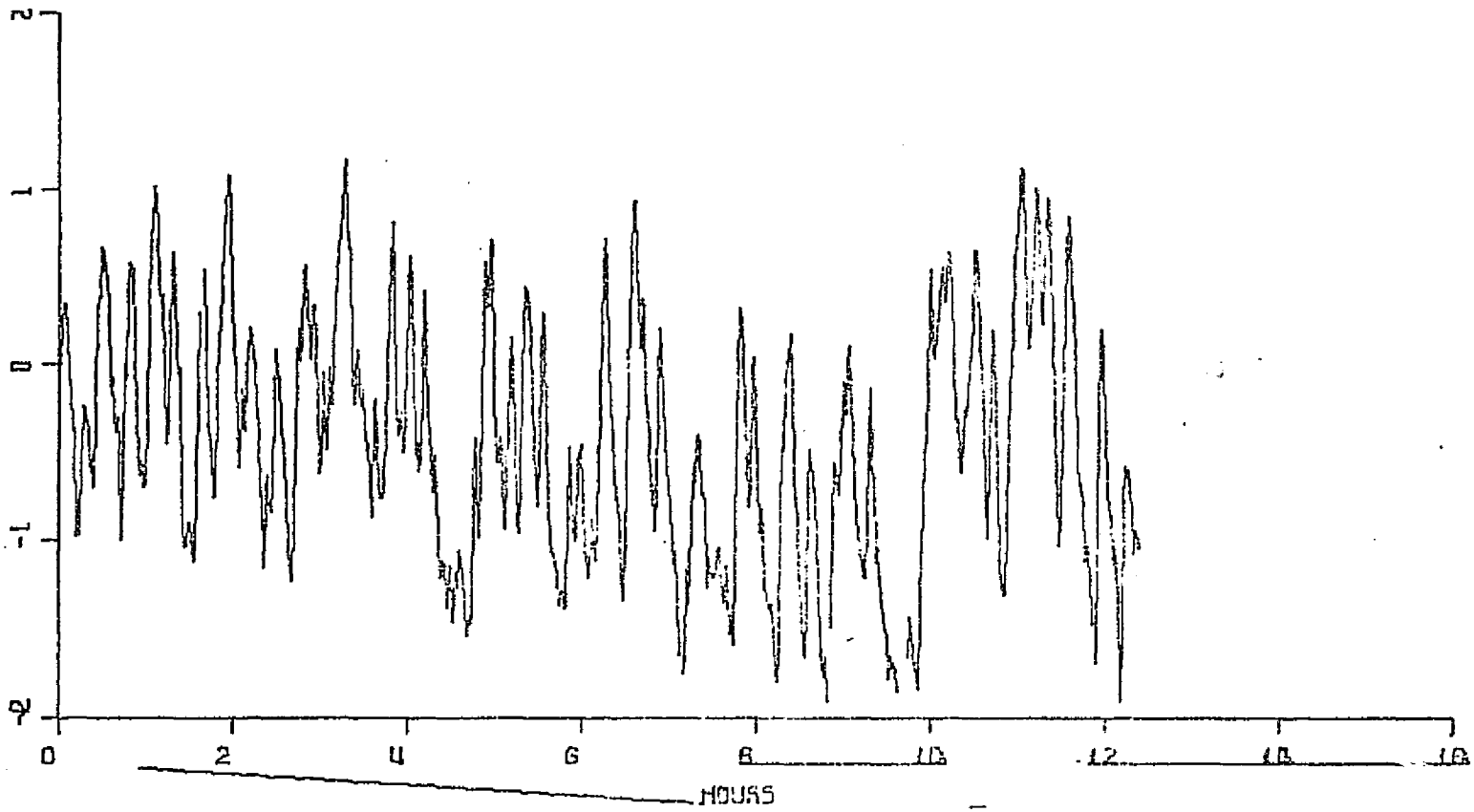

REFERENCE VALUE	-720.02080	MERU
MEAN	-720.41500	MERU
SIGMA	.6861	MERU
TREND	-.0[illegible]748	MERU /HOURS
SIGMA/TREND	.5729	HOURS
RUNNING PERIOD	71.68	SECONDS
ADJACENT POINTS 10	OUT OF 653	SKIPLED
MINNY 056M 3		

Fig 7

THE ABOVE DATA WERE PROCESSED BY SLIDING AND AVERAGING [illegible] SECOND CONTINUOUS DATA SAMPLES. THE APPROXIMATE FILTER CHARACTERISTICS DERIVED ARE:

(-2) Effective Bandwidth
rad/s

SKIPPER K TEST LABORATORY/BEDFORD FLIGHT FACILITY
SCS TEST LAB [illegible] 5/27/75 BM

MINI-MIORC ORD IMU TEST CHANNEL M4 TILT METER
MAY 21 TO MAY 22, 1975 RUN 056

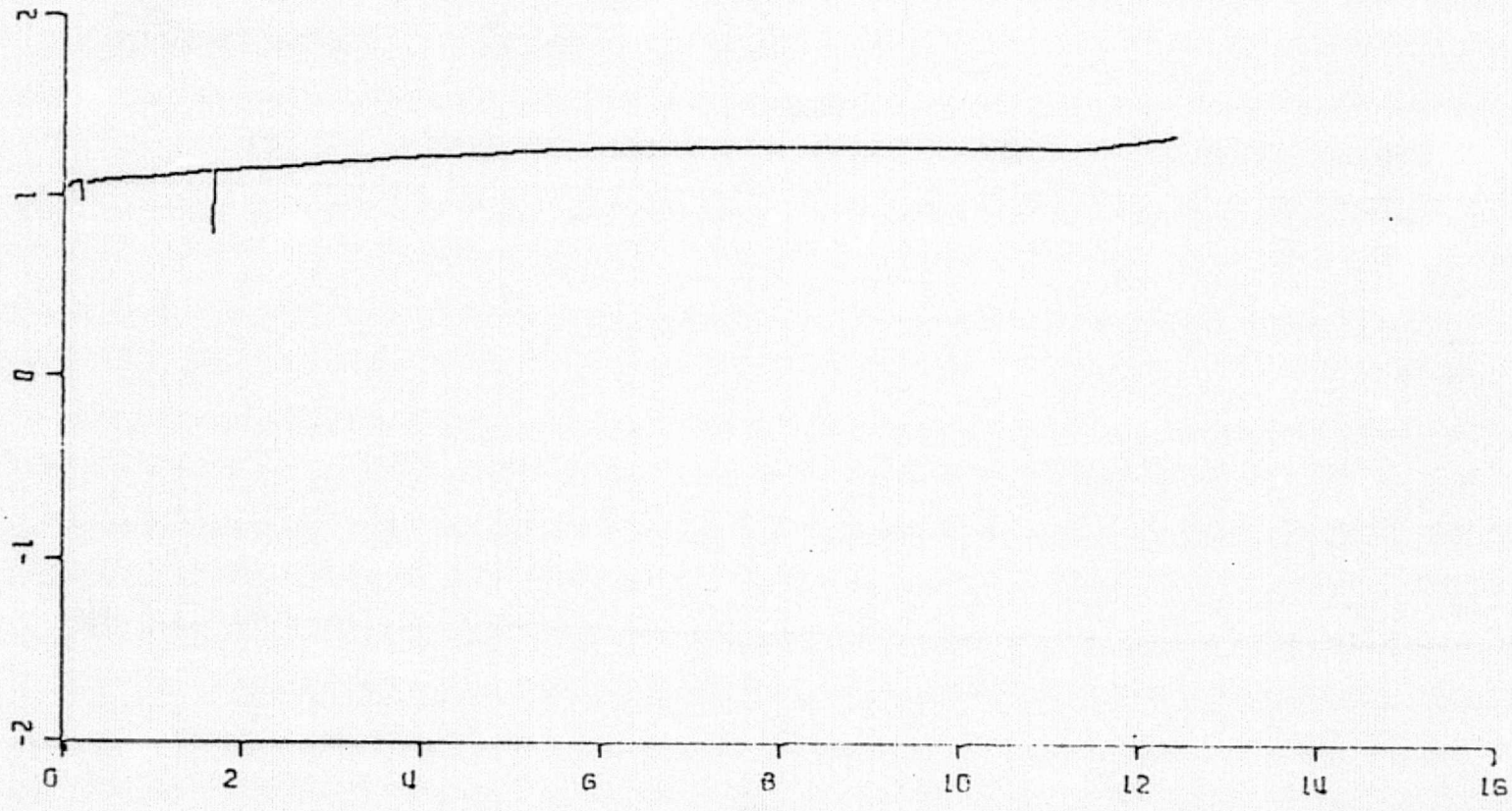

REFERENCE VALUE	1.8390000	ARC SEC
MEAN	3.0783632	ARC SEC
SIGMA	.07254	ARC SEC
TREND	.01796	ARC SEC/HOURS
SIGMA/TREND	.03369	ARC SEC
AVERAGING PERIOD	71.68	SECONDS
REJECTED POINTS 2	OUT OF 623	SAMPLES
MINNY 056M 4		

Fig. 8

THE ABOVE DATA WERE PROCESSED BY SLIDING AND AVERAGING [illegible] SECOND CONTINUOUS DATA SAMPLES. THE APPROXIMATE FILTER CHARACTERISTICS DERIVED ARE:

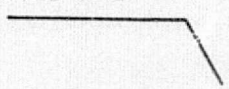

SKIPPER K TEST LABORATORY/BEDFORD FLIGHT FACILITY

MINI-MIDAC GAD IMU TEST CHANNEL M4 TILT METER
MAY 21 TO MAY 22, 1975 RUN 056

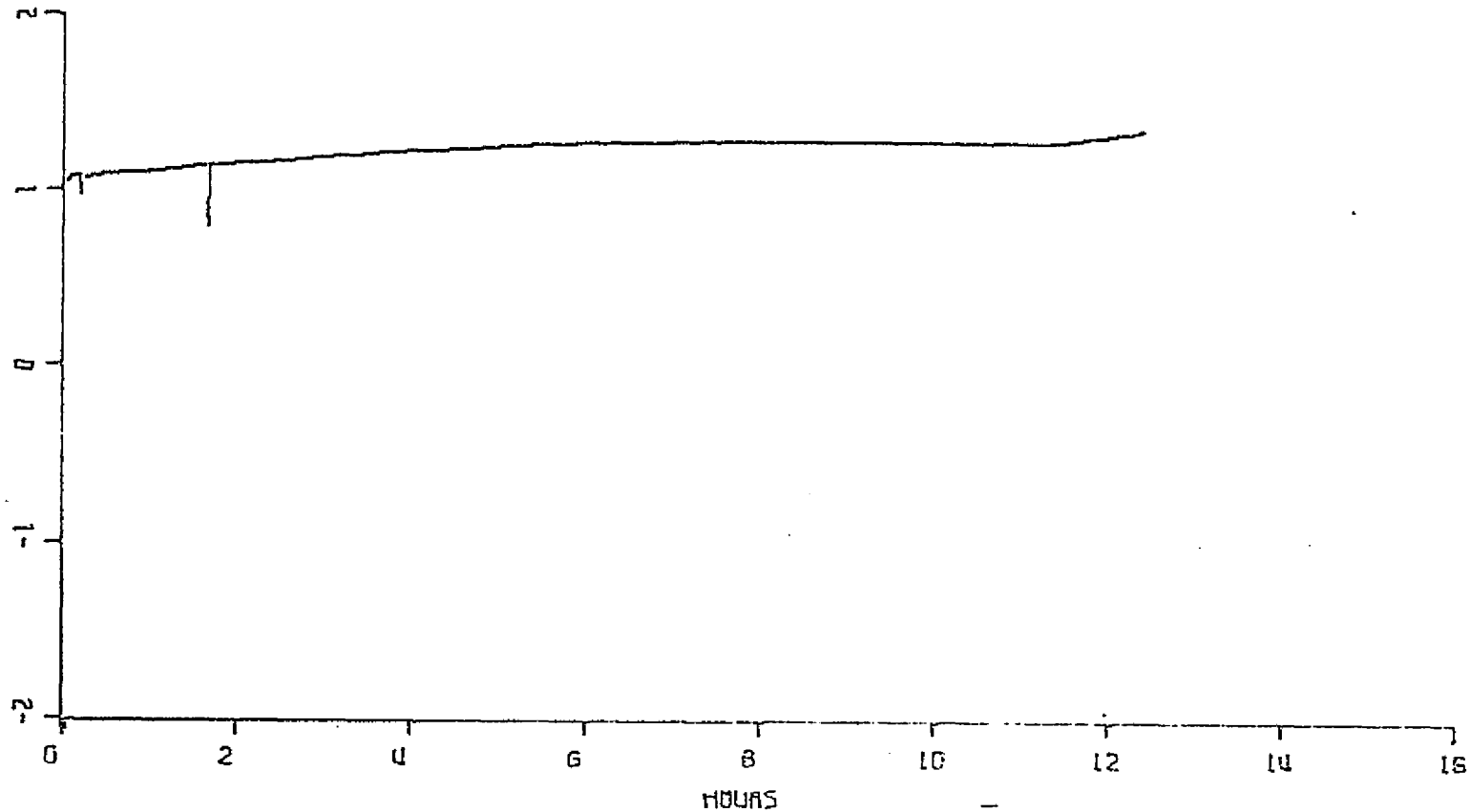

REFERENCE VALUE	1.8390000	ARC SEC
MEAN	3.0783632	ARC SEC
SIGMA	.07254	ARC SEC
TREND	.01796	ARC SEC/HOURS
SIGMA/TREND	.03369	ARC SEC
AVERAGING PERIOD	71.63	SECONDS
REJECTED POINTS 2	OUT OF 623	SAMPLES
MINNY 056M 4		

Fig. 8

THE ABOVE DATA WERE PROCESSED BY SLIDING AND AVERAGING [illegible] SECOND CONTINUOUS DATA SAMPLES. THE APPROXIMATE FILTER CHARACTERISTICS DERIVED ARE:

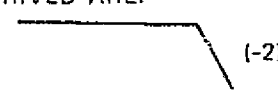

SKIPPER K TEST LABORATORY/BEDFORD FLIGHT FACILITY

MULTI-MIDAC CHANNEL M1 TWX DAD-IRU TEST 20.48 SEC/SAMPLES
MAY 22 TO MAY 28, 1975 GSFC RUN 059

ROLL AXIS

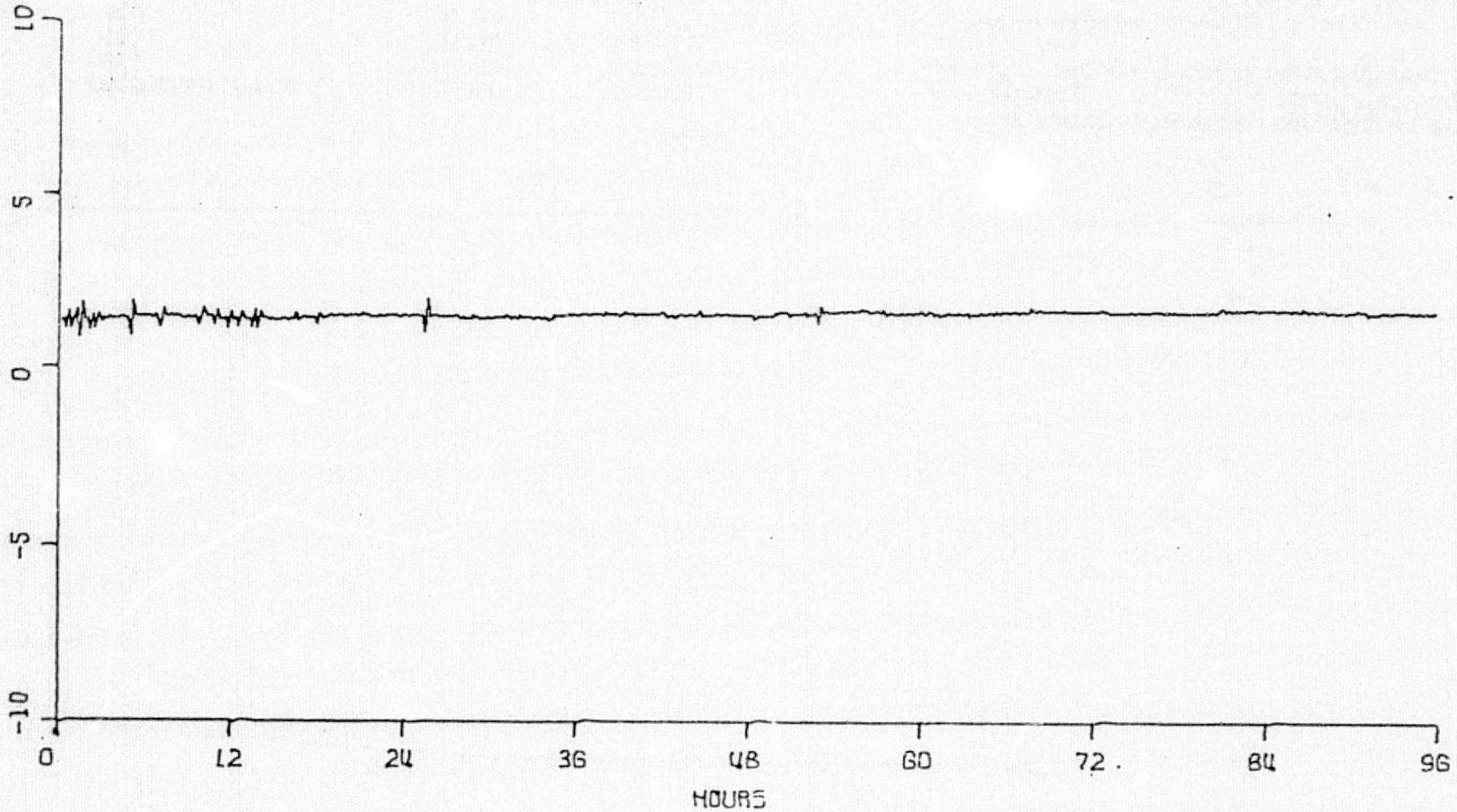

REFERENCE VALUE	53.000000	MERU
MEAN	54.537159	MERU
SIGMA	.1271	MERU
TREND	.003274	MERU /HOURS
SIGMA/TREND	.0390	HOURS
AVERAGING PERIOD	675.84	SECONDS
REJECTED POINTS 0	OUT OF 511	SAMPLES

MINNY 059M 1

Fig 9

SDS TEST LAB LSK 6/4/75 BV

[illegible] CHANNEL ML TNX OAO-IRU TEST 20.48 SEC/SAMPLES
MAY 22 TO MAY 28, 1975 GSFC RUN 059

ROLL AXIS

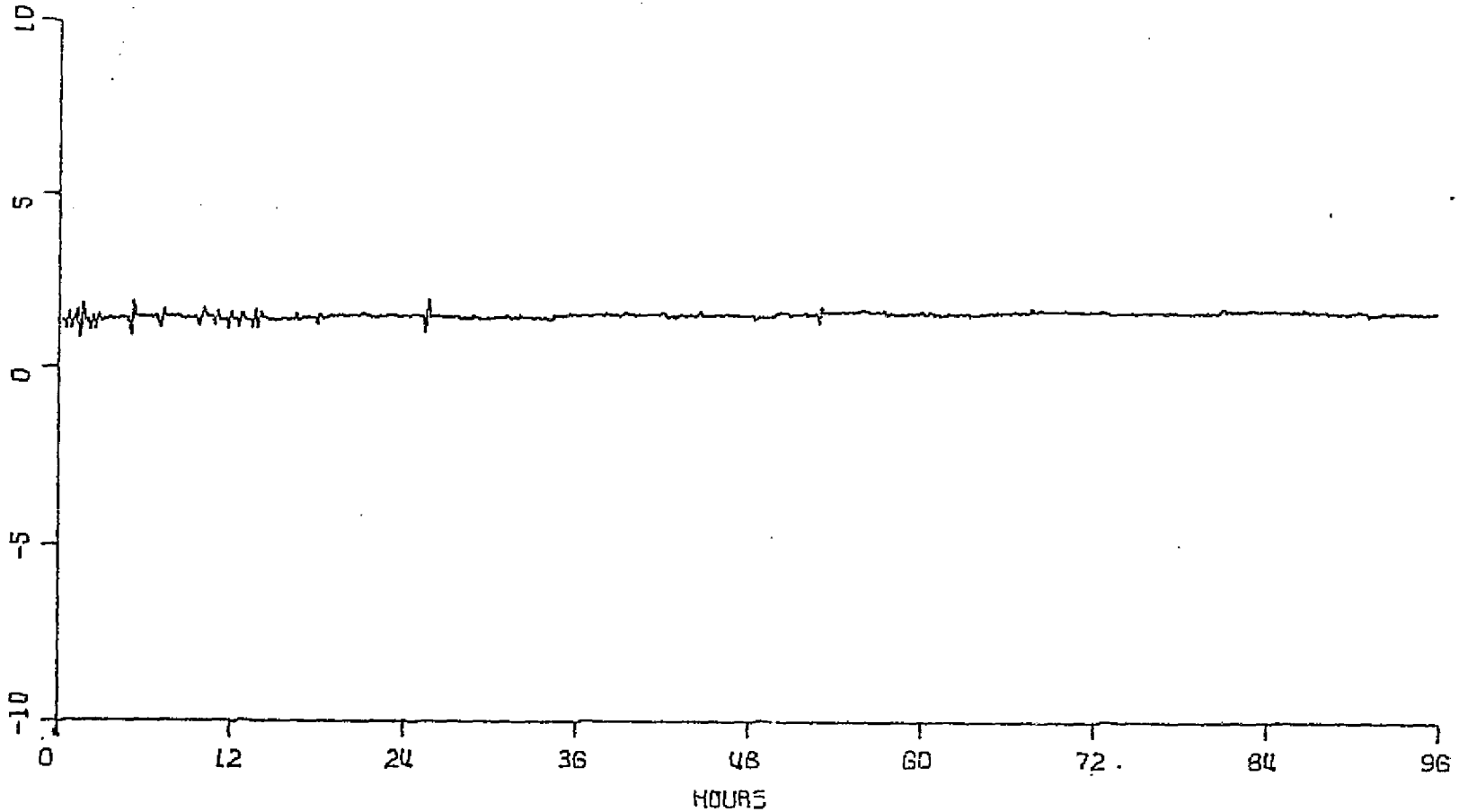

REFERENCE VALUE	53.000000	MERU
MEAN	54.537159	MERU
SIGMA	.1271	MERU
TREND	.003274	MERU /HOURS
SIGMA/TREND	.0390[illegible]	MERU
AVERAGING PERIOD	675.84	SECONDS
REJECTED POINTS 0	OUT OF 511	SAMPLES

MINNY 059M L

Fig 9

505 TEST LAB LSK 6/4/75 BV

MINI-MIDAC CHANNEL M2 TWY OAO-IRU TEST 20.48 SEC/SAMPLES
MAY 22 TO MAY 28, 1975 GSFC RUN 059

PITCH AXIS

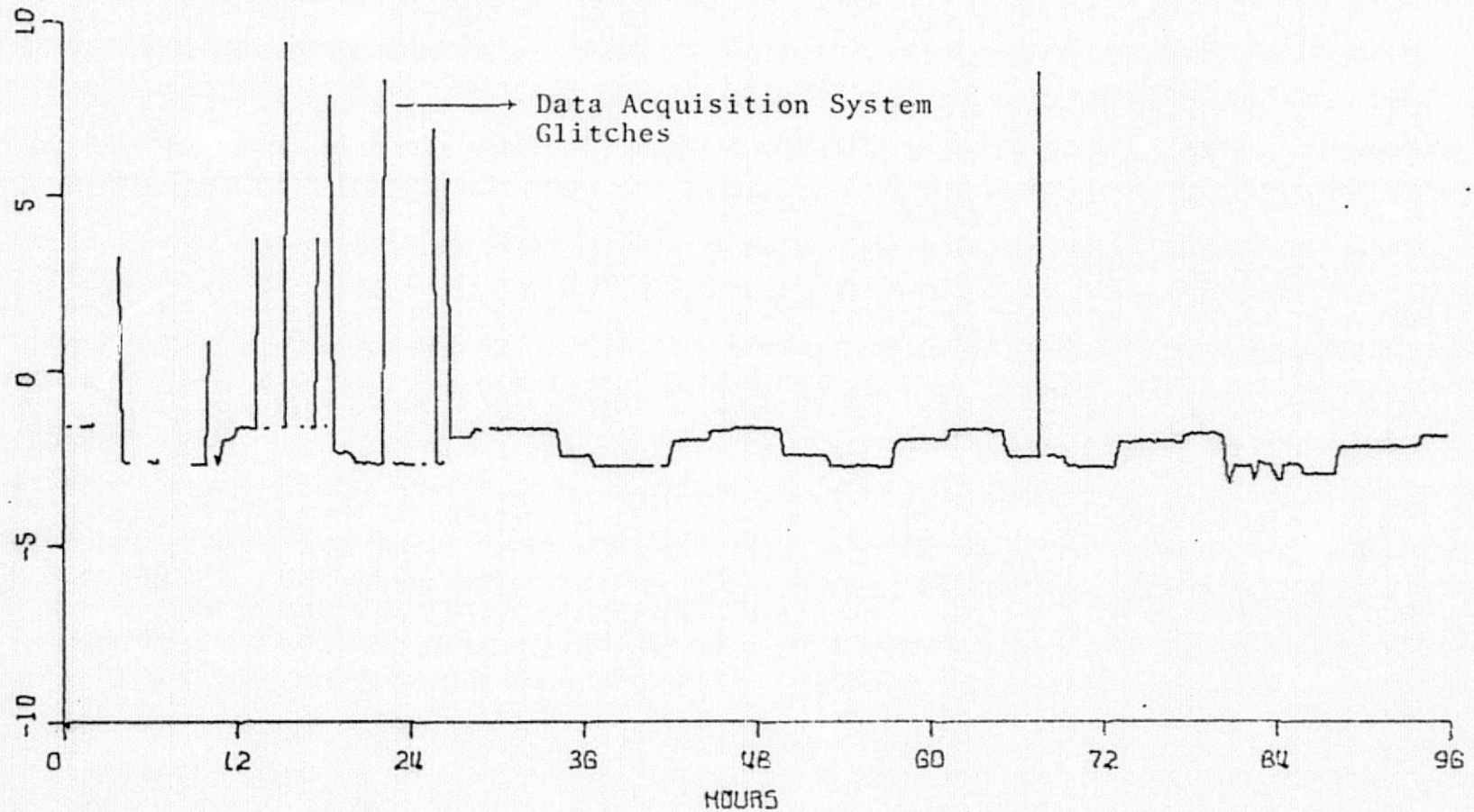

REFERENCE VALUE	-780.00000	MERU
MEAN	-782.00962	MERU
SIGMA	1.6393	MERU
TREND	-.01613	MERU /HOURS
SIGMA/TREND	1.5828	MERU
AVERAGING PERIOD	675.84	SECONDS
REJECTED POINTS 49	OUT OF 511	SAMPLES

MINNY 059M 2

Fig 10

505 TEST LAB LSK 6/4/75 BV

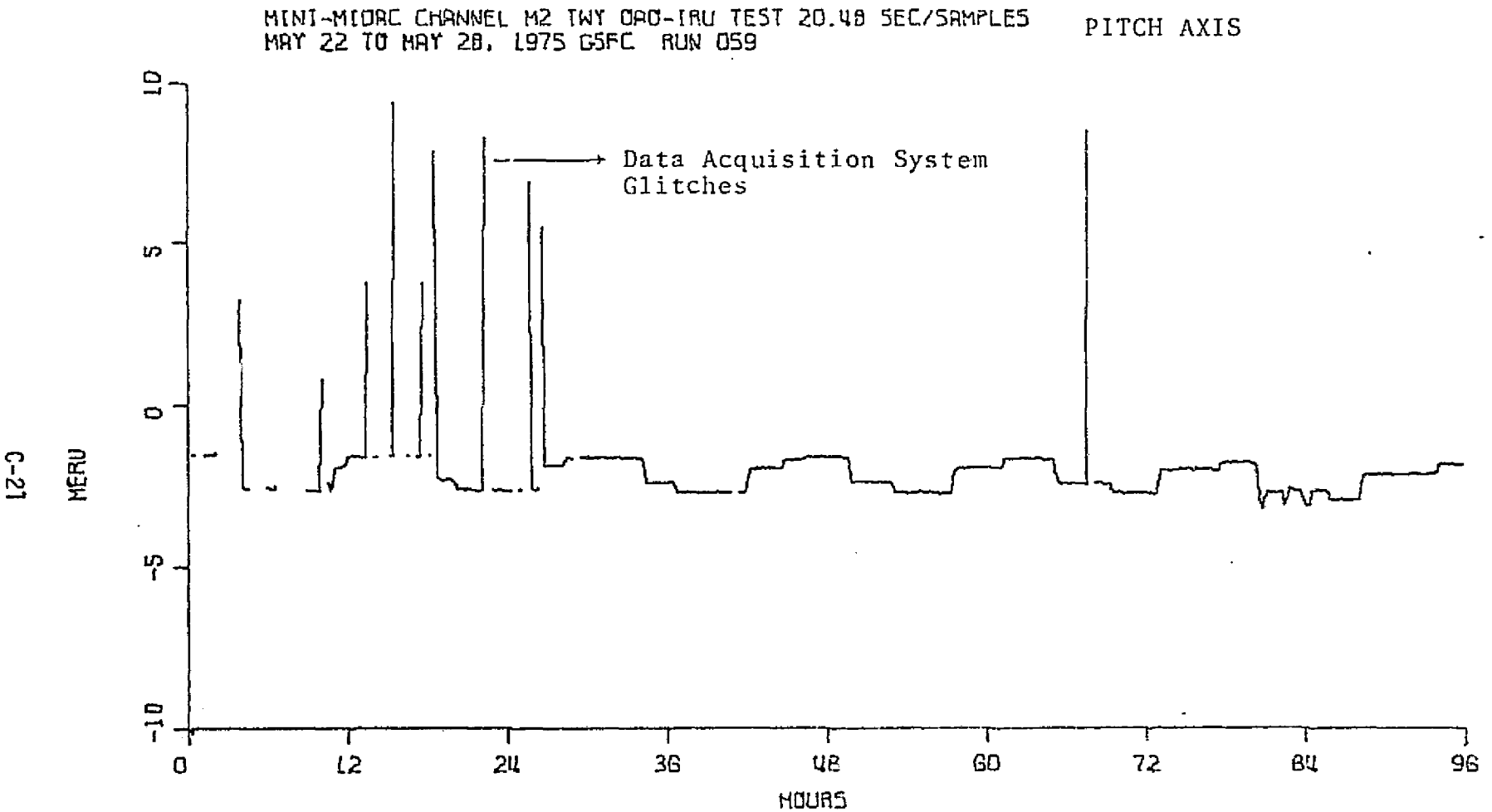

REFERENCE VALUE	-780.00000	MERU
MEAN	-782.00962	MERU
SIGMA	1.6393	MERU
TREND	-.01613	MERU /HOURS
SIGMA/TREND	1.5828	MERU
AVERAGING PERIOD	675.84	SECONDS
REJECTED POINTS 49	OUT OF 511	SAMPLES

MINNY 059M 2

Fig 10

585 TEST LAB LSK 6/4/75 BV

MINI-MIDRC CHANNEL M3 TWZ ORO-IRU TEST 20.48 SEC/SAMPLES
MAY 22 TO MAY 28, 1975 GSFC RUN 059

YAW AXIS

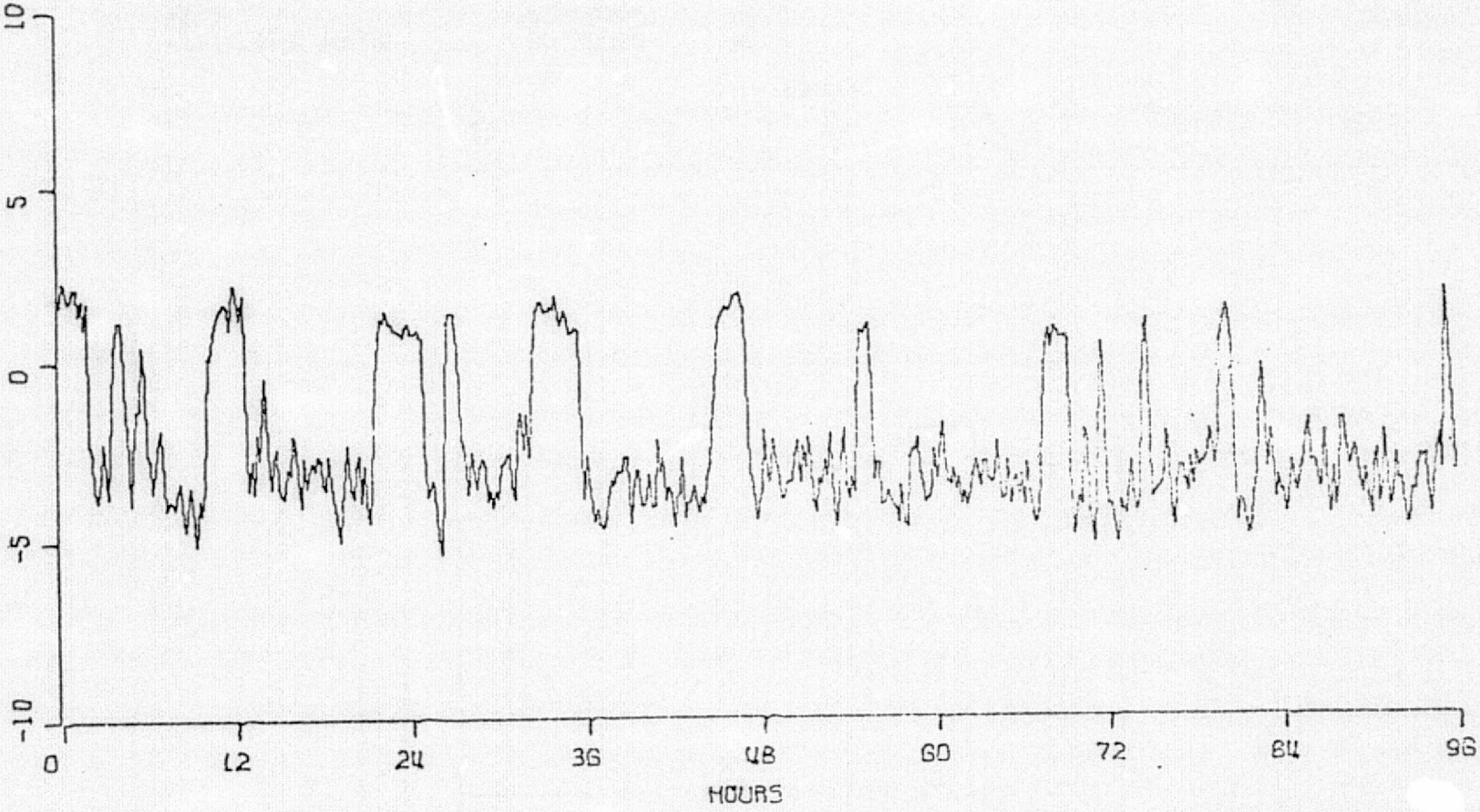

REFERENCE VALUE	-720.00000	MERU
MEAN	-722.35223	MERU
SIGMA	1.9524	MERU
TREND	-.01894	MERU /HOURS
SIGMA/TREND	1.8605	MERU
AVERAGING PERIOD	675.84	SECONDS
REJECTED POINTS 0	OUT OF 511	SAMPLES

MINNY 059M 3

Fig 11

SDS TEST LAB LSK 6/4/75 BV

GYRO	RUN	SEGMENT NUMBER	SEGMENT POINT COUNT	TIME (MINUTES)	TREND (MERU)	RESIDUE (ARCSEC) MAX	MIN	SIGMA
ROL	054	1	9216	30.720	53.696	0.307	-0.455	0.102
ROL	054	2	9216	30.720	53.685	0.411	-0.386	0.117
ROL	054	3	9216	30.720	53.719	0.726	-0.415	0.178
ROL	054	4	9216	30.720	53.708	0.462	-0.683	0.135
ROL	054	5	9216	30.720	53.702	0.356	-0.440	0.113
ROL	054	6	9216	30.720	53.702	0.636	-0.467	0.141
ROL	054	7	9216	30.720	53.725	0.494	-0.574	0.155
ROL	054	8	9216	30.720	53.685	0.549	-0.396	0.129
ROL	054	9	9216	30.720	53.759	0.757	-0.590	0.196
ROL	054	10	9216	30.720	53.719	0.398	-0.324	0.102
ROL	054	11	9216	30.720	53.736	0.451	-0.607	0.168
ROL	054	12	9216	30.720	53.730	0.441	-0.449	0.140
ROL	054	13	9216	30.720	53.736	0.569	-0.317	0.127
ROL	054	14	9216	30.720	53.748	0.283	-0.727	0.169
ROL	054	15	9216	30.720	53.748	0.253	-0.516	0.111
ROL	054	16	9216	30.720	53.787	0.590	-0.450	0.147
ROL	054	17	9216	30.720	53.793	0.518	-0.561	0.161

RECORDED FROM: 9 pm 20 MAY -- 6 am 21 MAY 1975

TABLE I

GYRO	RUN	SEGMENT NUMBER	SEGMENT POINT COUNT	TIME (MINUTES)	TREND (MERU)	RESIDUE (ARCSEC) MAX	MIN	SIGMA
PIT	057	1	9216	30.720	- 79.272	0.401	-0.269	0.092
PIT	057	2	9216	30.720	- 79.371	0.323	-0.319	0.096
PIT	057	3	9216	30.720	- 79.327	0.338	-0.408	0.108
PIT	057	4	9216	30.720	- 79.355	0.491	-0.175	0.100
PIT	057	5	9216	30.720	-779.410	0.665	-0.291	0.156
PIT	057	6	9216	30.720	- 79.488	0.627	-0.328	0.137
PIT	057	7	9216	30.720	-779.322	0.379	-1.490	0.434
PIT	057	8	9216	30.720	-779.255	0.412	-0.345	0.118
PIT	057	9	9216	30.720	- 79.305	0.944	-0.452	0.290
PIT	057	10	9216	30.720	-779.344	0.253	-0.516	0.129
PIT	057	11	9216	30.720	-779.211	0.292	-0.328	0.088
PIT	057	12	9216	30.720	-779.216	0.440	-0.362	0.114
PIT	)))-	0	326	1.087	-779.280	0.337	-0.135	0.083

RECORDED FROM: 10 am -- 4 pm 21 MAY 1975

TABLE 2

GYRO	RUN	SEGMENT NUMBER	SEGMENT POINT COUNT	TIME (MINUTES)	TREND (MERU)	RESIDUE (ARCSEC) MAX	MIN	SIGMA
Y[illegible]	058	1	9216	30.720	- 20.176	2.652	-3.187	1.672
Y[illegible]	058	2	9216	30.720	-720.120	3.332	-0.331	0.969
Y[illegible]	058	3	9216	30.720	-719.999	7.321	-0.298	2.192
Y[illegible]	058	4	9216	30.720	-719.599	0.782	-5.135	1.[illegible]
Y[illegible]	058	5	9216	30.720	-720.364	3.325	-1.502	1.[illegible]
Y[illegible]	058	6	9216	30.720	- 20.231	0.913	-5.477	1.[illegible]
Y[illegible]	058	7	9216	30.720	-719.844	4.619	-2.220	2.[illegible]
Y[illegible]	058	8	9216	30.720	- 20.159	0.389	-4.517	1.177
Y[illegible]	058	9	9216	30.720	-720.746	6.035	-0.444	1.[illegible]
Y[illegible]	058	10	9216	30.720	-720.552	0.840	-7.444	2.451
Y[illegible]	058	11	9216	30.720	-720.248	1.635	-2.192	[illegible]
Y[illegible]	058	12	9216	30.720	-720.995	0.799	-2.738	[illegible]
Y[illegible]	058	13	9216	30.720	-720.243	1.517	-5.536	1.[illegible]
Y[illegible]	058	14	9216	30.720	-720.591	6.422	-0.[illegible]	1.[illegible]
Y[illegible]	058	15	9216	30.720	-721.028	2.454	-1.[illegible]	1.[illegible]
Y[illegible]	058	16	9216	30.720	-720.751	4.[illegible]	-3.[illegible]	2.[illegible]
Y[illegible]	058	17	9216	30.720	-720.862	2.521	-3.995	1.[illegible]

RECORDED FROM: 11 pm 22 MAY -- 8 am 23 MAY 1975

TABLE 3

ORO IAU TEST GSFC
ATTITUDE ERROR ROLL AXIS
20 TO 21 MAY 1975
NSL#1

DEVIATION BETWEEN 0.2 SECOND DATA POINTS AND 30 MINUTE, BEST FIT MODEL.
THE DEVIATIONS ARE SAMPLED AT 36 SECOND INTERVALS.

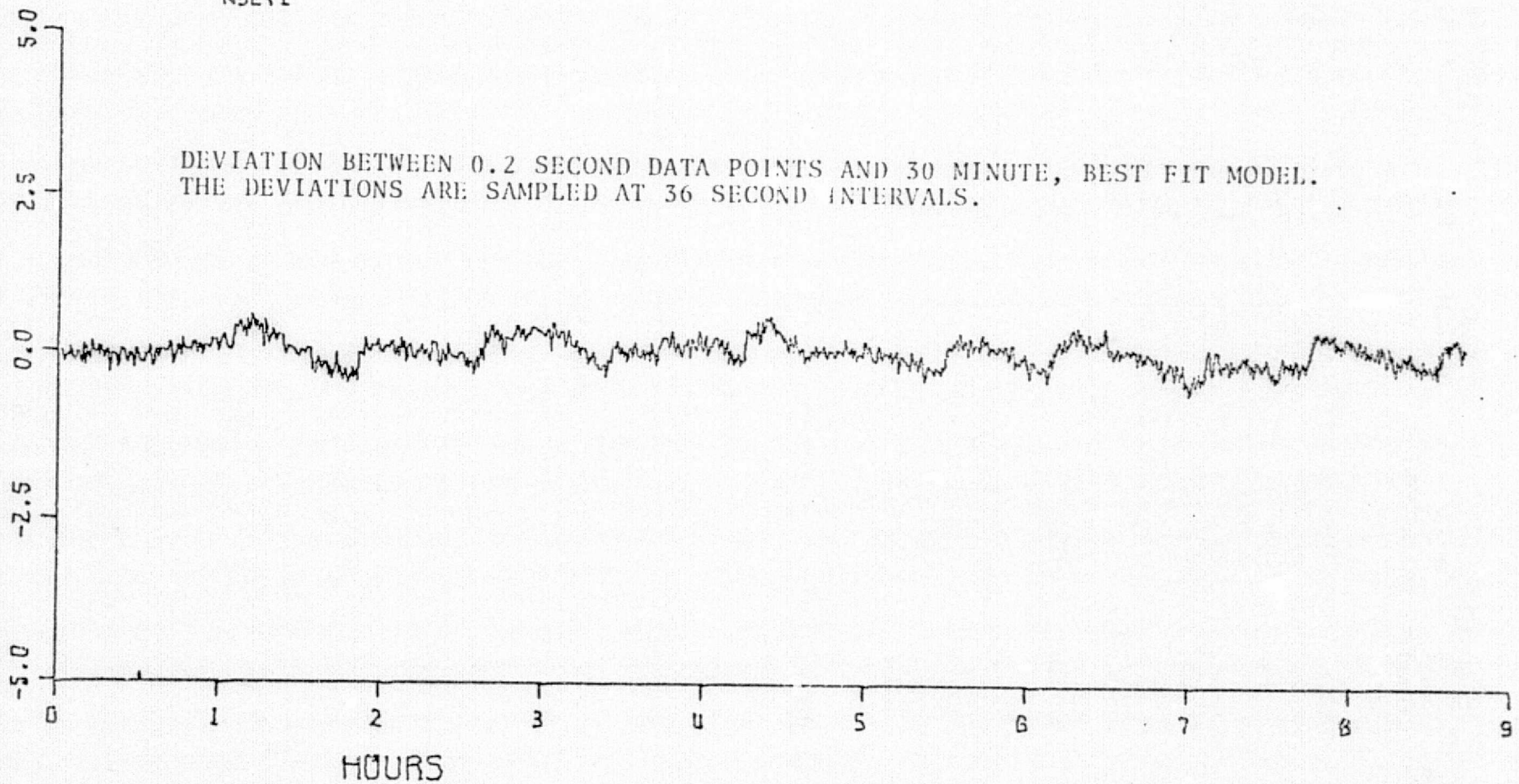

MEAN	.02817928	ARCSEC
SIGMA	.1984	ARCSEC
TREND	-.005067	ARCSEC /HOURS
SIGMA/TREND	.1980	ARCSEC
SAMPLE PERIOD	36.00	SECONDS
REJECTED POINTS 0	OUT OF 671	SAMPLES

Fig 12

SOS TEST LAB IS K.G.B.

ORO IRU TEST GSFC
ATTITUDE ERROR PITCH AXIS
21 TO 22 MAY 1975
NSLSL

DEVIATION BETWEEN 0.2 SECOND DATA POINTS AND 30 MINUTE, BEST FIT MODEL.
THE DEVIATIONS ARE SAMPLED AT 36 SECOND INTERVALS.

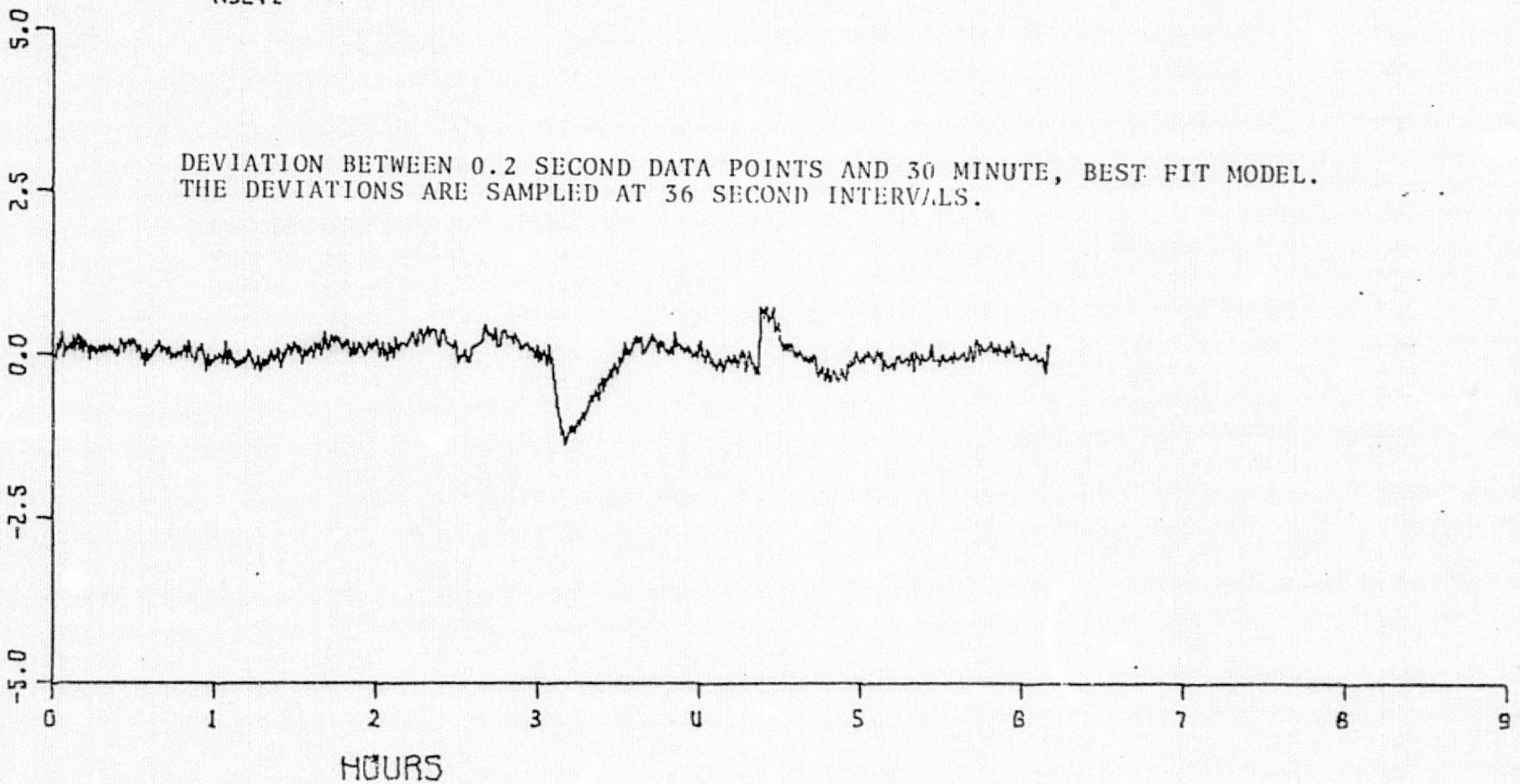

MEAN	-.008869693	ARCSEC	
SIGMA	.2685	ARCSEC	
TREND	-.01739	ARCSEC	/HOURS
SIGMA/TREND	.2667	ARCSEC	
SAMPLE PERIOD	36.00	SECONDS	
REJECTED POINTS 0	OUT OF 617	SAMPLES	

Fig 13

SDS TEST LAB L5 K G.R.B.

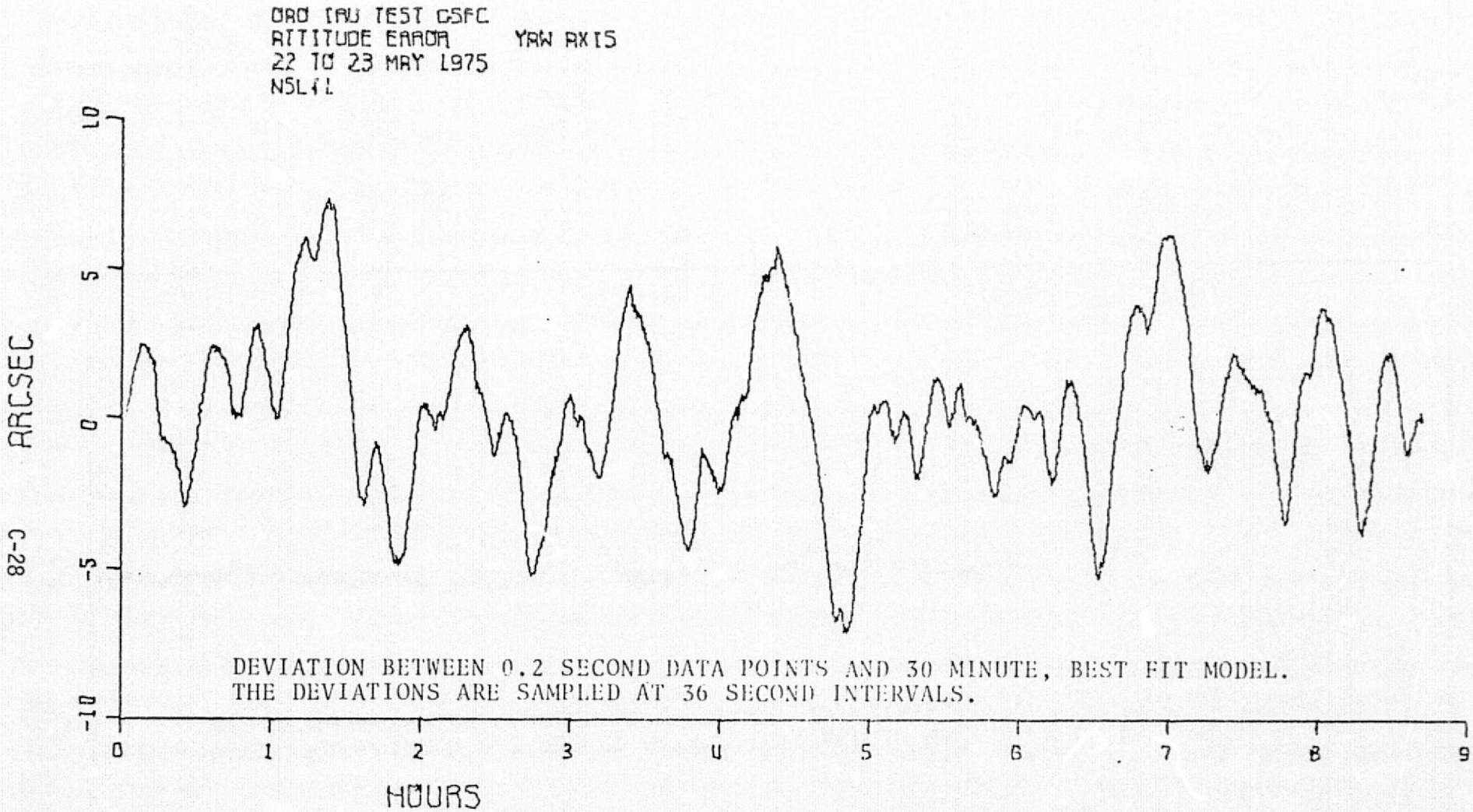

DEVIATION BETWEEN 0.2 SECOND DATA POINTS AND 30 MINUTE, BEST FIT MODEL.
THE DEVIATIONS ARE SAMPLED AT 36 SECOND INTERVALS.

MEAN	.2039577	ARCSEC	
SIGMA	2.6978	ARCSEC	
TREND	-.04560	ARCSEC	/HOURS
SIGMA/TREND	2.6934	ARCSEC	
SAMPLE PERIOD	36.00	SECONDS	
REJECTED POINTS 0	OUT OF 871	SAMPLES	

Fig 14

SDS TEST LAB L5 K G.R.B.

TO: R. Harris

FROM: R. Carson

DATE: 6 November 1975

SUBJECT: OAO-IRU Engineering Model Data at TRW September 1975

Approximately sixty hours of gyro data was obtained from the OAO-IRU Engineering Model at TRW, Redondo Beach, California during September 1975. This data is displayed in both time and power spectral density plots. The time histories provide an indication of the overall instrument performance and the PSD data can indicate the performance that can be expected in a particular frequency range. A brief description of the data accumulated is enclosed.

Time Plots

Three data sets were recorded simultaneously for each of the three instruments and are shown in Figures 1 through 9. The details of each set are described below:

Data Set	Run	Sample Period	Length of Test	Date
1	72	.32 seconds	9 hours	8-9 Sept
2	73	2.56 seconds	32 hours	9-10 Sept
3	74	2.56 seconds	16 hours	10-11 Sept

It can be seen from the time plots that the output of each gyro is consistent from test to test. It should also be noted that the roll and pitch instruments exhibit approximately 0.1 meru jumps within three stable states. It is further observed that these discontinuities occur simultaneously and are quite deterministic

with an overall period of approximately 17 hours. The yaw gryo on the other hand is quite erratic with frequent spikes of approximately 3 meru and occasional spikes greater than 10 meru. Needless to say, the erratic behavior of the yaw gyro and the discontinuities in the roll and pitch instruments are not considered normal. However this performance is an improvement by approximately a factor of 10 over that which was observed at GSFC in June. The roll and pitch gyros would be considered quite acceptable without the jumps. Again it is felt that the anomolous behavior of the instruments is the result of an unknown malfunction within the Engineering Model.

PSD Plots

The results of the PSD analysis are shown in Figures 10 through 18. The data are plotted as single sided PSDs (i.e., all the energy exists in the frequency range of 0 to ∞) in rate and have units of "meru^2/Hz". Selected portions of each of the three data sets were chosen to characterize the instrument output under various conditions and different frequency ranges. Figures 10 through 12 are the PSD of approximately 1.5 hours from data set 1 with no discontinuities. Figures 13 through 15 are the resultant PSDs of approximately 12 hours from data set 3 with several jumps. Figures 16 through 18 show the PSD plots of the first 24 hours of data set 2.

Each of the PSDs has two distinct characteristics: a positive slope at the high frequencies and a negative slope at the low frequencies. The positive slopes are proportional to f^2 and are attributed to quantization noise due to the sampling process. It will be noted that the levels of the PSDs calculated from 2.56 second data samples (Runs 73 and 74) are eight times higher than those calculated using 0.32 second samples (Run 72). This is consistent with modelling quantization noise as a white process in angle and band limited at the Nyquist frequency of the sample

rate. The remainder of this memo will concentrate on the low frequency characteristics which are attributed to the gyros and to the system.

Figures 10 and 11 illustrate the behavior of the roll and pitch instruments without the presence of jumps and compares favorably with previously obtained data with other 2FBG-6F gyros. Figure 12 further illustrates the erratic behavior of the yaw axis gyro. At the low frequencies, the PSD of the yaw gyro is approximately 100 times greater than those for the other two axes even though the data used to generate the yaw PSD plot did not include any spikes. Figures 13 through 18 are the PSDs of each instrument when spikes or discontinuities are present. The deterministic jumps in each of the axes not only increases the magnitude of the PSD but also change its characteristics at the lower frequencies.

RCC/alk

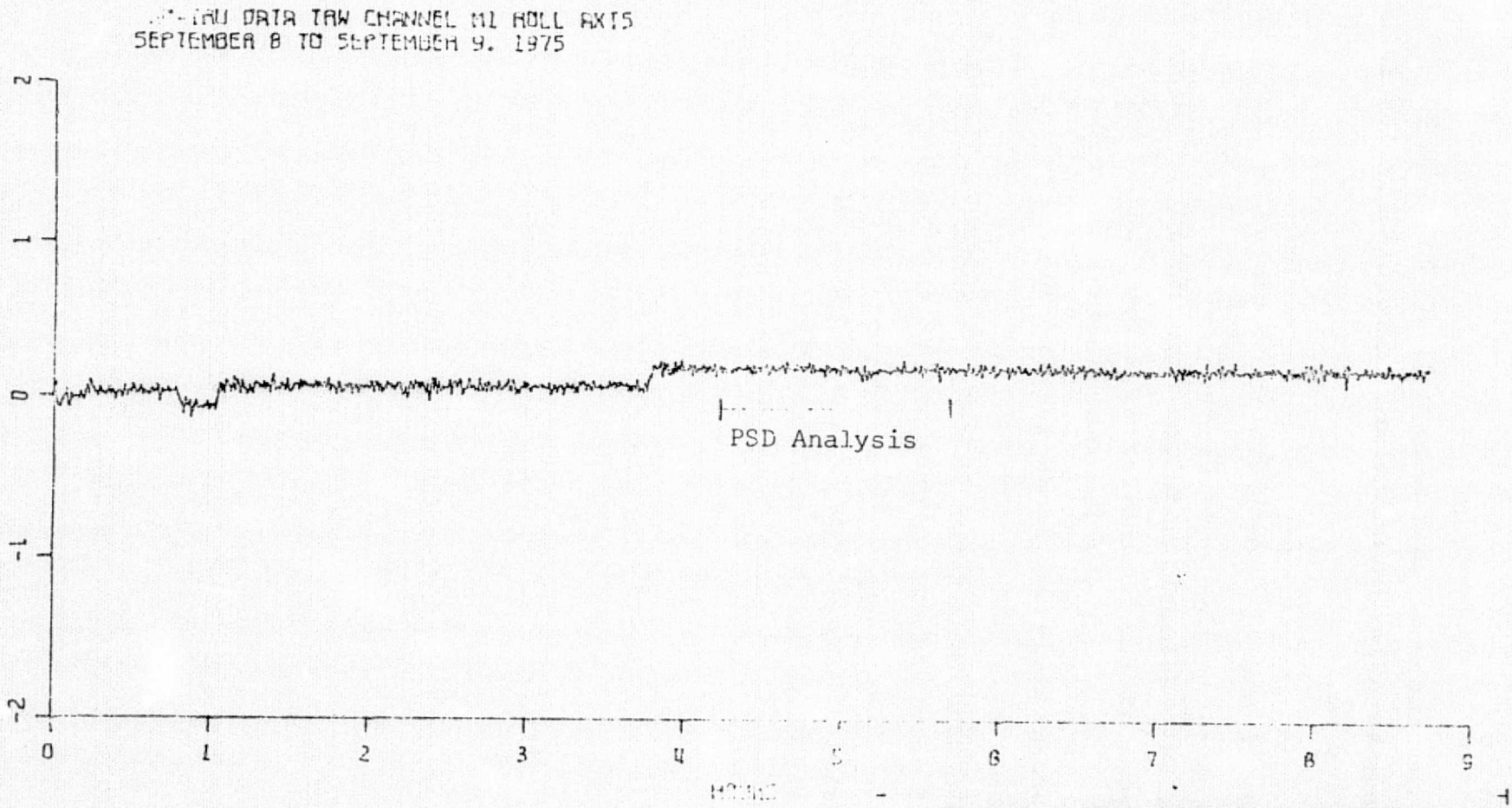

REFERENCE VALUE	[illegible]	[illegible]
MEAN	[illegible]	[illegible]
[illegible]	[illegible]	[illegible]
[illegible]	[illegible]	[illegible]
[illegible]	[illegible]	[illegible]
[illegible]	[illegible]	[illegible]
[illegible]	[illegible]	[illegible]

THE ABOVE DATA WERE PROCESSED BY SLIDING AND AVERAGING 1120.32 SECOND CONTINUOUS DATA SAMPLES. THE APPROXIMATE FILTER CHARACTERISTICS DERIVED ARE:

(-2) Effective Bandwidth
0.014 rad/s

SKIPPER K TEST LABORATORY/BEDFORD FLIGHT FACILITY

FIGURE 1

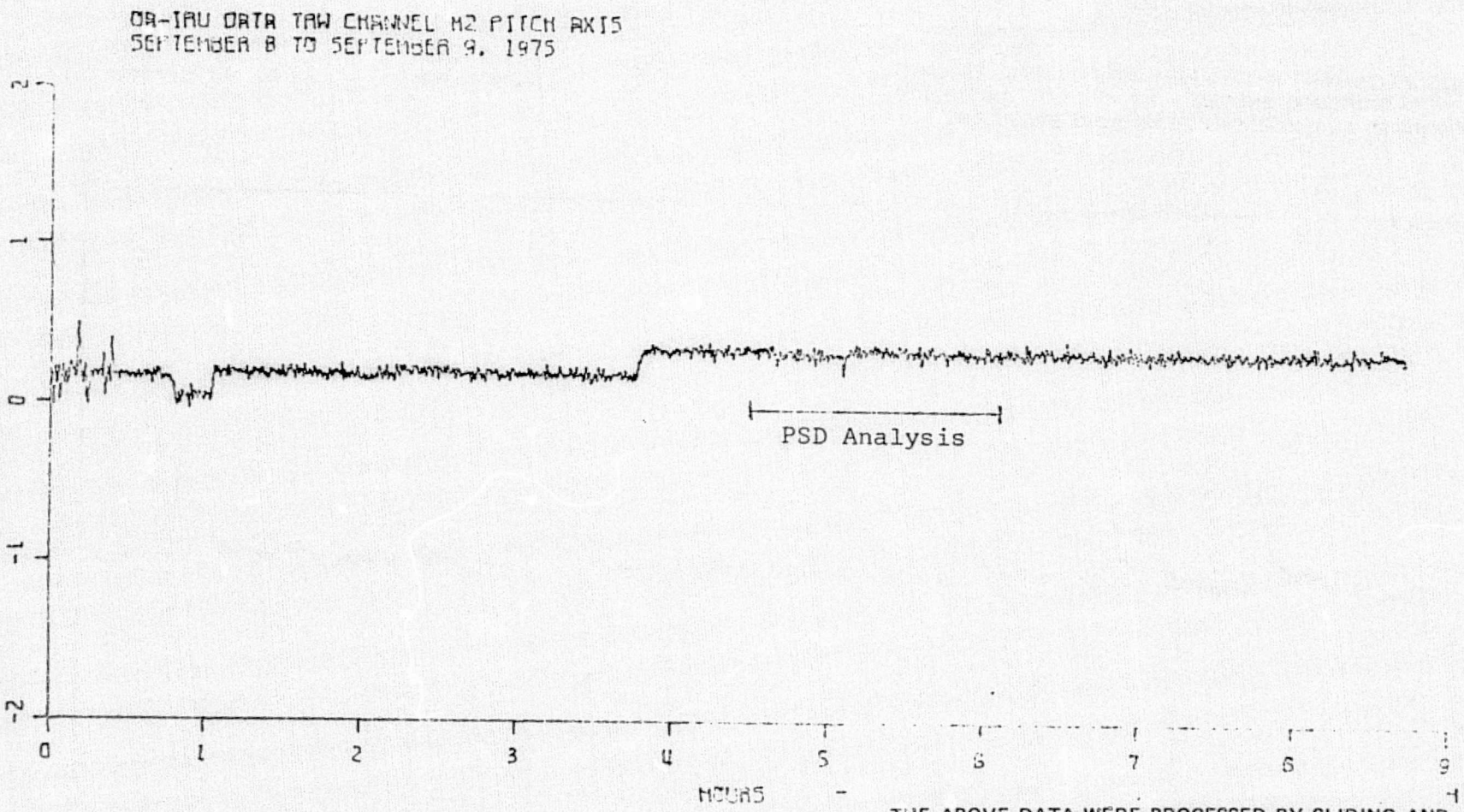

REFERENCE VALUE

THE ABOVE DATA WERE PROCESSED BY SLIDING AND AVERAGING 1120 , 32 SECOND CONTINUOUS DATA SAMPLES. THE APPROXIMATE FILTER CHARACTERISTICS DERIVED ARE:

(-2) Effective Bandwidth
0.014 rad/s

SKIPPER K TEST LABORATORY/BEDFORD FLIGHT FACILITY

FIGURE 2

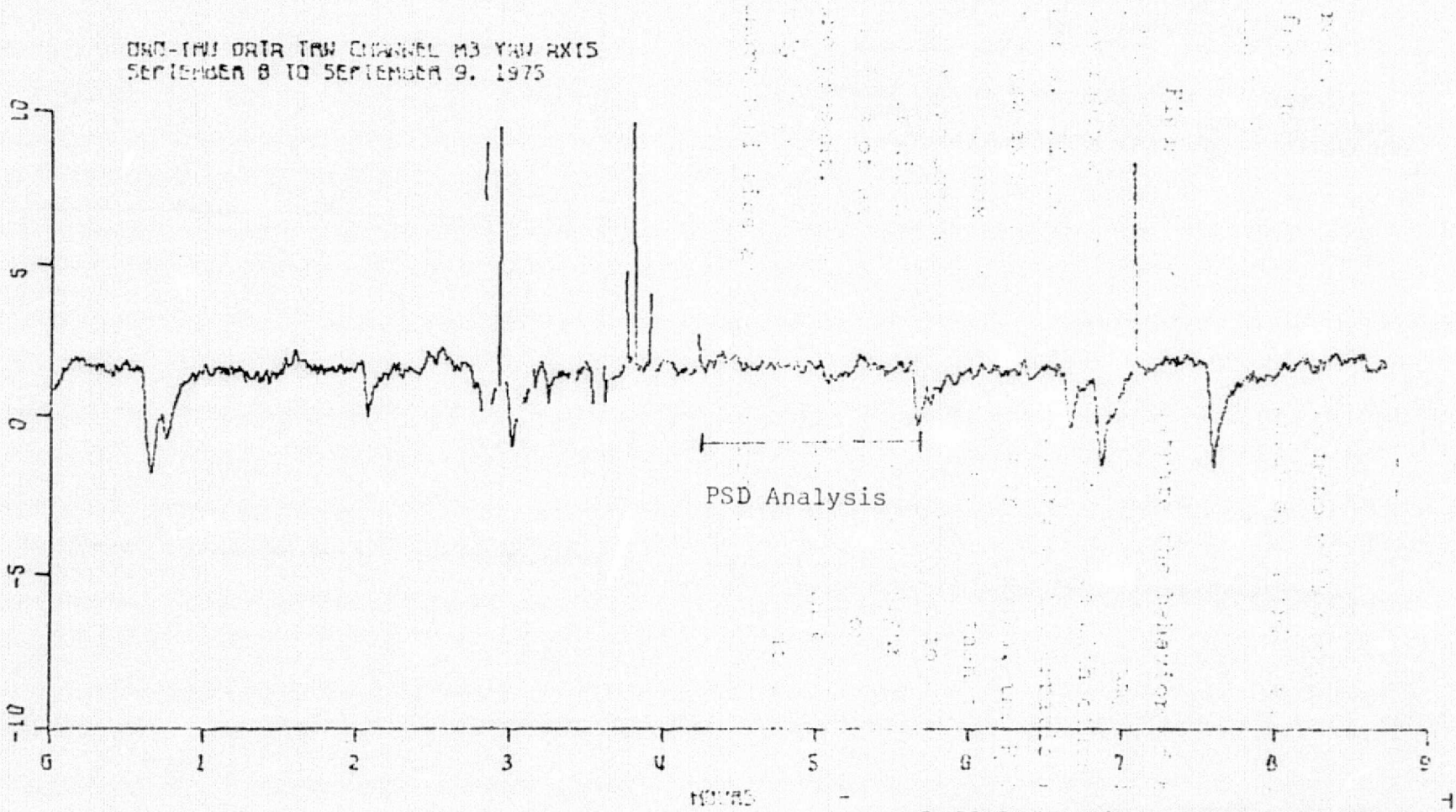

REFERENCE VALUE	-643.04949	MERU
MEAN	-641.67097	MERU
STDAR	.6965	MERU
TREND	.01214	MERU /HOUR
STDEV/TREND	.0458	MERU
AVERAGING PERIOD	35.6M	SEC/MIN
NUMBER POINTS 23	OUT OF 600	SAMPLES
DATA-[illegible] 01:2M :3		

THE ABOVE DATA WERE PROCESSED BY SLIDING AND AVERAGING 112 , 32 SECOND CONTINUOUS DATA SAMPLES. THE APPROXIMATE FILTER CHARACTERISTICS DERIVED ARE:

(-2) Effective Bandwidth

0.014 rad/s

SKIPPER K TEST LABORATORY/BEDFORD FLIGHT FACILITY

FIGURE 3

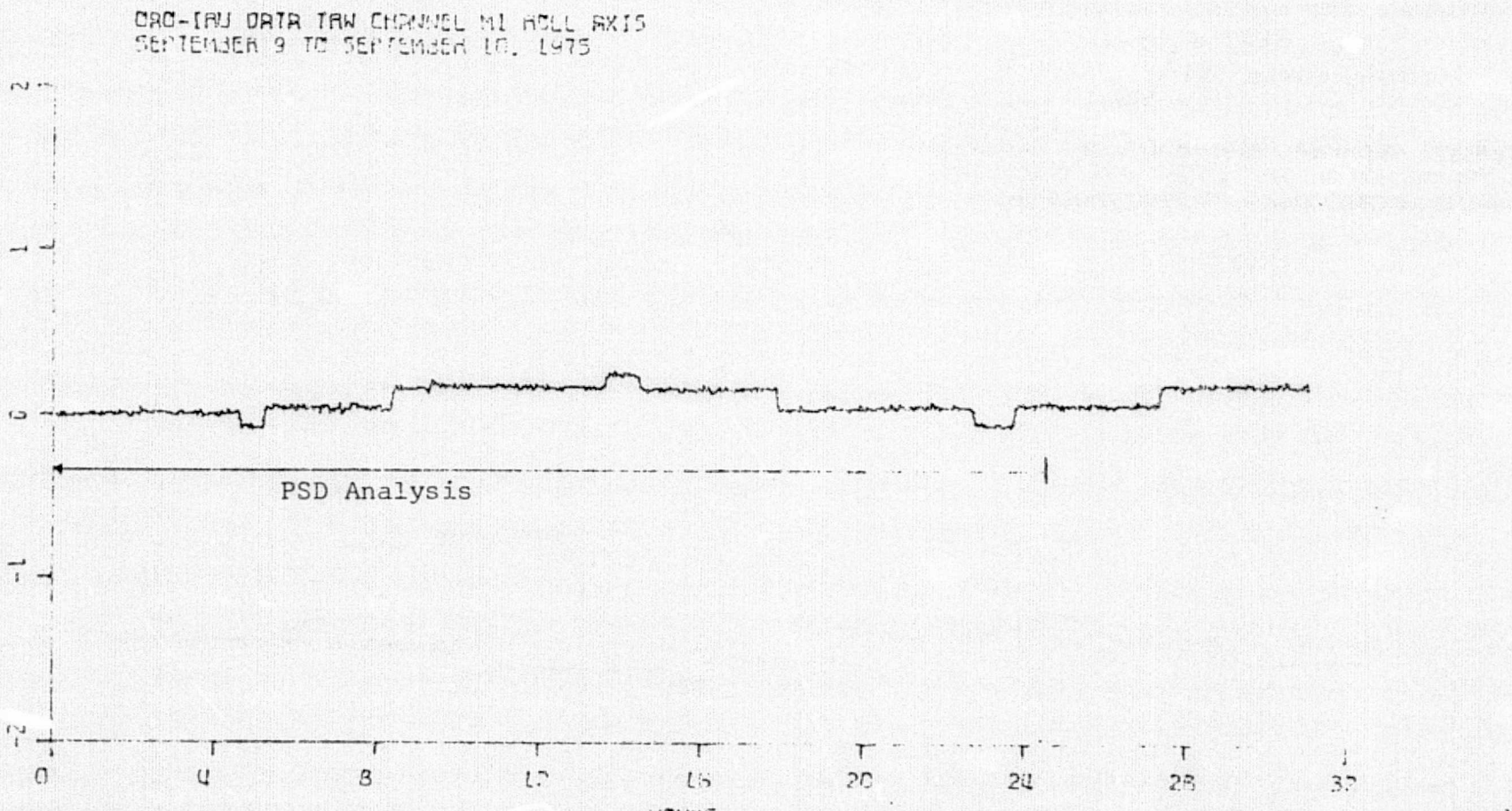

REFERENCE VALUE

THE ABOVE DATA WERE PROCESSED BY SLIDING AND AVERAGING 56.00, 3.56 SECOND CONTINUOUS DATA SAMPLES. THE APPROXIMATE FILTER CHARACTERISTICS DERIVED ARE:

(-2) Effective Bandwidth
0.0035 rad/s

SKIPPER K TEST LABORATORY/BEDFORD FLIGHT FACILITY

FIGURE 4

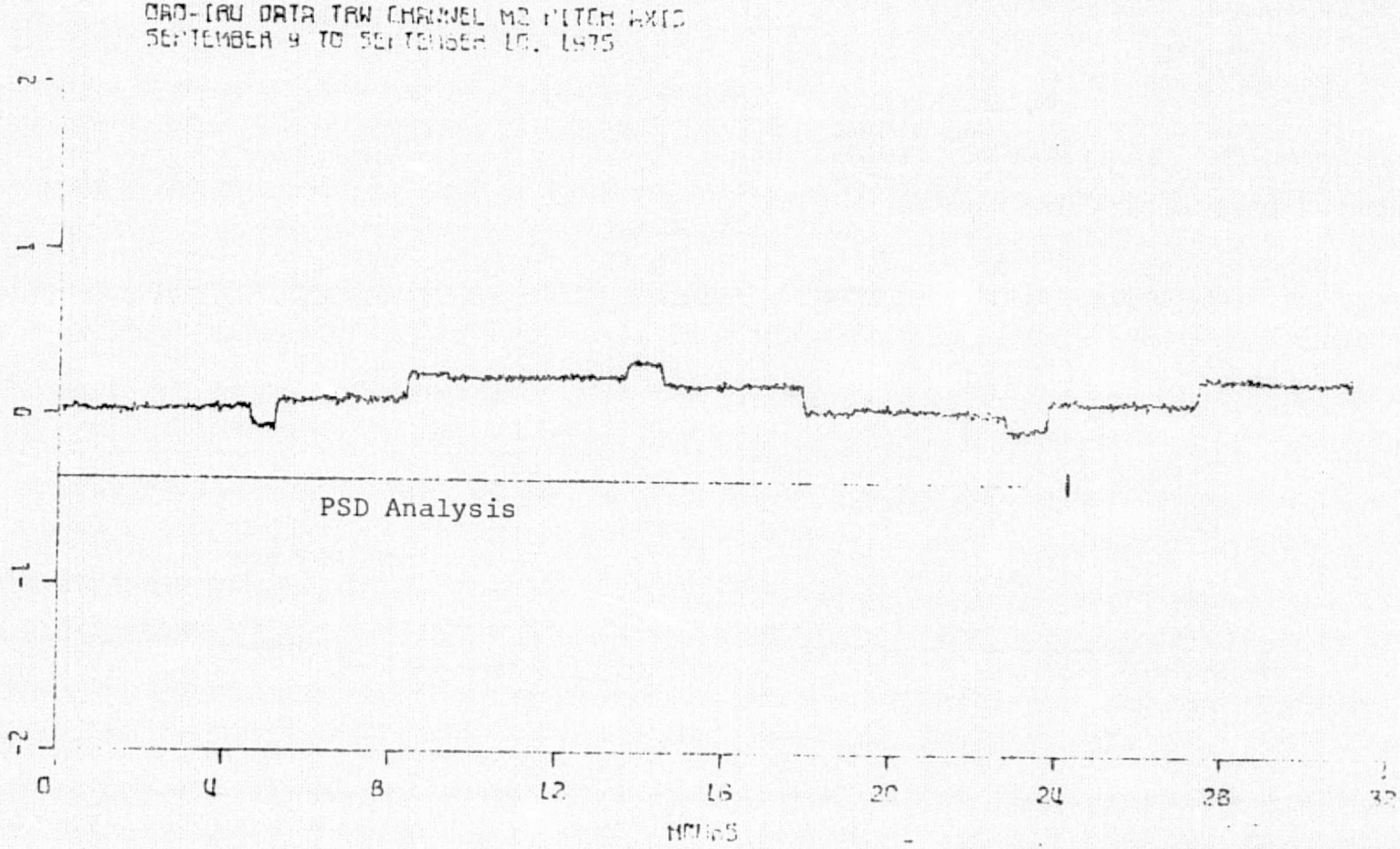

MEASURED VALUE

THE ABOVE DATA WERE PROCESSED BY SLIDING AND AVERAGING 50.0 , 256 SECOND CONTINUOUS DATA SAMPLES. THE APPROXIMATE FILTER CHARACTERISTICS DERIVED ARE:

(-2) Effective Bandwidth
0.0035 rad/s

SKIPPER K TEST LABORATORY/BEDFORD FLIGHT FACILITY

FIGURE 5

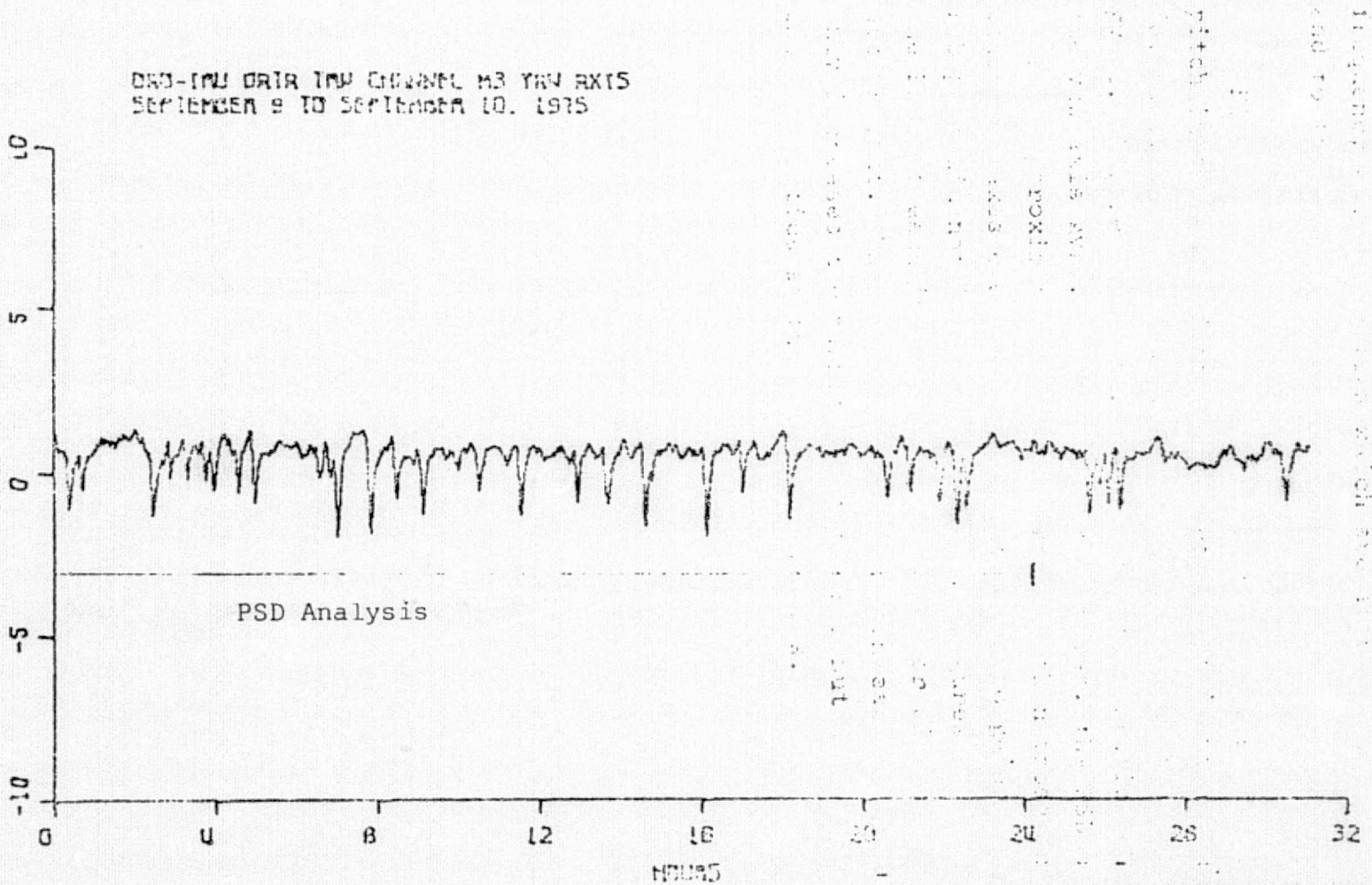

REFERENCE VALUE	-0V2.33V30	MERU
MERU	-0V1.87V82	MERU
STORM	.N.07	MERU
TREND	-.[illegible]	[illegible]
STANDARD DEVIATION	.[illegible]	[illegible]
[illegible]	[illegible]	[illegible]
[illegible]	[illegible]	[illegible]
[illegible]	[illegible]	[illegible]

THE ABOVE DATA WERE PROCESSED BY SLIDING AND AVERAGING 56.0 , 2.5% SECOND CONTINUOUS DATA SAMPLES. THE APPROXIMATE FILTER CHARACTERISTICS DERIVED ARE:

(-2) Effective Bandwidth
0.0035 rad/s

[illegible] TEST LABORATORY/BEDFORD FLIGHT FACILITY

CMG-IRU DATA TRW CHANNEL M1 ROLL AXIS
SEPTEMBER 10 TO SEPTEMBER 11, 1975

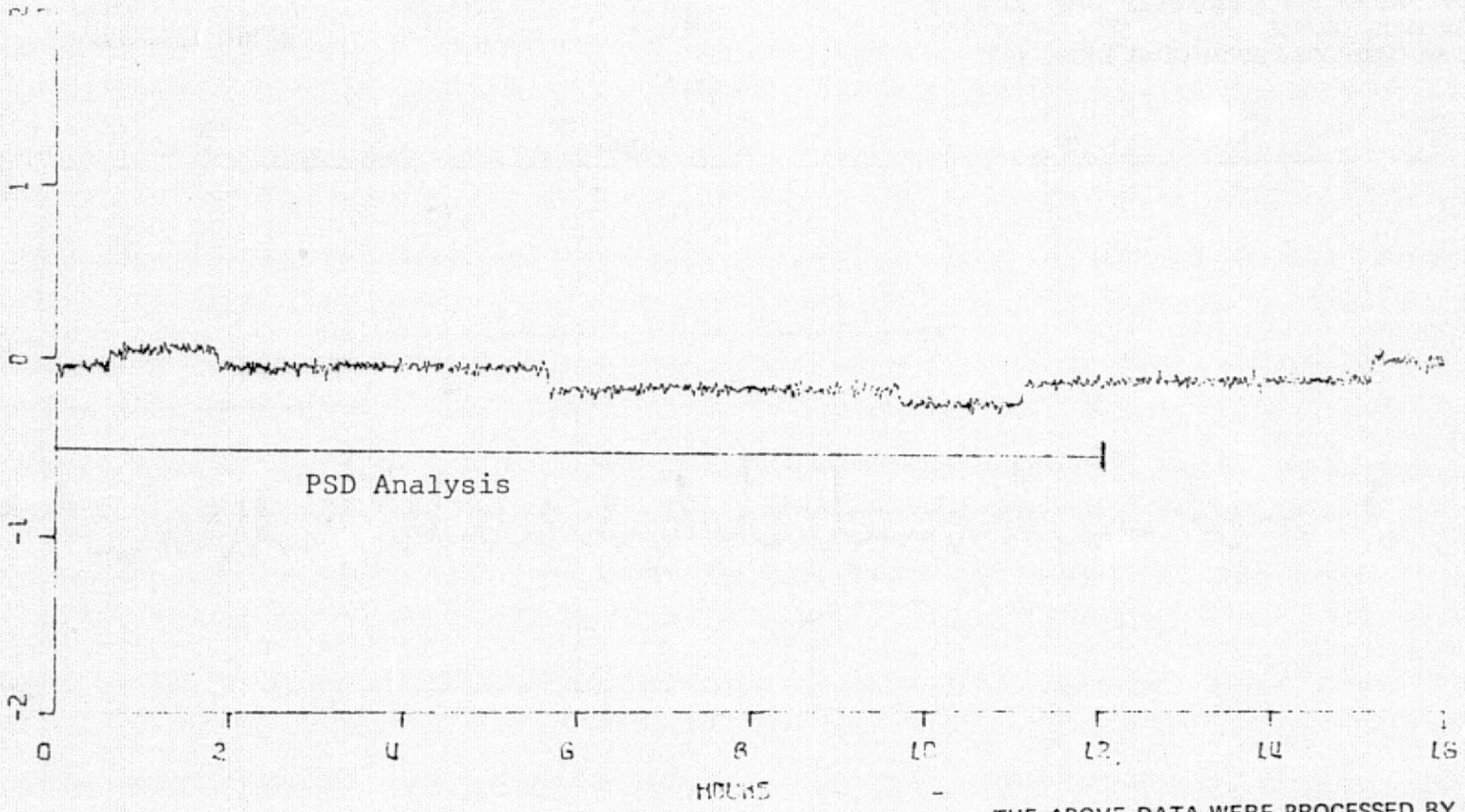

REFERENCE VALUE

THE ABOVE DATA WERE PROCESSED BY SLIDING AND AVERAGING 240 , 2.56 SECOND CONTINUOUS DATA SAMPLES. THE APPROXIMATE FILTER CHARACTERISTICS DERIVED ARE:

(-2) Effective Bandwidth
rad/s
0.007

SKIPPER K TEST LABORATORY/BEDFORD FLIGHT FACILITY

FIGURE 7

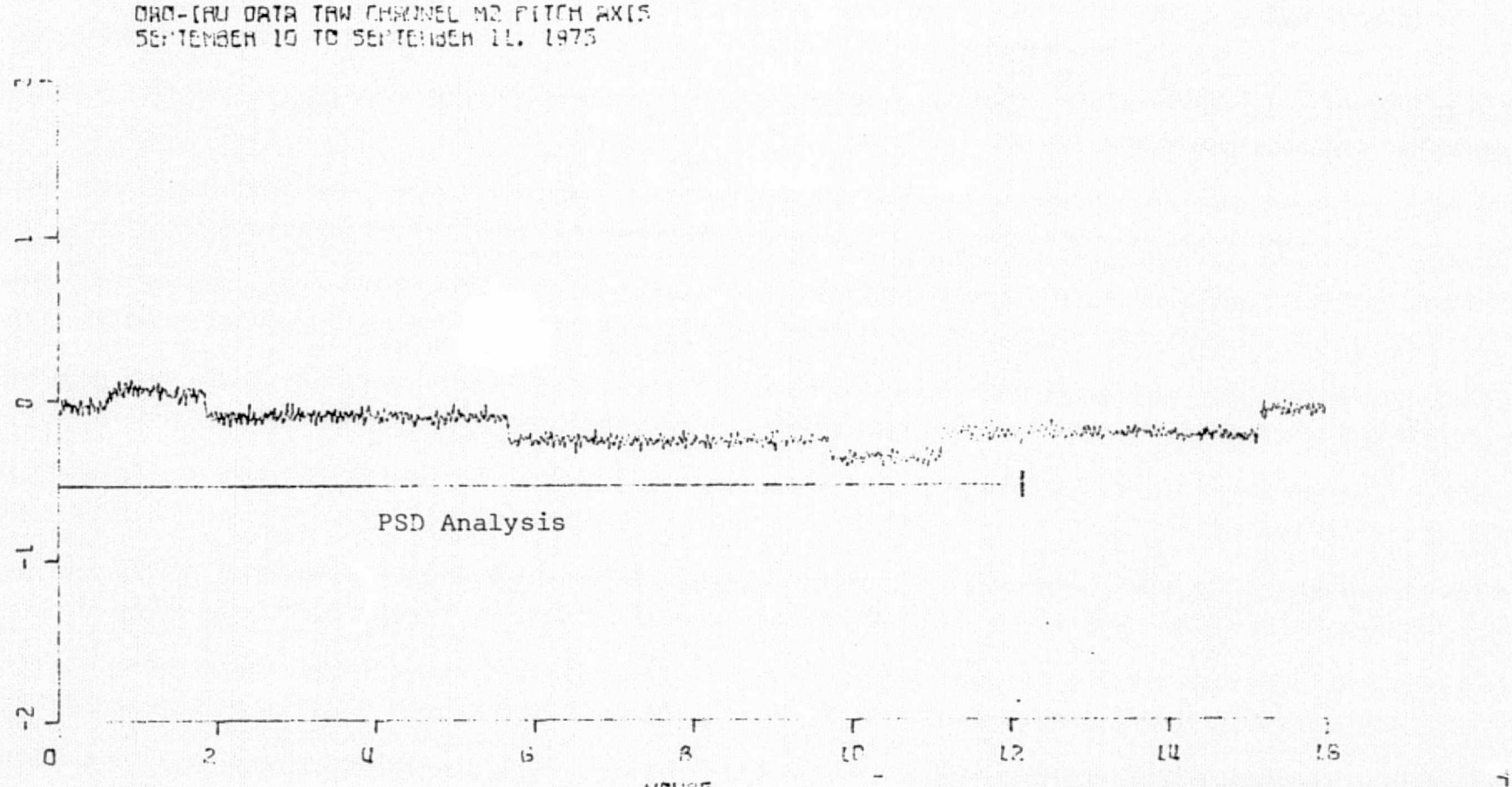

PSD Analysis

THE ABOVE DATA WERE PROCESSED BY SLIDING AND AVERAGING 2.56 , 2.56 SECOND CONTINUOUS DATA SAMPLES. THE APPROXIMATE FILTER CHARACTERISTICS DERIVED ARE:

(-2) Effective Bandwidth
0.007 rad/s

SKIPPER K TEST LABORATORY/BEDFORD FLIGHT FACILITY

FIGURE 8

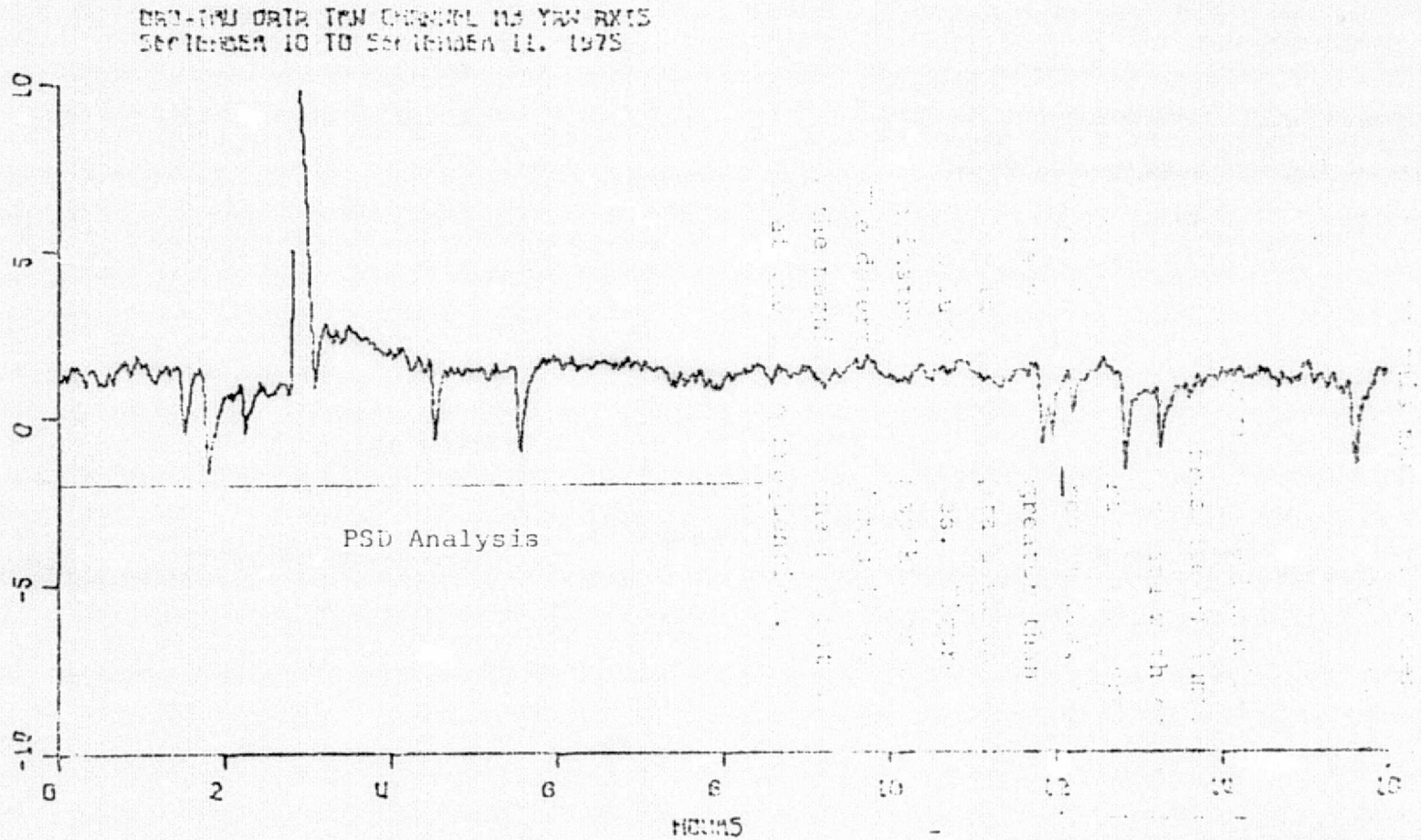

REFERENCE VALUE	-8N2.99593	MEAN
MEAN	-8N1.78121	MEAN
SIGMA	.8104	MEAN
TREND	-.08407	MEAN
SIGMA/TREND	.7967	MEAN
AVERAGING PERIOD	71.13	SE
ADJUSTED POINTS 4	OUT OF 513	SE
DAO-TAU STRM 3		

FIGURE 9

THE ABOVE DATA WERE PROCESSED BY SLIDING AND AVERAGING 240, 2.5 SECOND CONTINUOUS DATA SAMPLES. THE APPROXIMATE FILTER CHARACTERISTICS DERIVED ARE:

(-2) Effective Bandwidth
0.007 rad/s

SKIPPER K TEST LABORATORY/BEDFORD FLIGHT FACILITY

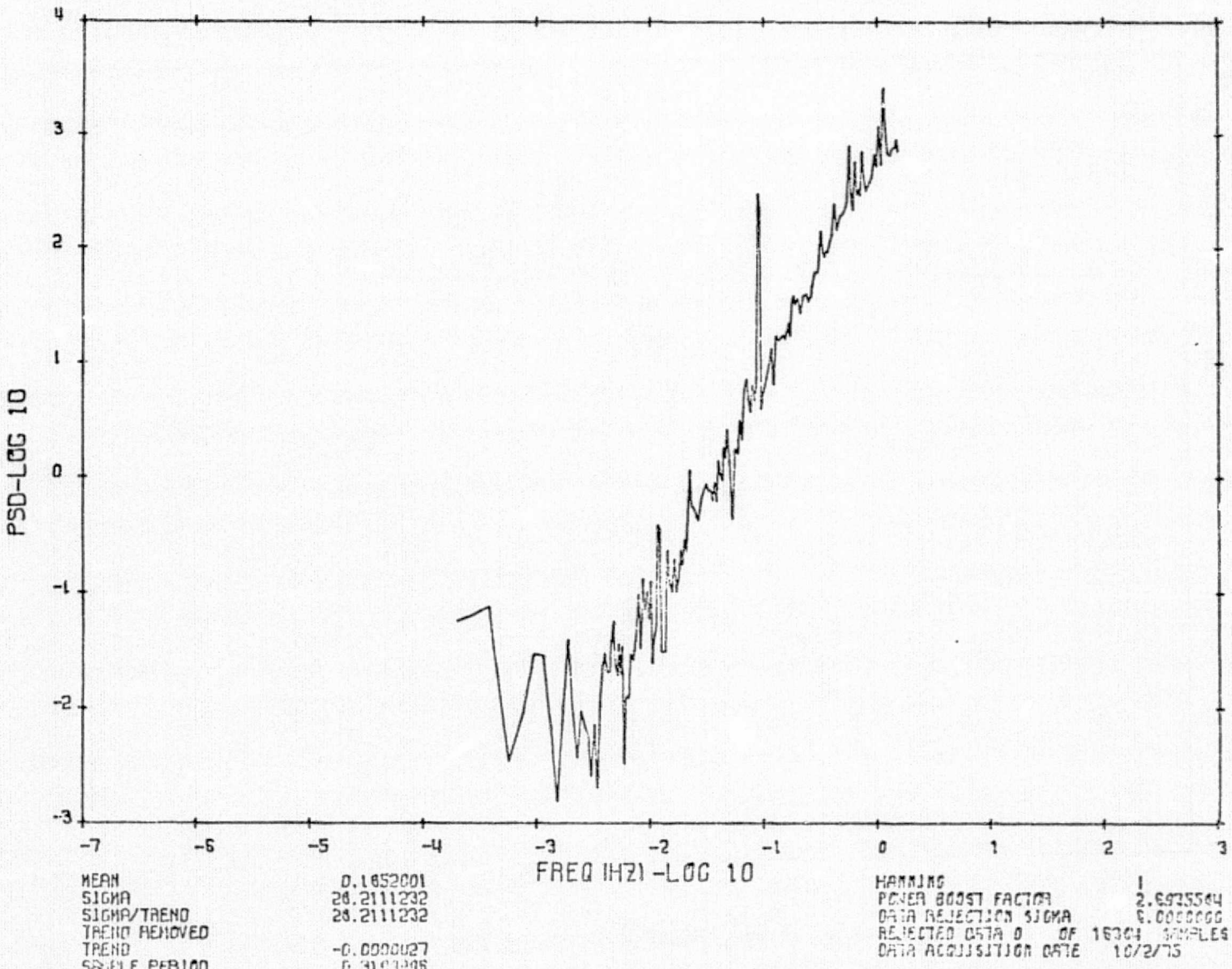

MEAN	0.1652001	HANNING	1
SIGMA	28.2111232	POWER BOOST FACTOR	2.6875564
SIGMA/TREND	28.2111232	DATA REJECTION SIGMA	6.0000000
TREND REMOVED		REJECTED DATA 0 OF 16384 SAMPLES	
TREND	-0.0000027	DATA ACQUISITION DATE	10/2/75
SAMPLE PERIOD	0.3100306		

FIGURE 10

PITCH (0A0-IRU) 72

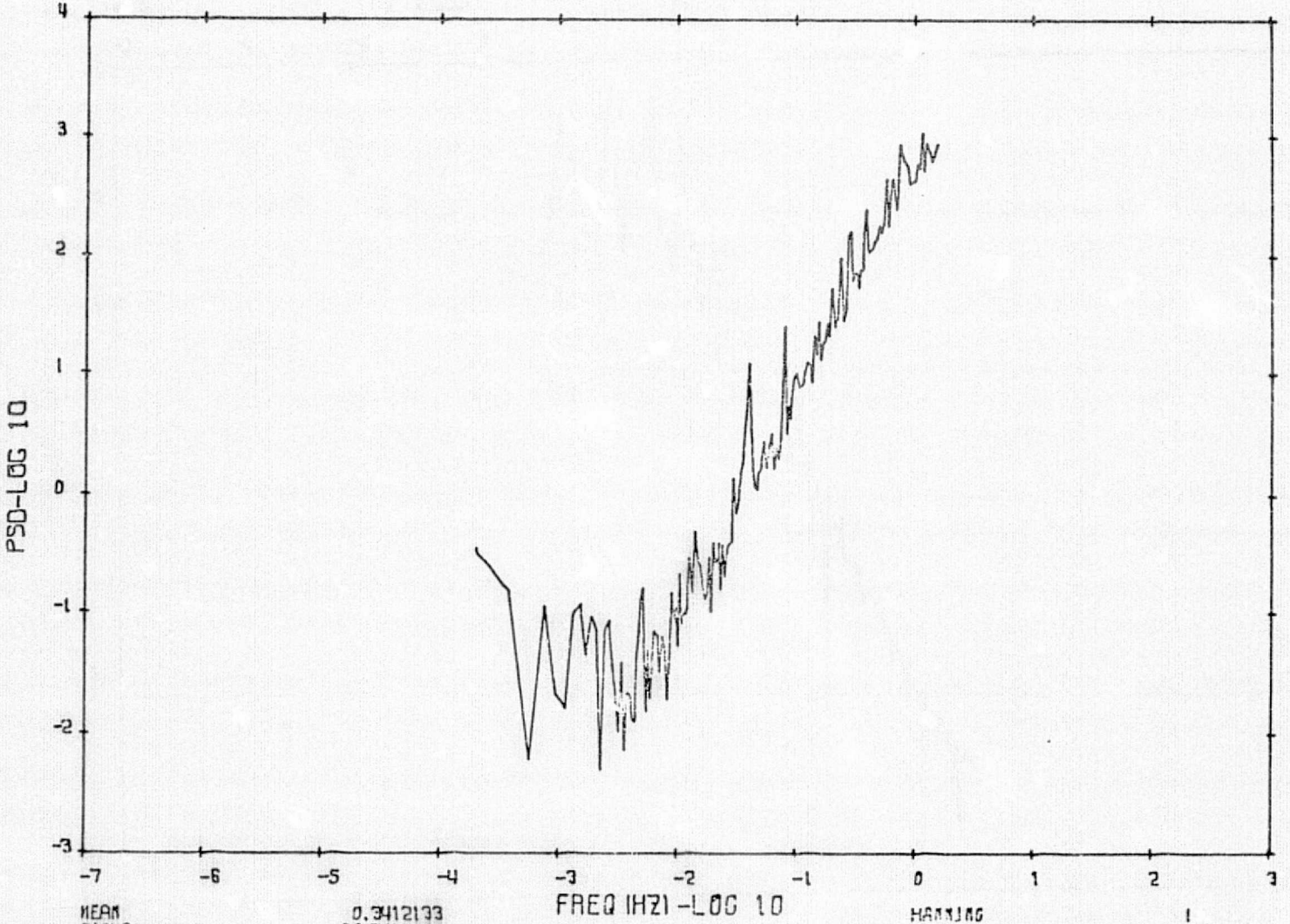

MEAN	0.3412133
SIGMA	25.7633260
SIGMA/TREND	25.7633260
TREND REMOVED	
TREND	-0.0000006
SAMPLE PERIOD	0.3199395

HANNING	!
POWER BOOST FACTOR	2.6665640
DATA REJECTION SIGMA	6.0000000
REJECTED DATA 0 OF	16384 SAMPLES
DATA ACQUISITION DATE	10/2/75

FIGURE 11

YAW (OAO-IRU) 72

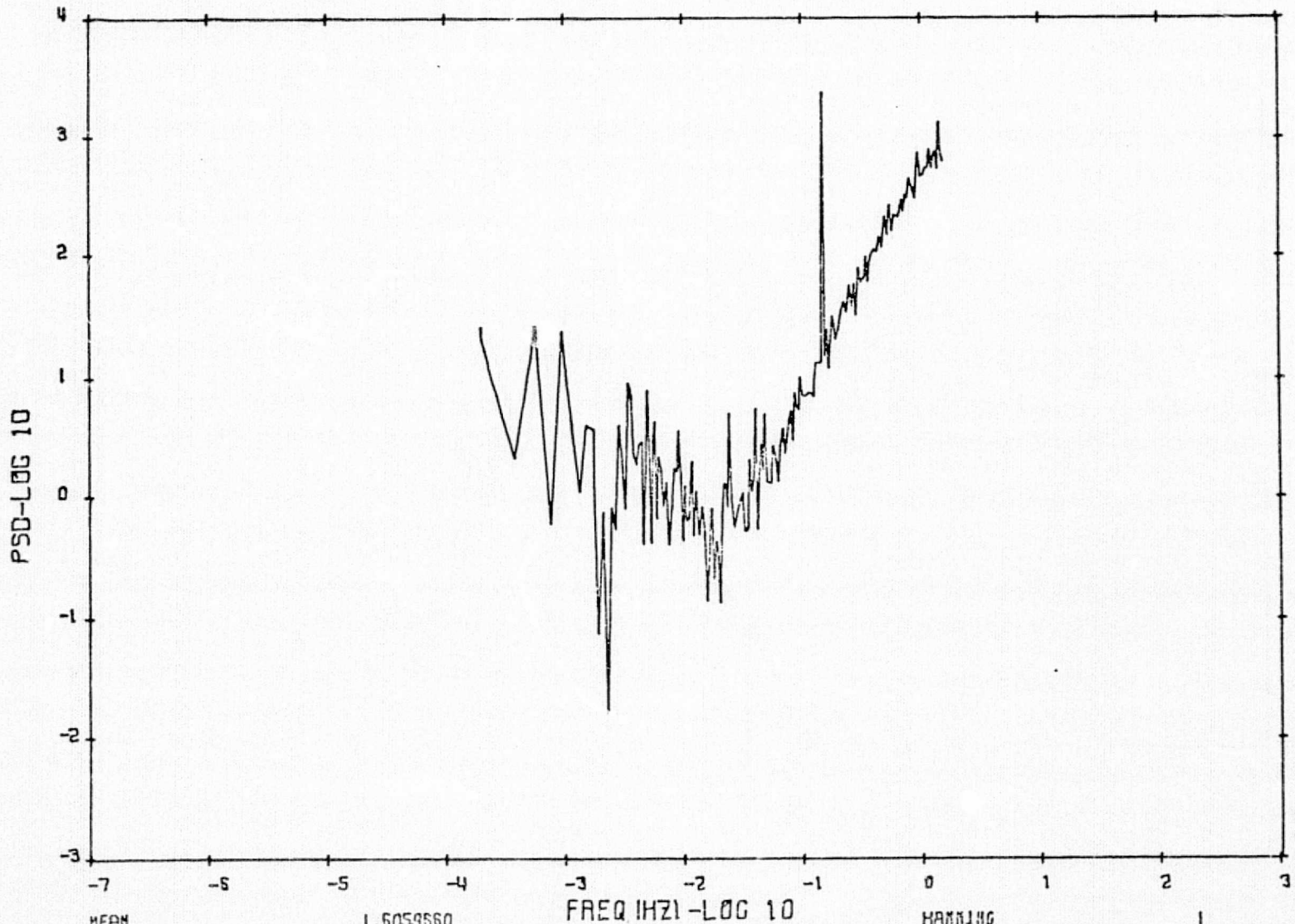

MEAN	1.6059660
SIGMA	24.0373760
SIGMA/TREND	24.0373760
TREND REMOVED	
TREND	-0.0000129
SAMPLE PERIOD	0.3125000

HANNING	1
POWER BOOST FACTOR	2.0069606
DATA REJECTION SIGMA	6.0000000
REJECTED DATA 3 OF	16384 SAMPLES
DATA ACQUISITION DATE	10/2/75

FIGURE 12

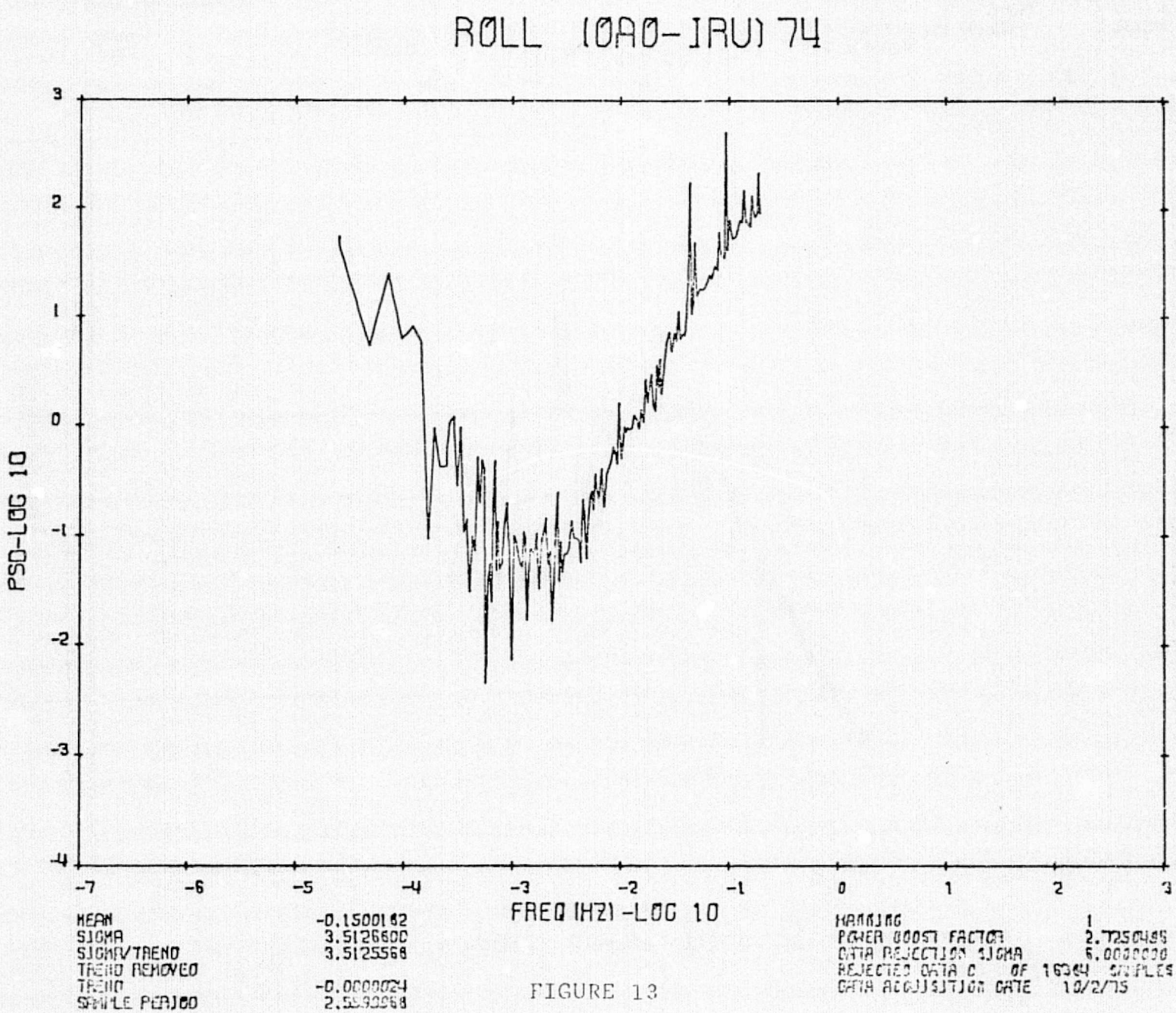
ROLL (OAO-IRU) 74
PSD-LOG 10
FREQ (HZ) -LOG 10
3
2
1
0
-1
-2
-3
-4
-7
-6
-5
-4
-3
-2
-1
0
1
2
3
MEAN -0.1500162
SIGMA 3.5126600
SIGMA/TREND 3.5125568
TREND REMOVED
TREND -0.0000024
SAMPLE PERIOD 2.5000068
HANNING 1
POWER BOOST FACTOR 2.7250495
DATA REJECTION SIGMA 6.0000000
REJECTED DATA 0 OF 16384 SAMPLES
DATA ACQUISITION DATE 10/2/75

FIGURE 13

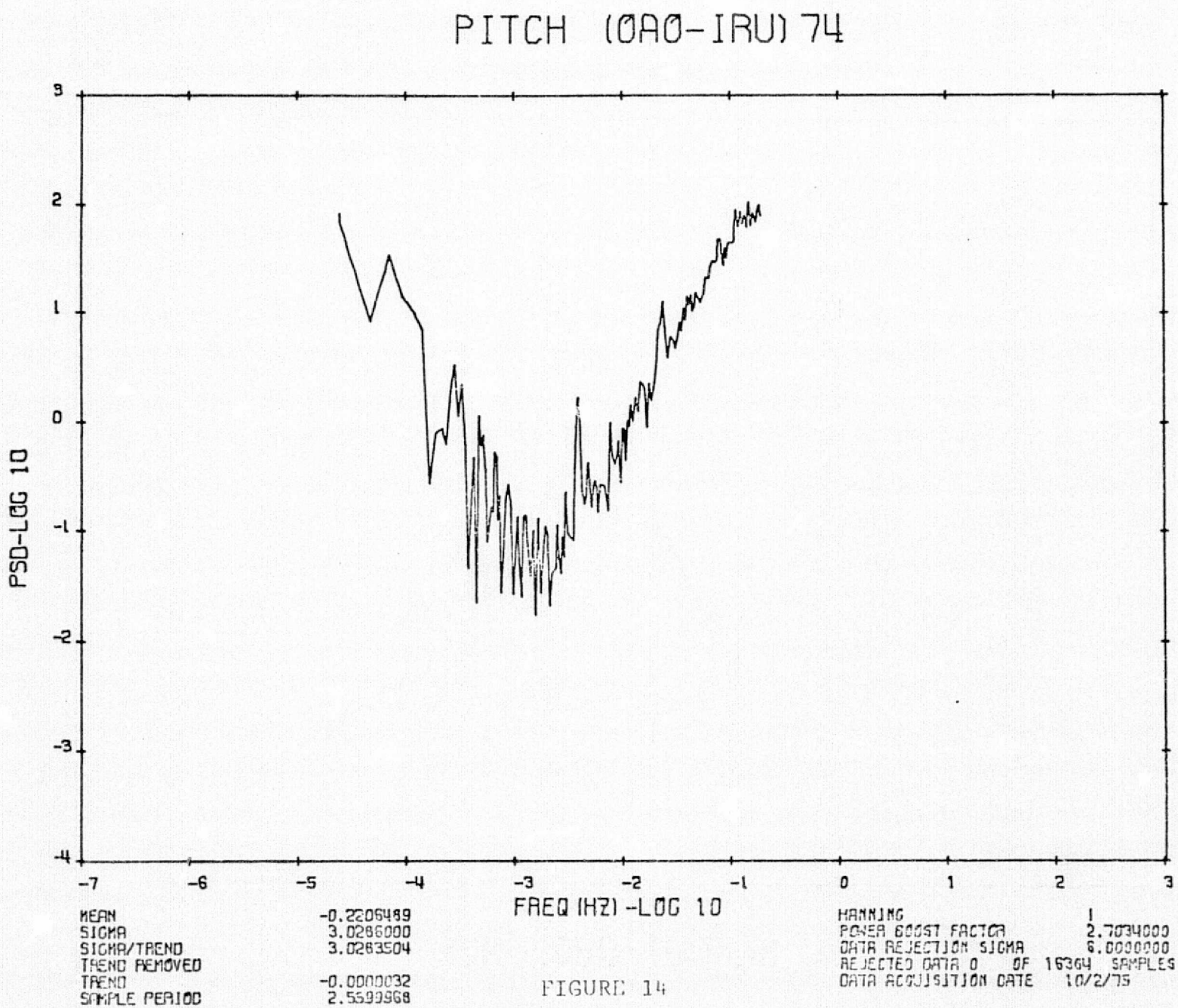
PITCH (0A0-IRU) 74
PSD-LOG 10
3
2
1
0
-1
-2
-3
-4
-7
-6
-5
-4
-3
-2
-1
0
1
2
3
FREQ (HZ) -LOG 10
MEAN -0.2206489
SIGMA 3.0286000
SIGMA/TREND 3.0283504
TREND REMOVED
TREND -0.0000032
SAMPLE PERIOD 2.5599968
HANNING 1
POWER BOOST FACTOR 2.7034000
DATA REJECTION SIGMA 6.0000000
REJECTED DATA 0 OF 16384 SAMPLES
DATA ACQUISITION DATE 10/2/75

FIGURE 14

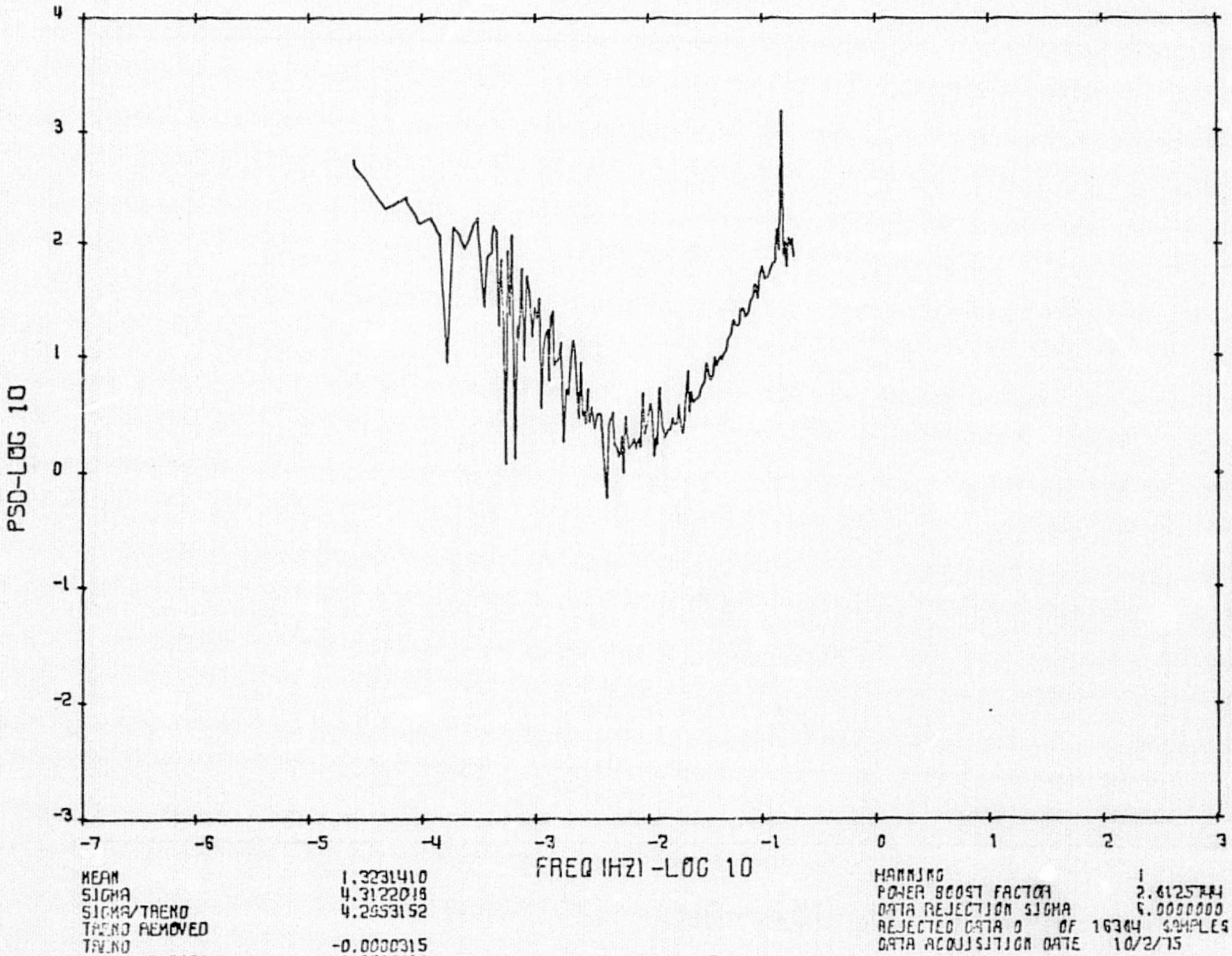

FIGURE 15

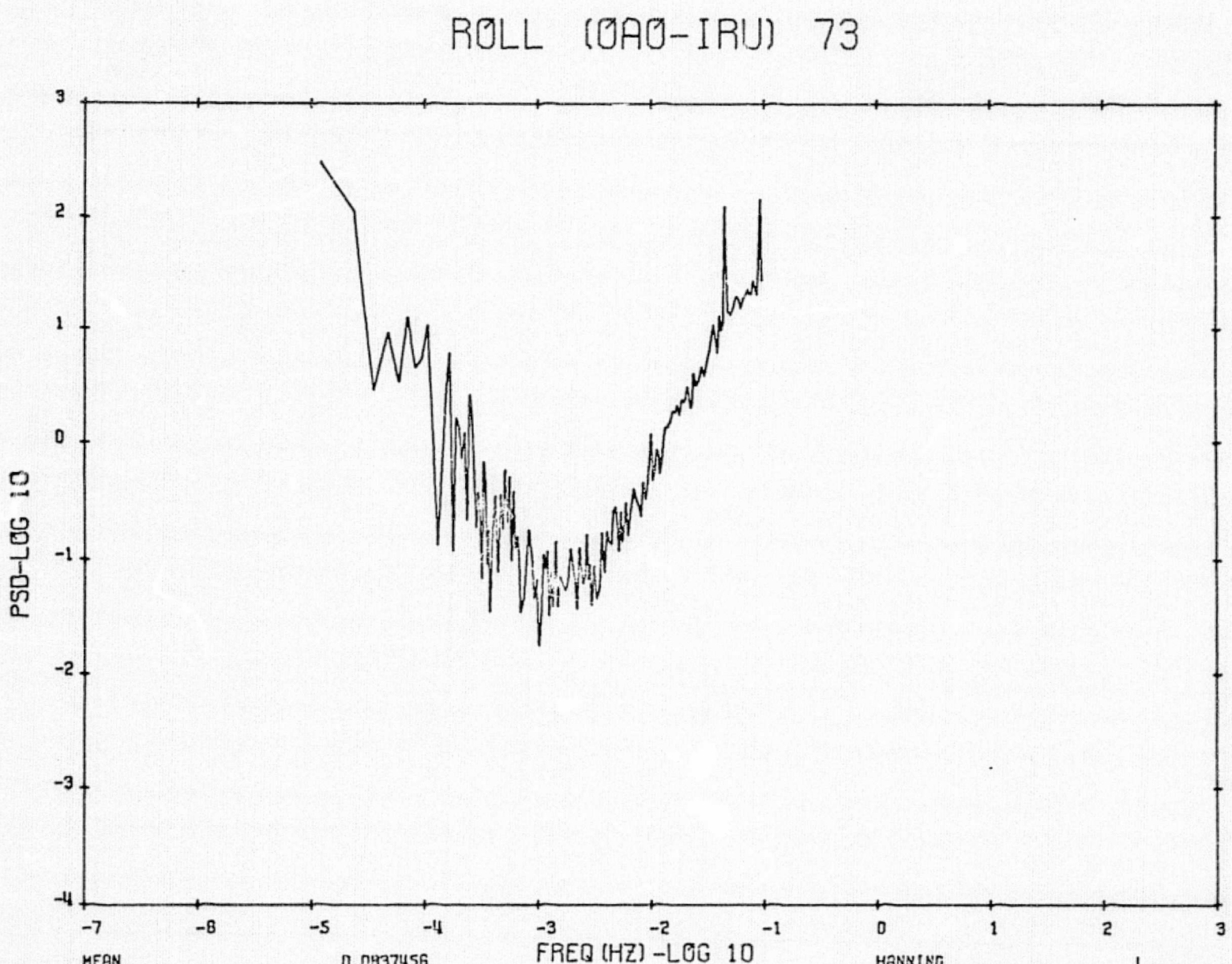

MEAN	0.0837456	HANNING	1
SIGMA	1.3671160	POWER BOOST FACTOR	2.6883136
SIGMA/TREND	1.3000800	DATA REJECTION SIGMA	6.0000000
TREND REMOVED		REJECTED DATA 0 OF 16384 SAMPLES	
TREND	0.0000010	DATA ACQUISITION DATE	9/10/75
SAMPLE PERIOD	5.1159536		

FIGURE 16

PITCH (0A0-IRU) 73

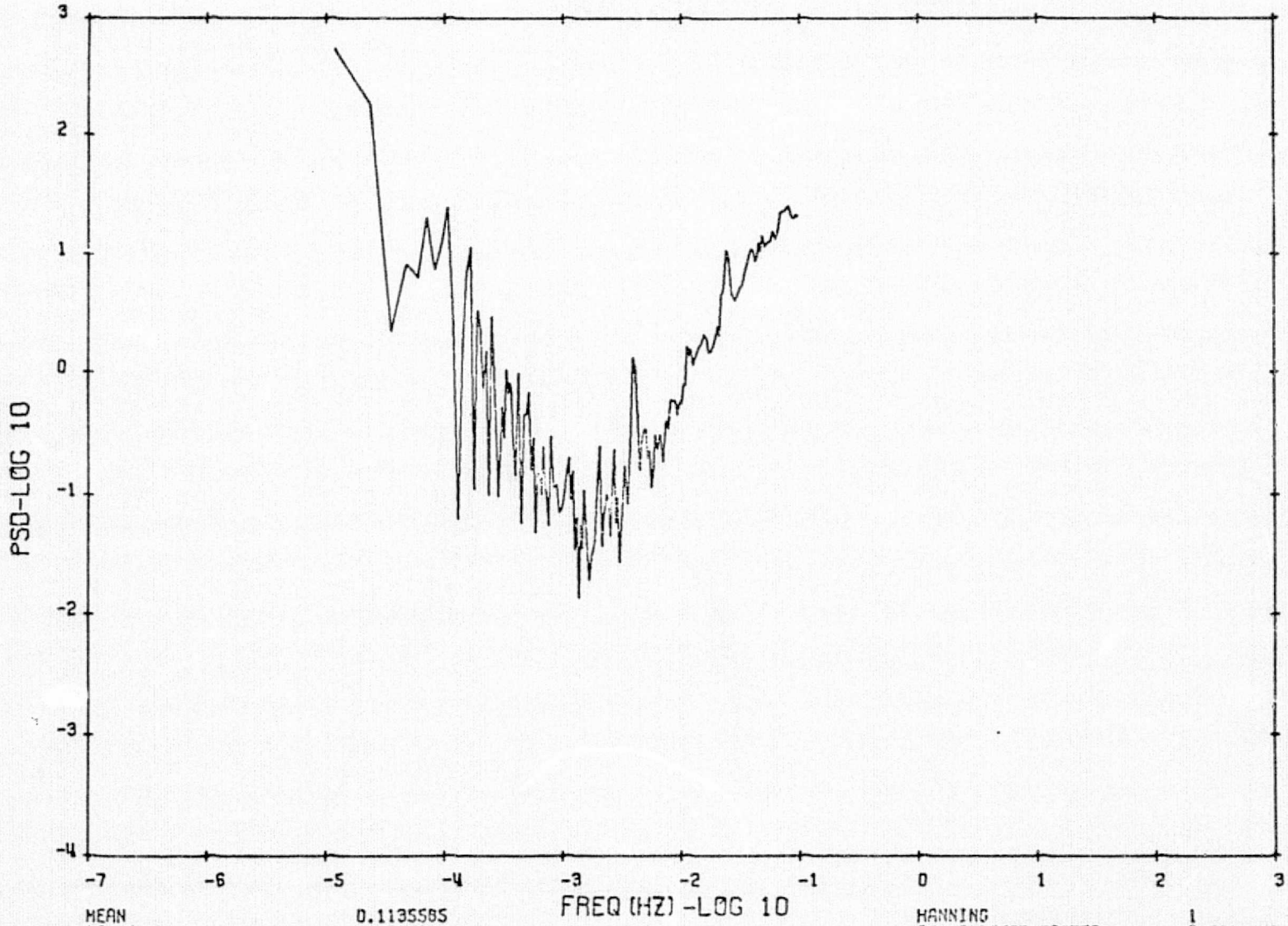

MEAN	0.1135585	HANNING	1
SIGMA	1.1011910	POWER BOOST FACTOR	2.6816448
SIGMA/TREND	1.1011570	DATA REJECTION SIGMA	6.0000000
TREND REMOVED		REJECTED DATA 0 OF	16384 SAMPLES
TREND	0.0000004	DATA ACQUISITION DATE	9/10/75
SAMPLE PERIOD	5.1155536		

FIGURE 17

YAW (0A0-IRU) 73

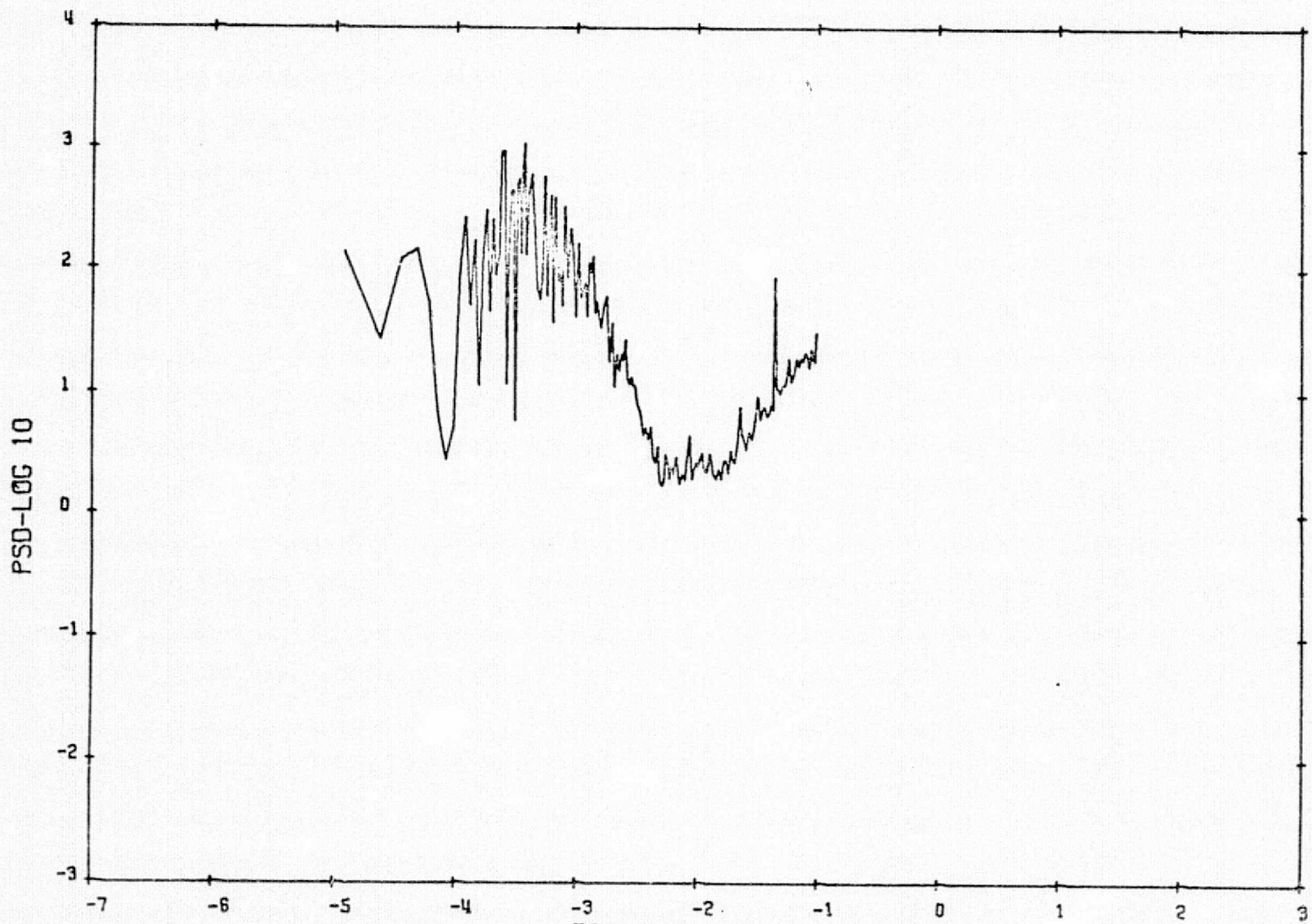

MEAN	0.4648734	HANNING	1
SIGMA	1.2565710	POWER BOOST FACTOR	2.6900633
SIGMA/TREND	1.2561930	DATA REJECTION SIGMA	6.0000000
TREND REMOVED		REJECTED DATA 0 OF 16384 SAMPLES	
TREND	-0.0000013	DATA ACQUISITION DATE	9/10/73
SAMPLE PERIOD	5.1150936		

FIGURE 18

APPENDIX D

REAL TIME DISGNOSTIC DATA

FOLDOUT FRAME

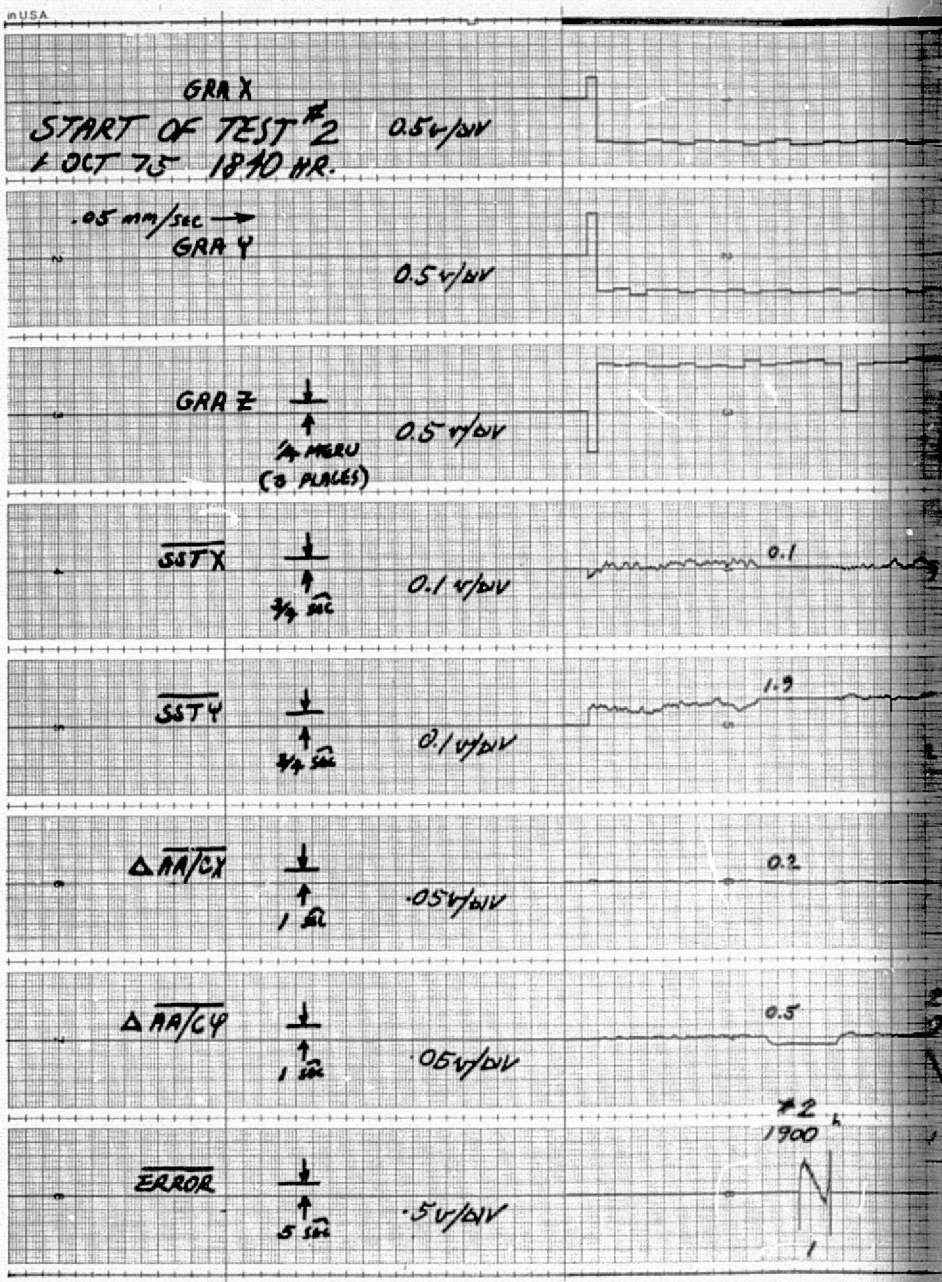

FOLDOUT FRAME 2

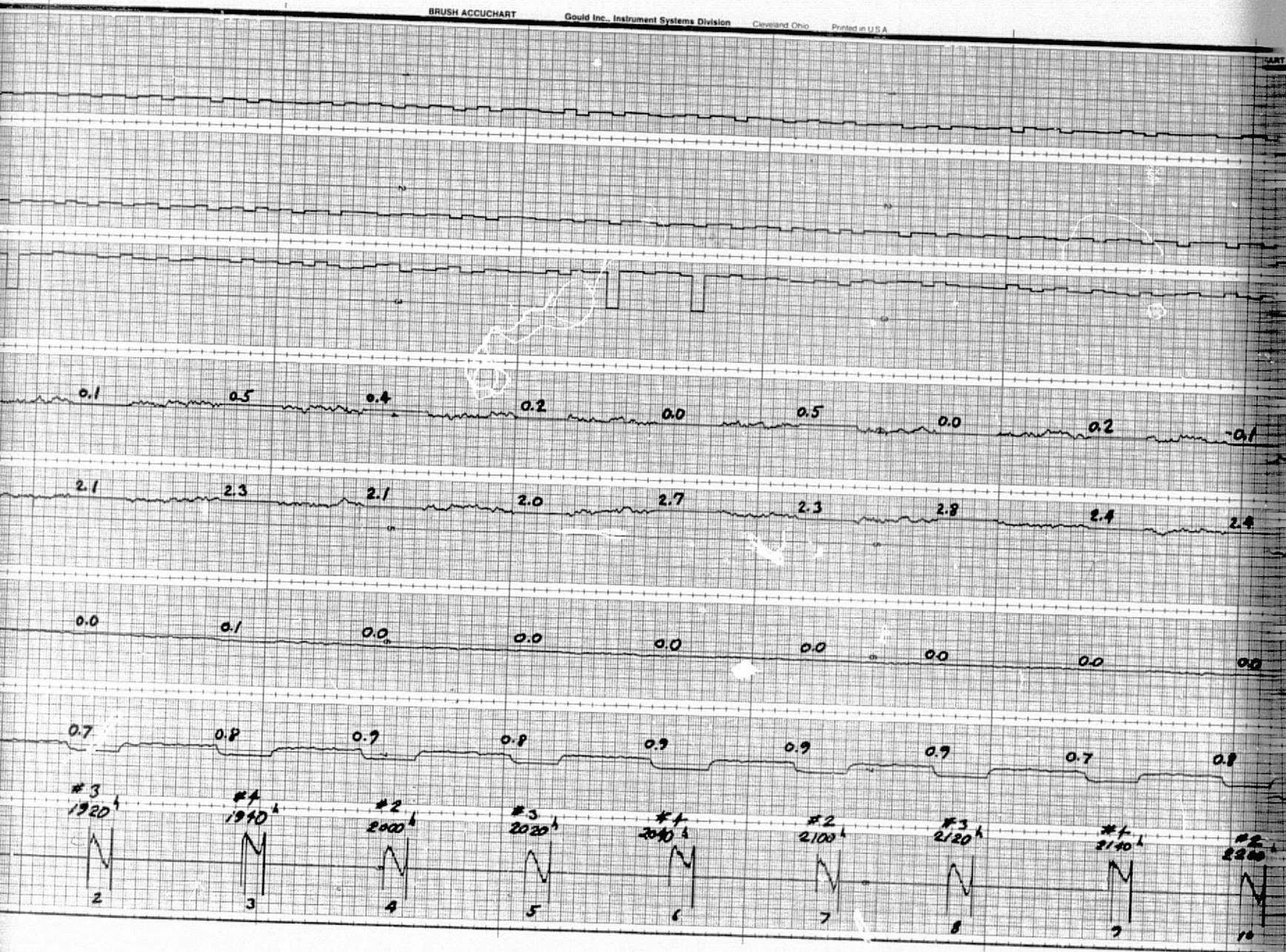

FOLDOUT FRAME 3

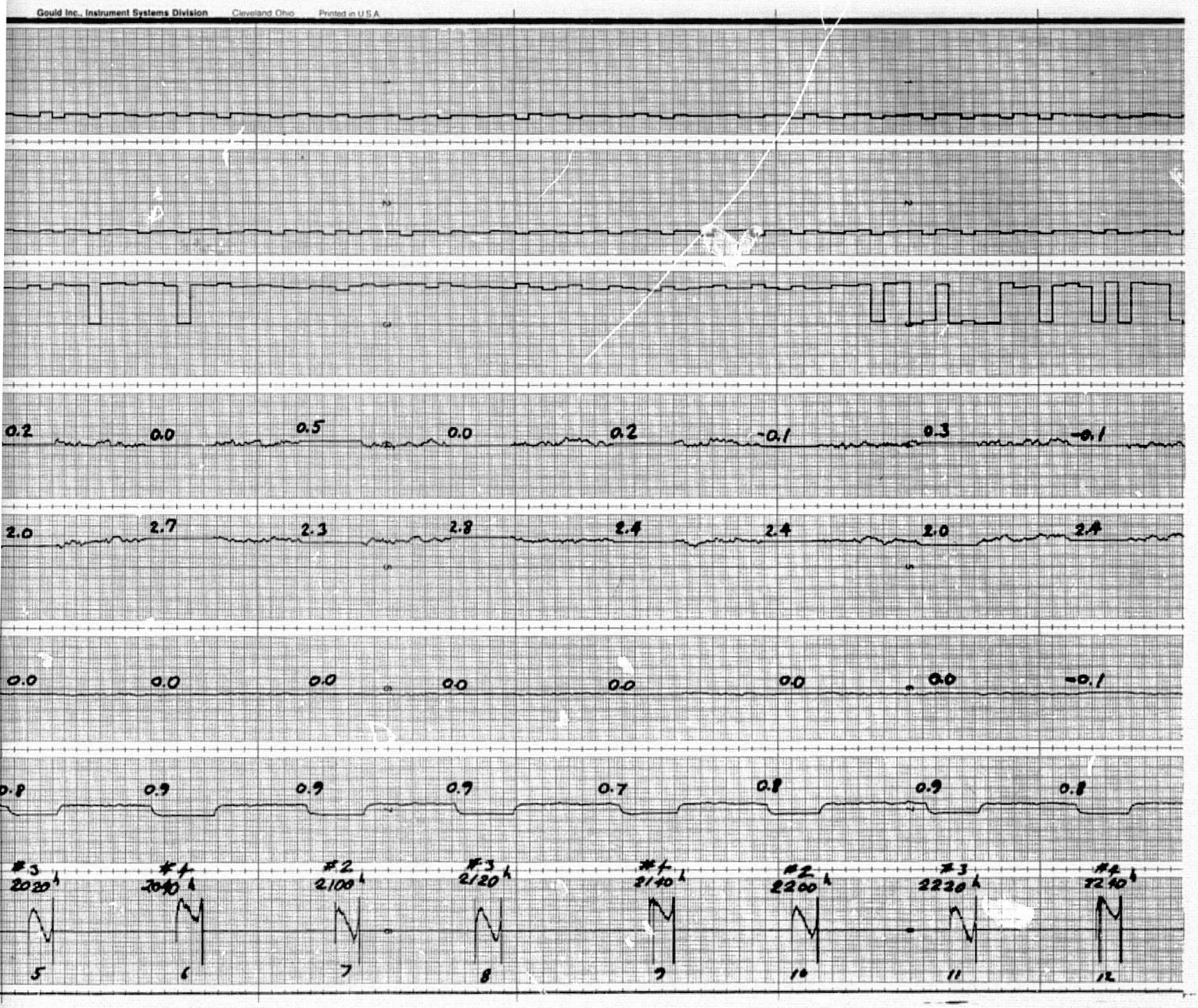

Figure D-1. Strapdown System Test Run No. 1

FOLDOUT FRAME 1

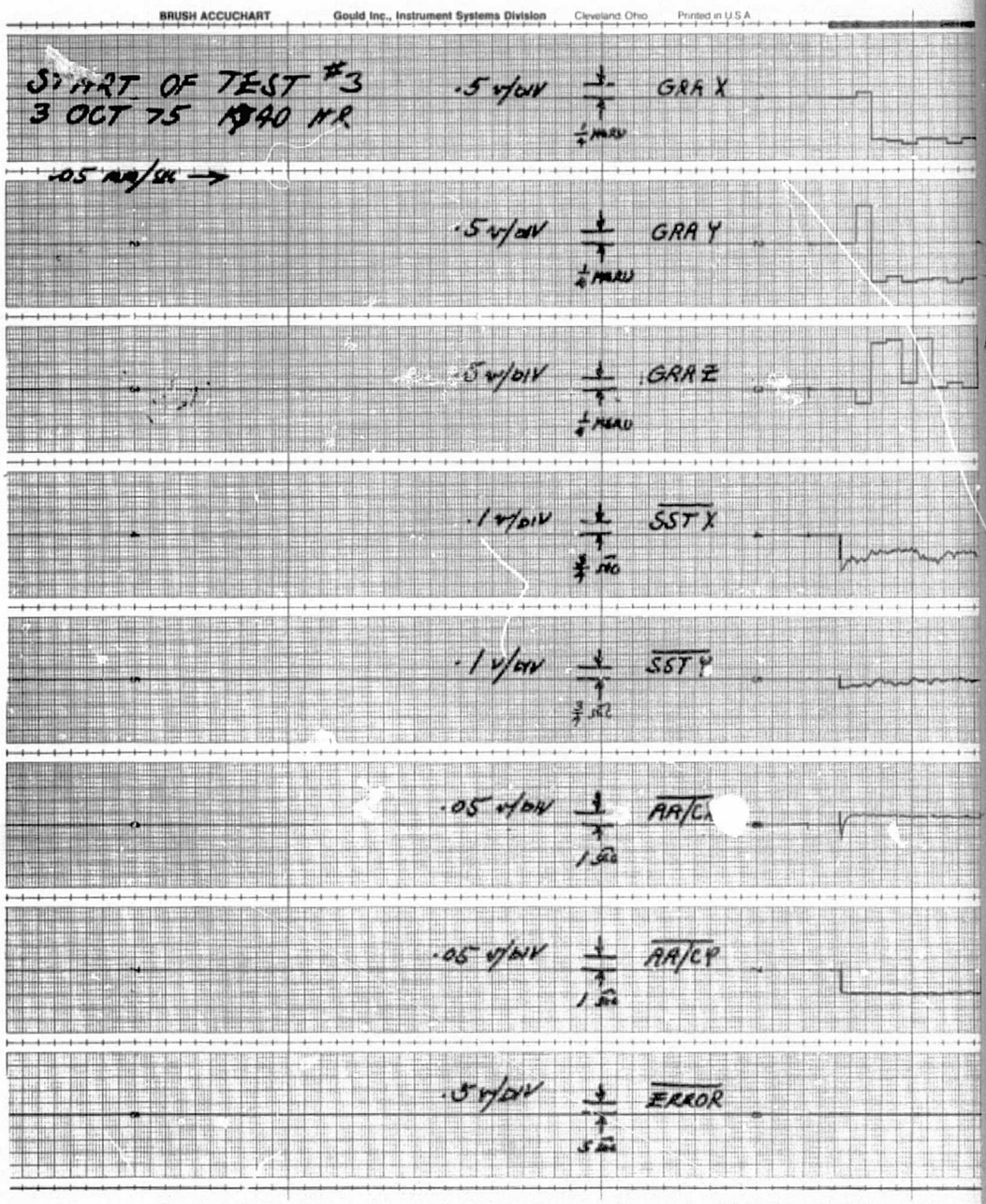

FOLDOUT FRAME 2

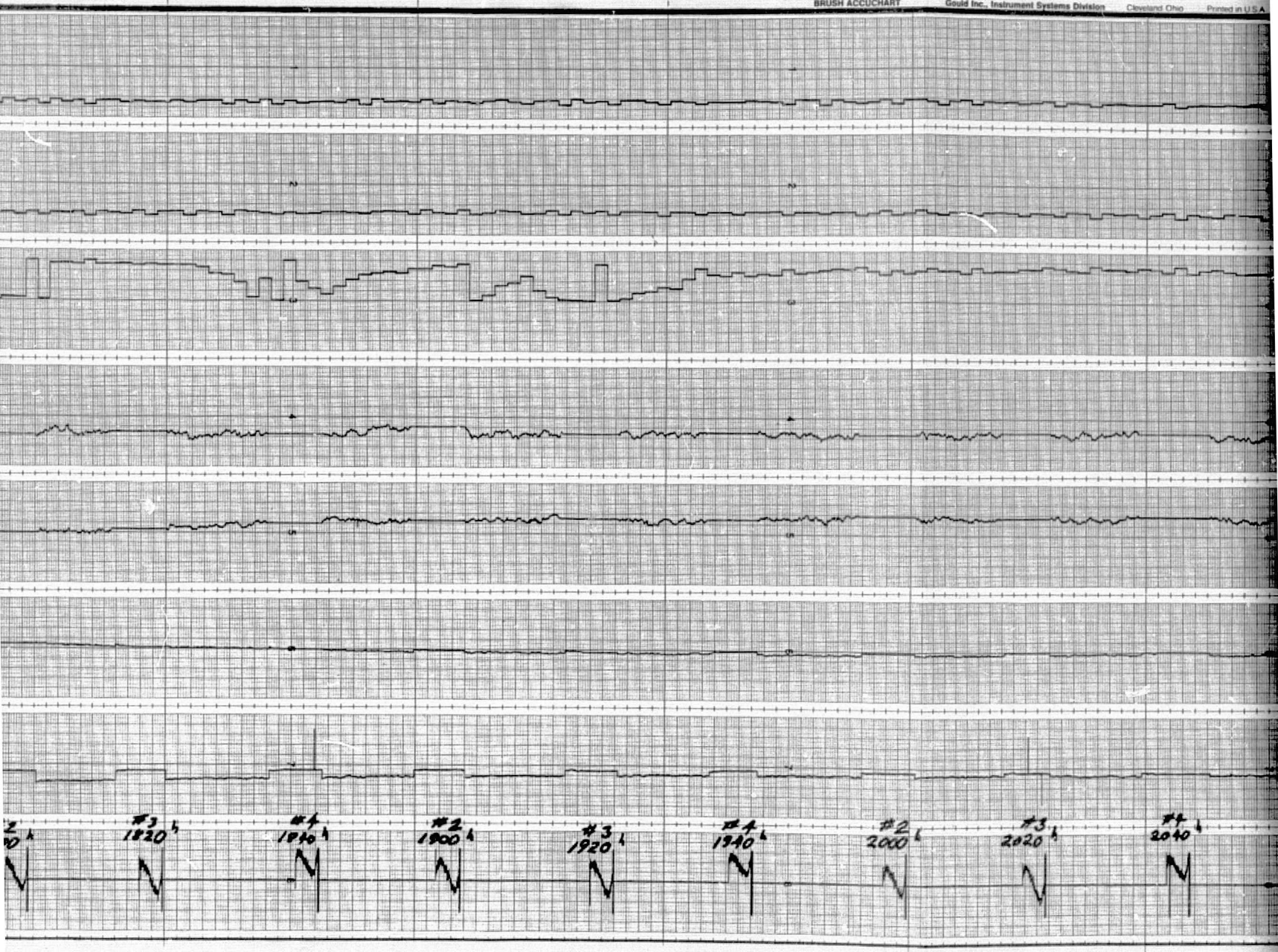

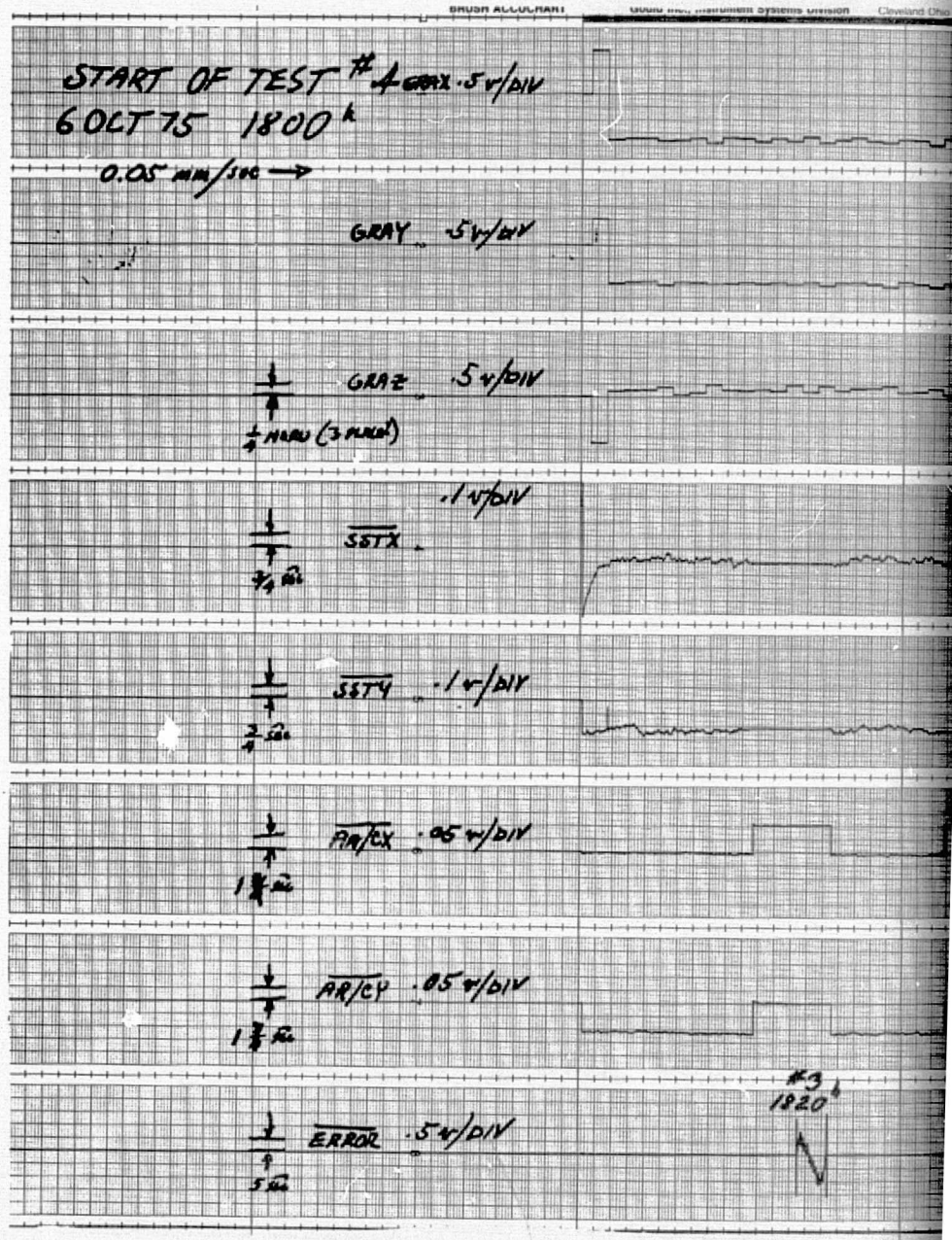

FOLDOUT FRAME 1

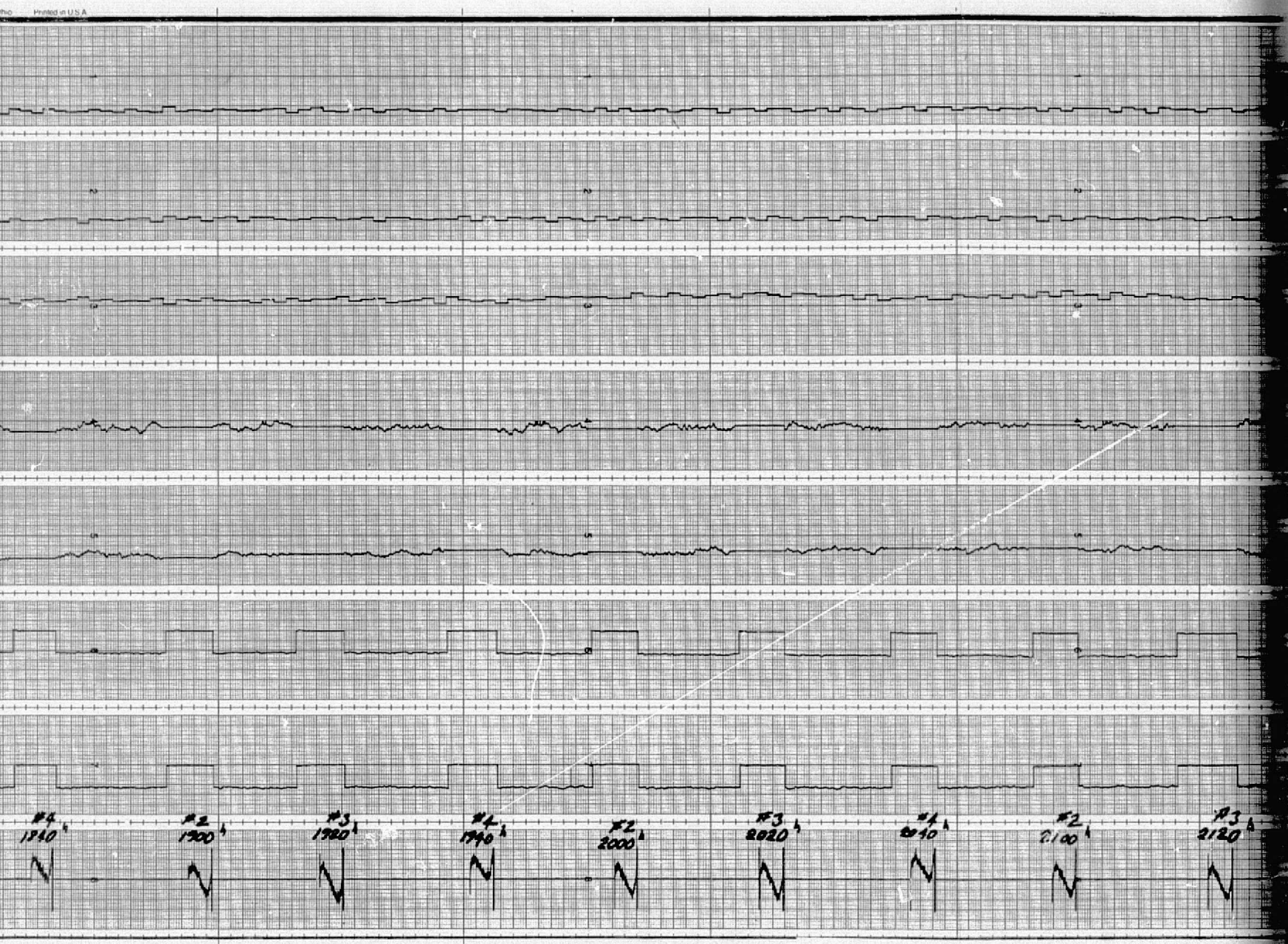

FOLDOUT FRAME 2

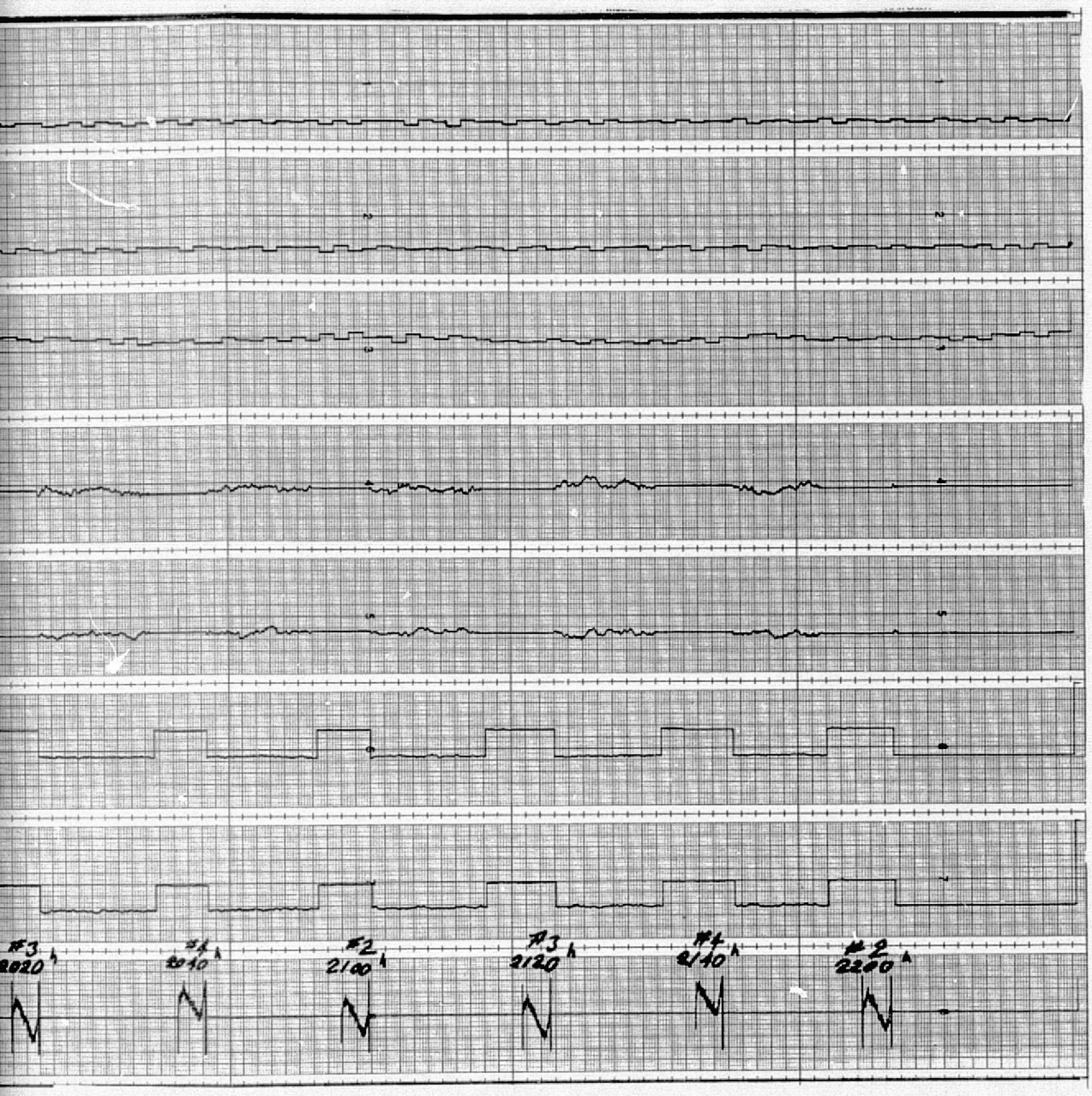

Figure D-3. Strapdown System
Test Run No. 3

FOLDOUT FRAME 3

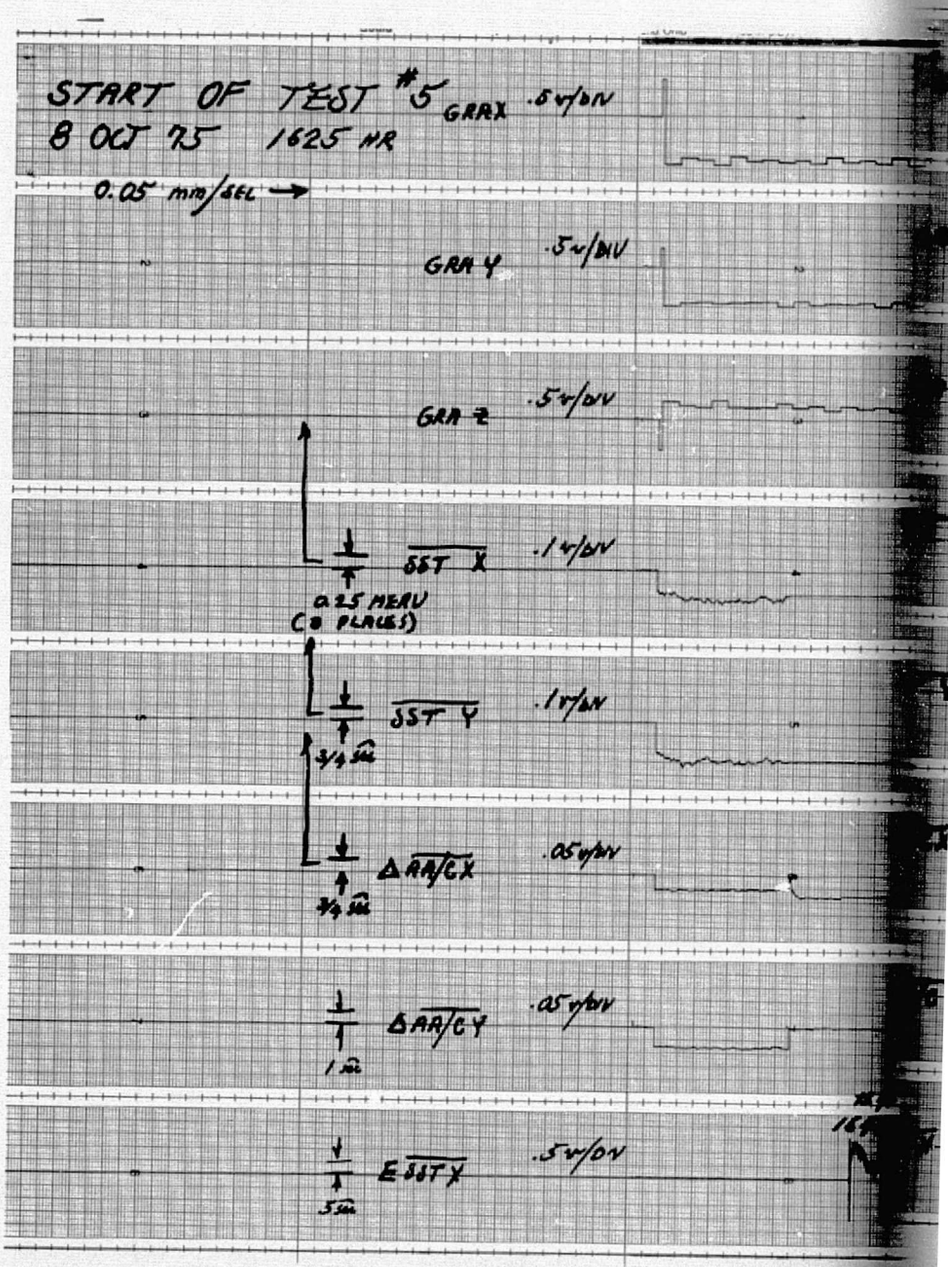

FOLDOUT FRAME

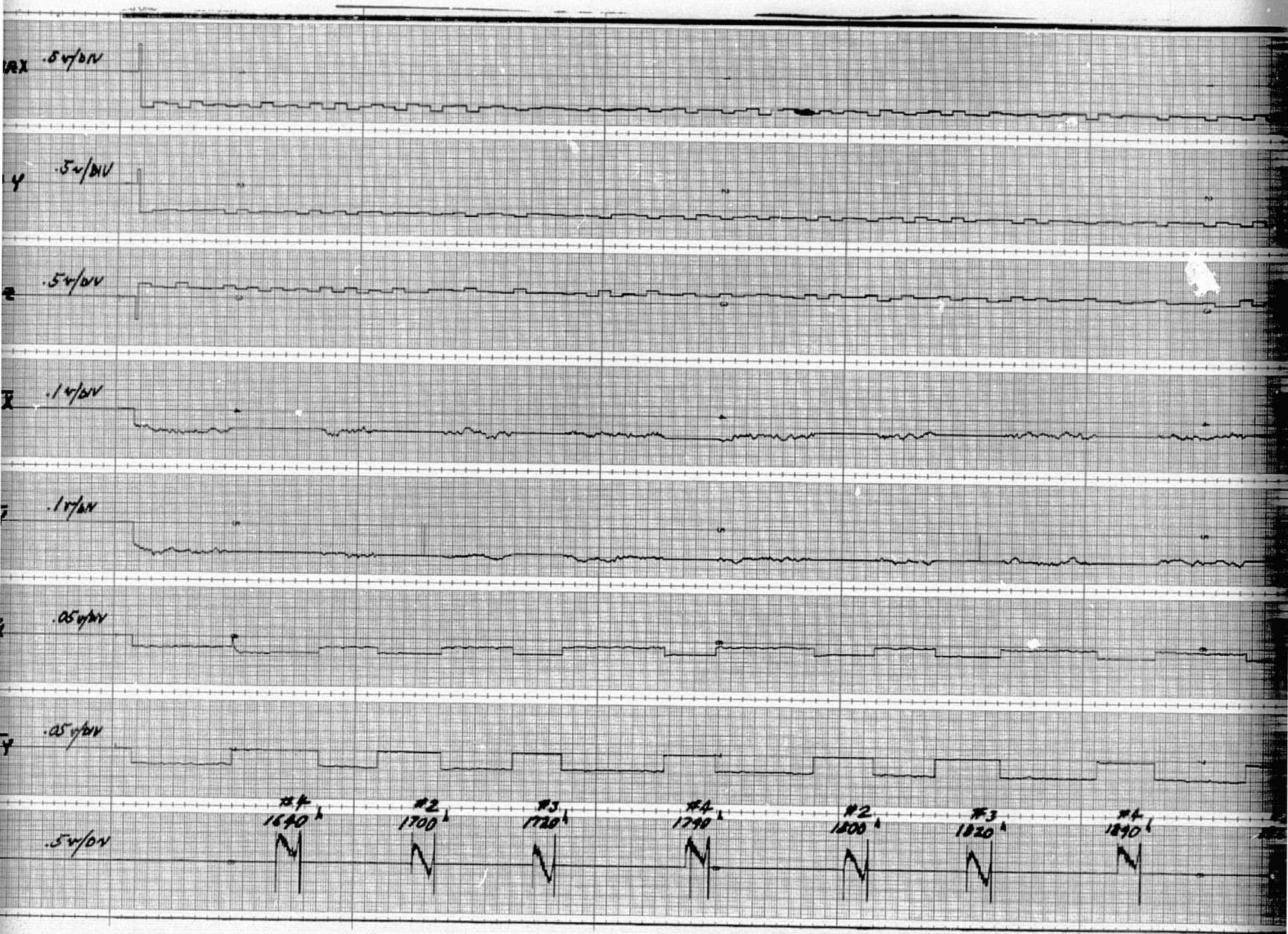

FOLDOUT FRAME 2

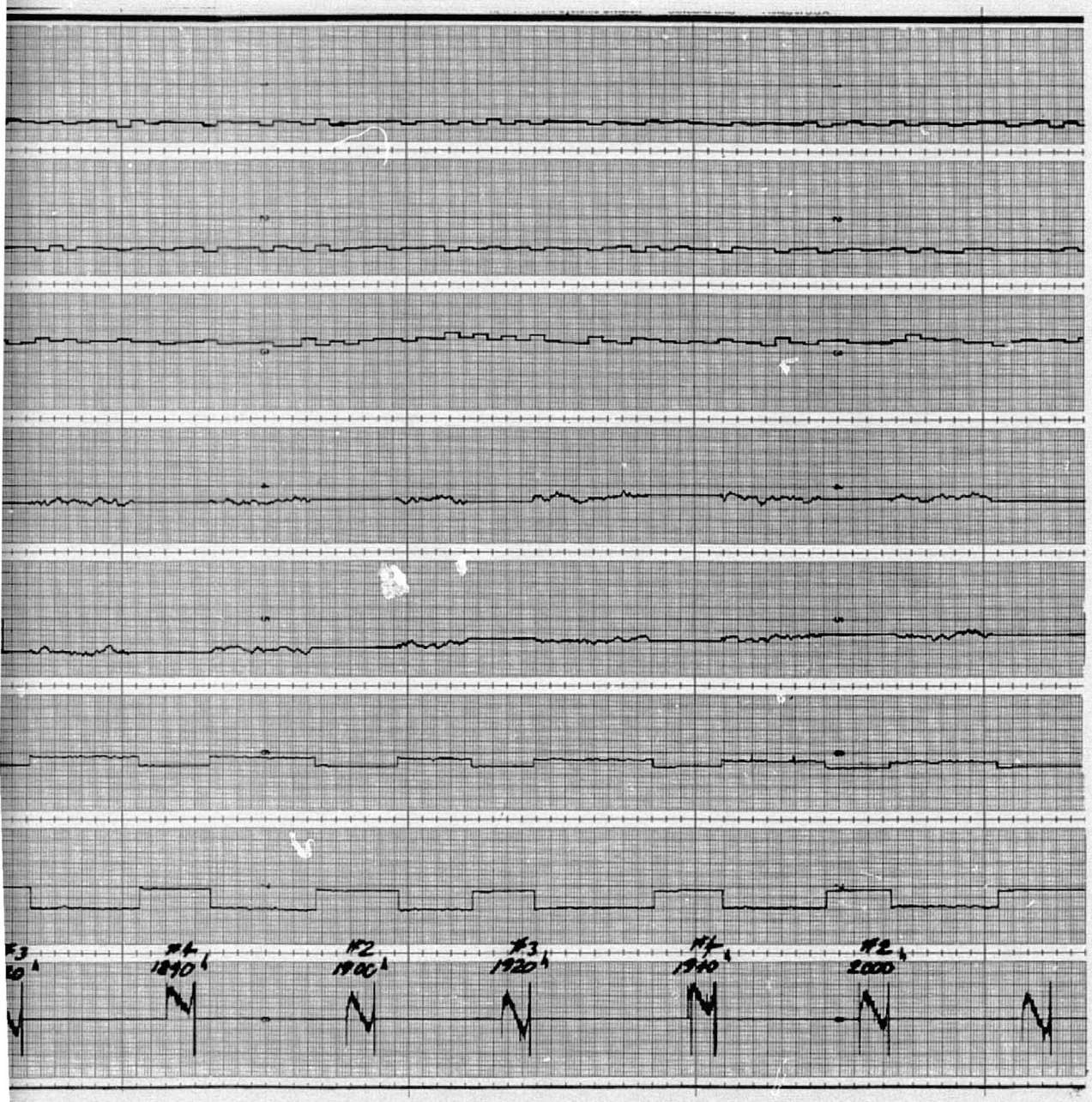

Figure D-4. Strapdown System Test Run No. 4

FOLDOUT FRAME 3

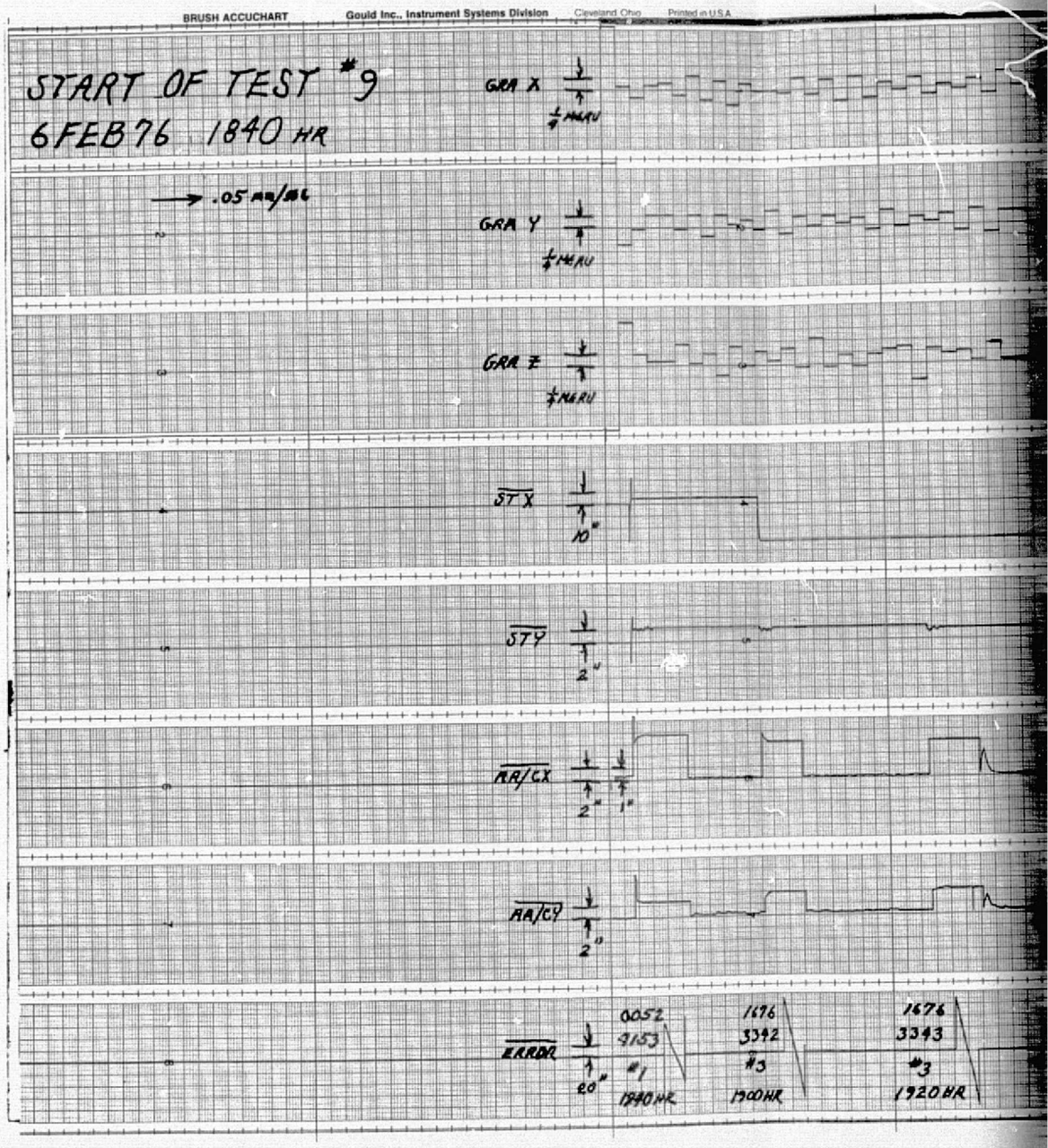

FOLDOUT FRAME

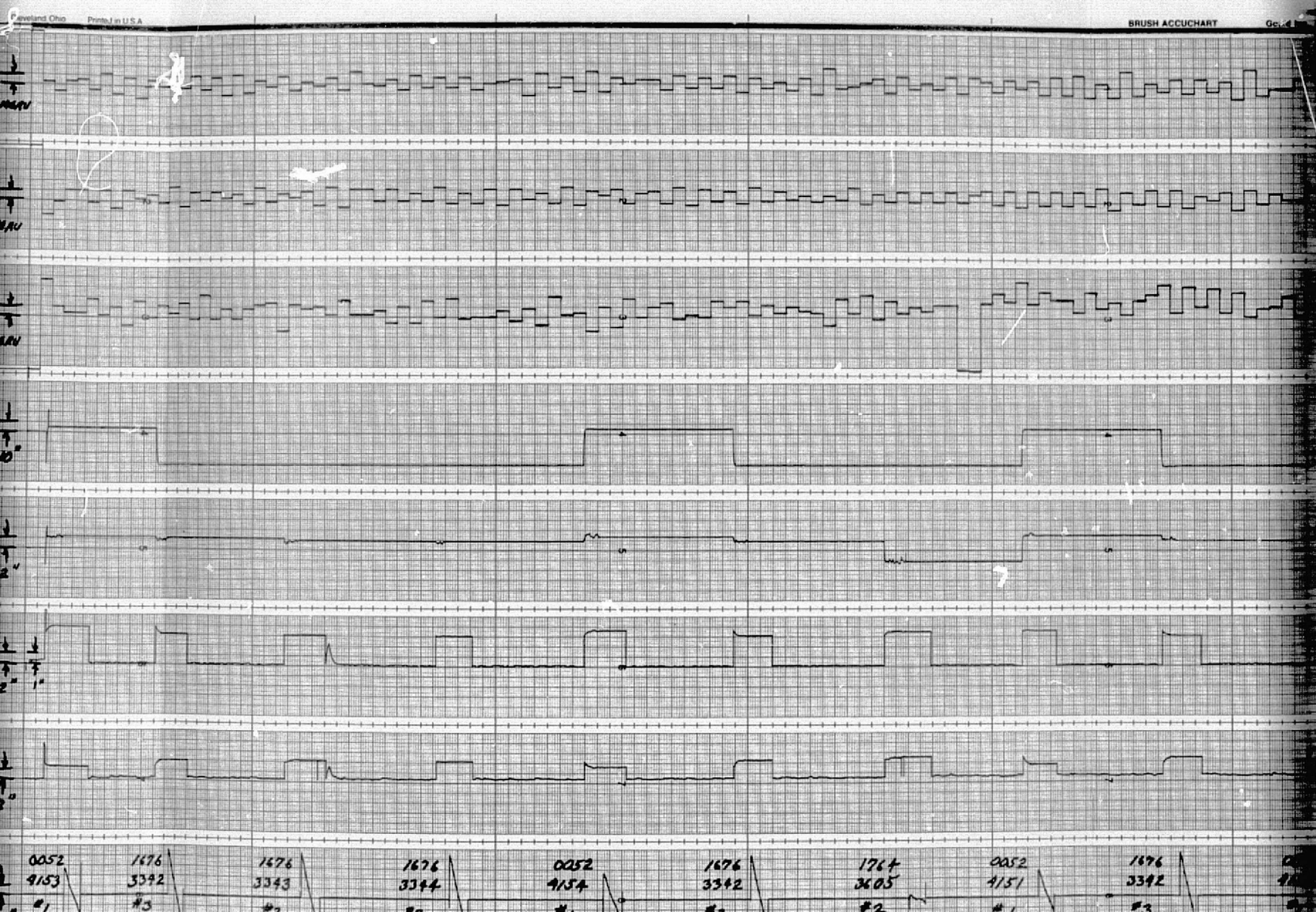

FOLDOUT FRAME 2

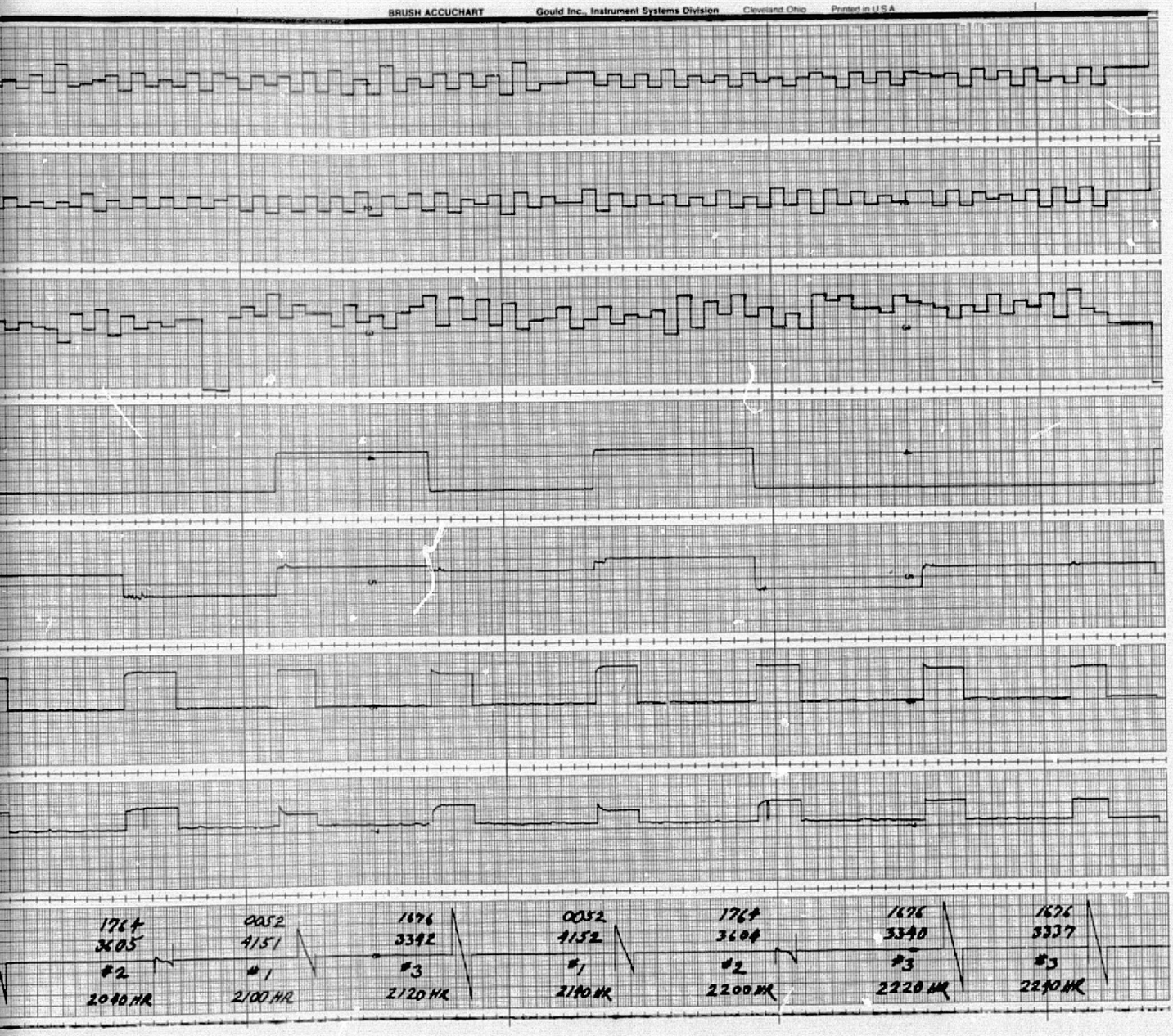

FOLDOUT FRAME 3

Figure D-5. Gimbal System Test Run No. 1

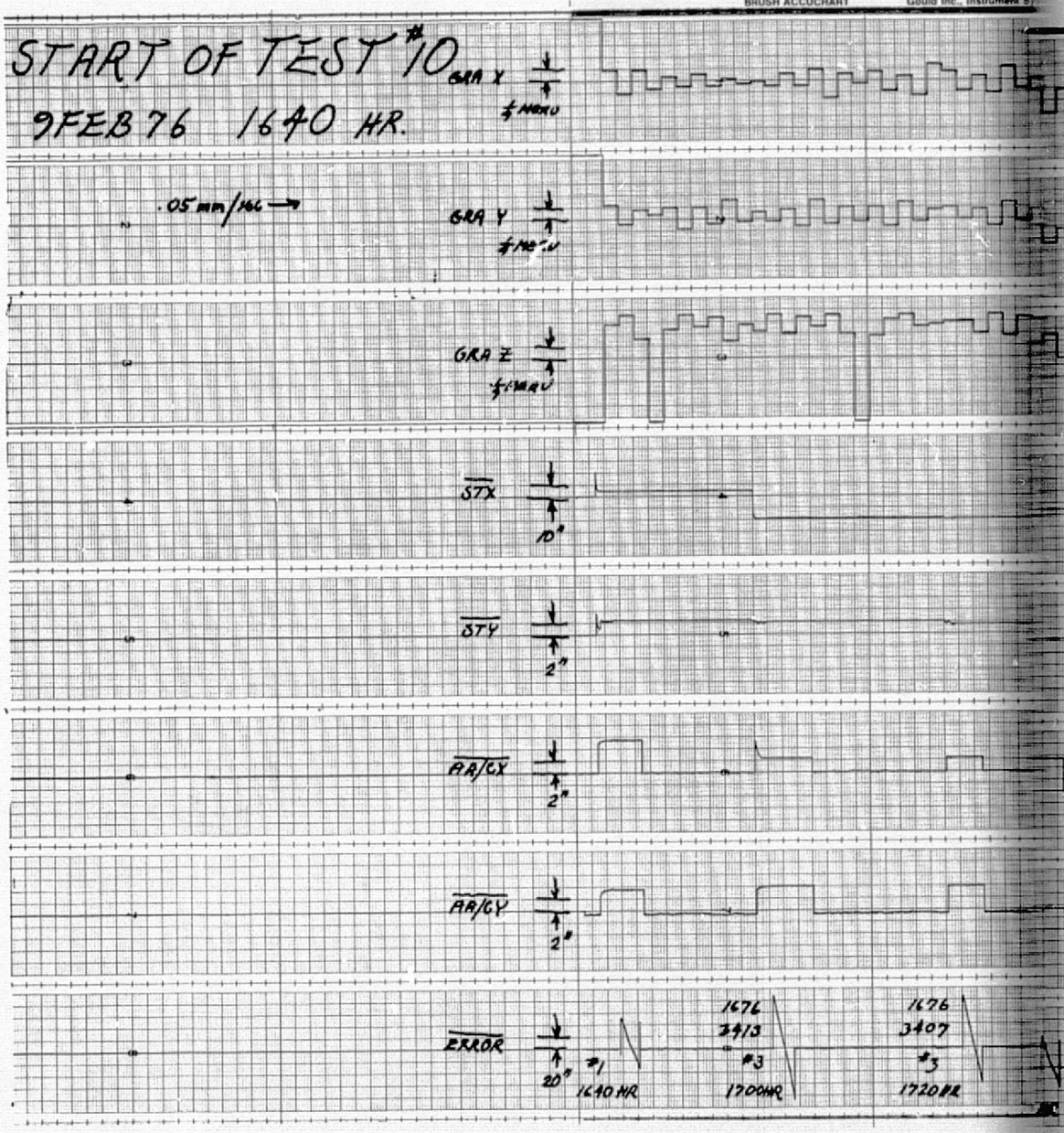

BRUSH ACCUCHART Gould Inc., Instrument Systems Division Cleveland Ohio Printed in U.S.A.

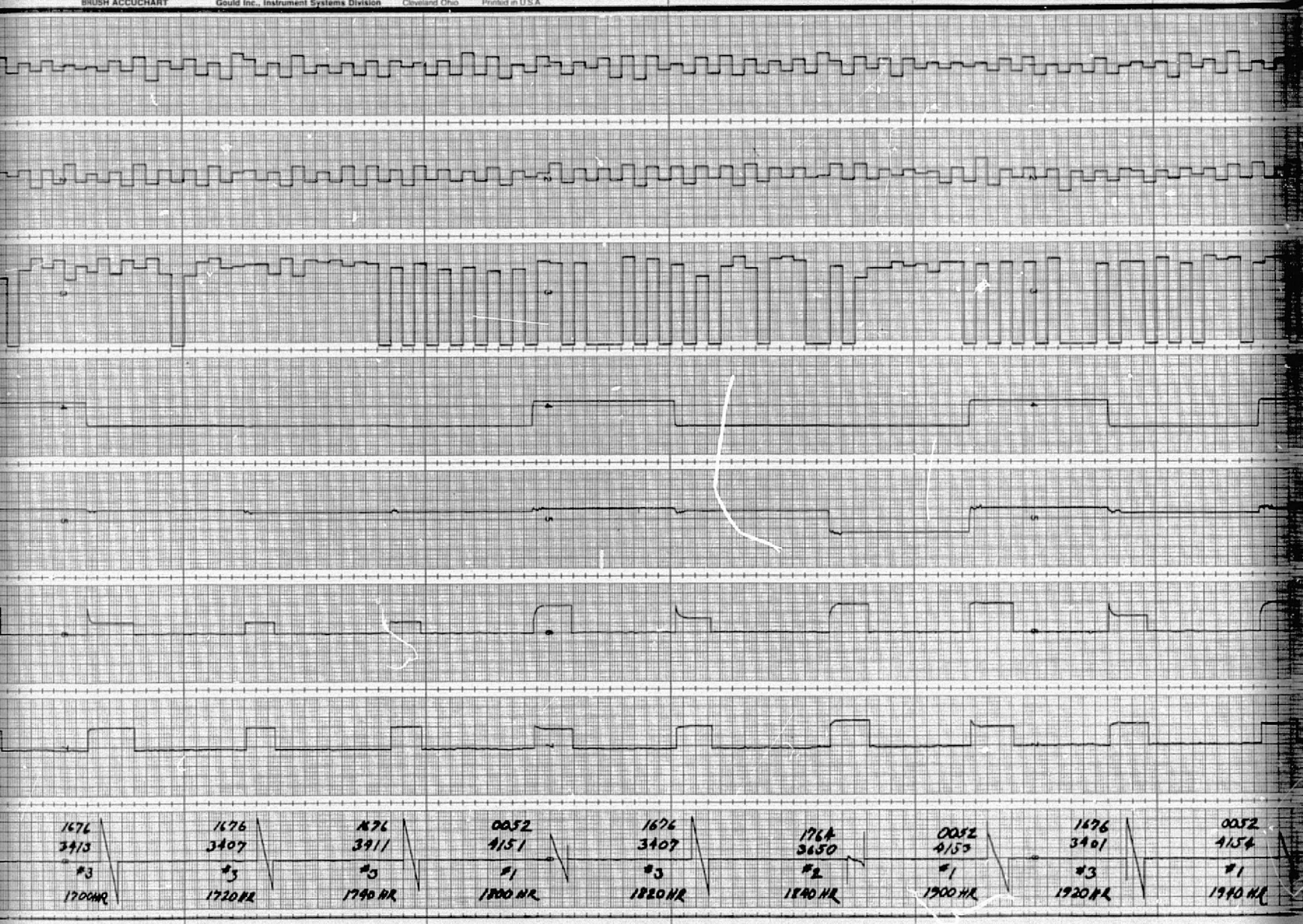

WATERMARK FRAME 2

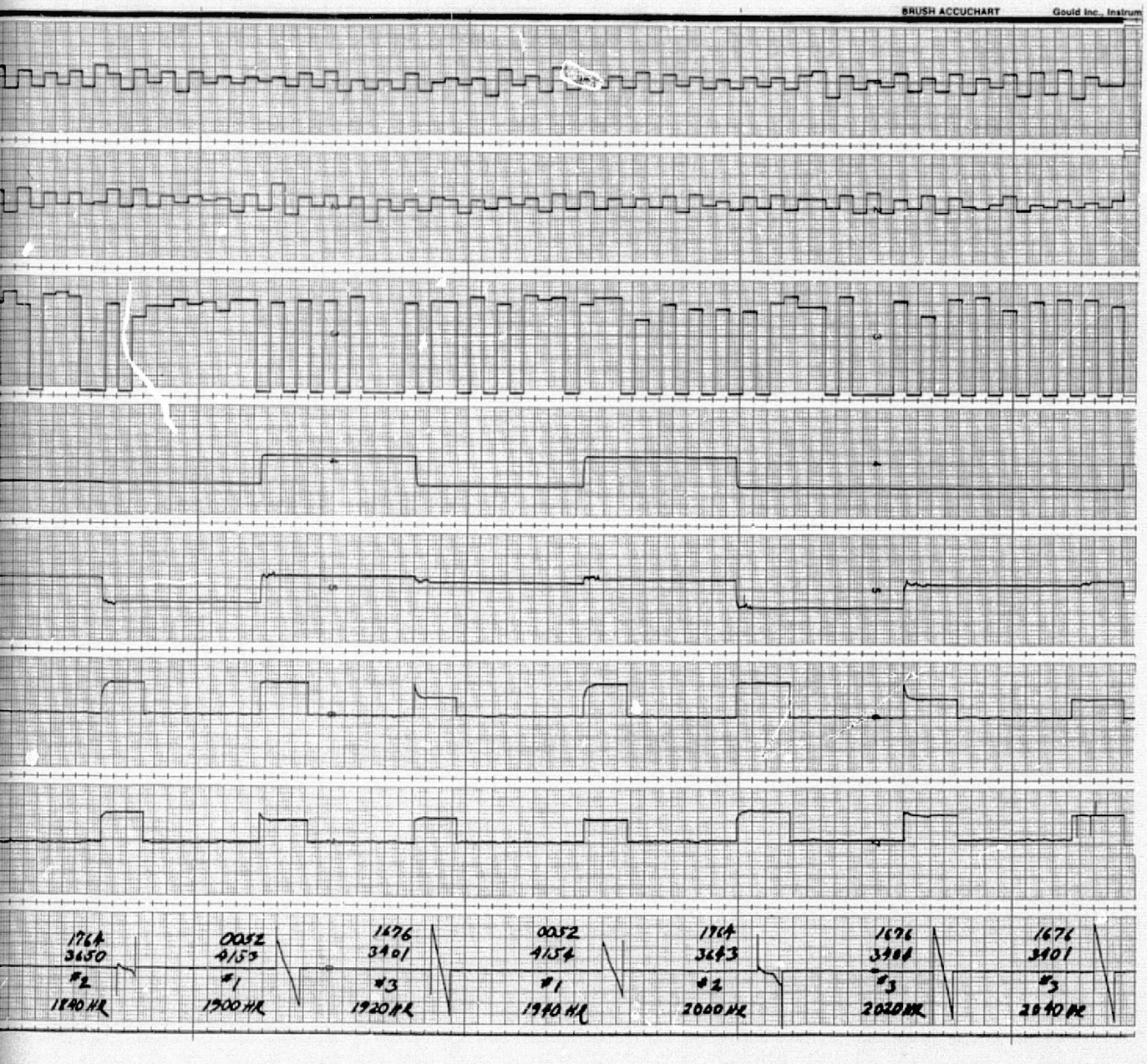

FOLDOUT FRAME 3

Figure D-6. Gimbal System Test Run No. 2

land, Ohio Printed in U.S.A.

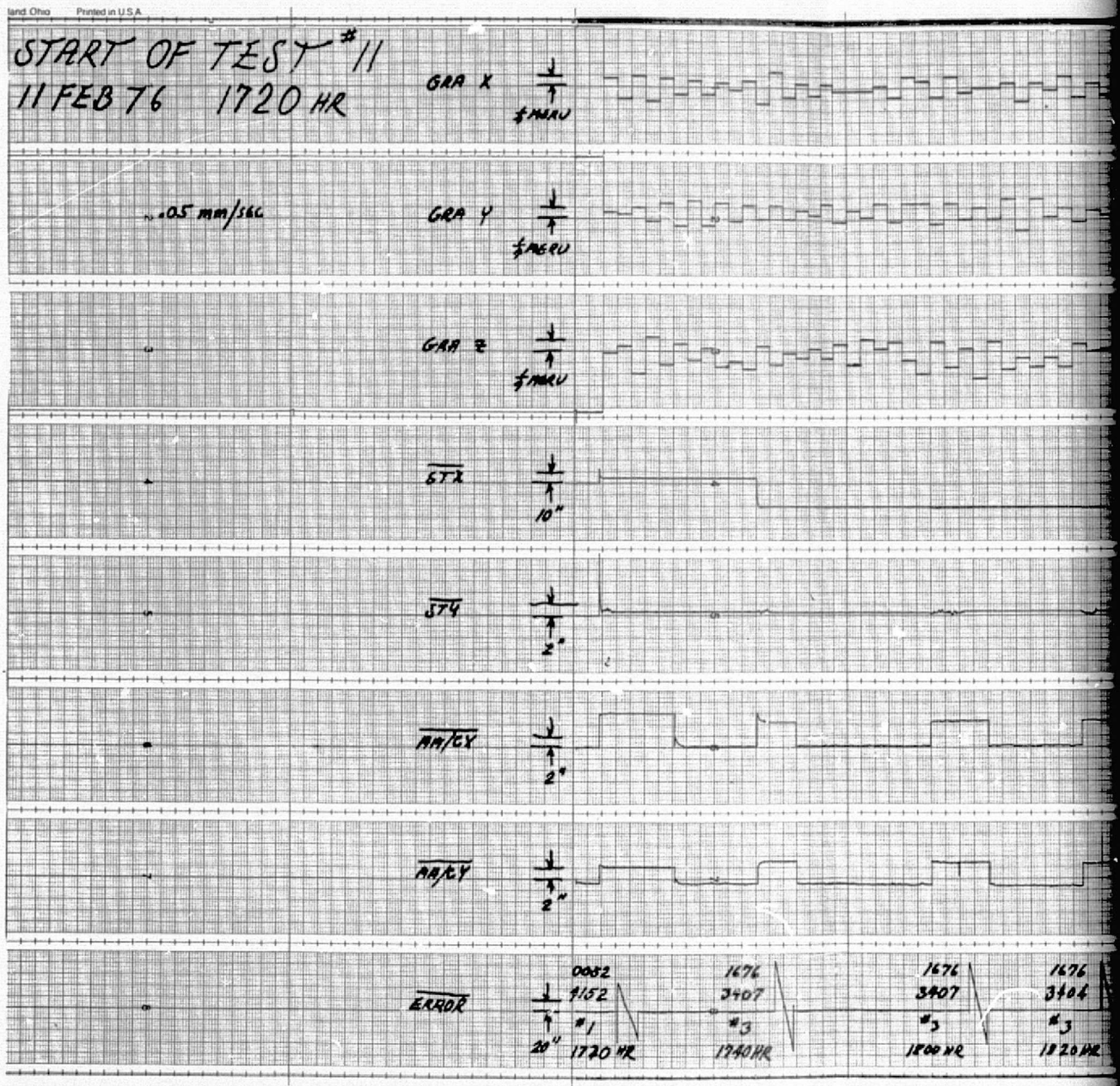

FOLDOUT FRAME

BRUSH ACCUCHART Gould Inc., Instrument Systems Division Cleveland, Ohio Printed in U.S.A.

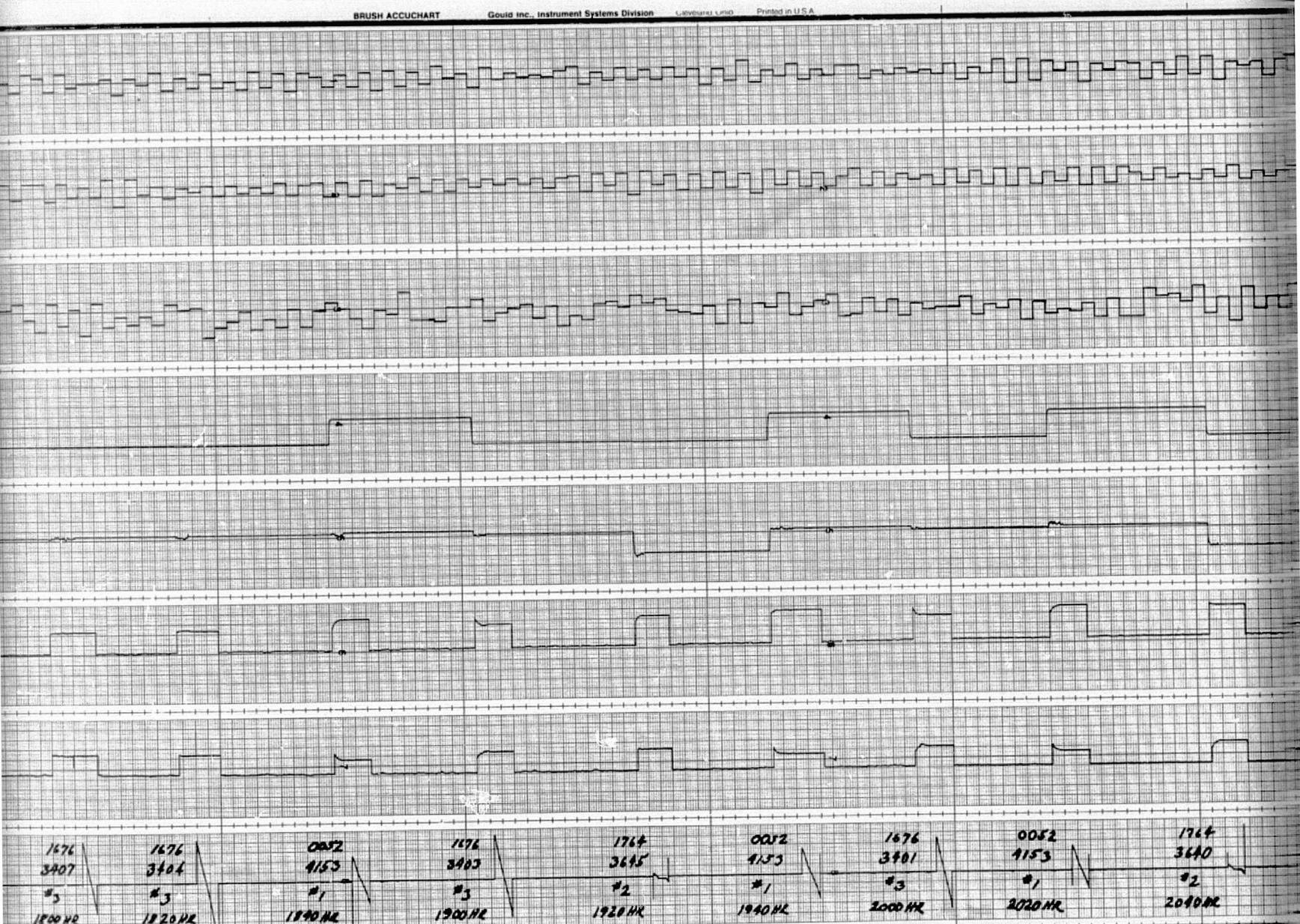

FOLDOUT FRAME 2

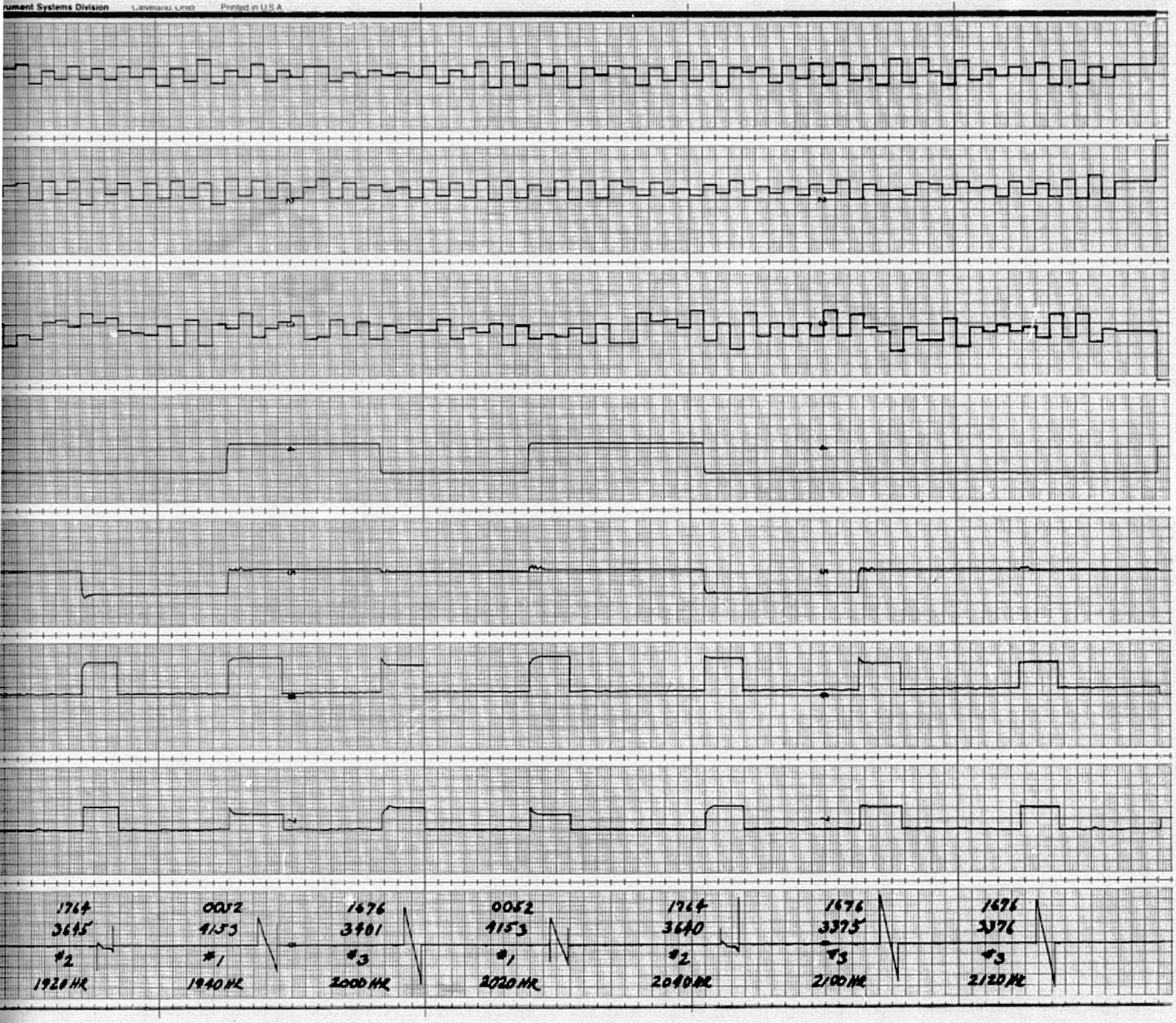

Figure D-7. Gimbal System
Test Run No. 3

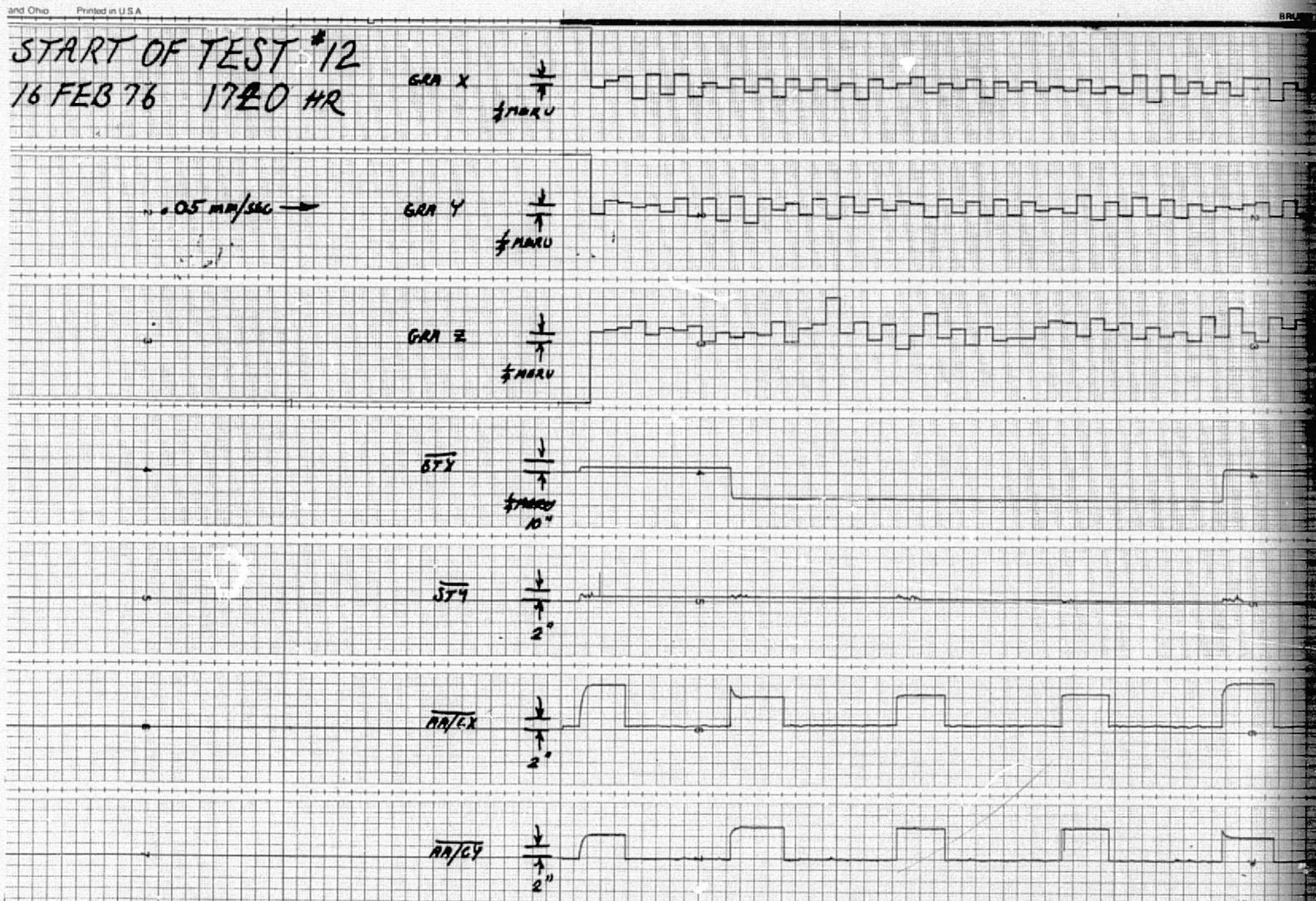

FOLDOUT FRAME 1

RUSH ACCUCHART Gould Inc., Instrument Systems Division Cleveland Ohio Printed in U.S.A.

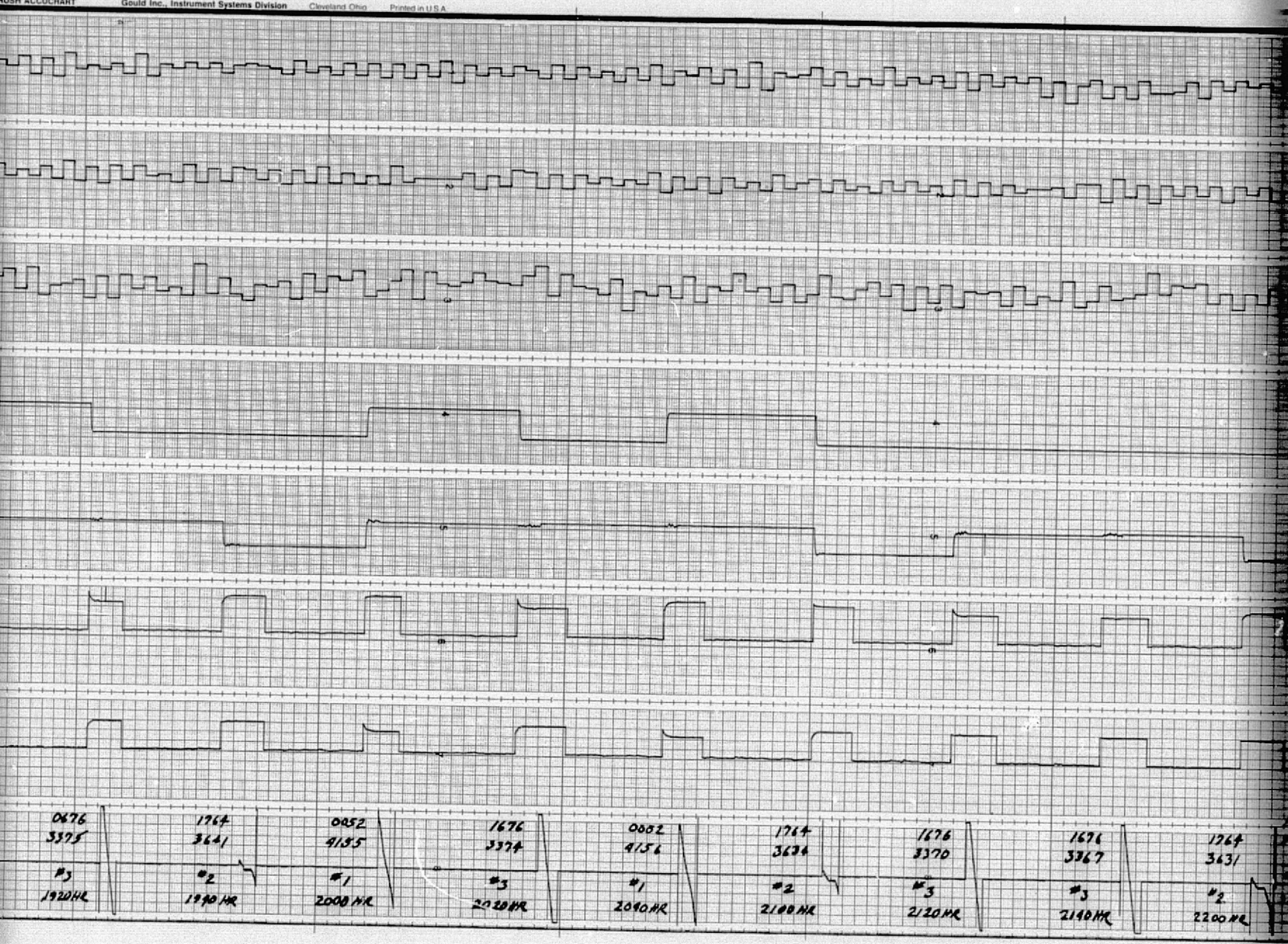

FOLDOUT FRAME 2

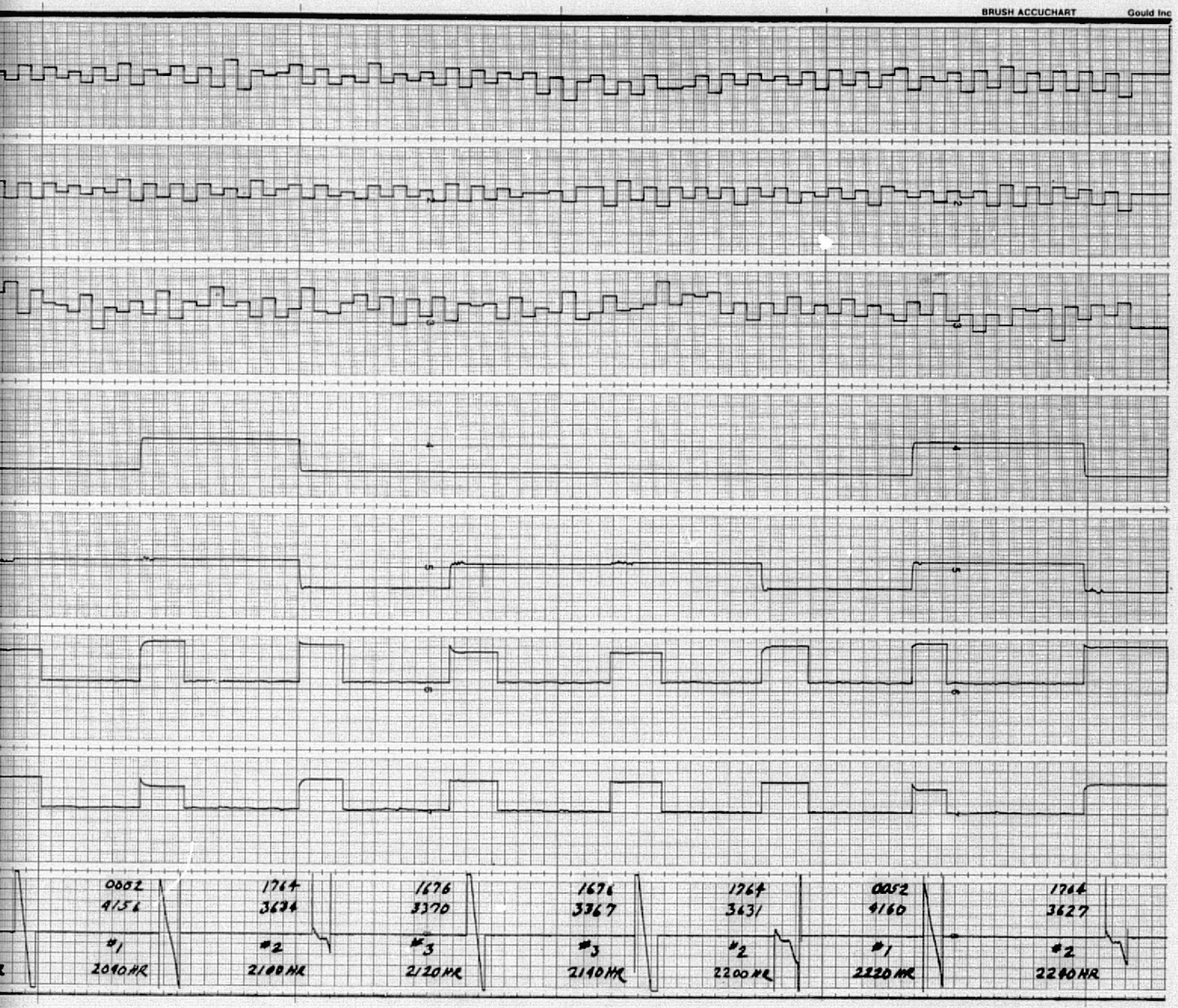

Figure D-8. Gimbal System Test Run No. 4

FOLDOUT FRAME 3

APPENDIX E

FLOW DIAGRAMS OF LABORATORY COMPUTER PROGRAMS

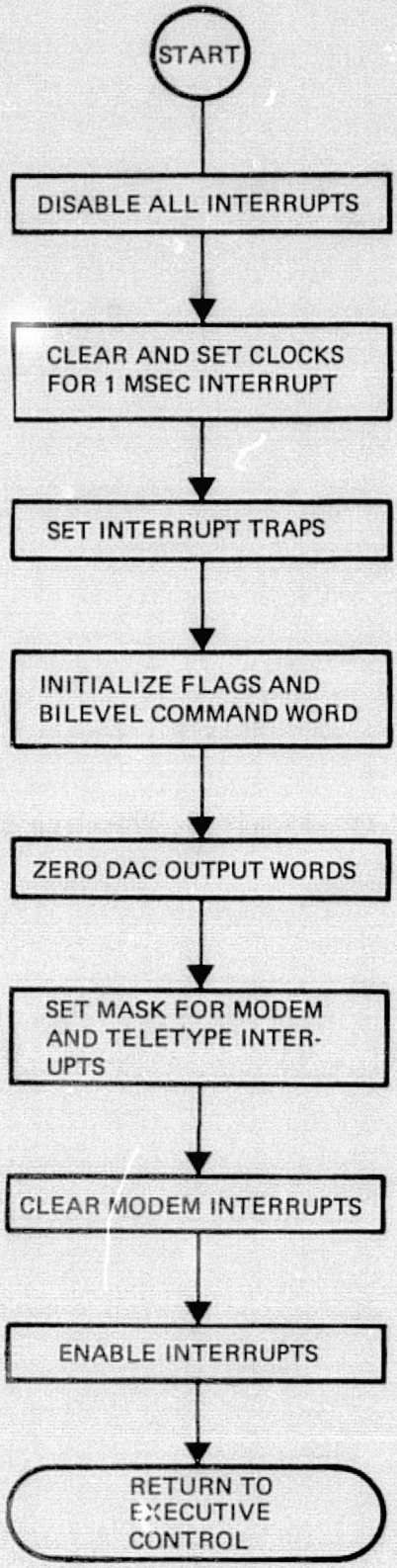

SUE Program Flow Charts (1 of 7)

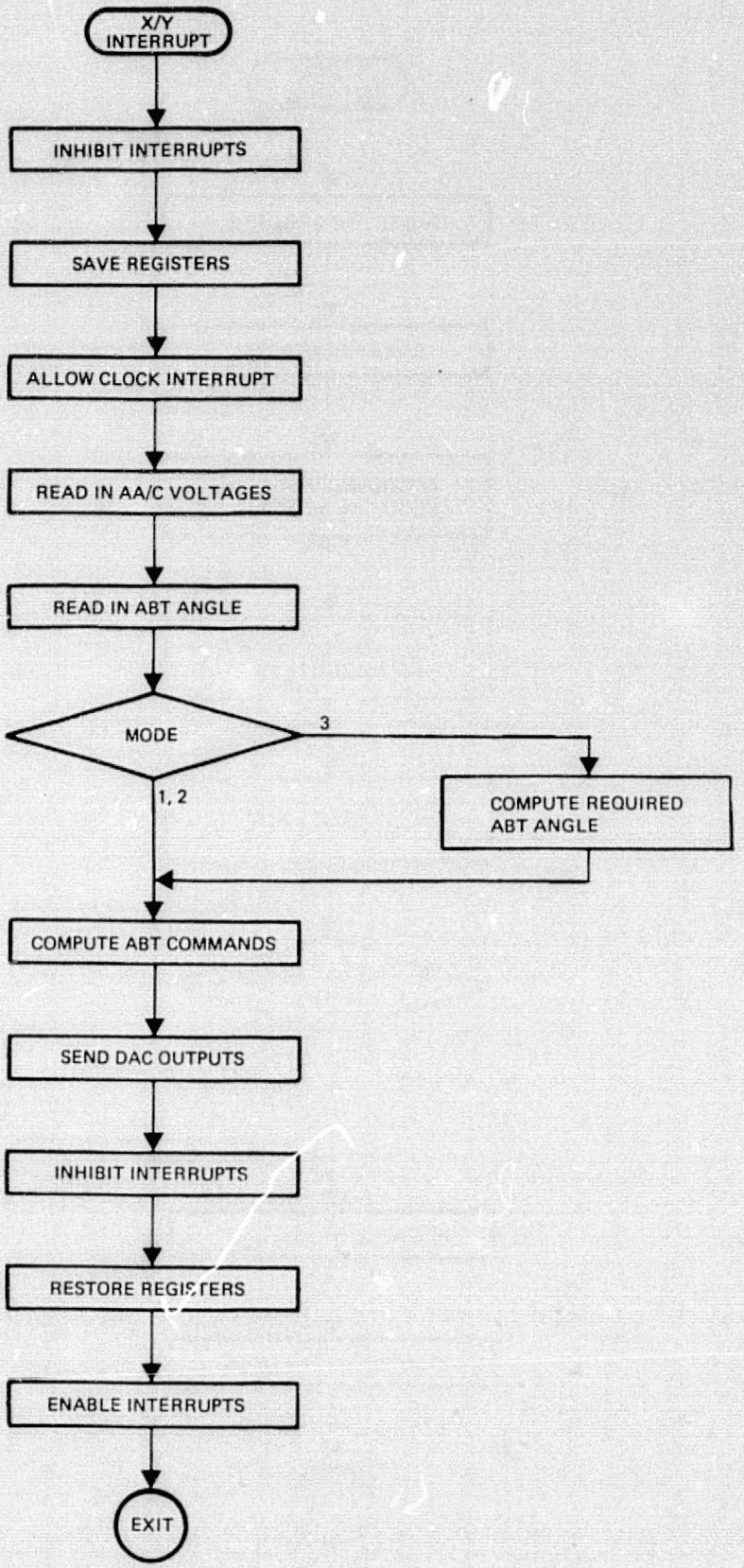

SUE Program Flow Charts (2 of 7)

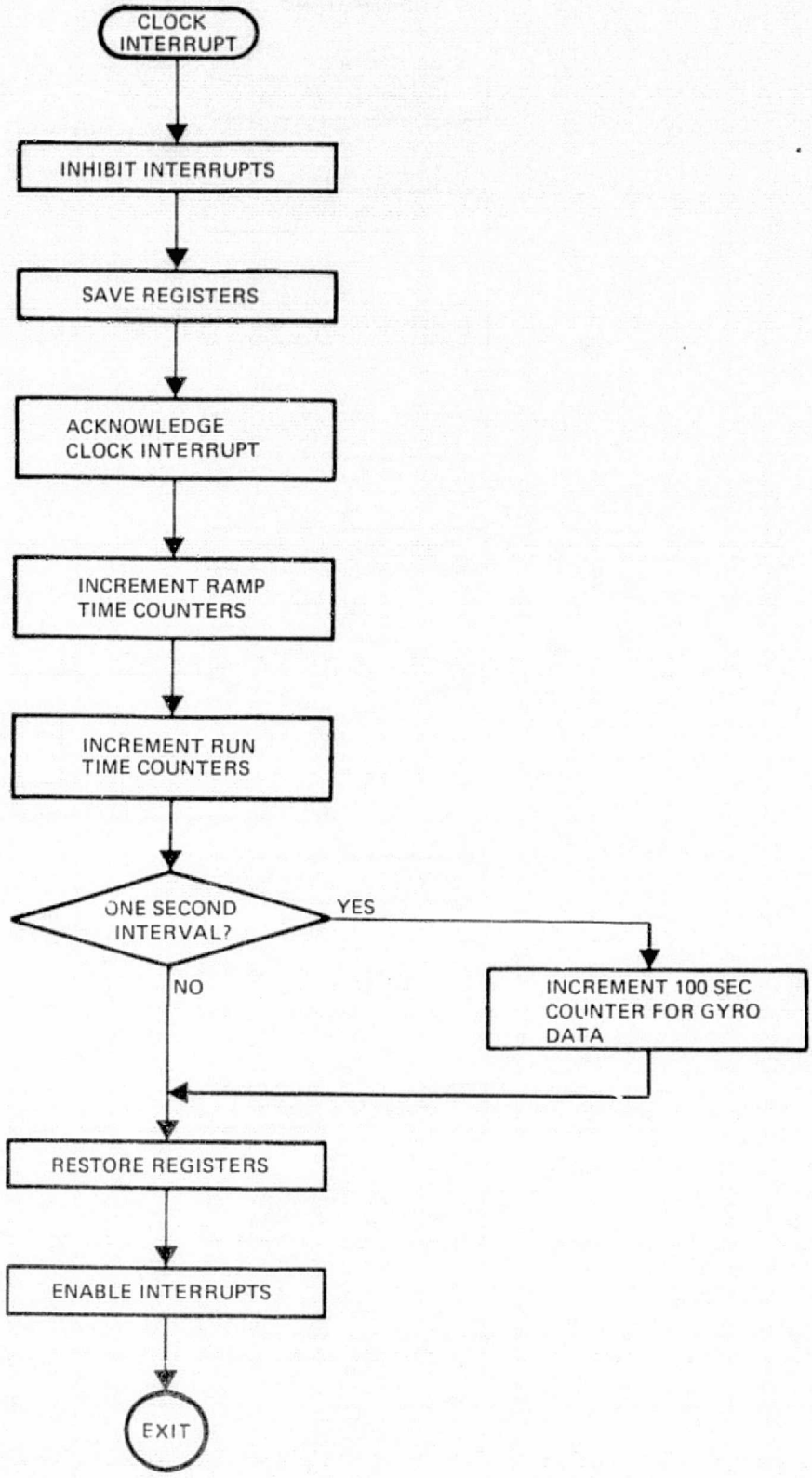

SUE Program Flow Charts (3 of 7)

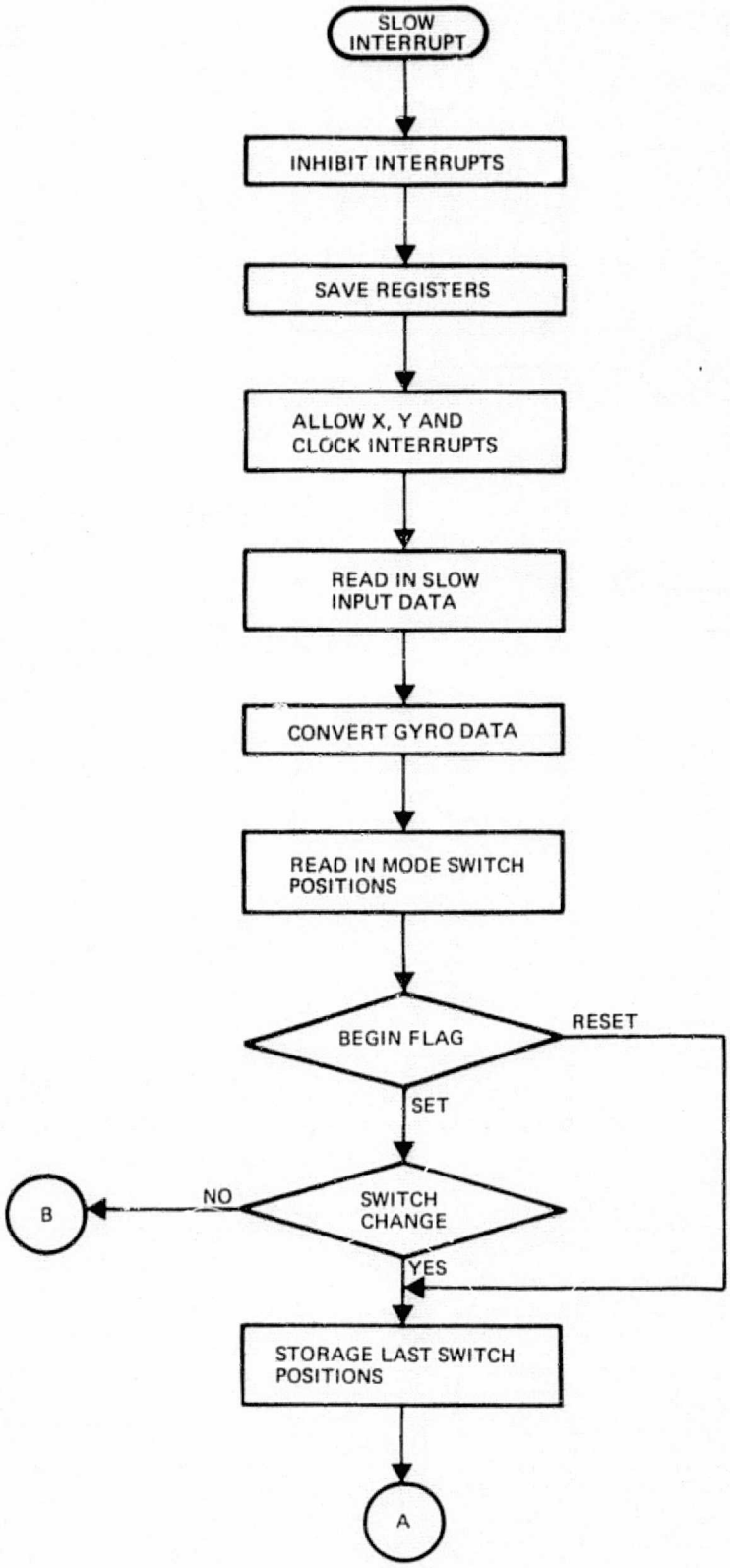

SUE Program Flow Charts (4 of 7)

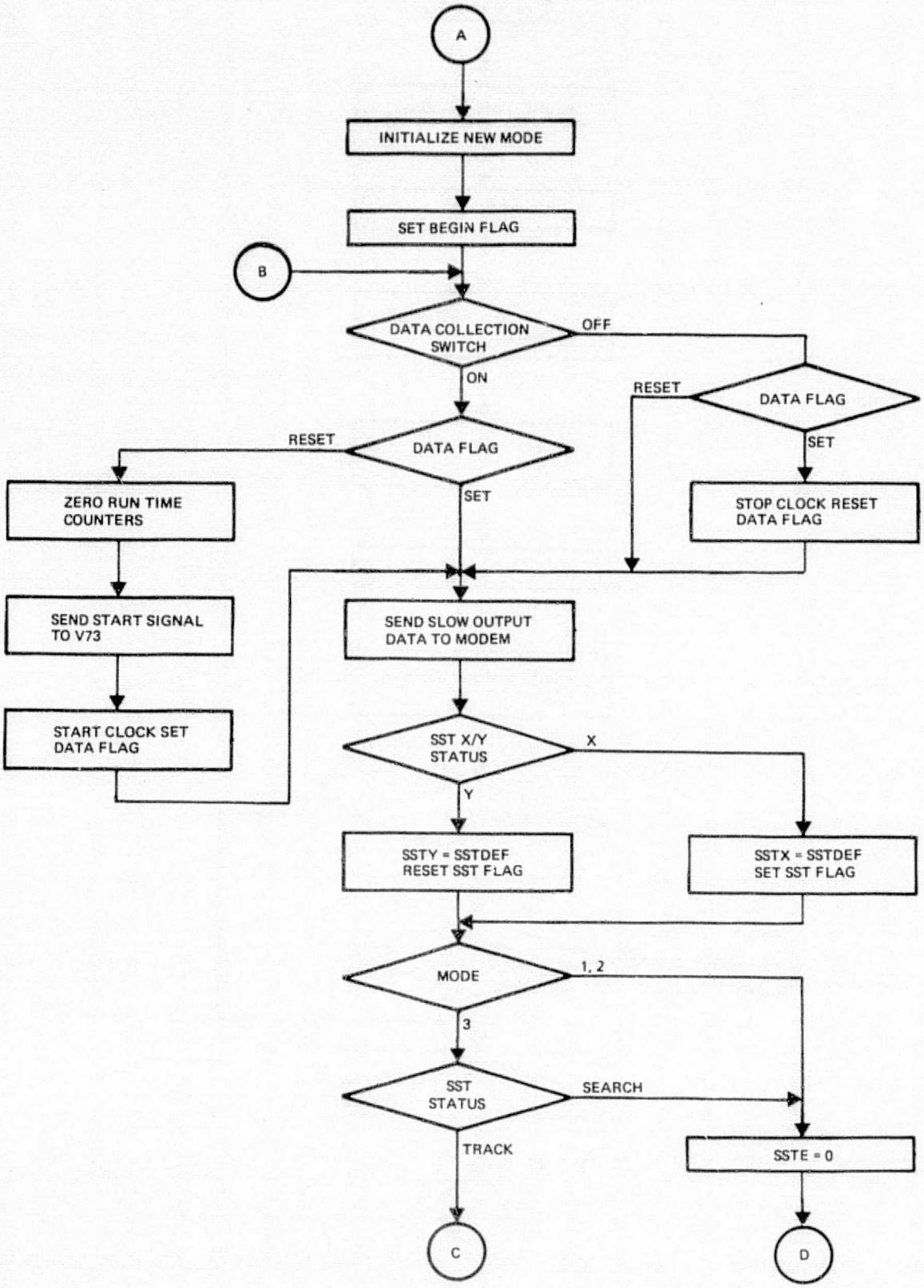

SUE Program Flow Charts (5 of 7)

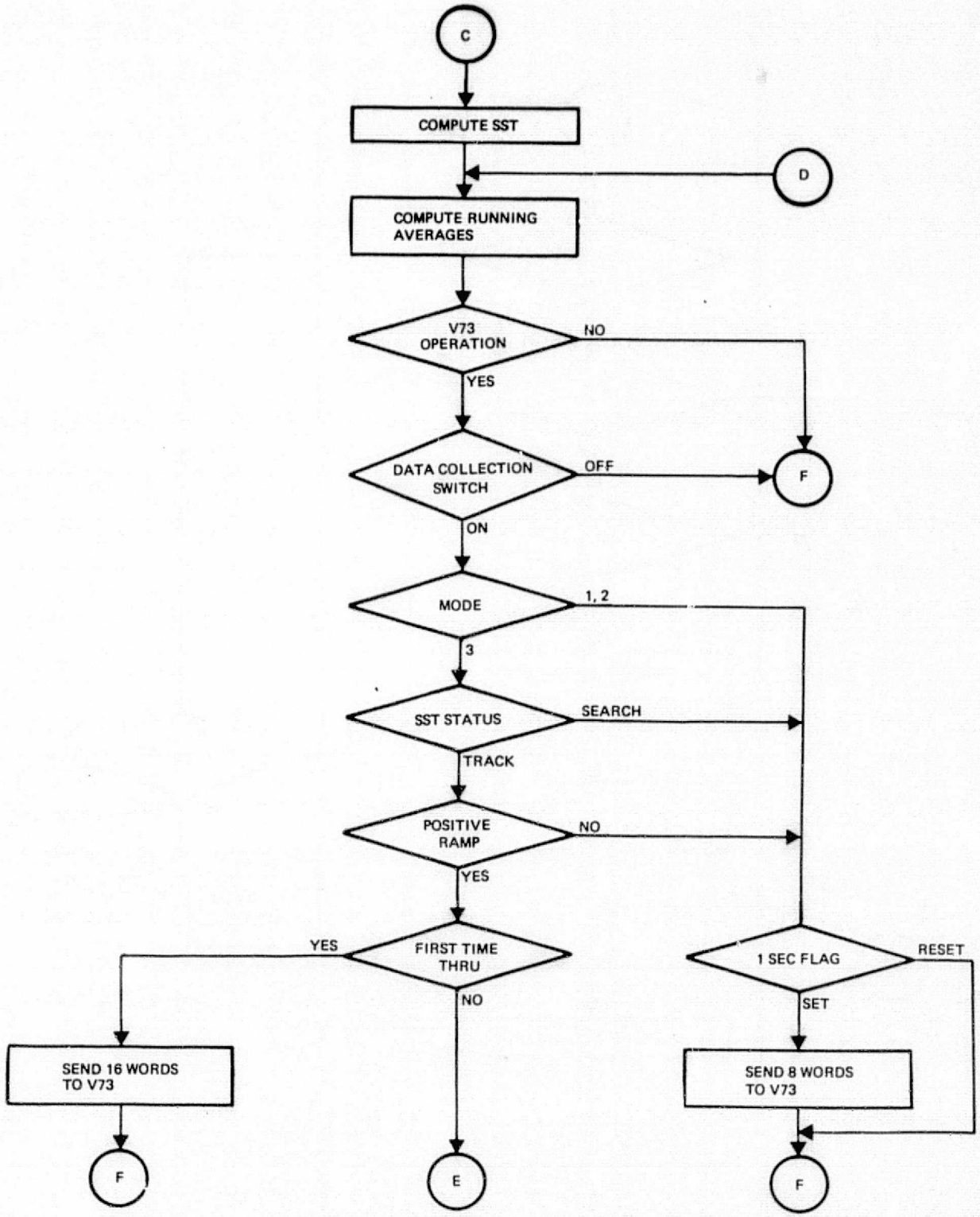

SUE Program Flow Charts (6 of 7)

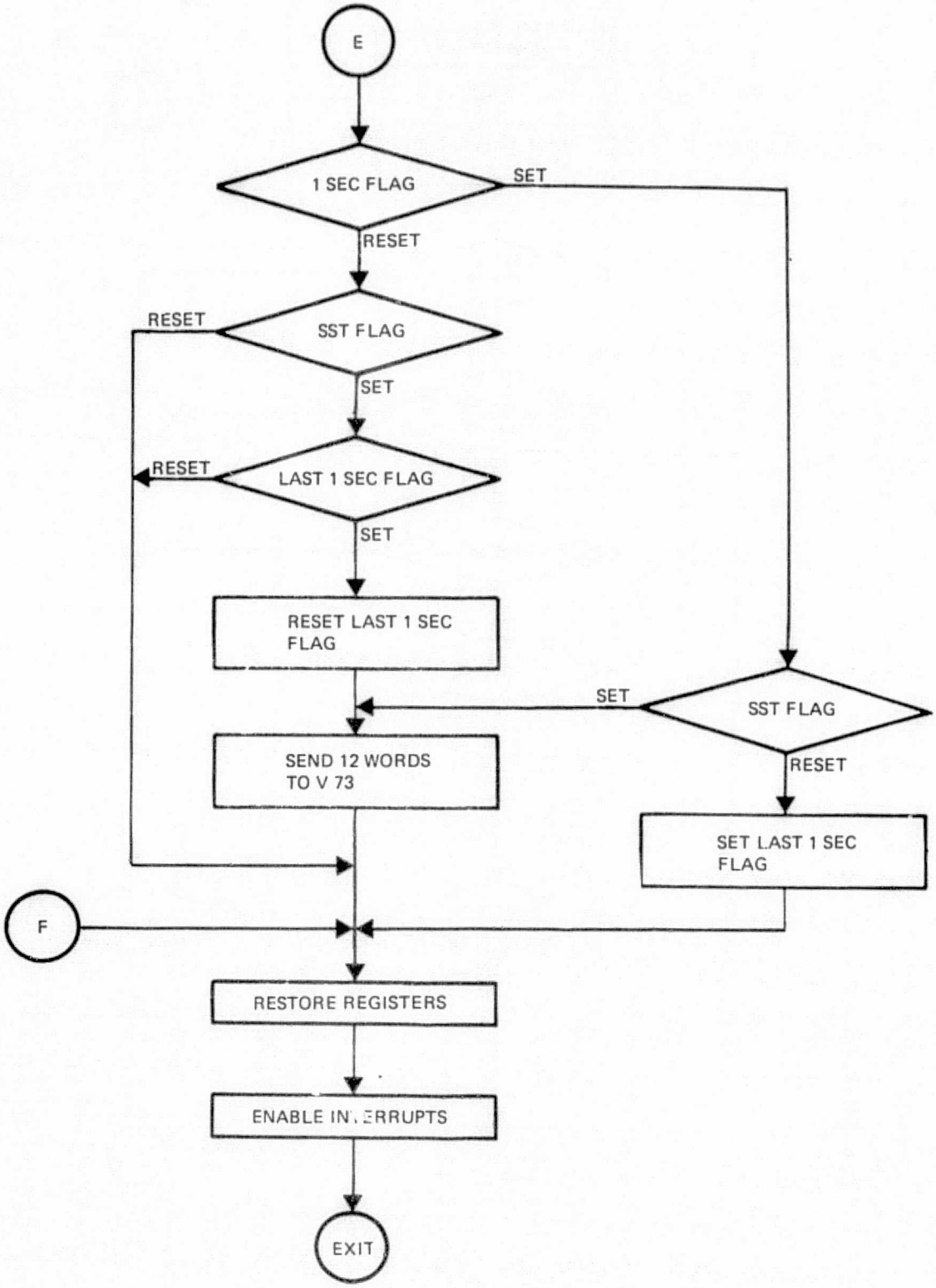

SUE Program Flow Charts (7 of 7)

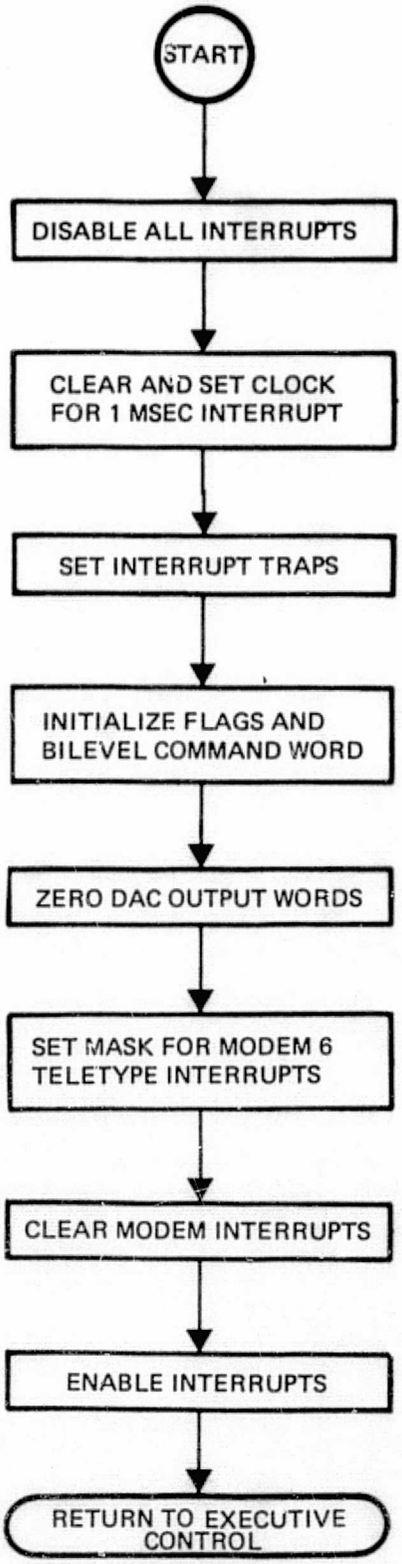

GWEN Program Flow Charts (1 of 7)

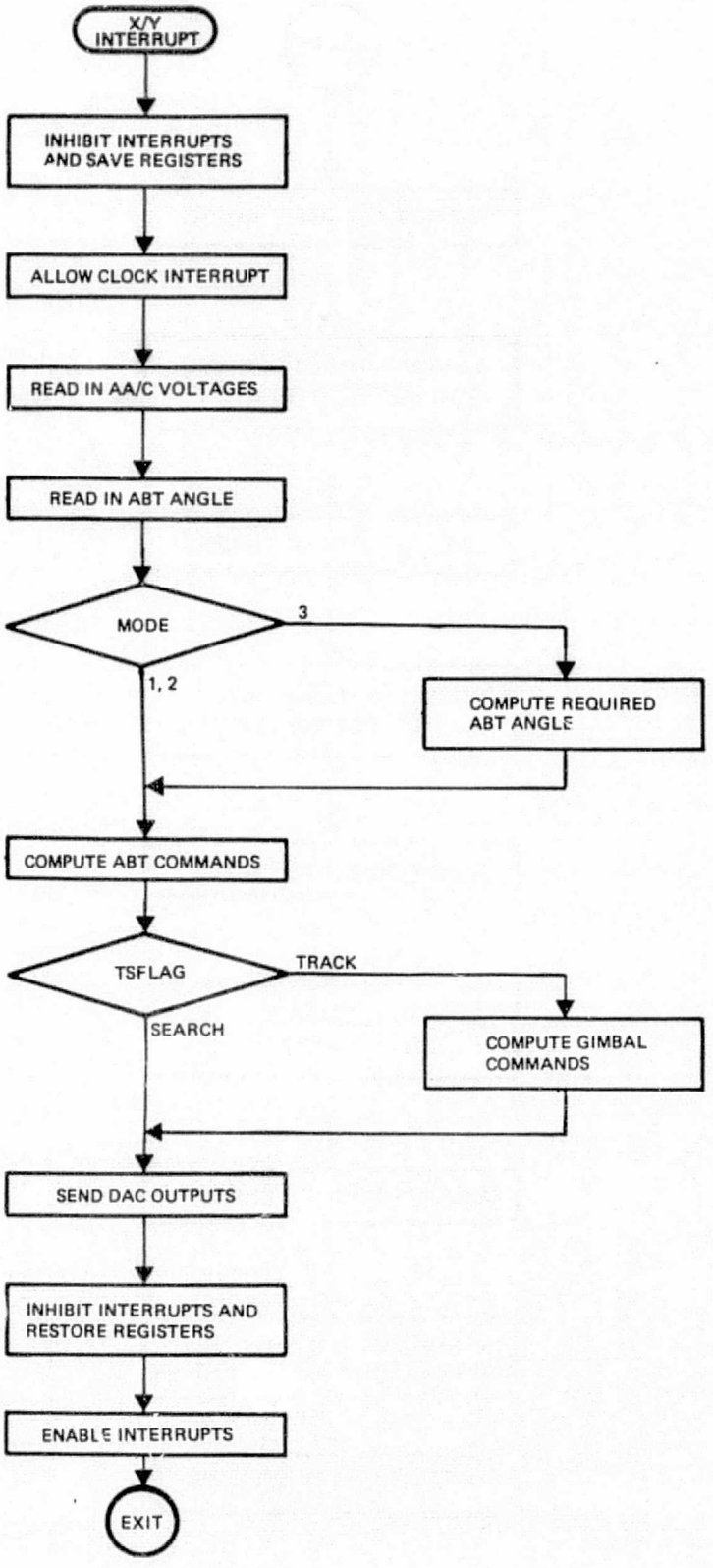

GWEN Program Flow Charts (2 of 7)

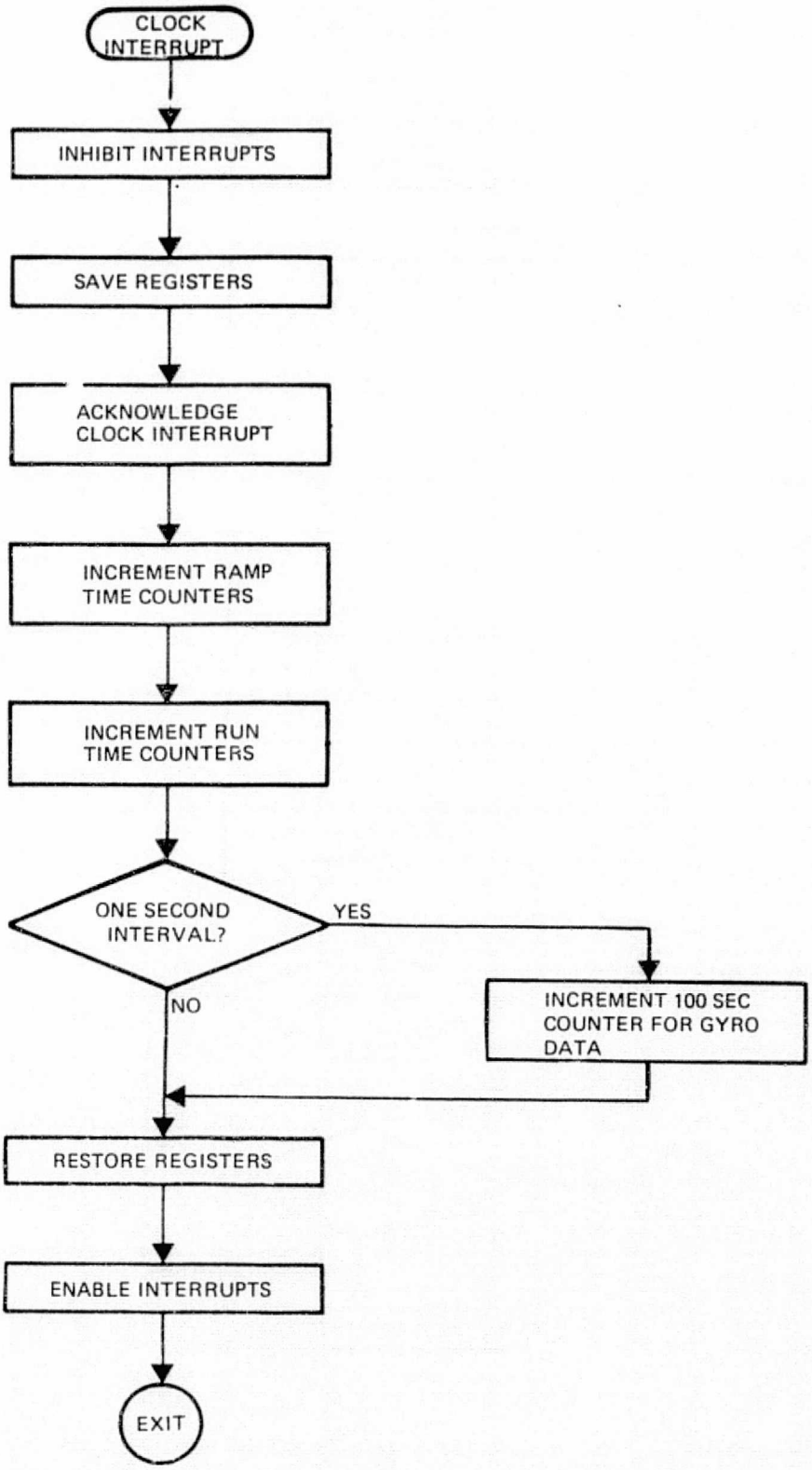

GWEN Program Flow Charts (3 of 7)

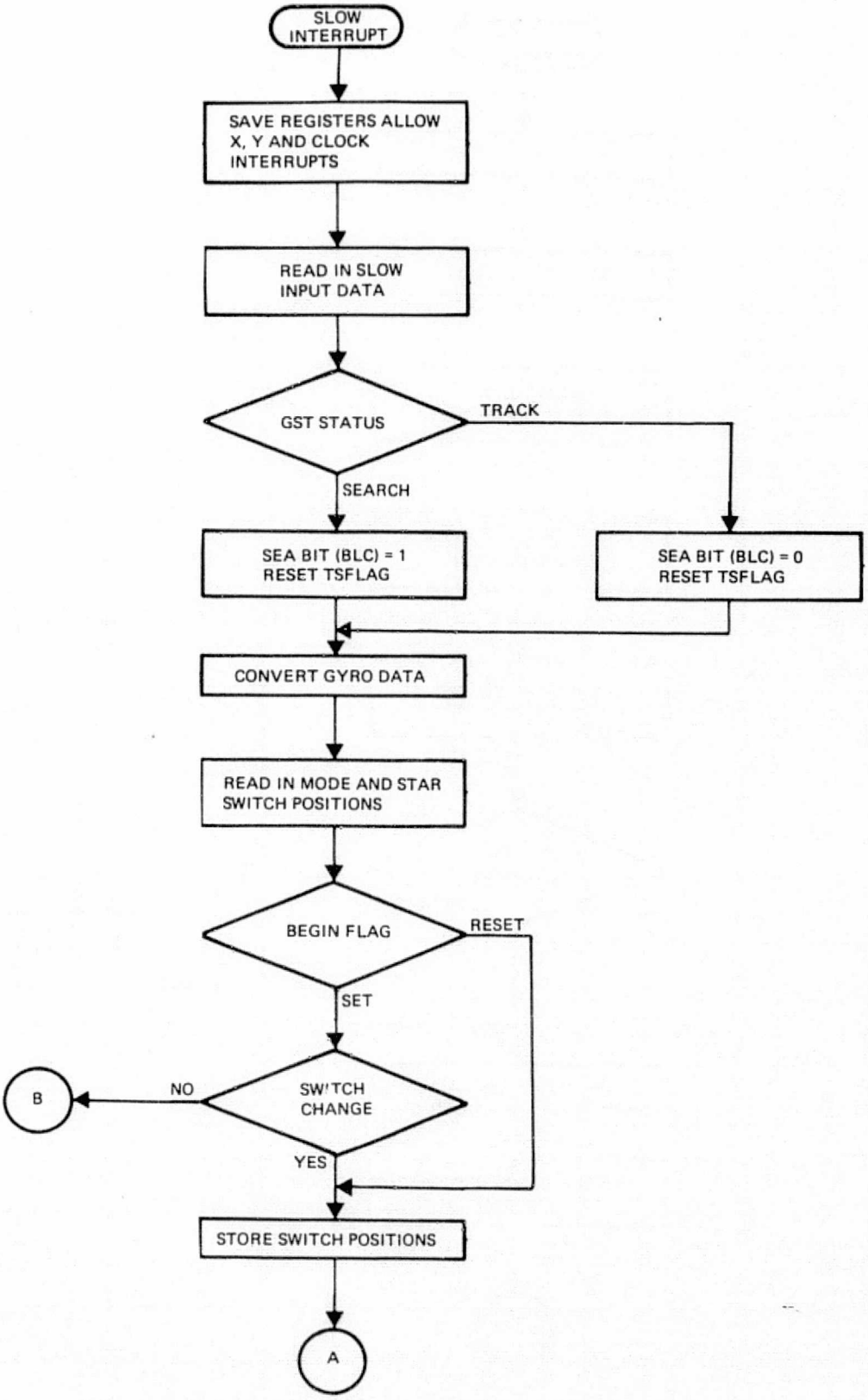

GWEN Program Flow Charts (4 of 7)

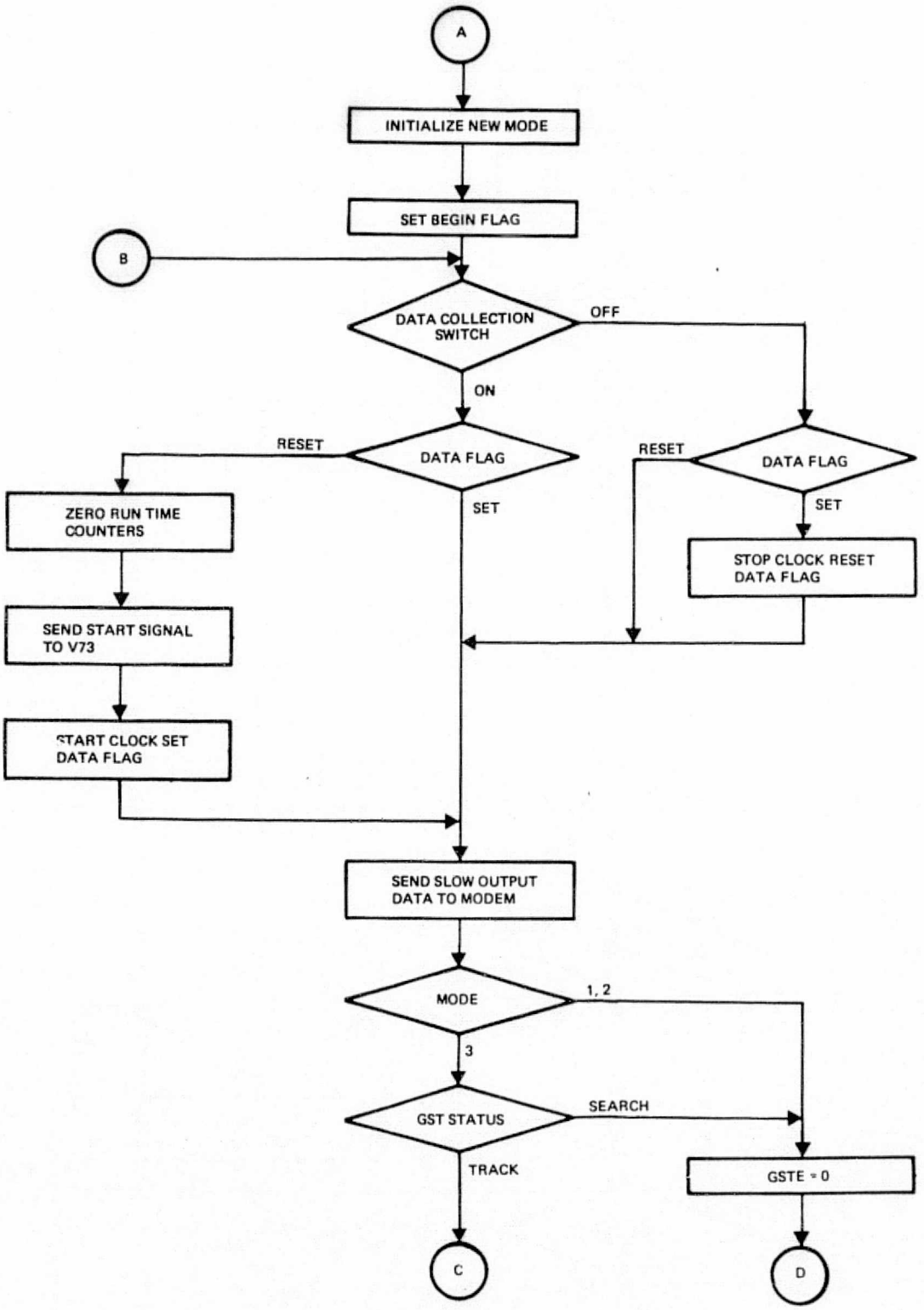

GWEN Program Flow Charts (5 of 7)

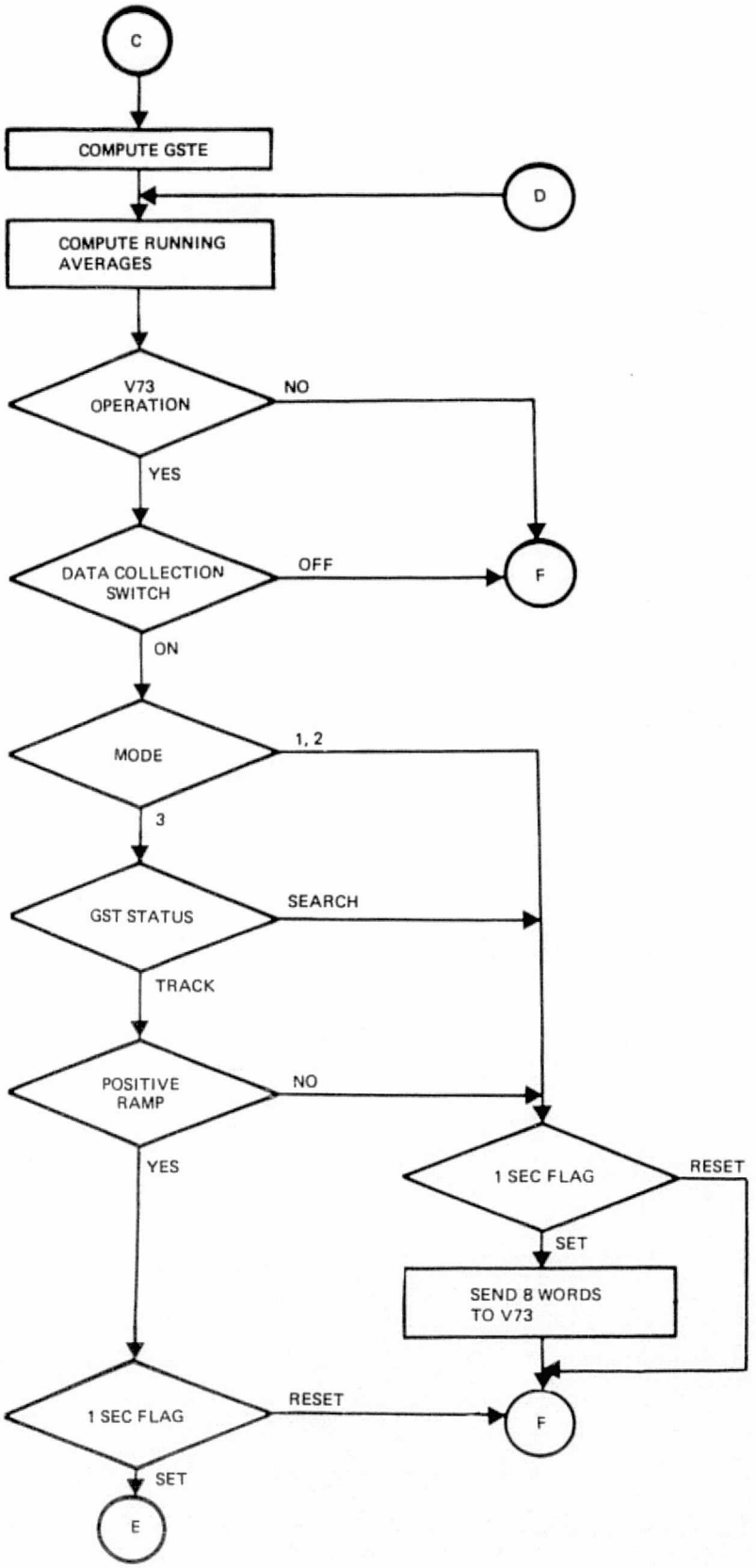

GWEN Program Flow Charts (6 of 7)

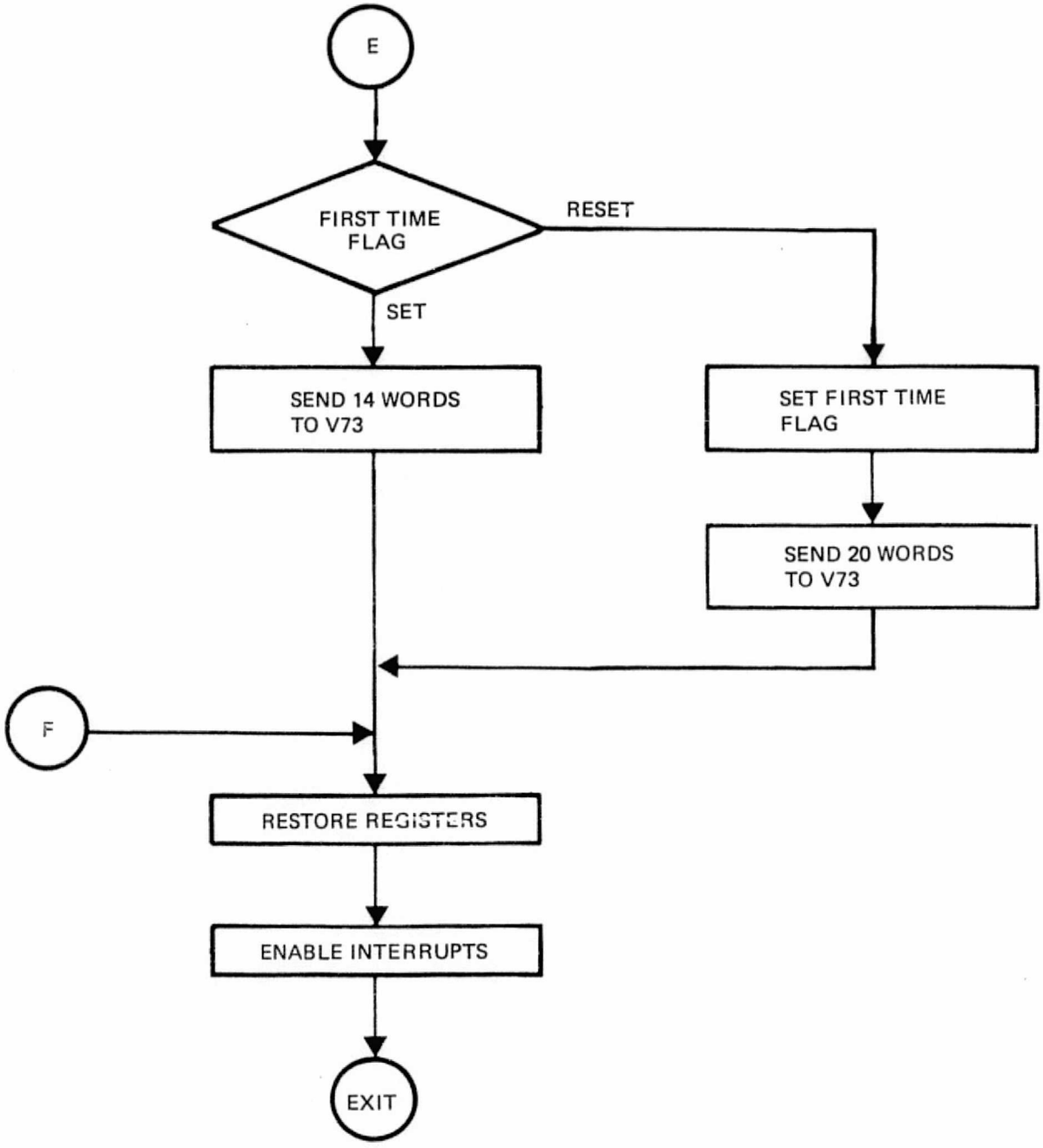

GWEN Program Flow Charts (7 of 7)